

IMPACT OF CLIMATE CHANGE IN THE SOUTHERN MEDITERRANEAN
OF TURKEY:
A METHOD TO ASSESS OYMAPINAR RESERVOIR'S INFLOW
PROJECTIONS

A THESIS SUBMITTED TO
THE GRADUATE SCHOOL OF NATURAL AND APPLIED SCIENCES
OF
MIDDLE EAST TECHNICAL UNIVERSITY

BY

BUKET MESTA YOLERI

IN PARTIAL FULFILLMENT OF THE REQUIREMENTS
FOR
THE DEGREE OF DOCTOR OF PHILOSOPHY
IN
EARTH SYSTEM SCIENCE

JUNE 2022

Approval of the thesis:

**IMPACT OF CLIMATE CHANGE IN THE SOUTHERN
MEDITERRANEAN OF TURKEY:
A METHOD TO ASSESS OYMAPINAR RESERVOIR'S INFLOW
PROJECTIONS**

submitted by **BUKET MESTA YOLERİ** in partial fulfillment of the requirements for the degree of **Doctor of Philosophy in Earth System Science, Middle East Technical University** by,

Prof. Dr. Halil Kalıpçılar
Dean, Graduate School of **Natural and Applied Sciences**

Prof. Dr. Bülent G. Akınoğlu
Head of the Department, **Earth System Science**

Prof. Dr. Elçin Kentel Erdoğan
Supervisor, **Earth System Science, METU**

Prof. Dr. İsmail Yücel
Co-Supervisor, **Civil Engineering, METU**

Examining Committee Members:

Prof. Dr. Head of the Ex. Committee Meryem Beklioğlu
Biology, METU

Prof. Dr. Supervisor Elçin Kentel Erdoğan
Supervisor, Earth System Science, METU

Prof. Dr. Member Aynur Şensoy Şorman
Civil Eng., Eskişehir Technical Univ.

Assoc. Prof. Dr. Member Emre Alp
Environmental Eng., METU

Asst. Prof. Dr. Member Önder Koçyiğit
Civil Eng., Gazi Univ.

Date: 20.06.2022

I hereby declare that all information in this document has been obtained and presented in accordance with academic rules and ethical conduct. I also declare that, as required by these rules and conduct, I have fully cited and referenced all material and results that are not original to this work.

Name Last name : Buket Mesta Yoleri

Signature :

ABSTRACT

IMPACT OF CLIMATE CHANGE IN THE SOUTHERN MEDITERRANEAN OF TURKEY: A METHOD TO ASSESS OYMAPINAR RESERVOIR'S INFLOW PROJECTIONS

Mesta Yoleri, Buket
Doctor of Philosophy, Earth System Science
Supervisor: Prof. Dr. Elçin Kentel Erdoğan
Co-Supervisor: Prof. Dr. İsmail Yücel

June 2022, 352 pages

Assessment of trends in climatological parameters observed in the last decades and the climate change projections through modeling studies indicated a high potential of increasing temperatures, decreasing precipitation, and runoff for Southern Europe and the Mediterranean basin. Within the scope of this study, climate change analysis for Antalya and its surrounding basins is conducted and the effects of climate change on streamflow in Oymapınar Basin and inflow of Oymapınar HEPP that is used for energy production are investigated. Climate change analyses are carried out using CORDEX Regional Climate Models and MRI's (Japan Meteorological Research Institute) super high-resolution MRI-AGCM and NHRCM models. Precipitation and temperature projections are carried out using each of these models and also through ensemble analysis. HBV-light and HEC-HMS are used for hydrological modeling of the Oymapınar basin to identify likely impacts on streamflow as well as for short-, medium- and long-term analysis of the Oymapınar HEPP reservoir inflow. Almost all of the climate models used in the study predict a decrease in areal precipitation

means in the study area in the medium and long-term, and an increase in temperature for short-, medium- and long-term both for RCP4.5 and RCP8.5 scenarios. It is estimated that climate change effects that are expected to be experienced in temperature and precipitation will reduce the inflows to the Oymapınar HEPP reservoir, especially in the long term. In order to minimize the potential negative impacts of the variations in precipitation and temperature caused by climate change, and their effects on water resources and hydropower production, it seems necessary to develop effective adaptation strategies and start implementing them in a tiered manner.

Keywords: Temperature, Precipitation, Hydrological Modeling, Multi-model Ensemble Analysis, High-Resolution Climate Models

ÖZ

GÜNEY AKDENİZ, TÜRKİYE’DE İKLİM DEĞİŞİKLİĞİNİN ETKİSİ: OYMAPINAR REZERVUARI GİRİŞ AKIM TAHMİNLERİNİN DEĞERLENDİRİLMESİ İÇİN BİR YAKLAŞIM

Mesta Yoleri, Buket
Doktora, Yer Sistem Bilimleri
Tez Yöneticisi: Prof. Dr. Elçin Kentel Erdoğan
Ortak Tez Yöneticisi: Prof. Dr. İsmail Yücel

Haziran 2022, 352 sayfa

İklim parametrelerinde son yıllarda gözlemlenen eğilimlerin incelenmesi ve modelleme çalışmaları ile elde edilen iklim değişikliği projeksiyonları, Güney Avrupa ve Akdeniz havzasını içeren bölgede sıcaklıklarda artış, yağış ve yüzey akışlarındaysa azalmalara işaret etmektedir. Bu çalışma kapsamında, Antalya ve çevre havzaları için iklim değişikliği analizleri gerçekleştirilmiş, iklim değişikliğinin Oymapınar Havzası’ndaki su kaynakları ve Oymapınar HES giriş akımlarına etkileri araştırılmıştır. İklim değişikliği analizleri için CORDEX Bölgesel İklim Modelleri ve Japon Meteorolojik Araştırma Enstitüsü (MRI: Japan Meteorological Reserach Institute) tarafından geliştirilmiş olan süper yüksek çözünürlüklü Küresel (MRI-AGCM) ve Bölgesel (NHRCM) İklim Modelleri kullanılmıştır. Yağış ve sıcaklık projeksiyonları hem tüm bu modeller tek tek kullanılarak hem de bütünleşik olarak hesaplanmıştır. Hidrolojik modelleme için hem HBV-light hem de HEC-HMS modellerinden yararlanılmıştır. Oymapınar HES rezervuarına gelecek olan su miktarları kısa, orta ve uzun vade için tahmin edilmiş ve enerji üretimleri hesaplanmıştır. Çalışmada kullanılan iklim modellerinin hemen hepsi hem RCP4.5

hem de RCP8.5 senaryoları için çalışma alanında orta ve uzun vadede alansal yağış ortalamalarında düşme, sıcaklıklardaysa kısa vade de dahil olmak üzere artış tahmin etmektedir. Sıcaklık ve yağışlarda yaşanması beklenen bu iklim değişikliği etkilerinin özellikle orta ve kısa vadede Oymapınar HES rezervuarına girecek akımları azaltacağı ve buna paralel olarak, HES'in yıllık enerji üretimlerinin kısa vadeye kıyasla orta ve uzun vadede düşeceği tahmin edilmiştir. İklim değişikliğinin yağış ve sıcaklıklarda yaratacağı farklılaşmalar ve bunların su kaynakları ve hidroelektrik enerji üretimine etkilerinin bölgedeki halkı ve doğal çevreyi minimum düzeyde etkilemesini sağlayabilmek için etkili adaptasyon stratejilerinin geliştirilmesi ve kademeli olarak uygulamaya alınmaya başlanması gerekli görünmektedir.

Anahtar Kelimeler: Sıcaklık, Yağış, Hidrolojik Modelleme, Çoklu Model Bütünleşik Analizi, Yüksek Çözünürlüklü İklim Modelleri

ACKNOWLEDGMENTS

I would like to express my deepest gratitude and special thanks to my supervisor Prof. Dr. Elçin Kentel Erdoğan for her guidance, valuable advice, motivation, and support throughout my Ph.D. study. Also, I would like to express my deepest appreciation to her for providing me with ideas and points of view to explore new insights and approaches throughout the research.

I also would like to express my profound gratitude to my co-supervisor Prof. Dr. İsmail Yücel for his guidance and kind encouragement throughout the research.

I am also thankful to Thesis Examining Committee Members, Prof. Dr. Meryem Tekol, and Assoc. Prof. Dr. Emre Alp for their advice and constructive feedback which were of greatest assistance throughout the research and also Prof. Dr. Aynur Şensoy Şorman and Asst. Prof. Dr. Önder Koçyiğit for their valuable review and feedback.

Last but not the least, I would like to give my deepest thanks to my husband Can Yoleri, and my sister Banu Altuğ for their endless patience and support throughout my Ph.D. study.

The research leading to these results is funded by the Scientific and Technological Research Council of Turkey (TÜBİTAK) under the project with the title “Assessment of Climate Change Impacts on Streamflow and Hydropower in Antalya, Turkey” and grant number TUBİTAK 118Y365.

TABLE OF CONTENTS

ABSTRACT	v
ÖZ.....	vii
ACKNOWLEDGMENTS	ix
TABLE OF CONTENTS	x
LIST OF TABLES	xv
LIST OF FIGURES	xviii
LIST OF ABBREVIATIONS	xxii
LIST OF SYMBOLS.....	xxviii
CHAPTERS	
1 INTRODUCTION.....	1
1.1 Introduction.....	1
1.2 The Significance of the Study.....	2
1.3 Objectives and Scope of the Study	3
1.4 Description of Thesis	6
2 LITERATURE REVIEW	9
2.1 Climate Change and Impacts in Mediterranean and Turkey	9
2.2 Climate Change Modeling and Ensemble Analysis	13
2.3 Hydrological Modeling and Climate Change Impact Assessment	16
3 CASE STUDY.....	21

3.1	Study Area.....	21
3.1.1	Climate Analysis Study Area.....	22
3.1.2	Hydrological Modeling and Impact Analysis Study Area.....	24
3.1.2.1	Land Cover and Canopy	28
3.1.2.2	Geology, Hydrogeology and Soil	30
3.1.2.3	Hydrology	31
3.2	Data	34
3.2.1	Meteorological Observation Data	34
3.2.2	Data from Climate Models.....	41
3.2.3	Historical Streamflow Data.....	45
4	METHODOLOGY	47
4.1	Climate Analysis Methodology.....	49
4.1.1	Analysis of Temperature and Precipitation Climatology.....	49
4.1.2	Evaluation of Climate Simulations	50
4.1.3	Analysis for Future Changes in Temperature and Precipitation	51
4.2	Hydrological Modeling Methodology.....	54
4.2.1	Analysis of Oymapınar Streamflow Data	55
4.2.2	Basin Properties and Development of Basin Model	57
4.2.3	Hydrometeorological Parameters.....	64
4.2.4	Calibration and Validation of Hydrologic Models	71
4.2.5	Statistical Performance Indicators (SPIs) Used in Hydrological Modeling Performance Evaluation	73
4.3	Streamflow Impact Assessment Methodology.....	76

4.3.1	Use of Individual RCM Outputs for Streamflow Simulations (Q1-Q12).....	78
4.3.2	Use of Ensembled Temperature and Precipitation for Streamflow Simulations (Q13, Q14).....	79
4.3.3	Use of Streamflow Simulations of Individual RCMs in Ensemble Streamflow Generation (Q15, Q16)	82
5	RESULTS AND DISCUSSION.....	85
5.1	Climate Analysis.....	85
5.1.1	Analysis of Temperature and Precipitation Climatology	87
5.1.2	Analysis of Simulation Performances of Climate Models	90
5.1.2.1	Performance of Climate Model Simulations in Representing Spatial Variability of Temperature and Precipitation Climatology.....	91
5.1.2.2	Performance of Climate Model Simulations in Representing Temporal Variability of Temperature and Precipitation Climatology	94
5.1.2.3	Performance of Raw versus Bias-Adjusted RCM Outputs in Representing Temporal Variability of Precipitation Climatology	97
5.1.3	Analysis of Potential Impacts of Climate Change on Temperature and Precipitation.....	103
5.1.3.1	Analysis of Temperature and Precipitation Projections for the CASA	103
5.1.3.2	Analysis of Temperature and Precipitation Projections for the Akseki MS	111
5.2	Hydrological Modeling.....	122
5.2.1	Surface Flow Analysis of Oymapınar Basin	123
5.2.2	Hydrological Model Development, Calibration and Validation in HBV-light.....	131

5.2.3	Hydrological Model Development, Calibration and Validation in HEC-HMS.....	137
5.2.4	Comparison of Model Efficiencies and Model Selection	140
5.3	Streamflow Impact Assessment	143
5.3.1	Analysis of Streamflow Projections using Individual RCMs (Q1-Q12)	145
5.3.1.1	Validation of Historical Streamflow Simulations (Q1 to Q12) and Comparison with Observed Flows.....	145
5.3.1.2	Future Streamflow Projections (for Q1 to Q12).....	150
5.3.2	Analysis of Streamflow Projections using Ensembled Temperature and Precipitation (Q13 and Q14).....	153
5.3.3	Analysis of Streamflow Projections using Ensembled Streamflow (Q15 and Q16)	156
5.3.4	Analysis of Potential Impacts of Climate Change on Streamflow .	161
6	CONCLUSIONS.....	169
6.1	Summary and Conclusions.....	169
6.2	Recommendations for Future Research	178
	REFERENCES	183
	APPENDICES	207
A.	PAPER 1: SUPERENSEMBLES OF RAW AND BIAS-ADJUSTED REGIONAL CLIMATE MODELS FOR MEDITERRANEAN REGION, TURKEY	207
B.	PAPER 2: CHANGES IN PRECIPITATION CLIMATOLOGY FOR THE EASTERN MEDITERRANEAN USING CORDEX RCMS, NHRCM AND MRI-AGCM.....	228

C. PAPER 3: EFFECT OF CLIMATE CHANGE ON SURFACE AIR TEMPERATURE AT EASTERN MEDITERRANEAN, TURKEY	248
D. PAPER 4: IMPROVING PRECIPITATION ESTIMATES FOR TURKEY WITH MULTIMODEL ENSEMBLE: A COMPARISON OF NONLINEAR ARTIFICIAL NEURAL NETWORK METHOD WITH LINEAR METHODS 297	
E. DAILY HYDROGRAPHS FROM HISTORICAL (1971-2005) STREAMFLOW SIMULATIONS (Q1 TO Q12).....	342
F. DAILY HYDROGRAPHS FROM HISTORICAL (1971-2005) STREAMFLOW SIMULATIONS USING ENSEMBLED TEMPERATURE AND PRECIPITATION (Q13 AND Q14).....	348
CURRICULUM VITAE	349

LIST OF TABLES

TABLES

Table 3.1 Annual and seasonal mean temperature (°C) climatology for the period between 1966-2005	26
Table 3.2 Annual and seasonal mean daily precipitation (mm/day) climatology for the period between 1966-2005	26
Table 3.3 Distribution of different land cover types in the Oymapınar basin	29
Table 3.4 Oymapınar basin morphologic parameters	34
Table 3.5 The list and details of meteorological stations in the CASA	36
Table 3.6 List of CORDEX RCMs used in this study	43
Table 3.7 List of bias-adjusted RCMs	44
Table 4.1 Timeframes of the simulation outputs of climate models used in the study	53
Table 4.2 Distribution of elevation bands and relevant vegetation zones in unit basin area	59
Table 4.3 Application of Thiessen Polygon method for the model basin in WMS software	66
Table 4.4 Elevation bands in model basin	68
Table 4.5 Components of basin and meteorological models in HEC-HMS hydrological model	69
Table 4.6 Threshold values for SPIs used in this study	76
Table 4.7 The list of CORDEX RCMs used for the generation of ensembled time series	81
Table 5.1 Aggregated Performance Indicator (API) values for climate models (Spatial Variability of Climatology)	94

Table 5.2 Aggregated Performance Indicator (API) values for climate models (Temporal Variability of Climatology)	96
Table 5.3 Analysis of the SPI values for the daily temperature data of individual models and ensembled outputs for training and test data sets for the Akseki MS	113
Table 5.4 Analysis of the SPI values for the daily precipitation data of individual models and ensembled outputs for training and test data sets for the Akseki MS	114
Table 5.5 The SPI values for the continuous temperature time series in comparison with the observed time series for the period between 1971 and 2003 for the Akseki MS	115
Table 5.6 The SPI values for the continuous precipitation time series in comparison with the observed time series for the period between 1971 and 2003 for the Akseki MS	116
Table 5.7 Change in annual mean temperature (°C) projected for the Akseki MS	120
Table 5.8 Percent change in annual mean precipitation (%) projected for the Akseki MS	121
Table 5.9 Surface areas of Oymapınar subbasins.....	125
Table 5.10 Area ratios of total drainage areas discharging through streamgages .	125
Table 5.11 Fluctuations in SPI values for HBV-light model due to uncertainties in calibration (for 100 calibration runs).....	135
Table 5.12 Comparison of simulation efficiencies of Model 1, Model 2, and Model 3	136
Table 5.13 Simulation performance classification of calibrated HBV-light model	136
Table 5.14 Simulation performance classification of calibrated HEC-HMS model	139
Table 5.15 Comparison of simulation performances of hydrological models in HEC-HMS and HBV-light.....	140

Table 5.16 Statistical Performance Indicators for monthly streamflow simulations (Q1 to Q12) to replicate the observed streamflow at the Sinanhoca streamgage between 1971 and 2005	148
Table 5.17 Statistical Performance Indicators for monthly mean streamflows (hm^3/d) for Q13 and Q14 in comparison with the streamflow simulations Q1 to Q12	154
Table 5.18 Statistical Performance Indicators for ensembled monthly mean (hm^3/d) streamflows (Q15 and Q16) in comparison to the streamflow simulations Q1 to Q12	157

LIST OF FIGURES

FIGURES

Figure 2.1. Hydrological Modeling Types (modified from Singh, 1998 and Xu, 2002)	17
Figure 3.1. The location of the study area	22
Figure 3.2. Map of the Climate Analysis Study Area (CASA), showing the locations of the meteorological stations used in this study	23
Figure 3.3. Map of the Hydrological Modeling Study Area (HMSA)	25
Figure 3.4. Oymapınar basin topography and hypsometric curve.....	27
Figure 3.5. Oymapınar basin slope map	28
Figure 3.6. Land cover types in the Oymapınar basin (EEA, 2018)	29
Figure 3.7. Topographical map showing Manavgat-İbradı-Cevizli aquifer and Manavgat, Oymapınar surface water basins (Koray Üstebay et al., 2018)	31
Figure 4.1. Study flowsheet.....	47
Figure 4.2. Oymapınar basin boundaries and its subbasins.....	56
Figure 4.3. HBV-light simulation algorithm (Normand et al., 2010).....	60
Figure 4.4. Elevation- precipitation relationship in the basin (Koray Üstebay et al., 2018).....	69
Figure 5.1. Annual mean temperature and precipitation climatology (for 1966-2005 period) maps of the CASA	88
Figure 5.2. Mean annual temperature and precipitation climatology anomaly at MSs from CASA mean.	90
Figure 5.3. Taylor diagrams for the climate models compared with the observed temperature and precipitation climatology concerning the spatial variability in the CASA	93

Figure 5.4. Taylor diagrams for the climate models compared with the observed temperature and precipitation climatology concerning the temporal variability in the CASA.....	95
Figure 5.5. Comparison of statistical performance indicators (SPIs) with observed for single (raw and bias-adjusted) regional climate models (RCMs) and superensembles (SEs) for test dataset.....	99
Figure 5.6. Comparison of raw and bias-adjusted regional climate models (RCMs), and three superensembles (SEs) with observed monthly average precipitation ...	101
Figure 5.7. Boxplot showing projected change in temperature climatology for (a) short-, (b) medium-, (c) long-term future under RCP4.5 and RCP8.5 scenarios .	104
Figure 5.8. Boxplot showing percent change in annual precipitation climatology projected by climate models for (a) short-, (b) medium-, (c) long-term future....	107
Figure 5.9. Areal average changes at basins in the CASA for short-, medium, and long-term future based on the mean projection by 12 CORDEX RCMs, and individual projection of MRI-AGCM_NHRCM	110
Figure 5.10. Historic and future (RCP4.5 scenario) temperature simulations by 12 CORDEX RCMs compared with ensembled (SE and SME) outputs for the Akseki MS.....	117
Figure 5.11. Historic and future (RCP8.5 scenario) temperature simulations by 12 CORDEX RCMs compared with ensembled (SE and SME) outputs for the Akseki MS.....	118
Figure 5.12. Historic and future (RCP4.5 scenario) precipitation simulations by 12 CORDEX RCMs compared with ensembled (SE and SME) outputs for the Akseki MS.....	118
Figure 5.13. Historic and future (RCP8.5 scenario) precipitation simulations by 12 CORDEX RCMs compared with ensembled (SE and SME) outputs for the Akseki MS.....	119
Figure 5.14. Oymapınar basin boundaries and its subbasins	123
Figure 5.15. Long-term mean monthly and annual streamflows in Manavgat River for the period between 1987 and 2015.....	124

Figure 5.16. Comparison of hydrographs of Sinanhoca and Şahapköprü streamgages (1992 to 2012)	127
Figure 5.17. Linear Regression analysis of flow rates at Şahapköprü and Sinanhoca streamgages	127
Figure 5.18. Comparison of calculated (with DAR method) and observed streamflows at Sinanhoca streamgage	128
Figure 5.19. Comparison of Oymapınar Inflow estimates with Sinanhoca streamgage hydrograph.....	129
Figure 5.20. Regression analysis of Oymapınar inflow with streamflow observed at Sinanhoca streamgage	130
Figure 5.21. Comparison of Oymapınar Inflow generated using regression function with the DSI’s estimated inflows and observed streamflow at the Sinanhoca streamgage.....	131
Figure 5.22. The change in SPI values for different “Number of Parameters” and “Number of Model Runs” parameters in GAP tool.....	134
Figure 5.23. Comparison of modeled (HBV-light) and observed hydrographs of Sinanhoca streamgage for calibration and validation periods	137
Figure 5.24. Comparison of modeled (HEC-HMS) and observed hydrographs of Sinanhoca streamgage for the calibration and validation periods	138
Figure 5.25. Comparison of modeled hydrographs in HEC-HMS and HBV-light with the observed hydrograph	141
Figure 5.26. Study flow to obtain Streamflow Impact Assessment results.....	144
Figure 5.27. Monthly hydrographs of the streamflow simulations (Q1-Q12) in the hydrological model based on the historical time series of RCMs	146
Figure 5.28. Empirical cumulative distribution function and comparison of observed and modeled daily mean flows (m^3/s)	150
Figure 5.29. Historic and future streamflow simulations from individual model runs of 12 CORDEX RCMs (Q1 to Q12)	151
Figure 5.30. Historic observed streamflow and simulated streamflows using ensembled meteorologic time series.....	155

Figure 5.31. Historic observed streamflow and ensembled streamflow simulation results	158
Figure 5.32. Historic and future (RCP4.5 scenario) ensembled total annual streamflow estimations (Q15 and Q16) in comparison to Q1 to Q12	160
Figure 5.33. Historic and future (RCP8.5 scenario) ensembled total annual streamflow estimations (Q15 and Q16) in comparison to Q1 to Q12	160
Figure 5.34. Historic and future streamflow simulations for the Sinanhoca streamgange	162
Figure 5.35. Projected percent change in the mean annual total flow at the Sinanhoca streamgange for RCP4.5 on the top panel and RCP8.5 on the bottom panel	163
Figure 5.36. Historic and future estimates of the mean annual total inflow of the Oymapınar Reservoir	166
Figure 5.37. Projected percent change in the mean annual total inflow of the Oymapınar Reservoir for RCP4.5 and RCP8.5.....	167

LIST OF ABBREVIATIONS

ABBREVIATIONS

AGI	Streamgauge operated by DSI
ANN	Artificial Neural Network
ASL	Above Sea Level
API	Aggregated Performance Index
AR5	The Fifth Assessment Report of IPCC
AR6	The Sixth Assessment Report of IPCC
Avg	Average
CASA	Climate Analysis Study Area
CDF-t	Cumulative Distribution Function Transform
CLC	CORINE Land Cover
CLMcom	Climate Limited-area Modelling Community
CMIP	Coupled Model Intercomparison Project
CN	Curve Number
CNRM	National Centre for Meteorological Research in France
CO ₂	Carbon dioxide
CO ₂ -eq.	Carbon dioxide equivalent
CORDEX	Coordinated Regional Climate Downscaling Experiment
CRMS	centered root-mean-square
<i>Corr (or r)</i>	Pearson's correlation coefficient

DAR	Drainage area ratio
DBS	Distribution Based Scaling
DC	Deficit and Constant Method
DEM	Digital Elevation Model
DJF	December, January, February
DMI	Danish Meteorological Institute
DSI	State Hydraulic Works of Turkey
DTS	Distance to the sea
EAWR	East Atlantic West Russia
EC	European Commission
EEA	European Environment Agency
Eionet	European Environment Information and Observation Network
ESGF	Earth System Grid Federation
EU	European Union
EURO-CORDEX	European-COordinated Regional Downscaling EXperiment
FAO	Food and Agriculture Organization of the United Nations
GA	Genetic Algorithm
GAP	Genetic Algorithm and Powel optimization
GCM	General Circulation Model/Global Climate Model
GHG	Greenhouse Gas

GIS	Geographic Information Systems
HBV	Swedish Meteorological and Hydrological Institute's modeling software Hydrologiska Byråns Vattenbalansavdelning
HEC-HMS	U.S. Army Corps of Engineers Hydrologic Engineering Center- Hydrologic Modeling Software
HEPP	Hydroelectrical Power Plant
HMSA	Hydrological Modeling Study Area
HWDI	Heatwave Duration Index
IDW	Inverse Distance Weighting
IPCC	Intergovernmental Panel on Climate Change
IPSL	Institut Pierre-Simon Laplace
IQR	Interquartile range
JJA	June, August, July
JSPS	Japan Society for the Promotion of Science
<i>KGE</i>	Klingt-Gupta efficiency coefficient
KHGM	(former) General Directorate of Rural Affairs of Turkey
KNMI	Royal Netherlands Meteorological Institute
MAM	March, April, May
METNO	Norwegian Meteorological Institute
MESAN	MESoscale ANalysis system
MLR	Multiple Linear Regression
MME	Multi-model ensemble
MoEU	Ministry of Environment and Urbanization of Turkey

MOHC	Met Office Hadley Centre
MRI	Japan Meteorological Research Institute
MRI-AGCM	Atmospheric Global Climate Model of MRI
MS	Meteorological Station
NAO	North Atlantic Oscillation
NCAR	National Center for Atmospheric Research
NCEP	National Centers for Environmental Prediction
NASA	The National Aeronautics and Space Administration of USA
NHRCM	Non-hydrostatic Regional Climate Model of MRI
NP	Number of Parameters
<i>NSE</i>	Nash–Sutcliffe efficiency coefficient
<i>p</i>	Probability
<i>PBIAS</i>	Percent bias
PBWA	Performance-based weighted average
PPE	Perturbed physics ensemble
ppm	Parts per million
PTQ-file	Precipitation-Temperature-Flow rate file
Q	Streamflow
QC	Quality check
QMap	Quantile Mapping
R	Reservoir inflow
<i>r</i> (or <i>Corr</i>)	Pearson’s correlation coefficient
R^2	Coefficient of determination

RB	Recession Baseflow or Exponential Recession
RCM	Regional Climate Model
RCP	Representative Concentration Pathways
RCP4.5	Representative Concentration Pathway radiative forcing 4.5W/m ²
RCP8.5	Representative Concentration Pathway radiative forcing 8.5W/m ²
RD	Reference Data
<i>RMSE</i>	Root Mean Square Error
RSR	The ratio of <i>RMSE</i> to the standard deviation of observed data set
SA	Study Area
SD (or σ)	Standard deviation
SE	Superensemble
SMA	Soil Moisture Accounting
SME	Simple Mean Ensemble
SMHI	Swedish Meteorological and Hydrological Institute
SON	September, October, November
SPI	Statistical Performance Indicator
SRES	Special Report on Emissions Scenarios
SRTM	Shuttle Radar Topography Mission
TSMS	The Turkish State Meteorological Service
TUBITAK	The Scientific and Technological Research Council of Turkey
<i>var</i>	variance
<i>VE</i>	Volume Error

WCRP	World Climate Research Programme
WFDEI	Watch Forcing Data - ERA-Interim
WMS	Watershed Modelling System

LIST OF SYMBOLS

SYMBOLS

σ	Standard deviation
μ	Mean
Δ	Delta indicating the change
Σ	Summation
\forall	For any

CHAPTER 1

INTRODUCTION

1.1 Introduction

IPCC in its AR6 (2022) reports that adverse impacts of climate change are likely to continue in the future. For the Mediterranean Region in addition to the increasing trend in mean air temperature that is highly likely to persist, mean precipitation is expected to decrease and water scarcity is exacerbated (IPCC, 2022). In that respect, in the case that the global increase in temperature relative to 1850-1900 reaches 2°C by mid 21st century, within the domain of Europe, unlike other regions in the domain (i.e., western and central Europe, eastern Europe, and northern Europe) climate change is expected (with high confidence) to create the regional impact of a decrease in precipitation and increase in drought (hydrological, ecological and agricultural) for the Mediterranean region (IPCC, 2022). Additionally, water scarcity due to potential changes in the hydrological cycle creates challenges in the allocation of water resources for various uses, catchment management, and further impacts of potentially cumulative and even irreversible in nature (IPCC, 2014). Findings from several studies support these projections indicating that the Mediterranean can be classified as a hotspot regarding climate change impacts. Turkey located in the eastern Mediterranean is also vulnerable considering the risk of a decrease in volume of water resources and stability of water supply. Furthermore, recent climate studies indicated Mediterranean Region of Turkey is likely to be among the most severely impacted areas in Turkey (Yıldırım and Yücel, 2019; Aziz et al., 2020; Aziz and Yucel, 2021).

Hence, for sustainable and integrated planning, potential changes in precipitation and subsequent impacts on water resources should be evaluated. Evaluation of the

impacts on precipitation is vital for the identification of potential risks on resilience and/or operational efficiencies of existing infrastructure such as facilities for flood protection, drainage and irrigation, water supply, and hydropower plants (Bates et al., 2008). Assessment of impacts on catchment scale is crucial for the determination of optimal adaptation strategies and potential vulnerabilities. Furthermore, adaptation options are necessary to be designed with integrated demand-side as well as supply-side strategies. Therefore, catchment-scale analysis of impacts provides insight with much satisfactory detail compared to larger-scale analyses (Bates et al., 2008).

1.2 The Significance of the Study

Despite its increasing importance, the assessment of the climate change impacts is still an emerging field of study in Turkey and there are still a very limited number of published works based on the use of multi-model ensemble including several GCM/RCM combinations. Furthermore, localized studies on climate change impact assessment towards the development of adaptation measures are still numbered. Therefore, this study aims to assess the climate change impacts with an added focus on the impact on streamflow that is expected to have a potential impact on hydropower generation in the selected case study area that can be considered as the first step of adaptation and planning against likely severe impacts in the future.

Within that context, this study covers an assessment of potential climate change impacts on temperature and precipitation in a large study area including a major portion of the Mediterranean (and Aegean) coastline and also its inland that stretches through 10 of the 26 major basins and three of seven geographical regions of Turkey based on the projections from different climate models under two Representative Concentration Pathways (RCPs) defined in the fifth assessment report (AR5) of IPCC (i.e., RCP4.5 and RCP8.5) (IPCC, 2014) for the future timeframe until the end of the current century. Furthermore, the subsequent impact on future streamflow is assessed more in detail through hydrological modeling. The case study area selected

for streamflow impact assessment is the Manavgat River in the Middle Mediterranean (or Antalya) basin which necessitates integrated planning for flood protection, water use allocation, and planning for hydropower generation concerning potential climate change impacts. Hence, hydrological modeling is used for the assessment of impacts on streamflow of Manavgat River that feeds Oymapınar Hydroelectrical Power Plant (HEPP) based on recent climate projections.

The analyses in the study demonstrate a gradual increase in temperature by the end of the 21st century for both climate scenarios in the entire study area. Furthermore, inter-regionally variable changes in the mean total precipitation and a decrease in the inflow of the Oymapınar reservoir are verified.

1.3 Objectives and Scope of the Study

In addition to the analysis of the potential impacts on temperature, precipitation, and streamflow, the study also targets to test several methodologies for climate change impact analysis at different stages of the assessment. These include testing of ensembling methodologies in comparison to the multi-model analysis approach using individual raw and bias-adjusted RCMs of high-resolution climate models to achieve a better reproduction of the hydrometeorology of the study area. Additionally, tools with different hydrological modeling approaches are tested for their simulation performances. Hence, one of the main objectives of the study is to lay out the steps for an efficient study flow towards the climate change impact assessment in the study area in Turkey considering available data, information sources, and tools.

The study comprises three main components; Climate Analysis, Hydrological Modeling, and Streamflow Impact Analysis, to achieve the following targeted objectives along with the aforementioned main research objective:

- Climatological analysis of the study area (SA) based on historical observations.

- Comparison of high-resolution climate models to identify models with the highest simulation skills for temperature and precipitation in the SA.
- Dynamical downscaling of MRI-AGCM (Japan Meteorological Research Institute's Atmospheric Global Climate Model) model by the use of the regional climate model of MRI (Non-hydrostatic Regional Climate Model: NHRCM) to obtain high-resolution (5 km mesh size) climate projections for the SA.
- Development of a representative rainfall and runoff model for the Oymapınar basin.
- Comparison of two different hydrological modeling software with respect to modeling efficiencies and relevant advantages and disadvantages.

Study for Climate Analysis is conducted with multi-model ensemble analysis approach for a study area (from henceforth will be named as Climate Analysis Study Area or CASA) covering a major portion of western, southern, and central Turkey. It provides climatological analysis of temperature and precipitation in Turkey by the use of meteorological observations by the Turkish State Meteorological Service (TSMS). Following the climatological analysis, high-resolution climate models from the EURO-CORDEX database and from Japan Meteorological Research Institute (MRI) are analyzed for their skills to replicate temperature and precipitation in Turkey. After the validation of climate models, a 14-member ensemble is used to analyze potential changes in temperature and precipitation in Turkey.

The scope of the Climate Analysis and the relevant methodology are delineated to enable a comparison of different approaches for climate change impact analysis. Assessment of the climate change impacts is still an emerging field of study in Turkey and there are still a limited number of published works based on the use of multi-model ensembles including several GCM/RCM combinations. The methodology in this study is, therefore, developed to assess the adequacy and efficiency of various high-resolution climate models and methodologies. On this basis, the study targets to contribute to the relevant literature.

CORDEX RCMs, in the ensemble set in this study, are selected to enable a comparison with the results of other recently published research such as studies by Aziz et al. (2020) and Aziz and Yuçel (2021) that are based on multi-model ensemble analysis with a large ensemble set of models. Furthermore, two high-resolution MRI climate models, which were not used in any earlier studies in Turkey, are also added to the analysis for a comparison with the CORDEX RCMs.

Hence, the climate analysis includes a 14-member ensemble set comprising 12 (out of 20) of the RCMs (with daily outputs for the EUR-11 domain under both RCP4.5 and 8.5 scenarios) available at the ESFG database at the time of the analysis and two MRI climate models with comparable or smaller mesh size with the CORDEX RCMs. Additionally, the ensemble set in this study enables comparisons between RCMs that are based on a particular GCM (e.g., HIRHAM5, CCLM4-8-17, RACMO22E, RCA4 nested in the ICHEC-EC-EARTH model), and between GCMs that are used as the boundary condition for a particular RCM (e.g., climate simulations with RCA4 using boundary conditions of ICHEC-EC-EARTH, CNRM-CERFACS-CNRM-CM5, MOHC-HadGEM2-ES, IPSL-IPSL-CM5A-MR models), to verify their simulation skills for the SA.

In this study, NHRCM nested in MRI-AGCM is run for the specific domain of the CASA. Assessment through NHRCM is intended to achieve a good simulation performance by putting more emphasis on the area of concern.

Regarding the analysis of simulation performances, the bias-adjusted RCMs, produced by the CORDEX-Adjust project through post-processing with three commonly tested bias-adjustment methodologies, are selected from the CODEX Database to enable a comparison with raw RCMs. Furthermore, ensembling approaches, giving researchers certain advantages of improvement of the climate projections along with their ease of use in climate change impact assessment, are compared with those available simulation outputs to identify potential advantages or drawbacks. The second component of the research study, Hydrological Modeling, comprises mathematical modeling of the Oymapınar basin (Hydrological Modeling

Study Area or HMSA). The Oymapınar basin has a high surface water yield discharging to the Oymapınar Reservoir through the Manavgat River and is located in an area with complex topography. Hence, the basin located in a climate change hot-spot region is affected by orographic driving forces on hydrometeorology. Furthermore, the basin is under a relatively low anthropogenic impact (e.g., little abstraction and discharge, very few hydraulic control structures, and no reservoirs upstream of the basin) concerning the river discharge. Hence, based on these properties the Oymapınar basin boundaries are selected as the boundaries of the HMSA.

In the Hydrological Modeling component, rainfall-runoff models of the basin are developed by the use of two hydrological modeling software, HEC-HMS, and HBV-light, with modeling setups based on different approaches. The use of two software with different approaches aims to assess their relative efficiencies. After the development of a representative model for the Oymapınar basin, the hydrological model is used for further streamflow impact assessment using the projections from climate models. The results from the hydrological models are initially validated against historical streamflow data and then analyzed for potential future changes in streamflow discharging to the Oymapınar Reservoir. Similar to the Climate Analysis, the Streamflow Impact Analysis methodology is laid out to compare different methodologies and identify ranges of uncertainty in streamflow projections.

1.4 Description of Thesis

The first chapter of this thesis provides general background on the topic and the main motive of the research study. In this chapter aim and scope of this study are also described briefly. Chapter 2 gives a brief review of the literature and a description of similar studies related to the various parts of this study. The following chapter (Chapter 3) presents details on the study area and data used. Methodologies followed in different parts of the study are given in Chapter 4. Chapter 5 presents the findings from the Climate Analysis component of the study. Additionally, the results of

hydrological modeling using HEC-HMS and HBV-light software and details of the impact assessment are also given in Chapter 5 with relevant findings. Finally, Chapter 6 presents conclusions from the research study with relevant recommendations regarding the major study findings.

CHAPTER 2

LITERATURE REVIEW

2.1 Climate Change and Impacts in the Mediterranean and Turkey

Human-induced climate change is the most prominent candidate for being the most severe problem for the Earth system today. Increasing Greenhouse Gases (GHGs) emissions from anthropogenic activities cause a striking increase almost at an exponential rate in GHGs concentrations after the Industrial Revolution. Among the GHGs CO₂ is of particular concern due to its significantly long retention time. The atmospheric residence time for CO₂ exceeds 100 years. In fact, only two-thirds of emitted CO₂ is removed from the atmosphere after 100 years. Further removal to remain 20% of the emission takes 1000 years (Kharecha and Hansen, 2008). Increased emissions and atmospheric concentrations of GHGs are followed by severe impacts of climate change that are verified by the analysis of climate trends in recent years based on observations.

In its Sixth Assessment Report (AR6) the Intergovernmental Panel on Climate Change (IPCC) stresses that it is certain that the current global climate change is originated from the results of anthropogenic activities and has already caused various severe impacts on the Earth System including global warming, changes in the water cycle, impacts on biosphere, mean sea level rise, loss in mass of glacier and Arctic Sea ice, and last but not the least ocean acidification (IPCC, 2021). The AR6 reports a net increase in global mean surface temperature between 0.8°C and 1.3°C by 2019 compared to the second half of the 19th century. Climate change causing the shift of Mid-latitude storm tracks (IPCC, 2021) also catalyzed changes in the water cycle that is complicated in nature considering the local drivers influencing the formation of precipitation. Hence regional or even local variable impacts are observed on precipitation.

Historical climate data indicates an increase in global mean temperatures (global land average) since the 1980s whereas an increasing trend in mean temperatures in Turkey started in the 1990s but has shown a higher rate of increase compared to the global trend (Şen, 2018). Hence, risks regarding climate change impacts have become more pressing after that time, and relevant studies gained a higher pace in the last decade. Turkey's National Climate Change Adaptation Strategy and Action Plan published in 2012 by the Turkish Ministry of Environment and Urbanization (MoEU) emphasizes potential impacts on the water cycle and a decrease in Turkey's overall water resources. Strategic plan targets adaptation and mitigation strategies to deal with the risks regarding water resources due to climate change together with other environmental stresses that exacerbate such impacts. The plan describes "Integrated Management of Water Resources in Water Basins for Adaptation to Climate Change" as an action item for the adaptation to climate change (MoEU, 2012).

The Mediterranean region including Turkey is expected to be among the most vulnerable regions to climate change impacts (Giorgi and Lionello, 2008). Studies on the historical temperature records demonstrated that the increase in global mean temperature triggered the escalation of maximum and minimum temperatures in the Mediterranean basin and created downstream adverse impacts (Kostopoulou and Jones, 2005; Kuglitsch et al., 2010; Efthymiadis et al., 2011; Bartolini et al., 2012; Tanarhte et al., 2015). The increase in extreme temperatures augmented the summer heatwaves, fire risk, and other extreme climate events with heavy socio-economic and ecological impacts in the Mediterranean basin including Turkey. Kuglitsch et al. (2010) studied the change in heatwave number, length, and intensity in the eastern Mediterranean region (including Albania, Bosnia-Herzegovina, Bulgaria, Croatia, Cyprus, Greece, Israel, Romania, Serbia, Slovenia, Turkey) for the period between 1960-2006 and identified certain parts of Turkey including eastern Black Sea coastline, western, southwestern, and central Turkey as the "Hot spots" of heatwave changes along with the western Balkans. Kostopoulou and Jones (2005) reported an increase in the Heatwave Duration Index (HWDI) in continental areas and especially

in the central Balkan countries by analyzing historical meteorological data between 1958 and 2000 for the eastern Mediterranean region (Kostopoulou and Jones, 2005). Similarly, in their study in the central Mediterranean (i.e., central Italy), Bartolini et al. (2012) showed an increase of 0.9°C per 50 years. The results showed even higher trends in summer warming.

Studies analyzing the trends in temperature changes, heatwaves, and extreme temperature events based on observational data across Turkey also verified adverse impacts of climate change in Turkey (Tayanç et al. 2009; Cagatan and Unal, 2010; Toros, 2012; Unal et al., 2013; Gönençgil and Deniz, 2015, 2016; Altın and Barak, 2017; Erlat et al., 2021). Tayanç et al. (2009) analyzed the climate signal of temperature for the records between 1950 and 2004 and identified two periods concerning the temperature trends in the latter half of the 20th century; the first relatively cold period between the early 1960s and 1993 with the lowest temperature values on 1992–1993 owing to the eruption of Mount Pinatubo and a continuous warming period after 1993. The study showed significant warming for the south and southeastern Turkey, featuring increases in maximum and mean temperature series (Tayanç et al., 2009). Gönençgil and Deniz (2015, 2016) studied the seasonal maximum and minimum temperatures and found an increasing trend for warm spells and a decreasing trend for cold spells for the Mediterranean coastline in Turkey. Additionally, they have identified that the increasing trend of warming is more pronounced after the mid-1990s, whereas the onset of the decreasing trend of cold spells was in the mid-1980s (Gönençgil and Deniz, 2015, 2016).

Studies on heatwave trends in western Turkey showed the increase in the number of hot days and heatwaves, and in heatwave durations in recent decades. Accordingly, the increasing trend is more evident in inland stations with an even higher rate observed in the 2000s relative to the 1970s with a threshold date of 1998 identified for the initiation of increase in the frequency of heatwaves (Cagatan and Unal, 2010; Unal et al., 2013). Additionally, Unal et al. (2013) emphasized the significant correlation between the number of heatwaves and the fire occurrences for most of the stations in their study area.

Toros (2012) indicated the beginning of the 1980s as the start of the increasing trend in temperature and compared the monthly average temperatures in two decades before and after 1985. The comparison showed an increase in maximum and minimum temperatures. The analysis revealed a stronger increase in extreme maximum temperatures than the increase in extreme minimum temperatures (Toros, 2012). Similarly, the comparison of heatwave trends before and after 1985 by Erlat et al. (2021) demonstrated a statistically significant increase in heatwave conditions after 1984. Erlat et al. (2021) also reported more evident changes in the heatwave characteristics after the middle of the 1990s regarding the Black Sea and the Mediterranean coasts. In their study in the Adana Sub-region of the Eastern Mediterranean coast of Turkey, Altın and Barak (2017) showed a statistically significant positive anomaly for the number of summer and tropical days above the long-term average for the duration between 1993 - 2014.

Regarding the climate change impacts on hydrology Yucel et al. (2015) analyzed historical (1970 - 2010) monitoring data on streamflow, temperature, and precipitation in eastern Turkey covering five major basins of Turkey including the Tigris and Euphrates basins. Their findings delineated significant temperature increases that also lead to a shift in the timing of peak flows due to snowmelt-fed stream discharges. However, the change in the mean annual precipitation in the study area is estimated to be statistically non-significant (Yucel et al., 2015). Considering potential severe impacts of climate change aggravated by increasing atmospheric GHGs concentrations climate models are used to project potential future changes in climate parameters. The climate models provide data for further climate change impact assessment that forms the basis of planning sound mitigation and adaptation strategies.

Within that scope, studies for the assessment of impacts from climate change in Turkey by the use of projections from climate models were conducted to focus on potential impacts considering forestry, ecosystem dynamics, crop yield, energy, management of extreme events and reservoir planning, and tourism activities (Fujihara et al., 2008; Özdoğan, 2011; Sen et al., 2012; Deidda et al., 2013; Kara and

Yücel, 2015; Öztürk et al., 2015; Sunyer Pinya et al., 2015; Yılmaz, 2015; Kara et al., 2016; Demircan et al., 2017; Mehr and Kahya, 2017; Bucak et al., 2018; Dino and Akgül, 2019).

2.2 Climate Change Modeling and Ensemble Analysis

The main tool for the generation of projections on future climate change is Global Climate Models (GCMs). GCMs are based on the description of atmospheric processes through mathematically formulated physical laws to obtain future climate projections based on some predefined emission scenarios. GCMs are intended to provide general predictions on climate on a global scale and do not provide predictions with regional scale resolution because regional or local scale processes cannot be included in these models due to their complexity. Accuracies for local-scale assessments have limitations because GCMs lack detailed regional information, which is needed to resolve features at the catchment scale. In addition, due to their coarse resolution, GCMs have the disadvantage of relatively poor representation of some significant atmospheric processes such as orographic precipitation, conventional processes, and local scale hydrologic processes (Fujihara et al., 2008; Sato et al., 2012). Therefore, for precipitation GCMs do not provide sufficient resolution for assessment in regions where complex topography work as a significant factor in local processes (Sunyer Pinya et al., 2015; Lun et al., 2021; Park et al., 2021). Use of coarse scale GCM outputs directly for the purpose of assessment of local hydrological processes without any bias correction and further downscaling may create results with lower accuracy, particularly for assessments on a local scale (Sharma et al., 2007; Piani et al., 2010; Jaw et al., 2015).

In order to overcome such drawbacks and produce data with higher resolution, dynamical downscaling can be applied by the use of Regional Climate Models (RCMs) (Fujihara et al., 2008). Dynamical downscaling through RCMs uses outputs of GCMs as boundary conditions and generates higher resolution data (Kara and Yücel, 2015). RCMs generally have biases due to reasons such as imperfect

conceptualization or biases that are inherited from the GCM in which RCM is nested (Fujihara et al., 2008; López-Moreno et al., 2008; Teutschbein and Seibert, 2012). Hence, in order to obtain better accuracy of data that complies with local conditions, bias correction (or bias adjustment) through methodologies that range from simple scaling to complex bias correction methods is applied (Kara and Yücel, 2015). Although bias adjustment techniques have the advantage of being computationally inexpensive they may have certain weaknesses (IPCC, 2015). As a result, the use of different RCMs and different bias correction methodologies may create advantages and disadvantages for the simulation of different processes that might be more significant for certain locations, seasons, or periods for high-resolution climate projections.

Different designs and assumptions on atmospheric conditions and processes in the climate models as well as post-processing of the outputs by the use of different bias adjustment approaches create variability in the climate projections. Several studies on climate projections by the use of various climate models revealed uncertainties and significant variability of projections (López-Moreno et al., 2008; Sunyer Pinya et al., 2015) which leads to the main weakness of single model-based climate change analysis. On the other hand, the multi-model ensemble analysis approach aims to overcome the shortcomings of single-model analysis. Most studies indicate that ensemble analysis generates superior results over single model use and improves understanding of uncertainties (Tebaldi and Knutti, 2007; Sunyer Pinya et al., 2015). The use of different models with different model setups in the ensemble aims to diminish model biases due to poorly represented processes through offsetting by better-represented processes in other models in the ensemble.

Ensemble analysis includes the generation of ensemble projections by the use of individual models selected as ensemble members. In that respect, different approaches can be followed such as perturbed physics ensembles (PPEs) or so-called ensembles of opportunity or multi-model ensembles (MMEs). In the PPE approach, a climate model is run for variations in different parameters to detect parameter uncertainties and biases (Déqué et al., 2007; Lopez et al., 2009). In the MME

approach, a combination of a set of models is obtained (Tebaldi and Knutti, 2007) by the use of various methodologies such as simple averaging, weighted averaging, etc. Ensemble obtained by averaging all models is commonly used for climate change impact assessment studies (Kitoh, 2007; Özdoğan, 2011; Okkan and İnan, 2015) and actually is based on assigning equal weights to all ensemble members. In weighted averaging of ensemble members, model weights can be defined based on some predefined criteria such as performance metrics, statistical indicators, or similar (Giorgi and Mearns, 2002, 2003; Tebaldi and Knutti, 2007; Christensen et al., 2010). The method for selection of model weights can vary from simple to complicated approaches such as statistical analysis, regression, and neural network analysis (Giorgi and Mearns, 2002, 2003; Boulanger et al., 2006, 2007; Sirdas et al., 2007; Okkan and Kirdemir, 2016). Several studies testing the performance of ensemble analysis demonstrated improvement in the coherence of the results and better values of statistical performance indicators compared to single model analysis (Hagedorn et al., 2005; Tebaldi and Knutti, 2007; Sunyer Pinya et al., 2015). The use of ensembling in climate analysis is getting more common recently and studies are conducted on the topic to investigate different methodologies making them available for use in climate impact assessment (Lopez et al., 2009).

Among the methodologies to produce ensemble projections, the approach of Superensemble (SE) is based on the use of Multiple Linear Regression (MLR). In this approach, models in the ensemble are combined with weights or coefficients identified through MLR so as to obtain the best fit of the ensemble with the observed by the use of the least-squares method (Krishnamurti et al., 1999, 2000, 2016; Stefanova and Krishnamurti, 2002). Studies to assess the efficiency of SE verified improvement in performance indicators by SE relative to single model assessment and ensembling with model averaging (Krishnamurti et al., 1999, 2000, 2016; Yun et al., 2005; Cane and Milelli, 2010). Furthermore, the comparison of the efficiency of SE with the averaging of bias-adjusted model outputs indicated better results for SE. Hence, SE provides an aggregated bias adjustment in the model set by giving a weight to each ensemble member (even negative weights depending on the

convergence/divergence from the reference data) to minimize difference from observed (Krishnamurti et al., 1999, 2000; Yun et al., 2005).

For the dissemination of information to users of climate projections, to establish a framework of regional-scale climate projections, and to support the above-mentioned studies regarding regional climate modeling and impact assessment within the European domain the European-COordinated Regional Downscaling EXperiment (EURO-CORDEX) initiative was established by the World Climate Research Programme (WCRP). EURO-CORDEX publicizes data from RCM simulation results for the EURO domain via the Earth System Grid Federation (ESGF) which supports a publicly available and accessible online database (Jacob et al., 2020). Furthermore, to foster the climate change impact assessment studies EURO-CORDEX RCM projections post-processed for bias adjustment with different methods are also publicized under the CORDEX-Adjust project through the climate4impact portal on ESGF (IPCC, 2015).

2.3 Hydrological Modeling and Climate Change Impact Assessment

Hydrological models provide a tool for the simulation of river systems draining a designated catchment area. In general terms, modeling provides simplification of complex natural systems. Hence, hydrological modeling provides a better understanding of behaviors of the basin as the modeled system or various conditions as a complete single unit or as composed of its subunits each with specific features in itself (Xu, 2002). Hydrological models simulating the rainfall-runoff relationship of catchment areas and associated river systems are used for various purposes including predictions for varying or changing conditions, assessment of potential outcomes combined with the variations in hydrological elements that enable evaluation of alternative conditions and scenarios. Hence, hydrological models are frequently used as a significant tool for decision-making in catchment management and water use planning as well as for predictions and impact assessments for changing climate parameters.

Depending on the type of the study and outputs that are intended to be obtained, the type of hydrological model can be selected (Xu, 1999; Kour et al., 2016). The type of model (Figure 2.1) (Singh, 1998; Xu, 2002) that is most suitable for the purpose of the study should be decided based on the objective of the study, type of system to be modeled, hydrological response (i.e., flood, monthly or daily discharges, etc.) that is aimed to be simulated, data availability, and model resolution targeted to be achieved. This study is based on the mathematical hydrological modeling approach for the purpose of impact assessment on streamflow. Mathematical models or symbolic models target the simulation of the system and representation of important hydrological components and relations among those by the use of mathematical methods. The use of mathematical modeling in hydrological assessment is rigorously tested for its efficiency in similar studies in the literature (Prudhomme and Davies, 2009; Teutschbein and Seibert, 2012; Meenu et al., 2013; Kour et al., 2016).

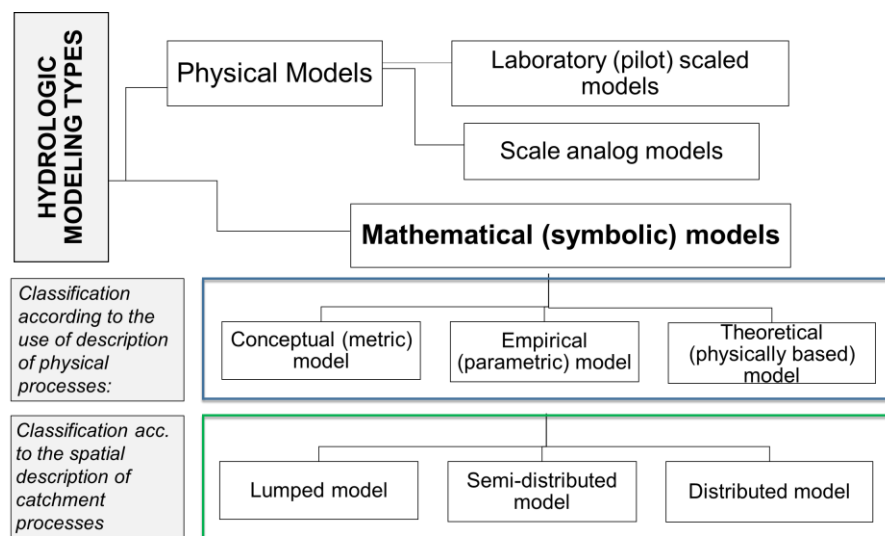


Figure 2.1. Hydrological Modeling Types (modified from Singh, 1998 and Xu, 2002)

According to the description of the hydrological processes in model setup, mathematical models are developed as Theoretical models, Empirical models, or

Conceptual models (Singh, 1998; Xu, 2002; Devi et al., 2015; Sitterson et al., 2018). Theoretical and empirical models can be accepted to be at the two extremes of mathematical modeling with respect to the methodology followed to include the physical process description in the mathematical model structure. Empirical models (e.g., regression models, correlation models, ANN models, etc.) are completely observation-based models and do not focus on the understanding of physical processes, whereas Theoretical models are based on the description of every hydrological process in the system by the use of finite difference equations (Xu, 2002; Devi et al., 2015). Conceptual modeling is between these two approaches and is based on semi-empirical equations with a physical basis. Model parameters are derived from field data and calibration (Devi et al., 2015; Sitterson et al., 2018). Hence, the simulation of basin hydrology (i.e., rainfall-runoff relationships) with a conceptual modeling approach enables the use of semi-empirical equations to define hydrological features of the basin that is further improved through parameter optimization by the use of available historical records to eliminate potential data gaps or biases in monitoring data (Wagener et al., 2001; Yener et al., 2007).

Depending on the detail in the spatial description of catchment processes, a mathematical model can be developed as lumped, in which the basin is simulated as a single homogeneous unit, semi-distributed, in which the basin is simulated as a composition of sub-basins with different but homogeneous features within themselves, or distributed that treat catchment as multiple units composed of elementary unit areas like a grid net and flows are passed from one grid point (node) to another as water drains through the basin (Devi et al., 2015; Sitterson et al., 2018). The selection of a suitable approach regarding spatial detail of the basin feature is based on the available data types and properties (topography, land use, vegetation cover, soil properties, etc.).

The selection of the duration of the hydrological simulation is also important in the model setup. Two main approaches are event-based modeling and continuous modeling. Event models are focused on the simulation of single storm events to verify the response of the model basin to the relevant event. Event models are to

simulate the basin hydrology during and immediately after a storm. On the other hand, a continuous simulation model enables the analysis of hydrology as a response to a series of storm events and the cumulative response of the basin (e.g., wet, dry conditions, etc.) in longer durations (Chu and Steinman, 2009). Hence, continuous models are developed by the use of long-term observed meteorologic and hydrologic data.

In this study, two different models, a complex and semi-distributed and a simpler conceptual hydrologic model are developed for the study basin to assess climate change impacts on streamflow. The first hydrologic modeling software used in this study is HEC-HMS (Scharffenberg, 2015) which is frequently used for the event (Knebl et al., 2005; Shahid et al., 2017) and continuous modeling (Fleming and Neary, 2004; Gyawali and Watkins, 2013; Halwatura and Najim, 2013) of basins across the world. Chu and Steinman (2009) tested HEC-HMS's efficiency in continuous and event modeling for the Mona Lake basin in the USA and verified its skill in replication of observed flows. HEC-HMS was used to model the Tonle Sap Lake basin in Cambodia by Chea and Oeurng (2017) satisfactorily. Du et al. (2012) successfully modeled the Qinhuai river with HEC-HMS to assess changes in runoff and flooding in the basin due to urbanization. Furthermore, HEC-HMS is used for climate change impact assessment studies in Tunga–Bhadra River basin in India (Meenu et al., 2013), Blue Nile River basin in Ethiopia (Yimer et al., 2009), Bagmati River basin in Nepal (Babel et al., 2014) through mathematical modeling of the basins by the use of climate projections. Several other studies from different regions of the world also used HEC-HMS to assess the risks combined with climate change-induced extreme events. On that subject, Cunderlik and Simonovic (2007) studied in Thames River basin in Canada, and Givati et al. (2016) studied the Ayalon basin in Israel. HEC-HMS was also successfully used in many studies in Mediterranean Region (Bouabid and Elalaoui, 2010; Givati et al., 2016; Aqnouy et al., 2018; Zapata-Sierra and Manzano-Agugliaro, 2019), and in Turkey (Yener et al., 2007; Yücel and Keskin, 2011; Yılmaz et al., 2012; Koçyiğit et al., 2017).

The other conceptual modeling software used in the study is the HBV-light model which is a version of HBV (Hydrologiska Byrns Vattenbalansavdelning) developed by SMHI (Swedish Meteorological and Hydrological Institute). HBV-light works with the multi-tank principle and enables semi-distributed hydrological modeling (Seibert, 2005). Although not as common as the HEC-HMS model, HBV-light has been used for several hydrological studies since the early 1970s. Rainfall-runoff simulation in HBV-light is generated based on the use of three main meteorological time series: precipitation, temperature, and evapotranspiration (Seibert, 1997). HBV-light is proven to be successfully used in hydrological assessment including climate change impact assessment studies across the world.

In their multi-model ensemble analysis study, Graham et al. (2007) used HBV to assess climate change impacts and potential changes in hydropower potential in the Lule River basin in Sweden. Dariane and Javadianzadeh (2016) used a modified version of HBV-light to successfully develop a conceptual lumped hydrological model of three basins in Iran. Osuch (2015) tested the effect of the climatologic drivers on hydrological model parameters by the use of HBV at four basins in Poland. Their study verified that the model parameters are dependent on the climate indices at a statistically significant level.

CHAPTER 3

CASE STUDY

As detailed in previous chapters, Turkey is located in a vulnerable region considering the potential future impacts of climate change. To identify potential local impacts, temperature and precipitation projections for a study area including a major portion of the coastline of the Mediterranean and Aegean seas and its hinterland are analyzed. Additionally, concerning further changes in local hydrology, the impact on streamflow is assessed for the case study area covering the Oymapınar basin through rainfall-runoff modeling. The objective of the streamflow impact assessment in the Oymapınar basin is to identify potential vulnerabilities in the case study area regarding changes in surface water, which requires to be addressed for future water resources management and adaptation planning, with a particular focus on water supply for hydropower.

This chapter describes the study areas used at different stages of the study and provides details on physical and hydrometeorological properties that are relevant to the climatologic and hydrologic assessment. Additionally, the details of the data used in these analyses are provided.

3.1 Study Area

The main components of the study are Climate Analysis, Hydrological Modeling, and Streamflow Impact Analysis. Each analysis is undertaken to focus on a specific study area or receptor of concern (Figure 3.1). The relevant descriptions are given in the following subsections.

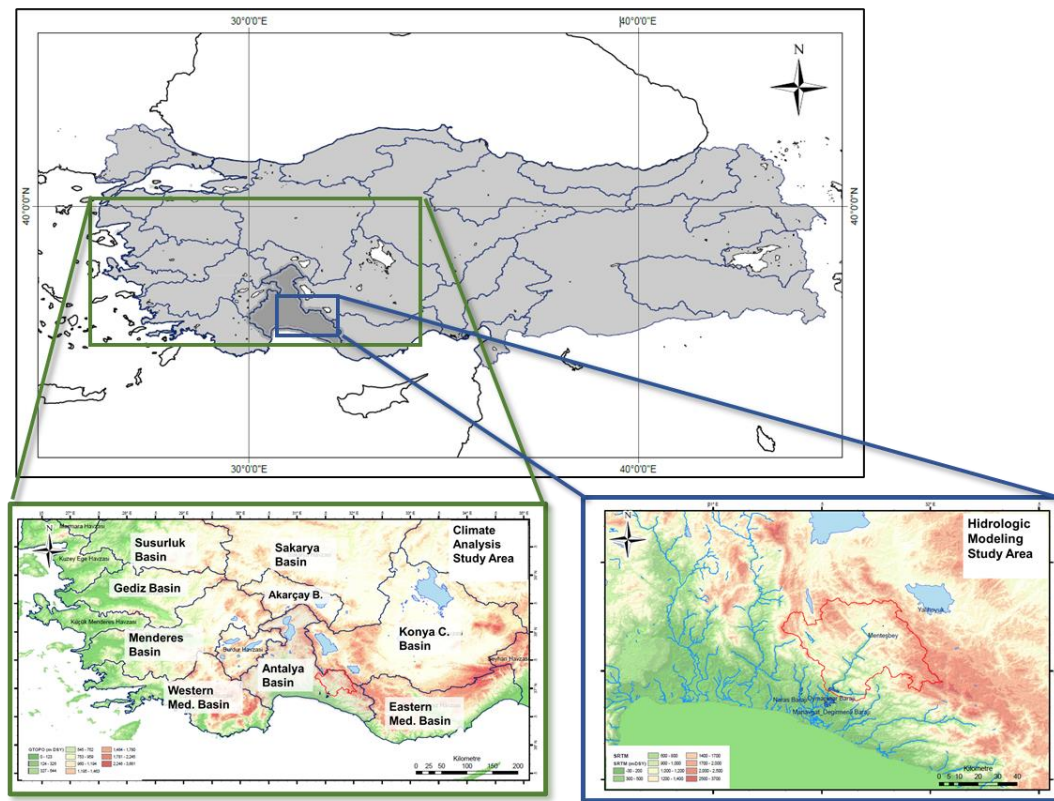


Figure 3.1. The location of the study area (lower left panel: Climate Analysis Study Area and lower right panel: Hydrological Modeling or Streamflow Impact Analysis Study Area)

3.1.1 Climate Analysis Study Area

The location of the study area is shown in Figure 3.1. In the study, regional-scale climate analysis is undertaken for a domain covering the Climate Analysis Study Area (CASA) comprising partially or fully, 10 of the major watersheds and three of the geographical regions of Turkey (Figure 3.2). The CASA is a part of the eastern Mediterranean basin and is located between Eastern Europe and the Middle East forming a transition zone between the two. The Mediterranean basin has a variable topography including geographical features such as gulfs, islands, and peninsulas, distinct basins, inland waters, and sharp topographical characteristics ranging from plain to mountainous landscapes that influence regional atmospheric circulation, and

add complexity to the local climate forcings (Lionello et al., 2006). Furthermore, several teleconnections such as North Atlantic Oscillation (NAO) and East Atlantic West Russia (EAWR) climate systems (Krichak et al., 2002; Evans, 2009) influence the regional climate along with the local processes. The Mediterranean Sea itself also exerts critical control over the climatology of the region (Hemming et al., 2010; Palatella et al., 2010). The Taurus Mountains stretching parallel to the southern Mediterranean coast forms the basin divide between southern basins (eastern, western, and middle Mediterranean basins) and basins located in the inland areas. The Taurus Mountains also form the boundary between the Mediterranean and Central Anatolia regions and act as a barrier to the effect of the Mediterranean Sea between the two regions creating diversified climatic conditions. On the western Aegean coast, on the other hand, the perpendicular stretch of the mountains to the coastline enables westerly flow to reach farther inland (Önol and Unal, 2014). Hence, complex topography and surrounding seas create diversified climatic conditions in each geographical region (Sensoy et al., 2008; Sensoy and Demircan, 2016).

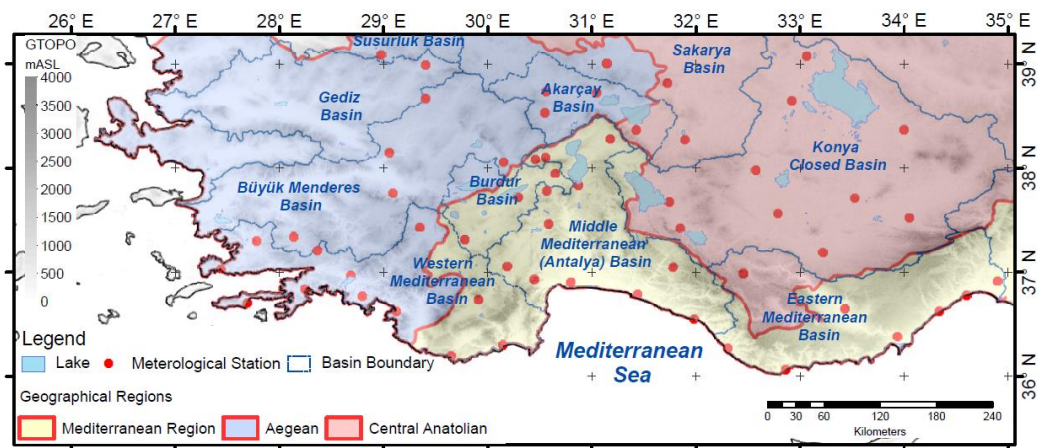


Figure 3.2. Map of the Climate Analysis Study Area (CASA), showing the locations of the meteorological stations used in this study

There are 131 meteorological monitoring stations operated by the Turkish State Meteorological Service between 1950 – 2005 in the CASA. However, the analysis of the quality of the monitoring data indicates that only 59 of these stations (Figure 3.2) provide continuous time series adequate for the purpose of the study. Further details on the historical monitoring data and a list of meteorological stations used in this study are given in Section 3.2.1.

3.1.2 Hydrological Modeling and Impact Analysis Study Area

The local climate change impact on streamflow is studied for an area limited to the Oymapınar basin and its vicinities (Figure 3.3). Hydrological Modeling Study Area (HMSA) or Streamflow Impact Assessment Area covers the area from which the surface flow drains into the Oymapınar HEPP through the Manavgat River network and the surrounding area including MSs that provide sufficient historical meteorological data time series. Details on the streamgages and meteorological stations in and around the Oymapınar basin in the HMSA are given in Section 3.2.

Oymapınar basin comprises approximately 1880 km² drainage area which is 75% of the entire Manavgat River basin. Downstream of Oymapınar HEPP, Manavgat River feeds Manavgat HEPP with an additional 118 km² drainage area. Reference data of the historical climate in and in the vicinity of the HMSA are obtained from seven meteorological stations, Bucak (7538), Akseki (8229), Antalya Airport (17300), Alanya (17310), Seydişehir (17898), Hadim (17928), Manavgat (17954), operated by TSMS (Figure 3.3). According to long-term historical meteorological data for the 1966-2005 period, the mean annual temperature for the MSs in the region ranges between 10°C and 19°C. The lowest and highest mean temperatures are observed in winter at Hadim MS (-0.15°C) and in summer at Antalya Airport MS (27°C), respectively (Table 3.1). Historical maximum mean summer temperatures at Akseki and Manavgat MSs located in the Manavgat basin are 26°C and 28.5°C, respectively, whereas, minimum mean winter temperatures at these stations for the same period are 1.5°C and 9°C, respectively.

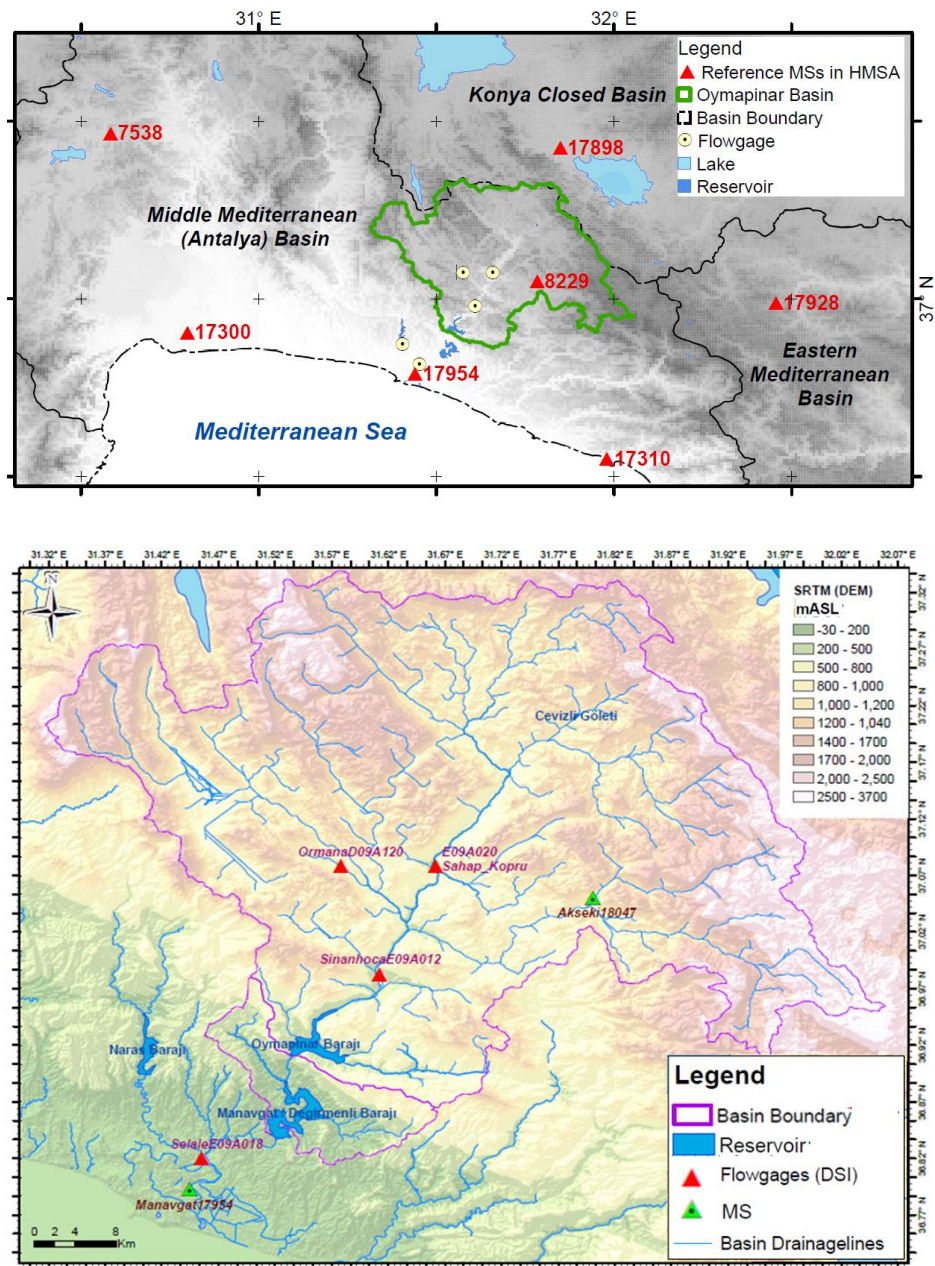


Figure 3.3. Map of the Hydrological Modeling Study Area (HMSA), top panel: Reference MSs around the Oymapınar basin in the HMSA; bottom panel: Oymapınar and Manavgat basins and streamgages on Manavgat River.

Table 3.1 Annual and seasonal mean temperature (°C) climatology for the period between 1966-2005

Meteorological Stations							
St ID	7538	8229	17300	17310	17898	17928	17954
St Name	Bucak	Akseki	Antalya Airport	Alanya	Seydişehir	Hadim	Manavgat
Elevation (mASL)	850	1150	64	6	1129	1552	38
DTS ¹ (km)	65	42	6	—	82	63	4
Annual	14.28	13.48	18.44	19.15	11.50	9.57	18.66
DJF ²	4.82	4.12	10.47	12.25	0.96	-0.15	11.14
MAM ²	12.41	11.26	16.28	16.95	10.47	8.18	16.43
JJA ²	24.51	23.49	27.03	26.32	21.78	19.36	26.62
SON ²	15.52	15.09	19.99	21.07	12.78	11.22	20.44

Table 3.2 Annual and seasonal mean daily precipitation (mm/day) climatology for the period between 1966-2005

Meteorological Stations							
St ID	7538	8229	17300	17310	17898	17928	17954
St Name	Bucak	Akseki	Antalya Airport	Alanya	Seydisehir	Hadim	Manavgat
Annual	2.03	4.58	3.04	3.00	2.03	1.78	3.02
DJF ²	3.23	7.78	7.29	6.52	3.89	3.38	7.10
MAM ²	2.11	3.36	2.11	2.22	1.93	1.80	1.89
JJA ²	0.71	0.71	0.14	0.19	0.52	0.44	0.15
SON ²	1.34	3.52	2.79	3.14	1.83	1.48	3.06

¹ DTS: Distance to the sea in km

² DJF: December, January, February, MAM: March, April, May, JJA: June, August, July, SON: September, October, November.

Oymapınar basin and its surroundings have an undulating topography with altitudes ranging from 100 mASL at the valley bottom to above 2500 mASL at the ridges bordering the basin in the north and northeast (Figure 3.4). The mean altitude of the basin is 1371 mASL. The highest altitudes are the northeast water divide of the basin where the Taurus mountain ridges stretch parallel to the coastline (in NW-NE direction) and exceed 2500 mASL. The hypsometric curve and the topographical map of the Oymapınar basin are given in Figure 3.4. The slope map of the basin is given in Figure 3.5.

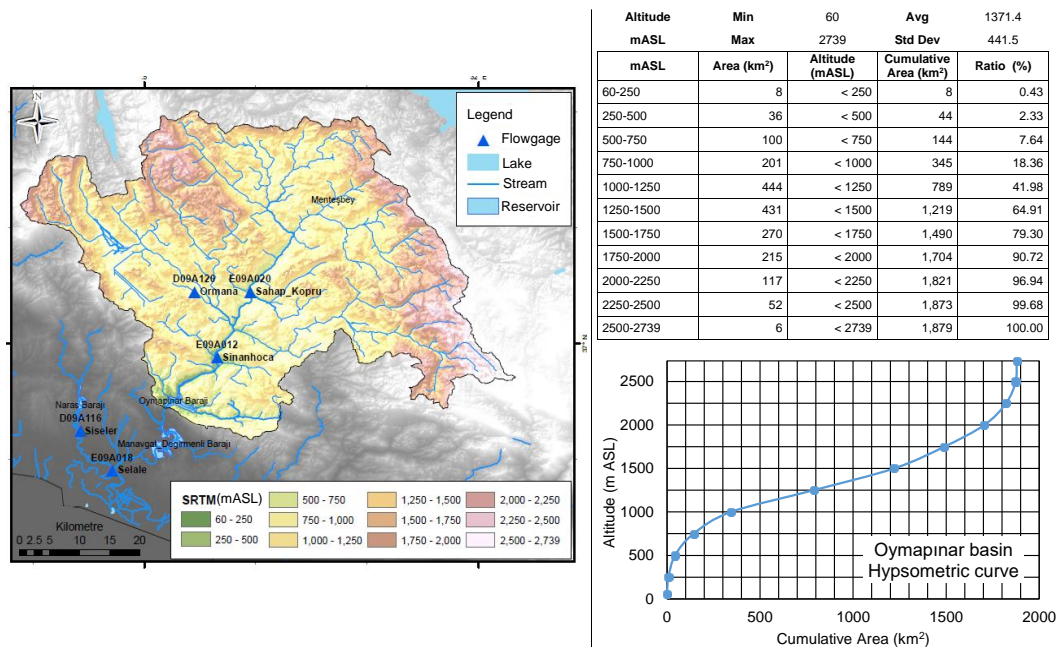


Figure 3.4. Oymapınar basin topography (NASA JPL, 2013) and hypsometric curve

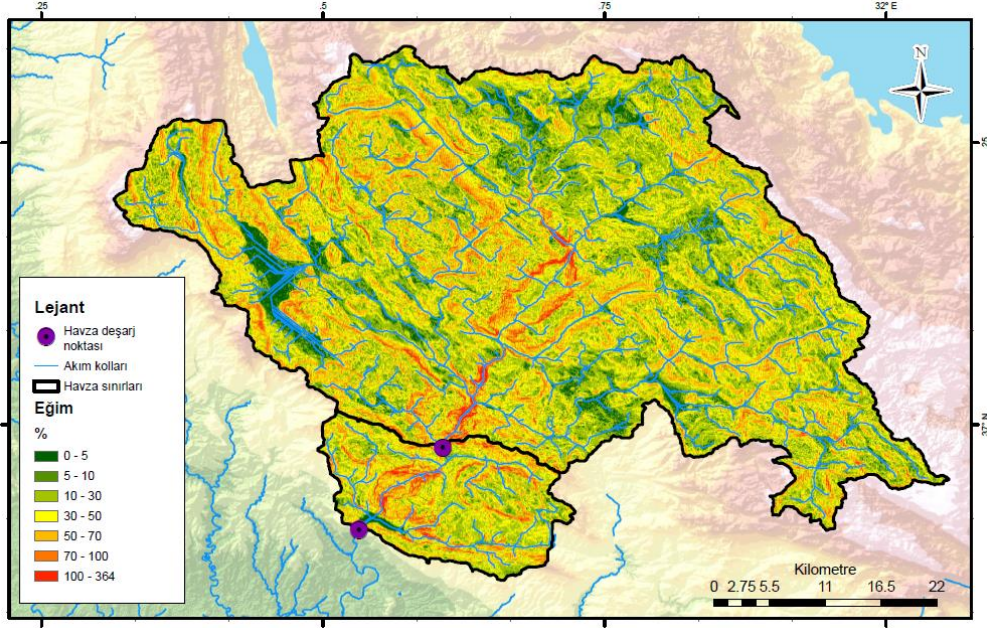


Figure 3.5. Oymapınar basin slope map

3.1.2.1 Land Cover and Canopy

Forests and seminatural areas cover most of the Manavgat basin. The agricultural areas mostly found in the valley bottom and at the south of the basin form the secondary land use in the basin (TÜBİTAK MAM, 2013). Vegetation and land cover types in the Oymapınar basin are assessed based on the Corine 2018 data (EEA, 2020). Oymapınar basin land cover map based on Corine 2018 is illustrated in Figure 3.6. Accordingly, the dominant land cover type in the Oymapınar basin is transitional woodland-shrub (36% of the basin). Land with coniferous forests, bare rocks, sparsely vegetated areas, lands with sclerophyllous vegetation are other major land cover types in the basin. The distribution of the land cover types within the basin is given in Table 3.4.

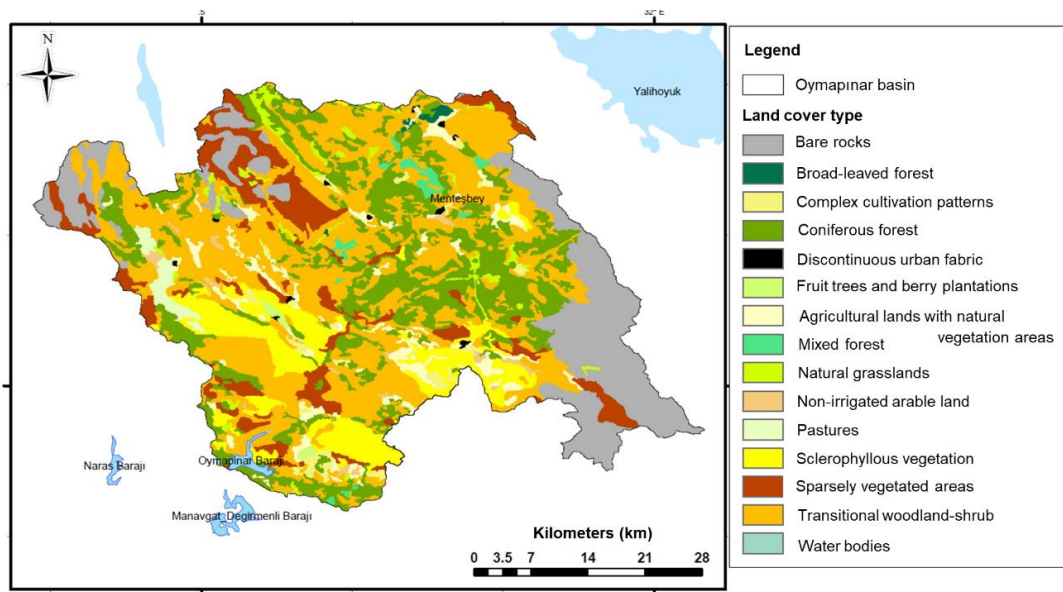


Figure 3.6. Land cover types in the Oymapınar basin, CLC 2018 (EEA, 2020)

Table 3.3 Distribution of different land cover types in the Oymapınar basin

Land cover type	Coverage	
	km ²	%
Transitional woodland-shrub	682	36.3
Coniferous forests	379	20.1
Bare rocks	280	14.9
Sparsely vegetated areas	170	9.0
Sclerophyllous vegetation	166	8.8
Land principally occupied by agriculture, with significant areas of natural vegetation	76	4.0
Natural grassland	33	1.7
Water body	6	0.3
Other	90	4.8

3.1.2.2 Geology, Hydrogeology, and Soil

Major formations within the HMSA are Antalya Miocene Basin in the south and Anamas Akseki relative autochthon in the north at higher elevations (Akay et al., 1985). In addition, at the northeast of the basin, the upstream of the Manavgat basin comprises nappes originated from the north (Akay et al., 1985). Within the HMSA the Antalya Miocene Formation comprises Oymapınar Limestone that is mainly composed of reef limestone and at the east of the Manavgat district Karpuzçay Formation that is mainly formed by shale-sandstone-conglomerate alternation. The coastline of the Manavgat basin which is located downstream of the Oymapınar basin is composed of Quarternary deposits (Akay et al., 1985).

The groundwater aquifer within the HMSA is Manavgat-İbradi-Cevizli Aquifer. The aquifer characteristics and the groundwater allocation is studied in detail by DSI within the scope of the Hydrological Survey of Manavgat-İbradi-Cevizli Aquifer (Koray Üstebay et al., 2018). According to the aquifer map provided in the Report of Hydrological Survey of Manavgat-İbradi-Cevizli Aquifer (Koray Üstebay et al., 2018), the aquifer area overlap with the surface flow drainage area of the Oymapınar basin at most of the upstream section (Figure 3.7). Furthermore, no important groundwater abstraction is identified within the upstream basin of the Oymapınar reservoir that may have a significant impact on the water balance of the basin.

The HMSA and its vicinities are majorly composed of lands with red Mediterranean soil (i.e., terra rosa) that is commonly found to cover limestone formations in the Mediterranean region. The soil classification by former KHGM (General Directorate of Rural Affairs) describes the lands in the area as lithosolic with inclinations exceeding 30% (KHGM, 1993). In addition to terra rosa known to be a soil type of low quality for agricultural purposes, although less common, lands covered with bare rock outcrops at the upstream of the basin and lands with alluvial and colluvial soils that are suitable for agricultural land use at the valley bottoms are found in the basin (KHGM, 1993).

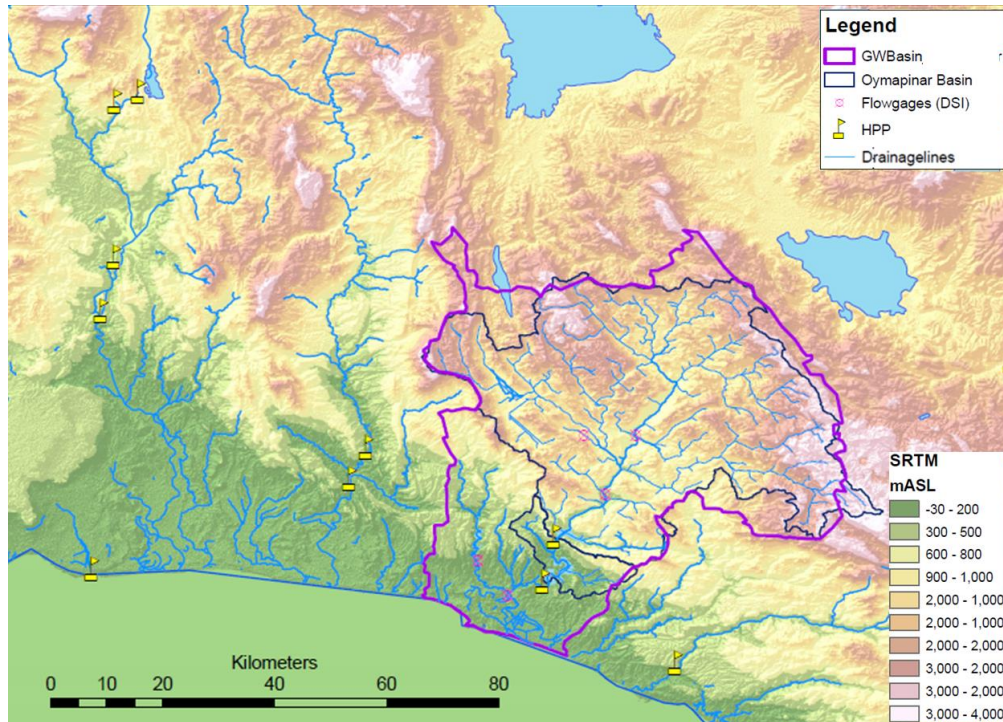


Figure 3.7. Topographical map showing Manavgat-İbradı-Cevizli aquifer and Manavgat, Oymapınar surface water basins (Koray Üstebay et al., 2018)

Based on the FAO/UNESCO World Soil Map, soils in the area are classified as Leptosols which are commonly found in the Mediterranean basin at steep slopes and undulating topography. Leptisols generally cover lands in karstic landscapes with degraded vegetation cover and are shallow soils under erosion impact (Kurucu and Esetlili, 2018).

3.1.2.3 Hydrology

Manavgat River is the largest stream within the streamflow impact assessment area. It is also the largest river in the Middle Mediterranean basin other streams in the area are mostly creeks of an ephemeral character. Manavgat River running through the basin with an approximately 90 km stream length originates from the east part of the

western Taurus Mountains. The river crosses conglomerate units and flows into the valley forming the Manavgat Waterfall downstream and discharges into the Mediterranean Sea 6-7 km south of the Manavgat district (Koray Üstebay et al., 2018).

A few natural springs in the basin discharges into the Manavgat River. Among those, Dumanlı spring has the highest flow rate. Dumanlı spring emerging from inside the Oynapınar reservoir area discharges directly into the reservoir and has a significant contribution to the reservoir inflow (Koray Üstebay et al., 2018; H. Coşkun, personal communication, September 10, 2019). Other major natural springs within the Oymapınar basin are Sinanhoca-Evga, Değirmenlik- Sugözü and Üzümdere springs. No natural lakes are located within the Oymapınar basin. Akseki-Cevizli pond is located in the northeastern part of the Oymapınar basin, on the Kalın creek that is an upstream tributary of the Manavgat River. Akseki-Cevizli pond is operated by DSI for agricultural irrigation of 220 hectares of land (Yolsu Mühendislik, 2018; Koray Üstebay et al., 2018). Other agricultural irrigation facilities abstracting surface water from Manavgat River operated by DSI include Manavgat – Oymapınar pumped irrigation infrastructure, Manavgat right bank irrigation infrastructure, and Manavgat - Ulualan irrigation facility all of which are located downstream of Oymapınar HEPP (Yolsu Mühendislik, 2018). Three reservoirs in operation in the Manavgat basin are Oymapınar reservoir, Manavgat reservoir, and Naras reservoir. The Naras reservoir which is located outside of the Oymapınar basin on Kargı creek, the east tributary of Manavgat River, is operated by DSI for irrigation and flood protection purposes. Downstream of the Naras reservoir, Kargı creek flows into the mainstream of Manavgat River at a point downstream of Oymapınar and Manavgat reservoirs. Other than the Akseki-Cevizli irrigation pond there are no reservoirs or ponds located within the Oymapınar basin (Koray Üstebay et al., 2018).

Analysis of the observed streamflow in Manavgat River at streamgages operated by DSI for the period between 1987-2015 indicates that the mean annual total flow at the Sinanhoca streamgage at the upstream of Oymapınar HEPP is 2039 hm³/yr (see Section 5.2 for details). Downstream at Şelale streamgage (downstream of

Oymapınar and Manavgat HEPPs, see Figure 3.3) total annual streamflow of Manavgat River reaches 3951 hm³/yr.

Oymapınar Reservoir and HEPP (Oymapınar HEPP) on the Manavgat River is the eighth largest HEPP in Turkey and is operated to supply electricity for industrial use at the Antalya Seydişehir Aluminum Production Facilities (TÜBİTAK MAM, 2013). HEPP is under operation since 1984 with an installed capacity of 540 MW and an annual hydropower generation of 1620 GWh (DSI, n.d.). According to the 30-year operation data of the Oymapınar reservoir for the duration between 1985-2014, there is no water supply from the reservoir for potable or irrigational purposes (Yolsu Mühendislik, 2018). The reservoir is used only for the purpose of hydropower generation. The water used in hydropower generation forms the main outflow from the reservoir. Other outflows are water loss due to evaporation from the reservoir lake surface and ecological water release which is the minimum outflow from the lake to sustain the downstream aquatic environment (Yolsu Mühendislik, 2018). Annual ecological water release is around 10% of the volume of water used for hydropower generation (Yolsu Mühendislik, 2018). Manavgat HEPP with 48 MW installed capacity is located downstream of the Oymapınar HEPP. Therefore, operational discharges from Oymapınar HEPP are significant concerning the operation and flood protection of the downstream Manavgat HEPP.

The river network and drainage lines in the Oymapınar basin and the boundaries of the basin are determined by the use of WMS (Watershed Modelling System) software based on the digital elevation model (EUDEM v1.1. (EEA, 2016)) of the basin. After the delineation of the basin relevant morphologic parameters are also calculated by the use of WMS software Morphological parameters of the Oymapınar basin are given in Table 3.5.

Table 3.4 Oymapınar basin morphologic parameters

Surface area (km ²)	Mean slope	Shape factor	Perimeter (km)	Mean elevation (mASL)
1886	0.31	1.51	374	1369

3.2 Data

3.2.1 Meteorological Observation Data

For the climatologic analysis, monitoring data from MSs operated by TSMS are used. According to the communication with TSMS, there are 131 MSs across the CASA operated for the period between 1950 and 2005. After a three-staged quality check (QC) process, 59 of the MSs among a total of 131 stations (Table 3.6) are selected as reference stations to provide daily time series adequate for climatologic analysis. Among the selected stations 12 are located within Antalya Basin including the Oymapınar basin, the streamflow impact assessment study area.

The meteorological data are processed with the assumption that the quality of the data is ensured by the QC processes of the TSMS. Hence, the QC of the meteorological data in this study is limited to the steps taken with the sole purpose of obtaining long-term time series with minor checks to eliminate potential minor errors.

The QC process in this study is applied based on the following criteria:

1. Data time series of all stations are examined so as to determine the monthly data gaps in precipitation records. The months with less than 20 days of data are eliminated.
2. 2005 is the last year of historical simulations of climate models. Therefore, stations with at least 30 years of records in the 1966-2005 period are selected

as candidate stations, and stations with less than 30 years of data are eliminated from the list of selected stations.

3. Candidate stations that have a data gap of more than 10 successive years are eliminated from the list and the remaining stations are selected for further analysis.

The period between 1966 and 2005, for which the highest number of MSs with continuous time series is found and the maximum size of the reference data set could be obtained for a good representation of the CASA climatology, is identified as the reference period.

Daily time series of observed temperature and precipitation are used for the climatologic and long-term historical analysis. After the determination of the final list of selected stations (hereinafter referred to as reference MSs) seasonal and annual climatologies for temperature and precipitation are calculated for each station. For the calculation of the climatology values, the entire time series available for the duration between 1966 and 2005 is used. The observed daily time series are also used as reference data for the analysis of simulation skills of climate models. The final time series of 59 MSs used for climatologic analysis will hereinafter be referred to as Reference Data (RD).

Table 3.5 The list and details of meteorological stations in the CASA

Station ID	Station Name	Province	District	Latitude (°)	Longitude (°)	Elevation (m ASL)	Length of time series (years) ³
4947	Dumlupınar KK	Kütahya		38.85	29.97	1250	<30
4956	Bayat	Afyon		38.98	30.93	1100	<30
5477	Çay KK	Afyon		38.70	31.03	1020	<30
5643⁴	Şuhut	Afyon		38.53	30.55	1130	35
5800	Eşme KK	Uşak		38.40	28.97	810	<30
5986	Çivril KK	Denizli		38.30	29.73	840	<30
6513	Şarkikaraağaç	Isparta		38.08	31.37	1180	<30
6679	Atabey KK	Isparta		37.95	30.65	1000	38
6840	Çardak	Denizli		37.83	29.67	920	<30
6854	Aksu KK	Isparta		37.80	31.07	1200	<30
7367	Sütçüler	Isparta		37.48	31.00	1000	<30
7373	Üzümlü	Konya		37.55	31.60	1275	<30
7538	Bucak	Burdur		37.47	30.58	850	33
7686	Turgut	Muğla		37.38	28.03	500	<30
7899	Cevizli	Antalya		37.18	31.77	1150	<30
7902	Ahırlı	Konya		37.25	32.12	1150	<30
8046	Göhlisar	Burdur		37.15	29.50	990	<30
8073	Bozkır	Konya		37.20	32.25	1180	<30
8229	Akseki	Antalya		37.05	31.78	1150	32
8327	Turgutreis	Muğla		37.02	27.25	5	<30
8355	Bük Forest	Antalya		36.93	30.45	475	30
8364	Serik	Antalya		36.92	31.10	50	<30

³ Length of time series (years): Total number of years for continuous time series obtained for the period between 1966-2005

⁴ Reference MSs selected for climatologic analysis (length of time series ≥ 30 years) are written in bold.

Table 3.5 (continued)

Station ID	Station Name	Province	District	Latitude (°)	Longitude (°)	Elevation (m ASL)	Length of time series (years) ³
8372	Güzelsu	Antalya		36.90	31.85	1250	<30
8402	Tarsus	Mersin		36.92	34.90	33	<30
8498	Gündoğmuş	Antalya		36.82	32.00	930	<30
8713	Kemer	Antalya		36.60	30.57	10	<30
8717	Güzelbağ	Antalya		36.73	31.90	500	<30
8880	Kumluca KK	Antalya		36.38	30.28	60	<30
9022	Tausus Rural Aff.	Mersin		36.92	34.90	11	34
9023	Gözlü Düç	Konya		38.45	32.37	930	<30
9025	Atınova Düç	Konya		38.72	32.22	1100	<30
17185	Uşak Airport	Uşak	Center	38.68	29.47	874	<30
17188	Uşak	Uşak	Center	38.67	29.40	919	40
17189	Afyon Airport	Afyon	Center	38.73	30.60	1001	<30
17190	Afyon	Afyon	Center	38.74	30.56	1034	40
17191	Cihanbeyli	Konya	Cihanbeyli	38.65	32.92	973	40
17192	Aksaray	Aksaray	Center	38.37	34.00	970	40
17237	Denizli	Denizli	Merkez-efendi	37.76	29.09	425	40
17238	Burdur	Burdur	Center	37.72	30.29	957	40
17239	Akşehir	Konya	Akşehir	38.37	31.43	1002	40
17240	Isparta	Isparta	Center	37.78	30.57	997	40
17241	Isparta Airport	Isparta	Gönen	37.86	30.37	869	<30
17242	Beyşehir	Konya	Beyşehir	37.68	31.75	1141	40
17244	Konya Airport	Konya	Selçuklu	37.98	32.57	1031	40
17245	Konya	Konya	Meram	37.87	32.47	1029	<30
17246	Karaman	Karaman	Center	37.19	33.22	1018	40
17248	Ereğli	Konya	Ereğli	37.53	34.05	1046	40
17257	Çardak Airport	Denizli	Çardak	37.79	29.70	848	<30
17290	Bodrum	Muğla	Bodrum	37.03	27.44	26	40
17291	Milas-Bodrum Airport	Muğla	Milas	37.25	27.66	11	<30
17292	Muğla	Muğla	Menteşe	37.21	28.37	646	40

Table 3.5 (continued)

Station ID	Station Name	Province	District	Latitude (°)	Longitude (°)	Elevation (m ASL)	Length of time series (years) ³
17293	İmsik-Bodrum Airport	Muğla	Bodrum	37.14	27.67	60	<30
17294	Dalaman	Muğla	Dalaman	36.77	28.80	12	40
17295	Dalaman Airport	Muğla	Dalaman	36.72	28.79	5	<30
17296	Fethiye	Muğla	Fethiye	36.63	29.12	3	40
17297	Datça	Muğla	Datça	36.71	27.69	28	40
17298	Marmaris	Muğla	Marmaris	36.84	28.25	16	40
17300	Antalya Airport	Antalya	Muratpaşa	36.91	30.80	64	40
17302	Antalya	Antalya	Muratpaşa	36.89	30.68	47	<30
17310	Alanya	Antalya	Alanya	36.55	31.98	6	40
17320	Anamur	Mersin	Anamur	36.07	32.86	2	40
17330	Silifke	Mersin	Silifke	36.38	33.94	10	40
17340	Mersin	Mersin	Yenişehir	36.78	34.60	7	40
17375	Finike	Antalya	Finike	36.30	30.15	2	40
17380	Kaş	Antalya	Kaş	36.20	29.65	153	30
17627	T.reis Marina	Muğla	Bodrum	37.00	27.26	6	<30
17744	Altınova Tıgem	Konya	Kadınhanı	38.72	32.18	1002	<30
17746	Demirci	Manisa	Demirci	39.03	28.65	855	<30
17747	Dumlupınar	Kütahya	Dumlupınar	38.85	29.98	1250	<30
17748	Simav	Kütahya	Simav	39.09	28.98	809	40
17750	Gediz	Kütahya	Gediz	38.99	29.40	736	33
17752	Emirdağ	Afyon	Emirdağ	39.01	31.15	983	40
17753	Bayat	Afyon	Bayat	38.97	30.92	1100	<30
17754	Kulu	Konya	Kulu	39.08	33.07	1005	40
17793	Çay	Afyon	Çay	38.59	31.03	996	<30
17796	Bolvadin	Afyon	Bolvadin	38.73	31.05	1018	38
17798	Yunak	Konya	Yunak	38.82	31.73	1148	35
17823	Yakasenek	Afyon	Sultandağı	38.55	31.17	1150	<30
17824	Güney	Denizli	Güney	38.15	29.06	825	40
17825	Çivril	Denizli	Çivril	38.26	29.71	824	<30
17826	Senirkent	Isparta	Senirkent	38.10	30.56	959	38

Table 3.5 (continued)

Station ID	Station Name	Province	District	Latitude (°)	Longitude (°)	Elevation (m ASL)	Length of time series (years) ³
17827	Eşme	Uşak	Eşme	38.40	28.99	809	<30
17828	Yalvaç	Isparta	Yalvaç	38.28	31.18	1096	32
17829	Şuhut	Afyon	Şuhut	38.53	30.57	1140	<30
17832	Ilgın	Konya	Ilgın	38.28	31.89	1036	40
17855	Çardak	Denizli		37.82	29.67	864	<30
17862	Dinar	Afyon	Dinar	38.06	30.15	864	40
17863	Şarkikaraağaç	Isparta	Şarkikaraağaç	38.06	31.36	1158	<30
17864	Uluborlu	Isparta	Uluborlu	38.09	30.46	1025	38
17865	Anamas	Isparta	Aksu	37.80	31.07	1240	<30
17867	Akköy	Denizli	Pamukkale	37.96	29.07	198	<30
17882	Eğirdir	Isparta	Eğirdir	37.84	30.87	920	39
17884	Milas	Muğla	Milas	37.30	27.78	57	40
17885	Atabey	Isparta	Atabey	37.95	30.64	1000	<30
17886	Yatağan	Muğla	Yatağan	37.34	28.14	365	38
17887	Bucak	Burdur		37.45	30.58	852	<30
17890	Acıpayam	Denizli	Acıpayam	37.43	29.35	941	38
17891	Göhlisar	Burdur	Göhlisar	37.14	29.53	990	<30
17892	Tefenni	Burdur	Tefenni	37.32	29.78	1142	40
17893	Sütçüler	Isparta	Sütçüler	37.49	30.97	985	<30
17895	Boztepe Tigem	Antalya	Aksu	36.94	30.90	10	<30
17897	Gözlü Tigem	Konya	Sarayönü	38.49	32.46	111	<30
17898	Seydişehir	Konya	Seydişehir	37.43	31.85	1129	40
17900	Çumra	Konya	Çumra	37.57	32.79	1014	35
17902	Karapınar	Konya	Karapınar	37.71	33.53	996	40
17915	Belek	Antalya	Serik	36.86	31.06	6	<30
17924	Köyceğiz	Muğla	Köyceğiz	36.97	28.69	24	40
17926	Korkuteli	Antalya	Korkuteli	37.06	30.19	1017	38
17927	İbradi	Antalya	İbradi	37.10	31.60	1036	<30
17928	Hadim	Konya	Hadim	36.99	32.46	1552	40
17951	Kumluca	Antalya	Kumluca	36.36	30.30	60	<30
17952	Elmalı	Antalya	Elmalı	36.74	29.91	1095	40

Table 3.5 (continued)

Station ID	Station Name	Province	District	Latitude (°)	Longitude (°)	Elevation (m ASL)	Length of time series (years) ³
17953	Kemer	Antalya	Kemer	36.59	30.57	10	<30
17954	Manavgat	Antalya	Manavgat	36.79	31.44	38	37
17956	Mut	Mersin	Mut	36.65	33.43	340	34
17958	Erdemli	Mersin	Erdemli	36.63	34.34	7	40
17964	Islahiye	Gaziantep		37.03	36.63	518	<30
17970	Kale-Demre	Antalya	Demre	36.24	29.98	25	<30
17974	Gazipaşa	Antalya	Gazipaşa	36.27	32.30	21	36
17975	Gazipaşa Airport	Antalya	Gazipaşa	36.30	32.30	32	<30
17978	Tarsus	Mersin	Tarsus	36.89	34.96	12	<30
18011	Beşkonak Forest	Antalya	Manavgat	37.14	31.19	142	<30
18012	Gündoğmuş Forest Depot	Antalya	Gündoğmuş	36.80	32.00	898	<30
18014	Gebiz Forest	Antalya	Serik	37.10	30.93	78	<30
18015	Bük Forest	Antalya	Korkuteli	36.97	30.43	489	<30
18047	Akseki	Antalya	Akseki	37.05	31.80	1063	<30
18306	Serik	Antalya	Serik	36.95	31.12	94	<30
18486	Ahırlı	Konya	Ahırlı	37.24	32.11	1185	<30
18489	Bozkır	Konya	Bozkır	37.18	32.25	1170	<30
18610	Cevizli Tekebeli	Antalya	Akseki	37.25	31.77	1420	<30
18611	Bedan	Antalya	Gündoğmuş	36.79	32.28	1672	<30

Apart from the climatological analysis, the historical meteorological data are also used to calibrate the hydrologic model of the Oymapınar basin. For that purpose, daily time series of temperature, precipitation, sun duration, and long-term mean temperature and evaporation data available from the MSs that are closest and most representative of the Oymapınar basin are used (Figure 3.3). The details of the meteorological data used in the hydrological modeling and relevant MSs are provided in Section 4.2.3.

3.2.2 Data from Climate Models

The second part of the Climate Analysis comprises the use of climate model simulation outputs. Daily precipitation and temperature data from the historical and future simulations of the climate models are used for this part of the study. The historical simulation outputs of the climate models are validated through a benchmark with the RD for the determination of the models with better simulation skills in the CASA. Then the future projections on temperature and precipitation are analyzed for the determination of potential impacts of climate change in the CASA. Finally, the future climate projections are used for the streamflow projections to identify the climate change impact on streamflow in the Manavgat River feeding the Oymapınar HEPP.

For the assessment of climate change impacts, two RCPs are taken into consideration. Two RCPs represent different CO₂ emissions and resulting atmospheric CO₂ concentrations that are expected to create different final radiative forcings in the year 2100. Two emission scenarios used in the study are:

- RCP4.5 scenario which is a medium mitigation scenario assuming an increase in radiative forcing stabilizing at approximately 4.5Wm^{-2} after 2100 (atmospheric GHGs concentration approximately 650 ppm CO₂-equivalent (CO₂-eq.) in 2100 and stabilization after 2100), and
- RCP8.5 scenario that represents the “business as usual” condition without mitigations for climate change. This scenario assumes high emissions causing the increase in the radiative forcing to reach approximately 8.5Wm^{-2} near 2100 (in terms of atmospheric GHGs concentration: >1370 ppm CO₂-eq. in 2100) (Taylor, 2009; Moss et al., 2010).

The Climate Analysis includes simulation results of 14 high-resolution climate models. The 14-member ensemble includes 12 RCMs from the CORDEX database and two climate models from MRI. The list of the CORDEX climate models is given in Table 3.7. Climate projections from CORDEX RCMs are based on simulations

for the EURO domain with 11° grid resolution and use CMIP5 (the fifth phase of the Coupled Model Intercomparison Project) GCMs as driving models. As it is seen in Table 3.7, CORDEX RCMs in the ensemble include a combination of six different RCMs using four different CMIP5 GCMs. This is aimed to enable a comparison between different RCM/GCM combinations to identify potential advantages/disadvantages regarding climate projections with the focus on the CASA.

Apart from the non-bias adjusted or raw outputs of the CORDEX RCMs, outputs post-processed for bias adjustment are also included in the study for a comparison of the simulation skills. Within that scope, RCM outputs bias-adjusted within the scope of the CORDEX-Adjust Project that is publicly available from the CORDEX database are used. The bias-adjusted simulation outputs are used to analyze uncertainties involved with climate projections and to identify any improvements on raw projections, if there are, provided by various bias-adjustment methods specific to the CASA. In total, nine bias-adjusted RCM outputs are used in the study. These include outputs processed by the use of Quantile Mapping (QMap), Distribution Based Scaling (DBS), and Cumulative Distribution Function Transform (CDF-t) methods. Among these outputs, bias-adjusted outputs using the QMap method (Gudmundsson et al., 2012) are generated by the Norwegian Meteorological Institute (METNO) based on MESAN (MESoscale ANalysis system) (Landelius et al., 2016) reference data. Outputs using the DBS45 method (Yang et al., 2010) are generated by Swedish Meteorological and Hydrological Institute (SMHI) based on MESAN data, and outputs using the CDFT method (Vrac et al., 2016) are generated by Pierre Simon Laplace Institute (IPSL) based on WFDEI (Watch Forcing Data - ERA-Interim) (Weedon et al., 2014) reference data. The list of bias-adjusted outputs used in this study is given in Table 3.8. The daily outputs of raw RCMs from the EURO-CORDEX Project and their bias-adjusted outputs are obtained from the web-based ESGF and climate4impact portals (ESGF, 2020; IS-ENES, n.d.).

Table 3.6 List of CORDEX RCMs used in this study

Institute	RCM	GCM			
		ICHEC-EC-EARTH	CNRM-CERFACS-CNRM-CM5	MOHC-HadGEM2-ES	IPSL-IPSL-CM5A-MR
Danish Meteorological Institute (DMI)	HIRHAM5	X			
Climate Limited-area Modelling Community (CLMcom)	CCLM4-8-17	X	X	X	
The Royal Netherlands Meteorological Institute (KNMI)	RACMO22E	X		X	
Swedish Meteorological and Hydrological Institute (SMHI)	RCA4	X	X	X	X
National Centre for Meteorological Research in France (CNRM)	ALADIN53		X		
National Center for Atmospheric Research (NCAR), National Centers for Environmental Prediction (NCEP)	WRF331F				X

Table 3.7 List of bias-adjusted RCMs

Driving Model	RCM	Bias Adjustment Method
CNRM-CERFACS-CNRM-CM5	SMHI-RCA4	CDFT21-WFDEI
		QMAP-MESAN
		DBS45-MESAN
ICHEC-EC-EARTH	SMHI-RCA4	CDFT21-WFDEI
		QMAP-MESAN
		DBS45-MESAN
ICHEC-EC-EARTH	KNMI-RACMO22E	CDFT21-WFDEI
		QMAP-MESAN
		DBS45-MESAN
ICHEC-EC-EARTH	DMI-HIRHAM5	CDFT21-WFDEI
		QMAP-MESAN
		DBS45-MESAN

In addition to the CORDEX RCMs, simulation results of a high-resolution atmospheric climate model, MRI-AGCM, and MRI’s NHRCM nested in MRI-AGCM are also used. The mesh sizes of MRI-AGCM and NHRCM used in this study are 20 km (0.1875°) and 5 km, respectively. The daily outputs of the MRI-AGCM for the study area are provided by the Japan MRI for the study. Furthermore, climate simulations with NHRCM are undertaken within the scope of this study for the domain limited to the CASA in collaboration with MRI by dynamical downscaling of MRI-AGCM outputs generated by MRI. The dynamical downscaling works using NHRCM are undertaken in Japan MRI facilities in collaboration with the MRI experts within the scope of the bilateral research collaboration supported by TUBITAK and Japan Society for the Promotion of Science under the TUBITAK project with the title of “Assessment of Climate Change Impacts on Streamflow and Hydropower in Antalya, Turkey” [Grant Number 118Y365].

3.2.3 Historical Streamflow Data

The hydrological model of the Oymapınar basin is developed by the use of the daily observed flow rates of the Manavgat River and its tributaries. Based on the examination of the river network, and historical daily flow rates provided by DSI, Sinanhoca streamgage (Flowgage ID: E09A012) is selected to be used for the development of the rainfall-runoff model of the Oymapınar basin. The historical monitoring data for the streamgages within the basin and daily operation data (daily reservoir inflow data) are also analyzed for the development of the conceptual basin model. The location of the streamgages in the Oymapınar basin and its vicinities are shown in Figure 3.3. Details on the data processing for the observed daily streamflows, use of the relevant data in hydrological model development are detailed in Section 4.2.3.

CHAPTER 4

METHODOLOGY

Details on the analysis methodologies used for the assessment are described in detail with relevant reasons for selection. Figure 4.1 illustrates the flowchart of the study methodology indicating subtasks completed to attain the targeted outcomes from Climate Analysis, Hydrological Modeling, and Streamflow Impact Analysis components.

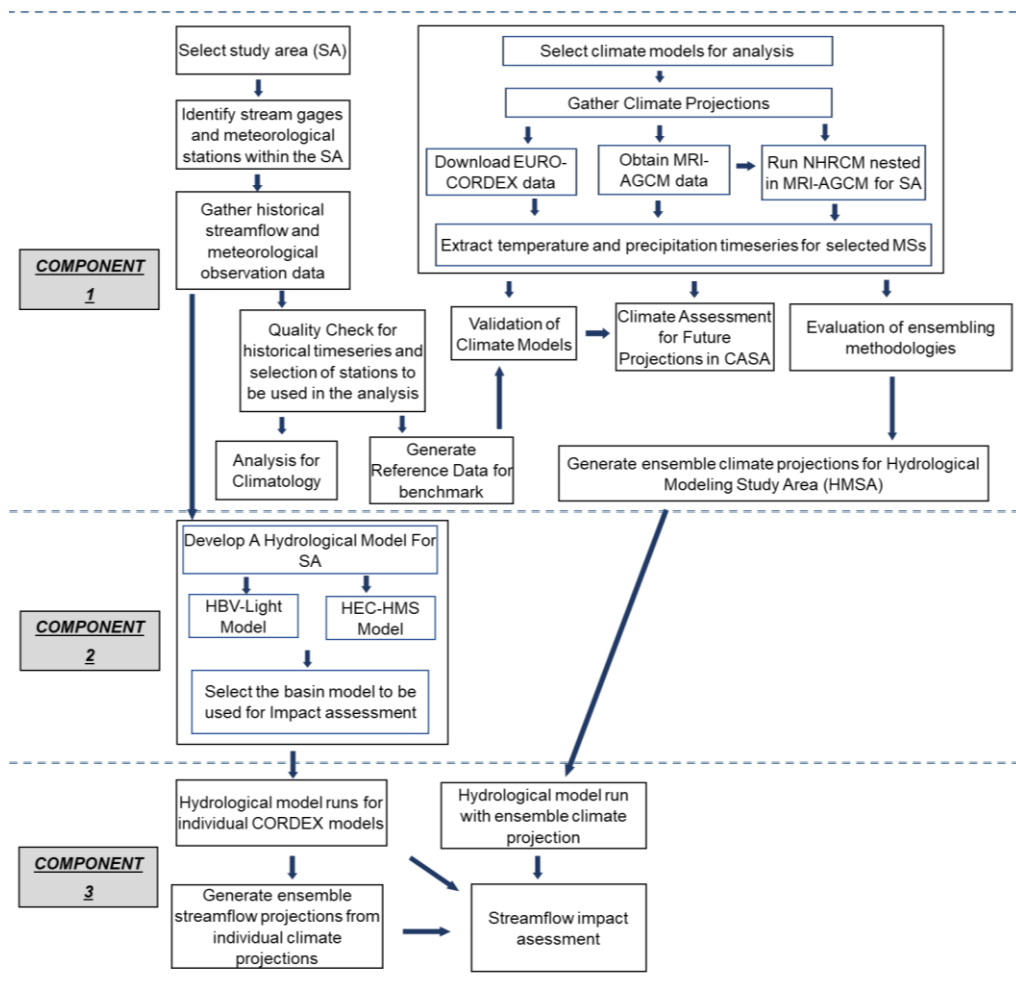


Figure 4.1. Study flowsheet

The first component (See Figure 4.1, Component 1), Climate Analysis, includes the analysis of current temperature and precipitation climatology at the CASA. This is followed by the multi-model ensemble analysis of 14 climate models. Climate models are validated through a benchmark of their historical simulation outputs against the RD to identify the models with the potentially highest skill in future projections. After the validation, the 14-member ensemble is used to analyze potential changes in temperature and precipitation in the CASA.

An additional step in the multi-model ensemble analysis is the comparison of commonly used ensembling methodologies to evaluate their efficiencies. For that purpose, the ensembled projections are also compared with individual models used in the ensemble and with their bias-adjusted versions in order to identify potential advantages and disadvantages.

Hydrological Modeling component (See Figure 4.1, Component 2) comprises the development of mathematical rainfall-runoff models of the basin by the use of two parametric modeling software: HEC-HMS (U.S. Army Corps of Engineers Hydrologic Engineering Center- Hydrologic Modeling Software), and HBV-light (Swedish Meteorological and Hydrological Institute's model Hydrologiska Byrns Vattenbalansavdelning). Two models developed with modeling softwares using different approaches in model setups are compared for their efficiency in simulating basin hydrology and also for their advantages and disadvantages in use. The hydrological model of the Oymapınar basin developed in this study component is used for the streamflow impact assessment in the third component of the study.

Streamflow Impact Analysis (See Figure 4.1, Component 3) is done by the use of 12 CORDEX RCMs that provide time series of projections for the period between 2020-2100. Firstly, the hydrological model is run using the projections of individual models. The streamflow projections from individual climate model runs are used to generate ensemble projection for the streamflow by the use of Multi-model Ensemble development methodologies described in Section 4.3.2.

In addition, the hydrological model is run using the ensemble (i.e., MME) temperature and precipitation data series. For this purpose, MME data series of temperature and precipitation are firstly generated from individual RCM projections by using MME methodologies and then used as input in hydrological modeling.

The results of the streamflow simulations are validated through a benchmark of historical results with observed flow rate at Sinahoca streamgauge. Following that the future streamflow projections that have indicated satisfactory simulation efficiency are analyzed for the assessment of the potential future changes in streamflow discharging to Oymapınar Reservoir.

4.1 Climate Analysis Methodology

4.1.1 Analysis of Temperature and Precipitation Climatology

Long-term annual and seasonal climatology of temperature and precipitation in the CASA are analyzed using the RD described in Section 3.2.1. Annual and seasonal (winter: December, January, February, spring: March, April, May, summer: June, July, August, and fall: September, October, November) climatologies are calculated based on at least 30 years of time series of daily mean temperature and daily total precipitation for the period of 1966-2005. Climatology data for 59 MSs across the CASA are converted to surface data with inverse distance weighted (IDW) interpolation method, and climatology maps are developed using the Spatial Analyst tool of ArcGIS 10.0. Climatology maps represent the observed present spatial variability of climatology in the CASA and highlight intraregional variability and the range of mean temperature and precipitation shaped by the current climate forcings.

4.1.2 Evaluation of Climate Simulations

Temperature and precipitation data from the climate models (Section 3.2.2) are validated through a benchmark with the reference data. Within that scope, raw and bias-adjusted outputs of historical simulations are analyzed for their skills to replicate the spatial variability of mean temperature and precipitation. The simulation skills are evaluated based on the statistical performance indicator (SPI) parameters and Taylor diagram. The SPI parameters used for the Climate Analysis are Pearson correlation coefficient (*Corr*), root mean square error (*RMSE*), percent bias (*PBIAS*), and bias as suggested by Moriassi et al. (2015). In addition to the calculation of individual SPI parameters an aggregated indicator parameter is generated for the models based on these three SPIs. An aggregated performance index (API) is calculated based on the average of the rankings (ranking from the best to worst indicator value) of the models for each SPI separately. The final API value of each model represents the relative simulation skill of the models. The final API values are used for the ranking of the models with respect to their simulation skills in which the lower the API value means that higher simulation skill is achieved. Analysis by the use of SPIs is also applied to the ensemble outputs generated from climate models by the use of different ensembling methodologies in order to have a benchmark with the efficiency of individual model outputs.

Another method used in this study for the evaluation of the simulation skills is the comparison of the modeled outputs with the RD through the Taylor diagram (Taylor, 2001, 2005). Taylor diagram is among the most common means of depicting the relative performance skill of models respecting the convergence to the reference data in terms of correlation (*Corr*), centered root-mean-square (CRMS), and variation (i.e., standard deviation, SD). However, the diagram does not include information on the scale of overall bias (Taylor, 2005). The analysis for overall bias is included in the evaluation through the use of SPIs and API as described above.

4.1.3 Analysis for Future Changes in Temperature and Precipitation

Potential changes in mean temperature and precipitation in the CASA are assessed by the analysis of results from a 14-member ensemble. For the analysis, results from individual models as well as their ensembled outputs are used together. Potential future changes in temperature and precipitation are calculated based on the difference between the modeled results for historical (i.e., reference period) and future periods. In that context, potential changes are calculated for 59 MSs separately, and as the average of all MSs to represent the areal average of the entire CASA. The impact identified for all MSs is then used to develop potential impact maps by the use of the IDW method. The analysis aims to obtain interpretations of the spatial variability of impacts that might be influenced by different climate forcings under climate change impact.

Due to the differences in model setups, intermodel variability is frequently observed in multi-model ensembles. This enables the assessment of uncertainties regarding climate projections. On the other hand, for further impact assessment and use of the projections in subsequent analysis and modeling (e.g., hydrological modeling), ensemble outputs are also generated to reduce uncertainty in projections. The use of ensemble outputs may have several advantages and drawbacks in impact assessment studies. The details regarding the ensemble approaches and potential restrictions and benefits relative to the individual model outputs are discussed in Sections 4.3.2, 5.1.3.2, and the research papers presented in Appendices.

One of the ensembling methodologies used to generate ensemble outputs for climate analysis in this study is a performance-based weighted average (PBWA). PBWA is calculated by using only the ensemble members that are identified with the highest skills to replicate temperature or precipitation climatology for CASA. PBWA is calculated for all MSs in the CASA as a weighted average of the projected impacts based on the normalized API values of each model. For the calculation of PBWA projections, the five best-performing climate models are used in this study. Details of the PBWA approach are given in Mesta et al. (2022) in Appendices B and C. In

addition to the PBWA, the mean value of the ensemble, the average value of the projections from 14 climate models at all MSs, is also used for the analysis. Other methodologies used in this study to generate ensemble outputs for streamflow impact assessment are detailed in Section 4.3.2.

Within the scope of Climate Analysis, potential future changes in mean temperature and precipitation are analyzed for the short (2020-2030), medium (2031-2050), and long-term (2051-2100) future. For that purpose, the long-term means of simulation results of the climate models for the reference period are compared with the long-term means of projections for the relevant future period. It should be noted that although the reference period in the study is determined to represent the period between 1966 and 2005, for certain CORDEX RCMs reference period is restricted to the period between 1970 and 2005 due to the length of the available simulation runs. Similarly, for the MRI models depending on the length of the historical and future simulation runs the period of the analysis is limited to 1980-2001 for the present and 2080-2100 for the future. The lengths of the modeled time series for present and future periods from 14 climate models are given in Table 4.1.

Table 4.1 Timeframes of the simulation outputs of climate models used in the study

Model ID ⁵	Climate Model (RCM/GCM)		Output Period	
	Driving GCM	RCM	Historic	Future (Scenarios)
M1	MRI-AGCM		1979-2003	2075-2100 (RCP8.5)
M2	MRI-AGCM	NHRCM	1980-2001	2080-2100 (RCP8.5)
M3 ⁶	CNRM-CM5	ALADIN53	1951-2005	2006-2100 (RCP4.5, RCP8.5)
M4 ⁶	CNRM-CM5	CCLM4-8-17	1950-2005	2006-2100 (RCP4.5, RCP8.5)
M5 ⁶	CNRM-CM5	RCA4	1970-2005	2006-2100 (RCP4.5, RCP8.5)
M6 ⁶	EC-EARTH	CCLM4-8-17	1949-2005	2006-2100 (RCP4.5, RCP8.5)
M7 ⁶	EC-EARTH	HIRHAM5	1951-2005	2006-2100 (RCP4.5, RCP8.5)
M8 ⁶	EC-EARTH	RACMO22E	1950-2005	2006-2100 (RCP4.5, RCP8.5)
M9 ⁶	EC-EARTH	RCA4	1970-2005	2006-2100 (RCP4.5, RCP8.5)
M10 ⁶	CM5A-MR	RCA4	1970-2005	2006-2100 (RCP4.5, RCP8.5)
M11 ⁶	CM5A-MR	WRF331F	1951-2005	2006-2100 (RCP4.5, RCP8.5)
M12 ⁶	HadGEM2-ES	CCLM4-8-17	1949-2005	2006-2100 (RCP4.5, RCP8.5)
M13 ⁶	HadGEM2-ES	RACMO22E	1950-2005	2006-2100 (RCP4.5, RCP8.5)
M14 ⁶	HadGEM2-ES	RCA4	1970-2005	2006-2100 (RCP4.5, RCP8.5)

An additional step in the analysis of the projections on climate change impact on temperature and precipitation is the statistical significance testing. The objective of the statistical significance testing is to differentiate between climate signals

⁵ Model ID's used in the study

⁶ Models from the CORDEX Database: ESGF, Earth System Grid Federation website, <https://esgf-node.llnl.gov/search/esgf-llnl/>, (CoG version v4.0.0b2, ESGF P2P Version v4.0.4)

represented by the projections from the internal variability or noise generated by the model. For that purpose, the most common methodology is the use of the Student's t-test (Decremer et al., 2014). In this study, the significance of the change in precipitation is tested by the use of a variation of Student's t-test, Welch's two-sample t-test (or unequal variances t-test). In order to identify the statistical significance of the projected temperature and precipitation change for each MS in CASA, the t-test is applied to the annual mean time series from the climate model projections for the reference versus future short-, medium- and long-term periods. The significance is tested by the use of a threshold value of 95% probability confidence level. Hence, for the probability (p) value less than or equal to 0.05 the change in the meteorologic parameter is classified as statistically significant (i.e., due to the climate signal). The statistical significance probability values for MSs across CASA are converted to surface data by the use of the IDW approach and the information of statistical significance (or non-significance) of the projected impacts is shown on the Climate Analysis maps for potential future change in temperature and precipitation for each of the 14 climate models.

4.2 Hydrological Modeling Methodology

The study methodology is based on the modeling of rainfall-runoff processes in the basin of concern by the use of two parametric modeling software in order to make a comparison of the modeling efficiencies. Two hydrological models, a complex and semi-distributed model developed in HEC-HMS and a simpler conceptual model developed in HBV-light, are obtained within the scope of the Hydrological Modelling component of the study. In line with the objectives and scope of this study continuous modeling approach is followed for hydrological modeling. The final calibrated model is used in subsequent assessment of climate change impact on streamflow into the Oymapınar reservoir. For the development of a conceptual model of the basin, initially, basin properties, hydrometeorology of the basin, and monitoring data available for the basin are analyzed.

4.2.1 Analysis of Oymapınar Streamflow Data

In order to determine the morphology of the Oymapınar basin, the drainage lines and stream network in the Oymapınar basin are analyzed by the use of hydrologic modeling software WMS (Watershed Modelling System) based on EUDEM v1.1 (EEA, 2016). Following the development of the streamflow network, the Oymapınar basin is delineated to define its subbasins and basin boundaries (Figure 4.2). The subbasins of the Oymapınar basin are formed based on the location of the streamgages in the basin that provides long-term historical streamflow data for hydrological modeling.

Because there is no streamgage located at the inlet of the Oymapınar reservoir to monitor the reservoir inflow, the streamflow data from the nearest streamgage are used in hydrological modeling. Şahapköprü (streamgage ID: E09A020) and Sinanhoca (streamgage ID: E09A012) streamgages located on the Manavgat mainstream upstream of Oymapınar reservoir provide long-term continuous daily streamflow observation data. Although the Sinanhoca streamgage located approximately 10.5 km upstream of the Oymapınar reservoir is an indicator of the reservoir inflow, an additional 200 km² drainage area and direct groundwater discharge (i.e., Dumanlı spring) into the reservoir create a difference in the volume of inflow from the flow rate at Sinanhoca streamgage.

In order to generate time series for Oymapınar inflow, the streamflow monitoring data from the flow gages within the Oymapınar basin are analyzed to delineate surface flow relationships within the basin.

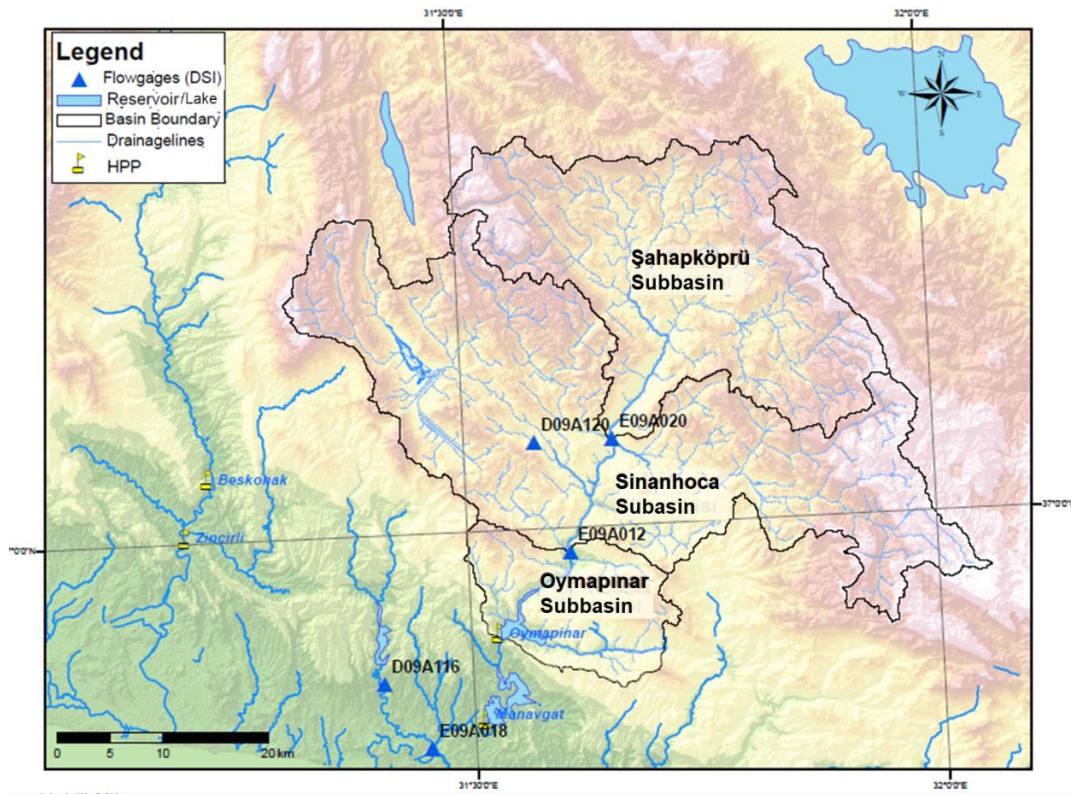


Figure 4.2. Oymapınar basin boundaries and its subbasins

Streamflow observations from Şahapköprü and Sinanhoca streamgages for the period between 1992-2012 are analyzed to determine any relationship with the basin area ratio. Additionally, the adequacy of the drainage area ratio (DAR) method (Emerson et al., 2005; Asquith et al., 2006; Hortness, 2006; Archfield and Vogel, 2010; Zelelew and Alfredsen, 2014; Ergen and Kentel, 2016) for the basin is evaluated for these streamgages. The correlation of observed streamflows and regression analysis between the relevant data series are assessed.

The estimated inflow data for Oymapınar that is provided by DSI is also analyzed. The estimated reservoir inflow data obtained from DSI and used in the analysis are originally generated by DSI based on reservoir water balance and operational data. Hence, reservoir inflow is calculated using the reservoir outflow and potential evaporation from the reservoir surface. The time series for the estimated daily

reservoir inflow provided by DSI covers the period between 2007 and 2017. For the flow analysis, the estimated inflows are compared with the flow rates observed at the Sinanhoca streamgage for 11 years period. Observation of the relevant daily hydrographs reveals that the high and low flow periods in both hydrographs display a similar pattern. Nevertheless, the daily inflow hydrograph also displays spurious fluctuations that can be described as too frequent to be natural. Hence, for the analysis of the relationship of the flow rates, the time series of estimated inflow is required to be smoothed to remove the likely noise. Therefore, the flow rate analysis for Oymapınar inflow is conducted by the use of total monthly flows. Consequently, the regression analysis of flows is done using monthly total volumes. The R^2 value and the regression function obtained from the analysis are found to be satisfactory to be used for the conversion of the Sinanhoca streamgage flow data to reservoir inflows. Hence, the obtained regression function is used for the calculation of the projections of Oymapınar reservoir inflow.

4.2.2 Basin Properties and Development of Basin Model

For the rainfall and runoff modeling in HBV-light and HEC-HMS, firstly a basin model is formed. The basin model includes the basin parameters and their basin-specific values that govern the rainfall-runoff behavior of the basin. Hence, in the first stage of the hydrological modeling basin properties are assessed and data on related parameters are compiled to develop the conceptual basin model. Within that scope, the surface characteristics of the basin are mathematically defined by the use of a digital elevation model of the basin. For the mathematical expression of the basin topography EU-DEM v1.1 (EEA, 2016) (Spatial Resolution: 25 m, upgrade was coordinated by the European Environment Agency (EEA) in the frame of the EU Copernicus Programme) and SRTM DEM (Spatial Resolution: 90 m, produced by Shuttle Radar Topography Mission) are used. The EU-DEM is analyzed by the use of WMS modeling software developed by US Aquaveo. With the analysis drainage lines in the basin are determined, the boundaries of the model basin and its subbasins

are delineated and morphological parameters are calculated. Thereafter, the hypsometric curve of the basin is developed in ArcGIS 10.0 based on the DEM to analyze the elevation range of the basin. Furthermore, the slope map of the basin is generated to obtain information on the surface slopes that have significant control over the runoff – infiltration process in the basin.

Concerning the basin surface properties, characteristics and distribution of soil types (i.e., texture and composition, permeability, drainage property of soil, hydrological properties of soil, etc.), vegetation and land use types (i.e., land cover types, the ratio of impermeable surfaces, etc.) are also studied by the use of international soil and land use databases and maps. Data on soil and drainage properties and the vegetation cover of the basin are gathered from soil maps (Ross et al., 2018) and the CORINE database (EEA, 2020), respectively. The CORINE Land Cover (CLC) (EEA, 2020) inventory was produced with a geometric accuracy of better than 100 m by The National Reference Centres Land Cover (NRC/LC) operating under Eionet (European Environment Information and Observation Network) that is integrated by EEA (European Environment Agency).

The basin model in HBV-light includes a description of the elevation bands within the basin. Each elevation band is assumed to extend within a specified elevation range. Additionally, for each elevation band, relevant vegetation cover types are identified in the model. The maximum number of vegetation zones that can be defined in an elevation band in HBV-light is three. Therefore, according to the basin topography, seven elevation bands each including three vegetation zones are defined to form the basin model in HBV-light. Furthermore, unlike the HEC-HMS model, which simulates the hydrological elements for the entire subbasin or basin area, HBV-light executes the calculations of hydrological elements for a unit basin area. Therefore, parameter values for the physical properties of the basin (i.e., Confined Parameters) are calculated per unit basin area. The values of the Confined Parameters for the model basin calculated for the unit basin area are given in Table 4.2.

Table 4.2 Distribution of elevation bands and relevant vegetation zones in the unit basin area

Elevation range (m ASL)		200-600	600-1000	1000-1300	1300-1700	1700-2000	2000-2400	2400-2700	Total
Approx. mean elevation (m ASL)		400	800	1150	1500.5	1850.5	2200	2550	
Elevation band		1	2	3	4	5	6	7	
Vegetation cover type		Vegetation zones							
Urban area or bare rock surfaces	1	0	5.10 E-05	1.68 E-03	9.70 E-03	0.0607	0.0845	0.0113	0.1680
Soil surfaces with vegetation cover composed of grass or shrubs	2	5.85 E-03	0.0503	0.0813	0.0550	0.0457	7.40 E-03	0	0.2460
Forests	3	7.10 E-03	0.0614	0.2183	0.2506	0.0484	1.60 E-04	0	0.5860
Total		0.0130	0.1120	0.3010	0.3150	0.1550	0.0920	0.0110	1

In HBV-light the basin surface properties defined by the Confined Parameters are assumed to remain constant throughout the modeling period and form the basis of rainfall-runoff simulation. On the other hand, other parameters (i.e., Free Parameters in HBV-light) governing the dynamic hydrological processes in the basin are optimized during the calibration of the hydrological model in HBV-light. The optimization of parameters enables a better representation of the basin to simulate rainfall-runoff processes (Şorman 2005; Şorman et al., 2009, 2020).

HBV-light uses free parameters for the simulation of the hydrological elements in the basin through its Snow, Soil Moisture, Response, and Routing routines. The Snow Routine defines rainfall/snow partition of precipitation, snowmelt runoff, and freezing conditions. The Soil Moisture Routine defines soil moisture storage and groundwater recharge processes. The Response Routine defines percolation, groundwater storage, and recession of discharge. Routing Routine simulates changes

in the surface runoff hydrograph on its flow path. Hence, the Free Parameters enable numerical definition of the hydrological processes in the basin. The estimated values for Free Parameters are initially defined by the modeler depending on the basin properties and further optimized during the calibration process to obtain a better fit of the simulated flow with the observed flow at the outlet of the basin.

The basin model setup uses the aforementioned model routines that contribute to the flow simulation in HBV-light based on the algorithm depicted in Figure 4.3 (Normand et al., 2010).

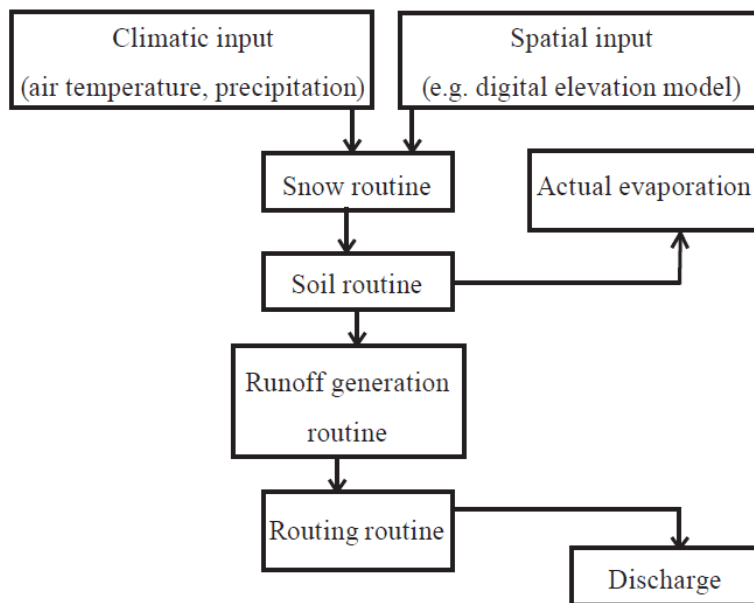


Figure 4.3. HBV-light simulation algorithm (Normand et al., 2010)

Different from the HBV-light model setup, HEC-HMS enables the selection of different physical models to represent the hydrological elements in the basin. This facilitates simulation of the rainfall-runoff relationship in the basin by the use of different deterministic models that fit best to the basin and hydrometeorology properties as well as the hydrological modeling scope and data availability.

For the hydrological modeling of the Oymapınar basin in HEC-HMS the basin model is developed by selecting the physical modeling approaches and relevant parameters for the following components.

1. Physical properties of the basin: Information on the surface area and location of the basin is defined in the basin model. Hydrological elements of the basin, coordinates of the basin outlet are entered in the conceptual model.
2. Vegetation cover (canopy) in the basin: For the simulation of the attenuation and storage due to the canopy, parameters related to the vegetation cover are required to be identified. Based on the data availability and the ease-of-use simple canopy method is selected in the basin model.
3. Surface depression storage features of the basin: The surface physical properties of the basin that affect the surface depression storage and create losses from excess rainfall volume before the formation of run-off are used by the surface method selected in the basin model. The mathematical expression of the surface depression storage in this method calculates the losses due to evaporation and infiltration from the surface depression storage. Based on the data availability and the ease-of-use simple surface method is selected in the basin model.
4. Basin properties controlling loss from precipitation volume and the infiltration/runoff partition of the basin: Hydrological soil properties, geology, land cover, topography (slope), etc., are the basin features that influence the accumulation of the excess rainfall on the surface to form the surface runoff. Various approaches can be used in the HEC-HMS basin model for the simulation of losses from the surface runoff. In addition to the evaporation from the surface, loss due to infiltration followed by interflow and percolation comprise the relevant losses. The remaining volume accumulates on the surface and forms the surface runoff that drains into the stream network in the basin. HEC-HMS enables the use of several different methodologies (i.e., SCS Curve Number method, Grid-based SCS Curve

Number method, Soil Moisture Accounting method, etc.). Several studies in the literature verify the use of the SCS Curve Number (CN) method for event-based modeling, and Soil Moisture Accounting (SMA) and Deficit and Constant (DC) methods for continuous hydrological modeling successfully (Chu and Steinman, 2009; Halwatura and Najim, 2013; De Silva et al., 2014; Gebre, 2015; Azmat et al., 2016; Gumindoga et al., 2017; Erşahin, 2020). DC method uses four parameters that are initially defined for the model development. These are initial deficit, maximum deficit, constant rate (of infiltration), and the ratio of impermeable surfaces in the basin, which are used for the calculation of the infiltration from the surface based on topsoil and unsaturated zone properties. The DC method uses one soil layer assumption to simulate the control of soil moisture on the infiltration from the surface. The use of the DC method with the canopy method in the hydrological model enables volume loss due to evapotranspiration to be included in the simulation. Moreover, the DC approach enables the influence of fluctuations in the soil moisture between storm events and drying of the soil layer during dry periods to be included in hydrological modeling (Scharffenberg, 2015).

On the other hand, the SMA method that can be used as an alternative to the DC method is based on a three-layer model to simulate loss due to infiltration and interflow in soil and unsaturated zone. The method calculates infiltration, storage, percolation, and interflow for Soil, Groundwater1, and Groundwater2 layers. For the simulation of loss with the SMA method numerical values of 14 parameters related to the hydrological properties of these layers, including thickness, permeability, storage capacity, and initial saturation ratio, are required to be defined.

During the development and calibration of the hydrological model, both methods are tried and compared for their efficiency to simulate the study basin. For the model calibration, the DC method is found to produce higher simulation efficiency. Furthermore, the SMA method uses 14 parameters

governing the process, which is considered to increase uncertainty in the model due to parametrization. Hence due to ease-of-use and better simulation efficiency, the DC method is selected for the hydrological modeling of the Oymapınar basin.

5. Basin properties controlling the transformation of excess rainfall to actual or direct runoff: HEC-HMS enables the use of various approaches (i.e., SCS Unit Hydrograph method, Kinematic Wave method, ModClark method, etc.) for the transformation of the surface runoff into the hydrograph of direct flow that joins into the flow in the stream network. SCS Unit Hydrograph method was successfully used in hydrological modeling studies in the literature both for the event and continuous modeling (Azmat et al., 2016, Bhuiyan et al., 2017, Fang et al., 2018; Erşahin, 2020). Additionally, The only parameter required for the SCS Unit Hydrograph method is the lag time parameter, which makes the method to be easier to be used compared to other methods. Hence SCS Unit Hydrograph method is used for the hydrological modeling of the Oymapınar basin.
6. Baseflow component that defines groundwater discharge and runoff recession: Among the baseflow methods that can be used in HEC-HMS modeling (i.e., Bounded Reservoir Baseflow method, Constant Monthly Baseflow method, Linear Reservoir Baseflow method, Nonlinear Boussinesq Baseflow method, and Recession Baseflow method), the Exponential Recession or Recession Baseflow (RB) method is selected for the hydrological modeling of the basin, because it is suitable to be used for the modeling of basins where exponential recession of discharge is seen after a rainfall event (Scharffenberg, 2015). RB method includes natural attenuation and storage of the basin in the simulation of groundwater discharge into the river network and can be successfully used for event and continuous modeling (Feldman, 2000). Furthermore, several studies on the hydrological modeling of karstic basins located in the greater Mediterranean basin

successfully used the RB method (Angelidis et al., 2010; Kotsifakis et al., 2015; Givati et al., 2016).

4.2.3 Hydrometeorological Parameters

Precipitation and temperature time series that control the surface flow formation in a basin are required for the simulation of the hydrological processes and streamflow. Additionally, observed streamflow time series are used for the model calibration. For the hydrological modeling, hydrometeorological monitoring data with daily timesteps are used in the study. These hydrometeorological time series are commonly used for rainfall-runoff modeling both in HEC-HMS and HBV-light. The same daily historical time series for temperature, precipitation, and flow rate are used for the model development both in HEC-HMS and HBV-light.

Meteorologic Model in HEC-HMS

Unlike the HBV-light model which basically relies on the time series of the aforementioned hydrometeorological parameters for rainfall-runoff simulation hydrological model development in HEC-HMS necessitates the development of a meteorological model along with the basin model as a main component of the hydrological model. The meteorological model defines the limits and significant parameters for the hydrometeorological conditions specific to the basin (or subbasins). The meteorological model in HEC-HMS comprises parameters on precipitation, temperature, sun duration, and evaporation (Yener et al., 2007; Mesta et al., 2021). Similar to the basin model, HEC-HMS enables the use of various approaches in the meteorological model for the calculation of precipitation, rainfall/snow partition, snow melting, evaporation, and solar irradiance or sun duration in hydrological simulation. The values for the parameters regarding the components of the meteorological model depending on the selected simulation approaches are identified for the development of the meteorological model in HEC-

HMS. The methods selected for the meteorological model in HEC-HMS and the hydrometeorological data used for the simulation of flow are described below.

1. Historical flow data: After the quality check and analysis, the operational data of the Oymapınar reservoir and HEPP and the estimated daily reservoir inflow time series provided by DSI are found to be inadequate to be used for hydrological model development and calibration. The total drainage area of the Sinanhoca streamgage, which provides long-term historical streamflow time series for Manavgat River mainstream, composes a major portion (89%) of the Oymapınar basin. Furthermore, the analysis of the historical streamflow data verifies a linear relationship between the flow and area of the subbasins, particularly for upstream of the Manavgat River. Also, analysis of the monitoring data and the location of the streamgages in the basin indicates that the Sinanhoca streamgage operated by DSI is the most representative streamgage for the modeling of the Oymapınar basin. Therefore, the historical daily streamflow monitoring data from the Sinanhoca streamgage are used for hydrological model development, calibration, and validation.
2. Historical precipitation data: Thiessen polygon method is used to obtain areal precipitation values from the meteorological stations located in and around the HMSA. Thiessen Polygon method indicates that among the three MSs (Manavgat MS: 17954, Akseki MS: 8229/18047, and Seydişehir MS: 17898) that provide meteorological time series of sufficient length Akseki represents 86% of the hydrological model basin. The area ratios of the MSs calculated by the Thiessen Polygon method are shown in Table 4.3. Furthermore, evaluation of the duration of continuous time series provided by the MSs indicates Akseki MS provides the longest continuous time series of historical meteorology data overlapping the period of streamflow monitoring at Sinanhoca streamgage compared to other MSs in the region. Consequently, Akseki MS (MS ID: 8229/18047) operated by TSMS within the Oymapınar basin is found to be the most suitable and representative for hydrological

modeling. Hence, historical daily precipitation data observed at Akseki MS is used for hydrological model development.

Table 4.3 Application of Thiessen Polygon method for the model basin in WMS software

Thiessen Polygon Map	Area Ratios of Thiessen Polygons		
	km ²	% Ratio	
	Akseki MS	1440	86
	Manavgat MS	186	11
	Seydişehir MS	56	3
	Total basin	1682	100

- Historical temperature, evaporation, sun duration, and other meteorological data: Observed daily temperature data from Akseki MS are used in hydrological modeling. The Manavgat MS (MS ID: 17954) is identified to be the closest MS to the HMSA that has historical sun duration monitoring. However, historical daily sun duration records from Manavgat MS are limited to the period between September 1984 and January 2012. Therefore, daily sun duration hours for the simulation period are obtained from long-term daily sun duration mean values calculated from 27 years of time series from Manavgat MS.

For evaporation rather than the observational data, evaporation calculated by HEC-HMS is used. The meteorological model in HEC-HMS enables the selection of the Priestley Taylor method for the calculation of evaporation. Priestley Taylor method uses sun duration data in the energy balance approach for the calculation of soil moisture and evapotranspiration. Hence, daily temperature time series from Akseki MS and sun duration time series from Manavgat MS are used in the model for the simulation of evapotranspiration based on the Priestley Taylor method. The use of the Priestley Taylor method for hydrological modeling of the study area is tested through a comparison with the use of the alternative Monthly Average method in HEC-HMS, in which the long-term monthly mean pan evaporation data is used. Similar simulation efficiencies are obtained from both evapotranspiration methods. Therefore, considering the objective of the study, to obtain projections on future streamflow, the Priestley Taylor method is selected for the meteorological model.

4. Snow/rainfall partitioning and snowmelt processes are simulated by HEC-HMS using the Temperature Index approach based on the properties of the elevation zones defined for the basin. The Temperature Index method is suitable to be used for modeling basins with coniferous forest vegetation cover (Melloh, 1999). The study basin also includes a similar type of vegetation cover as the dominant land cover. Temperature is found to be the most important control over the snowmelt that contributes to surface flow in a basin. Furthermore, the use of temperature, which is easily monitored and commonly available as long-term time series of historical data. Therefore, the Temperature Index method that relies on the temperature data as the main parameter in the calculation has the advantage over alternative methods that are based on parameters that are relatively difficult to monitor (Anderson, 2006). Additionally, the variation of temperature with respect to the elevation (i.e., the use of lapse rate) is also easily applied and therefore, can be practically used in the simulation of snow using the Temperature Index

method (Anderson, 2006). Moreover, temperature parameter is known to be generally simulated with high efficiency by climate models which brings another advantage of the use of the Temperature Index method in hydrological modeling for future projections. The Temperature Index method uses elevation, temperature, and precipitation data to calculate rainfall/snow partitioning, rainfall excess/ snowmelt contribution to runoff to include the orographic influence on basin hydrology. The elevation zones in the HEC-HMS model are defined in compliance with the elevation bands used in the HBV-light model (Table 4.4).

Table 4.4 Elevation bands in model basin

Elevation band	Approximate mean elevation (mASL)	Altitude range (mASL)	Surface area ratio in the basin (%)
1	400	200-600	1.29
2	800	600-1000	11.21
3	1150	1000-1300	30.07
4	1500	1300-1700	31.52
5	1850	1700-2000	15.50
6	2200	2000-2400	9.26
7	2550	2400-2741	1.16

HEC-HMS uses the identified elevation zones in the basin to simulate the influence of elevation on temperature and precipitation (Scharffenberg, 2015). The elevation-precipitation relationship specific to the Oymapınar basin used in the HEC-HMS model is obtained from the Hydrogeological Survey Report of Manavgat-İbradı-Cevizli Aquifer (Koray Üstebay et al., 2018). The survey report provides an analysis of the elevation – precipitation relationship (Figure 4.4) based on the data from 13 MSs located in the region (Koray Üstebay et al., 2018). A summary of the methods used in the HEC-HMS hydrological model in the study is given in Table 4.5.

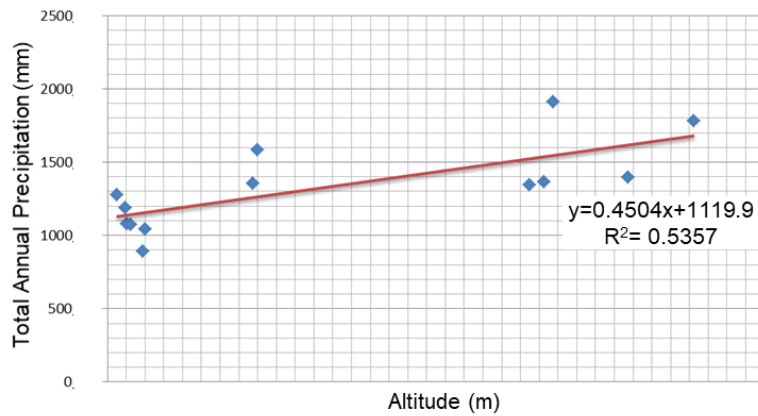


Figure 4.4. Elevation- precipitation relationship in the basin (Koray Üstebay et al., 2018)

Table 4.5 Components of the basin and meteorological models in the HEC-HMS hydrological model

Basin Model		Meteorologic Model	
Model Component	Selected Approach	Model Component	Selected Approach
Canopy Method	Simple canopy method	Precipitation	Specified Hyetograph method
Surface Method (Surface depression storage)	Simple surface method	Evapotranspiration	Priestley Taylor method
Loss Method (Loss from precipitation and runoff volume)	Deficit and Constant Loss method	Snowmelt	Temperature Index method
Transform Method (Transformation of runoff to direct flow)	SCS Unit Hydrograph method		
Baseflow Method (Groundwater discharge)	Recession Method		

Hydrometeorological Parameters in HBV-light

As described above, hydrometeorological time series for temperature, precipitation, and flow rate are used for the model development in the HBV-light. HBV-light uses a PTQ-file (Precipitation-Temperature-Flow rate file) as the input of the rainfall-runoff model (Seibert, 2005). The file includes precipitation, temperature, and discharge time series. For the HBV-light model, the same daily historical time series as the HEC-HMS model are used. These include historical daily flow rate data from Sinanhoca streamgage, precipitation, and temperature data from Akseki MS.

Additionally, in the HBV-light model, evaporation data is optionally used for simulation in addition to the precipitation and temperature. HBV-light calculates daily evaporation values by the use of the long-term mean evaporation and long-term mean temperature data in combination with the daily temperature time series (Seibert, 2005). The long-term mean monthly evaporation and long-term mean monthly temperature from the historical data of Manavgat MS are used in the model for the adjustment of the daily evaporation in the basin. Manavgat MS data are selected to be used for long-term mean monthly evaporation and temperature time series due to the data availability.

The simulation of the snow is governed by the snow routine in HBV-light by the use of precipitation and temperature time series in the PTQ file. HBV-light makes use of the degree-day method to calculate the snow-melt and snowpack, as well as to decide whether the precipitation falls as snow or rain (Seibert, 2005). Relevant calculations are executed for each elevation zone of the basin defined in HBV-light with a temperature correction factor for elevation assumed to be -0.6°C per 100 m (Seibert, 2005).

4.2.4 Calibration and Validation of Hydrologic Models

Hydrological models developed in HBV-light and HEC-HMS are calibrated for the optimization of the parameter values to increase the simulation efficiency of the models. Following the calibration, hydrological models are validated to verify the simulation efficiencies. The calibration and validation periods in the hydrological model are identified according to the timeframes for which continuous hydrometeorological time series of monitoring data are available. As a result, the period between the 2013-2016 water years, and 2017 water year are selected for calibration and validation, respectively. HBV-light and HEC-HMS models are initially calibrated and then validated for the aforementioned periods by the use of relevant historical observation data. For both conditions, the hydrological simulation is run for daily time steps to generate the daily mean flow rate at Sinanhoca streamgage.

One of the most explicit differences in hydrological modeling between HBV-light and HEC-HMS is the distinct optimization and calibration approaches used in the software. HBV-light uses a stochastic optimization tool based on the Genetic Algorithm (GA) approach, whereas the HEC-HMS calibration tool is based on a deterministic approach.

HBV-light Genetic Algorithm and Powel (GAP) optimization tool works for the minimization of the difference between observed and modeled hydrographs by searching for the global optimum solution for the objective function defined through the model setup. GA approach, used in the GAP tool, mimics the natural genetic evolutionary process to achieve the optimum value of the potential solution represented with the objective function. The optimization process in GA evaluates the performance efficiency (calculated using statistical performance indicators) of the parameter sets (i.e., individuals or chromosomes in GA) with respect to their convergence with the observed and continuous iterative optimization process until the best fit is obtained or the pre-set iteration number is reached. Pairs from parameter sets that show higher performance with respect to the SPIs are randomly

selected for the formation of the next generation of parameter sets (i.e., individuals) through crossing-over. At each generation, individuals are evaluated for their fitness (i.e., convergence to the observed solution). In an iterative process that moves towards the determination of an optimum parameter set the best possible solution for objective function is achieved (Whitley, 1994; Seibert, 2000).

In the study, for optimization in the GAP tool of HBV-light, the GA parameters are initially optimized through a trial-error process in order to avoid overfitting that diminishes the simulation efficiency but to allow sufficient iterations for the optimization of the parameters. After identifying the GA parameters in the HBV-light model, GAP optimization is used for the calibration of the hydrologic model. Due to the stochastic nature of GAP optimization to manage the uncertainties combined with the solution, calibration is recommended to be executed multiple times (Vis et al., 2015). Therefore, hydrological model calibration in the GAP optimization tool is repeated 100 times to include the uncertainties in the analysis.

Hydrological model calibration in HEC-HMS is conducted by the use of the automated calibration tool of HEC-HMS in combination with manual calibration. The automated calibration tool in HEC-HMS (ver.4.1) enables the use of two deterministic optimization approaches, Nelder Mead and Univariate Gradient methods. Nelder Mead method is generally used for the solution of linear optimization problems, whereas Univariate Gradient optimization works on the solution with one parameter/variant optimized at once, and the optimum value of each parameter is determined separately for the local optimum solution. Due to the different advantages and disadvantages of these methods both are used in the calibration in an alternating way to obtain the best fit for the flow simulation. The automated calibration tool in HEC-HMS is run to achieve the best fit of hydrographs in terms of statistical performance indicator parameters detailed in the following subsection. Manual calibration is done in addition to the automated calibration to obtain the most representative model hydrograph for the basin concerning the hydrological components of the hydrograph (i.e., the volume of runoff, loss, or attenuation due to canopy, base flow, etc.) and basin drainage characteristics.

4.2.5 Statistical Performance Indicators (SPIs) Used in Hydrological Modeling Performance Evaluation

The parameter optimization during calibration of the model and verification of the model efficiency during the validation is done based on the comparison of the modeled streamflow (Q_t^{model}) with the observed streamflow (Q_t^{observed}) by the use of statistical performance indicator parameters. SPIs used in calibration and validation in this study are Nash–Sutcliffe efficiency coefficient (NSE) (Equation 1), Coefficient of determination (R^2) (Equation 3), Root Mean Square Error ($RMSE$) (Equation 4), Volume Error (VE) (Equation 5) and Klingt-Gupta efficiency coefficient (KGE) (Equation 6).

$$NSE = 1 - \frac{\sum_{t=1}^{n_t} (Q_t^{\text{model}} - Q_t^{\text{observed}})^2}{\sum_{t=1}^{n_t} (Q_t^{\text{observed}} - \bar{Q}^{\text{observed}})^2} \quad (1)$$

$$r = \frac{\sum_{t=1}^{n_t} [(Q_t^{\text{observed}} - \bar{Q}^{\text{observed}}) \times (Q_t^{\text{model}} - \bar{Q}^{\text{model}})]}{\sqrt{\sum_{t=1}^{n_t} (Q_t^{\text{observed}} - \bar{Q}^{\text{observed}})^2 \times \sum_{t=1}^{n_t} (Q_t^{\text{model}} - \bar{Q}^{\text{model}})^2}} \quad (2)$$

$$R^2 = r^2 \quad (3)$$

$$RMSE = \sqrt{\frac{1}{n_t} \sum_{t=1}^{n_t} (Q_t^{\text{observed}} - Q_t^{\text{model}})^2} \quad (4)$$

$$VE = 1 - \frac{|\sum_{t=1}^{n_t} (Q_t^{\text{observed}} - Q_t^{\text{model}})|}{\sum_{t=1}^{n_t} (Q_t^{\text{observed}})} \quad (5)$$

$$KGE = 1 - \sqrt{(r - 1)^2 + (\alpha - 1)^2 + (\beta - 1)^2} \quad (6)$$

$$\alpha = \frac{\sigma^{\text{model}}}{\sigma^{\text{observed}}} \quad \text{or} \quad \alpha = \frac{\text{var}^{\text{model}}}{\text{var}^{\text{observed}}} \quad (7)$$

$$\beta = \frac{\bar{Q}^{model}}{\bar{Q}^{observed}} \quad (8)$$

where, n_t is the total number of observations, Q_t^{model} and $Q_t^{observed}$ are the modeled and observed flow rates, respectively, at the time of t , and \bar{Q}^{model} and $\bar{Q}^{observed}$, are the mean of modeled and observed flow rates, respectively. Additionally, $\sigma^{observed}$, σ^{model} , and $var^{observed}$, var^{model} are standard deviation and variance of observed and modeled data sets, respectively.

NSE (Equation 1) ranges between $[-\infty, 1]$ with $NSE=1$ indicating perfect fit of the model with the observed and $NSE=0$ indicating the model performance equal to the performance of the use of the mean of observed data (Moriasi et al., 2007).

Pearson's correlation coefficient, r (or Corr) (Equation 2) and *Coefficient of determination, R^2* (Equation 3), are indicators of the linear relationship between model and observed data series. The r value ranges between $[-1, 1]$ and R^2 ranges between $[0, 1]$. An r value of zero means that there is no linear relationship, whereas $r = \pm 1$ means perfect positive or negative linear relationship (Gupta et al., 1999; Moriasi et al., 2007).

RMSE (Equation 4) is an error-based indicator, the unit, and value of which changes depending on the type of data that is being evaluated. The lower value of *RMSE* indicates the better model performance showing better convergence of the modeled to the observed. Hence, the optimal value is 0 indicating no residual error or difference between observed and modeled data. Therefore, *RMSE* ranges between $[0, \infty]$ (Moriasi et al., 2007). Because the unit and the size of *RMSE* depends on the analyzed data there are no threshold values identified for *RMSE* to indicate model performance. Nevertheless, Singh et al. (2005) classifies *RMSE* less than the standard deviation of the data set as an indication of low model error. According to Moriasi et al. (2007), *RMSE* less than 70% of the standard deviation indicates that the model has satisfactory efficiency.

VE (Equation 5) is a bias-based indicator similar to Percent Bias ($PBIAS$) and Relative Volume Error (RVE) and indicates the ratio of the cumulative error to the total observed volume. $VE=1$ is the optimal value indicating that the value of cumulative error is 0. HBV-light enables the selection of VE as the SPI to be used in the optimization tool. In this study, VE is preferred over $PBIAS$ and RVE because, similar to other SPIs used in this study, VE convergence to 1 means improvement in the modeling efficiency. There are no threshold values for VE identified in the literature for the classification of modeling performance. Therefore, threshold values for classification based on VE are calculated using the threshold values defined for $PBIAS$ by Moriasi et al. (2015).

KGE (Equation 6) combines different efficiency indicators. These are Pearson's correlation coefficient r (Equation 2), the ratio of the variability α (Equation 7) calculated by the use of standard deviation or variance of modeled and observed data sets, and bias indicator β (Equation 8) calculated as the ratio of the means of observed and modeled data sets. The optimal value of three components at the perfect fit of modeled and observed data is 1. Hence, the optimal value for KGE is also 1 and similar to NSE it ranges between $[-\infty, 1]$ (Gupta et al., 2009). KGE is preferred in some studies in order to overcome some limitations of NSE (Knoben et al., 2019). In the evaluation of model performance, convergence of KGE and its r, α, β to 1 is used as the indicator of improved model efficiency. There are still no standard threshold values identified in the literature for the classification of efficiency based on KGE , and various threshold values are used for the evaluation of model performance. Nevertheless, as a general practice, negative values of KGE indicate unsatisfactory model performance (Knoben et al., 2019). Additionally, in their studies, Rogelis et al. (2016) and Thiemig et al. (2015) used 0.5 as the threshold value for modified KGE (Gupta, 2009) and accepted model efficiency as unsatisfactory for KGE value less than 0.5.

The threshold values for the SPIs used in this study for the classification of simulation efficiency of the hydrological model are given in Table 4.6.

Table 4.6 Threshold values for SPIs used in this study

SPI ⁷	Performance class			
	Very good	Good	Satisfactory	Not satisfactory
R^2	$R^2 > 0.85$	$0.75 < R^2 \leq 0.85$	$0.60 < R^2 \leq 0.75$	$R^2 \leq 0.60$
NSE	$NSE > 0.8$	$0.7 < NSE \leq 0.8$	$0.5 < NSE \leq 0.7$	$NSE \leq 0.5$
VE	$VE > 0.95$	$0.9 < VE \leq 0.95$	$0.85 < VE \leq 0.9$	$VE \leq 0.85$
$\frac{RMSE}{\sigma_{observed}}$	$0.00 \leq RMSE/\sigma \leq 0.50$	$0.50 < RMSE/\sigma \leq 0.60$	$0.60 < RMSE/\sigma \leq 0.70$	$RMSE/\sigma > 0.70$
	Good	Intermediate	Poor	Very poor
KGE	$KGE \geq 0.75$	$0.75 > KGE \geq 0.5$	$0.5 > KGE > 0.0$	$KGE \leq 0.0$

4.3 Streamflow Impact Assessment Methodology

Comparison of hydrological models calibrated in HEC-HMS and HBV-light to simulate the model basin in this study (See Section 5.2.4 for details) shows slightly better simulation efficiency for the HEC-HMS model of the basin. Additionally, HEC-HMS is evaluated to produce a better physical and hydrometeorological description of the basin hydrology. As a result, the hydrological HEC-HMS model of the study basin that is verified to have good simulation skills is selected to be used for streamflow impact assessment in the Oymapınar basin. For the assessment of the climate change impact on Manavgat River streamflow and Oymapınar reservoir inflow, precipitation, and temperature projections of climate models are used. In that context, the potential future changes in streamflow and Oymapınar reservoir inflow

⁷ R^2 , NSE threshold values are based on Moriasi et al. (2015), KGE threshold values are based on (Thiemig et al. (2014) and Rogelis (2016), threshold values for $RMSE$ /standard deviation of observed data set ratio (i.e., RSR) are based on Moriasi et al. (2007), VE threshold values are adapted from the threshold values defined for $PBIAS$ by Moriasi et al. (2015) (Very good: $PBIAS < \pm 5\%$, Good: $5\% \leq PBIAS < \pm 10\%$, Satisfactory: $\pm 10\% \leq PBIAS < \pm 15\%$).

compared to the present condition (1971-2005) are assessed for the short- (2020-2030), medium- (2031-2050), and long-term (2051-2099) future. For the assessment of the impact on streamflow, three approaches are used in the analysis:

- The hydrological model is run by the use of simulation outputs of 12 CORDEX RCMs for the historical period between 1971-2005 and the future period until 2099 to generate 12 streamflow simulations. From hereafter, these are referred to as streamflow simulations from individual climate model runs or daily streamflow series Q1 to Q12.
- The hydrological model is run with two ensemble precipitation and temperature projection series obtained using ensembling methods (Superensemble and Simple Mean Ensemble) to generate two streamflow time series for the historical period between 1971-2005 and the future period until 2099 each. From hereafter, these are referred to as streamflow simulations from ensemble model runs or daily streamflow series Q13 and Q14.
- Ensembled streamflow time series are generated using 12 streamflow simulations from individual climate model runs in the hydrological model. Ensembling methods are applied to streamflow series Q1 to Q12 to generate ensembled streamflow simulations. In this approach, two ensembled streamflow time series are formed by the use of Superensemble and Simple Mean Ensemble methods. For that purpose, ensembling is applied to 12 monthly streamflow time series and monthly ensembled streamflow time series are obtained. From hereafter, these are referred to as monthly ensembled streamflow projection series Q15 and Q16.

The analysis methodologies followed for the assessment are described in the below subsections.

4.3.1 Use of Individual RCM Outputs for Streamflow Simulations (Q1-Q12)

Historical and future simulation outputs for daily temperature and precipitation time series obtained from 12 CORDEX RCMs for the modeling grid closest to the Akseki MS are used to run the calibrated hydrological model of the basin. Model runs with daily time-steps for durations from 1971 to 2005 to represent the historic streamflow conditions and from 2006 to 2099 to represent future streamflow projections based on RCP4.5 and RCP8.5 climate change scenario conditions are used to obtain daily streamflow time series at the Sinanhoca streamgage (i.e., streamflow projections from individual climate model runs Q1 to Q12), at the outlet of the modeling basin. The streamflow simulation outputs from individual climate model use are initially validated through a comparison with observed streamflow at the Sinanhoca streamgage. Thereafter, similar to the Climate Analysis for the CASA, the potential impact is assessed through the analysis of percent change in the streamflow for:

1. Short-term future between 2020-2030 for RCP4.5 and RCP8.5 scenarios,
2. Medium-term future between 2031-2050 for RCP4.5 and RCP8.5 scenarios,
and
3. Long-term future between 2051-2100 for RCP4.5 and RCP8.5 scenarios.

Furthermore, using the regression model of Sinahoca streamgage and Oymapınar inflow, the monthly inflow time series for the Oymapınar reservoir is calculated. The calculated inflows are used for the impact assessment as potential percent change projected for the future periods described above. Finally, the annual total flow series for historic and future terms are analyzed through the unequal variances t-test (or Welch's two-sample t-test) with the threshold of the confidence level of 95% to identify the significance of the change in streamflow in the future.

4.3.2 Use of Ensembled Temperature and Precipitation for Streamflow Simulations (Q13, Q14)

For this approach, historical and future simulation outputs for daily temperature and precipitation time series obtained from 12 CORDEX RCMs for the modeling grid closest to the Akseki MS are used to produce ensemble outputs for temperature and precipitation. The ensembling approaches for MME aim to reduce the uncertainty and bias in projections by forming a composition of the outputs of climate models in the ensemble using various methodologies (e.g., simple averaging, weighted averaging, regression, ANN, etc.). In this study, two ensembling methodologies are applied to obtain ensemble outputs. These are Superensemble (SE) and Simple Mean Ensemble (SME). The methodologies used in these approaches are described below.

Ensemble outputs from the SME method are calculated using Equation (9) (Cane and Milelli, 2010). SME approach gives equal weights to all ensemble member climate models and uses the anomalies simulated by the models to calculate ensemble output as the average of models.

$$SME_{i,t}^M = \bar{O}_i + \frac{1}{M} \sum_{j=1}^M (RCM_{i,t}^j - \overline{RCM_t^j}), \forall i, \forall t \quad (9)$$

where, $SME_{i,t}^M$ is the SME ensemble generated using all RCMs (i.e., 12 RCM outputs are used in this study, see Table 4.7) at grid i for day t , $j = 1, 2, \dots, M$, is the number of ensemble member climate models; thus $M = 12$ in this study, $i = 1, 2, \dots, N$, is the number of model grids used in the analysis. Here, only the modeling grid closest to the Akseki MS is used for hydrological model input generation, therefore $i = 1$. $t = 1, 2, \dots, T$, is the number of data points (i.e., specific day of the projection) in the data series in ensemble calculation. $RCM_{i,t}^j$ is the j^{th} RCM prediction at grid i for

day t . \overline{O}_i is the mean observation or observed climatology value at grid i (Equation 10), and \overline{RCM}_i^j is the climatology determined by $RCM j$ (Equation 11).

$$\overline{O}_i = \frac{1}{T} \sum_{t=1}^T O_{i,t}, \forall i \quad (10)$$

where, $O_{i,t}$ is the observed precipitation at grid i at day t .

$$\overline{RCM}_i^j = \frac{1}{T} \sum_{t=1}^T RCM_{i,t}^j, \forall i, \forall j \quad (11)$$

SE approach is based on the Multiple Linear Regression (MLR) method. In this approach that is suggested by Krishnamurti et al. (1999, 2000) Equation 12 is used to calculate ensemble outputs:

$$SE_{i,t}^M = \overline{O}_i + \sum_{j=1}^M a_j (RCM_{i,t}^j - \overline{RCM}_i^j), \forall i, \forall t \quad (12)$$

where, $SE_{i,t}^M$ is the SE generated using RCMs in the ensemble set at grid i for day t , a_j is the weight of $RCM j$ optimized for the training period to minimize the difference between observed and modeled precipitation at grid i based on the conventional multiple linear regression.

The weights assigned to the ensemble member climate models are determined by the use of the Least Square Method (LSM). The optimum for the objective function is the possible minimal solution of G_i (Equation 13) that means the highest convergence of

SE ($SE_{i,t}^M$) with observed value ($O_{i,t}$). The optimum a_j values that minimize G_i (i.e., total error) are identified for a training period or data set.

$$G_i = \sum_{t=1}^T (SE_{i,t}^M - O_{i,t})^2, \forall i \quad (13)$$

As described above, the SME approach uses equal weights for all 12 ensemble members (See Table 4.7) and does not require any training data set, whereas the weights in the SE approach are identified by calibration (or training) based on the training period or (data set). After the calibration, the efficiency of the SE is verified by benchmarking with the observed data based on SPIs (*Corr*, *RMSE*, *PBIAS*). For the training of SE historical simulation outputs of climate models (1971-2005) are used. The calculated weights determined during training are used to generate time series of future periods.

Table 4.7 The list of CORDEX RCMs used for the generation of ensembled time series

GCM	RCM	Model No
CNRM-CM5	CCLM4-8-17	M1
CNRM-CM5	ALADIN53	M2
CNRM-CM5	RCA4	M3
EC-EARTH	CCLM4-8-17	M4
EC-EARTH	RACMO22E	M5
EC-EARTH	HIRHAM5	M6
EC-EARTH	RCA4	M7
CM5A-MR	WRF331F	M8
CM5A-MR	RCA4	M9
HadGEM2-ES	CCLM4-8-17	M10
HadGEM2-ES	RACMO22E	M11
HadGEM2-ES	RCA4	M12

In the study, simulated temperature and precipitation time series for the Akseki MS are used to obtain SME and SE outputs. The efficiencies of SME and SE outputs are compared with that of the individual ensemble members. After testing the efficiency of ensemble outputs, the daily time series for future periods under RCP4.5 and RCP8.5 scenarios are generated by the use of weights determined. Finally, the ensembled temperature and precipitation time series are used as the input of the calibrated hydrological model in HEC-HMS to generate streamflow simulations for historical and future periods. The result (streamflow simulations from ensemble model runs Q13 and Q14) is evaluated through a benchmark with historical streamflow observations together with the streamflow simulations from individual model runs (Q1 to Q12). The analysis results indicated that although for climate parameters (temperature, and precipitation) ensemble outputs provide advantages in simulation skills, the use of the daily ensembled data in streamflow simulations displayed unsatisfactory performance (See Section 5.3.2 for details). Hence, the outputs from this approach are eliminated from the streamflow projections used in impact assessment.

4.3.3 Use of Streamflow Simulations of Individual RCMs in Ensemble Streamflow Generation (Q15, Q16)

For this approach, the streamflow series (Q1-Q12) of the individual climate model runs in the hydrological model for the period 1971 - 2005 are used. Twelve daily time series for simulated streamflow for the historical period are initially converted to monthly time series and then used to generate monthly ensemble streamflow at Sinanhoca streamgauge. For the ensembling of streamflow simulations, SE and SME methods described in the preceding subsection are used. The efficiencies of monthly ensemble streamflows (Q15 and Q16) are compared with the efficiencies of streamflow simulations with individual climate model runs (Q1-Q12). After testing the efficiency of ensemble outputs, the monthly streamflow projections are generated for future periods under RCP4.5 and RCP8.5 scenarios. The analysis results

demonstrated that both SE and SME methods produce satisfactory results and even certain advantages over the results from individual climate model runs in the hydrological model (See Section 5.3.3 for details). Therefore, monthly ensemble streamflow projections for Sinanhoca streamgage (Q15, Q16) are used in the impact assessment study together with the streamflow projections from individual climate model runs (Q1 to Q12).

CHAPTER 5

RESULTS AND DISCUSSION

This chapter presents the results of the study. As detailed in Chapter 4, the study comprises three main components, Climate Analysis, Hydrological Modeling, and Streamflow Impact Assessment. This chapter elaborates on the results of each component in different sections. Section 5.1 covers the results of the Climate Analysis which includes the subsections on the analysis of observed climatology in the CASA (Section 5.1.1), analysis of the simulation performances of climate models (Section 5.1.2), and assessment of potential impacts of climate change on temperature and precipitation in the CASA and at Akseki MS (Section 5.1.3). In Section 5.2, the hydrological model development processes in HEC-HMS and HBV-light, and the simulation efficiency of the models are discussed in detail in relevant subsections. Finally, Section 5.3 presents the details of the Streamflow Impact Assessment component of the study for Manavgat River and Oymapınar reservoir inflow. The subsections of Section 5.3 discuss the results from different approaches used in this study for future streamflow projections for the Oymapınar basin (Section 5.3.1 to 5.3.3) and conclude with potential ranges of change in the streamflow and reservoir inflow considering future RCP4.5 and 8.5 radiative forcing scenarios for short-, medium- and long-term future (Section 5.3.4).

5.1 Climate Analysis

The Climate Analysis, Component 1 of this study includes an analysis of observed and simulated daily time series of precipitation and temperature for historic (1966-2005) and future (short-term: 2006-2020, medium-term: 2021-2050, long-term: 2051-2199). The study is undertaken for the MSs in the CASA. A summary of the results of the analysis within the scope of Component 1 is given in the below

sections. The details and findings of the study are presented in four articles attached (from hereinafter will be referred to as Paper 1 to 4). The list of the papers presented in the Appendices of this thesis is as follows:

1. Mesta, B., & Kentel, E. (2022). Superensembles of raw and bias-adjusted regional climate models for Mediterranean region, Turkey. *International Journal of Climatology*. 42(4), 2566-2585.

(See Appendix A)

2. Mesta, B., Sasaki, H., Nakaegawa, T., & Kentel, E. (2022). Changes in precipitation climatology for the Eastern Mediterranean using CORDEX RCMs, NHRCM and MRI-AGCM. *Atmospheric Research*, Volume 272, 2022, 106140.

(See Appendix B)

3. Mesta, B., Sasaki, H., Nakaegawa, T., & Kentel, E. (submitted). Effect of Climate Change on Surface Air Temperature at Eastern Mediterranean, Turkey.

In review.

(See Appendix C)

4. Mesta, B., Akgun, O.B., Kentel, E. (submitted). Improving precipitation estimates for Turkey with multi-model ensemble: A comparison of nonlinear artificial neural network method with linear methods.

In review.

(See Appendix D)

5.1.1 Analysis of Temperature and Precipitation Climatology

The climatologic properties of the CASA are assessed through the analysis of daily mean temperature and daily total precipitation observations for the period from 1966 to 2005 at 59 MSs. Accordingly, throughout the CASA (at 59 MSs) the climatological annual mean temperature range between 10°C and 20°C for the period between 1966 and 2005. The climatological annual mean temperature in coastal areas is 18°C or higher, whereas at the inland stations the mean annual temperature drops down to 10°C at some parts of the CASA (See Figure 5.1). The coastal stations are observed to have higher mean temperatures for all seasons compared to inland stations in CASA. For the MSs in the CASA coldest mean temperature for the winter season is recorded at Hadim MS (MS: 17928, at 1500mASL) in the Eastern Mediterranean Basin and Kulu MS (MS: 17754, at 1000mASL) in the Central Anatolia region. At these stations, the long-term mean for winter temperature is slightly less than 0°C (Figure 5.1). For the summer season, Mut MS (MS: 17956) in the eastern Mediterranean Basin is recorded to have the highest long-term mean seasonal temperature (28°C). The long-term mean temperature difference between the winter and summer seasons is between 14°C and 21°C across the CASA.

Analysis of the long-term precipitation data for the same observation period indicates the highest precipitation seasonality for coastal MSs, for which the annual precipitation is mostly received as rain during the winter season (Figure 5.1). During the summer season, the mean precipitation may even drop to zero at the coastal MSs. However, the coastal stations still receive annual mean precipitation over 2 mm/day which is higher than the mean annual precipitation at the inland stations. The MSs in Central Anatolia, particularly in Konya Closed Basin, have the lowest annual mean precipitation (less than 1mm/day) (Figure 5.1). The wet seasons for this region are winter and spring.

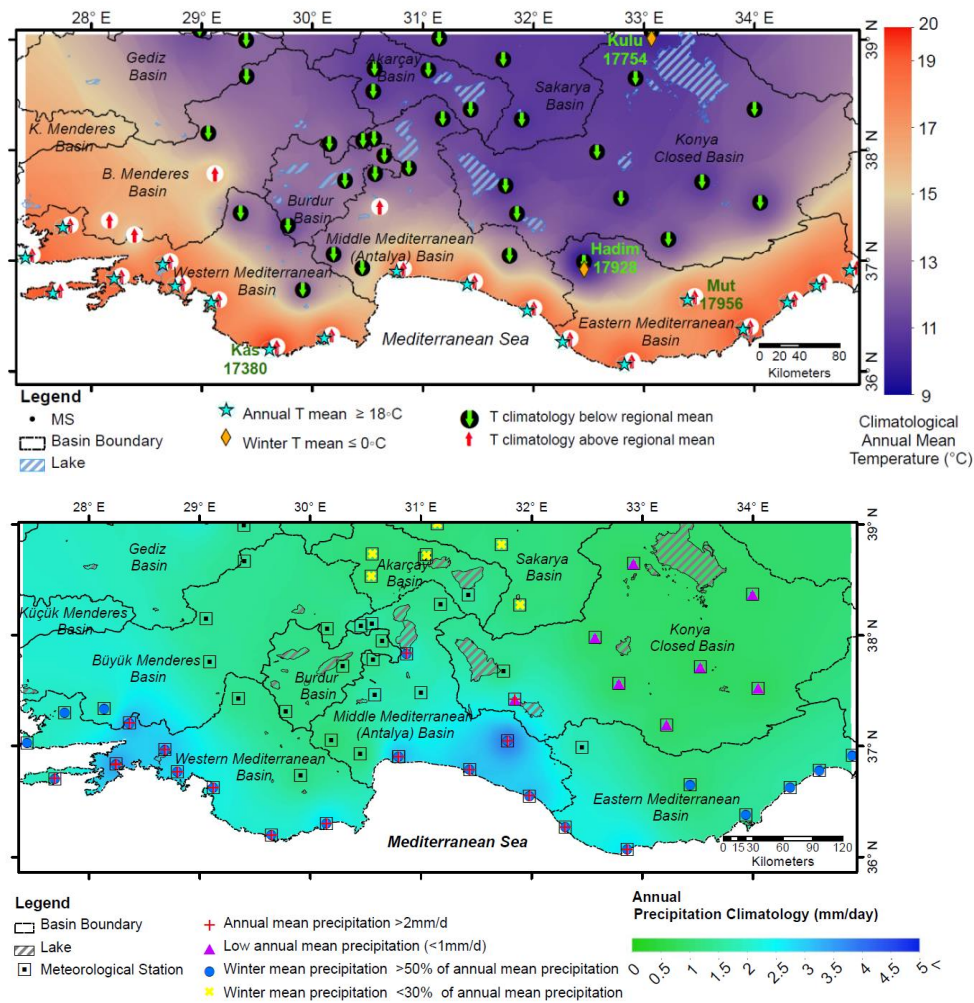


Figure 5.1. Annual mean temperature (upper panel) and precipitation (lower panel) climatology (for 1966-2005 period) maps of the CASA

The spatial variability of temperature and precipitation climatology in the CASA is illustrated in Figure 5.2. The maps in Figure 5.2 show the deviation of the annual means for each meteorological station from the areal mean of the CASA (i.e., the arithmetic average of 59 MSs) for the period between 1966 and 2005.

The maps are formed by the use of the IDW method for the interpolation of $\Delta \bar{T}_i$ values to convert the point data calculated for the stations to the surface data for the

entire study area. The spatial climatic anomaly (i.e., deviation from the areal mean) for stations, $\Delta\bar{T}_i$, is calculated as:

$$\Delta\bar{T}_i = \bar{T}_i - \bar{T} \quad (14)$$

where, \bar{T}_i represents the long-term average of the mean annual temperature at station i , and \bar{T} is the mean temperature of the study area for the same period:

$$\bar{T} = \frac{\sum_{i=1}^n \bar{T}_i}{n} \quad (15)$$

where n is the total number of stations in the study area.

The upper and lower panels in Figure 5.2 show mean temperature and mean precipitation climatology maps, respectively. Below each map the \bar{T} value calculated for the CASA is given.

As seen in Figure 5.2, the spatial variability of temperature is significantly influenced by the topographical features of the CASA. The Taurus Mountains in the south running parallel to the coastline defines the boundary for the coastal climatology zone with higher annual mean temperature and precipitation, whereas in the west the topology of mountain ranges extending in a west-east direction lets the milder climate conditions reach further inland.

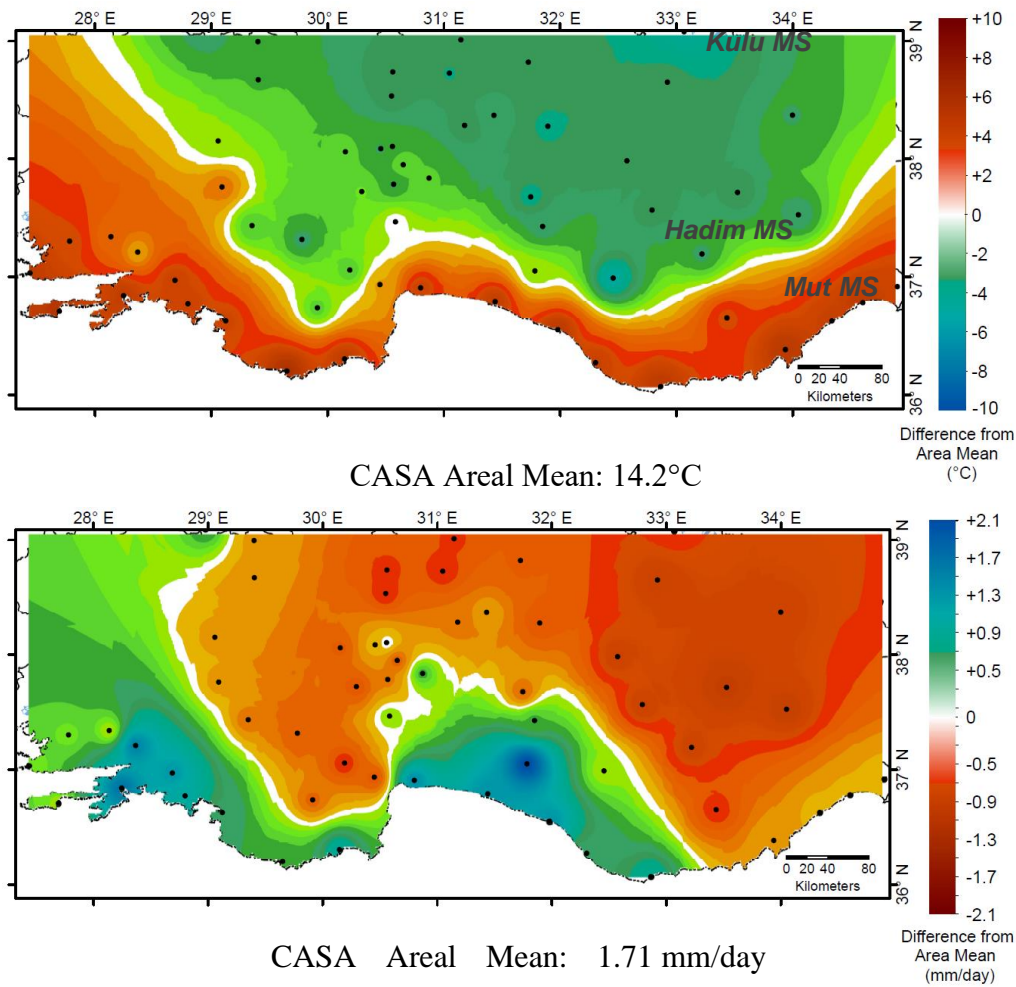


Figure 5.2. Mean annual temperature (top panel) and precipitation (bottom panel) climatology anomaly at MSs from CASA mean.

Further analysis of baseline climatology in the CASA is detailed in Paper 2 and Paper 3 in Appendices B and C.

5.1.2 Analysis of Simulation Performances of Climate Models

This section provides the analysis of the performance of the climate model simulations to replicate the observed temperature and precipitation. In that scope,

historic time series of 14 raw (i.e., non-bias adjusted) high-resolution climate models, 12 bias-adjusted CORDEX RCMs, and ensembled series generated from raw and/or bias-adjusted RCMs are validated through a comparison with the RD (i.e., observed data) of the same period.

5.1.2.1 Performance of Climate Model Simulations in Representing Spatial Variability of Temperature and Precipitation Climatology

As detailed in Chapter 2, for the simulation of meteorologic parameters that are influenced by local processes such as precipitation, GCMs do not provide sufficient resolution to replicate local conditions and may include significant biases (Fujihara et al., 2008; Sato et al., 2012; Sunyer Pinya et al., 2015; Lun et al., 2021; Park et al., 2021). Therefore, for the purpose of basin-scale hydrological impact assessment, high-resolution climate models are selected to be used in this study. However, even the high-resolution RCMs may include biases that are inherited from their driving GCMs or due to poor parametrization (Sharma et al., 2007; Piani et al., 2010; Jaw et al., 2015). Hence, before the use of climate simulations for impact assessment purposes the models are required to be validated. For the analysis of the performance of model simulations to represent spatial variability of temperature and precipitation climatology in CASA, 14 raw high-resolution climate models (i.e., 12 CORDEX RCMs and 2 MRI climate models) are used. The spatial variability is analyzed through a benchmark of RD from 59 MSs across the CASA. For the evaluation of the simulation performances of the climate models for temperature and precipitation in the CASA regarding the spatial variability of climatology, historical simulations by the climate models are compared with the observed (See the Taylor diagrams in Figure 5.3). To evaluate the simulation performances, the performance indicators, *Corr*, *RMSE*, and bias (*PBIAS* for precipitation and *Bias* for temperature), and API calculated from the ranking of models according to these indicators are used. The API values calculated for the climate models are given in Table 5.1.

Based on a combined evaluation of the Taylor diagram and performance indicators, the below listed five climate models are identified to have the highest simulation performances in the replication of baseline temperature climatology. These are:

- M1: MRI-AGCM
- M2: MRI-AGCM_NHRCM
- M7: EC-EARTH_HIRHAM5
- M12: HadGEM2-ES_CCLM4-8-17
- M14: HadGEM2-ES_RCA4

For precipitation, five climate models identified to have the highest simulation performances in the replication of baseline climatology are:

- M2: MRI-AGCM_NHRCM
- M6: EC-EARTH_CCLM4-8-17
- M7: EC-EARTH_HIRHAM5
- M8: EC-EARTH_RACMO22E
- M14: HadGEM2-ES_RCA4

In the 14-member ensemble, M3: CNRM-CM5_ALADIN53 is found to perform worst both for temperature and precipitation. On the other hand, as seen above, M2: MRI-AGCM_NHRCM, M7:EC-EARTH_HIRHAM5, and M14: HadGEM2-ES_RCA4 are among the best performing models both for temperature and precipitation climatology. However, M8: EC-EARTH_RACMO22E which performed well for precipitation is seen to perform relatively poorly for temperature.

The analysis of simulation performances indicated a significant variation in the modeling skills of 14 models. Furthermore, significant intra-regional variability is observed regarding the simulation performances of the models. Hence, some climate models may perform particularly poorly for certain MSs and for certain seasons (e.g.,

summer season or inland MSs). Therefore, for hydrological impact assessment purposes modeling skills are required to be evaluated with a focus on the local scale of the hydrological assessment (e.g. hydrological modeling area) and the particular study objective (e.g., assessment for water supply or flood risk). A detailed analysis of the performances of climate models in the 14-member ensemble for simulation of temperature and precipitation in the CASA is given in Paper 2 and Paper 3 in Appendices B and C.

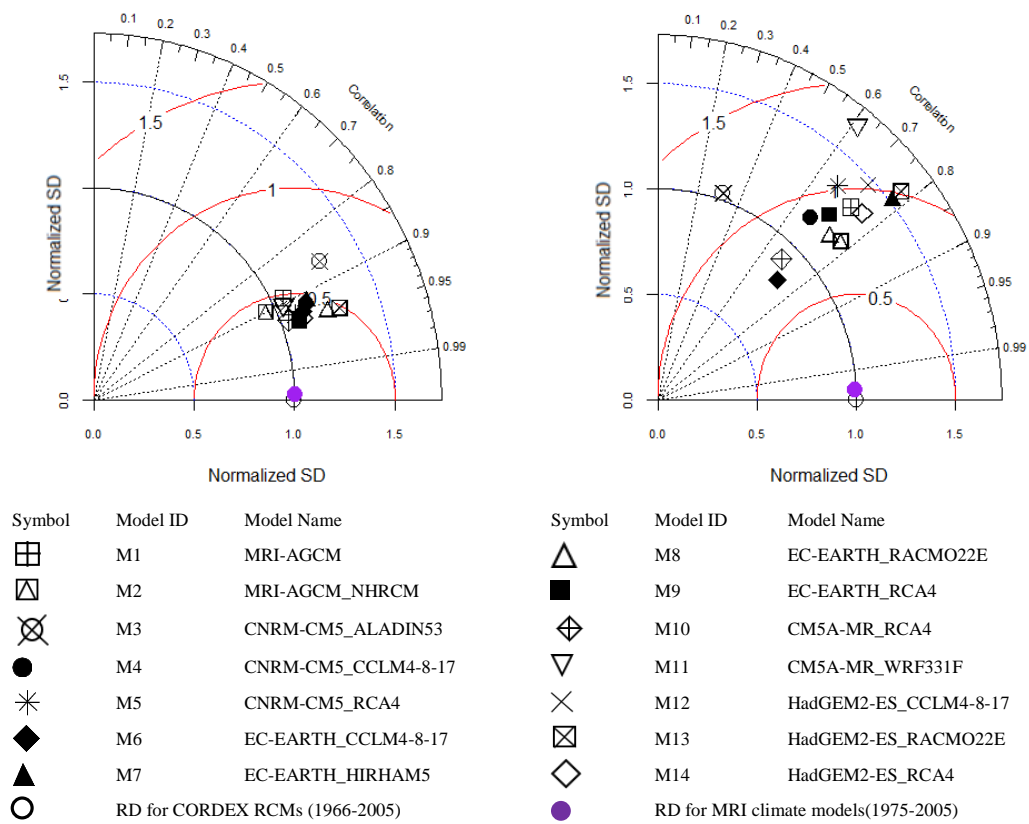


Figure 5.3. Taylor diagrams for the climate models compared with the observed temperature and precipitation climatology concerning the spatial variability in the CASA (left panel: temperature, right panel: precipitation)

Table 5.1 Aggregated Performance Indicator (API) values for climate models (Spatial Variability of Climatology)

ID	Model Name	API for Temperature ⁸	API for Precipitation ⁸
M1	MRI-AGCM	5.00	8.00
M2	MRI-AGCM_NHRCM	5.33	1.67
M3	CNRM-CM5_ALADIN53	14.00	11.67
M4	CNRM-CM5_CCLM4-8-17	8.67	12.67
M5	CNRM-CM5_RCA4	9.00	7.00
M6	EC-EARTH_CCLM4-8-17	7.67	3.00
M7	EC-EARTH_HIRHAM5	5.67	4.00
M8	EC-EARTH_RACMO22E	9.33	5.00
M9	EC-EARTH_RCA4	9.00	6.67
M10	CM5A-MR_RCA4	6.00	10.00
M11	CM5A-MR_WRF331F	8.00	13.33
M12	HadGEM2-ES_CCLM4-8-17	5.33	10.00
M13	HadGEM2-ES_RACMO22E	7.33	7.67
M14	HadGEM2-ES_RCA4	4.67	4.33

5.1.2.2 Performance of Climate Model Simulations in Representing Temporal Variability of Temperature and Precipitation Climatology

The performance of 14 raw high-resolution climate models' simulations to represent temporal variability of temperature and precipitation climatology in CASA is also analyzed through a benchmark of RD from 59 MSs across the CASA. For the analysis, the historical time series of annual means of temperature and precipitation on average of the CASA (i.e., the average of 59 MSs) calculated for each climate

⁸ the best values are indicated in bold.

model for the period between 1966 and 2005 are compared with the observed means through the use of Taylor diagram (Figure 5.4) and API (Table 5.2) values. For MRI models the historical period is taken between 1980 and 2001.

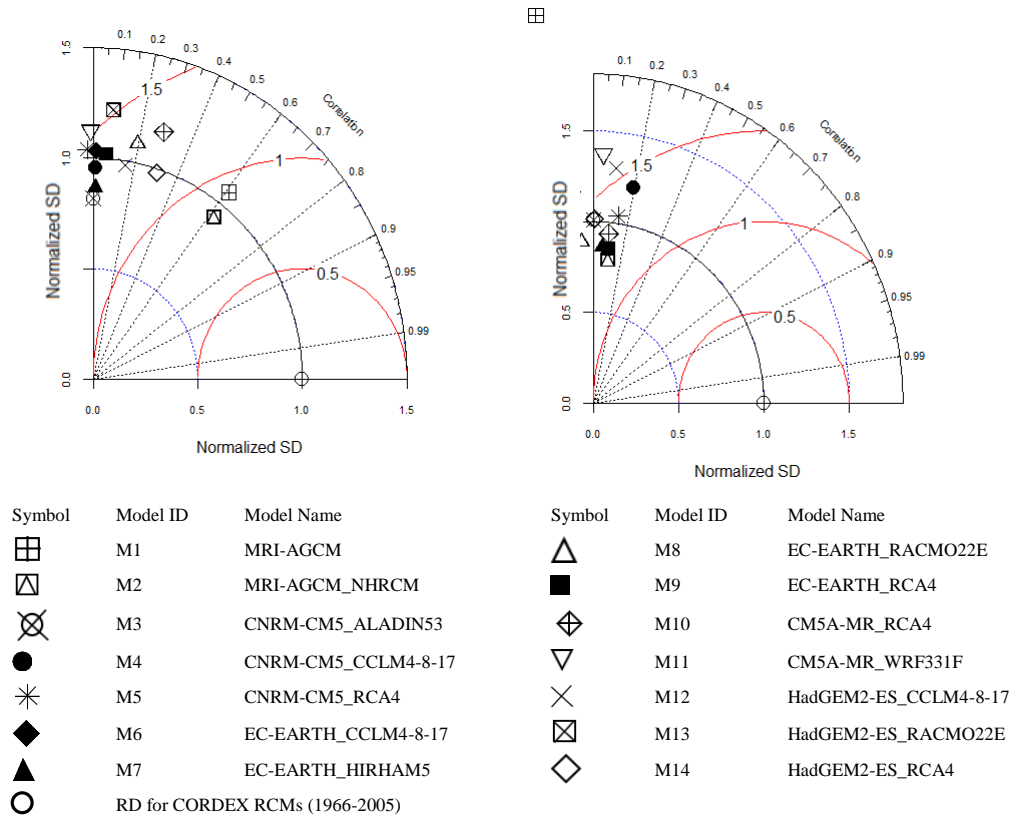


Figure 5.4. Taylor diagrams for the climate models compared with the observed temperature and precipitation climatology concerning the temporal variability in the CASA (left panel: temperature, right panel: precipitation)

Table 5.2 Aggregated Performance Indicator (API) values for climate models (Temporal Variability of Climatology)

ID	Model Name	API for Temperature ⁸	API for Precipitation ⁸
M1	MRI-AGCM	1.33	11.00
M2	MRI-AGCM_NHRCM	1.67	2.33
M3	CNRM-CM5_ALADIN53	13.33	8.67
M4	CNRM-CM5_CCLM4-8-17	9.33	9.67
M5	CNRM-CM5_RCA4	11.33	3.67
M6	EC-EARTH_CCLM4-8-17	8.33	7.00
M7	EC-EARTH_HIRHAM5	6.33	4.33
M8	EC-EARTH_RACMO22E	10.33	8.00
M9	EC-EARTH_RCA4	10.67	3.00
M10	CM5A-MR_RCA4	5.67	9.00
M11	CM5A-MR_WRF331F	8.67	11.33
M12	HadGEM2-ES_CCLM4-8-17	4.00	9.00
M13	HadGEM2-ES_RACMO22E	9.67	11.33
M14	HadGEM2-ES_RCA4	4.33	6.67

Based on a combined evaluation of the Taylor diagram and performance indicators, the below listed five climate models are identified to have the highest simulation performances in the replication of baseline temperature climatology. These are:

- M1: MRI-AGCM
- M2: MRI-AGCM_NHRCM
- M10: CM5A-MR_RCA4
- M12: HadGEM2-ES_CCLM4-8-17
- M14: HadGEM2-ES_RCA4

For precipitation, five climate models identified to have the highest simulation performances in the replication of baseline climatology are:

- M2: MRI-AGCM_NHRCM
- M5: CNRM-CM5_RCA4
- M7: EC-EARTH_HIRHAM5

- M9: EC-EARTH_RCA4
- M14: HadGEM2-ES_RCA4

The climate models' performances to replicate interannual variability in actual observations are significantly affected by the model setups such as assumptions on initial atmospheric and meteorological conditions. Hence, all of the models in the ensemble are seen to have worse performance for the replication of the interannual variability of temperature and precipitation compared to the performance to replicate the spatial variability of climatology.

5.1.2.3 Performance of Raw versus Bias-Adjusted RCM Outputs in Representing Temporal Variability of Precipitation Climatology

A multi-model analysis is done in order to evaluate the simulation performances of raw/non-bias adjusted CORDEX RCMs in comparison with the bias-adjusted CORDEX RCMs. The analysis is done on selected eight MSs located in the HMSA. The ensemble set included four raw and twelve bias-adjusted CORDEX RCMs (i.e., each RCM post-processed with CDFt, QMAP, and DBS methods for bias adjustment). The findings from the analysis verified that the simulation performances to replicate the climatology and temporal variability of precipitation in the region are significantly diversified not only for the raw RCMs but also for the bias-adjusted outputs. Furthermore, when the specific MSs or specific seasonal conditions are taken into consideration the analysis demonstrated that the bias-adjusted outputs from the CORDEX database (a product of the CORDEX-Adjust Project) do not necessarily provide an improvement in the simulation performance of precipitation outputs of raw RCMs (Figure 5.5 and Figure 5.6). As seen from Figure 5.5, for Karaman MS raw RCMs provide better results regarding *Corr*, *RMSE*, and *PBIAS* values, in general. Furthermore, concerning the *Corr* values the bias-adjusted outputs for RCM3 (EC-EARTH_RACMO22E) are observed to perform

worse than the raw RCMs for Karaman, Anamur, and Seydişehir MSs. Hence, the bias-adjusted RCMs from the CORDEX database should be used only after adequate validation through a comparison of historical outputs with observed data.

A detailed comparison of the performances of raw and bias-adjusted climate models for the simulation of seasonal and annual precipitation is given in Paper 1 in Appendix A.

Additionally, to assess potential improvement in estimations of precipitation, ensembled outputs obtained through Superensemble (SE) method are also analyzed for their simulation performances in comparison to the individual raw and bias-adjusted RCMs. For that purpose, three types of ensembled outputs (i.e., SE_RCM, SE_BARCM, SE_All) are generated by the use of raw and bias-adjusted RCMs in the ensemble set. Among the three ensembled output types that are produced by the use of the SE approach SE_RCM is formed from four raw RCMs only, SE_BARCM is formed from 12 bias-adjusted RCMs only, and SE_All is formed using all models in the ensemble set (i.e., 4 raw and 12 bias-adjusted RCM outputs). The analysis is done on selected eight MSs located in the HMSA.

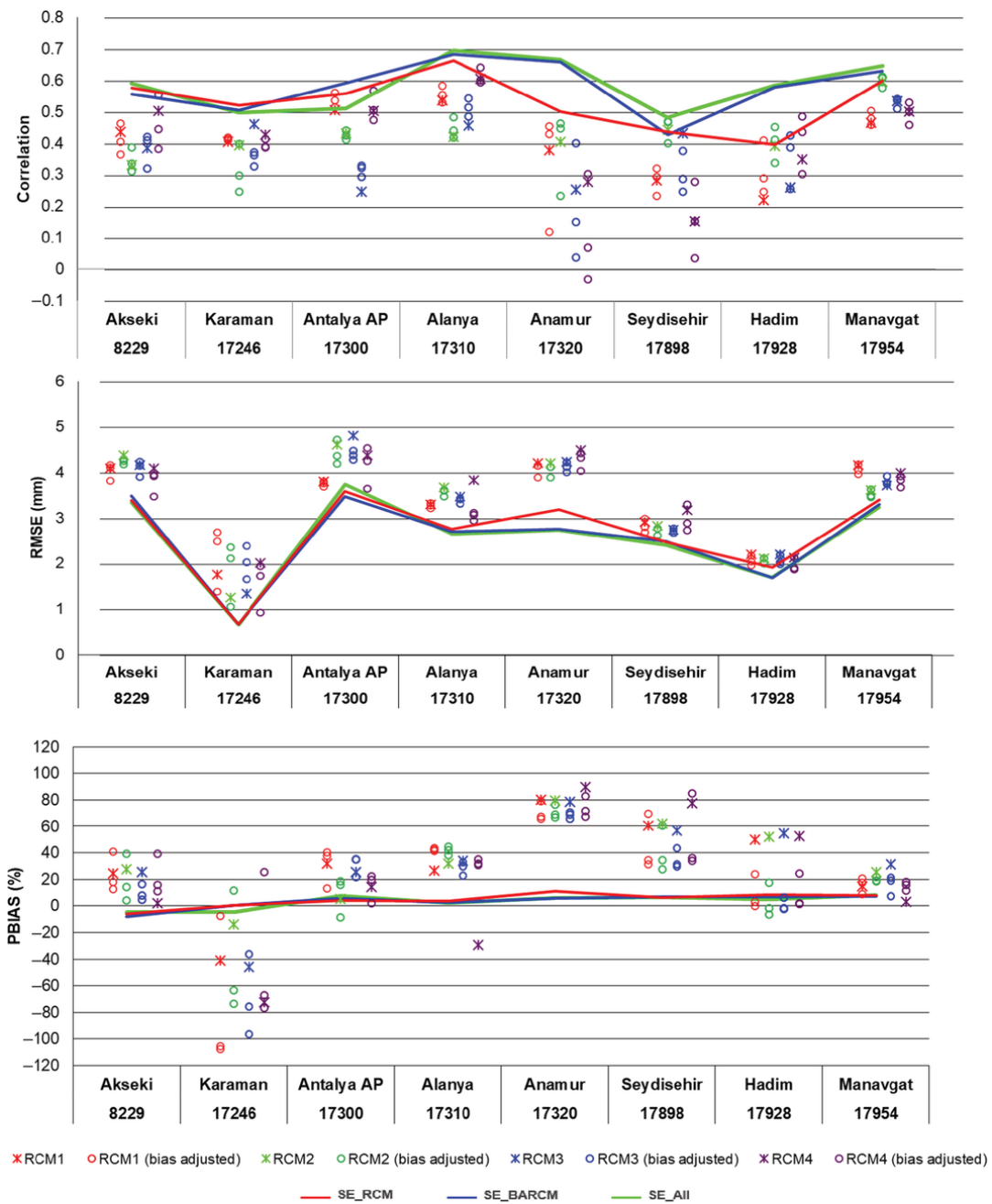


Figure 5.5. Comparison of statistical performance indicators (SPIs) with observed for single (raw and bias-adjusted) regional climate models (RCMs) and superensembles (SEs) for the test dataset

The comparison of the simulation performances of ensembled outputs with individual RCMs indicated that all three SE outputs are seen to improve the simulation performances regarding the *PBIAS*, *RMSE*, and *Corr* values (Figure 5.5), particularly for annual climatology. The analysis also indicated that SE improved correlation (up to 42%) and *RMSE* (between 20 and 72%) for the monthly precipitation time series of the historical simulations from the individual climate models, respecting the best-performing RCM. Furthermore, total bias is also significantly reduced by SE verifying the better performance of SEs over the raw and bias-adjusted models concerning these performance indicators. Taylor diagrams in Figure 5.6 also verify improvement in the simulation performance for precipitation by SE compared to both raw and bias-adjusted outputs for all eight MSs in the HMSA. However, concerning the seasonality and variability of precipitation, some limitations are still observed for SE outputs which should be taken into consideration for the use of outputs for further impact assessment purposes. The detailed analysis of SE outputs in comparison with the individual RCMs is given in Paper 1 in Appendix A.

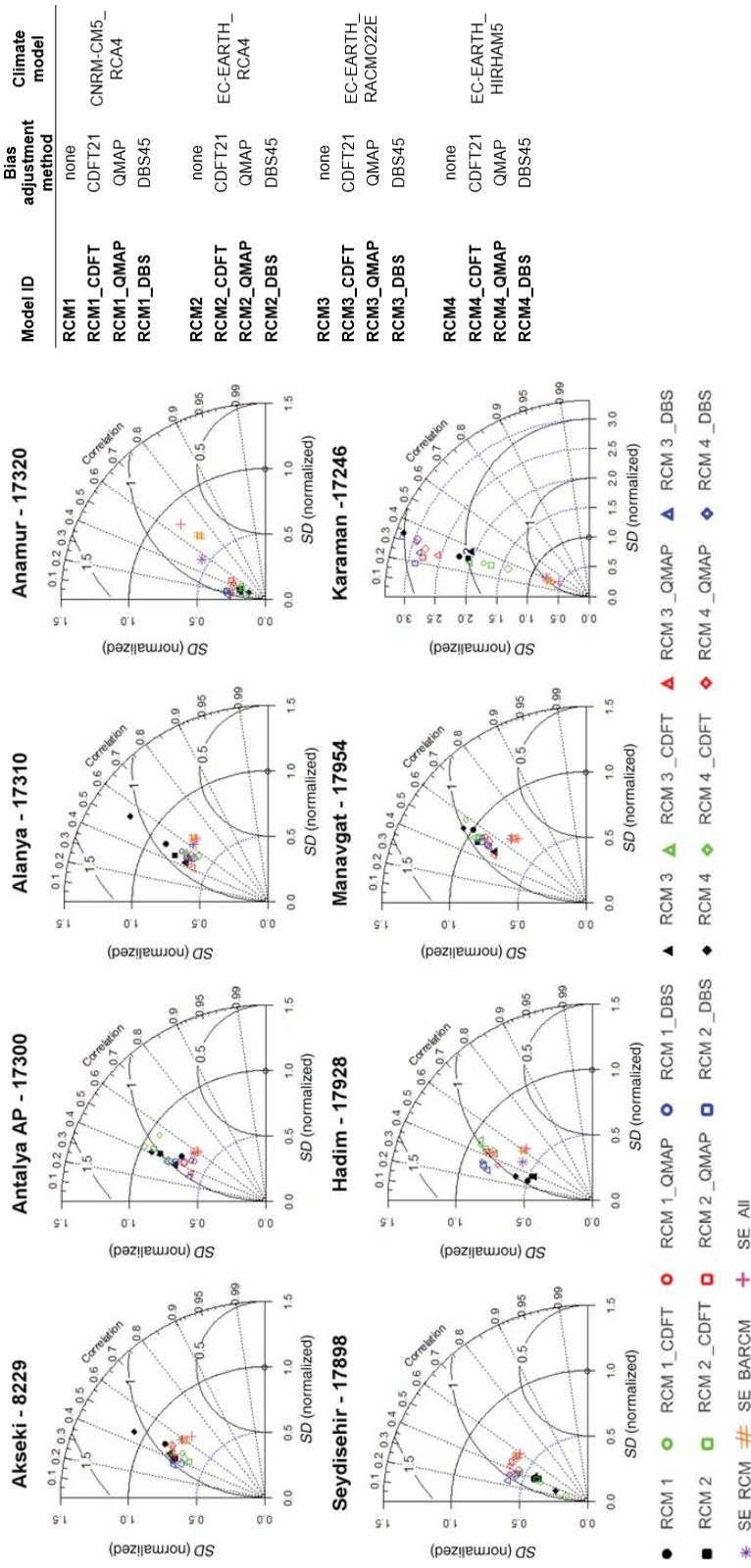


Figure 5.6. Comparison of raw and bias-adjusted regional climate models (RCMs), and three superensembles (SEs) (SE_RCM: SE of raw RCMs, SE_BARCM: SE of bias-adjusted RCMs, SE_All: SE of all RCMs including raw and bias-adjusted) with observed monthly average precipitation

Consequently, the analysis results (detailed in Paper 1 in Appendix A) indicated that the bias-adjusted outputs may improve simulation performances for certain locations, certain seasons, or periods while it may degrade the simulation performances for other locations and seasons. Therefore, the bias-adjusted RCM outputs should again be used by taking into consideration of the local-scale conditions and the purpose of the study.

Furthermore, the analysis of 14 raw (Section 5.1.2.1 and 5.1.2.2), and 12 bias-adjusted RCMs verifying high inter-model variability of the modeling skills shows the importance of the multi-model analysis for the assessment of uncertainties. Additionally, the analysis of potential improvements and drawbacks of the use of ensembled outputs indicated that ensembled outputs provide certain benefits such as:

- Improvement in the simulation performances with respect to the SPI's including *Corr*, and *RMSE*.
- Bias adjustment and reduction in the total bias in the simulations.

Thus, reduction of the uncertainty in the estimations is achieved through ensembled time series. On the other hand, ensembled outputs obtained in this study have the limitation of reducing the variability of the parameter simulated by the climate models and fail to represent the observed low-frequency events (detailed in Paper 1 in Appendix A).

Hence, for the impact analysis on temperature and precipitation in CASA and at Akseki MS (Section 5.1.3), multi-model analysis is applied by the use of raw high-resolution climate models. The analysis includes an evaluation of potential uncertainties by taking the range of variability shown by all models in the ensemble set. In addition, to obtain information on the general trend for the projections, a simple ensembling method (i.e., PBWA) is used to assess changes in the temperature and precipitation in the overall CASA (Section 5.1.3.1). For Akseki MS, with the purpose of further streamflow impact assessment two more complex ensembling approaches (SE, and SME) are used (Section 5.1.3.2).

5.1.3 Analysis of Potential Impacts of Climate Change on Temperature and Precipitation

This section presents the results of the analysis of potential future impacts on temperature and precipitation based on climate projections. The analysis is done at two different scales. The first analysis is for the CASA (including 59 MSs) based on the projections by 14 raw (i.e., non-bias adjusted) high-resolution climate models (Section 5.1.3.1). Following that analysis is done with the purpose of providing inputs for subsequent streamflow impact assessment for the Oymapınar basin (Section 5.1.3.2). Assessment for the Oymapınar basin includes the analysis for Akseki MS in the basin and is based on the projections by 12 raw CORDEX RCMs and ensembled series generated from these RCMs.

5.1.3.1 Analysis of Temperature and Precipitation Projections for the CASA

The potential changes in mean temperature and precipitation due to climate change in the CASA are assessed for the short- (2020-2030), medium- (2031-2050), and long-term (2051-2099) future based on the projections of 12 CORDEX RCMs for RCP4.5 and 8.5 scenarios. Additionally, projections by MRI's climate models for the RCP8.5 scenario for the 2080-2100 period are analyzed.

For the analysis, changes in the mean temperature and precipitation at 59 MSs in the CASA are determined from the difference of the long-term means projected for the relevant future periods from the historical means (of 1966-2005 period for CORDEX RCMS and 1981-2000 for MRI's models) simulated by climate models. Furthermore, the statistical significance of the projected changes is tested by the use of Welch's test as detailed in Section 4.1.3, and Paper 2 and Paper 3 in Appendices B and C.

The boxplots of the projected change in the mean temperature (°C) and percent change in the mean precipitation (%) for (a) short-, (b) medium-, (c) long-term future under RCP4.5 and RCP8.5 scenarios are given in Figure 5.7 and 5.8, respectively. In the boxplots, in Figures 5.7 and 5.8, the upper whisker boundary indicates the

largest data within 1.5 IQR (interquartile range, i.e., the difference between 75th and 25th percentiles) above the 75th percentile, and the lower whisker indicates the smallest data within 1.5 IQR below the 25th percentile of the projections for each climate model. The boxplots of the MRI's climate models for the long-term demonstrate only the RCP8.5 projections for the long-term future covering the period of 2080 to 2099.

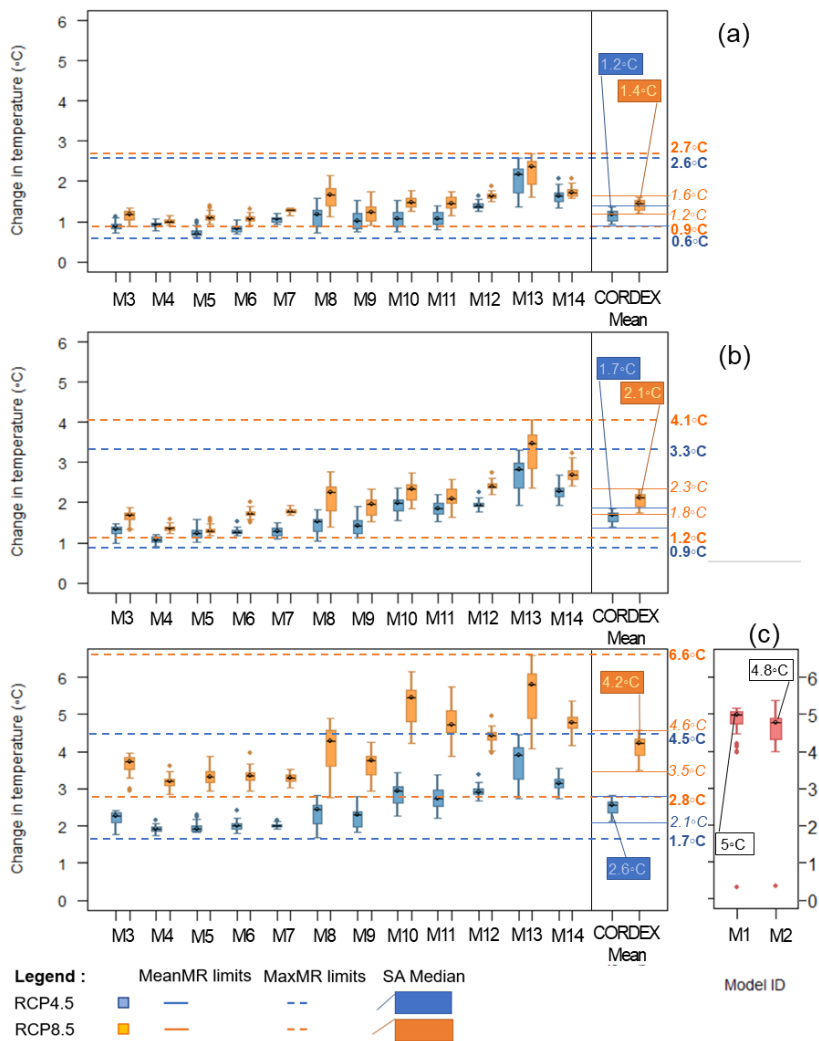


Figure 5.7. Boxplot showing projected change in temperature climatology for (a) short-, (b) medium-, (c) long-term future under RCP4.5 and RCP8.5 scenarios

As seen in Figure 5.7, the analysis of the 14-member ensemble for temperature verifies that:

- The projections by all models agree on a gradual increase in the mean temperature in the entire CASA (i.e., 59 MSs) during the 21st century for both RCP4.5 and 8.5 scenarios.
- The temperature increases at all MSs and for all future terms are projected to be statistically significant (with a 95% confidence level) under both scenarios.
- The projections on temperature increase for the RCP4.5 scenario from 12 CORDEX RCMs range between 0.6°C and 2.6°C for short-term, 0.9°C and 3.3°C for medium-term, and 1.7°C and 4.5°C for the long-term future across the CASA.
- The ensemble means of 12 CORDEX RCMs regarding the RCP4.5 scenario for the short-, medium- and long-term future indicate a 1.2°C, 1.6°C, and 2.5°C increase in the mean temperature on average of 59 MSs (i.e., areal average).
- The projections on temperature increase for the RCP8.5 scenario from 12 CORDEX RCMs range between 0.9°C and 2.7°C for short-, 1.2°C and 4°C for medium-, and 2.8°C and 6.6°C for long-term future.
- For the RCP8.5 scenario, for the short-, medium- and long-term future, the ensemble means of 12 CORDEX RCMs show 1.4°C, 2.1°C, 4.1°C increase in the mean temperature on average of 59 MSs.
- The projections by MRI's climate models for the long-term future under the RCP8.5 scenario show statistically significant temperature increases in the range of 4°C to 5.2°C and 4°C to 5.4°C, based on M1 and M2, respectively.
- The areal mean for temperature change is projected as 4.9°C by M1, and 4.7°C by M2.

The multi-model analysis for annual mean temperature change in the CASA is in agreement with the increase in the annual mean temperature in the land portion of the Mediterranean, ranging between 0.9 to 5.6°C for different emission scenarios as identified by the AR6 of IPCC to be very likely compared to the historic period of 1980-2000 (Ali et al., 2022).

Additionally, the ensemble mean projections for the RCP4.5 scenario are similar to the findings by Johns et al. (2003). Johns et al. (2003) in their study verified a statistically significant 1.5°C and 2.7°C increase in the annual mean temperature in Southern Europe in the 2040s (2030-2059) and in 2080s (2070-2100), respectively, under the SRES B1 scenario which is comparable with the RCP4.5 scenario of the AR6. The findings by Gualdi et al. (2013) revealed a steady increase in the mean temperature in the Mediterranean for the short-, and medium-term future. Their findings indicated a slightly higher increase (an increase over 2°C) under the SRES A1B scenario which is comparable with the RCP6 scenario, based on the assumption of approximately 200 ppm CO₂-eq. higher atmospheric GHG concentrations and 1.5W/m² higher radiative forcing than the RCP4.5 scenario of the AR6.

For the high emission RCP8.5 scenario which is comparable with the A1FI and A2 scenarios of the SRES, the ensemble mean projections of the 14-member ensemble set in this study are similar to the findings from Johns et al. (2003) and Giorgi and Lionello (2008). Johns et al. (2003) verified an increase of 2.2°C and 5.4°C for the annual mean temperature in the 2040s and 2080s, respectively, in Southern Europe, under the SRES A1Fi scenario. Similarly, based on the results from the Prudence project and data adapted from Déqué et al. (2005) in the southern Mediterranean study area including Italy and Greece, Giorgi and Lionello (2008) indicated a temperature increase under the SRES A2 scenario for the last 30 years of 21st century (2071-2100). Their findings are in agreement with the above-given findings and reveal a temperature increase in the range of 2.7°C and 4.2°C based on GCMs, and 3.9°C and 6.8°C based on RCMs. On the other hand, the findings by Seguí et al. (2010) on an increase in annual temperature in the range of 1.5°C and 1.7°C for the A2 scenario in the Mediterranean region of France for the future time period between

2035-2065 is lower than the projections analyzed in this study for the CASA which covers a significant portion of the Anatolian Peninsula.

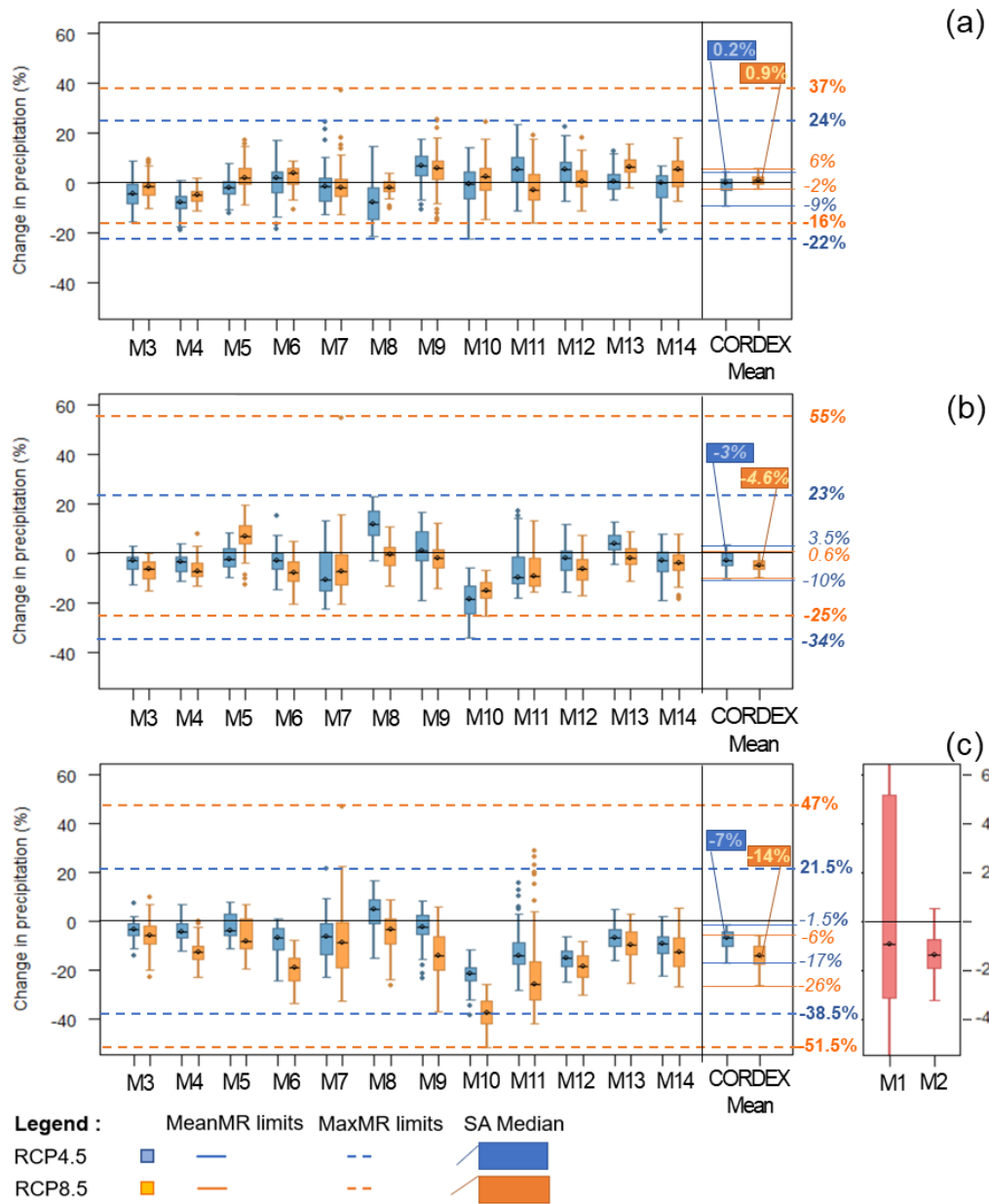


Figure 5.8. Boxplot showing percent change in annual precipitation climatology projected by climate models for (a) short-, (b) medium-, (c) long-term future (In (c) MRI's maximum model range for M1: MRI's AGCM extends beyond the limit of y axis in the plot, it ranges between -69% to 120%)

Analysis of the projections from the 14-member ensemble for precipitation reveals the following findings that are also seen in the boxplots in Figure 5.8.

- Projections for the CASA indicate significant intra-regional variability in the size and type (i.e., decrease or increase) of impact on precipitation.
- Under the RCP4.5 scenario, the projections on percent change in the mean precipitation from 12 CORDEX RCMs for 59 MSs in the CASA range between -22% and 24% for short-, -34% and 23% for medium-, and -38.5% and 21.5% for long-term future.
- Concerning the CASA on average, the ensemble means of CORDEX RCMs indicate a 0.5%, 2.7%, and 7% decrease in precipitation for the short-, medium-, and long-term future under the RCP4.5 scenario, respectively.
- Under the RCP8.5 scenario, the projections of CORDEX RCMs on percent change in the mean precipitation range between -16% and 37% for short-, -25% and 55% for medium-, and -51.5% and 47% for long-term future at 59 MSs across the CASA.
- On average for the entire CASA, the ensemble means for 12 RCMs show +1.3%, -4.6%, and -14% change in precipitation for short-, medium-, and long-term future under the RCP8.5 scenario, respectively.
- Based on the projections by MRI-AGCM_NHRCM on average of the CASA a 14% decrease in the mean annual precipitation is calculated for the long-term future period between 2080 and 2099 compared to the historical period between 1981 and 2000. A statistically significant level of change in precipitation is projected for the long-term future between 2080 and 2099 under the RCP8.5 scenario for more than 40% of the MSs in the SA.

The IPCC's AR6 highlights a likely decrease in precipitation in the range of 4% to 22% in most parts of the Mediterranean at the end of this century, depending on the projection scenario (Ali et al., 2022). The ensemble mean in this study is within the range of the projections underlined in the AR6, however, the projections for the RCP8.5 scenario in the CASA are lower than the projected maximum increase mentioned by the AR6 for the Mediterranean basin.

The analysis of the potential change in the mean precipitation in Mediterranean mountains (including Taurus, Pyrenees, Apennines, Dinaric Alps, Pintos, and Atlas) under the SRES B1 scenario which is comparable to the RCP4.5 scenario by Bravo et al. (2008) indicated a decrease in precipitation in the range of 2.5 and 5.7% for 2055s (2040-2069) and 2085s (2070-2099). For the SRES A1FI scenario, comparable with the RCP8.5, their findings revealed 5.9 and 13% decreases for 2055s and 2085s, respectively. Thus, the findings in this study are similar to those findings. However, for the CASA a slightly more intensified decrease is projected for RCP4.5 in the long term. Furthermore, Bravo et al. (2008) demonstrated that among the Mediterranean mountain ranges the highest decrease in precipitation is expected for the Taurus mountains. For the A1Fi scenario 8.8% (2055s) and 22.4% (2085s) decreases, and for B1 scenario 4.1% (2055s) and 9.4% (2085s) decreases are estimated. A comparison of their findings with the analysis results for Akseki MS (See Section 5.1.3.2 Table 5.8) verifies similar projections for the Akseki MS based on the 14-member ensemble mean. However, the Akseki MS located at 1150 m altitude in the western Taurus mountains is projected to experience a slightly higher decrease (-11.8%) for the RCP 4.5, and a slightly lower decrease (20%) for the RCP8.5 scenario compared to the projections indicated by Bravo et al. (2008) (i.e., 9.4% and 22.4% for B1 and A1Fi scenarios) for the 2085s.

Seguí et al. (2010) identified a much lower decrease in the mean precipitation (i.e., 3 to 4%) for the future time period between 2035-2065 in the Mediterranean region

of France under the SRES A2 scenario, compared to the decrease projected in the CASA.

A comparison of the projected changes in the mean temperature and precipitation across the basins in the CASA verifies an inverse linear relationship (Figure 5.9). The increase in the mean temperature at the basins is projected to be parallel to a decrease in the mean precipitation at all basins within the CASA.

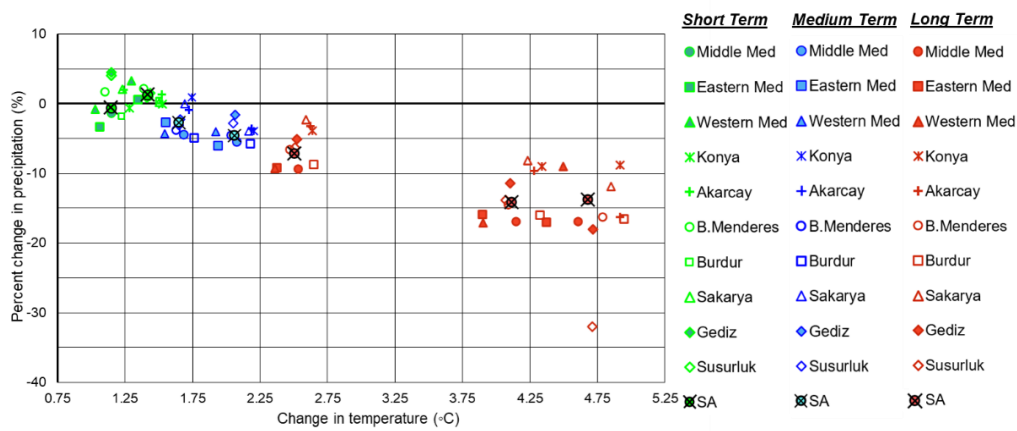


Figure 5.9. Areal average changes at basins in the CASA for short-, medium, and long-term future based on the mean projection by 12 CORDEX RCMs, and individual projection of MRI-AGCM_NHRCM (Both RCP4.5 and RCP8.5 projections for the same basin are shown with the same symbol and color)

Further details on the analysis results for the assessment of likely climate change impacts on mean temperature and precipitation are provided in Paper 2 and Paper 3 in Appendices B and C.

Consequently, the analysis of the projected changes in annual temperature and precipitation throughout the CASA indicates a statistically significant and gradual increase in temperature throughout the 21st century, and a statistically significant decrease in precipitation at a significant portion of the CASA, for the second half of the century. The concurrent impacts on temperature and precipitation in the CASA

are expected to aggravate the stress on the water resources and increase the drought risk in the region, particularly in inland basins where the increase in temperature is likely to be more pronounced due to the intensification of the dry climate characteristics. The IPCC's AR6 stresses the drying in the Mediterranean in the last decades and emphasizes a highly likely aggravation of droughts during this century (Ali et al., 2022) such as the potential drying of the major freshwater lake of Turkey (i.e., Lake Beyşehir) in Konya Closed Basin (Bucak et al., 2017), which is also located approximately 25 km to the north of the HMSA. Furthermore, the study by Yilmaz et al. (2021) revealed that elevated evapotranspiration due to increased temperature under both RCP4.5 and 8.5 scenarios intensifies water loss from inland surface water bodies and may even cause the complete loss of some of them (Yilmaz et al, 2021).

Similarly, the analysis results in this study show that the impacts are likely to increase with time and exacerbate the risk of water stress. Intensified impacts are particularly very likely after the onset of a significant level of decrease in the precipitation in the long-term future (i.e., in the second half of the 21st century). Therefore, tiered adaptation strategies are considered to be necessary to minimize the increased risks and vulnerabilities regarding the climate change impacts on water resources.

5.1.3.2 Analysis of Temperature and Precipitation Projections for the Akseki MS

For the subsequent streamflow impact assessment for the Oymapınar basin in Component 3 of the study (Section 5.3), the meteorological parameters simulated by RCMs are validated specifically for the modeling basin before the use in the hydrological modeling. Furthermore, to benefit from the advantages of the ensembling two different approaches are analyzed in order to obtain a better efficiency for the simulation of the streamflow at the model basin. The potential

improvement by ensembling for hydrological impact assessment (Section 5.3) is evaluated for two conditions:

1. Ensembling of meteorological time series for the Akseki MS to be used as input of the hydrological model.
2. Ensembling of the streamflows simulated for individual climate models for the Akseki MS.

This subsection details the results of validation of the individual climate models for the Akseki MS and production and testing of the simulation performance of ensembled time series for precipitation and temperature at the Akseki MS. The results of the latter approach, ensembling of the streamflow time series, are detailed in Section 5.3.

Generation of the ensembled temperature and precipitation time series and analysis of simulation performances in comparison to the individual RCMs

The temperature and precipitation simulations of the individual climate models for the model grid closest to the Akseki MS are initially ensembled using SME and SE methods. The ensembling of the daily time series aims to decrease variability in estimations and provide bias adjustment in the climate simulations.

The ensembled time series generated with SME methodology is formed using equal weights for the anomalies simulated by each model for historic (1971-2005) and future (2006-2099) RCP4.5 and 8.5 scenario conditions. For the application of the SE method, data series resampled from the historic period are initially used for the training of the SE to determine the weights of modeled anomalies. The weights identified during training are then used to generate continuous time series for historic and future periods. Depending on the available observed meteorological data for the Akseki MS in the historical period, the training and validation of SE are done by the use of data collected between January 1971 and December 2003. The list of 12 CORDEX RCMs used for the generation of ensembled time series by SME and SE approaches is given in Section 4.3.2 (Table 4.7).

For the development of the SE model, the data for the Akseki MS from between 1971 and 2003 are firstly resampled to obtain randomly partitioned two data sets, training and test (i.e., validation) data sets. The training (i.e., calibration) data set is formed to include 75% of the entire time series and the test data set to include the remaining 25 %. The same data points (same point in time) are used for the data sets from the observed and modeled temperature and precipitation. The efficiency of the ensembled training and test data sets generated using SE and SME approaches to replicate the observed daily data in comparison with the efficiency of the individual models are shown in Tables 5.3 and 5.4 for temperature and precipitation, respectively.

Table 5.3 Analysis of the SPI values for the daily temperature data of individual models and ensembled outputs for training and test data sets for the Akseki MS

ID	Climate Model		Training			Test		
	GCM	RCM	Corr	RMSE (°C)	PBIAS (%)	Corr	RMSE (°C)	PBIAS (%)
M1	CNRM-CM5	CCLM4-8-17	0.83	7.66	-44.43	0.83	7.66	-44.62
M2	CNRM-CM5	ALADIN53	0.89	6.87	-41.61	0.89	6.81	-41.09
M3	CNRM-CM5	RCA4	0.86	7.05	-40.87	0.86	7.02	-40.72
M4	EC-EARTH	CCLM4-8-17	0.84	7.50	-43.37	0.84	7.46	-42.61
M5	EC-EARTH	RACMO22E	0.87	9.05	-57.42	0.87	9.00	-56.57
M6	EC-EARTH	HIRHAM5	0.87	6.18	-34.27	0.86	6.24	-34.01
M7	EC-EARTH	RCA4	0.86	7.36	-43.86	0.85	7.33	-43.14
M8	CM5A-MR	WRF331F	0.87	5.46	-25.57	0.87	5.44	-25.47
M9	CM5A-MR	RCA4	0.87	6.68	-37.72	0.87	6.76	-38.10
M10	HadGEM2-ES	CCLM4-8-17	0.86	6.45	-34.36	0.86	6.31	-32.81
M11	HadGEM2-ES	RACMO22E	0.87	8.08	-48.09	0.87	7.91	-46.93
M12	HadGEM2-ES	RCA4	0.87	6.18	-33.55	0.86	6.16	-32.80
SE			0.93⁹	3.19	-0.11	0.92	3.22	0.32
SME			0.92	3.25	-0.12	0.92	3.25	0.35

⁹ best values are indicated in bold

Table 5.4 Analysis of the SPI values for the daily precipitation data of individual models and ensembled outputs for training and test data sets for the Akseki MS

ID	Climate Model		Training			Test		
	GCM	RCM	<i>Corr</i>	<i>RMSE</i> (mm)	<i>PBIAS</i> (%)	<i>Corr</i>	<i>RMSE</i> (mm)	<i>PBIAS</i> (%)
	M1	CNRM-CM5	CCLM4-8-17	0.07	13.61	-15.06	0.04	12.56
M2	CNRM-CM5	ALADIN53	0.07	16.36	23.95	0.05	15.02	41.88
M3	CNRM-CM5	RCA4	0.09	14.04	-27.77	0.11	12.28	-26.36
M4	EC-EARTH	CCLM4-8-17	0.05	13.42	-36.04	0.03	11.98	-29.7
M5	EC-EARTH	RACMO22E	0.05	14.53	-30.86	0.06	12.96	-24.71
M6	EC-EARTH	HIRHAM5	0.04	16.61	-8.08	0.09	14.78	0.17
M7	EC-EARTH	RCA4	0.06	13.92	-39.74	0.04	12.63	-31.13
M8	CM5A-MR	WRF331F	0.05	14.94	-5.18	0.09	14.41	16
M9	CM5A-MR	RCA4	0.06	14.25	-38.82	0.06	12.73	-39.09
M10	HadGEM2-ES	CCLM4-8-17	0.06	14.18	-16.44	0.07	13.15	-5.57
M11	HadGEM2-ES	RACMO22E	0.08	16.12	8.21	0.09	15.21	21.77
M12	HadGEM2-ES	RCA4	0.06	15.01	-20.95	0.09	13.17	-20.17
SE			0.14 ⁹	11.75	-2.64	0.16	10.3	8.96
SME			0.14	12.05	-2.42	0.16	10.57	8.22

As seen in Tables 5.3 and 5.4, SE and SME provide a significant improvement in the efficiency of the simulations to replicate observed data both for training and test data sets. The ensembled daily time series of temperature and precipitation achieve the best *Corr*, *RMSE*, and *PBIAS* values for training compared with the individual models. For test data sets, ensembled outputs again provide the best *Corr*, *RMSE*, and *PBIAS* values for temperature. For precipitation, ensembled outputs of test data sets provide the best *Corr* and *RMSE* values. Although the *PBIAS* value for the test data set of precipitation is not the best among the models, it is still at a satisfactory level.

As a result, ensembling of daily temperature and precipitation data with SE and SME indicates satisfactory performance and therefore is used for the generation of

meteorological inputs of the hydrological model (Section 5.3.2) in flow simulations. The efficiency of the continuous daily (ensembled and individual RCMs') time series is also verified by a comparison with the observed time series for monthly and annual time steps. The SPI values calculated for the monthly and annual temperature and precipitation time series are shown in Tables 5.5 and 5.6, respectively. As seen in Tables 5.5 and 5.6, the continuous time series generated with the SE model and SME provide satisfactory results for monthly and annual time steps and generated better values for RMSE and PBIAS compared to the individual RCMs.

Table 5.5 The SPI values for the continuous temperature time series in comparison with the observed time series for the period between 1971 and 2003 for the Akseki MS

ID	Climate Model		Monthly mean time series			Annual mean time series		
	GCM	RCM	Corr	RMSE (°C)	PBIAS (%)	Corr	RMSE (°C)	PBIAS (%)
M1	CNRM-CM5	CCLM4-8-17	0.95	6.51	44.61	0.22	6.13	44.46
M2	CNRM-CM5	ALADIN53	0.97	5.97	41.66	0.18	5.69	41.21
M3	CNRM-CM5	RCA4	0.95	6.02	40.97	0.19	5.65	40.77
M4	EC-EARTH	CCLM4-8-17	0.95	6.33	43.29	0.22	5.98	43.26
M5	EC-EARTH	RACMO22E	0.96	8.13	57.47	0.28	7.83	57.05
M6	EC-EARTH	HIRHAM5	0.97	5.11	34.27	0.60	4.74	34.46
M7	EC-EARTH	RCA4	0.95	6.38	43.84	0.15	6.06	43.80
M8	CM5A-MR	WRF331F	0.96	4.07	25.65	0.28	3.57	25.49
M9	CM5A-MR	RCA4	0.96	5.62	37.98	0.16	5.23	37.64
M10	HadGEM2-ES	CCLM4-8-17	0.96	5.16	34.13	0.32	4.77	34.36
M11	HadGEM2-ES	RACMO22E	0.95	7.06	48.05	0.32	6.66	48.32
M12	HadGEM2-ES	RCA4	0.96	5.07	33.48	0.25	4.70	33.80
SE			0.98 ⁹	1.61	0.00	0.54	0.69	0.35
SME			0.98	1.66	0.00	0.47	0.71	0.39

Table 5.6 The SPI values for the continuous precipitation time series in comparison with the observed time series for the period between 1971 and 2003 for the Akseki MS

ID	Climate Model		Monthly mean time series			Annual mean time series		
	GCM	RCM	<i>Corr</i>	<i>RMSE</i> (mm)	<i>PBIAS</i> (%)	<i>Corr</i>	<i>RMSE</i> (mm)	<i>PBIAS</i> (%)
M1	CNRM-CM5	CCLM4-8-17	0.43	3.67	12.66	0.33	0.95	11.76
M2	CNRM-CM5	ALADIN53	0.32	4.6	-28.3	0.27	1.56	-31.05
M3	CNRM-CM5	RCA4	0.51	3.73	27.09	0.38	1.3	26.83
M4	EC-EARTH	CCLM4-8-17	0.39	3.89	34.28	-0.14	1.6	33.55
M5	EC-EARTH	RACMO22E	0.47	3.84	29.06	-0.25	1.59	27.52
M6	EC-EARTH	HIRHAM5	0.5	4.16	6.04	0.25	1.01	6.54
M7	EC-EARTH	RCA4	0.44	3.92	37.58	-0.19	1.74	36.9
M8	CM5A-MR	WRF331F	0.37	4.16	-0.22	-0.09	1.05	-1.34
M9	CM5A-MR	RCA4	0.44	4.06	38.45	-0.12	1.74	39.22
M10	HadGEM2-ES	CCLM4-8-17	0.52	3.54	14.01	0.07	1.17	14.64
M11	HadGEM2-ES	RACMO22E	0.57	4.24	-11.53	0.26	1.26	-11.24
M12	HadGEM2-ES	RCA4	0.51	3.92	20.62	0.34	1.23	20.24
SE			0.65⁹	3.35	-0.15	0.34	0.72	-1.16
SME			0.65	2.97	-0.28	0.26	0.74	-0.99

Potential future changes in temperature and precipitation at Akseki MS

For the analysis of potential short-, medium-, and long-term future impacts, climate model simulations for the future (2006-2099) period under RCP4.5 and 8.5 scenarios of temperature and precipitation are compared with the historic (1971-2005) simulations. The annual mean temperature at the Akseki MS simulated for the historic period and for the future period under RCP4.5 and 8.5 scenarios are shown in Figures 5.10 and 5.11, respectively. The annual total precipitation time series calculated from the daily time series of 12 individual RCMs in comparison with the ensembled time series for the Akseki MS are illustrated in Figures 5.12 and 5.13 for RCP4.5 and 8.5 scenarios, respectively.

As seen in Figures 5.10 to 5.13, SE and SME provide a better representation of the mean climatology of temperature and precipitation for the historic period than the individual models and the average of the 12 models, which is seen to underestimate

the mean precipitation and temperature climatology for the Akseki MS. SE and SME are seen to provide bias adjustment, particularly for mean temperature. However, interannual variability in the observed precipitation is underrepresented by the ensembled time series. Hence, in this study, both of the ensembling approaches, based on the weighted averaging of the modeled anomalies, are seen to improve the correlation and bias indicators but at the same time cause the ensembled time series to be mostly concentrated around the mean climatology. This result might be interpreted as a limitation of the linear methodologies in general, particularly in the representation of parameters such as precipitation that are of non-linear nature.

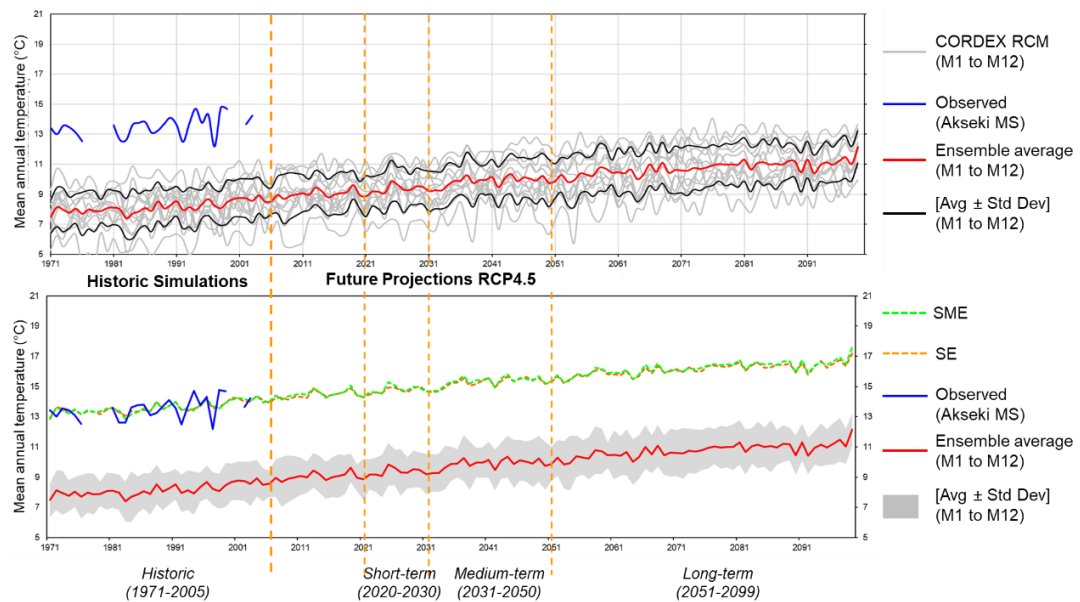


Figure 5.10. Historic and future (RCP4.5 scenario) temperature simulations by 12 CORDEX RCMs compared with ensembled (SE and SME) outputs for the Akseki MS

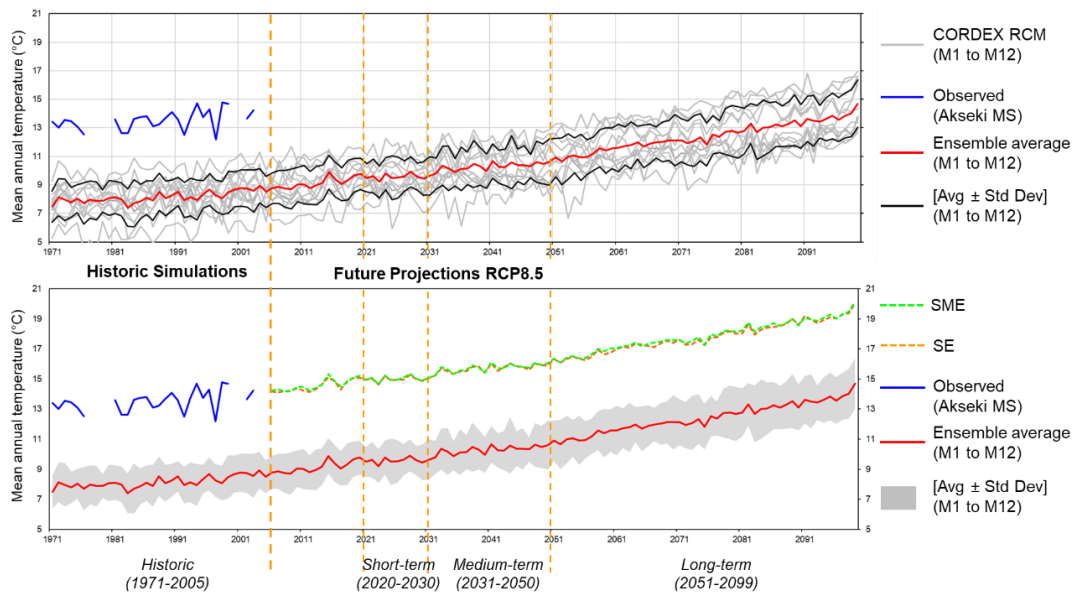


Figure 5.11. Historic and future (RCP8.5 scenario) temperature simulations by 12 CORDEX RCMs compared with ensembled (SE and SME) outputs for the Akseki MS

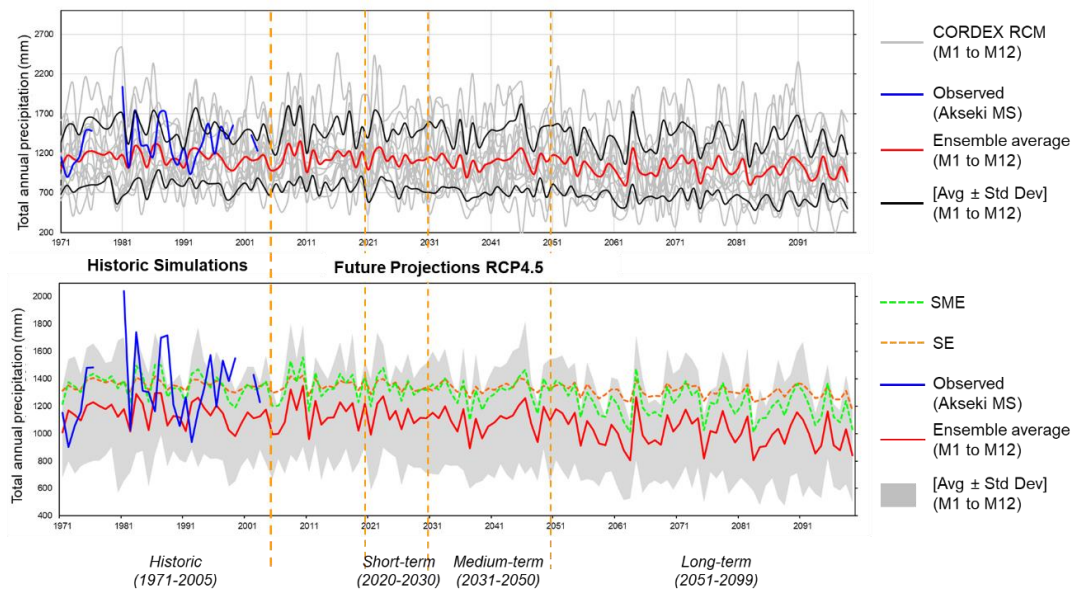


Figure 5.12. Historic and future (RCP4.5 scenario) precipitation simulations by 12 CORDEX RCMs compared with ensembled (SE and SME) outputs for the Akseki MS

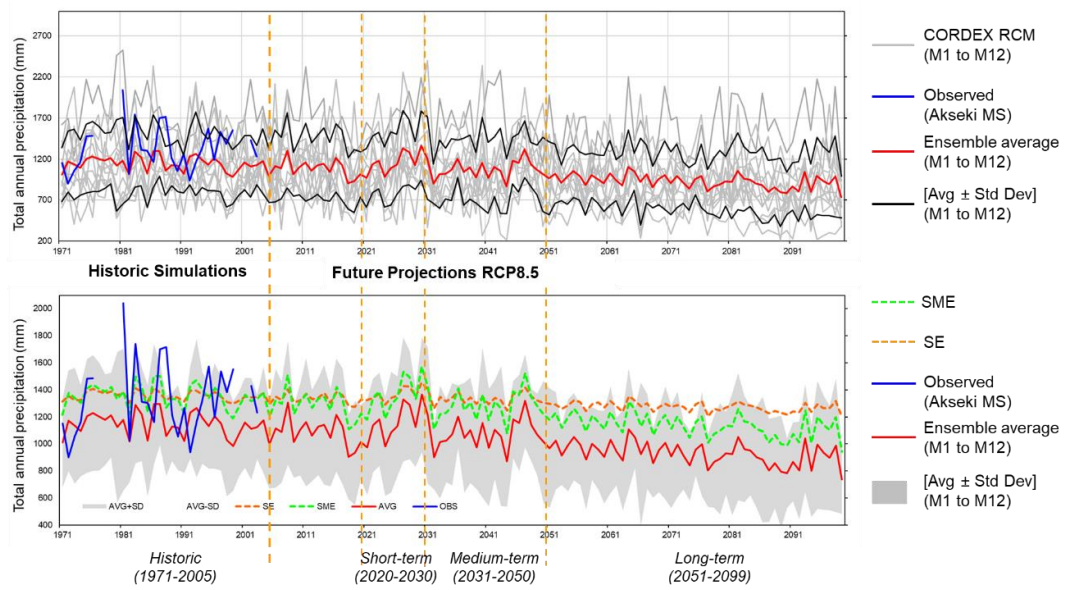


Figure 5.13. Historic and future (RCP8.5 scenario) precipitation simulations by 12 CORDEX RCMs compared with ensembled (SE and SME) outputs for the Akseki MS

The change in the mean annual temperature ($^{\circ}\text{C}$) and percent change in annual mean precipitation (%) at the Akseki MS based on the individual RCMs' and ensembled projections under RCP4.5 and 8.5 scenarios are given in Tables 5.7 and 5.8, respectively.

Table 5.7 Change in annual mean temperature (°C) projected for the Akseki MS

CORDEX RCM	Short term		Medium term		Long term	
	RCP4.5	RCP8.5	RCP4.5	RCP8.5	RCP4.5	RCP8.5
CNRM-CM5_ALADIN53	0.88	1.18	1.39	1.72	2.27	3.69
CNRM-CM5_CCLM4-8-17	1.02	1.07	1.14	1.42	1.99	3.32
CNRM-CM5_RCA4	0.83	1.25	1.39	1.45	2.16	3.59
EC-EARTH_CCLM4-8-17	0.89	1.19	1.33	1.77	2.09	3.44
EC-EARTH_HIRHAM5	1.08	1.29	1.33	1.87	2.11	3.48
EC-EARTH_RACMO22E	1.26	1.82	1.72	2.34	2.69	4.64
EC-EARTH_RCA4	1.13	1.35	1.61	2.08	2.44	3.97
CM5A-MR_RCA4	1.32	1.72	2.28	2.63	3.24	5.78
CM5A-MR_WRF331F	1.05	1.43	1.80	2.05	2.71	4.66
HadGEM2-ES_CCLM4-8-17	1.48	1.69	2.04	2.47	3.03	4.49
HadGEM2-ES_RACMO22E	2.16	2.41	2.99	3.74	4.22	6.15
HadGEM2-ES_RCA4	1.69	1.82	2.37	2.77	3.32	4.98
<i>CORDEX Mean</i>	1.23	1.52	1.78	2.19	2.69	4.35
SE	1.1	1.4	1.6	2.1	2.5	4.2
SME	1.2	1.4	1.7	2.1	2.6	4.3

Accordingly, for the Akseki MS, all models agree on a gradual increase in the annual mean temperature up to 2100 for both scenarios. 12 CORDEX RCMs project a long-term increase between 2 and 4°C for RCP4.5 and 3 and 6°C for the RCP8.5 scenario. Similarly SE and SME project a gradual increase up to 2100 that is expected to reach around 2.5°C for the RCP4.5 scenario and exceed 4°C for the RCP8.5 scenario.

Regarding the projections for total annual precipitation at the Akseki MS, all of the 12 RCMs and the ensembled outputs indicate a decrease in the long-term future under both RCP4.5 and 8.5 scenarios. Under the RCP4.5 scenario the projections of 12 RCMs on the percent decrease in precipitation at the Akseki MS range between 1% and 30%. For the RCP8.5 scenario the projections for the percent decrease in precipitation range between 9% and 47%. Ensembled projections by SE and SME indicate a 3% and 8% decrease for RCP4.5, respectively. For RCP8.5 a decrease of around 5% and 12% is projected for the Akseki MS by SE and SME.

Table 5.8 Percent change in annual mean precipitation (%) projected for the Akseki MS

CORDEX RCM	Short term		Medium term		Long term	
	RCP4.5	RCP8.5	RCP4.5	RCP8.5	RCP4.5	RCP8.5
CNRM-CM5_ALADIN53	-1.17	-0.57	-2.22	-4.03	-4.12	-8.56
CNRM-CM5_CCLM4-8-17	-5.61	2.05	-1.51	-5.58	-1.00	-11.18
CNRM-CM5_RCA4	-2.93	14.60	-3.54	2.03	-9.61	-17.69
EC-EARTH_CCLM4-8-17	-0.06	-1.08	0.48	-5.81	-6.56	-17.81
EC-EARTH_HIRHAM5	1.71	-7.95	-15.81	-12.49	-13.82	-21.52
EC-EARTH_RACMO22E	-17.30	0.69	11.66	-3.05	-1.03	-9.22
EC-EARTH_RCA4	9.48	6.81	0.74	-5.52	-4.49	-15.54
CM5A-MR_RCA4	2.71	-6.65	-28.29	-13.71	-29.62	-46.56
CM5A-MR_WRF331F	9.03	-2.20	-11.00	-7.23	-16.96	-28.86
HadGEM2-ES_CCLM4-8-17	5.90	-1.50	-0.81	-2.60	-16.79	-19.12
HadGEM2-ES_RACMO22E	-3.72	3.63	5.19	-1.90	-14.39	-16.19
HadGEM2-ES_RCA4	-10.20	-3.56	-6.45	-11.90	-22.62	-24.29
<i>CORDEX Mean</i>	-1.01	0.35	-4.30	-5.98	-11.75	-19.71
SE	-0.3	0.6	-1.0	-1.2	-2.9	-4.7
SME	-0.5	0.2	-2.5	-3.7	-7.8	-12.3

The analysis of climate projections for the Taurus mountains by Bravo et al. (2008) indicated 2.3°C and 3.2°C increases in the mean temperature for 2055s and 2085s, respectively, under the SRES B1 (comparable with RCP4.5) scenario and 3.2°C and 5.3°C increases for 2055s and 2085s, respectively, under the SRES A1Fi (comparable with RCP8.5) scenario. Additionally, for the mean precipitation, they found the highest decrease in precipitation for the Taurus mountains compared to the other Mediterranean mountains (Bravo et al., 2008). Their findings showed 4.1% (2055s) and 9.4% (2085s) decreases under the SRES B1 and decreases of 8.8% (2055s) and 22.4% (2085s) for the SRES A1FI scenario. Although their findings are not directly comparable with the results in this study due to the difference in the future time frames (i.e., 2055s: 2040-2069, 2085s: 2070-2099 (Bravo et al., 2008) vs. medium-term: 2031-2050, long-term: 2051-2099 in this study) and area of

analysis (Akseki MS in western Taurus vs. entire Taurus Mountain ranges) the results are seen to be in general agreement, particularly for temperature, and both for the ensemble mean and SE and SME projections. For precipitation, the CORDEX ensemble mean projection is seen to be very similar to the results by Bravo et al. (2008). But the SE and SME projections are slightly lower for Akseki MS compared to the findings by Bravo et al. (2008).

5.2 Hydrological Modeling

Following the Climate Analysis for the CASA (See Figure 4.1, Component 1), Hydrological Modeling (Component 2 in Figure 4.1) is conducted. The Hydrological Modeling is undertaken for the selected case study area comprising the Oymapınar basin, which is named as Hydrological Modeling Study Area or HMSA in this thesis. The hydrological model of the Oymapınar basin is then used in Streamflow Impact Analysis (Component 3 in Figure 4.1).

The initial stage of Hydrological Modeling is the development of mathematical rainfall-runoff models of the basin by the use of HEC-HMS, and HBV-light. Following that, the simulation efficiencies of the calibrated hydrological models in HEC-HMS, and HBV-light, which use different conceptual modeling approaches, are compared. The hydrological model of the basin that has better representation performances for the basin hydrology is selected to be further used in Component 3 of the study.

Details of the hydrological model development and calibration, results of the verification of model efficiencies, and evaluations regarding encountered advantages and disadvantages of the use of modeling softwares in the study are detailed in the following subsections.

5.2.1 Surface Flow Analysis of Oymapınar Basin

Within the scope of the study, a hydrological model to enable simulation of the inflow into the Oymapınar basin is required regarding the objective of the study. The basin topography based on EU-DEM v1.1 (EEA, 2016) is analyzed by the use of hydrologic modeling software WMS to delineate drainage lines, stream network, and boundaries of the Oymapınar basin. The subbasins of the Oymapınar basin are also formed based on the location of the streamgages in the basin that provides long-term historical streamflow data (See Figure 5.14). There are no streamgages located at the inlet of the reservoir that provides historical daily inflow data for the reservoir. The streamgages located on the Manavgat River mainstem are Şahapköprü (streamgage ID: E09A20), Sinanhoca (streamgage ID: E09A012), and Şelale (streamgage ID: E09A018) streamgages (See Figure 5.14).

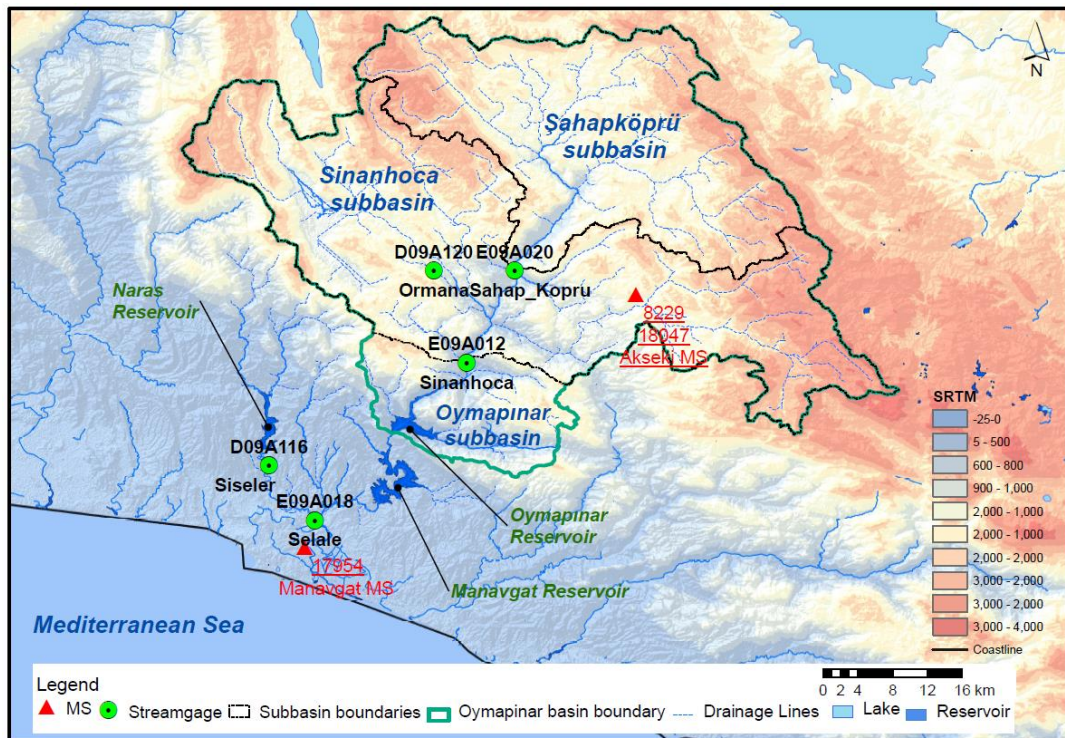


Figure 5.14. Oymapınar basin boundaries and its subbasins

As seen in Figure 5.15, analysis of the observed streamflow in Manavgat River at streamgages operated by DSI for the period between 1987-2015 indicates that the mean annual total flow at the Sinanhoca streamgage upstream of Oymapınar HEPP is 2039 hm³/yr. Downstream (downstream of Oymapınar and Manavgat HEPPs), at Şelale streamgage, total annual streamflow of Manavgat River reaches 3951 hm³/yr.

Downstream on Manavgat mainstream at Şelale streamgage, the highest monthly flow is observed in January whereas, upstream of Oymapınar HEPP, the peak monthly flow is observed in April. The peak flow in April at higher altitudes is interpreted to be due to the spring meltwater contribution both as surface runoff and discharge from karstic springs fed by higher altitudes of the basin.

Based on the long-term mean monthly flows, the highest monthly flow at the Sinanhoca streamgage is 295 hm³/mo in April. On the other hand, downstream at Şelale streamgage, at 4 mASL altitude, annual peak flow is created by the winter precipitation received as rainfall and it reaches 513 hm³/mo in January. After January the streamflow at Şelale streamgage gradually decreases.

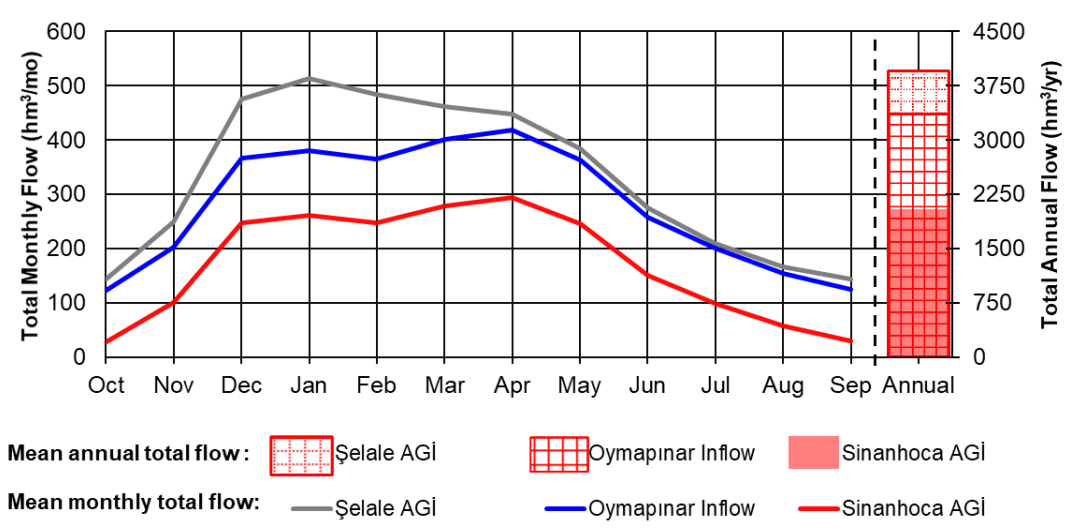


Figure 5.15. Long-term mean monthly and annual streamflows in Manavgat River for the period between 1987 and 2015

The Oymapınar inflow data indicated in Figure 5.15 is given for comparison purposes and is generated after the completion of the basin and river flow analysis of the Oymapınar basin, as detailed below. As mentioned above, no historical daily monitoring is available for the Oymapınar reservoir inflows. Therefore, nearest streamflow data are used for the determination of the Oymapınar inflows. For that purpose, the streamflow monitoring data from the flow gages on the Manavgat mainstream and its tributaries located within the Oymapınar basin are analyzed to delineate surface flow relationships within the basin.

Şahapköprü (streamgage ID: E09A020) and Sinanhoca (streamgage ID: E09A012) streamgages located upstream of Oymapınar reservoir on the Manavgat mainstream provide long-term continuous daily streamflow observation data. Total drainage areas of Şahapköprü and Sinanhoca streamgages are 680 km² and 1680 km², respectively. The cumulative drainage area of the Oymapınar basin feeding the Oymapınar reservoir and HEPP inflow is 1890 km². Relevant surface areas of subbasins and the relevant basin area ratios of each are provided in Tables 5.9 and 5.10.

Table 5.9 Surface areas of Oymapınar subbasins

Subbasin	Surface area (km²)	Cumulative surface area for the total basin (km²)
Şahapköprü	677	677
Sinanhoca	1005	1682
Oymapınar	204	1886

Table 5.10 Area ratios of total drainage areas discharging through streamgages

	Streamgage	Şahapköprü	Sinanhoca	Oymapınar
Streamgage	<i>Total Drainage Area (km²)</i>	<i>677</i>	<i>1682</i>	<i>1886</i>
Şahapköprü	<i>677</i>	1.00	2.48	2.78
Sinanhoca	<i>1682</i>	0.40	1.00	1.12
Oymapınar	<i>1886</i>	0.36	0.89	1.00

Accordingly, the basin area ratio of the Sinanhoca subbasin to the Şahapköprü subbasin is 2.5. Additionally, the basin area ratio of the Oymapınar basin to Şahapköprü and Sinanhoca subbasins are 2.8 and 1.1, respectively. Streamflow monitoring from Şahapköprü and Sinanhoca streamgages are analyzed to determine the relationship with the basin area ratio. Daily streamflow time series from both gages are compared for the period between 1992 and 2012. The hydrographs for both streamgages for 21 years period are shown in Figure 5.16. The comparison of the hydrographs indicates the same high and low flow periods and the same peak flow times for both streamgages. The Pearson's correlation coefficient (*Corr*) calculated for these flow time series is 0.92. The regression analysis of the flow at two streamgages is illustrated in Figure 5.17.

Accordingly, drainage basins for Sinanhoca and Şahapköprü streamgages are concluded to have significantly similar rainfall-runoff relationships. The drainage area ratio (DAR) method (Emerson et al., 2005; Asquith et al., 2006; Hortness, 2006; Archfield and Vogel, 2010; Zelelew and Alfredsen, 2014; Ergen and Kentel, 2016) is tested for Sinanhoca streamgage basin. For that purpose, the flow rate at Sinanhoca streamgage is calculated by the use of the DAR method on the streamflow at Şahapköprü gage. The calculated streamflow at Sinanhoca gage is compared with the observed flows and the *Corr* value is calculated. The *Corr* value for calculated and observed daily streamflow at Sinanhoca gage is 0.92. The regression analysis of calculated and observed time series of streamflow is shown in Figure 5.18.

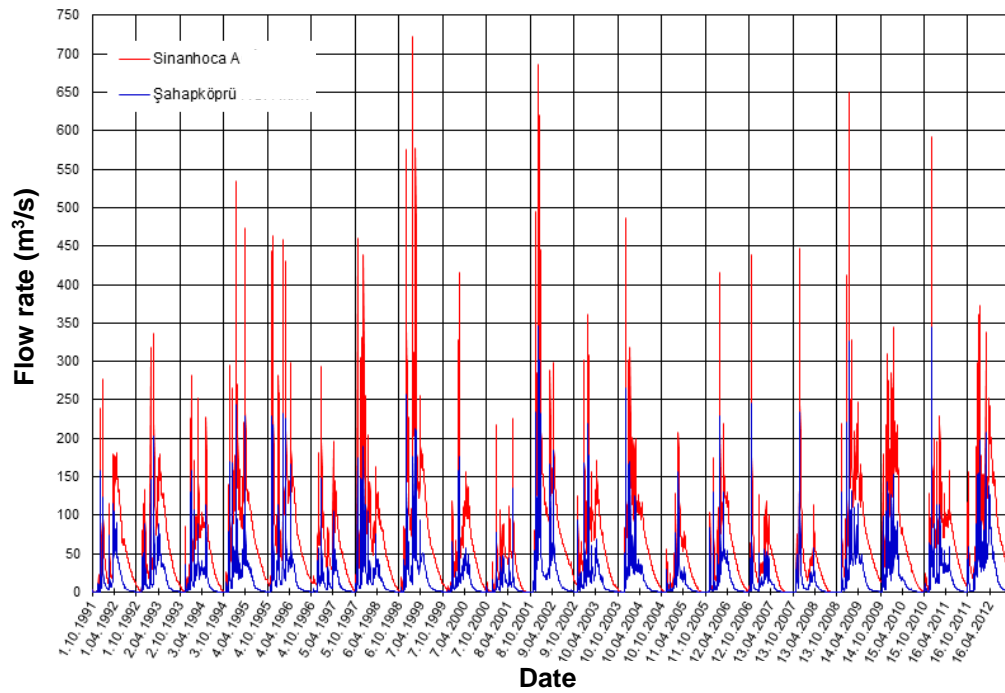


Figure 5.16. Comparison of hydrographs of Sinanhoca and Şahapköprü streamgages (1992 to 2012)

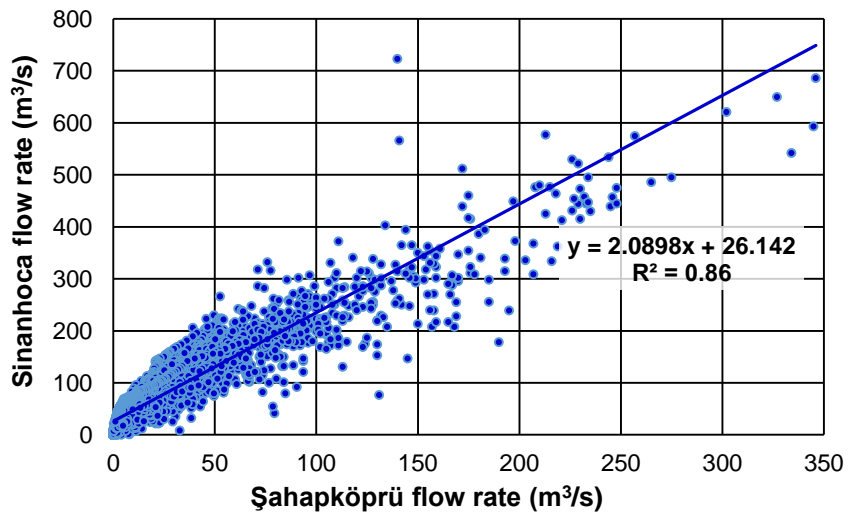


Figure 5.17. Linear Regression analysis of flow rates at Şahapköprü and Sinanhoca streamgages

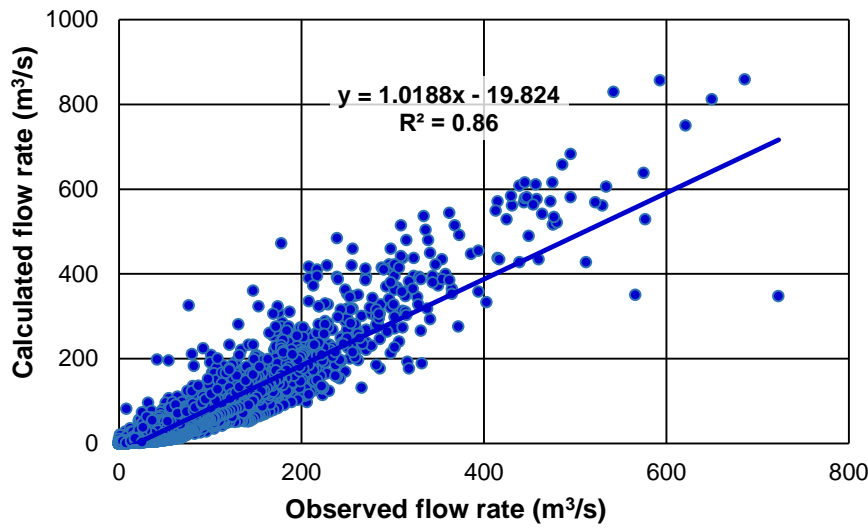


Figure 5.18. Comparison of calculated (with DAR method) and observed streamflows at Sinanhoca streamgage

The flow analysis is also conducted to delineate the relationship between Oymapinar inflow and streamflow at Sinanhoca streamgage. Although there is no streamflow monitoring for the inflow into the Oymapinar reservoir, the daily reservoir inflow is estimated by DSI. The time series for reservoir inflow estimates provided by DSI covers the period between 2007 and 2017. For the analysis, the estimated inflow data is compared with the streamflow observed at Sinanhoca streamgage for 11 years period. The relevant daily hydrographs formed by the use of both time series are given in Figure 5.19.

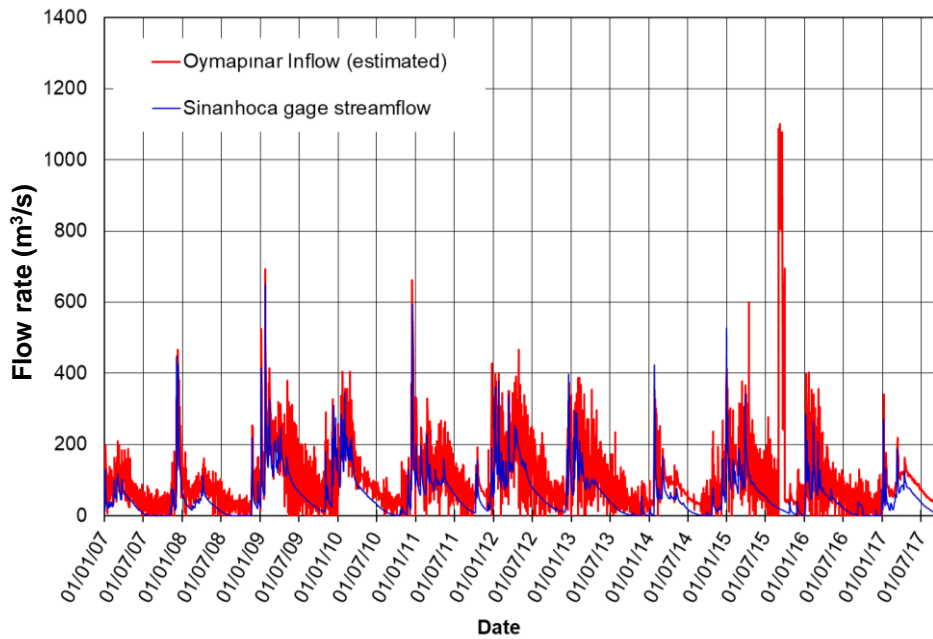


Figure 5.19. Comparison of Oymapinar Inflow estimates with Sinanhoca streamgage hydrograph

The superimposition of both hydrographs shows a similar seasonality for the streamflows, and high and low flow periods are seen to generally overlap. Although there are certain periods during which the estimated reservoir inflow significantly diverges from the trend in the streamflow at Sinanhoca streamgage (i.e., estimates after 2015). For further analysis of the relationship between the flow rates, the estimated inflow time series is required to be smoothed to remove the likely noise, that is seen to create erroneous fluctuations in the time series. Therefore, the flow rate analysis is conducted by the use of monthly total flows.

The Pearson correlation coefficient for reservoir inflow and Sinanhoca streamgage streamflow based on monthly total flows for 11 years period is 0.98, verifying a strong linear relationship between the two flows. Furthermore, regression analysis supports the linear relationship and demonstrates a similarity with the drainage area ratio ($y=1.1215x$) between the two basins. The regression analysis of Oymapinar

inflow with Sinanhoca streamflow in comparison with the drainage area ratio is shown in Figure 5.20.

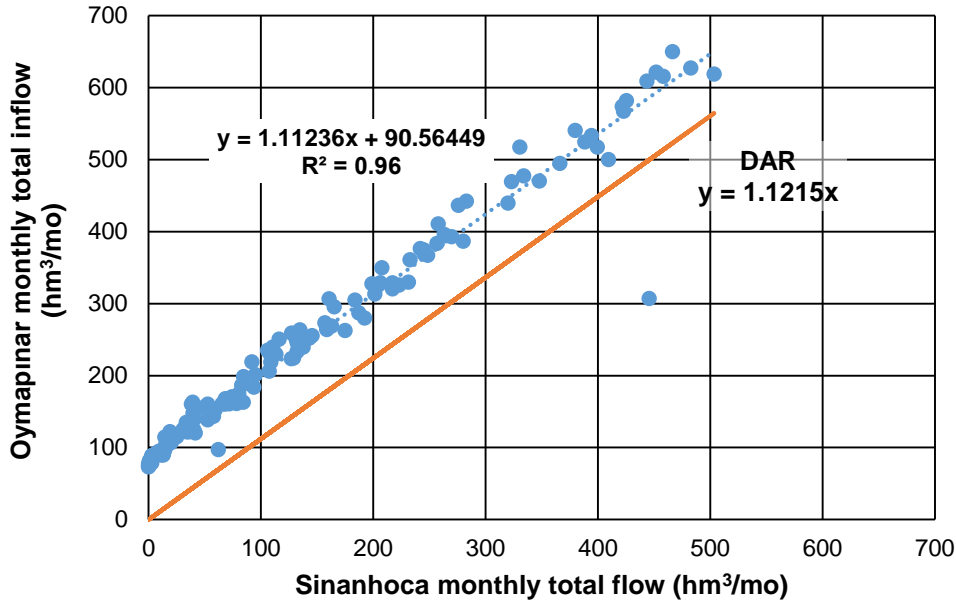


Figure 5.20. Regression analysis of Oymapınar inflow with streamflow observed at Sinanhoca streamgauge

The regression analysis of 11-year period monthly total flows indicates 0.96 R^2 . The regression function generated by the analysis with a high coefficient of determination verifies the linear relationship of the streamflow connected with the relative basin area ratios as well as the contribution of the direct groundwater discharge into the Oymapınar reservoir on top of the surface flow from the Manavgat River. Figure 5.21 gives a comparison of the calculated Oymapınar inflow generated using the regression function with the Oymapınar inflow estimates by DSI. The calculated Oymapınar inflow is obtained by the use of the regression function with observed streamflow at Sinanhoca streamgauge. The comparison in Figure 5.21 shows that regression model used for the conversion of Sinanhoca streamflow into the

Oymapınar inflow data provides satisfactory results. Consequently, the regression function generated through this analysis is used for the conversion of the simulated flow rates from the hydrological model into Oymapınar Inflows.

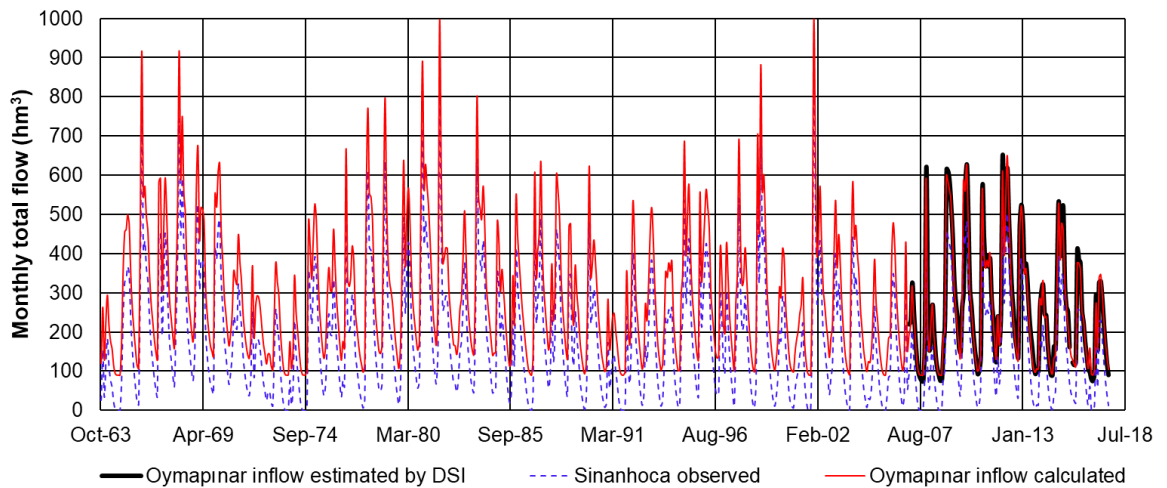


Figure 5.21. Comparison of Oymapınar Inflow generated using regression function with the DSI’s estimated inflows and observed streamflow at the Sinanhoca streamgage

5.2.2 Hydrological Model Development, Calibration and Validation in HBV-light

The hydrological model of the Oymapınar basin is developed in HBV-light according to the methodology detailed in Chapter 4. Confined parameters in the basin model that are identified based on topography and surface properties of the basin are assumed to be constant in the HBV-light model throughout the simulation duration. Free parameters that are used in the semi-empirical functions defining hydrological processes in the basin are optimized during the calibration of the model. In order to obtain a hydrological model with satisfactory simulation performance,

the model is calibrated in HBV-light by the use of the automated optimization tool. Depending on the availability of continuous daily time series of observed precipitation, temperature, and flow rate, the hydrological model is calibrated for the period between the 2013 and 2016 water years. After the optimization of the model parameters to obtain the best possible model of the basin in HBV-light, the model's skill to represent the basin hydrology is tested by a validation run using the time series of observed data for the 2017 water year. For the calibration and validation of the hydrological model, SPI's described in Chapter 4 are used.

As detailed in Chapter 4, the automated optimization tool in HBV-light uses Genetic Algorithm and Powel optimization module that is based on a stochastic Genetic Algorithm approach. The GAP optimization tool runs an iterative process to obtain the global optimum solution of the objective function of the model that provides the best fit of the simulated flow to the observed flow.

Before the use of the GAP tool for calibration of the model, the parameters that define the iterative optimization process in the Genetic Algorithm are identified by trial runs. The determination of GAP parameters is aimed to adjust the optimization tool for the model process in order to avoid overfitting that diminishes the simulation efficiency but to allow sufficient iterations for the optimization of the parameters.

The parameters of the GAP module under Population, Reproduction, and Model settings are selected as follows:

- To define the Number of Parameters (NP) under Population Settings 13 runs are conducted by using values within the range of 50 -1000 (the maximum number of parameters in parameter set allowed in the HBV-light is 1000) to observe the change in the *NSE*, *KGE* and *VE*. It is observed that NP=650 value provides the best values for the SPI's in general, whereas for values less than 650 uncertainty creates a natural fluctuation in SPI's (Figure 5.22). Hence, the NP value is taken as 650.

- The Number of Model Runs and the Number of Runs for Local Optimization (Powell) under the Model Settings define the number of iterative cycles to be used in the optimization process. GAP tool uses the GA algorithm to search for the global optimum in an iterative process defined by the Number of Model Runs parameter and then uses the Powell method for local optimization at the defined global optimum point to find the best solution. To define the most efficient numbers, the model is run for values ranging between 5000 and 22000, and between 1000 and 4400 for the number of cycles of the GA and Powell algorithm, respectively. The different values for these parameters are seen to create no significant change in SPI values obtained from the model (Figure 5.22).
- Other parameters related to the details of crossing-over calculations in GA under the Reproduction Settings such as the probability of mutations and similar are taken as the default values defined in the GAP optimization tool.

As a result, the GAP module is used with 650 parameters in each parameter set for every generation to be run for 5000 cycles of GA to reach the global optimum and 1000 cycles for local optimization with the Powell Algorithm. Furthermore, due to the stochastic nature of the GA approach, the calibration process with the GAP module is repeated 100 times to analyze for the involved uncertainty. For the automated calibration in the optimization tool, the main goodness of fit measure to define the fitness of the solution for the objective function is selected as *NSE*.

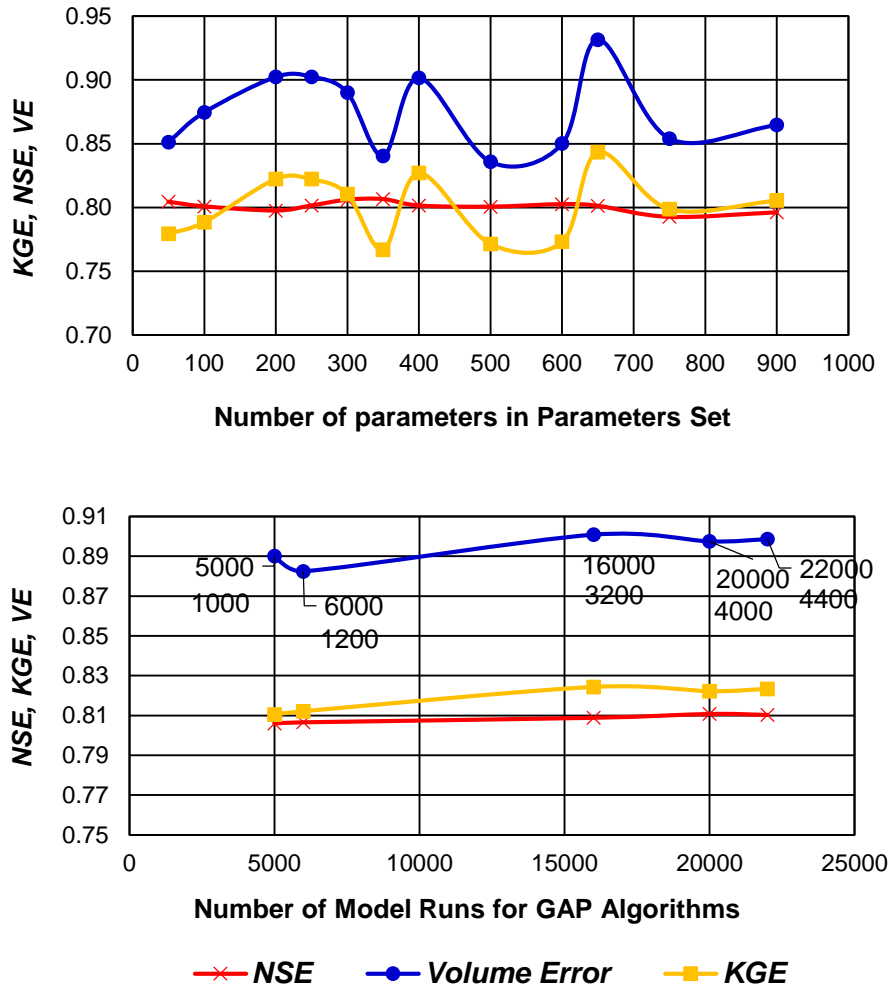


Figure 5.22. The change in SPI values for different “Number of Parameters” and “Number of Model Runs” parameters in GAP tool

The results from 100 calibration runs of the model for the period between 2013-2016 water years with the GAP optimization tool in HBV-light are analyzed to determine potential ranges of model efficiency. The statistical analysis of the optimum parameter sets generated in 100 calibration runs is given in Table 5.11. As it is seen in Table 5.11, even the minimum values of the SPI’s achieved at the end of 100 calibration runs indicate satisfactory model performance. Furthermore, the small range of fluctuations in *NSE* (between 0.79 and 0.81) due to the uncertainty of GAP

optimization indicates that the uncertainty in the model is insignificant. Similarly, the ranges of uncertainty for other SPI's are also at acceptable levels. The SPI values given for the *NSE*-Maximum in Table 5.11 show the SPI values that are obtained by the calibration run that achieved the best *NSE* value among all 100 calibration runs.

Table 5.11 Fluctuations in SPI values for HBV-light model due to uncertainties in calibration (for 100 calibration runs)

	<i>NSE</i>	<i>R</i> ²	<i>VE</i>	<i>KGE</i>
Minimum	0.79	0.80	0.80	0.75
Mean	0.80	0.82	0.87	0.80
Median	0.80	0.81	0.87	0.81
Maximum	0.81	0.83	0.92	0.83
<i>NSE</i>-Maximum	0.81	0.82	0.91	0.83

Three alternatives of the calibrated hydrological model of the basin are formed based on the results of 100 calibration runs. These are Model 1, using the parameter values that generated the highest *NSE* in 100 calibration runs, Model 2, using the mean of the parameter values obtained from 100 calibration runs, and Model 3, using the median of the parameter values obtained from 100 calibration runs. The SPI values of three HBV-light model alternatives are compared for calibration (2013-2016) and validation (2017) periods. The results are given in Table 5.12. Accordingly, Model 3, using the median parameter values from 100 calibration runs, is selected as the final calibrated HBV-light model.

Table 5.12 Comparison of simulation efficiencies of Model 1, Model 2, and Model 3

SPI	Model 1		Model 2		Model 3	
	Calibration (2013-2016)	Validation (2017)	Calibration (2013-2016)	Validation (2017)	Calibration (2013-2016)	Validation (2017)
<i>r</i>	0.90	0.88	0.90	0.89	0.90	0.90
<i>NSE</i>	0.81	0.67	0.79	0.70	0.80	0.70
<i>R²</i>	0.82	0.78	0.81	0.80	0.81	0.81
<i>RMSE</i>	1.28	1.21	1.35	1.16	1.32	1.16
<i>KGE</i>	0.83	0.64	0.79	0.67	0.81	0.65
<i>VE</i>	0.91	0.74	0.85	0.81	0.87	0.76

The comparison of the SPI values from Model 3 with the threshold values for the classification of simulation efficiency of the hydrological model is given in Table 5.13. The comparison of simulated and observed hydrographs for calibration and validation periods is illustrated in Figure 5.23.

Table 5.13 Simulation performance classification of calibrated HBV-light model

SPI	Unit	Performance classification			Model results	
		Satisfactory	Good	Very good	Calibration (2013-2016)	Validation (2017)
<i>NSE</i>	-	0.5-0.7	0.7-0.8	0.8-1	0.80	0.70
<i>R²</i>	-	0.6-0.75	0.75-0.85	0.85-1	0.81	0.81
<i>RMSE</i>	mm	-	-	-	1.32	1.16
<i>RMSE/σ_{obs}</i>	-	0.6-0.7	0.5-0.6	0-0.5	0.45	0.60
<i>VE</i>	-	0.85-0.9	0.9-0.95	0.95-1	0.87	0.77
<i>KGE</i>	-	0.5-0.75	0.75-1		0.81	0.65
<i>r</i>	-				0.90	0.90
<i>α</i>	-				0.89	1.24
<i>β</i>	-				0.87	1.23

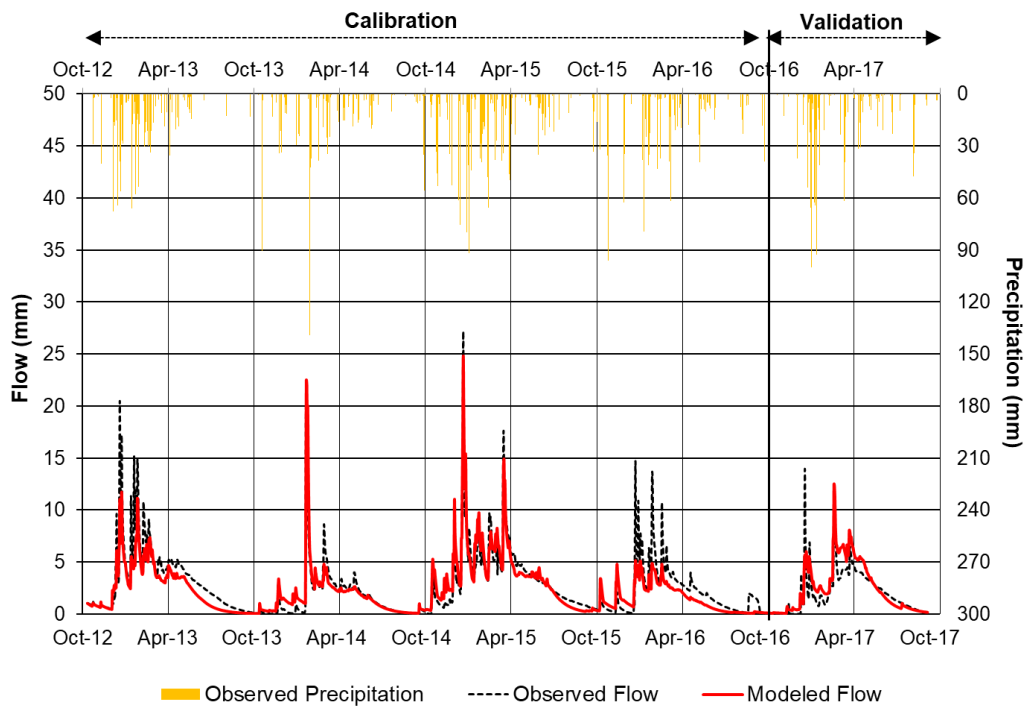


Figure 5.23. Comparison of modeled (HBV-light) and observed hydrographs of Sinanhoca streamgauge for calibration and validation periods

5.2.3 Hydrological Model Development, Calibration and Validation in HEC-HMS

The hydrological model of the Oymapınar basin, delineated in WMS, is developed in HEC-HMS according to the surface and vegetation cover properties by following the methodology detailed in Chapter 3. Following the development of the model, basin parameters are optimized through calibration of the model based on the observed streamflow at Sinanhoca streamgauge for the duration between the 2013 and 2016 water years. The efficiency of the calibrated model to represent basin hydrology is tested with validation for observed flow rates in the 2017 water year. For the optimization of the model in the automated calibration tool of HEC-HMS,

NSE is selected as the main SPI. Furthermore, manual calibration is also used to improve the simulated hydrograph to have a better fit with the observed hydrograph with respect to hydrological components (e.g., baseflow and recession, losses due to surface depression and canopy, etc.). The comparison of the simulated hydrograph from the calibrated model with the observed hydrograph of the Sinanhoca streamgage is shown in Figure 5.24.

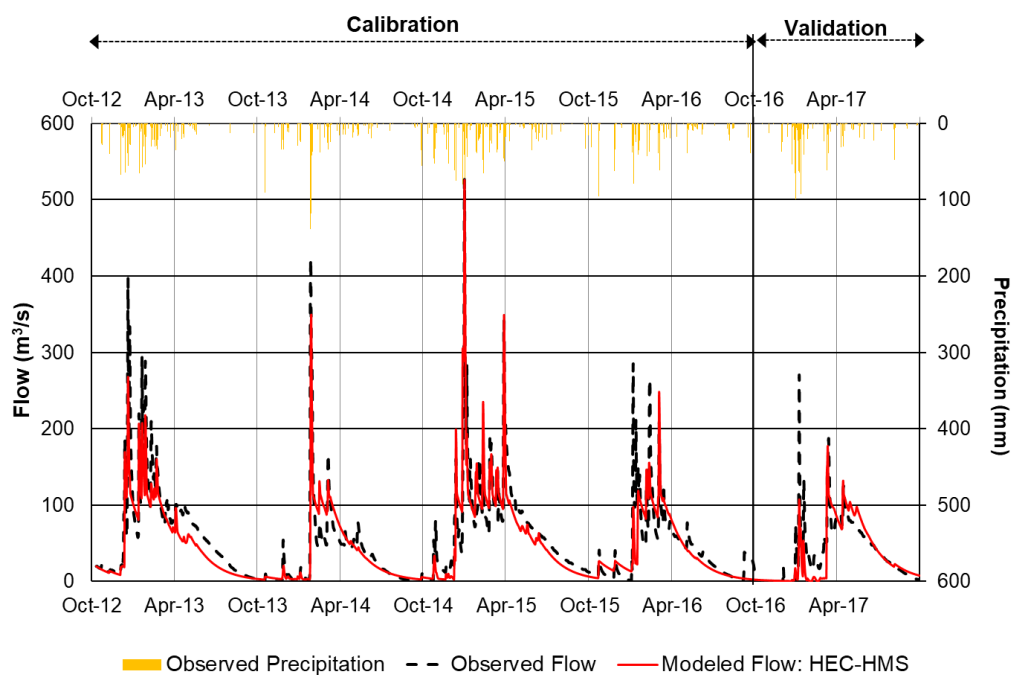


Figure 5.24. Comparison of modeled (HEC-HMS) and observed hydrographs of Sinanhoca streamgage for the calibration and validation periods

As seen in Figure 5.24, the calibrated model has satisfactory performance and simulates the Sinanhoca hydrograph with a good fit with the observed. For the validation period, the performance of the model is seen to decrease. However, the

calibrated model still achieves a satisfactory representation of the peak flows during spring and the decrease in the surface flow at the start of the dry period.

NSE that is used for the automated calibration of the model is known to give higher weight to high flows compared to low flows. Hence manual calibration is particularly used to improve the hydrologic simulation to have a better representation of the low flow periods and a better fit with the flow recession in the observed hydrograph which creates a relative decrease in the final *NSE* value obtained from the calibrated model. Hence, other SPI's are also taken into consideration during the calibration of the model in HEC-HMS. Regarding the intended use of basin hydrograph, assessment of the streamflow during the dry season and low flow periods is important. Therefore, the model is calibrated with a trade-off of the representation of peak flows against a better representation of the base flow and low flow periods. The SPI values calculated for calibration and validation periods and the comparison with the thresholds for classification of modeling efficiency are shown in Table 5.14. The SPI values of the HEC-HMS model verify good/very good simulation performance both for calibration and validation periods.

Table 5.14 Simulation performance classification of calibrated HEC-HMS model

SPI	Unit	Performance classification			Model results	
		Satisfactory	Good	Very good	Calibration (2013-2016)	Validation (2017)
<i>NSE</i>	-	0.5-0.7	0.7-0.8	0.8-1	0.78	0.74
<i>R²</i>	-	0.6-0.75	0.75-0.85	0.85-1	0.79	0.72
<i>RMSE</i>	mm	-	-	-	26.87	20.87
<i>RMSE/σ_{obs}</i>	-	0.6-0.7	0.5-0.6	0-0.5	0.47	0.56
<i>VE</i>	-	0.85-0.9	0.9-0.95	0.95-1	0.90	0.93
<i>KGE</i>	-	0.5-0.75	0.75-1		0.84	0.83
<i>r</i>	-				0.89	0.85
<i>α</i>	-				0.93	1.02
<i>β</i>	-				0.90	0.93

5.2.4 Comparison of Model Efficiencies and Model Selection

In order to compare the results from hydrological models in HBV-light and HEC-HMS, the streamflow simulated in HBV-light for the unit basin area is converted to the total flow from the model basin. The calculated SPI values for the calibrated hydrological models and regarding classifications of simulation performances for calibration and validation periods are compared in Table 5.15. Furthermore, simulated hydrographs from both models are compared with the observed hydrograph of Sinanhoca streamgauge for calibration and validation periods in Figure 5.25.

Table 5.15 Comparison of simulation performances of hydrological models in HEC-HMS and HBV-light

SPI	Performance classification			HBV-light model		HEC-HMS model	
	Satisfactory	Good	Very good	Calibration (2013-2016)	Validation (2017)	Calibration (2013-2016)	Validation (2017)
<i>NSE</i>	0.5-0.7	0.7-0.8	0.8-1	0.80	0.70	0.78	0.74
<i>R²</i>	0.6-0.75	0.75-0.85	0.85-1	0.81	0.81	0.79	0.72
<i>RMSE/σ_{obs}</i>	0.6-0.7	0.5-0.6	0-0.5	0.45	0.60	0.47	0.56
<i>VE</i>	0.85-0.9	0.9-0.95	0.95-1	0.87	0.77	0.90	0.93
<i>KGE</i>	0.5-0.75	0.75-1		0.81	0.65	0.84	0.83
<i>r</i>				0.90	0.90	0.89	0.85
<i>α</i>				0.89	1.24	0.93	1.02
<i>β</i>				0.87	1.23	0.90	0.93

Color coding for simulation performance classes:

Satisfactory	Good	Very good
--------------	------	-----------

Accordingly, for calibration and validation periods, the HBV-light model achieves simulation performances between satisfactory and very good for most of the SPIs except for Volume Error (*VE*) indicating unsatisfactory simulation performance for

the validation period. For the HEC-HMS model, SPIs indicate simulation performances between satisfactory and very good for both calibration and validation periods. Regarding the *VE*, the HEC-HMS model shows even better simulation performance for the validation period. On the other hand, for the HEC-HMS model, the values of other SPIs are seen to drop slightly for the validation period, although the simulation performances of the model still remain between satisfactory and very good. Hence, with respect to the SPIs, the HEC-HMS model shows relatively better simulation skills compared to the HBV-light model.

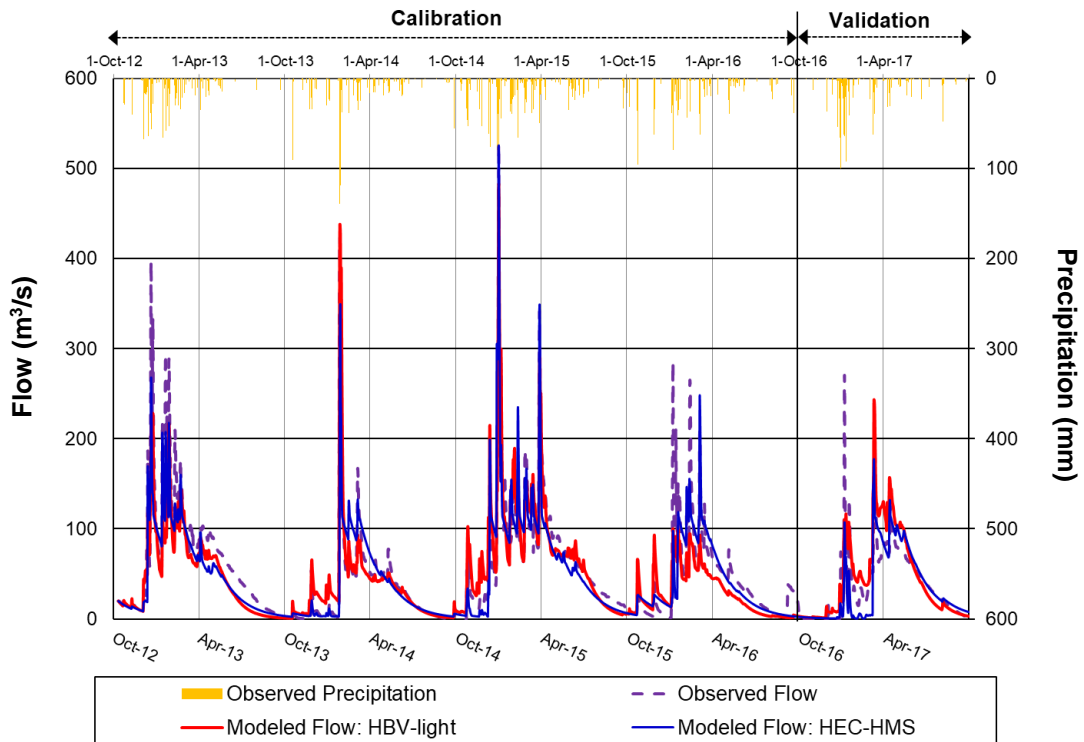


Figure 5.25. Comparison of modeled hydrographs in HEC-HMS and HBV-light with the observed hydrograph

Examination of the simulated hydrographs in comparison with the observed hydrograph shows that both models tend to underestimate the peak flows, in general.

For the early periods of simulation, both models are observed to generate very similar results. However, at later stages, HEC-HMS is seen to provide a slightly better simulation for the recession curve in the hydrograph. This is considered to result in relatively better SPI values of the HEC-HMS model for the validation period compared to the HBV-light model.

Respecting the model development and calibration in HEC-HMS and HBV-light software, HBV-light can be designated as less data-intensive compared to the HEC-HMS. HBV-light enables the development of the model with low knowledge of basin properties and parameter values assigned to represent the basin hydrology because the automated optimization module enables searching for the global optimum regardless of the initial values assigned to the calibrated parameters (i.e., Free Parameters, Section 4.2.2). However, the automated calibration tool of HEC-HMS works on the local optimum which is considerably influenced by the initial values assigned to the basin parameters related to the hydrological properties.

As a result, in HBV-light the modules used for the basin model development and calibration can be classified as more user-friendly. Hence, HBV-light requires less time for model development and calibration compared to HEC-HMS. Therefore, considering similar performance efficiencies achieved in both models, it is to say that, HBV-light has advantages over HEC-HMS due to its ease of use, particularly for basins where not much data and background information are available and can be preferred for certain study objectives over HEC-HMS.

Nevertheless, the ease-of-use of HBV-light created by its relatively simple model algorithm compared to HEC-HMS is also interpreted to cause certain weaknesses of HBV-light. As detailed in Chapter 4, unlike HEC-HMS, HBV-light uses certain predefined physical models for the mathematical expression of hydrological processes which reduces the flexibility of the model to simulate the basin. HEC-HMS enables selection of the adequate physical approaches to simulate the elements of hydrological and meteorologic conditions of the basin. Furthermore, owing to its stochastic optimization tool calibration in the HBV-light model is scarcely

dependent on the initial parameters related to the basin hydrology which reduces the control of the modeler over the basin hydrology defined in the model, particularly for users less proficient in HBV-light. Consequently, concerning the representation of the hydrological processes in the Oymapınar basin, the model developed in HEC-HMS is considered to be more representative and selected to be used for further analysis of the climate change impact on streamflow detailed in consecutive sections.

5.3 Streamflow Impact Assessment

The study aims to assess impacts on the streamflow and to obtain an indication of the likely impact on the water supply for hydropower in the Oymapınar basin. The hydrological model calibrated in Component 2 (See Figure 4.1) is used for the Climate Change Streamflow Impact Assessment (Component 3) in the study and Component 3 focuses on the research of likely impacts on Manavgat River flow feeding the Oymapınar reservoir.

Historical and future runs of the hydrological model with the temperature and precipitation time series from 12 CORDEX RCMs (See Table 4.7 in Section 4.3.2) are used for the simulation of the streamflow in the basin. The comparison of streamflow simulations from historical and future periods is used to calculate potential changes in streamflow in Manavgat River at the outlet of the model basin (i.e., Sinanhoca streamgage). The streamflows simulated by the hydrological model are used to obtain inflows into the Oymapınar reservoir based on the regression model obtained in the flow analysis for the Oymapınar basin (Section 5.2.1). The study flow to obtain the results presented and discussed in this section is shown in Figure 5.26. The relevant results and evaluations are detailed in the consecutive subsections.

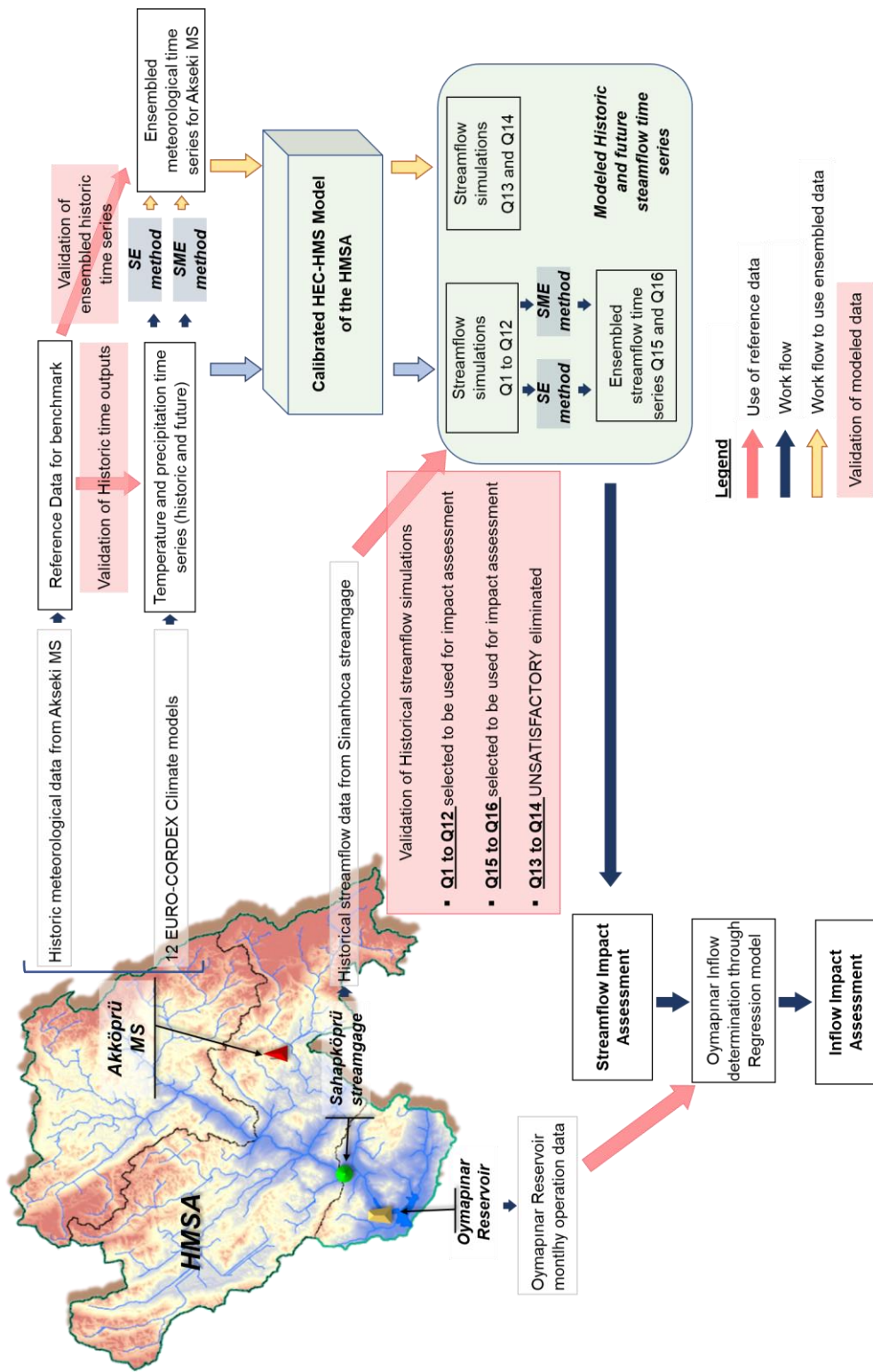


Figure 5.26. Study flow to obtain Streamflow Impact Assessment results

5.3.1 Analysis of Streamflow Projections using Individual RCMs (Q1-Q12)

For the assessment of the climate change impact on streamflow calibrated model is used to simulate the streamflow based on the meteorological outputs of 12 CORDEX RCMs (See Table 4.7 in Section 4.3.2). Simulated streamflows from Q1 to Q12 generated by using historic and future simulations of RCMs from M1 to M12 represent historic (1971 to 2005) and future (2020 to 2030 for short-, 2031 to 2050 for medium-, and 2051 to 2099 for long-term future) flow rates at the Sinanhoca streamgauge. The relevant methodology is detailed in Section 4.3.1.

5.3.1.1 Validation of Historical Streamflow Simulations (Q1 to Q12) and Comparison with Observed Flows

The hydrological model is run by the use of the climate forcings simulated by 12 CORDEX RCMs that provide continuous time series for the historical period between 1971 and 2005 and the future period between 2006 and 2099. The time series of two main climatologic parameters, temperature and precipitation that control the rainfall-runoff relationship in the basin are used to run the hydrological model. The streamflow simulations from the hydrological model runs based on historical simulations of 12 individual climate models are validated against the observed streamflow in the same period. The daily hydrographs generated from the historical streamflow simulations (Q1 to Q12) superimposed with the observed streamflow are provided in Appendix E. The monthly hydrographs produced from the daily time series are displayed in Figure 5.27.

The SPI values indicating the performance efficiency of streamflow simulations obtained from the individual climate model runs in the hydrological model based on the monthly streamflow time series are given in Table 5.16.

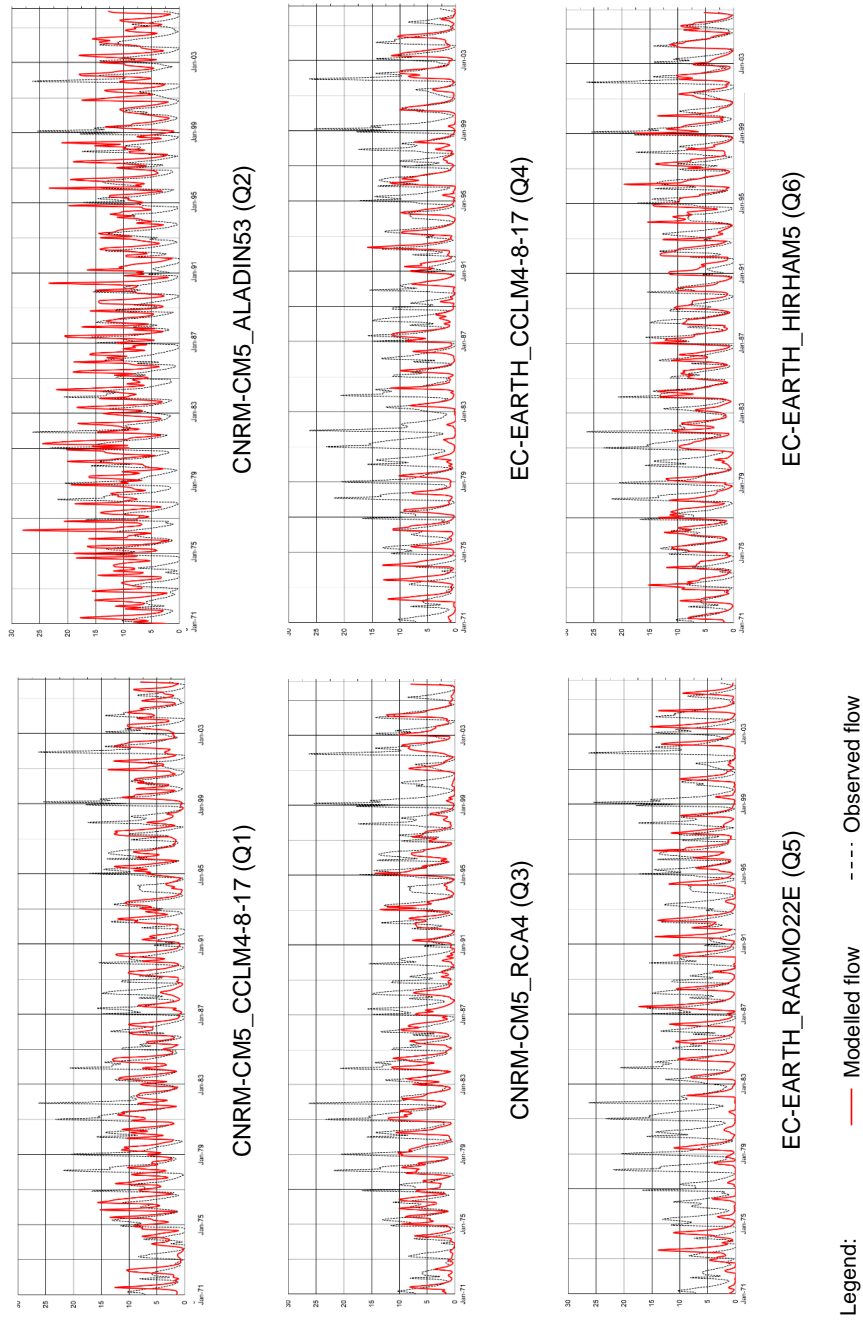


Figure 5.27. Monthly hydrographs of the streamflow simulations (Q1-Q12) in the hydrological model based on the historical (1971 to 2005) time series of RCMs (In all graphs x axis: dates in months of the year, y axis: monthly mean flow rates (hm^3/d))

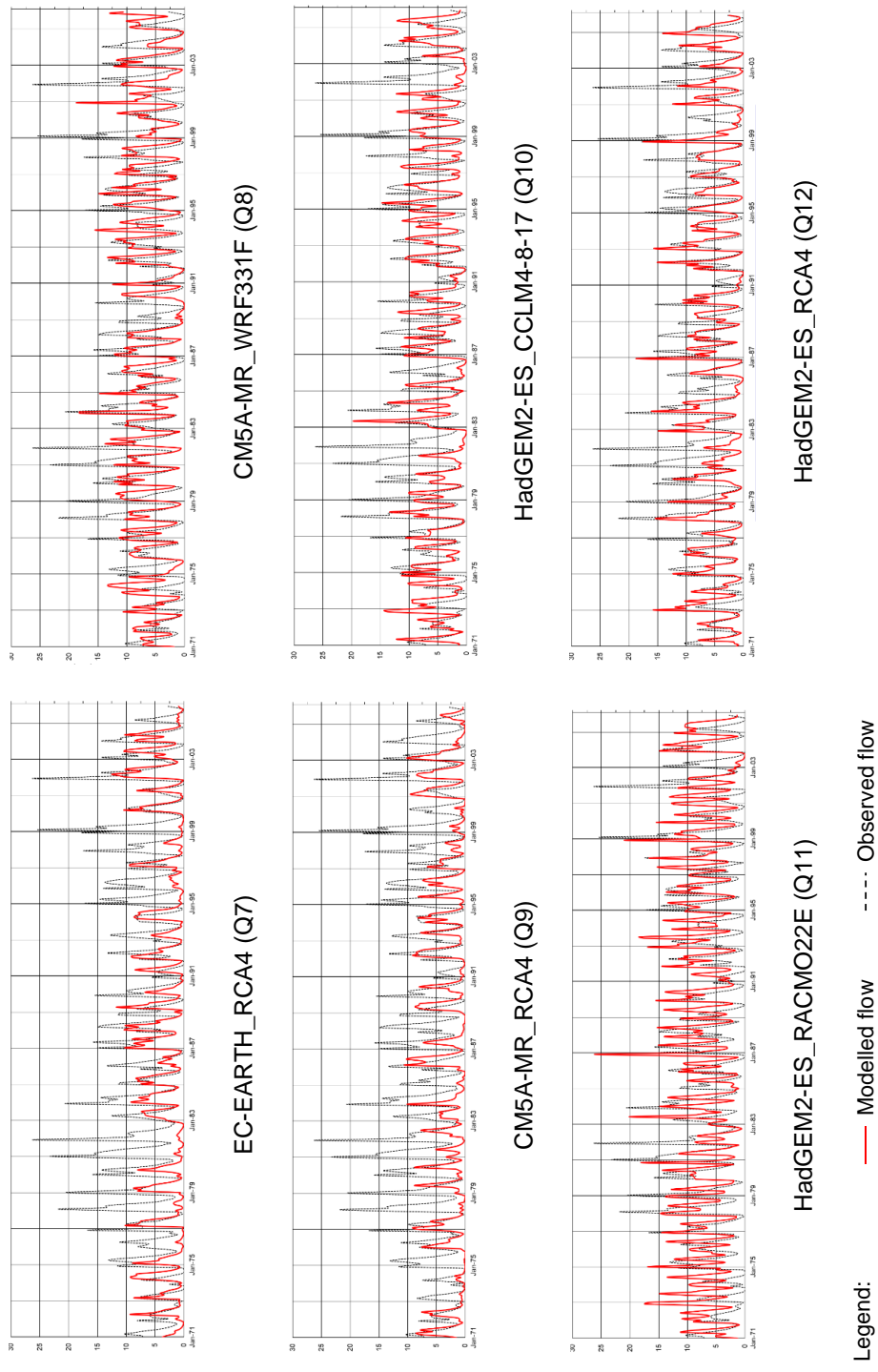


Figure 5.27. (continued)

Table 5.16 Statistical Performance Indicators for monthly streamflow simulations (Q1 to Q12) to replicate the observed streamflow at the Sinanhoca streamgauge between 1971 and 2005

Climate Model	CNRM-CM5_ALADIN53	CNRM-CM5_CCLM4-8-17	CNRM-CM5_RCA4	EC-EARTH_CCLM4-8-17	EC-EARTH_HIRHAM5	EC-EARTH_RACMO22E	EC-EARTH_RCA4	CM5A-MR_RCA4	CM5A-MR_WRF331F	HadGEM2-ES_CCLM4-8-17	HadGEM2-ES_RACMO22E	HadGEM2-ES_RCA4
<i>Corr</i>	0.32	0.26	0.43 ¹⁰	0.13	0.43	-0.12	0.21	0.16	0.33	0.25	0.25	0.43
<i>R</i> ²	0.10	0.07	0.19	0.02	0.19	0.01	0.05	0.03	0.11	0.06	0.06	0.19
<i>NSE</i>	-0.73	-0.16	-0.09	-0.67	0.04	-1.12	-0.47	-0.60	-0.10	-0.21	-0.37	0.02
<i>PBIAS</i> (%)	-55.9	12.6	39.8	53.0	11.3	57.5	49.5	58.1	-1.6	18.6	-20.5	23.1
<i>RMSE</i> (<i>hm</i> ³)	6.42	5.26	5.09	6.31	4.79	7.11	5.92	6.18	5.11	5.38	5.72	4.85
<i>RSR</i>	1.32	1.08	1.04	1.29	0.98	1.46	1.21	1.27	1.05	1.10	1.17	0.99
<i>VE</i>	0.44	0.87	0.60	0.47	0.89	0.42	0.50	0.42	0.98	0.81	0.80	0.77
<i>KGE</i>	0.12	0.19	0.22	-0.08	0.38	-0.29	-0.01	-0.12	0.30	0.19	0.21	0.34

Accordingly, among the 12 streamflow simulations, the EC-EARTH_HIRHAM5 generated relatively high SPIs indicating relatively good skills for all SPIs for the replication of the historical monthly streamflow. HadGEM2-ES_RCA4, CM5A-MR_WRF331F, CNRM-CM5_RCA4, and CNRM-CM5_CCLM4-8-17 are other RCMs that provided relatively better simulation performances than the other RCMs in the ensemble. Among these models, CNRM-CM5_RCA4, EC-EARTH_HIRHAM5, and HadGEM2-ES_RCA4 show the best correlations with the observed monthly mean streamflows, whereas the other models have relatively poor

¹⁰ The three-best values for each SPI are indicated in bold

skills for correlation compared to these three models. On the other hand, the other well-performing two models (i.e., CM5A-MR_WRF331F, and CNRM-CM5_CCLM4-8-17) have relatively good skills regarding the bias parameters. Furthermore, respecting the Volume Error, CM5A-MR_WRF331F is seen to provide "very good" and CNRM-CM5_CCLM4-8-17 and EC-EARTH_HIRHAM5 verify "satisfactory" level performance (See Table 4.6 and Section 4.2.5 for performance level thresholds of SPIs). In addition, the three RCMs (CCLM4-8-17, RACMO22E, RCA4) nested in the HadGEM2-ES are seen to generate relatively high *VE* values that are close to the satisfactory level. Among the 12 RCMs, EC-EARTH_RACMO22E performed relatively poorly in streamflow simulation compared to the other climate model runs. This is considered because of the weakness of EC-EARTH_RACMO22E in the hydrological model to estimate peak flows which also cause high bias and low correlation with the observed. Furthermore, as seen in Figure 5.27, among 12 models some are seen to be particularly weak in the simulation of the peak flows (e.g., CNRM-CM5_RCA4, HadGEM2-ES_RCA4), whereas some others are weak in the simulation of the low flows (e.g., CNRM-CM5_ALADIN53, HadGEM2-ES_RACMO22E).

To analyze the high and low flow conditions simulated for the 12-RCMs, daily mean flow rates (m^3/s) are ranked from smallest to largest and compared with the observed flow rates through a scatter plot and for their cumulative distribution function (CDF) curves (Figure 5.28). Accordingly, Q6, Q8, Q11, and Q12 generated flow rates that are the most similar to the flow rates observed in the basin. However, Q8 and Q12 are seen to slightly overestimate high and underestimate low flows, whereas Q6 slightly underestimates flow rates in general and Q11 overestimates high flows. Among 12 flow simulations, Q9 is observed to distinctly underestimate and Q2 overestimate flow in the basin.

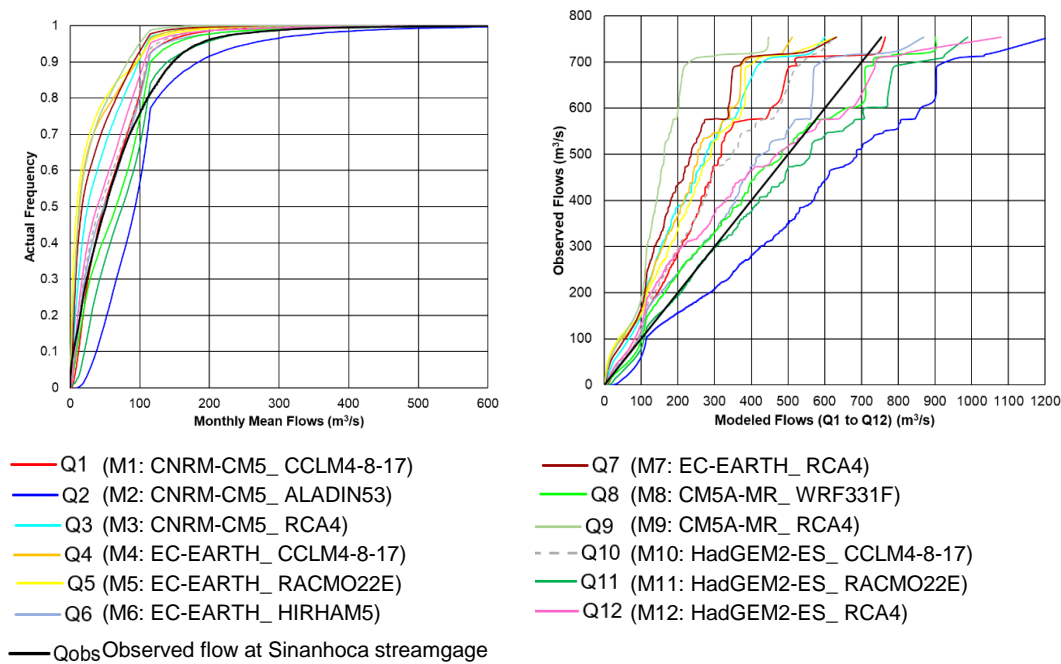


Figure 5.28. Empirical cumulative distribution function and comparison of observed and modeled daily mean flows (m^3/s)

5.3.1.2 Future Streamflow Projections (for Q1 to Q12)

At the next step of the analysis, future projections by 12 RCMs are used to analyze the effect of the climate change signal on streamflow. For that purpose, the calibrated hydrological model is run by the use of future temperature and precipitation projections for the RCP4.5 and RCP8.5 scenarios by the individual climate models. The streamflow projections (Q1 to Q12) in the means of annual total flows for RCP4.5 and 8.5 scenarios by individual climate model runs are illustrated in Figure 5.29. As seen in Figure 5.29, annual total streamflow simulations for historic and future periods based on 12 RCMs are highly variable. On the other hand, the ensemble mean of simulations of Q1 to Q12 tends to underestimate the historical streamflow. Regarding the future projections, a decrease in the streamflow is observed for both of the scenarios by taking the general trend in the signal generated

displayed by the ensemble mean. Furthermore, for the RCP8.5 scenario, the decreasing trend is more pronounced than it is for the RCP4.5 scenario. In the long-term future under the higher radiative forcing of the RCP8.5 scenario which is likely to cause a more pronounced decrease in the precipitation for the entire CASA (See Section 5.1.3.1) and also for the Akseki MS (See Section 5.1.3.2) than the RCP4.5 scenario, a higher impact on the streamflow is also projected. Furthermore, the concurrent increase in the temperature which is again projected to be more pronounced for the RCP8.5 scenario is considered to aggravate the impact on surface waters.

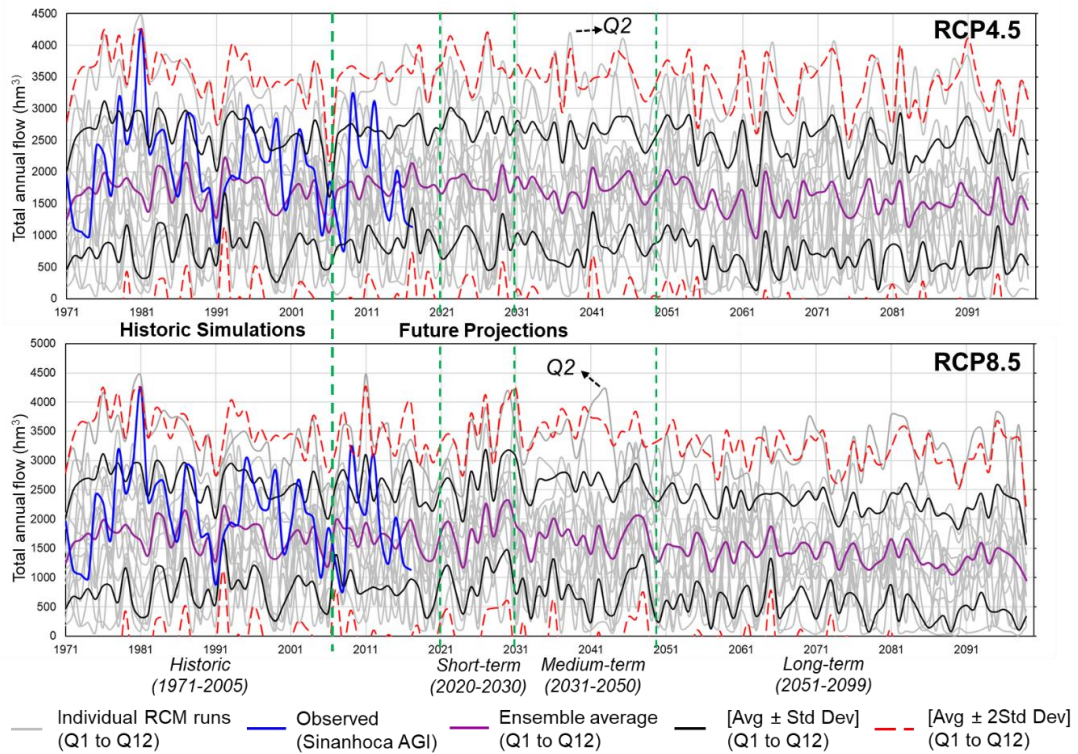


Figure 5.29. Historic and future (RCP4.5 on the top panel and 8.5 scenarios on the bottom panel) streamflow simulations from individual model runs of 12 CORDEX RCMs (Q1 to Q12)

As seen in Figure 5.29, analysis of the projections based on different RCMs for outliers indicates that Q2 (i.e., projections based on CNRM-CM5_ALADIN53) projected under both scenario conditions forms outliers (exceeding mean+2Standard deviations of the ensemble indicated with dotted red line in Figure 5.29) for a significant portion of the projections (approximately one-third of the projections for total annual flow).

The significance of the projected change in annual total streamflow is tested by the use of Welch's two-sample t-test with a threshold of confidence level of 95%. Accordingly, for the RCP4.5 scenario, seven of the streamflow simulations (Q5, Q6, Q8, Q9, Q10, Q11, and Q12) which are based on projections by the RCMs nested on HadGEM2-ES and CM5A-MR and EC-EARTH_RACMO22E indicate a significant level change in the streamflow in Manavgat River for the second half of the 21st century. On the other hand, for the first half of the century that is analyzed as the short-, and medium-term future most of the projections do not indicate a significant level change in the streamflow under the RCP4.5 scenario. For the short-term Q8 and Q10, and for the medium-term Q5 and Q9 are the only projections that indicate a significant change in streamflow for the RCP4.5 scenario.

The streamflow projections for the RCP8.5 scenario based on 10 out of 12 models (all projections except Q3 and Q7) agree on a significant change in streamflow for the long-term future. On the other hand, for the short-term none of the 12 projections, and for the medium-term future only Q5 indicates a significant level of change with a confidence level of 95% in the streamflow for the RCP8.5 scenario.

Finally, the analysis results are processed to determine the potential impact on the streamflow as percent change projections, based on the climate change signal indicated by each CORDEX RCM. For that purpose, the change in the total mean annual flow for the historic period is compared to the total mean annual flow projected for short-, medium- and long-term future periods. The projected changes in streamflow of Manavgat River at the Sinanhoca streamgage and in the inflow to Oymapinar reservoir are detailed in Section 5.3.4.

5.3.2 Analysis of Streamflow Projections using Ensembled Temperature and Precipitation (Q13 and Q14)

Ensembling of daily temperature and precipitation data with SE and SME shows satisfactory results regarding the simulation performances to replicate mean climatologic conditions. Therefore it is used for the generation of meteorological inputs of the hydrological model (Section 5.1.3.2) in flow simulations. The ensembled daily historic and future time series of temperature and precipitation are used to run the calibrated hydrological model. The historical streamflow simulation results for ensembled inputs are compared with the observed streamflow data of Sinanhoca streamgauge to verify the simulation efficiencies. The daily hydrographs of historical and future simulations of streamflow (Q13 and Q14) based on the ensembled meteorologic time series are given in Appendix F. Figure 5.30 illustrate the monthly hydrographs for Q13 (i.e., based on inputs generated with SE) and Q14 (i.e., based on inputs generated with SME) superimposed with the observed hydrograph of Sinanhoca streamgauge. As seen in Figure 5.30, despite the improvement in the temperature and precipitation estimations regarding the SPI values, the use of the ensembled meteorological time series resulted in poor streamflow simulations.

A closer look at the rainfall-runoff relationship in the model basin simulated in the hydrological model shows that the streamflow is significantly influenced by the occurrence of precipitation events that are higher than the average conditions. Hence, SE and SME which reduce low-frequency events as a tradeoff for a better representation of the mean conditions underestimate the precipitation events that are over the mean precipitation which causes an underestimation of the streamflow.

Furthermore, the SPI values (Table 5.17) calculated for the simulated monthly streamflows also verify unsatisfactory performance to replicate the observed streamflow. As seen in Table 5.17, for most of the SPIs, the streamflow simulation with ensembled meteorologic time series generated values close to or even poorer than the worst-performing streamflow simulation of individual climate model runs

(Q1 to Q12). Historical period Q13 and Q14 simulations are observed to have significantly high bias and high volumetric error. Hence, Q13 and Q14 are not used for the assessment of the climate change impact on streamflow.

Table 5.17 Statistical Performance Indicators for monthly mean streamflows (hm^3/d) for Q13 and Q14 in comparison with the streamflow simulations Q1 to Q12

SPI	Q1 to Q12		Q13	Q14
	Best	Worst	SE	SME
<i>Corr</i>	0.43	-0.12	0.29	0.5¹¹
<i>R²</i>	0.19	0.01	0.09	0.25
<i>NSE</i>	0.04	-1.12	-1.04	-0.38
<i>PBIAS (%)</i>	-1.6	58.1	87.09	65.81
<i>RMSE (hm^3/d)</i>	4.79	7.11	6.97	5.73
<i>RSR</i>	0.98	1.46	1.43	1.17
<i>VE</i>	0.98	0.42	0.13	0.34
<i>KGE</i>	0.38	-0.29	-0.41	0.02

¹¹ The best values for each SPI are indicated in bold

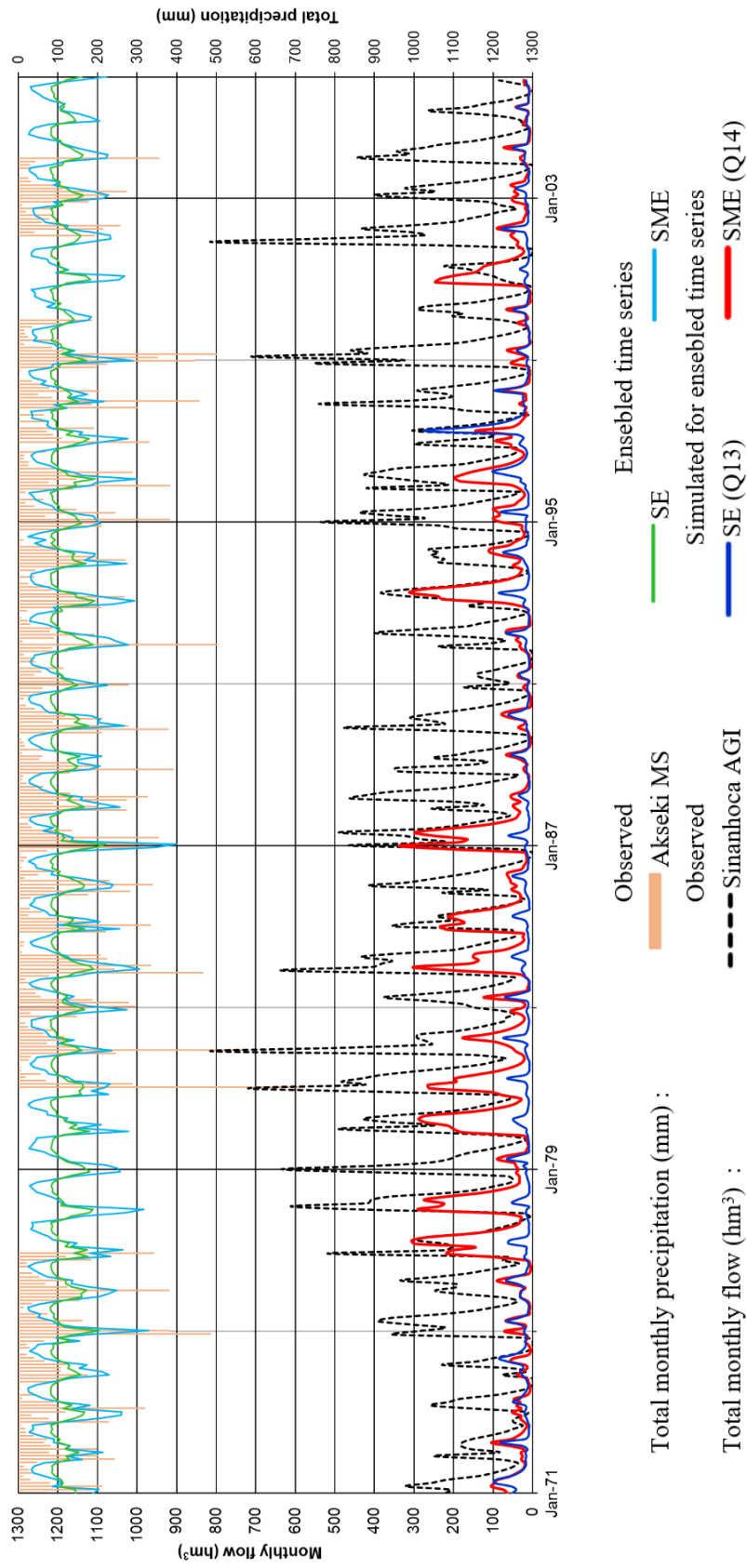


Figure 5.30. Historic observed streamflow and simulated streamflows using ensemble meteorologic time series (observed and ensemble monthly total precipitations in the same period are also shown in the graph for comparison)

5.3.3 Analysis of Streamflow Projections using Ensembled Streamflow (Q15 and Q16)

In order to take advantage of the MME approach to improve the simulation performances regarding the SPIs, the streamflow simulations from 12 individual climate model runs (Q1 to Q12) are used to obtain ensembled streamflow time series (Q15 and Q16). Q15 and Q16 are generated by the use of SE and SME methods for streamflow. Similar to the methodology followed for the MME of meteorologic parameters detailed in Section 5.1.3.2 training and test data sets for the SE model are formed through resampling of the monthly flow data for the period between 1971 and 2005. Resampling is done by random partitioning of the data set into training and test data sets to include 75% and 25 % of the entire data set. The same data points (same point in time) are used for the data sets from the observed and modeled streamflow. After the generation of the ensembled monthly streamflows for the historical period (1971 to 2005), the efficiencies of Q15 and Q16 to replicate observed flows are compared with that of simulated streamflows, Q1 to Q12. The SPI values for Q15 and Q16 compared with the best and worst SPI values obtained for the simulations Q1 to Q12 are given in Table 5.18. Accordingly, ensembled streamflow generated using the SE approach (Q15) achieved the best simulation performances regarding all SPIs. For Q15, *Corr* and *VE* values are in the “satisfactory” and “very good” range, respectively. Furthermore, the *KGE* value is at the threshold for satisfactory performance (See Table 4.6 in Section 4.2.5 for SPI threshold values). Both of the ensembling approaches are observed to be significantly successful in the reduction of the bias in total flow volume achieving the ideal *VE* value of 1.

Table 5.18 Statistical Performance Indicators for ensembled monthly mean (hm^3/d) streamflows (Q15 and Q16) in comparison to the streamflow simulations Q1 to Q12

SPI	Q1 to Q12		Q15	Q16
	Best	Worst	SE	SME
<i>Corr</i>	0.43	-0.12	0.62 ¹¹	0.45
<i>R</i> ²	0.19	0.01	0.39	0.21
<i>NSE</i>	0.04	-1.12	0.39	0.21
<i>PBIAS</i> (%)	-1.6	58.1	0	0
<i>RMSE</i> (hm^3/d)	4.79	7.11	3.83	4.35
<i>RSR</i>	0.98	1.46	0.78	0.89
<i>VE</i>	0.98	0.42	1	1
<i>KGE</i>	0.38	-0.29	0.49	0.21

Figure 5.31 displays the monthly total streamflows ensembled using SE and SME (Q15 and Q16) in comparison with the observed streamflows at the Sinanhoca streamgage. As seen in Figure 5.31, although the ensembled streamflows, Q15 and Q16, are superior to the simulations of individual model runs (Q1 to Q12) regarding the SPIs, they still perform relatively poorly to replicate the high flows and peaks as well as the low flows and dry conditions. Nevertheless, the SE approach is seen to provide a better representation of the variability in the streamflow than the SME approach does.

Hence, Q15 and Q16 achieve a better representation of the observed mean flow conditions and the general trend than the streamflow simulations from Q1 to Q12 but still remain relatively weak to represent the variability of flow compared to some of the simulated streamflows from Q1 to Q12. Consequently, unlike the use of ensembled meteorological time series in hydrological modeling, detailed in Section 5.3.2, which generated unsatisfactory streamflow estimations, the approach of ensembling of the streamflows Q1 to Q12 is verified to generate satisfactory results although some limitations that should be taken into consideration still exist.

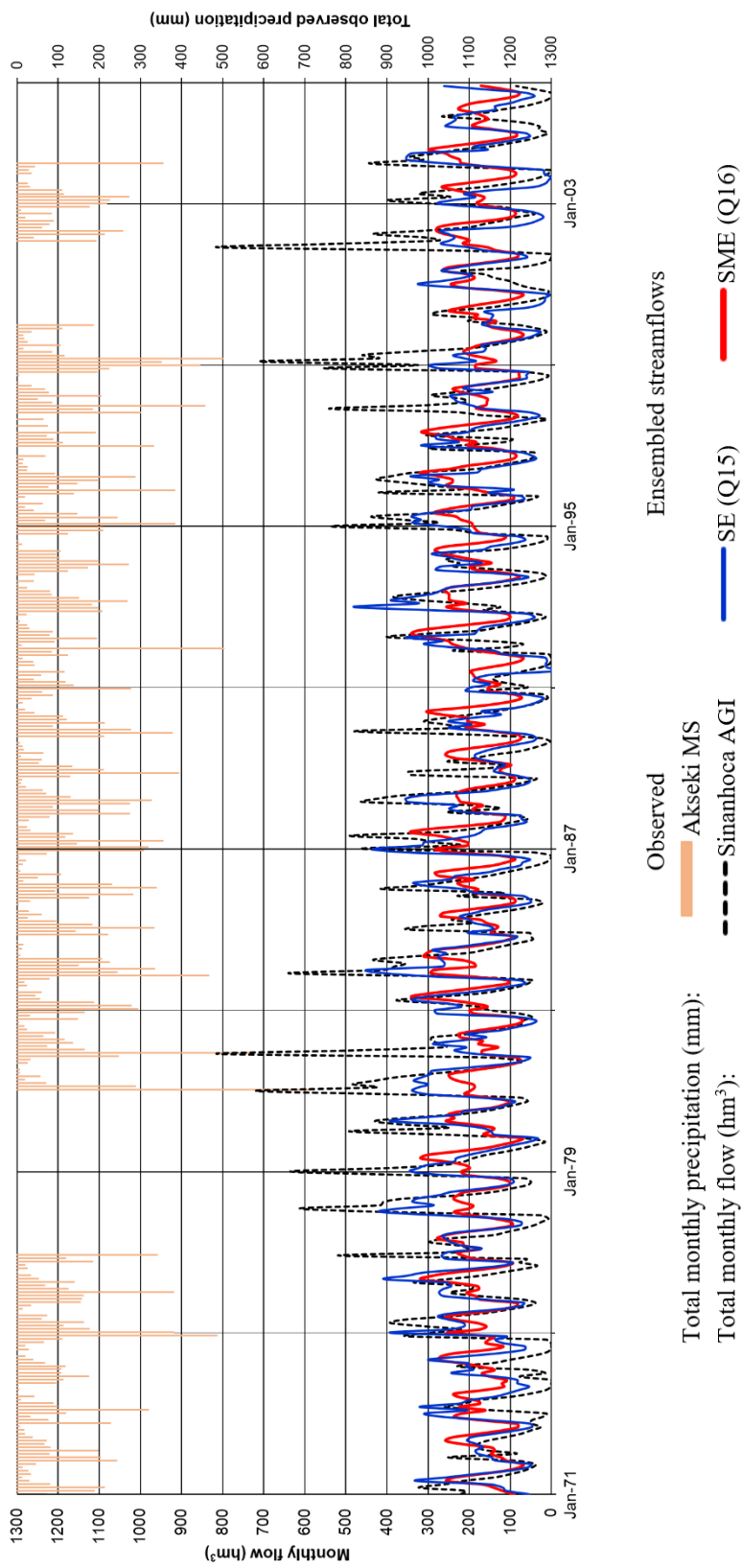


Figure 5.31. Historic observed streamflow and ensemble streamflow simulation results (the observed monthly total precipitation for the same period is also shown in the graph for comparison)

Ensembled streamflow time series are also generated for the future projections under RCP4.5 and 8.5 scenario conditions by the use of SE and SME approaches (i.e., Q15 and Q16 for the future). The streamflow simulation results for historic (1971 to 2005) and future (2006 to 2099, RCP4.5 and 8.5) periods including ensembled flows (Q15 and Q16) and individual flow projections (Q1 to Q12) are shown in Figures 5.32 and 5.33 for RCP4.5 and RCP8.5 scenarios, respectively. As seen in Figures 5.32 and 5.33, ensembled projections by SE and SME display a similar trend with the average of the flow projections from Q1 to Q12 (solid black line in the lower panel of Figures 5.32 and 5.33). Regarding the interannual variability and the range of changes in total flow Q15 and Q16 are better than the simple average of streamflows from Q1 to Q12, although they are still relatively weak to capture the observed variability in streamflow and cause the lower and higher extreme values (i.e, low-frequency conditions) simulated in Q1 to Q12 to be lost in a tradeoff of reduction of the overall bias.

To determine the significance of the change indicated by the ensembled streamflow projections for Q15 and Q16 Welch's two-sample t-test with a threshold of the confidence level of 95% is used. Accordingly, Q15 and Q16 indicate a significant level change in the streamflow for the second half of the 21st century under both RCP4.5 and 8.5 scenarios. On the other hand, for short-, and medium-term Q16 generated with SME indicates no significant level of change with a 95% confidence level under either scenario conditions, whereas Q15 generated with SE indicates a significant level change for medium-term for the RCP4.5 scenario.

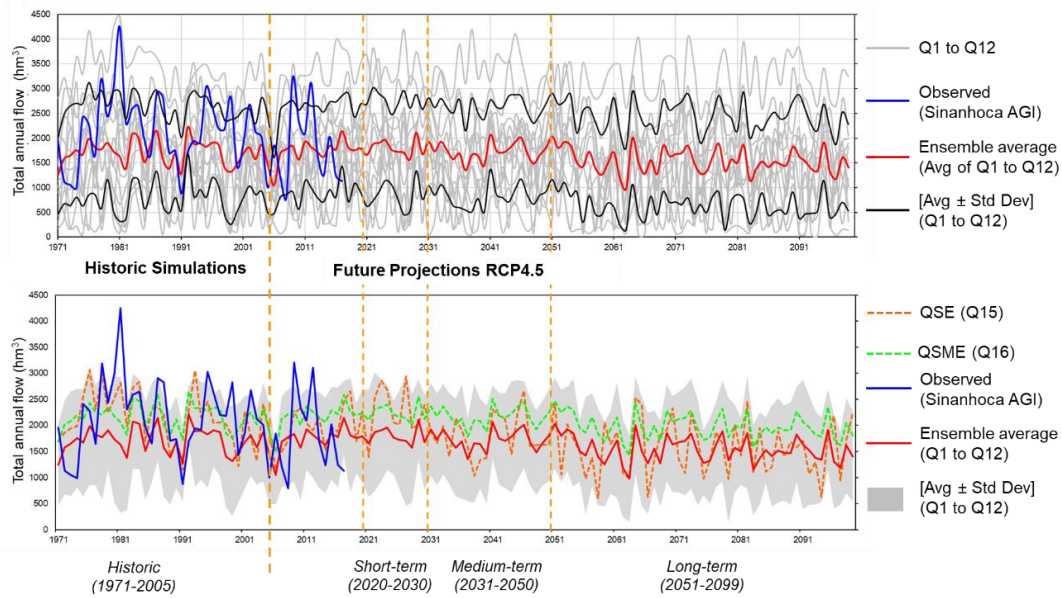


Figure 5.32. Historic and future (RCP4.5 scenario) ensembled total annual streamflow estimations (Q15 and Q16) in comparison to Q1 to Q12

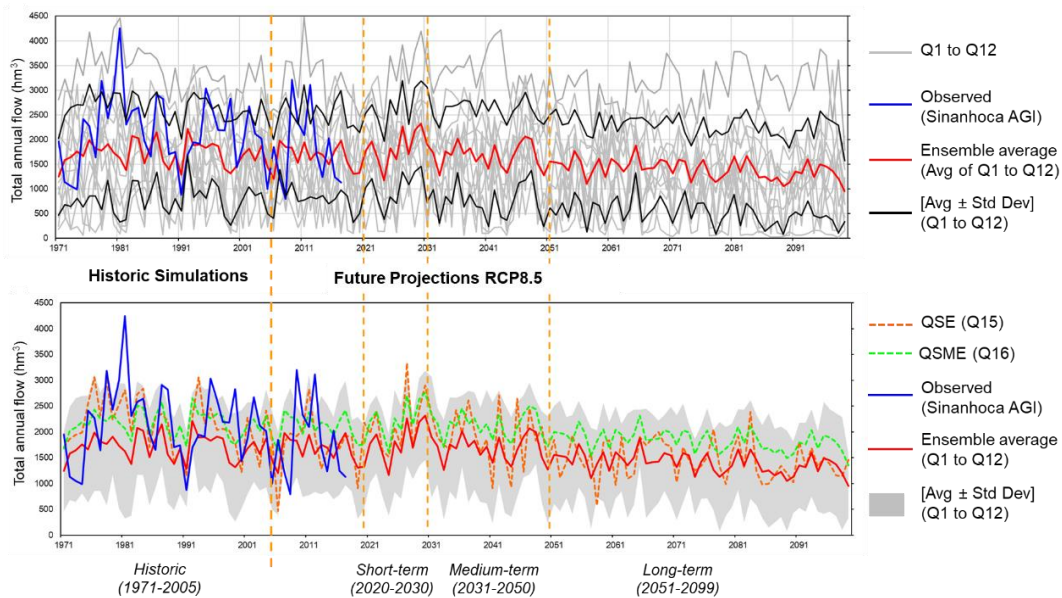
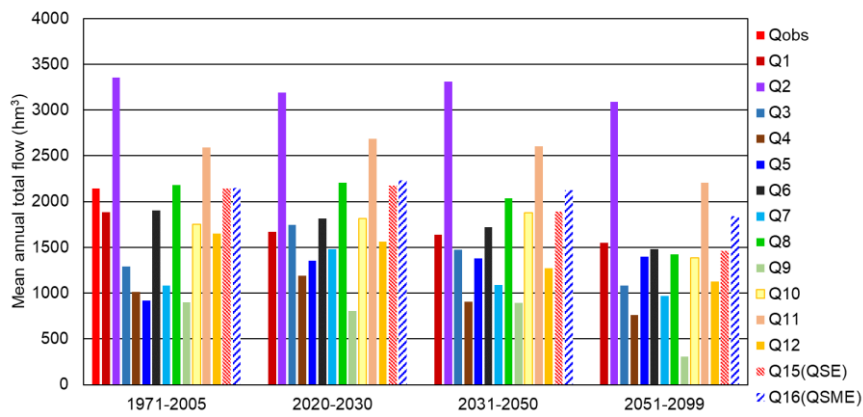
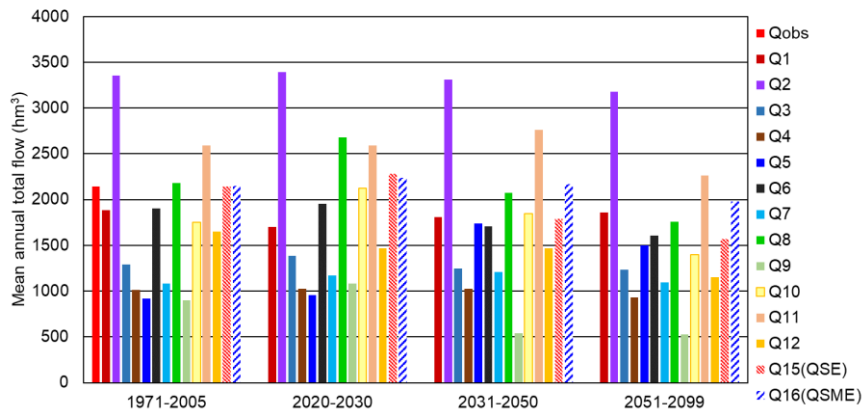


Figure 5.33. Historic and future (RCP8.5 scenario) ensembled total annual streamflow estimations (Q15 and Q16) in comparison to Q1 to Q12

The historic and future ensembled streamflows are processed to determine potential impact on the streamflow for RCP4.5 and 8.5 scenarios. The projected changes in streamflow of Manavgat River at Sinanhoca streamgage and in the inflow to Oymapınar reservoir are detailed in Section 5.3.4.

5.3.4 Analysis of Potential Impacts of Climate Change on Streamflow

The mean annual total flows calculated for the historical and future terms for the model basin (i.e., Sinanhoca streamgage) are shown in Figure 5.34. The projections on the percent change in mean annual total streamflows are depicted in Figure 5.35. Accordingly, except for Q5 (i.e., streamflow simulation based on EC-EARTH_RACMO22E simulations), the streamflow simulations based on the projections by all models under the RCP8.5 scenario indicate a decrease in the streamflow in the range of 8% to 66%. The ensembled streamflows, Q15 from the SE method and Q16 from the SME method, indicate a 32% and 14.5% decrease, respectively. For the RCP4.5 scenario, the projected decrease for the long-term is 27% and 8% for Q15 and Q16, respectively. For the projections according to simulations of Q1 to Q12 excluding Q5, the change in the annual total streamflow range between 1.2% (increase) and -41.5 (decrease).



- | | | | |
|----|----------------------------|-----|-------------------------------|
| Q1 | (M1: CNRM-CM5_ CCLM4-8-17) | Q7 | (M7: EC-EARTH_ RCA4) |
| Q2 | (M2: CNRM-CM5_ ALADIN53) | Q8 | (M8: CM5A-MR_ WRF331F) |
| Q3 | (M3: CNRM-CM5_ RCA4) | Q9 | (M9: CM5A-MR_ RCA4) |
| Q4 | (M4: EC-EARTH_ CCLM4-8-17) | Q10 | (M10: HadGEM2-ES_ CCLM4-8-17) |
| Q5 | (M5: EC-EARTH_ RACMO22E) | Q11 | (M11: HadGEM2-ES_ RACMO22E) |
| Q6 | (M6: EC-EARTH_ HIRHAM5) | Q12 | (M12: HadGEM2-ES_ RCA4) |

Figure 5.34. Historic and future (RCP4.5 on the top panel and RCP8.5 on the bottom panel) streamflow simulations for the Sinanhoca streamgage

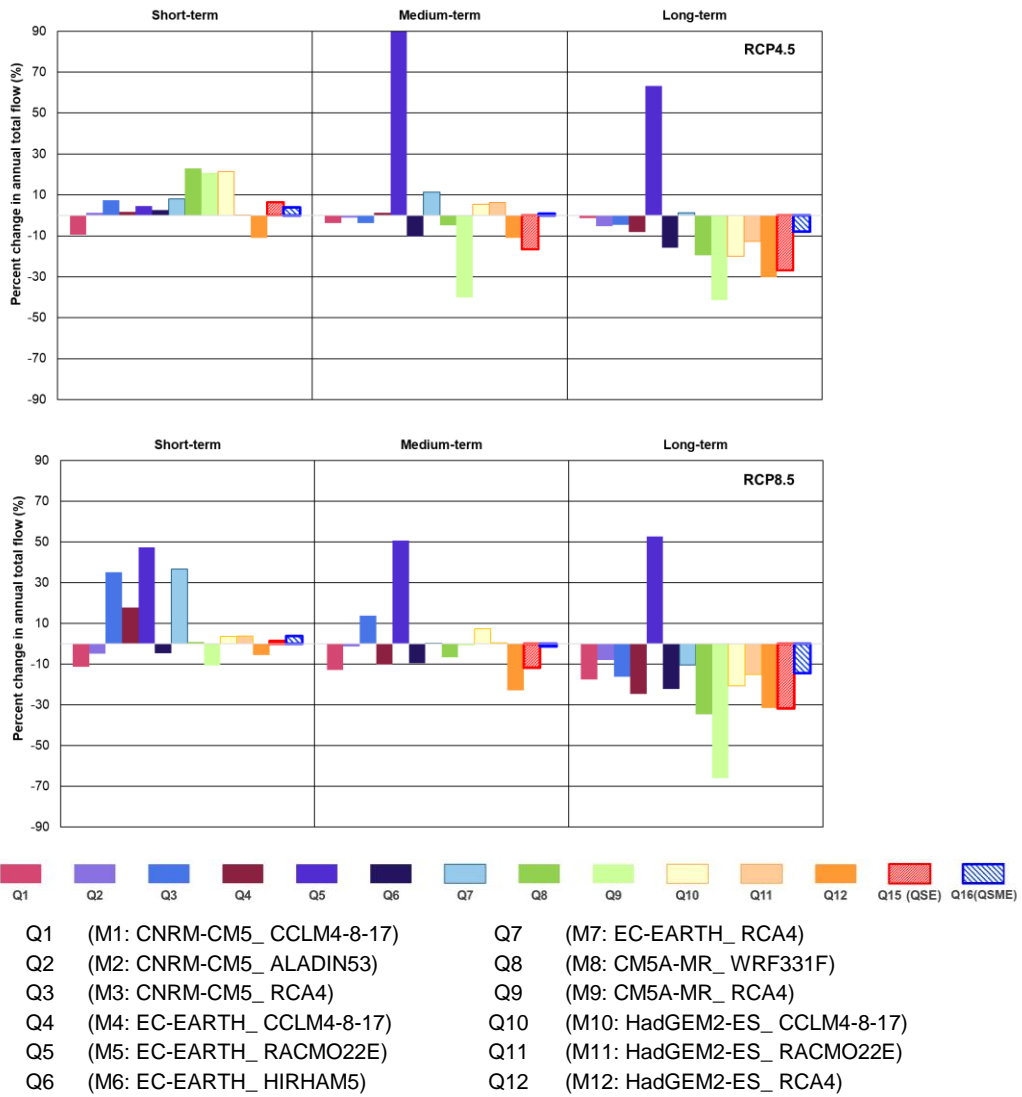


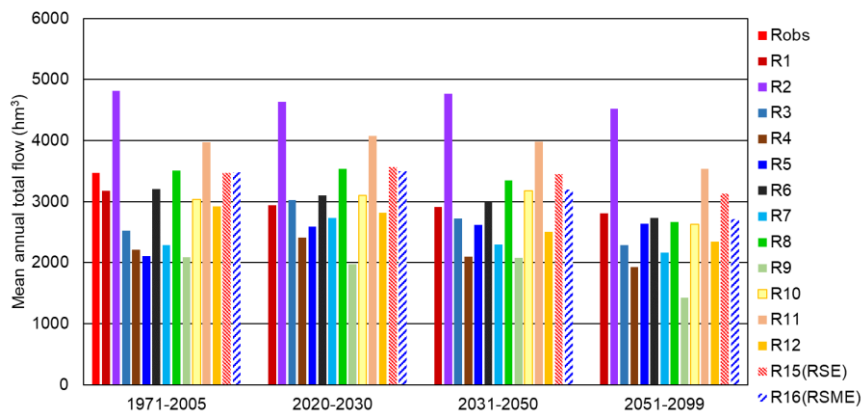
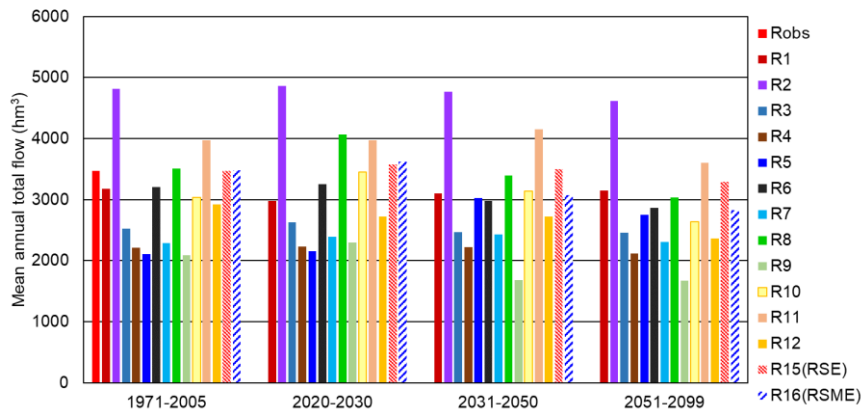
Figure 5.35. Projected percent change in the mean annual total flow at the Sinanhoca streamgage for RCP4.5 on the top panel and RCP8.5 on the bottom panel

The same analysis is done for the Oymapınar reservoir inflows (R1 to R12) by the use of the regression model of the relationship between streamflow at Sinanhoca streamgauge and Oymapınar reservoir inflow. The mean annual total inflows for the historical and future terms are illustrated in Figure 5.36. The projections on the percent change in mean annual total inflows are shown in Figure 5.37. Accordingly, similar to the Manavgat River streamflow projections, except for R5, the streamflow simulations based on the projections by all models under the RCP8.5 scenario indicate a decrease in the reservoir inflows in the range of 5.5% to 32%. The inflows (R15 and R16) calculated from the ensembled streamflows, Q15 from the SE method and Q16 from the SME method, indicate a 22% and 10% decrease, respectively. For the RCP4.5 scenario, the projected decrease for the long-term is 19% and 5% for R15 and R16, respectively. For the projections according to simulated inflows R1 to R12 excluding R5, the change in the annual total streamflow range between 0.5% (increase) and -20% (decrease).

Regarding the climate change impacts in the Mediterranean, IPCC's AR6 emphasizes the very likely decrease in the annual runoff and streamflow during the low flow seasons. The decrease is identified to be in a range of 5 to 70% and is likely to impact the hydropower generation in the region (Ali et al., 2022). The findings from the multi-model analysis in this study (excluding R5) reveal similar projections showing a statistically significant decrease in the Oymapınar reservoir inflow up to 20% for RCP4.5 and 32% for RCP8.5 conditions for the second half of this century.

The potential impact on hydropower generation due to future changes in streamflow is also assessed within the scope of the TUBITAK Project with the Title of "Assessment of Climate Change Impacts on Streamflow and Hydropower in Antalya (Project Number: 365Y118)". The relevant research study used the monthly total streamflow (i.e., Q8 in this study) and Oymapınar reservoir inflow (i.e., R8 in this study) time series based on CM5A-MR_WRF331F (i.e., M8 in this study) that is verified to have the lowest total bias regarding the mean annual precipitation compared to other CORDEX RCMs (See Table 5.6 in Section 5.1.3.2) (Kentel et al., 2021).

The analysis by Kentel et al. (2021) of potential changes in hydropower generation in the Oymapınar HEPP determined that a decrease in the streamflow in the long-term future for RCP4.5 and 8.5 scenarios is likely to cause a drop in hydropower generation efficiency compared to the available production capacity of the HEPP. On the other hand, due to current limitations to operation, such as restrictions due to flood protection of the downstream reservoirs, Oymapınar HEPP is operated with a total annual hydropower generation rate of around 1000 GWh, which is already around 20% lower than its capacity (i.e., approximately 1200 GWh). Thus, assuming that the baseline operation conditions remain unchanged the decrease in the Oymapınar Inflow is projected to create a decrease in the current hydropower generation for the RCP8.5 scenario in the long-term future (Kentel et al., 2021). Under such conditions, Kentel et al. (2021) project an approximate 10% decrease in the total annual hydropower generation compared to the current energy generation (i.e., 900 GWh) in the Oymapınar HEPP.



- | | | | |
|----|----------------------------|-----|-------------------------------|
| R1 | (M1: CNRM-CM5_ CCLM4-8-17) | R7 | (M7: EC-EARTH_ RCA4) |
| R2 | (M2: CNRM-CM5_ ALADIN53) | R8 | (M8: CM5A-MR_ WRF331F) |
| R3 | (M3: CNRM-CM5_ RCA4) | R9 | (M9: CM5A-MR_ RCA4) |
| R4 | (M4: EC-EARTH_ CCLM4-8-17) | R10 | (M10: HadGEM2-ES_ CCLM4-8-17) |
| R5 | (M5: EC-EARTH_ RACMO22E) | R11 | (M11: HadGEM2-ES_ RACMO22E) |
| R6 | (M6: EC-EARTH_ HIRHAM5) | R12 | (M12: HadGEM2-ES_ RCA4) |

Figure 5.36. Historic and future (RCP4.5 on the top panel and RCP8.5 on the bottom panel) estimates of the mean annual total inflow of the Oymapınar Reservoir

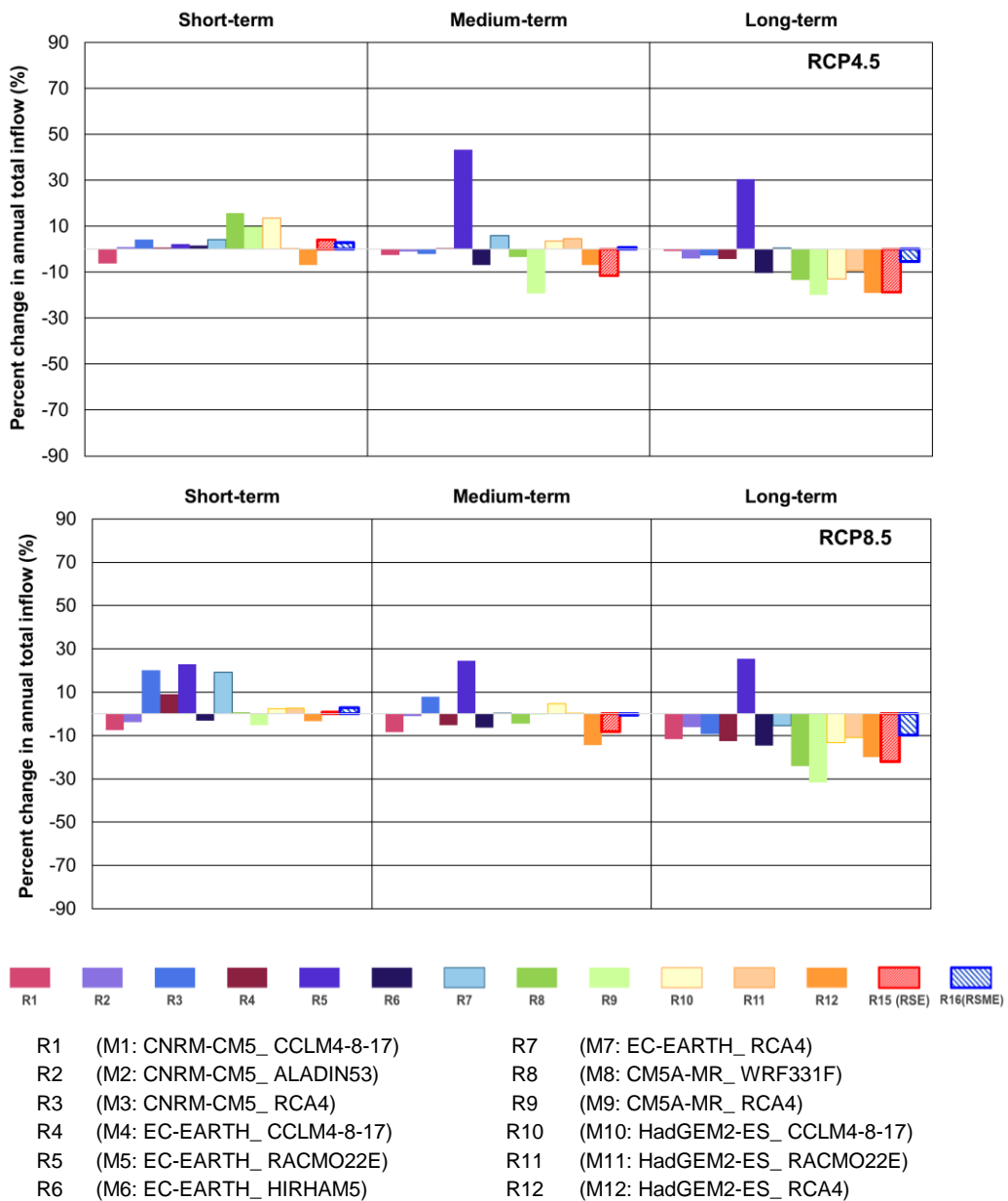


Figure 5.37. Projected percent change in the mean annual total inflow of the Oymapinar Reservoir for RCP4.5 on the top panel and RCP8.5 on the bottom panel

CHAPTER 6

CONCLUSIONS

6.1 Summary and Conclusions

This study assesses potential climate change impacts on temperature and precipitation in Southern Mediterranean Turkey extending and its hinterland covering 10 major surfacewater basins. Furthermore, the impact of climate change on the streamflow of the Manavgat River feeding the Oymapınar reservoir is assessed in the study. The details of and findings from the multi-model analysis of high-resolution climate models and subsequent impact analysis for the Oymapınar basin using hydrological modeling are presented in this thesis.

The study includes three main components, Climate Analysis, Hydrological Modeling, and Streamflow Impact Analysis.

The main findings and conclusions from these components are as follows:

Component 1, Climate Analysis:

- The analysis of the observed precipitation and temperature at 59 MSs across the CASA from 1966 to 2005 indicates that:
 - The annual mean temperature climatology range between 10°C and 20°C across the CASA and the mean temperature difference between the winter and summer seasons is between 14°C and 21°C for the region.
 - Konya Closed Basin has the lowest annual mean precipitation (less than 1mm/day) among the basins in the CASA.
 - Coastal areas receive more mean annual precipitation than inland areas but have a very high seasonality. For coastal stations, annual

precipitation is mostly received during the winter season, and mean precipitation drops significantly, even to zero, during the dry season.

- The spatial variability of climatology is significantly influenced by the topographical features of the CASA. The Taurus Mountains extending parallel to the coastline in the south form the boundary for the coastal climatology zone which has a relatively high annual mean temperature (18°C or higher) and total precipitation. On the other hand, in the west, the topology of mountain ranges lets the milder climate conditions reach further inland from the coastal areas.
- The multi-model analysis of the simulation performances of high-resolution raw and bias-adjusted climate models indicates that:
 - Simulation performances of 14 raw climate models are distinctly variable. Also, intra-regional variability is observed regarding the simulation performances of the models.
 - The bias-adjusted outputs of CORDEX RCMs are verified to have better simulation performances for certain locations, certain seasons, or periods while they are shown to perform poorly for other locations in the CASA (e.g., better simulation for coastal stations than the inland stations) and periods (e.g. poor performance for summer season). This creates even higher diversification of the simulation performances and the future projections for the CASA.
 - Due to the high diversification of modeling performances raw and bias-adjusted RCM outputs should be used only after validation for the scale and the objective specific to the study (e.g., impacts on water supply or flood risk).
- The multi-model analysis of the simulation performances of individual models in the 14-member ensemble showed that:

- MRI-AGCM_NHRCM, EC-EARTH_HIRHAM5, and HadGEM2-ES_RCA4 are found to be the best performing models in the 14-member ensemble both for temperature and precipitation climatology in the CASA.
- Among 14 models, CNRM-CM5_ALADIN53 is found to be the weakest to replicate the observed temperature and precipitation climatology in the CASA.
- The analysis results of the ensembling methods SE and SME are as follows:
 - The ensembling methods are found to provide improvement in the estimations of temperature and precipitation climatology.
 - Ensembled outputs are observed to have better Corr and RMSE values.
 - Ensembling is observed to reduce overall bias.
 - The skills of the ensembled data series are found to be highly affected by the simulation performances of the input data series (i.e., climate models).
 - Better results are seen to be observed for larger ensemble sets.
 - Ensembling generates output time series that are mostly concentrated around the mean climatology.
 - Ensembling is seen to reduce the variability of the climate simulations, which causes the ensembled outputs to fail to replicate the observed low-frequency events.
 - The limitations of ensembled outputs are interpreted to be originated from the limitations of the linear methodologies used for ensembling, particularly concerning the parameters such as precipitation that are of non-linear in nature.
- The multi-model analysis of 14 climate models for potential changes in the temperature in the CASA verifies that:

- The projections by all models agree on a gradual increase in the mean temperature in the entire CASA during the 21st century for both RCP4.5 and 8.5 scenarios.
 - The temperature increase at all MSs and for all future terms is projected to be statistically significant (with a 95% confidence level) under both scenarios.
 - Based on the average of 12 CORDEX RCMs' RCP4.5 scenario projections, the areal average for the CASA (i.e., 59-MS average) for potential temperature increase is 1.2°C, 1.6°C, and 2.5°C for the short-, medium- and long-term future.
 - For the RCP8.5 scenario, the 12-model average of the short-, medium- and long-term future projections for potential temperature increase on the CASA average are 1.4°C, 2.1°C, and 4.1°C, respectively.
 - The projections by MRI's climate models for the long-term future covering the period between 2080 and 2099 indicate a statistically significant temperature increase under the RCP8.5 scenario. The projections by MRI-AGCM and MRI-AGCM_NHRCM show an increase in temperature in the range of 4°C to 5.2°C and 4°C to 5.4°C across the CASA, respectively.
- The multi-model analysis of 14 climate models for potential changes in the precipitation in the CASA reveals the following:
 - Projections for the CASA indicate significant intra-regional variability in the size and type (i.e., decrease or increase) of the impact on precipitation.
 - Concerning the CASA on average, the average of 12 CORDEX RCMs' projections indicate a 0.5%, 2.7%, and 7% decrease in precipitation for the short-, medium-, and long-term future under the RCP4.5 scenario, respectively.

- Under the RCP8.5 scenario, the average of 12 CORDEX RCMs' projections shows +1.3%, -4.6%, and -14% change in precipitation on average of the CASA for short-, medium-, and long-term future, respectively.
 - Based on the projections by MRI-AGCM_NHRCM on average of the CASA a 14% decrease in the mean annual precipitation is calculated for the long-term future period between 2080 and 2099 compared to the historical 1981 to 2000 period. A statistically significant level of change in precipitation is projected for the long-term future between 2080 and 2099 under the RCP8.5 scenario for more than 40% of the MSs in the SA.
- The concurrent impacts of climate change on temperature and precipitation in the CASA are expected to aggravate the stress on the water resources and increase the drought risk in the region, particularly for the inland basins where the increase in temperature is likely to be more pronounced due to the intensification of the dry climate characteristics.
 - The impacts that are projected to increase with time are likely to exacerbate risks to water supply, particularly after the onset of a significant level of decrease in precipitation in the long-term future in the second half of the 21st century. Therefore, tiered adaptation strategies are considered to be necessary to minimize the increased risks and vulnerabilities regarding the climate change impacts on water resources.

Component 2, Hydrological Modeling:

- Both of the hydrological models developed in HBV-light and HEC-HMS provide satisfactory results for the simulation of the streamflow at the modeling basin.
- HEC-HMS model provided slightly better values for SPI's for the validation period.

- In modeling, HBV-light has the advantage of its ease of use, due to being less data-intensive, more user-friendly, and requiring less time for model development and calibration compared to the HEC-HMS.
- However, HEC-HMS enables better control by the user over the hydrological modeling algorithm for different elements of the basin hydrology and hydrometeorology.

Component 3, Streamflow Impact Analysis:

- The validation of the streamflow simulations in HEC-HMS (Q1 to Q12) based on the historic temperature and precipitation time series of 12 CORDEX RCMs indicates that:
 - Among the 12 CORDEX RCMs, the use of historic time series from EC-EARTH_HIRHAM5 generated relatively higher SPIs indicating better performance for the replication of the historical monthly streamflow compared to other models.
 - HadGEM2-ES_RCA4, CM5A-MR_WRF331F, CNRM-CM5_RCA4, and CNRM-CM5_CCLM4-8-17 are other RCMs, for which the use of historic time series shows relatively better streamflow simulation performances among other RCMs in the ensemble.
 - The use of the EC-EARTH_RACMO22E time series performs relatively poorly in streamflow simulation compared to the others in the ensemble.
 - Analysis of the range of the daily mean flow rates simulated by the climate model outputs in comparison to the observed flow rates in the basin verifies that Q9 of CM5A-MR_ RCA4 is observed to distinctly underestimate and Q2 of CNRM-CM5_ ALADIN53 to overestimate streamflow in the basin.
 - Regarding the range of daily flow rate observed in the basin, Q6 of EC-EARTH_HIRHAM5, Q8 of CM5A-MR_WRF331F, Q11 of HadGEM2-ES_RACMO22E, and Q12 of HadGEM2-ES_RCA4 are found to replicate the streamflow in the basin better.

- The validation of the streamflow simulations in HEC-HMS (Q13 and Q14) based on ensembled temperature and precipitation time series indicates that:
 - Although SE and SME methods are seen to provide significant improvement in the SPI values for temperature and precipitation simulations the use of the ensembled meteorological time series in hydrological modeling resulted in poor streamflow simulations.
 - The poor performance of the use of ensembled meteorological time series in the streamflow simulation is due to the reduction of the variability of the hydrometeorological parameters (particularly precipitation). SE and SME fail to represent relatively lower-frequency events in the time series as a tradeoff for a better representation of the mean meteorological conditions. Therefore, the precipitation events that are over the mean precipitation are underestimated by the ensembled precipitation which leads to a significant underestimation of the streamflow by the HEC-HMS model.

- The validation of the ensembled streamflows(Q15 and Q16) indicates that:
 - The monthly total streamflows ensembled using SE and SME (Q15 and Q16) in comparison with the observed streamflows at the Sinanhoca streamgage provide better SPI values compared to the individual streamflow simulations (Q1 to Q12) in the ensemble.
 - Ensembled streamflows are seen to provide a better representation of the observed mean flow conditions but remain relatively weak to replicate the high flows and peaks as well as the low flows and dry conditions.
 - The SE approach is seen to provide a better representation of the variability in the streamflow than the SME approach does.

- Analysis of the potential change in the Manavgat River streamflow due to climate change indicates that:

- For short-, and medium-term streamflow, simulations on most of the RCMs and the SME streamflow do not show a statistically significant change in the streamflow under either scenario.
 - Individual streamflow simulations of 12 RCMs (Q1 to Q12) and the ensembled streamflow time series (Q15 and Q16) indicate a statistically significant level (with a 95% confidence level) of change in the streamflow for the second half of the 21st century under the RCP8.5 scenario, in general. For the RCP4.5 scenario, seven of 12 models and the ensembled streamflows indicate a significant level of change for the long-term future.
 - The streamflow simulations based on the projections by all RCMs, except for Q5 (i.e., streamflow simulation based on EC-EARTH_RACMO22E outputs), under the RCP8.5 scenario indicate a decrease in the streamflow in the range of 8% to 66% for the long-term future.
 - For the RCP4.5 scenario, the projected change in the annual total streamflow range between 1.2% (increase) and -41.5 (decrease).
 - The ensembled streamflows, Q15 from the SE method and Q16 from the SME method, indicate a 32% and 14.5% decrease under the RCP8.5 scenario in the long-term future, respectively. For the RCP4.5 scenario, the projected decrease for the long-term is 27% and 8% for Q15 and Q16, respectively.
- Analysis of the potential change in the Oymapınar reservoir inflow due to climate change indicates that:
 - Under the RCP8.5 scenario, a decrease in the range between 5.5% and 32%, and under the RCP4.5 scenario, a change in the range between 0.5% (increase) and -20% (decrease) is projected for the long-term future.

- Based on the ensembled streamflows QSE and QSME, under the RCP8.5 scenario, 22%, and 10% decreases are projected for the long-term future, respectively. For the RCP4.5 scenario, the projected decreases in the reservoir inflow in the long-term future are 19% and 5%.

As summarized above significant interregional and intermodel variability is identified regarding the simulation skills of the climate models in the ensemble set in this study. The validation of the climate models to be used for the climate change impact assessment for the CASA, Akseki MS and HMSA, and for the Manavgat River streamflow verifies significant variability among the climate models. For example, CM5A-MR_WRF331F which is determined to have relatively better simulation skills for the Akseki MS due to its low total bias compared to other models in the ensemble is identified to perform relatively poorly for the CASA on average.

Nevertheless, considering analysis results on various assessment parameters (e.g., evaluation for CASA or HMSA, evaluation for temperature, precipitation, or streamflow simulation) in this study the following models can be classified to perform best for most of the analyses for the study areas in this research.

- MRI-AGCM_NHRCM is verified to have better simulation skills both for interannual and spatial variability of temperature and precipitation in the CASA.
- EC-EARTH_HIRHAM5 and HadGEM2-ES_RCA4 are verified to perform well to replicate interannual and spatial variability of temperature and precipitation in the CASA and relatively in Akseki MS. Additionally, these two models are identified to have better results for the simulation of the streamflow to replicate the daily flow rate and mean annual streamflow in the Oymapınar basin compared to other CORDEX RCMs.

As IPCC's AR6 emphasizes Mediterranean region is vulnerable to highly likely "interconnected" hazards and risks which is triggered by climate change (Ali et al., 2022). In that respect, adaptation strategies are required to minimize such hazards including but not limited to loss and degradation of ecosystem elements and services, aridification, crop losses, water scarcity, and public and ecological safety risks due to extreme events, and to build resilience in the socio-economic and ecological environment in the future.

6.2 Recommendations for Future Research

This study focuses on the changes in the temperature and precipitation climatology and streamflow due to climate change and therefore mostly analyzes the results for monthly and annual time series. Although the hydrological modeling is based on the daily time series, no detailed analysis of daily time-scale results is included in this study. For the risk analysis on low-frequency and small-time scale, extreme events (e.g., wet and dry extremes on the daily time scale, flood due to extreme storm events, and similar) the analysis of daily results and associated extreme analysis is considered as the subject of potential future studies.

The detailed analysis of the change in the climatological means in this study provides information on the potential future trends and vulnerability of water resources. However, concerning the ecological and socioeconomic vulnerabilities, potential changes in some additional meteorological parameters such as maximum and minimum temperatures, maximum precipitation, and also seasonal total and mean precipitations also have significant importance due to potential hazards and risks (e.g., heatwaves and extremely cold days, wildfires, agricultural droughts, flash floods, etc.). Draft lists of hydrometeorological parameters for future research studies regarding the hazards likely to be induced by climate change may include but are not limited to the following:

- Changes in seasonal mean temperatures, Growing Season Length, and/or the number of annual Growing Degree Days, Heating Degree Days, and Cooling Degree Days (Peterson et al., 2001; Crespi et al., 2020).
- Changes in the number and intensity of extreme temperatures (maximum and minimum values of daily maximum temperature, and minimum temperature, number of days with daily maximum temperature exceeding 25°C (i.e., summer days) and 30°C (i.e., hot days), and daily minimum temperature over 20°C (i.e., tropical nights), frost days, changes in warm and cold spell duration indices), intra-annual Extreme Temperature Range, heatwave frequency, intensity and duration (e.g., Heat Wave Duration Index). Days with fire danger exceeding a threshold (Peterson et al., 2001; Donat et al., 2013; Crespi et al., 2020).
- Changes in the seasonal mean and total precipitation, and simple precipitation intensity index (Peterson et al., 2001; Crespi et al., 2020).
- Changes in the extreme precipitation events (maximum 1-day precipitation, maximum consecutive 5-day precipitation), extreme precipitation total (i.e., the total sum of daily precipitation over a certain period exceeding the 95th and/or 99th percentile of the reference interval), maximum lengths of dry and wet spells (Peterson et al., 2001; Donat et al., 2013; Crespi et al., 2020).
- Changes in the seasonality and inter-annual variability of discharge.
- Changes in the River Flood Index, frequency, magnitude, and duration of 10-year and 100-year flood events (Crespi et al., 2020).
- Aridity and drought (e.g., Standardized Precipitation Index Aridity Index, and drought intensity), changes in the number of consecutive dry days, duration and magnitude of meteorological, and soil moisture droughts, Water stress index (i.e., use-to-resource ratio) (Raskin et al., 1997; Byers et al., 2018; Crespi et al., 2020).
- Changes in the evapotranspiration and connected indices such as the Standardized Precipitation Evapotranspiration Index (Crespi et al., 2020).

A limitation of the hydrological model developed for impact assessment in this study is that the calibration and validation periods are restricted to the time frames for which continuous hydrometeorological time series of monitoring data (i.e., temperature, precipitation, and streamflow) are available. Hence, due to the data availability, the period for calibration has to be restricted to four (2013-2016 water years), whereas the validation period is restricted to one (2017) water year duration. As a better practice, where data is available, calibration and validation periods should be selected for longer durations. Hence, in the future, if additional continuous historical hydrometeorological data are generated, calibration and validation of the hydrological model can be improved using longer time series of historical data. Within the scope of this study, the results from several ensembling approaches are used to improve the estimations as well as to reduce the significant divergence in the multi-model projections. The ensembling approaches examined in this study (e.g., SME, SE, PBWA, and analysis of the ensemble average values) are linear methods that provide significant ease of use compared to other complex non-linear and/or probabilistic approaches. However, linear methods may have limitations in the estimation of parameters of non-linear nature. Hence, as a future study the use of non-linear ensembling methods and research on the improvements of easy-to-apply linear approaches are considered to be useful.

The analysis of bias-adjusted CORDEX RCMs from the CORDEX-Adjust project verified variable simulation skills. Furthermore, regarding the improvements in the estimations particularly for seasonal climatology and total bias, the bias-adjusted outputs are found not to be significantly superior to raw RCM or ensembled outputs which also have their limitations. The weakness of the available bias-adjusted RCMs in the CORDEX database is considered to be mainly originated from the reference data (i.e., climate reanalysis data with relatively low resolution or containing biases from the local conditions) used for bias adjustment. Hence, for a potential future study on climate change analysis (particularly for local and seasonal assessment purposes), bias adjustment using observed meteorological data from ground-based meteorological stations is recommended to be used over the bias-adjusted RCMs

from the CORDEX database unless the bias-adjusted outputs from the CORDEX database are verified to have good simulation skills for the related study purpose.

In this study, the combined analysis of changes in temperature and precipitation climatologies indicated a distinct inversely correlated linear relationship. Furthermore, the analysis demonstrated that the inland basins with a semi-arid climate are likely to have a more intense temperature increase which is interpreted to be combined with increased dryness due to lower latent heat flux. Hence, a future study is recommended to include an analysis of the projections on evaporation along with the other hydrometeorological parameters.

REFERENCES

- Akay, E., Uysal, S., Poisson, A., Cravatte, J., & Müller, C. (1985). Stratigraphy of the Antalya Neogene basin. *Bull. Geol. Soc. Turkey*, 28, 105-119.
- Ali, E., Cramer W., Carnicer J., Georgopoulou E., Hilmi N.J.M., Le Cozannet G., & Lionello P. (2022). Cross-Chapter Paper 4: Mediterranean Region. In: *Climate Change 2022: Impacts, Adaptation, and Vulnerability. Contribution of Working Group II to the Sixth Assessment Report of the Intergovernmental Panel on Climate Change* [H.-O. Pörtner, D.C. Roberts, M. Tignor, E.S. Poloczanska, K. Mintenbeck, A. Alegria, M. Craig, S. Langsdorf, S. Löschke, V. Möller, A. Okem, B. Rama (eds.)]. Cambridge University Press. In Press.
- Altın, T. B., & Barak, B. (2017). Trends and changes in tropical and summer days at the Adana Sub-Region of the Mediterranean Region, Southern Turkey. *Atmospheric Research*, 196, 182-199.
- Anderson, E. A. (2006). Snow accumulation and ablation model–SNOW-17. US National Weather Service, Silver Spring, MD.
- Angelidis, P., Mystakidis, G., Lalikidou, S., Hrisanthou, V., & Kotsovinos, N. (2010). Computation of hydrographs in Evros river basin. *European Water*, 31, 33-42.
- Aqnouy, M., El Messari, J. E., Boudila, A., Bouizrou, I., & Mansour, M. R. (2018). Application of hydrological model" HEC HMS" In a Mediterranean watershed (Oued Laou, Northern of Morocco). *International Journal of Innovation and Applied Studies*, 24(4), 1773-1781.
- Archfield, S. A., & Vogel, R. M. (2010). Map correlation method: Selection of a reference streamgage to estimate daily streamflow at ungaged catchments. *Water resources research*, 46(10).

- Asquith, W. H., Roussel, M. C., & Vrabel, J. (2006). Statewide analysis of the drainage-area ratio method for 34 streamflow percentile ranges in Texas (No. 2006-5286). US Geological Survey.
- Aziz, R., & Yucel, I. (2021). Assessing nonstationarity impacts for historical and projected extreme precipitation in Turkey. *Theoretical and Applied Climatology*, 143, 1213-1226. doi:10.1007/s00704-020-03503-x
- Aziz, R., Yucel, I., & Yozgatligil, C. (2020). Nonstationarity impacts on frequency analysis of yearly and seasonal extreme temperature in Turkey. *Atmospheric Research*, 238, 1-13. doi:10.1016/j.atmosres.2020.104875
- Azmat, M., Choi, M., Kim, T. W., & Liaqat, U. W. (2016). Hydrological modeling to simulate streamflow under changing climate in a scarcely gauged cryosphere catchment. *Environmental Earth Sciences*, 75(3), 186.
- Babel, M. S., Bhusal, S. P., Wahid, S. M., & Agarwal, A. (2014). Climate change and water resources in the Bagmati River Basin, Nepal. *Theoretical and Applied Climatology*, 115 (3-4), 639-654.
- Bartolini, G., Di Stefano, V., Maracchi, G., & Orlandini, S. (2012). Mediterranean warming is especially due to summer season. *Theoretical and Applied Climatology*, 107(1), 279-295.
- Bates, B. C., Kundzewicz, Z. W., Wu, S., & Palutikof, J. P. (2008). *Climate Change and Water*. Technical paper of the intergovernmental panel on climate change. IPCC Secretariat, Geneva, 210.
- Bhuiyan, H. A., McNairn, H., Powers, J., & Merzouki, A. (2017). Application of HEC-HMS in a cold region watershed and use of RADARSAT-2 soil moisture in initializing the model. *Hydrology*, 4(1), 9.
- Bouabid, R., & Elalaoui, C. A. (2010). Impact of climate change on water resources in Morocco: The case of Sebou Basin. *Séminaires Méditerranéens*, 9, 57-62.

- Boulanger, J. P., Martinez, F., & Segura, E. C. (2006). Projection of future climate change conditions using IPCC simulations, neural networks and Bayesian statistics. Part 1: Temperature mean state and seasonal cycle in South America. *Climate Dynamics*, 27(2-3), 233-259.
- Boulanger, J. P., Martinez, F., & Segura, E. C. (2007). Projection of future climate change conditions using IPCC simulations, neural networks and Bayesian statistics. Part 2: precipitation mean state and seasonal cycle in South America. *Climate Dynamics*, 28(2-3), 255-271.
- Bravo, D. N., Araújo, M. B., Lasanta, T., & Moreno, J. I. L. (2008). Climate change in Mediterranean mountains during the 21st century. *Ambio*, 280-285.
- Bucak, T., Trolle, D., Andersen, H. E., Thodsen, H., Erdoğan, Ş., Bezirci, G., Filiz, N., Jeppesen, E., Beklioğlu, M. (2017). Future water availability in the largest freshwater Mediterranean lake is at great risk as evidenced from simulations with the SWAT model. *Sci Total Environ.* 581–582:413–425.
- Bucak, T., Trolle, D., Tavşanoğlu, Ü. N., Çakıroğlu, A. İ., Özen, A., Jeppesen, E., & Beklioğlu, M. (2018). Modeling the effects of climatic and land use changes on phytoplankton and water quality of the largest Turkish freshwater lake: Lake Beyşehir. *Science of the Total Environment*, 621, 802-816. doi:10.1016/j.scitotenv.2017.11.258
- Byers, E., Gidden, M., Leclère, D., Balkovic, J., Burek, P., Ebi, K., Greve, P., Grey, D., Havlik, P., Hillers, A., Johnson, N., Kahil, T., Krey, V., Langan, S., Nakicenovic, N., Novak, R., Obersteiner, M., Pachauri, S., Palazzo, A., Parkinson, S., Rao, N. D., Rogelj, J., Satoh, Y., Wada, Y., Willaarts, B., & Riahi, K. (2018). Global exposure and vulnerability to multi-sector development and climate change hotspots. *Environmental Research Letters*, 13(5), 055012. <https://doi.org/10.1088/1748-9326/aabf45>
- Cagatan, K., & Unal, Y. (2010, May). Heat Wave Tendency in the Western Part of Turkey and Its Relation to Circulation Patterns. In EGU General Assembly Conference Abstracts (p. 8507).
- Cane, D., & Milelli, M. (2010). Multimodel Super Ensemble technique for quantitative precipitation forecasts in Piemonte region. *Natural Hazards & Earth System Sciences*, 10(2), 265-273.

- Chea, S., & Oeurng, C. (2017). Flow simulation in an ungaged catchment of Tonle Sap Lake Basin in Cambodia: Application of the HEC-HMS model. *Water Utility Journal*, 17, 3-17.
- Christensen, J. H., Kjellström, E., Giorgi, F., Lenderink, G., & Rummukainen, M. (2010). Weight assignment in regional climate models. *Climate Research*, 44(2-3), 179-194.
- Chu, X., & Steinman, A. (2009). Event and Continuous Hydrologic Modeling with HEC-HMS. *Journal of Irrigation and Drainage Engineering*, 135(1), 119-124.
- Crespi, A., Terzi, S., Cocuccioni, S., Zebisch, M., Berckmans, J., & Füssel, H. M. (2020). Climate-related hazard indices for Europe. ETC-CCA Technical Paper, 1, European Topic Centre on Climate Change Impacts, Vulnerability and Adaptation. ETC/CCA, Bologna, Italy. doi:https://doi.org/10.25424/cmcc/climate_related_hazard_indices_europe_2020
- Cunderlik, J. M., & Simonovic, S. P. (2007). Inverse flood risk modelling under changing climatic conditions. *Hydrological Processes: An International Journal*, 21(5), 563-577.
- Darlane, A. B., & Javadianzadeh, M. M. (2016). Towards an Efficient Rainfall–Runoff Model through Partitioning Scheme. *Water*, 8(2), 63.
- Decremer, D., Chung, C. E., Ekman, A. M., & Brandefelt, J. (2014). Which significance test performs the best in climate simulations?. *Tellus A: Dynamic Meteorology and Oceanography*, 66(1), 23139.
- Deidda, R., Marrocu, M., Caroletti, G., Pusceddu, G., Langousis, G., Langousis, A., Lucarini, V., Puliga, M., Speranza, A. (2013). Regional climate models' performance in representing precipitation and temperature over selected Mediterranean areas. *Hydrology and Earth System Sciences*, 17, 5041-5059. doi:10.5194/hess-17-5041-2013.

- Demircan, M., Gürkan, H., Eskiöglu, O., Arabacı, H., & Coşkun, M. (2017). Climate Change Projections for Turkey: Three Models and Two Scenarios. *Turkish Journal of Water Science & Management*, 1(1), 22-43.
- Déqué, M., Jones, R.G., Wild, M., Giorgi, F., Christensen, J.H., Hassell, D.C., Vidale, P.L., Rockel, B., Jacob, D., Kjellström, E., de Castro, M., Kucharski, F., van den Hurk, B. (2005). Global high resolution versus Limited Area Model climate change projections over Europe: quantifying confidence level from PRUDENCE results. *Clim Dyn*, . 25, 653–670. doi:10.1007/S00382-005-0052-1.
- Déqué, M., Rowell, D. P., Lüthi, D., Giorgi, F., Christensen, J. H., Rockel, B., & van den Hurk, B. J. J. M. (2007). An intercomparison of regional climate simulations for Europe: assessing uncertainties in model projections. *Climatic Change*, 81(1), 53-70.
- De Silva, M. M. G. T., Weerakoon, S. B., & Herath, S. (2014). Modeling of event and continuous flow hydrographs with HEC–HMS: case study in the Kelani River Basin, Sri Lanka. *Journal of Hydrologic Engineering*, 19(4), 800-806.
- Devlet Su İşleri (DSİ). (n.d.). “Hidroelektrik Santral Projeleri Listesi”. <http://www2.dsi.gov.tr/skatablo /Tablo1.htm>. Latest access: 17.08.2018.
- Devi, G. K., Ganasri, B. P., & Dwarakish, G. S. (2015). A review on hydrological models. *Aquatic Procedia*, 4(1), 1001-1007.
- Dino, I. G., & Akgül, C. M. (2019). Impact of climate change on the existing residential building stock in Turkey: An analysis on energy use, greenhouse gas emissions and occupant comfort. *Renewable Energy*, 141, 828-846. doi:10.1016/j.renene.2019.03.150.
- Donat, M. G., Alexander, L. V., Yang, H., Durre, I., Vose, R., & Caesar, J. (2013). Global land-based datasets for monitoring climatic extremes. *Bulletin of the American Meteorological Society*, 94(7), 997-1006.

- Du, J., Qian, L., Rui, H., Zuo, T., Zheng, D., Xu, Y., & Xu, C. Y. (2012). Assessing the effects of urbanization on annual runoff and flood events using an integrated hydrological modeling system for Qinhuai River basin, China. *Journal of Hydrology*, 464, 127-139.
- EEA (European Environment Agency). (2016). Copernicus Programme Land Monitoring Service. "EU-DEM v1.1". Retrieved from: <https://land.copernicus.eu/pan-european/satellite-derived-products/eu-dem/eu-dem-v1.1>. Latest access: 17.08.2018.
- EEA. (2020) "Corine Land Cover (CLC) 2018, Version 2020_20u1"_. Retrieved from: <https://land.copernicus.eu/pan-european/corine-land-cover>. Latest access: 10.07.2020.
- Efthymiadis, D., Goodess, C. M., & Jones, P. D. (2011). Trends in Mediterranean gridded temperature extremes and large-scale circulation influences. *Natural Hazards and Earth System Sciences*, 11(8), 2199-2214.
- Emerson, D. G., Vecchia, A. V., & Dahl, A. L. (2005). Evaluation of drainage-area ratio method used to estimate streamflow for the Red River of the North Basin, North Dakota and Minnesota.
- Ergen, K., & Kentel, E. (2016). An integrated map correlation method and multiple-source sites drainage-area ratio method for estimating streamflows at ungauged catchments: A case study of the Western Black Sea Region, Turkey. *Journal of environmental management*, 166, 309-320.
- Erlat, E., Türkeş, M., & Aydın-Kandemir, F. (2021). Observed changes and trends in heatwave characteristics in Turkey since 1950. *Theoretical and Applied Climatology*, 145(1), 137-157.
- Erşahin, B. (2020). Simulation of streamflow using hydrologic modeling system HEC-HMS (Master's thesis, Middle East Technical University).

- ESGF. (2020). Earth System Grid Federation website. CoG version v4.0.0b2, ESGF P2P Version v4.0.4. <https://esgf-node.llnl.gov/search/esgf-llnl/>. Latest access: 05.06.2020.
- Evans, J.P. (2009). 21st century climate change in the Middle East. *Climatic Change*, 92(3–4), 417–432.
- Feldman, A. D. (2000). Hydrologic modeling system HEC-HMS: Technical Reference Manual. Hydrologic Engineering Center. US Army Corps of Engineers.
- Fang, G., Yuan, Y., Gao, Y., Huang, X., & Guo, Y. (2018). Assessing the effects of urbanization on flood events with urban agglomeration polders type of flood control pattern using the HEC-HMS model in the Qinhuai River basin, China. *Water*, 10(8), 1003.
- Fleming, M., & Neary, V. (2004). Continuous Hydrologic Modeling Study with the Hydrologic Modeling System. *Journal of Hydrologic Engineering*, 9(3), 175-183.
- Fujihara, Y., Tanaka, K., Watanabe, T., Nagano, T., & Kojiri, T. (2008). Assessing the impacts of climate change on the water resources of the Seyhan River Basin in Turkey: Use of dynamically downscaled data for hydrologic simulations. *Journal of Hydrology*, 353(1-2), 33-48.
- Gebre, S. L. (2015). Application of the HEC-HMS model for runoff simulation of Upper Blue Nile River Basin. *Hydrology: Current Research*, 6(2), 1.
- Giorgi, F., & Bi, X. (2005). Updated regional precipitation and temperature changes for the 21st century from ensembles of recent AOGCM simulations. *Geophysical Research Letters*, 32(21).
- Giorgi, F., & Lionello, P. (2008). Climate change projections for the Mediterranean region. *Global and Planetary Change*, 63, 90-104. doi:10.1016/j.gloplacha.2007.09.005.

- Giorgi, F., & Mearns, L. O. (2002). Calculation of average, uncertainty range, and reliability of regional climate changes from AOGCM simulations via the “reliability ensemble averaging”(REA) method. *Journal of Climate*, 15(10), 1141-1158.
- Giorgi, F., & Mearns, L. O. (2003). Probability of regional climate change based on the Reliability Ensemble Averaging (REA) method. *Geophysical research letters*, 30(12).
- Givati, A., Gochis, D., Rummeler, T., & Kunstmann, H. (2016). Comparing one-way and two-way coupled hydrometeorological forecasting systems for flood forecasting in the Mediterranean region. *Hydrology*, 3(2), 19.
- Gönençgil, B., & Deniz, Z. A. (2015). Trends of summer daily maximum temperature extremes in Turkey. *Physical Geography*, 36(4), 268-281.
- Gönençgil, B., & Deniz, Z. A. (2016). Extreme maximum and minimum air temperature in Mediterranean coasts in Turkey. *Geography, Environment, Sustainability*, 9(1), 59-70.
- Graham, L. P., Andréasson, J., & Carlsson, B. (2007). Assessing climate change impacts on hydrology from an ensemble of regional climate models, model scales and linking methods—a case study on the Lule River basin. *Climatic Change*, 81(1), 293-307.
- Gualdi, S., Somot, S., May, W., Castellari, S., Déqué, M., Adani, M., Artale, V., Bellucci, A., Breitgand, J. S., Carillo, A., Cornes, R., Dell’Aquila, A., Dubois, C., Efthymiadis, D., Elizalde, A., Gimeno, L., Goodess, C.M., Harzallah, A., Krichak, S.O., Kuglitsch, F.G., Leckebusch, F.G., L’Hévéder, B., Li, L., Lionello, P., Luterbacher, J., Mariotti, A., Navarra, A., Nieto, R., Nissen, K.M., Oddo, P., Ruti, P., Sanna, A., Sannino, G., Scoccimarro, E., Sevault, F., Struglia, M. V., Toret, A., Ulbrich, U. & Xoplaki, E. (2013). Future climate projections. In *Regional assessment of climate change in the Mediterranean* (pp. 53-118). Springer, Dordrecht.

- Gudmundsson, L., Bremnes, J.B., Haugen, J.E. & Engen-Skaugen, T. (2012). Downscaling RCM precipitation to the station scale using statistical transformations—a comparison of methods. *Hydrology and Earth System Sciences*, 16(9), 3383–3390.
- Gumindoga, W., Rwasoka, D. T., Nhapi, I., & Dube, T. (2017). Ungauged runoff simulation in Upper Manyame Catchment, Zimbabwe: Application of the HEC-HMS model. *Physics and Chemistry of the Earth, Parts A/B/C*, 100, 371-382.
- Gupta, H. V., Sorooshian, S., & Yapo, P. O. (1999). Status of automatic calibration for hydrologic models: Comparison with multilevel expert calibration. *Journal of hydrologic engineering*, 4(2), 135-143.
- Gupta, H. V., Kling, H., Yilmaz, K. K., and Martinez, G. F. (2009). Decomposition of the mean squared error and NSE performance criteria: Implications for improving hydrological modelling. *J. Hydrol.*, 377, 80–91.
- Gyawali, R., & Watkins, D.W. (2013). Continuous hydrologic modeling of snow-affected watersheds in the Great Lakes Basin using HEC-HMS”. *Journal of Hydrologic Engineering*, 18(1), 29-39.
- Hagedorn, R., Doblas-Reyes, F. J., & Palmer, T. N. (2005). The rationale behind the success of multi-model ensembles in seasonal forecasting—I. Basic concept. *Tellus A: Dynamic Meteorology and Oceanography*, 57(3), 219-233.
- Halwatura, D., & Najim, M. M. M. (2013). Application of the HEC-HMS model for runoff simulation in a tropical catchment. *Environmental modelling & software*, 46, 155-162.
- Hemming, D., Buontempo, C., Burke, E., Collins, M., & Kaye, N. (2010). How uncertain are climate model projections of water availability indicators across the Middle East? *Philosophical Transactions of the Royal Society A*, 368, 5117-5135. doi:10.1098/rsta.2010.0174

- Hortness, J. E. (2006). Estimating low-flow frequency statistics for unregulated streams in Idaho. US Department of the Interior, US Geological Survey.
- IPCC. (2014). Climate Change 2014: “Synthesis Report. Contribution of Working Groups I, II and III to the Fifth Assessment Report of the Intergovernmental Panel on Climate Change” [Core Writing Team, R.K. Pachauri and L.A. Meyer (eds.)]. IPCC, Geneva, Switzerland, 151 pp.
- IPCC. (2015) Workshop report of the intergovernmental panel on climate change workshop on regional climate projections and their use in impacts and risk analysis studies. In: Stocker, T.F., Qin, D., Plattner, G.-K. and Tignor, M. (Eds.) IPCC Working Group I technical support unit. Bern, Switzerland: University of Bern, p. 171.
- IPCC. (2021). Climate Change 2021: The Physical Science Basis. Contribution of Working Group I to the Sixth Assessment Report of the Intergovernmental Panel on Climate Change [Masson-Delmotte, V., P. Zhai, A. Pirani, S.L. Connors, C. Péan, S. Berger, N. Caud, Y. Chen, L. Goldfarb, M.I. Gomis, M. Huang, K. Leitzell, E. Lonnoy, J.B.R. Matthews, T.K. Maycock, T. Waterfield, O. Yelekçi, R. Yu, and B. Zhou (eds.)]. Cambridge University Press. In Press.
- IPCC. (2022). Climate Change 2022: Impacts, Adaptation, and Vulnerability. Contribution of Working Group II to the Sixth Assessment Report of the Intergovernmental Panel on Climate Change [Pörtner, H.-O. , Roberts, D.C. , Tignor, M. , Poloczanska, E.S. , Mintenbeck, K. , Alegría, A., Craig, M., Langsdorf, S., Löschke, S., Möller, V., Okem, A., Rama, B. (eds.)]. Cambridge University Press. In Press.
- IS-ENES. (n.d.). “Infrastructure for the European network for earth system modelling”. Climate4Impact website. <https://climate4impact.eu/impactportal/data/esgfsearch.jsp>. Latest access: 05.06.2020.
- Jacob, D., Teichmann, C., Sobolowski, S., Katragkou, E., Anders, I., Belda, M., ... & Wulfmeyer, V. (2020). Regional climate downscaling over Europe: perspectives from the EURO-CORDEX community. *Regional environmental change*, 20(2), 1-20.

- Jaw, T., Li, J., Hsu, K. L., Sorooshian, S., & Driouech, F. (2015). "Evaluation for Moroccan dynamically downscaled precipitation from GCM CHAM5 and its regional hydrologic response". *Journal of Hydrology: Regional Studies*, 3, 359-378.
- Johns, T.C., Gregory, J.M., Ingram, W.J., Johnson, C.E., Jones, A., Lowe, J.A., Mitchell, J.F.B., Roberts, D.L., Sexton, D.M.H., Stevenson, D.S., Tett, S.F.B., Woodage M.J. (2003). Anthropogenic climate change for 1860 to 2100 simulated with the HadCM3 model under updated emissions scenarios. *Clim Dyn* 20:583–612. DOI 10.1007/s00382-002-0296-y
- Kara, F., & Yucel, I. (2015). Climate change effects on extreme flows of water supply area in Istanbul: utility of regional climate models and downscaling method. *Environmental monitoring and assessment*, 187(9), 1-18.
- Kara, F., Yucel, I., & Akyurek, Z. (2016). Climate change impacts on extreme precipitation of water supply area in Istanbul: use of ensemble climate modelling and geo-statistical downscaling. *Hydrological Sciences Journal*, 61(14), 2481-2495.
- Kharecha, P. A., & Hansen, J. E. (2008). Implications of "peak oil" for atmospheric CO₂ and climate. *Global Biogeochemical Cycles*, 22(3).
- Köy Hizmetleri Genel Müdürlüğü (KHGM), T. B. K. H. G. (1993). 1/100 000 Ölçekli Toprak ve Arazi Kullanım Haritası (Antalya İli Arazi Varlığı) Tarım Orman ve Köy İşleri Bakanlığı Köy Hizmetleri Genel Müdürlüğü Yayınları. Ankara. (in Turkish).
- Kentel, E., Yücel, İ., Mesta, B., Akgün, Ö.B., Özcan, C., Ercan, E., Körpınar, A. S., Kaleli, M., Matur, İ. (2021). TÜBİTAK Antalya Havzası'nda İklim Değişikliğinin Debi ve HES Enerji Üretimine Etkilerinin İncelenmesi Projesi (Pr No: 118Y365), Proje Sonuç Raporu, TÜBİTAK, Ankara. (in Turkish).
- Kitoh, A. (2007). Future climate projections around Turkey by global climate models. Final report of the Research Project on the Impact of Climate Changes On Agricultural Production System In Arid Areas (ICCAP). ICCAP Publication 10

- Knebl, M. R., Yang, Z. L., Hutchison, K., & Maidment, D. R. (2005). Regional scale flood modeling using NEXRAD rainfall, GIS, and HEC-HMS/RAS: a case study for the San Antonio River Basin Summer 2002 storm event. *Journal of Environmental Management*, 75(4), 325-336.
- Knoben, W. J., Freer, J. E., & Woods, R. A. (2019). Inherent benchmark or not? Comparing Nash–Sutcliffe and Kling–Gupta efficiency scores. *Hydrology and Earth System Sciences*, 23(10), 4323-4331.
- Koçyiğit, M., Akay, H., & Yanmaz, A. (2017). Estimation of Hydrologic Parameters of Kocanaz Watershed by a Hydrologic Model. *International Journal of Engineering and Applied Sciences*, 9(4), 42-50.
- Koray Üstebay, E., Keleş, A., Taşkın, İ. (2018). 9-20 Manavgat-İbradı-Cevizli Yeraltısuyu Alt Havzası Hidrojeolojik Etüt Raporu, DSİ 13. Bölge Müdürlüğü, Antalya (in Turkish).
- Kostopoulou, E., & Jones, P. D. (2005). Assessment of climate extremes in the Eastern Mediterranean. *Meteorology and Atmospheric Physics*, 89(1), 69-85.
- Kotsifakis, K. G., Psomas, A. G., Feloni, E. G., & Baltas, E. A. (2015, September). Rainfall-Runoff Modeling in an Experimental Watershed in Greece. In 14th International Conference on Environmental Science and Technology.
- Kour, R., Patel, N., & Krishna, A. P. (2016). Climate and hydrological models to assess the impact of climate change on hydrological regime: a review. *Arabian Journal of Geosciences*, 9(9), 544.
- Krichak, S. O., Kishcha, P., & Alpert, P. (2002). Decadal trends of main Eurasian oscillations and the Eastern Mediterranean precipitation. *Theoretical and Applied Climatology*, 72(3), 209-220.
- Krishnamurti, T. N., Kishtawal, C. M., LaRow, T. E., Bachiochi, D. R., Zhang, Z., Williford, C. E., ... & Surendran, S. (1999). Improved weather and seasonal climate forecasts from multimodel superensemble. *Science*, 285(5433), 1548-1550.

- Krishnamurti, T. N., Kishtawal, C. M., Zhang, Z., LaRow, T., Bachiochi, D., Williford, E., ... & Surendran, S. (2000). Multimodel ensemble forecasts for weather and seasonal climate. *Journal of Climate*, 13(23), 4196-4216.
- Krishnamurti, T. N., Kumar, V., Simon, A., Bhardwaj, A., Ghosh, T., & Ross, R. (2016). A review of multimodel superensemble forecasting for weather, seasonal climate, and hurricanes. *Reviews of Geophysics*, 54(2), 336-377.
- Kuglitsch, F. G., Toreti, A., Xoplaki, E., Della-Marta, P. M., Zerefos, C. S., Türkeş, M., & Luterbacher, J. (2010). Heat wave changes in the eastern Mediterranean since 1960. *Geophysical Research Letters*, 37(4).
- Kurucu, Y., & Esetlili, M.T. (2018). Rendzic Leptosols. In: Kapur S., Akça E., Günel H. (eds) *The Soils of Turkey*. World Soils Book Series. Springer, Cham.
- Landelius, T., Dahlgren, P., Gollvik, S., Jansson, A. and Olsson, E. (2016). A high-resolution regional reanalysis for Europe. Part 2: 2D analysis of surface temperature, precipitation, and wind. *Quarterly Journal of the Royal Meteorological Society*, 142(698), 2132–2142.
- Lionello, P., Malanotte-Rizzoli, P., Boscolo, R., Alpert, P., Artale, V., Li, L., . . . Xoplaki, E. (2006). The Mediterranean Climate: An Overview of the Main Characteristics and Issues. In P. Lionello, P. Malanotte-Rizzoli, & R. Boscolo, *Mediterranean Climate Variability*, Volume 4 (p. 438).
- Lopez, A., Fung, F., New, M., Watts, G., Weston, A., & Wilby, R. L. (2009). From climate model ensembles to climate change impacts and adaptation: A case study of water resource management in the southwest of England. *Water Resources Research*, 45(8).
- López-Moreno, J. I., Goyette, S., & Beniston, M. (2008). Climate change prediction over complex areas: spatial variability of uncertainties and predictions over the Pyrenees from a set of regional climate models. *International Journal of Climatology: A Journal of the Royal Meteorological Society*, 28(11), 1535-1550.

- Lun, Y., Liu, L., Cheng, L., Li, X., Li, H., & Xu, Z. (2021). Assessment of GCMs simulation performance for precipitation and temperature from CMIP5 to CMIP6 over the Tibetan Plateau. *International Journal of Climatology*.
- Meenu, R., Rehana, S., & Mujumdar, P. P. (2013). Assessment of hydrologic impacts of climate change in Tunga–Bhadra river basin, India with HEC-HMS and SDSM. *Hydrological Processes*, 27(11), 1572-1589.
- Mehr, A. D., & Kahya, E. (2017). Climate Change Impacts on Catchment-Scale Extreme Rainfall Variability: Case Study of Rize Province, Turkey. *Journal of Hydrologic Engineering*, 22(3), 1-11. doi:10.1061/(ASCE)HE.1943-5584.0001477.
- Melloh, R. A. (1999). A synopsis and comparison of selected snowmelt algorithms. US Army Corps of Engineers, CRREL Report 99-8, p.17.
- Mesta, B., Akgun, O. B., & Kentel, E. (2021). Alternative solutions for long missing streamflow data for sustainable water resources management. *International Journal of Water Resources Development*, 37(5), 882-905.
- Mesta, B., & Kentel, E. (2022). Superensembles of raw and bias-adjusted regional climate models for Mediterranean region, Turkey. *International Journal of Climatology*, 42(4), 2566-2585. <https://doi.org/10.1002/joc.7381>.
- Mesta, B., Sasaki, H., Nakaegawa, T., & Kentel, E. (2022). Changes in precipitation climatology for the Eastern Mediterranean using CORDEX RCMs, NHRCM and MRI-AGCM. *Atmospheric Research*, Volume 272, 2022, 106140, ISSN 0169-8095, <https://doi.org/10.1016/j.atmosres.2022.106140>.
- Moriasi, D. N., Arnold, J. G., Van Liew, M. W., Bingner, R. L., Harmel, R. D., & Veith, T. L. (2007). Model evaluation guidelines for systematic quantification of accuracy in watershed simulations. *Transactions of the ASABE*, 50(3), 885-900.

- Moriasi, D. N., Gitau, M. W., Pai, N., & Daggupati, P. (2015). Hydrologic and water quality models: Performance measures and evaluation criteria. *Transactions of the ASABE*, 58(6), 1763-1785.
- Moss, R. H., Edmonds, J. A., Hibbard, K. A., Manning, M. R., Rose, S. K., Van Vuuren, D. P., & Meehl, G. A. (2010). "The next generation of scenarios for climate change research and assessment". *Nature*, 463(7282), 747.
- NASA JPL (2013). NASA Shuttle Radar Topography Mission Global 1 arc second number [Data set]. NASA EOSDIS Land Processes DAAC. Latest access: 23.07.2020 Retrieved from: <https://doi.org/10.5067/MEaSURES/SRTM/SRTMGL1N.003>
- Normand, S., Konz, M., & Merz, J. (2010). An application of the HBV model to the Tamor Basin in Eastern Nepal. *Journal of Hydrology and meteorology*, 7(1), 49-58.
- Okkan, U., & Inan, G. (2015). Statistical downscaling of monthly reservoir inflows for Kemer watershed in Turkey: use of machine learning methods, multiple GCMs and emission scenarios. *International Journal of Climatology*, 35(11), 3274-3295.
- Okkan, U., & Kirdemir, U. (2016). Downscaling of monthly precipitation using CMIP5 climate models operated under RCPs. *Meteorological Applications*, 23(3), 514-528.
- Osuch, M. (2015). Sensitivity and uncertainty analysis of precipitation-runoff models for the Middle Vistula Basin. In *Stochastic Flood Forecasting System* (s. 61-81). Springer Cham.
- Öno1, B., & Unal, Y. S. (2014). Assessment of climate change simulations over climate zones of Turkey. *Regional Environmental Change*, 14(5), 1921-1935.
- Özdoğan, M. (2011). Modeling the impacts of climate change on wheat yields in Northwestern Turkey. *Agriculture, Ecosystems and Environment*, 141, 1-12. doi:10.1016/j.agee.2011.02.001.

- Öztürk, T., Ceber, Z. P., Türkeş, M., & Kurnaz, M. L. (2015). Projections of climate change in the Mediterranean Basin by using downscaled global climate model outputs. *International Journal of Climatology*, 35, 4276-4292. doi:10.1002/joc.4285.
- Palatella, L., Miglietta, M. M., Paradisi, P., & Lionello, P. (2010). Climate change assessment for Mediterranean agricultural areas by statistical downscaling. *Natural Hazards and Earth System Sciences*, 1647-1661. doi:10.5194/nhess-10-1647-201
- Park, C., Lee, G., Kim, G., & Cha, D. H. (2021). Future changes in precipitation for identified sub-regions in East Asia using bias-corrected multi-RCMs. *International Journal of Climatology*, 41(3), 1889-1904.
- Peterson, T. C., Folland, C., Gruza, G., Hogg, W., Mokssit, A., & Plummer, N. (2001). Report of the Activities of the Working Group on Climate Change Detection and Related Rapporteurs, 1998–2001, WMO, Rep. WCDMP-47, WMO-TD 1071, 143 pp., World Meteorological Organization, Geneva, Switzerland.
- Piani, C., Weedon, G. P., Best, M., Gomes, S. M., Viterbo, P., Hagemann, S.,... & Haerter, J. O. (2010). Statistical bias correction of global simulated daily precipitation and temperature for the application of hydrological models. *Journal of hydrology*, 395(3-4), 199-215.
- Prudhomme, C., Davies, H. (2009). Assessing uncertainties in climate change impact analyses on the river flow regimes in the UK. Part 2: future climate. *Climatic Change* 93, 197–222. <https://doi.org/10.1007/s10584-008-9461-6>.
- Raskin, P., Gleick, P., Kirshen, P., Pontius, G., & Strzepek, K. (1997). Water futures: assessment of long-range patterns and problems. Comprehensive assessment of the freshwater resources of the world. SEI.

- Republic of Turkey Ministry of Environment and Urbanization (MoEU). (2012). Turkey's National Climate Change Adaptation Strategy and Action Plan: 2011–2023. Ankara.
- Rogelis, M. C., Werner, M., Obregón, N., & Wright, N. (2016). Hydrological model assessment for flood early warning in a tropical high mountain basin. *Hydrology and Earth System Sciences Discussions*.
- Ross, C.W., Prihodko, L., Anchang, J.Y., Kumar, S.S., Ji, W., and Hanan, N.P. (2018). Global Hydrologic Soil Groups (HYSOGs250m) for Curve Number-Based Runoff Modeling. ORNL DAAC, Oak Ridge, Tennessee, USA. <https://doi.org/10.3334/ORNLDAAC/1566>.
- Sato, Y., Kojiri, T., Michihiro, Y., Suzuki, Y., & Nakakita, E. (2012). Estimates of Climate Change Impact on River Discharge in Japan Based on a Super-High-Resolution Climate Model. *Terrestrial, Atmospheric & Oceanic Sciences*, 23(5).
- Scharffenberg, W. (2015). Hydrologic Modeling System HEC-HMS: User's Manual, version 4.1 [online]. Davis: US Army Corps of Engineers, Hydrologic Engineering Center. Retrieved from: http://www.hec.usace.army.mil/software/hec-hms/documentation/HEC-HMS_Users_Manual_4.1.
- Seguí, P. Q., Ribes, A., Martín, E., Habets, F., & Boé, J. (2010). Comparison of three downscaling methods in simulating the impact of climate change on the hydrology of Mediterranean basins. *Journal of hydrology*, 383(1-2), 111-124.
- Seibert, J. (1997). Estimation of parameter uncertainty in the HBV model. *Nordic Hydrology*, 28(4/5), 247-262.
- Seibert, J. (2000). "Multi-criteria calibration of a conceptual runoff model using a genetic algorithm." *Hydrology and Earth System Sciences Discussions*, European Geosciences Union, 2000, 4 (2), pp.215-224. hal-00304596.

- Seibert, J. (2005). HBV Light Version 2. User's Manual. Department of Physical Geography and Quaternary Geology, Stockholm University, Stockholm, Sweden, 2005; p. 32.
- Şen, Z. (2018). Climate Change Impact on Floods. In: Flood Modeling, Prediction and Mitigation. Springer, Cham. p.337-379. https://doi.org/10.1007/978-3-319-52356-9_8
- Sen, B., Topcu, S., Türkeş, M., Sen, B., & Warner, J. F. (2012). Projecting climate change, drought conditions and crop productivity in Turkey. *Climate Research*, 52, 175-191. Doi:10.3354/cr01074.
- Sensoy, S., Demircan, M., Ulupinar, Y., & Balta, I. (2008). Climate of Turkey. Turkish State Meteorological Service, 401. http://212.174.109.9/FILES/genel/makale/31_climateofturkey.pdf
- Sensoy, S., & Demircan, M. (2016). Climate of Turkey. Turkish State Meteorological Service, Ankara, Turkey. https://www.researchgate.net/publication/296597022_Climate_of_Turkey.
- Shahid, M., Boccoardo, P., Usman, M., Albanese, A., & Qamar, M. (2017). Predicting Peak Flows in Real Time through Event Based Hydrologic Modeling for a Trans-Boundary River Catchment. *Water Resources Management*, 31, 793-810.
- Sharma, D., Das Gupta, A., & Babel, M. S. (2007). Spatial disaggregation of bias-corrected GCM precipitation for improved hydrologic simulation: Ping River Basin, Thailand. *Hydrology and Earth System Sciences*, 11(4), 1373-1390.
- Singh, V.P. (1988). *Hydrologic Systems. Volume 1: Rainfall-runoff modelling*. Prentice Hall, New Jersey.
- Singh, J., Knapp, H. V., Arnold, J. G., & Demissie, M. (2005). Hydrological modeling of the Iroquois river watershed using HSPF and SWAT 1. *JAWRA Journal of the American Water Resources Association*, 41(2), 343-360.

- Sirdas, S., Ross, R. S., Krishnamurti, T. N., & Chakraborty, A. (2007). Evaluation of the FSU synthetic superensemble performance for seasonal forecasts over the Euro-Mediterranean region. *Tellus A: Dynamic Meteorology and Oceanography*, 59(1), 50-70.
- Sitterson, J., Knightes, C., Parmar, R., Wolfe, K., Muche, M., & Avant, B. (2018). An overview of rainfall-runoff model types. Georgia: U.S. Environmental Protection Agency (EPA).
- Sorman, A., (2005) Use of satellite observed seasonal snow cover in hydrological modeling and snowmelt runoff prediction in upper Euphrates basin, Turkey. PhD Thesis. Middle East Technical University (METU) .
- Şorman, A. A., Şensoy, A., Tekeli, A. E., Şorman, A. Ü., & Akyürek, Z. (2009). Modelling and forecasting snowmelt runoff process using the HBV model in the eastern part of Turkey. *Hydrological Processes: An International Journal*, 23(7), 1031-1040.
- Sorman, A. A., Tas, E., Dogan, Y. O. (2020). Comparison of hydrological models in upper Aras Basin. *Pamukkale Üniversitesi Mühendislik Bilimleri Dergisi*, 26 (6), 1015-1022 Retrieved from: <https://dergipark.org.tr/en/pub/pajes/issue/57790/825410>
- Stefanova, L., & Krishnamurti, T. N. (2002). Interpretation of seasonal climate forecast using Brier skill score, the Florida State University superensemble, and the AMIP-I dataset. *Journal of Climate*, 15(5), 537-544.
- Sunyer Pinya, M. A., Hundecha, Y., Lawrence, D., Madsen, H., Willems, P., Martinkova, M., Vormoor, K., Bürger, G., Hanel, M., Kriaučiuniene, J., Loukas, A., Osuch, M., & Yücel, I. (2015). Inter-comparison of statistical downscaling methods for projection of extreme precipitation in Europe. *Hydrology and Earth System Sciences*, 19(4), 1827-1847. <https://doi.org/10.5194/hess-19-1827-2015>.
- Tanarhte, M., Hadjinicolaou, P., & Lelieveld, J. (2015). Heat wave characteristics in the eastern Mediterranean and Middle East using extreme value theory. *Climate Research*, 63(2), 99-113.

- Tayanç, M., İm, U., Doğruel, M., & Karaca, M. (2009). Climate change in Turkey for the last half century. *Climatic Change*, 94(3), 483-502.
- Taylor, K. E. (2001). Summarizing multiple aspects of model performance in a single diagram. *Journal of Geophysical Research: Atmospheres*, 106(D7), 7183-7192.
- Taylor, K. E. (2005). Taylor diagram primer. Retrived from: http://www.pcmdi.llnl.gov/about/staff/Taylor/CV/Taylor_diagram_primer.pdf.
- Taylor, K. E. (2009). A summary of the CMIP5 experiment design. Retrived from: http://cmip-pcmdi.llnl.gov/cmip5/docs/Taylor_CMIP5_design.pdf. Latest access: 17.08.2018.
- Tebaldi, C., & Knutti, R. (2007). The use of the multi-model ensemble in probabilistic climate projections. *Philosophical transactions of the royal society A: mathematical, physical and engineering sciences*, 365(1857), 2053-2075.
- Teutschbein, C., & Seibert, J. (2012). Bias correction of regional climate model simulations for hydrological climate-change impact studies: Review and evaluation of different methods. *Journal of hydrology*, 456, 12-29.
- Thiemig, V., Bisselink, B., Pappenberger, F., & Thielen, J. (2015). A pan-African medium-range ensemble flood forecast system. *Hydrol. Earth Syst. Sci*, 19(8), 3365-3385.
- Toros, H. (2012). Spatio-temporal variation of daily extreme temperatures over Turkey. *International Journal of Climatology*, 32(7), 1047-1055.
- TÜBİTAK MAM. (2013). Havza Koruma Eylem Planlarının Hazırlanması Projesi-Antalya Havzası, Proje kodu: 5118601. Proje sonuç raporu. Türkiye Bilimsel ve Teknik Araştırma Kurumu Marmara Araştırma Merkezi (TÜBİTAK MAM) Çevre Enstitüsü. Kocaeli. (in Turkish).

- Unal, Y. S., Tan, E., & Montes, S. S. (2013). Summer heat waves over western Turkey between 1965 and 2006. *Theoretical and Applied Climatology*, 112(1), 339-350.
- Vis, M., Knight, R., Pool, S., Wolfe, W., and Seibert, J. (2015). Model calibration criteria for estimating ecological flow characteristics. *Water*, 7(5), 2358-2381.
- Vrac, M., Noël, T. & Vautard, R. (2016). Bias correction of precipitation through singularity stochastic removal: because occurrences matter. *Journal of Geophysical Research: Atmospheres*, 121(10), 5237–5258.
- Wagener, T., Boyle, D. P., Lees, M. J., Wheater, H. S., Gupta, H. V., & Sorooshian, S. (2001). A framework for development and application of hydrological models, *Hydrol. Earth Syst. Sci.*, 5, 13–26, <https://doi.org/10.5194/hess-5-13-2001>, 2001.
- Weedon, G.P., Balsamo, G., Bellouin, N., Gomes, S., Best, M.J. & Viterbo, P. (2014). The WFDEI meteorological forcing data set: WATCH forcing data methodology applied to ERA-interim reanalysis data. *Water Resources Research*, 50. <https://doi.org/10.1002/2014WR015638>.
- Whitley, D. (1994). A genetic algorithm tutorial. *Statistics and computing* 4.2: 65-85.
- Xu, C.Y. (1999). From GCMs to river flow: a review of downscaling methods and hydrologic modelling approaches. *Pro Phys Geogr* 23:229–249
- Xu, C. Y. (2002). *Textbook of hydrologic models: Chapter 1 Modelling in Hydrology*. Uppsala University. Sweden. 50-59.
- Yang, W., Andréasson, J., Phil Graham, L., Olsson, J., Rosberg, J. & Wetterhall, F. (2010). Distribution-based scaling to improve usability of regional climate model projections for hydrological climate change impacts studies. *Hydrology Research*, 41(3–4), 211–229.

- Yener, M. K., Sorman, A. U., Sorman, A. A., Sensoy, A., & Gezgin, T. (2007). Modeling studies with HEC-HMS and runoff scenarios in Yuvacik Basin, Turkiye. *Int. Congr. River Basin Manage*, 4(2007), 621-634.
- Yıldırım, A., & Yücel, İ. (2019). Drought Analysis using CORDEX Simulations over the Mediterranean Climate Regions of Turkey.
- Yılmaz, A. G., Imteaz, M. A., & Ogwuda, O. (2012). Accuracy of HEC-HMS and LBRM models in simulating snow runoffs in Upper Euphrates Basin. *Journal of Hydrologic Engineering*, 17(2), 342-347.
- Yılmaz, A. G. (2015). The effects of climate change on historical and future extreme rainfall in Antalya, Turkey. *Hydrological Sciences Journal - Journal des Sciences Hydrologiques*, 60(12), 2148-2162. doi:10.1080/02626667.2014.945455.
- Yılmaz, G., Çolak, M. A., Özgencil, İ. K., Metin, M., Korkmaz, M., Ertuğrul, S., Soylier M., Bucak T., Tavşanoğlu Ü. N., Özkan K., Akyürek Z., Beklioğlu M. Jeppesen, E. (2021). Decadal changes in size, salinity, waterbirds, and fish in lakes of the Konya Closed Basin, Turkey, associated with climate change and increasing water abstraction for agriculture. *Inland Waters*, 11(4), 538-555. DOI: 10.1080/20442041.2021.1924034
- Yimer, G., Jonoski, A., & Griensven, A. V. (2009). Hydrological response of a catchment to climate change in the upper Beles river basin, upper blue Nile, Ethiopia. *Nile Basin Water Engineering Scientific Magazine*, 2, 49-59.
- Yolsu Mühendislik Hizmetleri. (2018). Antalya Havzası Master Plan Yapım İşİ Nihai Raporu 3.Bölüm – Hidroloji, Devlet Su İşleri Genel Müdürlüğü, 13. Bölge Müdürlüğü, Antalya (in Turkish).
- Yücel, I., & Keskin, F. (2011). Assessment of flash flood events using remote sensing and atmospheric model-derived precipitation in a hydrological model. *Int. Assoc. Hydrol. Sci.*, 344, 245-251.

- Yucel, I., Güventürk, A., & Sen, O. L. (2015). Climate change impacts on snowmelt runoff for mountainous transboundary basins in eastern Turkey. *International Journal of Climatology*, 35(2), 215-228.
- Yun, W. T., Stefanova, L., Mitra, A. K., Vijaya Kumar, T. S., Dewar, W., & Krishnamurti, T. N. (2005). A multi-model superensemble algorithm for seasonal climate prediction using DEMETER forecasts. *Tellus A: Dynamic Meteorology and Oceanography*, 57(3), 280-289.
- Zapata-Sierra, A. J., & Manzano-Agugliaro, F. (2019). Proposed methodology for evaluation of small hydropower sustainability in a Mediterranean climate. *Journal of cleaner production*, 214, 717-729.
- Zeleeuw, M. B., & Alfredsen, K. (2014). Use of cokriging and map correlation to study hydrological response patterns and select reference stream gauges for ungauged catchments. *Journal of Hydrologic Engineering*, 19(2), 388-406.

APPENDICES

A. PAPER 1: SUPERENSEMBLES OF RAW AND BIAS-ADJUSTED REGIONAL CLIMATE MODELS FOR MEDITERRANEAN REGION, TURKEY

This appendix was published as Mesta, B., & Kentel, E. (2022). Superensembles of raw and bias-adjusted regional climate models for Mediterranean region, Turkey. *International Journal of Climatology*, 42(4), 2566-2585. <https://doi.org/10.1002/joc.7381>.

RESEARCH ARTICLE

Superensembles of raw and bias-adjusted regional climate models for Mediterranean region, Turkey

Buket Mesta¹ | Elcin Kentel² 

¹Department of Earth System Science,
Middle East Technical University,
Ankara, Turkey

²Department of Civil Engineering, Middle
East Technical University, Ankara,
Turkey

Correspondence

Elcin Kentel, Department of Civil
Engineering, Water Resources Laboratory,
Middle East Technical University, K4
Bldg., 06800 Ankara, Turkey.
Email: ekentel@metu.edu.tr

Funding information

Scientific and Technological Research
Council of Turkey, Grant/Award Number:
118Y365

Abstract

For regional-scale studies on climate change and relevant impact assessment, the projections of regional climate models (RCMs) are used due to their advantage of high resolution and better representation of the local climate relative to the global climate models. However, direct use of RCM outputs is prone to uncertainties and biases that may significantly diminish the accuracy of results. EURO-COordinated Regional Downscaling EXperiment (CORDEX) initiative that is a part of the global Coordinated Regional Downscaling Experiment Project provides high-resolution RCM projections for the European domain and bias-adjusted regional projections under the “CORDEX-Adjust” Project for climate change impact assessment studies. This study aims to perform a multi-model analysis of precipitation data using bias-adjusted and raw/non-bias adjusted CORDEX RCMs to obtain an evaluation of their representativeness for local climate conditions and adequacy to be used for climate change impact assessment. For this purpose, the analysis focuses on four CORDEX RCMs and their 12 bias-adjusted versions generated with cumulative distribution function transformation, quantile mapping, and distribution-based scaling methodologies. For the analysis in total, 16 hindcast results of raw and bias-adjusted RCMs, and three superensembles (SEs) generated through multiple linear regression are compared for their performance regarding their goodness of fit to the ground-based precipitation monitoring data from eight meteorological stations in the Mediterranean region in Turkey. The analysis verified that the skill of individual simulations including the bias-adjusted outputs is significantly variable in spatial and temporal means. On the other hand, SE formed by using all 16 hindcast outputs has the highest skill for the representation of variability in precipitation in time as well as for the reproduction of annual climatology at all stations, although potential drawbacks concerning seasonality and the range of anomaly may still exist which might be significant depending on the specific aim of impact assessment.

KEYWORDS

bias-adjusted RCM, climate change impact assessment, Mediterranean region, multi-model ensembles, RCM, superensemble

1 | INTRODUCTION

Many globally observed indicators of climate change suggest potential significant impacts on the environmental conditions both regionally and globally, given that the climate is one of the main controls on the environment. Therefore, assessment of those impacts is a crucial part of adequate planning and management of the environment and natural resources on various scales. Numerous studies on climate change impacts rely on the projections from regional climate models (RCMs), particularly for regional and local assessments. RCMs provide sufficient resolution for such purposes and enable simulation of regional conditions through parametrization of local climate processes (Leung *et al.*, 2003). However, RCM outputs may contain systematic errors or biases (IPCC, 2015; Gutiérrez *et al.*, 2019) that may be inherited from the driving global climate models (GCMs) or caused by reasons such as imperfect conceptualization, discretization, and spatial averaging within grid cells (Fujihara *et al.*, 2008; López-Moreno *et al.*, 2008; Teutschbein and Seibert, 2012; Kara and Yucel, 2015). To overcome such drawbacks, researchers choose to use RCM outputs that are post-processed with statistical bias adjustment methods for climate change impact assessment.

Bias correction methodologies have the advantage of being computationally inexpensive but may have their limitations (IPCC, 2015). Different RCMs and different empirical bias correction methodologies may create advantages and disadvantages for the simulation of different processes that might be more significant for certain locations, seasons, or periods. The studies indicate significant uncertainties and inter-model variability for RCM results (López-Moreno *et al.*, 2008; Sunyer Pinya *et al.*, 2015) which is even more pronounced for regions with complex terrain features (Evans, 2009). In fact, the uncertainties from climate models (i.e., driving GCM and downscaling to obtain RCM) is verified to be the most dominant element of uncertainty in climate change impact assessment studies on hydrology (Chen *et al.*, 2011) along with the uncertainties from natural variability, selected emission scenario, and hydrological modelling (Lee *et al.*, 2017).

Therefore, before the use of climate model products the hindcast outputs should be validated through an evaluation of the goodness of fit with the local climate observations. On the other hand, due to the multi-dimensional variability and uncertainties of climate modelling, there is no standard method for the selection of the best or most representative model to be used in climate change impact assessments. Additionally, the single model assessment may cause poor justification due to the various advantage and disadvantages different models have.

Multi-model ensemble (MME) analysis is an approach to overcome this challenge. Studies indicate that the ensemble model generates superior results over single model use (Tebaldi and Knutti, 2007; Sunyer Pinya *et al.*, 2015). MME is reported to reduce the model biases by enabling the use of a set of models (Tebaldi and Knutti, 2007). In order to obtain MME outputs, different approaches can be used such as multi-model simple averaging or the use of multi-model weighted average based on some model performance metrics (Tebaldi and Knutti, 2007; Christensen *et al.*, 2010). Among these various techniques, the superensemble (SE) approach is suggested by Krishnamurti *et al.* (1999) and is based on the calculation of MME output by the use of a set of models with weights identified through multiple linear regression (MLR) so as to obtain the best fit between observed and MME output (Krishnamurti *et al.*, 1999; 2000; 2016; Stefanova and Krishnamurti, 2002).

EURO-COordinated Regional Downscaling EXperiment (CORDEX) initiative that is a part of the global CORDEX Project provides high-resolution RCM projections (Jacob *et al.*, 2020) and bias-adjusted regional projections under the “CORDEX-Adjust” Project (IPCC, 2015) for climate change impact assessment studies in European Domain. Certain studies have been conducted by the use of projections from CORDEX RCMs (from hereafter will be referred to as RCMs) and bias-adjusted RCMs from the CORDEX-Adjust database (from hereafter will be referred to as bias-adjusted RCMs) for the impact of climate change on the hydrological elements of the water cycle in the region of the eastern Mediterranean. Yucel *et al.* (2015) studied the effect of climate change in runoff volumes and shifts in seasonality in eastern Turkey created by a change in snowmelt runoff. Some other studies assessed the potential future changes in the water cycle (Onol and Semazzi, 2009; Black *et al.*, 2010; Onol *et al.*, 2014) and the potential of an increase in aridity in the region (Gao and Giorgi, 2008) by the use of RCMs. Onol and Semazzi (2009) report the potential of a decrease in precipitation for the winter season, the main wet season for the region, over southeastern Turkey. The decrease in winter precipitations is expected to have a significant impact on the region and its downstream in the eastern Mediterranean. Several studies validate the decreasing trend in total winter precipitation in south and southeastern Anatolian, and the Mediterranean, an increase in extremes, and the potential of increased aridity and water stress in the region that is defined to be vulnerable under climate change conditions (Gao and Giorgi, 2008; Yucel *et al.*, 2015; Türkeş *et al.*, 2016; Aziz *et al.*, 2020). Furthermore, the study by Giannaros *et al.* (2018) on the thermal bioclimate mapping of the southeast Mediterranean and

the Balkans with high-resolution climate modelling verified statistically significant warming trends that are expected to create potential concerns on public health as well as impacts on certain socioeconomic activities.

With its complex terrain and climatic features, the eastern Mediterranean attracts much attention for the projection of the climate impacts. Hence, for such a complex terrain with localized climate processes, the variability of the climate projections is required to be tested well. On the other hand, to the best of our knowledge, the number of studies testing the performance of climate models, RCMs, bias-adjusted RCMs, and ensemble models, against historical land-based climate records in Turkey is still limited. Additionally, the studies for the analysis of bias-adjusted RCM outputs available from the CORDEX database in the eastern Mediterranean are still numbered.

Aziz *et al.* (2020) in their study provide an ensemble analysis of 12 raw RCMs and 2 bias-adjusted RCMs. The accuracy of outputs is validated through a comparison with long-term temperature data from local meteorological stations (MSs). Study results indicate approximately 60% improvement in root mean square error (RMSE) and mean absolute error of RCMs using the distribution-based scaling (DBS) method by the Swedish Meteorological and Hydrological Institute (SMHI) compared to the non-bias adjusted outputs of CNRM-CERFACS-CNRM-CM5—CCLM4-8-7, and Institut Pierre Simon Laplace (IPSL)-IPSL-CM5A-MR—RCA4.

A study by Kentel *et al.* (2019) uses the results of 5 RCMs and makes a comparison with the 13 bias-adjusted RCMs. In their study, raw and bias-corrected (adjusted with DBS, cumulative distribution function transform [CDF-t], and quantile-mapping methods) hindcast outputs from RCMs are compared with historical monthly

precipitation time series from two local MSs. Analysis indicates that a group of bias-adjusted RCM outputs provides a relative improvement in the correlations and RMSE values regarding the goodness of fit with observation data, whereas some of the bias-adjusted versions in the study create a reduction in correlations (Kentel *et al.*, 2019).

MME analysis and use of MME outputs for the climate change impact assessment is used in various studies focusing on relevant impacts on hydrology, crop yields, and reservoir inflows for various basins in Turkey (Kitoh, 2007; Ozdogan, 2011; Okkan and Inan, 2015; Okkan and Kirdemir, 2016).

In this study, our objective is to test the accuracy and the representativeness of 4 RCMs and their 12 bias-adjusted versions. The RCMs and their bias-adjusted hindcast results for precipitation are analysed through a comparison with land-based historical observational records on daily precipitation. The performance of RCMs and the rate of improvement provided by the post-processed outputs are evaluated to define potential advantages and weaknesses in the case of use in climate change impact assessment such as hydrological assessment studies. Furthermore, MLR is used to generate SEs and the performance of single model projections compared to the ensembled series is evaluated. To summarize, this study comparatively evaluates performances of RCMs, bias-adjusted RCMs, and SEs in southern Turkey.

2 | DESCRIPTION OF THE STUDY AREA

The objective of this study is the multi-model analysis of climate models to assess the relative performance of

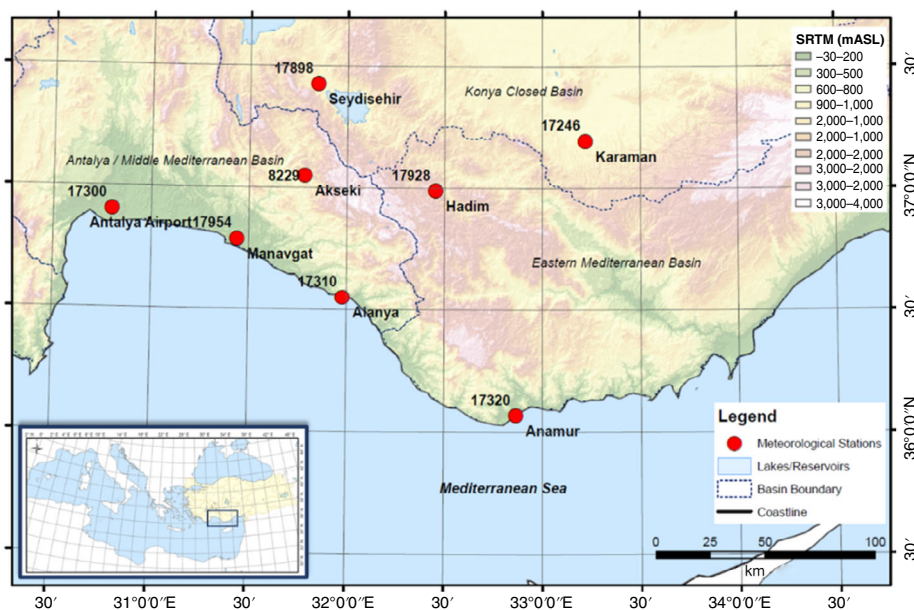


FIGURE 1 Location of the study area [Colour figure can be viewed at wileyonlinelibrary.com]

different RCMs for an approximate area of 20,000 km² in southern Turkey (Figure 1). The study focuses on the historical climate data for an area between 36°50′–37°70′N latitudes and 30°50′–33°15′E longitudes including the drainage divide of three main watersheds of Turkey.

The daily historical precipitation data that are used for this study are collected from eight local ground-based meteorological monitoring stations operated by the Turkish State Meteorological Services. Among the eight MSs, two of them (MS 17246: Karaman and MS 17898: Seydisehir) are in Konya closed basin located behind the water divide created by the Taurus mountain ridges that also act as a strong control on the local climate. The remaining six stations are in Middle and Eastern Mediterranean basins where a typical Mediterranean climate with mild winter and dry hot summer conditions prevail. Despite the relative proximity of these stations, the local topography and the Mediterranean Sea create complexity in local climate processes and divergent climatologic features for the stations in different watersheds. For example, according to the precipitation records between 1971 and 2005 Akseki station (MS 8229, 1,150 mASL) is located approximately 40 km inward Mediterranean coast and shows typical Mediterranean climate features with pronounced seasonality in precipitation intensity. Due to the orographic processes, Akseki station receives the highest precipitation in the middle Mediterranean basin. In the same basin, less than 45 km south the coastal Manavgat station (MS 17954) receives 20% less mean precipitation relative to Akseki. Seydisehir station (MS 17898) less than 45 km north and Hadim station (MS 17928) 60 km east of Akseki station are located at the leeward side of the mountain ridges forming their respective basin boundaries. Although these two stations

are located at a similar altitude range with Akseki station, they receive relatively half of its mean precipitation. Along with Seydisehir station, Karaman station (MS 17246) further east is located in a closed basin where cold semi-arid climate prevails receives significantly low total precipitation. The mean precipitation at Karaman station drops to 25% of Akseki Station. The physical barrier of the Taurus Mountains between different basins exerts a significant orographic impact shaping the regional climatology.

3 | DATA AND METHOD

3.1 | Reference data

In this study, the daily historical precipitation records from eight MSs based on readings from the manually operated rain gauges for the period between 1971 and 2005 are used as the benchmark for the analysis of the accuracy of climate models. The monthly average precipitation calculated from daily historical runs from climate models is compared with those of observations. The list of eight MSs operated by Turkish State Meteorological Services is given in Table 1. Figure 1 shows a location map of MSs indicating relevant drainage basins of each.

To obtain the monthly time series from each station daily data are put into a simple quality check process in which the months with more than 10 days of missing records are eliminated from the dataset. Similarly, for further analysis of seasonal and annual means, and climatological precipitation values, seasons missing more than 2 months and years missing more than two seasons are eliminated from the time series obtained for the analysis.

TABLE 1 List of meteorological stations in the study area

Station ID	Station name	Province	Basin name	Latitude (DD)	Longitude (DD)	Elevation (mASL)	Distance to the sea (km)
8229	Akseki	Antalya	Middle Mediterranean	37.05	31.78	1,150	42
17246	Karaman	Karaman	Konya closed basin	37.71	33.53	996	118
17300	Antalya Airport	Antalya	Middle Mediterranean	36.91	30.80	64	6
17310	Alanya	Antalya	Middle Mediterranean	36.55	31.98	6	—
17320	Anamur	Mersin	Eastern Mediterranean	38.06	30.15	2	—
17898	Seydisehir	Konya	Konya closed basin	37.43	31.85	1,129	82
17928	Hadim	Konya	Eastern Mediterranean	36.99	32.46	1,552	63
17954	Manavgat	Antalya	Middle Mediterranean	36.79	31.44	38	4

3.2 | Model data

Four different RCMs contribute to the multi-model assessment in this study. For analysis, the daily precipitation outputs from the historical runs of the RCMs are obtained from the CORDEX database. Furthermore, the analysis includes a comparative evaluation between raw and bias-adjusted outputs of the relevant climate models. The bias-adjusted outputs of RCMs are hindcast outputs available from the Climate4impact portal (IS-ENES, n.d.) of the European FP-7 IS-ENES2 project (Plieger *et al.*, 2015) and are produced by the post-processing of RCM outputs based on three different methodologies, quantile mapping (QMap), DBS, and CDF-t. Bias-adjusted outputs with the QMap method (Gudmundsson *et al.*, 2012) are produced by the Norwegian Meteorological Institute (METNO) and are calibrated according to the MESoscale ANalysis system (MESAN) reanalysis data that were produced by SMHI (Landelius *et al.*, 2016). Outputs generated by SMHI with DBS (DBS45) method (Yang *et al.*, 2010) are also calibrated according to MESAN. The third group of bias-adjusted outputs is RCM outputs processed with the CDFT method (Vrac *et al.*, 2016) by IPSL using the Watch Forcing Data methodology applied to ERA-Interim data (WFDEI) (Weedon *et al.*, 2014) as the benchmark.

Each of the 16 outputs is used for single model analysis for the determination of the goodness of fit for the simulation of historical climate. The goodness of fit

values for single models contributed to the multi-model analysis by providing an understanding of the range of simulation efficiency. Second, raw and bias-adjusted models are used in different combinations to develop MME results. The analysis is carried out for the period between 1971 and 2005 and aims to evaluate the efficiency of model outputs in the simulation of the historical climatic conditions and change in climate in time experienced in the study area. The RCMs and the bias-adjusted outputs used in this study are listed in Table 2 with the relevant Model Ids used in the below text.

Raw and bias-adjusted daily model outputs are used for the development of monthly, seasonal, and annual time series of average precipitation values at the RCM grids closest to the eight MSs.

3.3 | Method for MME formation

The analysis of the climate models for the adequacy to be used for impact assessment purposes includes ensemble formation using the climate outputs. Three SEs are developed in this study: (a) SE of four non-bias adjusted RCMs (from hereafter will be referred to as SE_RCM), (b) SE of 12 bias-adjusted RCMs (from hereafter will be referred to as SE_BARCM), and (c) SE of all 16 RCMs (from hereafter will be referred to as SE_All). SEs are formed with the monthly average precipitations and are based on the SE technique proposed by Krishnamurti *et al.* (1999, 2000).

TABLE 2 List of the RCMs used in this study

Driving model	RCM	Bias adjustment method	Model ID
CNRM-CERFACS-CNRM-CM5	SMHI-RCA4	—	RCM1
		CDFT21-WFDEI	RCM1_CDFT
		QMAP-MESAN	RCM1_QMAP
		DBS45-MESAN	RCM1_DBS
ICHEC-EC-EARTH	SMHI-RCA4	—	RCM2
		CDFT21-WFDEI	RCM2_CDFT
		QMAP-MESAN	RCM2_QMAP
		DBS45-MESAN	RCM2_DBS
ICHEC-EC-EARTH	KNMI-RACMO22E	—	RCM3
		CDFT21-WFDEI	RCM3_CDFT
		QMAP-MESAN	RCM3_QMAP
		DBS45-MESAN	RCM3_DBS
ICHEC-EC-EARTH	DMI-HIRHAM5	—	RCM4
		CDFT21-WFDEI	RCM4_CDFT
		QMAP-MESAN	RCM4_QMAP
		DBS45-MESAN	RCM4_DBS

Abbreviations: RCMs, regional climate models; SMHI, Swedish Meteorological and Hydrological Institute; DMI, Danish Climate Centre KNMI, Royal Netherlands Meteorological Institute.

The formation of the SEs using MLR with the SE approach is carried out according to Equation (1).

$$SE_type_{i,t} = \bar{O}_i + \sum_{j=1}^M a_j \left(RCM_{i,t}^j - \overline{RCM}_i^j \right), \forall i, \forall t \quad (1)$$

where $RCM_{i,t}^j$ is the estimation of RCM j at grid i for month t , $SE_type_{i,t}$ is the SE generated using $RCM_{i,t}^j$, a_j is the weight of RCM j that is optimized for the training period to minimize the difference between observed and estimation of the model at grid i based on the conventional MLR (Equation (4)), $type$ indicates which type of RCM models are ensembled. Here, as explained above, $type = RCM, BARCM, All$. Thus, M is 4, 12, and 16, for $type = RCM, BARCM, All$, respectively.

RCM_i^j is the climatology determined by RCM j (Equation (2)) for the training period T , and \bar{O}_i is the mean observation or observed climatology value at grid i (Equation (3)) for the same period.

$$\overline{RCM}_i^j = \frac{1}{T} \sum_{t=1}^T RCM_{i,t}^j, \forall i, \forall j \quad (2)$$

$$\bar{O}_i = \frac{1}{T} \sum_{t=1}^T O_{i,t}, \forall i \quad (3)$$

where $O_{i,t}$ is the observed data at grid i for month t .

The formation of SEs is carried out as a three-stage procedure:

1. Training for the determination of the model weights

Training data set for each model is formed through a random sampling of 75% of the data in time series of monthly average precipitations between 1971 and 2005. The same training data set is used for all models to enable the comparison between them for accuracy. The reference data are used as the benchmark for the training of MLR of the SE. The observed values of the same time and location with the model data points in the training set are used for the determination of optimal weightings for models. The MLR in the SE approach is trained so as to minimize the total error (G) at each grid based on the least-squares method as per Equation (4).

$$G_i = \sum_{t=1}^T (SE_type_{i,t} - O_{i,t})^2, \forall i \quad (4)$$

2. Test of the SE performance for the validation data set

The remaining 25% of the monthly average precipitation time series between 1971 and 2005 are used for the

evaluation of the performance of SEs. The performance of SEs for training and validation data sets is determined by the calculation of the statistical performance indicators (SPIs) of the goodness of fit with the reference data of the same point of time and location.

3. Evaluation of SE time series performance with respect to RCMs and bias-adjusted RCMs

After the calculation of model weights for each SE with training data sets and testing of the performance of SEs with validation data sets, continuous SE time series are formed by combining training and validation data. The SE time series are compared with the single models for their goodness of fit with respect to the observed and their adequacy for impact assessment. The comparison is done based on the monthly average precipitation time series for the period between 1971 and 2005.

3.4 | Model performance evaluation and performance measures

The evaluation includes comparison for the accuracy in representing the change of monthly precipitation in time for the period of study, the percent difference between observed and modelled precipitation climatology, and representation of extreme conditions that might be of particular concern in impact assessment on the environment such as impacts due to extreme events in hydrology, for example, long rainy periods which may cause floods, droughts, and so forth.

SPIs that are used in this study to compare the accuracy of hindcast outputs of raw and bias-adjusted RCMs, as well as SEs, are Correlation or Pearson's coefficient of correlation ($Corr$, Equation (5)), $RMSE$ (Equation (6)), and Percent BIAS ($PBIAS$, Equation (7)).

$$Corr(O_i RCM_i^j) = \frac{\sum_{t=1}^{n_t} [(O_{i,t} - \bar{O}_i) \times (RCM_{i,t}^j - \overline{RCM}_i^j)]}{\sqrt{\sum_{t=1}^{n_t} (O_{i,t} - \bar{O}_i)^2 \times \sum_{t=1}^{n_t} (RCM_{i,t}^j - \overline{RCM}_i^j)^2}} \quad (5)$$

$$RMSE = \sqrt{\frac{1}{n_t} \sum_{t=1}^{n_t} (O_{i,t} - RCM_{i,t}^j)^2} \quad (6)$$

$$PBIAS = \frac{\sum_{t=1}^{n_t} (O_{i,t} - RCM_{i,t}^j)}{\sum_{t=1}^{n_t} (O_{i,t})} \times 100 \quad (7)$$

In Equations (5)–(7), t stands for the time steps and the total number of precipitation data is n_t . $RCM_{i,t}^j$ stands for

the estimation of RCM j . In the case of the SEs, instead of $RCM_{i,t}^j$, $SE_{type_{i,t}}$ is used for SPIs calculation. The monthly average precipitations are expressed in mm/day.

4 | DEVELOPMENT OF SEs

Three SEs are formed following the procedure described in Section 3. The data set from each model and the SE outputs for training and test are evaluated with respect to the monthly averages of observations. The training results of the three SEs show better simulation performance than single models including raw RCMs and bias-adjusted outputs. Among the SE types, the ensemble set containing all 16 raw or bias-adjusted outputs (SE_All) is observed to have the best performance.

Although the correlation and RMSE values (Tables 3 and 4, respectively) for the test dataset mostly indicate to be slightly poorer compared to the training results, they still verify a better performance for SE outputs, in general. PBIAS values (Table 5) obtained for three SEs are

also satisfactory and verifies a reduction in the total error in projections (Figure 2). Note that in Figure 2, all four bias-adjusted versions of the corresponding RCM are represented by the same marker (i.e., empty circles). Rather than the analysis through randomly formed training and test datasets, a better analysis of the total error is obtained for the PBIAS through the use of continuous time series, which is detailed in the below section.

5 | ANALYSIS OF PERFORMANCE EFFICIENCY OF HINDCAST OUTPUTS

5.1 | Analysis of RCM and SE time series for the representation of change in precipitation in time

Continues time series of meteorological parameters are generally used for the climate change assessment. In order to evaluate the goodness of fit of the RCMs and SEs

TABLE 3 Correlation values for training and test

Station ID	Correlation Station name	SE_RCM		SE_BARCM		SE_All	
		Training	Test	Training	Test	Training	Test
8229	Akseki	0.59	0.58	0.63	0.56	0.68	0.59
17246	Karaman	0.39	0.52	0.36	0.50	0.45	0.50
17300	Antalya AP	0.57	0.56	0.61	0.59	0.63	0.51
17310	Alanya	0.61	0.66	0.66	0.68	0.67	0.70
17320	Anamur	0.57	0.50	0.72	0.66	0.73	0.67
17898	Seydisehir	0.60	0.44	0.65	0.43	0.66	0.48
17928	Hadim	0.54	0.40	0.63	0.58	0.66	0.58
17954	Manavgat	0.69	0.60	0.71	0.63	0.72	0.65

Abbreviations: RCM, regional climate model; SE, superensemble.

TABLE 4 RMSE (mm) values for training and test

Station ID	RMSE Station name	SE_RCM		SE_BARCM		SE_All	
		Training	Test	Training	Test	Training	Test
8229	Akseki	3.23	3.38	3.06	3.49	2.86	3.33
17246	Karaman	0.83	0.67	0.84	0.66	0.75	0.65
17300	Antalya AP	3.54	3.59	3.42	3.48	3.34	3.74
17310	Alanya	2.94	2.75	2.77	2.70	2.74	2.64
17320	Anamur	2.45	3.19	2.06	2.76	2.02	2.74
17898	Seydisehir	1.50	2.47	1.42	2.49	1.39	2.40
17928	Hadim	1.37	1.91	1.26	1.69	1.22	1.68
17954	Manavgat	2.55	3.40	2.48	3.30	2.44	3.23

Abbreviations: RCM, regional climate model; RMSE, root mean square error; SE, superensemble.

TABLE 5 PBIAS (%) values for training and test

Station ID	PBIAS Station name	SE_RCM		SE_BARCM		SE_All	
		Training	Test	Training	Test	Training	Test
8229	Akseki	1.87	-5.76	2.67	-8.24	1.51	-4.66
17246	Karaman	-0.19	0.64	-0.17	0.55	1.37	-4.54
17300	Antalya AP	-1.40	4.35	-1.80	5.61	-2.43	7.56
17310	Alanya	-1.29	3.71	-0.80	2.31	-0.72	2.07
17320	Anamur	-5.00	10.94	-2.69	5.88	-2.79	6.11
17898	Seydisehir	-2.32	6.04	-2.54	6.61	-2.53	6.59
17928	Hadim	-2.97	8.40	-2.36	6.67	-1.82	5.15
17954	Manavgat	-3.06	8.08	-2.85	7.54	-2.98	7.88

Abbreviations: RCMs, regional climate models; SEs, superensembles.

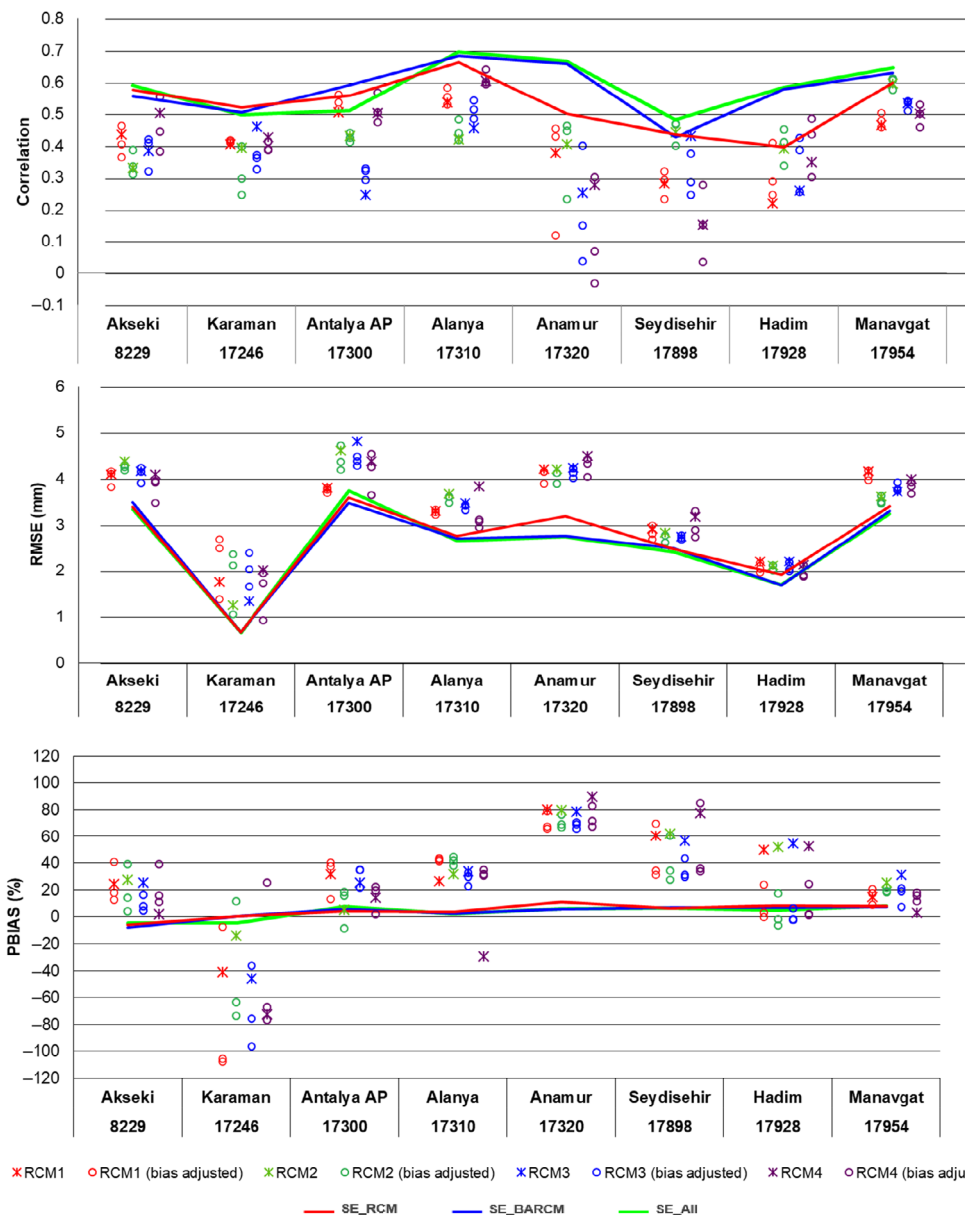


FIGURE 2 Comparison of statistical performance indicators (SPIs) with observed for single regional climate models (RCMs) and superensembles (SEs) for test dataset [Colour figure can be viewed at wileyonlinelibrary.com]

TABLE 6 Correlation, PBIAS (%), and RMSE (mm) values for SE and RCM time series

Station ID	SPI	4 RCMs		SE_RCM	12 BA RCMs		SE_BARCM	16 RCMs		SE_All
		Worst	Best		Worst	Best		Worst	Best	
8229 Akseki	Corr	0.41	0.49	0.59	0.35	0.51	0.61	0.35	0.51	0.66
	RMSE	4.42	3.84	3.27	4.01	3.62	3.23	4.42	3.62	2.98
	PBIAS	37.1	4.04	0.00	45.45	12.25	-16.26	45.45	4.04	-0.30
17300 Antalya AP	Corr	0.39	0.49	0.57	0.32	0.54	0.60	0.32	0.54	0.60
	RMSE	4.54	3.9	3.55	4.59	3.82	3.43	4.59	3.82	3.44
	PBIAS	23.34	12.96	0.00	26.85	-0.74	-0.34	26.85	-0.74	-0.52
17310 Alanya	Corr	0.44	0.54	0.62	0.42	0.56	0.67	0.42	0.56	0.68
	RMSE	4.02	3.46	2.9	3.57	3.21	2.75	4.02	3.21	2.72
	PBIAS	26.72	16.02	0.00	35.07	25.57	0.00	35.07	16.02	-0.01
17898 Seydisehir	Corr	0.33	0.44	0.54	0.2	0.47	0.57	0.20	0.47	0.59
	RMSE	2.50	2.18	1.79	2.65	1.95	1.75	2.65	1.95	1.70
	PBIAS	74.24	52.72	0.00	81.94	22.43	-0.01	81.94	22.43	-0.03
17928 Hadim	Corr	0.30	0.39	0.49	0.28	0.49	0.61	0.28	0.49	0.63
	RMSE	1.89	1.82	1.52	1.9	1.68	1.38	1.90	1.68	1.35
	PBIAS	48.19	42.45	0.00	17.47	0.45	0.00	48.19	0.45	-0.05
17954 Manavgat	Corr	0.50	0.56	0.66	0.47	0.58	0.68	0.47	0.58	0.7
	RMSE	3.70	3.41	2.79	3.57	3.31	2.71	3.70	3.31	2.66
	PBIAS	17.23	-1.14	0.00	13.79	-0.29	0.00	17.23	-0.29	0.00
17320 Anamur	Corr	0.31	0.41	0.55	0.12	0.5	0.71	0.12	0.50	0.68
	RMSE	3.70	3.52	2.66	3.66	3.22	2.24	3.70	3.22	2.39
	PBIAS	84.93	74.81	0.00	78.16	59.92	-1.90	84.93	59.92	-5.77
17246 Karaman	Corr	0.31	0.37	0.42	0.2	0.33	0.39	0.20	0.37	0.46
	RMSE	2.65	1.65	0.79	2.64	1.16	0.80	2.65	1.16	0.73
	PBIAS	-107.13	-30.47	0.00	-100.22	-4.46	0.00	-107.13	-4.46	0.00

Note: The best performing model for each station is given in bold.

Abbreviations: RCM, regional climate model; RMSE, root mean square error; SE, superensemble.

with respect to the observed precipitation over the period between 1971 and 2005, continuous monthly average time series are used. Table 6 shows the comparison of SPIs calculated for individual models in ensemble sets and relevant SEs based on the goodness of fit of the change of monthly precipitation in time. Figure 3 gives a comparison of the performance of raw and bias-adjusted RCM outputs in the ensemble set, and SEs with the reference data on Taylor diagrams. Our goal here is to evaluate the performances of readily available raw and bias-adjusted RCM outputs and SEs generated in this study. Similar to raw RCMs, bias-adjusted RCM outputs are obtained from CORDEX database. It should be noted here that bias-adjustments for these RCMs were carried out using reference data sets of WFDEI and MESAN while SEs generated in this study used datasets of MSs. SEs which are tuned using data of the study area,

combine prediction abilities of multiple models and adjust to local data. Thus, the cost of local data collection and ensembling should be taken into account while comparing raw and bias-adjusted RCM results with those of SEs.

As it is seen in Figure 3, the ranking of raw RCMs regarding the skill to reproduce the monthly time series differs at each MS. On the other hand, RCM4 shows the worst performance among the four RCMs at the majority of stations, particularly due to relatively higher RMSE values, whereas skill for the remaining three models is similar at most of the stations. Regarding the bias-adjusted outputs, the performance is even more diverse considering different MSs.

Comparison on Taylor diagram shows that depending on the methodology the bias-adjustment has added better simulation performance to raw models only for certain

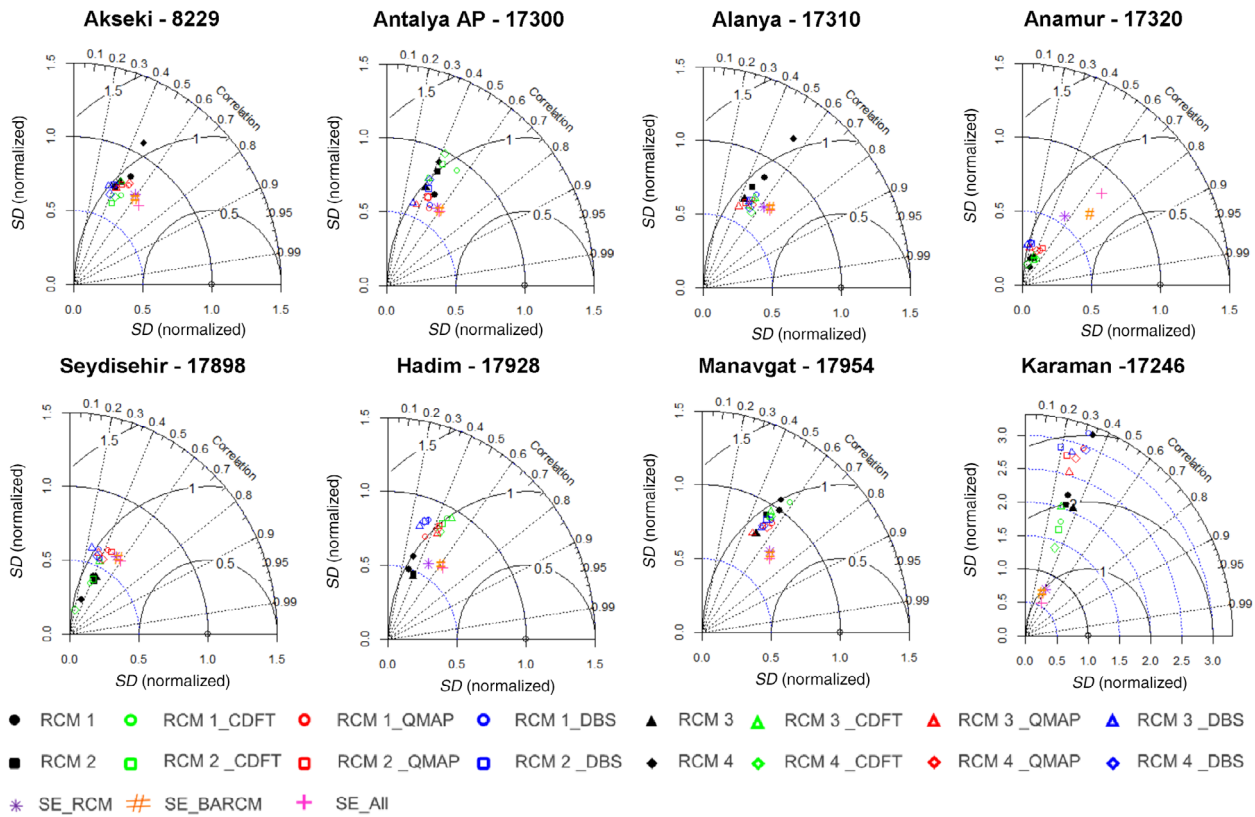


FIGURE 3 Comparison of raw and bias-adjusted regional climate models (RCMs), and three superensembles (SEs) (SE_RCM, SE_BARCM, SE_All) with observed monthly average precipitation [Colour figure can be viewed at wileyonlinelibrary.com]

MSs but not for all MSs. For example, CDFT bias-adjusted model outputs achieve better performance over other bias-adjusted versions for arid climate Karaman station, particularly due to reduction in error reflected by lower RMSE and PBIAS, but the same bias-adjusted outputs do not provide any significant improvement over raw RCMs for coastal Manavgat station. Furthermore, for Hadim station post-processing with the DBS method diminished the performance of climate models by increasing RMSE and decreasing the correlation coefficient for the precipitation time series. However, despite the variability of performances of individual models the analysis for eight stations agrees on a typical improvement provided by superensembling in the goodness of fit of the modelled with observed time series (Figure 3).

Ensembling provides up to 42% improvement in correlation and between 20 and 72% improvement in RMSE, relative to the best single model considering the change in monthly precipitation in time. It is seen that the higher the number of well-performing single models in an ensemble set and the better range of the performance of models in the set, the better performance obtained through ensembling (Table 6). The total bias is

significantly reduced with ensembling decreasing the PBIAS to zero for all SE_RCM formed by the raw RCMs and at four locations for SE_BARCM. For SE_All, PBIAS values are also reduced significantly, ranging between 0 and -5.77 with the highest PBIAS value in Anamur station (MS 17320). Hence, as it can be seen in Table 6, a comparison of 35-year monthly average precipitation time series validates the better performance of SEs over the raw and bias-adjusted models in ensemble member sets. Moreover, it can be concluded that among the tree SEs, SE_All formed by the use of all 16 RCM outputs provided the best performance in general.

For the verification of the improvement provided by ensembling regarding the representation of the reference data, the same analysis is repeated with two other reference data sets. The reference data that are originally used to produce the bias-adjusted RCMs, that is, MESAN reference data for QMAP and DBS45 bias-adjusted RCMs, and WFDEI reference data for CDFT bias-adjusted RCMs, are taken as the reference data for the reproduction of SE time series (SE_RCM, SE_BARCM, and SE_All). In addition, these reference data are used as the benchmark to calculate the performance measures for the evaluation of simulation skills.

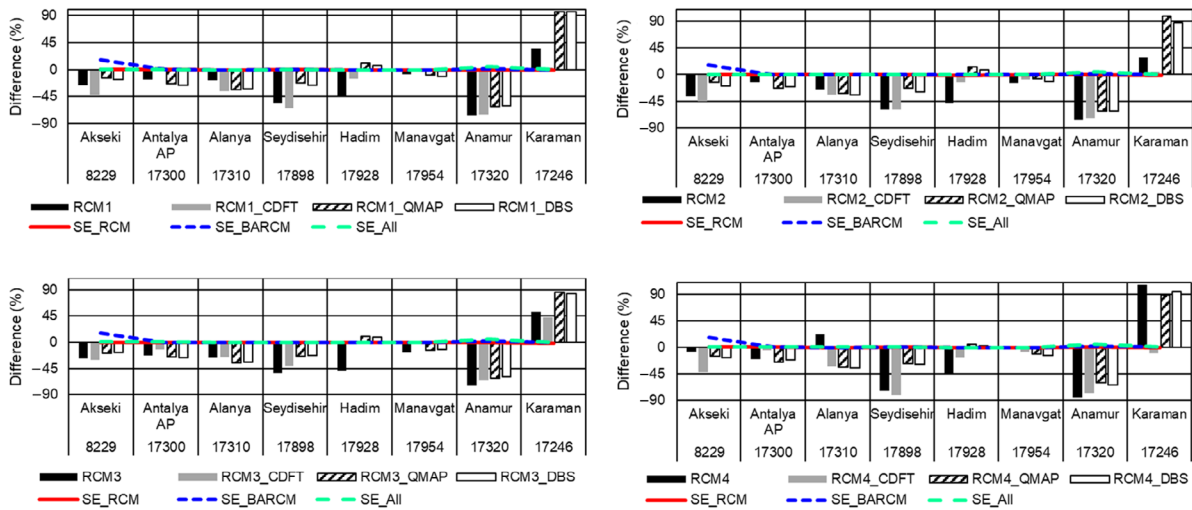


FIGURE 4 Percent difference of regional climate model (RCM)-calculated annual precipitation climatology from observed [Colour figure can be viewed at wileyonlinelibrary.com]

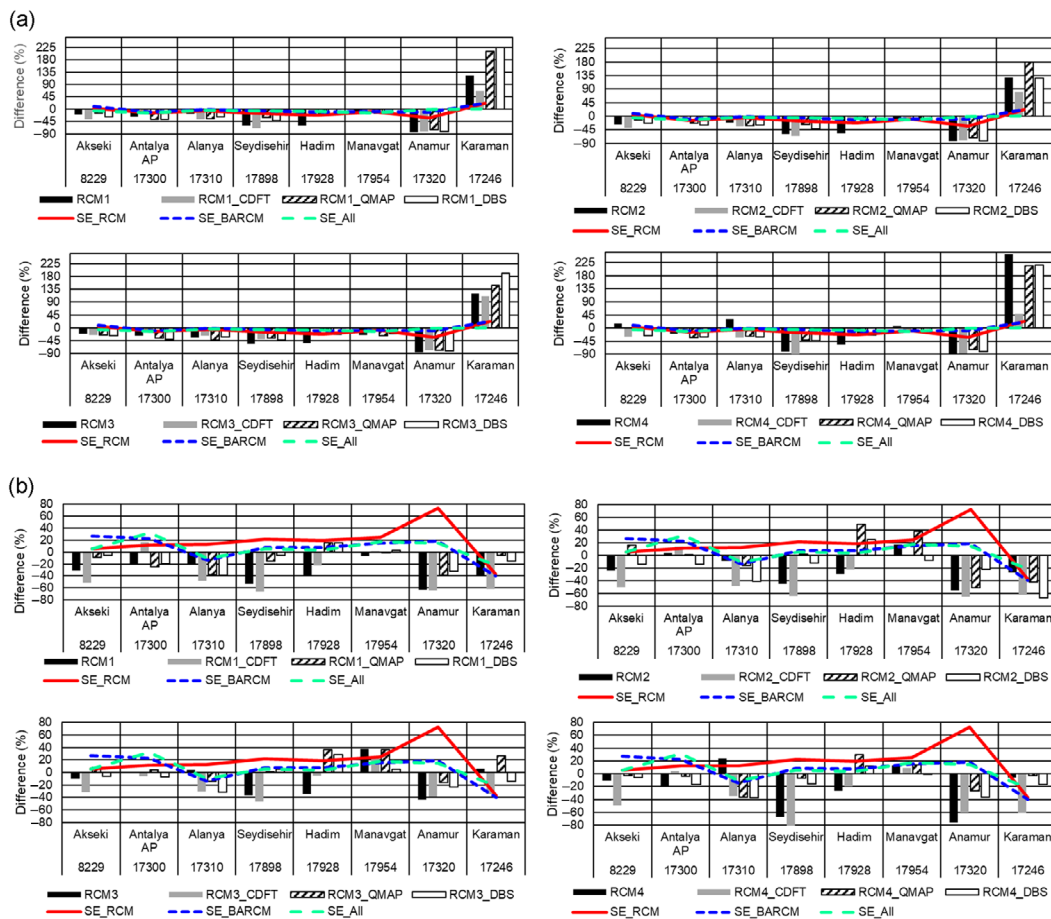


FIGURE 5 Percent difference of regional climate model (RCM)-calculated seasonal precipitation climatology from observed for winter and spring ((a) winter and (b) spring, top left is the comparison of RCM1 and its bias-adjusted versions with superensembles (SEs), top right is the comparison of RCM2 and its bias-adjusted versions with SEs, bottom left is the comparison of RCM3 and its bias-adjusted versions with SEs, bottom right is the comparison of RCM4 and its bias-adjusted versions with SEs) [Colour figure can be viewed at wileyonlinelibrary.com]

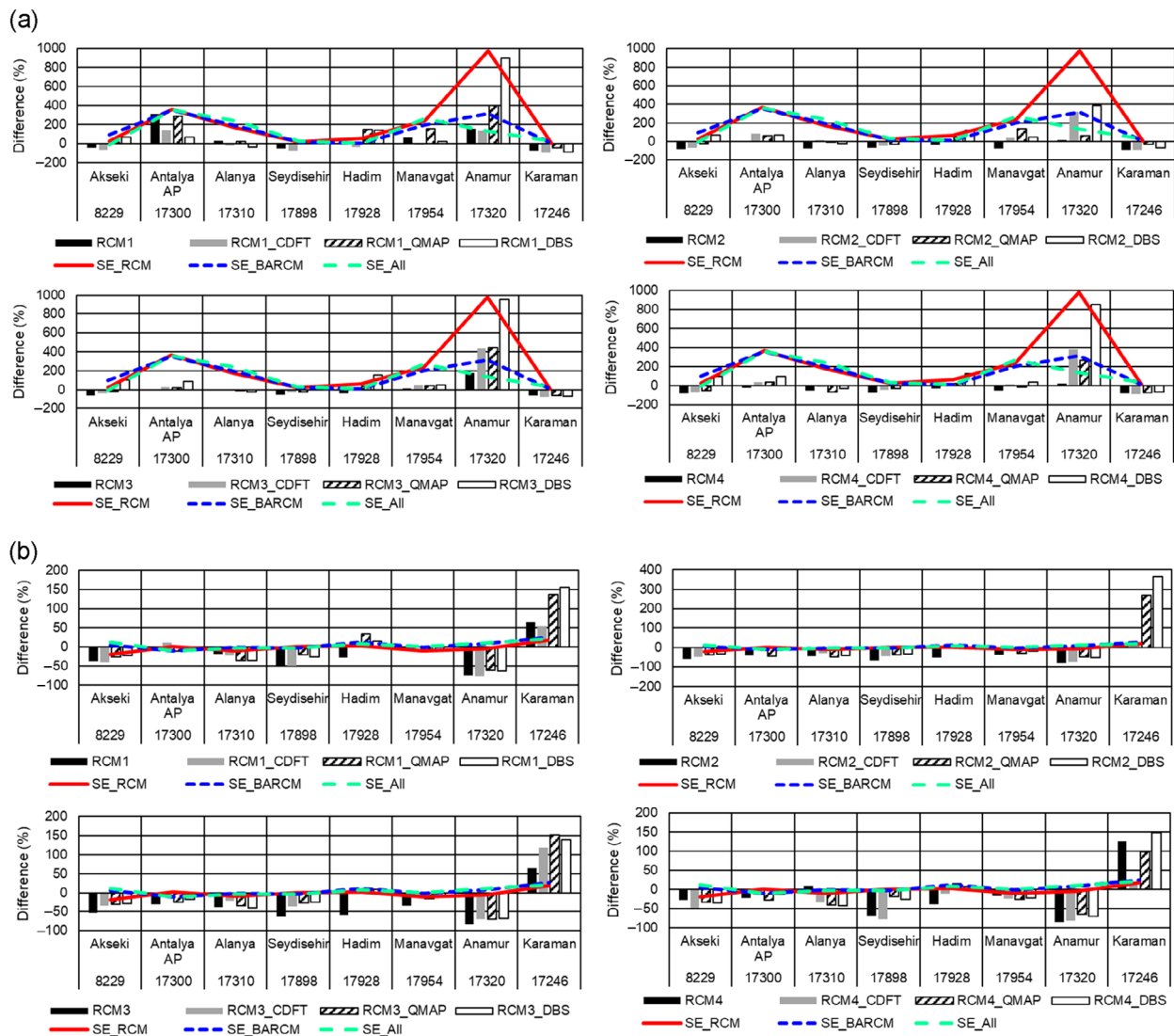


FIGURE 6 Percent difference of regional climate model (RCM)-calculated seasonal precipitation climatology from observed for summer and fall ((a) summer and (b) fall, for all seasons, top left is the comparison of RCM1 and its bias-adjusted versions with superensembles (SEs), top right is the comparison of RCM2 and its bias-adjusted versions with SEs, bottom left is the comparison of RCM3 and its bias-adjusted versions with SEs, bottom right is the comparison of RCM4 and its bias-adjusted versions with SEs) [Colour figure can be viewed at wileyonlinelibrary.com]

In order to enable a comparison between outputs of the use of different reference datasets, the analysis is done for the period between 1989 and 2003 that is the timeframe in which precipitation time series data are available for all eight MSs and all reference datasets. To distinguish the potential added-value of superensembling, the different raw and bias-adjusted RCMs, and calculated SE time series are evaluated in comparison with the benchmark of: (a) ground-based observation (OBS), (b) WFDEI, and (c) MESAN as reference data.

The analysis results are provided in Tables A1–A3, Appendix. As it can be seen in Appendix, regardless of the different reference datasets used for ensembling,

SE_All generated from 16 RCM outputs still provides the best performance in general.

5.2 | Analysis of RCMs and SE for the representation of precipitation climatology in study area

The precipitation climatology for eight MSs within the case study area is compared with the hindcast results of four RCMs. The bias-adjusted hindcast results and SE outputs are also included in the analysis to identify the type and degree of change added to the RCMs by post-processing for bias adjustment and ensembling.

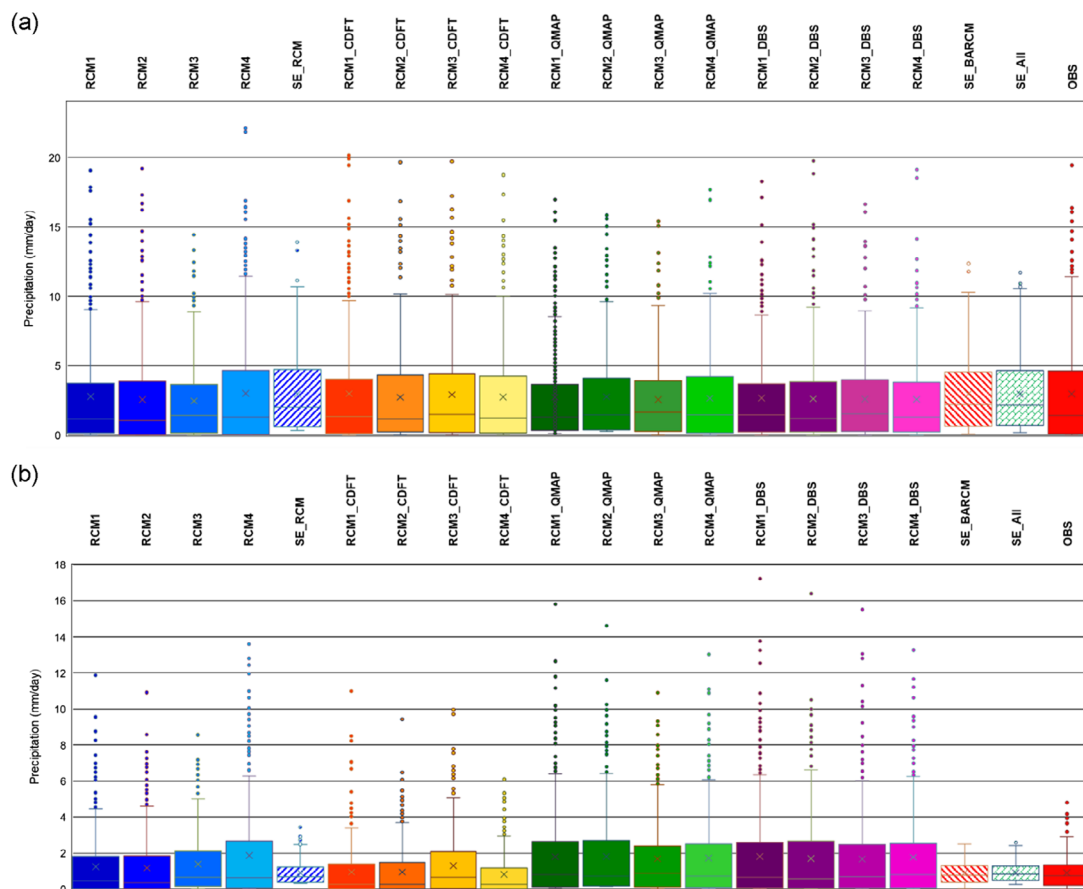


FIGURE 7 Box plot of observed and modelled monthly average precipitations at (a) Manavgat (MS 17954) and (b) Karaman (MS 17246) stations in the study period [Colour figure can be viewed at wileyonlinelibrary.com]

The percent difference in the annual climatology between modelled and observed shows that the best projections are obtained by the application of the SE to climate models (Figure 4). Considering the annual climatology, all four RCMs are seen to operate most successfully at Manavgat station (MS 17954). Additionally, at Hadim station (MS 17928) despite relatively poor projections from raw RCMs, bias adjustment methodologies create significant improvement in the reproduction of the annual climatology. On the other hand, at certain stations including Akseki (MS 8229), and Antalya AP (MS 17300) raw RCM outputs are seen to reproduce annual climatology better than the bias-adjusted outputs. Therefore, regarding the annual climatology, it is to say that not all bias adjustment methodologies create a decrease in simulation error at all locations. However, ensembling improves the estimation of annual climatology for all the stations.

Figures 5 and 6 depict the seasonal simulation performance of the raw RCMs in comparison with their bias-adjusted versions and with the SEs. Note that the y axis represents the percent difference of model estimations of seasonal precipitation climatology from the observed. As can be seen in Figures 5 and 6, the simulation

performance of RCMs regarding the accuracy of seasonal precipitation climatology also varies at different locations. At Karaman station (MS 17246) with a dry continental climate with cold winters, four RCMs and their bias-adjusted outputs tend to overestimate winter and fall precipitation and underestimate summer and spring precipitation, although variations are seen for different methods of bias adjustment. For all other seven locations with relatively high total precipitation, winter climatology is generally underestimated by four RCMs even after bias adjustment. Underestimation of winter precipitation is more pronounced in inland stations (e.g., Seydisehir, Hadim) compared to the coastal stations (Akseki, Antalya, Manavgat).

At all MSs for winter (Figure 5a), the wettest season of the year in the region, and for fall (Figure 6b), the climatology reproduced by SE has a low difference from observed relative to the other seasons. On the other hand, the size of the error of SEs in seasonal climatology increases for the reproduction of summer (Figure 6a) and spring (Figure 5b) climatology. The error in summer climatology for SEs is more pronounced at coastal MSs (Manavgat, Antalya, Alanya, and Anamur, Figure 6a). The SEs significantly overestimate the summer

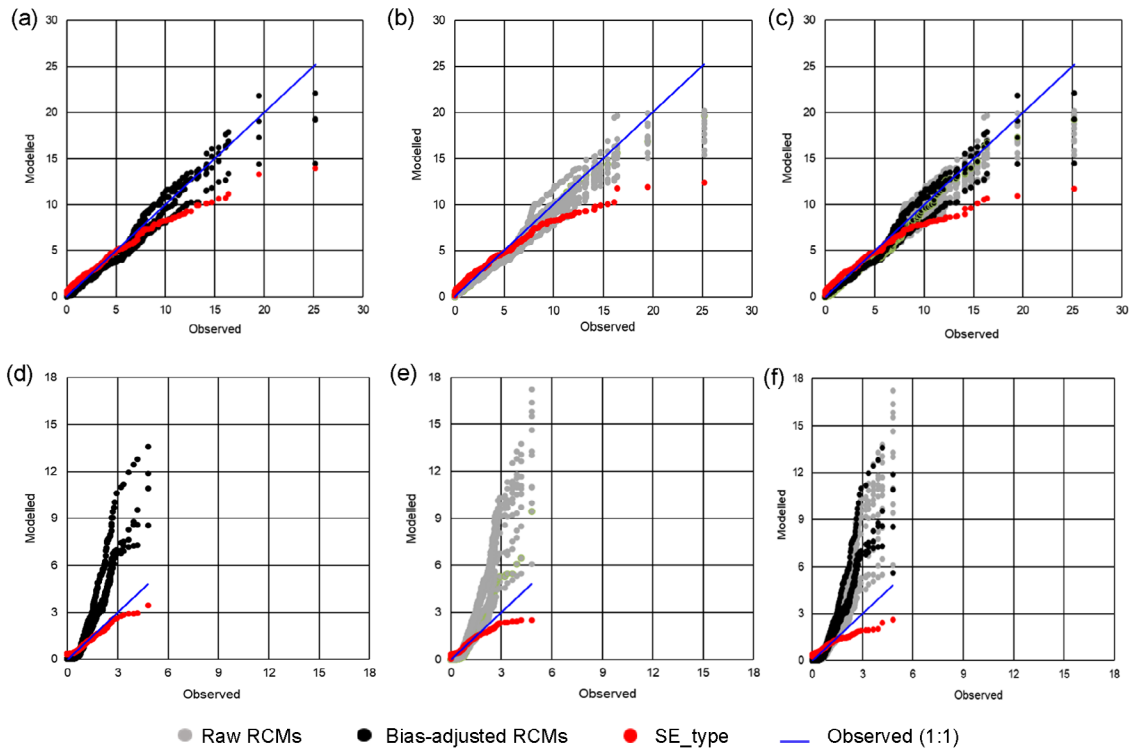


FIGURE 8 Quantile–quantile plots of modelled versus observed monthly average precipitation (mm/day) for Manavgat (MS 17954) and Karaman (MS 17246) stations (top row plots are for Manavgat station (MS 17954) (a) raw regional climate models (RCMs) and SE_RCM, (b) bias-adjusted RCMs and SE_BARCM, (c) raw and bias-adjusted RCMs, and SE_All; bottom row plots are for Karaman station (MS 17246), (d) raw RCMs and SE_RCM, (e) bias-adjusted RCMs and SE_BARCM, and (f) raw and bias-adjusted RCMs, and SE_All) [Colour figure can be viewed at wileyonlinelibrary.com]

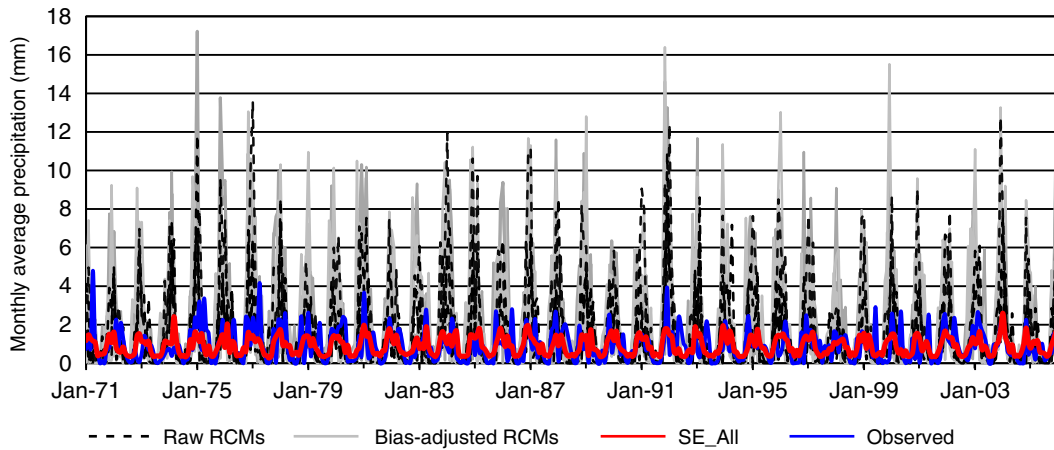


FIGURE 9 Comparison of time series of modelled versus observed monthly average precipitation at Karaman (MS 17246) station [Colour figure can be viewed at wileyonlinelibrary.com]

climatology with an error highly exceeding 100% of the observed for those stations, even though it is seen to perform very well for the reproduction of winter and fall climatology (Figures 5a and 6b, respectively) with errors remaining less than 13% at the majority of the coastal stations.

Hence, although SEs are seen to be successful in reproducing the annual climatology and seasonal climatology for winter and fall and outperform single raw and bias-adjusted models, for summer and spring they fail to reproduce the precipitation climatology. The error is highest in the SE_RCM that is composed mainly of raw

RCMs. For SEs, error in the summer climatology is particularly significant for Anamur, Manavgat, Alanya, and Antalya stations, all of which are coastal stations.

5.3 | Analysis of RCM and SE time series for the representation of the precipitation variability in the study area

The analysis of the ability to reproduce the variability of the monthly average precipitation indicates that although SEs outperform single models in reproducing the averages and intensity of the high return period events within the 25th–75th percentile range, it fails to predict the potential extreme events, as can be seen in Figure 7. Even though the single models composing SEs contain relatively higher variability by including estimations for extreme conditions (i.e., high, and low extremes) superensembling tends to reduce the extremes and concentrate the precipitation projections around the median value. Moreover, in Figure 7, it is seen that SE_All time series that have the best correlation and RMSE values at the majority of MSs incline most to force the extremes closer to the mean value. The same behaviour is observed both for coastal stations (e.g., Manavgat) with relatively high precipitation and for dry climate, inland stations (e.g., Karaman) (Figure 7).

The characteristic of SE outputs reducing wet and dry extremes is also evident from the quantile–quantile plots of modelled versus observed data (Figure 8). The reproduction of the time series around the precipitation climatology potentially creates lower accuracy in the simulation of hydrological extreme events such as dry spells and potential floods due to high storm events (Figure 9).

6 | CONCLUSION

In this study, a multi-model analysis is done using 4 raw RCMs and their 12 bias-adjusted outputs from the CORDEX database to evaluate the representativeness for local climate conditions at eight ground-based meteorological monitoring stations in Turkey. The analysis aims to test the adequacy of the climate model outputs to be used for climate change impact assessment. In addition to the hindcast outputs, three SEs are formed in this study to assess potential improvement and advantages of the use of ensembling which is a cost and time-effective method that can be practically used in impact assessment studies particularly for reducing climate model uncertainties.

Comparison of the raw RCMs and bias-adjusted outcomes with SEs verifies that bias-adjusted outcomes of

RCMs do not necessarily improve the quality of projection relevant to the purposive and/or areal focus of the study.

Analysis of a single model may cause biases in the assessment since not every model performs at its best at all locations as seen from the Taylor diagrams showing relatively weak performance of RCM4 at certain MSs. Similarly, as the range of SPI values, Taylor diagram comparisons and seasonal evaluation for each MS verify, the variability of the performance of bias-adjusted outputs to reproduce the inter- and intra-annual change in precipitation creates the necessity for testing against observed. Hence, parallel to the general understanding, in climate impact assessment studies, it is important to choose the use of multi-model analysis over single model analysis and to test and validate the performance of each model specific to the study area before use. This becomes more prominent particularly for regions with a complex topography and climate features such as Turkey and the Mediterranean basin.

Despite the variability of the individual models in ensemble sets, all SEs are seen to improve the goodness of fit of precipitation time series to the observed with an increase in correlation up to 42%, and an increase in RMSE up to 72% relative to the best single model in the study. However, SE is observed to be significantly affected by the performance of the composing single models. The better result is achieved by the use of bias-adjusted outputs compared to the raw climate projections. Moreover, SE_All is seen to perform best compared to SE_RCM and SE_BARCM which can be interpreted as the increased number of models has a positive impact on SE.

In this study, it is also seen that SE creates superior results over single models in reducing the total error and reproducing annual climatology. On the other hand, its performance may again vary depending on the seasonality of the study area. SE reduces the error in seasonal climatology relative to the single model analysis including raw and bias-adjusted RCMs for winter and fall seasons. However, it is seen that even the SE that has high performance in reproducing annual climatology and has a good correlation with the monthly average time series has the drawback of significant overestimation of summer climatology particularly at coastal MSs and has a poor simulation ability considering the extremes in precipitation. Both high storm events and dry periods are seen to be underestimated by the SE that causes the estimations to concentrate around the mean climatology. Therefore, it is concluded that superensembling improves correlation coefficient and RMSE but as a trade-off extremes are underrepresented. This effect of superensembling might be a significant concern for impact assessment studies

particularly for studies focusing on impacts of extreme hydrological conditions such as floods and drought conditions. Complete evaluation of the reproduction of wet and dry extremes should include analysis of daily datasets which is reserved as the topic of a future study.

ACKNOWLEDGEMENTS

The research leading to these results is funded by the Scientific and Technological Research Council of Turkey (TÜBİTAK) and an on-going project “Assessment of Climate Change Impacts on Streamflow and Hydropower in Antalya, Turkey” (Project ID: 118Y365). The authors thank the two anonymous reviewers whose comments and suggestions helped us to improve and clarify this manuscript and shape our future research.

AUTHOR CONTRIBUTIONS

Buket Mesta: Conceptualization; formal analysis; investigation; methodology; validation; visualization; writing – original draft; writing – review and editing. **Elcin Kentel:** Conceptualization; funding acquisition; methodology; project administration; supervision; validation; writing – review and editing.

ORCID

Elcin Kentel  <https://orcid.org/0000-0002-7477-0345>

REFERENCES

- Aziz, R., Yucel, I. and Yozgatligil, C. (2020) Nonstationarity impacts on frequency analysis of yearly and seasonal extreme temperature in Turkey. *Atmospheric Research*, 238, 104875.
- Black, E., Brayshaw, D.J. and Rambeau, C.M. (2010) Past, present, and future precipitation in the Middle East: insights from models and observations. *Philosophical Transactions of the Royal Society A: Mathematical, Physical and Engineering Sciences*, 368(1931), 5173–5184.
- Chen, J., Brissette, F.P., Poulin, A. and Leconte, R. (2011) Overall uncertainty study of the hydrological impacts of climate change for a Canadian watershed. *Water Resources Research*, 47(12), 1–16.
- Christensen, J.H., Kjellström, E., Giorgi, F., Lenderink, G. and Rummukainen, M. (2010) Weight assignment in regional climate models. *Climate Research*, 44(2–3), 179–194.
- Evans, J.P. (2009) 21st century climate change in the Middle East. *Climatic Change*, 92(3–4), 417–432.
- Fujihara, Y., Tanaka, K., Watanabe, T., Nagano, T. and Kojiri, T. (2008) Assessing the impacts of climate change on the water resources of the Seyhan River basin in Turkey: use of dynamically downscaled data for hydrologic simulations. *Journal of Hydrology*, 353(1–2), 33–48.
- Gao, X. and Giorgi, F. (2008) Increased aridity in the Mediterranean region under greenhouse gas forcing estimated from high resolution simulations with a regional climate model. *Global and Planetary Change*, 62, 195–209. <https://doi.org/10.1016/j.gloplacha.2008.02.002>.
- Giannaros, T.M., Kotroni, V., Lagouvardos, K. and Matzarakis, A. (2018) Climatology and trends of the Euro-Mediterranean thermal bioclimate. *International Journal of Climatology*, 38(8), 3290–3308.
- Gudmundsson, L., Bremnes, J.B., Haugen, J.E. and Engen-Skaugen, T. (2012) Downscaling RCM precipitation to the station scale using statistical transformations—a comparison of methods. *Hydrology and Earth System Sciences*, 16(9), 3383–3390.
- Gutiérrez, J.M., Maraun, D., Widmann, M., Huth, R., Hertig, E., Benestad, R., Roessler, O., Wibig, J., Wilcke, R., Kotlarski, S., San Martín, D., Herrera, S., Bedia, J., Casanueva, A., Manzananas, R., Iturbide, M., Vrac, M., Dubrovsky, M., Ribalaya, J., Pórtoles, J., Rätty, O., Räisänen, J., Hingray, B., Raynaud, D., Casado, M.J., Ramos, P., Zerener, T., Turco, M., Bosshard, T., Štěpánek, P., Bartholy, J., Pongracz, R., Keller, D.E., Fischer, A.M., Cardoso, R.M., Soares, P.M.M. and Czernecki, B. (2019) An intercomparison of a large ensemble of statistical downscaling methods over Europe: results from the VALUE perfect predictor cross-validation experiment. *International Journal of Climatology*, 39(9), 3750–3785.
- IPCC. (2015) Workshop report of the intergovernmental panel on climate change workshop on regional climate projections and their use in impacts and risk analysis studies. In: Stocker, T.F., Qin, D., Plattner, G.-K. and Tignor, M. (Eds.) *IPCC Working Group I technical support unit*. Bern, Switzerland: University of Bern, p. 171.
- IS-ENES (n.d.) Infrastructure for the European network for earth system modelling. Climate4Impact website. Available at: <https://climate4impact.eu/impactportal/data/esgsearch.jsp> [Accessed June 5 2020]
- Jacob, D., Teichmann, C., Sobolowski, S., Katragkou, E., Anders, I., Belda, M., et al. (2020) Regional climate downscaling over Europe: perspectives from the EURO-CORDEX community. *Regional Environmental Change*, 20(2), 1–20.
- Kara, F. and Yucel, I. (2015) Climate change effects on extreme flows of water supply area in Istanbul: utility of regional climate models and downscaling method. *Environmental Monitoring and Assessment*, 187(9), 580.
- Kentel, E., Mesta, B. & Akgun, O. B. (2019) Multi-model analysis of bias corrected and non-bias corrected RCM simulations for the assessment of uncertainties and representation of orographic impacts in Mediterranean region. AGUFM, 2019, A51Q-2824.
- Kitoh, A. (2007) Future climate projections around Turkey by global climate models. Final report of ICCAP.
- Krishnamurti, T.N., Kishtawal, C.M., LaRow, T.E., Bachiochi, D.R., Zhang, Z., Williford, C.E., et al. (1999) Improved weather and seasonal climate forecasts from multimodel superensemble. *Science*, 285(5433), 1548–1550.
- Krishnamurti, T.N., Kishtawal, C.M., Zhang, Z., LaRow, T., Bachiochi, D., Williford, E., et al. (2000) Multimodel ensemble forecasts for weather and seasonal climate. *Journal of Climate*, 13(23), 4196–4216.
- Krishnamurti, T.N., Kumar, V., Simon, A., Bhardwaj, A., Ghosh, T. and Ross, R. (2016) A review of multimodel superensemble forecasting for weather, seasonal climate, and hurricanes. *Reviews of Geophysics*, 54(2), 336–377.
- Landelius, T., Dahlgren, P., Gollvik, S., Jansson, A. and Olsson, E. (2016) A high-resolution regional reanalysis for Europe. Part 2:

- 2D analysis of surface temperature, precipitation, and wind. *Quarterly Journal of the Royal Meteorological Society*, 142(698), 2132–2142.
- Lee, J.K., Kim, Y.O. and Kim, Y. (2017) A new uncertainty analysis in the climate change impact assessment. *International Journal of Climatology*, 37(10), 3837–3846.
- Leung, L.R., Mearns, L.O., Giorgi, F. and Wilby, R.L. (2003) Regional climate research: needs and opportunities. *Bulletin of the American Meteorological Society*, 84(1), 89–95.
- López-Moreno, J.I., Goyette, S. and Beniston, M. (2008) Climate change prediction over complex areas: spatial variability of uncertainties and predictions over the Pyrenees from a set of regional climate models. *International Journal of Climatology: A Journal of the Royal Meteorological Society*, 28(11), 1535–1550.
- Okkan, U. and Inan, G. (2015) Statistical downscaling of monthly reservoir inflows for Kemer watershed in Turkey: use of machine learning methods, multiple GCMs and emission scenarios. *International Journal of Climatology*, 35(11), 3274–3295.
- Okkan, U. and Kirdemir, U. (2016) Downscaling of monthly precipitation using CMIP5 climate models operated under RCPs. *Meteorological Applications*, 23(3), 514–528.
- Onol, B. and Semazzi, F.H. (2009) Regionalization of climate change simulations over the eastern Mediterranean. *Journal of Climate*, 22, 1944–1961. <https://doi.org/10.1175/2008JCLI1807.1>.
- Onol, B., Bozkurt, D., Turuncoglu, U.U., Sen, O.L. and Dalfes, H.N. (2014) Evaluation of the twenty-first century RCM simulations driven by multiple GCMs over the eastern Mediterranean–Black Sea region. *Climate Dynamics*, 42(7–8), 1949–1965.
- Ozdogan, M. (2011) Modeling the impacts of climate change on wheat yields in northwestern Turkey. *Agriculture, Ecosystems & Environment*, 141(1–2), 1–12.
- Plieger, M., Som de Cerff, W., Pagé, C., Tatarinova, N., Cofiño, A., Vega Saldarriaga, M., et al. (2015) The climate4impact portal: bridging the CMIP5 and CORDEX data infrastructure to impact users. In: *EGU general assembly conference abstracts*, Vol. 17. Vienna, Austria: 2015 EGU General Assembly.
- Stefanova, L. and Krishnamurti, T.N. (2002) Interpretation of seasonal climate forecast using brier skill score, the Florida State University superensemble, and the AMIP-I dataset. *Journal of Climate*, 15(5), 537–544.
- Sunyer Pinya, M.A., Hundedcha, Y., Lawrence, D., Madsen, H., Willems, P., Martinkova, M., Vormoor, K., Bürger, G., Hanel, M., Kriaučiuniene, J., Loukas, A., Osuch, M. and Yücel, I. (2015) Inter-comparison of statistical downscaling methods for projection of extreme precipitation in Europe. *Hydrology and Earth System Sciences*, 19(4), 1827–1847. <https://doi.org/10.5194/hess-19-1827-2015>.
- Tebaldi, C. and Knutti, R. (2007) The use of the multi-model ensemble in probabilistic climate projections. *Philosophical Transactions of the Royal Society A: Mathematical, Physical, and Engineering Sciences*, 365(1857), 2053–2075.
- Teutschbein, C. and Seibert, J. (2012) Bias correction of regional climate model simulations for hydrological climate-change impact studies: review and evaluation of different methods. *Journal of Hydrology*, 456–457, 12–29. <https://doi.org/10.1016/j.jhydrol.2012.05.052>.
- Türkeş, M., Yozgatlıgil, C., Batmaz, İ., İyigün, C., Koç, E.K., Fahmi, F.M. and Aslan, S. (2016) Has the climate been changing in Turkey? Regional climate change signals based on a comparative statistical analysis of two consecutive time periods, 1950–1980 and 1981–2010. *Climate Research*, 70(1), 77–93.
- Vrac, M., Noël, T. and Vautard, R. (2016) Bias correction of precipitation through singularity stochastic removal: because occurrences matter. *Journal of Geophysical Research: Atmospheres*, 121(10), 5237–5258.
- Weedon, G.P., Balsamo, G., Bellouin, N., Gomes, S., Best, M.J. and Viterbo, P. (2014) The WFDEI meteorological forcing data set: WATCH forcing data methodology applied to ERA-interim reanalysis data. *Water Resources Research*, 50(9), 7505–7514. <https://doi.org/10.1002/2014WR015638>.
- Yang, W., Andréasson, J., Phil Graham, L., Olsson, J., Rosberg, J. and Wetterhall, F. (2010) Distribution-based scaling to improve usability of regional climate model projections for hydrological climate change impacts studies. *Hydrology Research*, 41(3–4), 211–229.
- Yucel, I., Guventurk, A. and Sen, O.L. (2015) Climate change impacts on snowmelt runoff for mountainous transboundary basins in eastern Turkey. *International Journal of Climatology*, 35(2), 215–228.

How to cite this article: Mesta, B., & Kentel, E. (2021). Superensembles of raw and bias-adjusted regional climate models for Mediterranean region, Turkey. *International Journal of Climatology*, 1–20. <https://doi.org/10.1002/joc.7381>

APPENDIX A: EVALUATION OF THE MONTHLY PRECIPITATION TIME SERIES OUTPUTS FOR THE SKILL OF THE REPRODUCTION BASED ON DIFFERENT REFERENCE DATA

TABLE A1 Correlation, PBIAS (%), and RMSE (mm) values indicating the goodness of fit to the ground-based observation reference data for the monthly time series of SE(OBS)^a and RCMs

Station ID	SPI	4 RCMs			12 BA RCMs			16 RCMs		
		Worst	Best	SE_RCM	Worst	Best	SE_BARCM	Worst	Best	SE_All
8229 Akseki	Corr	0.42	0.48	0.57	0.27	0.47	0.56	0.27	0.48	0.65
	RMSE	4.37	3.78	3.23	3.96	3.53	3.66	4.37	3.53	3.16
	PBIAS	23.6	11.6	-13.3	36.3	0.44	-53.2	36.3	0.44	-18.01
17300 Antalya AP	Corr	0.34	0.50	0.59	0.27	0.56	0.66	0.27	0.56	0.66
	RMSE	4.73	4.10	3.73	4.69	4.04	3.53	4.73	4.04	3.51
	PBIAS	30.2	15.7	0.00	32.7	-3.13	-1.37	32.7	3.13	-1.02
17310 Alanya	Corr	0.46	0.50	0.61	0.34	0.54	0.65	0.34	0.54	0.70
	RMSE	4.33	3.42	2.92	3.72	3.27	2.80	4.33	3.27	2.65
	PBIAS	-29.7	22.2	0.00	40.1	22.7	0.00	40.1	22.2	-0.18
17898 Seydisehir	Corr	0.24	0.51	0.55	0.10	0.46	0.54	0.10	0.51	0.66
	RMSE	2.72	2.26	1.92	2.85	2.10	1.94	2.85	2.10	1.72
	PBIAS	75.7	53.4	4.68	82.7	25.0	0.00	82.7	25.0	-0.38
17928 Hadim	Corr	0.29	0.48	0.54	0.25	0.48	0.59	0.25	0.48	0.65
	RMSE	1.76	1.56	1.34	1.85	1.63	1.29	1.85	1.56	1.21
	PBIAS	44.4	36.5	0.00	-21.0	6.00	0.00	44.4	6.00	-0.64
17954 Manavgat	Corr	0.49	0.54	0.66	0.41	0.55	0.67	0.41	0.55	0.70
	RMSE	3.73	3.44	2.77	3.65	3.29	2.74	3.73	3.29	2.65
	PBIAS	14.6	-4.13	0.00	15.4	-0.70	-0.37	15.4	-0.70	-0.18
17320 Anamur	Corr	0.34	0.47	0.57	0.10	0.53	0.69	0.10	0.53	0.70
	RMSE	3.48	3.31	2.47	3.44	3.06	2.17	3.48	3.06	2.17
	PBIAS	84.2	72.7	0.00	77.1	58.5	-1.61	84.2	58.5	-4.72
17246 Karaman	Corr	0.33	0.44	0.48	0.17	0.44	0.42	0.17	0.44	0.50
	RMSE	2.67	1.43	0.71	2.52	1.14	0.74	2.67	1.14	0.66
	PBIAS	-116	-24.6	0.00	-108	5.05	-0.17	-116	5.05	0.00

Note: The best performing model for each station is given in bold.

Abbreviations: RCM, regional climate model; RMSE, root mean square error; SE, superensemble.

^aSE(OBS): SE_RCM, SE_BARCM, or SE_All time series generated by the use of the ground-based observation reference data.

TABLE A2 Correlation, PBIAS (%), and RMSE (mm) values indicating the goodness of fit to the WFDEI reference data for the monthly time series of SE(WFDEI)^a and RCMs

Station ID	SPI	4 RCMs			12 BA RCMs			16 RCMs		
		Worst	Best	SE_RCM	Worst	Best	SE_BARCM	Worst	Best	SE_All
8229 Akseki	Corr	0.40	0.55	0.59	0.25	0.52	0.59	0.25	0.55	0.65
	RMSE	4.24	2.69	1.90	3.21	2.36	1.97	4.24	2.36	1.79
	PBIAS	-54.6	-5.15	4.43	-44.7	2.51	-22.6	-54.6	2.51	3.64
17300 Antalya AP	Corr	0.36	0.51	0.60	0.29	0.56	0.66	0.29	0.56	0.66
	RMSE	4.06	3.46	3.04	4.02	3.32	2.91	4.06	3.32	2.89
	PBIAS	20.9	4.52	0.00	23.8	2.01	-1.02	23.8	2.01	-0.72
17310 Alanya	Corr	0.49	0.53	0.67	0.37	0.57	0.68	0.37	0.57	0.72
	RMSE	4.04	2.98	2.42	3.26	2.82	2.37	4.04	2.82	2.24
	PBIAS	-35.1	18.9	0.00	37.6	19.5	0.00	37.6	18.9	-0.15
17898 Seydisehir	Corr	0.30	0.51	0.57	0.13	0.49	0.61	0.13	0.51	0.70
	RMSE	2.81	2.36	1.91	2.96	2.13	1.86	2.96	2.13	1.66
	PBIAS	77.1	56.0	0.00	83.7	29.3	0.00	83.7	29.3	-0.25
17928 Hadim	Corr	0.29	0.47	0.53	0.22	0.50	0.62	0.22	0.50	0.69
	RMSE	2.80	2.68	2.17	2.67	2.36	2.01	2.80	2.36	1.85
	PBIAS	60.9	55.3	0.00	38.3	14.8	-0.16	60.9	14.8	-1.28
17954 Manavgat	Corr	0.48	0.58	0.68	0.39	0.59	0.71	0.39	0.59	0.73
	RMSE	3.71	3.32	2.66	3.66	3.15	2.57	3.71	3.15	2.48
	PBIAS	14.02	-4.78	0.00	14.8	-1.33	-0.61	14.8	1.33	-0.24
17320 Anamur	Corr	0.33	0.45	0.56	0.10	0.52	0.69	0.10	0.52	0.70
	RMSE	3.15	2.98	2.22	3.11	2.71	1.95	3.15	2.71	1.98
	PBIAS	83.4	71.4	0.00	76.0	56.5	-1.11	83.4	56.5	-6.40
17246 Karaman	Corr	0.37	0.47	0.52	0.21	0.47	0.47	0.21	0.47	0.55
	RMSE	2.61	1.40	0.70	2.46	1.12	0.73	2.61	1.12	0.64
	PBIAS	-101	-16.2	0.00	-93.6	0.45	-0.15	-101	0.45	0.00

Note: The best performing model for each station is given in bold.

Abbreviations: RCM, regional climate model; RMSE, root mean square error; SE, superensemble.

^aSE(WFDEI): SE_RCM, SE_BARCM, or SE_All time series generated by the use of the WFDEI reference data.

TABLE A3 Correlation, PBIAS (%), and RMSE (mm) values indicating the goodness of fit to the MESAN reference data for the monthly time series of SE(MESAN)^a and RCMs

Station ID	SPI	4 RCMs			12 BA RCMs			16 RCMs		
		Worst	Best	SE_RCM	Worst	Best	SE_BARCM	Worst	Best	SE_All
8229 Akseki	Corr	0.40	0.51	0.56	0.25	0.49	0.57	0.25	0.51	0.60
	RMSE	4.16	3.06	2.40	3.39	2.90	2.56	4.16	2.90	2.23
	PBIAS	26.4	-8.23	4.58	38.58	1.33	-35.0	38.6	1.33	4.36
17300 Antalya AP	Corr	0.29	0.44	0.50	0.26	0.49	0.57	0.26	0.49	0.58
	RMSE	3.75	3.06	2.43	3.84	2.77	2.29	3.84	2.77	2.26
	PBIAS	-18.8	-1.66	0.00	-45.3	-0.10	-0.62	-45.3	-0.10	-0.21
17310 Alanya	Corr	0.48	0.54	0.65	0.36	0.59	0.68	0.36	0.59	0.69
	RMSE	4.27	2.62	1.94	2.72	2.25	1.88	4.27	2.25	1.84
	PBIAS	-86.3	-9.84	0.00	14.0	0.16	0.00	-86.3	-0.16	0.00
17898 Seydisehir	Corr	0.28	0.49	0.52	0.13	0.46	0.49	0.13	0.49	0.59
	RMSE	1.54	1.24	1.08	1.68	1.27	1.07	1.68	1.24	0.96
	PBIAS	67.0	36.6	0.00	76.5	-1.98	-0.06	76.5	-1.98	0.00
17928 Hadim	Corr	0.24	0.42	0.46	0.30	0.39	0.44	0.24	0.42	0.50
	RMSE	1.77	1.60	1.27	1.82	1.54	1.24	1.82	1.54	1.18
	PBIAS	52.8	46.1	0.00	25.5	-0.69	0.00	52.8	-0.69	0.00
17954 Manavgat	Corr	0.48	0.52	0.66	0.37	0.57	0.68	0.39	0.59	0.71
	RMSE	3.65	3.02	2.38	3.51	2.97	2.34	3.65	2.97	2.23
	PBIAS	-19.7	-0.85	0.00	-15.7	-0.46	-0.70	-19.7	-0.46	-0.53
17320 Anamur	Corr	0.32	0.45	0.55	0.11	0.52	0.66	0.11	0.52	0.68
	RMSE	2.88	2.71	2.16	2.86	2.50	1.95	2.88	2.50	2.00
	PBIAS	79.9	65.3	0.00	70.9	47.3	-1.75	79.9	47.3	-13.8
17246 Karaman	Corr	0.23	0.27	0.31	0.13	0.29	0.33	0.13	0.29	0.41
	RMSE	2.71	1.50	0.85	2.52	1.25	0.84	2.71	1.25	0.76
	PBIAS	-96.3	-13.3	0.00	-88.8	2.93	-0.09	-96.3	-2.93	0.00

Note: The best performing model for each station is given in bold.

Abbreviations: RCM, regional climate model; RMSE, root mean square error; SE, superensemble.

^aSE(MESAN): SE_RCM, SE_BARCM, or SE_All time series generated by the use of the MESAN reference data.

**B. PAPER 2: CHANGES IN PRECIPITATION CLIMATOLOGY FOR
THE EASTERN MEDITERRANEAN USING CORDEX RCMS, NHRCM
AND MRI-AGCM**

This appendix was published as Mesta, B., Sasaki, H., Nakaegawa, T., & Kentel, E. (2022). Changes in precipitation climatology for the Eastern Mediterranean using CORDEX RCMs, NHRCM and MRI-AGCM. *Atmospheric Research*, Volume 272, 2022, 106140, ISSN 0169-8095, <https://doi.org/10.1016/j.atmosres.2022.106140>.



Changes in precipitation climatology for the Eastern Mediterranean using CORDEX RCMs, NHRCM and MRI-AGCM

Buket Mesta^a, Hidetaka Sasaki^b, Toshiyuki Nakaegawa^b, Elçin Kentel^{c,*}

^a Department of Earth System Science, Middle East Technical University, Ankara, Turkey

^b Department of Applied Meteorology Research, Meteorological Research Institute, Tsukuba, Japan

^c Department of Civil Engineering, Middle East Technical University, Ankara, Turkey

ARTICLE INFO

Keywords:

Regional Climate Model
NHRCM
MRI-AGCM
Precipitation
Mediterranean

ABSTRACT

Mediterranean Basin is expected to be one of the regions most severely impacted by global climate change. However, the complex interactions of driving forces of climate in the region create a challenge for climate projections for the future. Findings from climate change studies support the inter-model and inter-regional variability of projections on climate change impacts. On the other hand, the studies on the evaluation of the simulation skills of high-resolution climate models for the region particularly for Turkey are still numbered. Hence, this study brings a 14-member ensemble together for the analysis of the performance efficiencies of 12 CORDEX RCMs and two high-resolution climate models, NHRCM and MRI-AGCM, of the Japanese Meteorological Research Institute (MRI). The skill of climate models to reproduce the spatial variability of baseline precipitation climatology is assessed through a benchmark with reference data from 59 ground-based meteorological stations across the study area. Additionally, potential changes in precipitation climatology in the short (2020–2030), medium (2031–2050), and long-term (2051–2100) future are studied with a 14-member ensemble analysis. Projections of 14 models show significant disagreement, especially in the short-term, but most models project a general decrease in the precipitation in the study area in medium- and long-term under both RCP4.5 and RCP8.5 scenarios. For RCP8.5 scenario, performance based weighted average of five climate models project a decrease in precipitation across the whole study area both for medium- and long-term future.

1. Introduction

Turkey, having Mediterranean climate characteristics is under the pressure of the climatic changes occurring in the Mediterranean Basin. According to the IPCC special report (IPCC, 2018), the Mediterranean region is adversely affected by climate change. The report highlights with medium confidence that the region is at risk of drought. The study of Giorgi and Lionello (2008) verifies that the Mediterranean region between the arid climate of North Africa and the temperate and rainy climate of Central Europe (i.e., the location of Turkey) is a potentially vulnerable region to the climatic changes induced by anthropogenic activities, for example, increasing concentrations of greenhouse gases. The findings from Giorgi (2006) support this argument defining the region as one of the most prominent ‘Hot-spots’ in terms of the response to global change and will experience a significant decrease in mean precipitation as well as intensified precipitation variability, particularly

for the dry (warm) season. Furthermore, subregional analysis of the Mediterranean Basin indicates that unlike the central Mediterranean that experiences the mitigating effect of Alps against drying, the eastern Mediterranean is expected to be particularly under heavy impact of precipitation reduction (Giorgi and Lionello, 2008). Since a critical amount of decrease in the precipitation is expected for this region, Spinoni et al. (2020) conducted a global study evaluating the severity, frequency, and peak conditions of future drought under two representative concentration pathways (RCPs), RCP4.5 and 8.5. They used two drought assessment indices, i.e., the standardized precipitation index (SPI) and the standardized precipitation-evapotranspiration index (SPEI) for assessment and found that more frequent and severe droughts are likely for the Mediterranean region.

Various studies focusing on the climate change impacts at different regions of Turkey were performed to project future climate change effects and possible outcomes in terms of different perspectives such as

* Corresponding author at: Department of Civil Engineering, Water Resources Laboratory, Middle East Technical University, Üniversiteler Mahallesi Dumlupınar Bulvarı No:1, 06800 Ankara, Turkey.

E-mail address: ekentel@metu.edu.tr (E. Kentel).

<https://doi.org/10.1016/j.atmosres.2022.106140>

Received 17 November 2021; Received in revised form 18 February 2022; Accepted 8 March 2022

Available online 13 March 2022

0169-8095/© 2022 Elsevier B.V. All rights reserved.

forestry, evapotranspiration, crop yield, energy, and tourism activities (Fujihara et al., 2008; Özdoğan, 2011; Sen et al., 2012; Deidda et al., 2013; Öztürk et al., 2015; Sunyer Pinya et al., 2015; Yilmaz, 2015; Demircan et al., 2017; Mehr and Kahya, 2017; Bucak et al., 2018; Dino and Akgül, 2019; Gorguner et al., 2019). Most of these studies cover the analysis based on a few models or for relatively small study areas.

Mehr and Kahya (2017) studied climate change impacts on extreme storm events in a catchment at the Black Sea coast in northern Turkey by the use of two GCM (General Circulation Model) /RCM (Regional Climate Model) combinations under SRES-A2 and RCP8.5 scenarios, respectively. The study of Demircan et al. (2017) included an assessment for Turkey in general and its surrounding region in the greater Mediterranean Basin using the RegCM4.3.4 RCM (the latest version of Regional Climate Model system RegCM updated by the International Center for Theoretical Physics) for dynamical downscaling of three GCMs under RCP4.5 and RCP8.5 scenarios. Dino and Akgül (2019), using an ensemble of 14 GCMs, studied the assessment of potential climate change impacts on energy use and CO₂ emissions from residential buildings due to the use of different cooling strategies. The study was performed for four cities (Izmir, Istanbul, Ankara, and Erzurum) in Turkey. Bucak et al. (2018) studied potential impacts on the largest freshwater lake in Turkey regarding the changes in significant parameters controlling the ecosystem dynamics under different climate change and land use scenarios. In their study, for the assessment of the limnological changes, hydrological models were operated using the outputs from three GCMs and the outputs of RegCM4 based on the boundary conditions of two GCMs.

In recent years, studies focusing on climate change and related impacts in the region are performed with larger climate model ensembles providing a broader view in the analysis of uncertainties. The study conducted by Deidda et al. (2013) evaluated 14 RCMs from the EU-FP6-ENSEMBLES project and identified four best-performing models for precipitation. The study covered several hydrological basins from different parts of the Mediterranean and Izmit Bay is the selected case study area in Turkey. Their findings show that among 14 GCM/RCM combinations four RCMs are the best performing for the study area, particularly for hydrological assessment. Similarly, Sunyer Pinya et al. (2015) compared eight statistical downscaling methods applied on 15 GCM/RCM combinations from the ENSEMBLES project for 11 catchments in different parts of Europe including the Omerli basin in Istanbul Province as the case study area. Their findings indicated an improvement in the projections with statistical downscaling methods particularly based on bias correction methodologies. Additionally, the climate projections in their study are shown to agree in general in an increase in extreme precipitations at the majority of study catchments, although models show distinct variability regarding the magnitude of the change.

In their study, Aziz and Yucel (2021) analyzed the climate non-stationarity based on the outputs of 12 CORDEX RCMs under the RCP8.5 scenarios based on the precipitation records of meteorological stations in various geographical regions of Turkey. Comparison of RCM outputs with observed data showed distinct inter-regional variability in performance skills of RCMs. Their findings show that among 12 CORDEX RCMs, RACMO22E and CCLM4-8-17 RCMs using HadGEM2 as the driving model have the highest simulation efficiency for precipitation in the Mediterranean Region extending parallel to the Mediterranean coast of Turkey. Additionally, CM5A-MR-RCA4 showed relatively high accuracy in simulations for almost all regions of Turkey. The analysis revealed inter-regional variability in changes in precipitation climatology and an increased risk of water scarcity particularly for eastern Anatolia and Mediterranean regions of Turkey (Aziz and Yucel, 2021).

The objective and scope of this study are the analysis of climate projections for a study region covering more than 200,000 km² area in western and southwestern Turkey, including the Mediterranean Region (from hereafter will be referred to as study area or SA) using high-resolution climate model outcomes. Twelve CORDEX RCMs for the EUR-11 domain along with two additional climate models generated by

the Japan Meteorological Agency (JMA) Meteorological Research Institute (MRI) are used in this study to carry out short-, medium- and long-term precipitation projections. The latter two models are the super high-resolution atmospheric climate model of MRI (MRI-AGCM), and MRI's RCM, Non-Hydrostatic Regional Climate Model (NHRCM) nested in the boundary conditions of the MRI-AGCM. The MRI-AGCM is an atmospheric general circulation model (AGCM) that was developed to improve the regional-scale representation of the climate integrated with the global-scale and long-term mean climate state. The horizontal resolution of the grid of this model is about 20 km (Mizuta et al., 2006), which corresponds to high-resolution GCM data. The study by Kusunoki (2018) verified that MRI-AGCM3.2 provides a simulation efficiency higher than or similar to CMIP5 models in reproducing the average seasonal precipitation in East Asia majorly because of its higher horizontal resolution and its cumulus convection scheme. MRI-AGCM was also used for future climate change studies in various parts of the world, including Central America (Nakaegawa et al., 2014; Kusunoki et al., 2019) and Australia (Nakaegawa et al., 2017).

McSweeney et al. (2015) tested the efficiency of MRICGCM3 among 43 CMIP5 GCMs through validation against ERA-40, ERA-Interim data and also CRU (temperature), and GPCP, CMAP (precipitation) datasets for Southeast Asia, Europe, and Africa domains to identify the most suitable models for downscaling with the purpose of the regional analysis. The GCM, MRI-CGCM3, analyzed in their study consists of the atmosphere-land model (MRI-AGCM3), which is interactively coupled with the aerosol model (MASINGAR mk-2) along with the ocean and sea-ice model (MRI.COM3) (Yukimoto et al., 2012). According to the overall evaluation of the models, MRI-CGCM3 was found to perform relatively poorly in the representation of Southeast Asian Summer Monsoon (significant biases) and West African Monsoon (biases) and replication of the annual temperature and precipitation cycles over Africa. On the other hand, regarding Europe MRI-CGCM3 was evaluated to have satisfactory results for the replication of the annual cycles of temperature and precipitation, circulation patterns, and storm tracks (McSweeney et al., 2015). Similarly, among the tested CMIP5 GCMs, CNRM-CM5, EC-EARTH, HadGEM2-ES that are also included as driving models of RCMs in our study are reported to be found satisfactory for the Europe domain regarding the same parameters. Although IPSL-CM5A-MR was reported to show weak performance particularly for the replication of the annual temperature and precipitation cycles in the Mediterranean (McSweeney et al., 2015).

NHRCM is a regional climate model which was developed by enhancing an operational non-hydrostatic model (NHM) of MRI and the Numerical Prediction Division of the Japan Meteorological Agency (NPD/JMA) (Sasaki et al., 2008, 2011). The performance of NHRCM for climate simulations was thoroughly tested by several studies in Japan. Sasaki et al. (2008) demonstrated strong simulation performance of NHRCM to reproduce the precipitation and surface temperature as well as the inter-annual variation of surface temperature. Furthermore, it is shown to perform well in the simulation of extreme storm events that is generally a challenging task for regional climate modeling. Sasaki and Kurihara (2008) analyzed and verified the high skill of NHRCM to represent the effect of topography on precipitation in river basins through a comparison of the elevation-precipitation relationship reproduced by NHRCM with the observed. Sasaki et al. (2011) demonstrated that NHRCM provides improved skills for local temperature and precipitation projections compared to AGCM. Additionally, it was tested for its performance for other parameters such as snow depth and storm tracks (Sasaki et al., 2012, 2013).

Furthermore, various other studies were carried out for the present and future climate simulations of various regions of the world using MRI-AGCM and NHRCM, and their model performances were evaluated by comparing them to other global and regional models (Saito et al., 2006; Kitoh et al., 2009, 2016; Pinzón et al., 2017; Varghese et al., 2020). Even though Turkey was included in some of these studies, this is the first study that covers a detailed comparison of these two models

with CORDEX RCMs for the Mediterranean region. In this study, NHRCM grid data are generated by nesting within MRI-AGCM with a 20-km grid spacing. The horizontal resolution of NHRCM is 5 km in this study and it is run for the domain that is limited to the study area of concern. NHRCM integration with MRI-AGCM boundary conditions was conducted for 20-year timeframes to simulate present (1980–2001) and future (2080–2100) climate conditions.

Given that the projections by CORDEX RCMs demonstrate inter-regional and inter-model variability, identification of the climate change impacts for the Mediterranean Region of Turkey that has a complex topography and climate features is a challenging task. Furthermore, to the best of our knowledge, the number of studies that include a comparison of various CORDEX RCMs for the projection skills for Turkey is still limited. Therefore, this study aims to provide a comparison of 12 CORDEX RCMs and two MRI climate models for the identification of the models with relatively better projection skills and to analyze the range of uncertainty in precipitation projections of this 14-member ensemble. Furthermore, the study provides a comparison of the projection efficiencies of a super high-resolution GCM with various high-resolution RCMs obtained through dynamical downscaling of CMIP5 GCMs and with NHRCM based on the same high-resolution GCM to analyze the size of relative biases in the precipitation projections of each model.

In this study, the skills of the models in reproducing the spatial variability in the climatology of the study area are evaluated. Performances of the climate models are evaluated using monitoring data from ground-based meteorological stations and three commonly used model performance evaluation parameters: the Pearson correlation coefficient (*Corr*), root mean square error (*RMSE*), and percent bias (*PBIAS*). Following that, the potential change in precipitation in the short-term (2020–2030), medium-term (2031–2050), and long-term (2051–2100) future and relevant uncertainties in projections are analyzed. One of the objectives of this study is to provide information on potential water scarcity or changes that might be expected to have a significant impact on potential receptors (i.e., water users) in the SA through the analysis of potential changes in the mean precipitation. In this regard, the findings from the analysis are aimed to serve the future planning for the use of water resources in Turkey. For this purpose, different from similar studies in the literature that use virtually identical (roughly 30 years) sections of the projections on climate of 21st century (Guo et al., 2018), the future time-series of projections are divided to aforementioned short-, medium- and long-term periods. Furthermore, to assess potential significant changes that are likely to influence the period means (particularly for the long-term future between 2051 and 2100) the smoothed future time-series of annual total precipitation projections of RCMs are also analyzed.

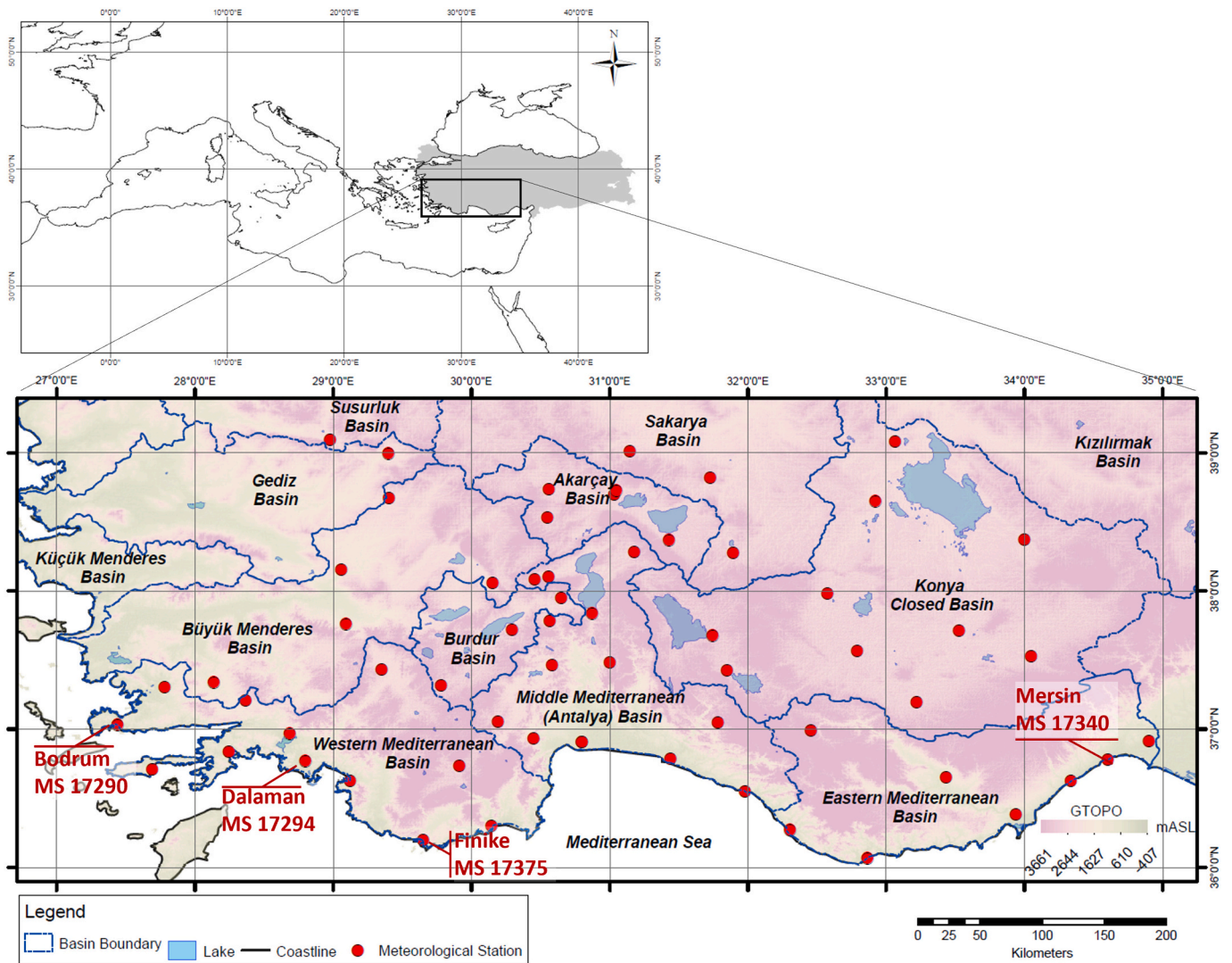


Fig. 1. Study area, showing the topography of the region with the locations of the meteorological stations used in this study (Overview map in the upper panel displays the Mediterranean Basin).

2. Study area

The region of interest in this study covers a major portion of Turkey where the temperate climate conditions, so-called Mediterranean climate features, are dominantly observed (Fig. 1). The study area (SA) includes partially or fully, 10 of the major watersheds in Turkey. Mild, wet winters and warm to hot, dry summers characterize climate of the study area located in the greater Mediterranean Basin (Cowling et al., 1996). The morphology of the region is complex due to sharp orographic features, distinct basins and gulfs, islands, and peninsulas of various sizes. This complex morphological structure strongly affects the atmospheric circulation in the region (Lionello et al., 2006). At the transition zone between eastern Europe and the Middle East, the regional climatology is affected not only by complex topography and inland water bodies but also by the Mediterranean Sea as well as by the factors affecting modes of variability controlling the precipitation patterns in Europe such as North Atlantic Oscillation (NAO) and East Atlantic West Russia (EAWR) climate systems (Krichak et al., 2002; Evans, 2009). As indicated previously, the Mediterranean Basin has significant trends in terms of precipitation and temperature due to climate change, which is likely to create strong impacts on the climatic behaviors of our study region.

3. Data and methods

3.1. Data

The historical datasets of the 59 meteorological stations (MSs) operated by the General Directorate of State Meteorological Service (DMI) of Turkey are used as the benchmark for the validation of the historical data from climate models. Daily historical precipitation records of the timeframe between 1966 and 2005 are used in this study. The locations of these MSs are shown in Fig. 1.

Analysis of climate projections is based on outputs of 14 climate models (Table 1). Among 14 climate models analyzed for the study area, 12 are RCMs for EUR-11 Domain with approximate grid resolutions of 12 km (0.11 degrees on a rotated coordinate system) available from the CORDEX database. Twelve climate models from the CORDEX database include the combination of five different RCMs (i.e., ALADIN53 of Centre National de Recherches Météorologiques (CNRM), CCLM4-8-17 of Climate Limited-area Modeling Community (CLM-Community), RCA4 of Swedish Meteorological and Hydrological Institute (SMHI), HIRHAM5 of Danish Meteorological Institute (DMI), and RACMO22E of Royal Netherlands Meteorological Institute (KNMI), and WRF331F of Institut Pierre-Simon Laplace (IPSL-INERIS)) based on the boundary conditions defined by four GCMs. The combination of 12 CORDEX RCMs is selected to enable the assessment of the performance of at least two

different RCMs taking the same GCM as the boundary conditions.

The outputs of the remaining two models are from climate models generated by MRI. These include the outputs of the super high-resolution AGCM and climate projections generated for the study area by dynamic downscaling with the use of MRI's NHRCM nested in the MRI-AGCM. Additionally, unlike other climate models used in this study, the NHRCM is run within the model domain limited to our study area in Fig. 1. Hence projections on local climate generated using NHRCM are expected to put more emphasis on the study area.

MRI-AGCM uses prescribed observation-based sea-surface temperatures (SST), while CMIP5 models project ocean conditions including SST based on ocean physics. For the present-day climate simulations, MRI-AGCM uses observed, historical SSTs, and sea ice concentrations. For the future climate simulations, future SSTs and sea ice concentrations are prescribed by combining three components: observed interannual variabilities, climatological future change in SSTs/sea-ice concentrations, and linear trend in SSTs/sea-ice concentrations for a future target period (Mizuta et al., 2008, 2014). The methodology used for the future simulations in MRI-AGCM for SST and sea-ice concentrations is similar to the methodology that is also used by HighResMIP (High Resolution Model Intercomparison Project), which is one of the CMIP6-endorsed MIPs (Haarsma et al., 2016).

For all the models, the historical and future projection data of the model grids closest to the 59 MSs are extracted from the model outputs using the R code developed by Kentel et al. (2019) for the analysis. Present climate conditions regenerated by CORDEX RCMs are obtained from the historical data for the period between 1966 (whenever available otherwise 1970) and 2005 whereas for MRI-AGCM and NHRCM present climatology is obtained from the outputs for the timeframe between 1980 and 2000. The historical data from climate models are used for the testing of the accuracy of these models through a comparison with the benchmark ground-based data. Additionally, the replicated present climatology is used for a comparison with the future climate projections to determine potential future changes in precipitation based on each climate model.

The future projections on precipitation are analyzed for three periods: short-term (2020–2030), medium-term (2031–2050), and long-term (2051–2100) future based on RCP4.5 and RCP8.5 scenarios for 12 CORDEX RCMs. For MRI models, due to the available data, future projections are analyzed only for the RCP8.5 scenario and for the long-term future impacts of the 2080–2100 period. The list of the names and relevant ID's of the MSs, climate models and basins used in this study are provided in Appendix A.

Table 1

List of the climate models used in the study.

Climate model (RCM/GCM)			Output period		Resolution	Source	Model number
Driving model/ GCM (institution)	Name	Institution	Historic	Future (scenarios)			
MRI-AGCM (MRI)		MRI	1979–2003	2075–2100 (RCP8.5)	0.1875°	MRI	M1
MRI-AGCM (MRI)	NHRCM	MRI	1980–2001	2080–2100 (RCP8.5)	5 km	MRI	M2
CNRM-CM5 (CNRM-CERFACS)	ALADIN53	CNRM	1951–2005	2006–2100 (RCP4.5, RCP8.5)	0.11°	CORDEX Db ^a	M3
CNRM-CM5 (CNRM-CERFACS)	CCLM4-8-17	CLM-Community	1950–2005	2006–2100 (RCP4.5, RCP8.5)	0.11°	CORDEX Db ^a	M4
CNRM-CM5 (CNRM-CERFACS)	RCA4	SMHI	1970–2005	2006–2100 (RCP4.5, RCP8.5)	0.11°	CORDEX Db ^a	M5
EC-EARTH (ICHEC)	CCLM4-8-17	CLM-Community	1949–2005	2006–2100 (RCP4.5, RCP8.5)	0.11°	CORDEX Db ^a	M6
EC-EARTH (ICHEC)	HIRHAM5	DMI	1951–2005	2006–2100 (RCP4.5, RCP8.5)	0.11°	CORDEX Db ^a	M7
EC-EARTH (ICHEC)	RACMO22E	KNMI	1950–2005	2006–2100 (RCP4.5, RCP8.5)	0.11°	CORDEX Db ^a	M8
EC-EARTH (ICHEC)	RCA4	SMHI	1970–2005	2006–2100 (RCP4.5, RCP8.5)	0.11°	CORDEX Db ^a	M9
CM5A-MR (IPSL)	RCA4	SMHI	1970–2005	2006–2100 (RCP4.5, RCP8.5)	0.11°	CORDEX Db ^a	M10
CM5A-MR (IPSL)	WRF331F	IPSL-INERIS	1951–2005	2006–2100 (RCP4.5, RCP8.5)	0.11°	CORDEX Db ^a	M11
HadGEM2-ES (MOHC)	CCLM4-8-17	CLM-Community	1949–2005	2006–2100 (RCP4.5, RCP8.5)	0.11°	CORDEX Db ^a	M12
HadGEM2-ES (MOHC)	RACMO22E	KNMI	1950–2005	2006–2100 (RCP4.5, RCP8.5)	0.11°	CORDEX Db ^a	M13
HadGEM2-ES (MOHC)	RCA4	SMHI	1970–2005	2006–2100 (RCP4.5, RCP8.5)	0.11°	CORDEX Db ^a	M14

^a CORDEX Database: ESGF, Earth System Grid Federation website, <https://esgf-node.llnl.gov/search/esgf-llnl/>, (CoG version v4.0.0b2, ESGF P2P Version v4.0.4).

3.2. Quality check for observed data and formation of baseline climatology

Observed data from ground-based manual precipitation records is used to analyze the baseline climatology in the study region as well as to form a benchmark in the validation of the climate models. The quality of the reference data has particular importance for model validation and evaluations in climate change impact assessment. Therefore, a preliminary quality check (QC) is applied to obtain reference data sets from observed data of meteorological stations. For that purpose, the daily time series of the observed data for each MS is screened for data gaps and potential errors. The data series for months with more than ten days of missing records are removed from the dataset and monthly average precipitation values are calculated. The monthly average precipitation time series obtained after screening and relevant climatology data (from hereafter will be referred to as Reference Data or RD) are used for the assessment of baseline distribution of precipitation that is represented with the baseline climatology maps of the study region, and as a benchmark for validation of climate models. In order to prevent potential biases in precipitation climatology calculations for seasonal and annual terms, monthly timeseries of RD are processed to exclude the seasons with more than two months of missing records and years with more than two seasons of missing records before the calculation of relevant climatologies.

3.3. Testing of model performance

To test the model performances historical outputs are compared with the RD over the reference period. The reference period of each model is selected based on its data availability for the historic period. The performance of climate models to reproduce the precipitation climatology is analyzed based on the accuracy of the areal representation concerning the spatial variation pattern in the region obtained using 59 MSs. The testing of model skills for reproducing spatial change in precipitation is done using statistical performance indicators and by comparison with the Taylor diagram.

Three statistical performance indicators used for testing are Pearson correlation coefficient (*Corr*), root mean square error (*RMSE*), and percent bias (*PBIAS*). The equations for relevant performance indicators are given as follows:

$$Corr = \frac{\sum_{i=1}^n (O_i - \bar{O})(M_i - \bar{M})}{\sqrt{\sum_{i=1}^n (O_i - \bar{O})^2 \sum_{i=1}^n (M_i - \bar{M})^2}} \quad (1)$$

$$RMSE = \sqrt{\frac{1}{n} \sum_{i=1}^n (M_i - O_i)^2} \quad (2)$$

$$PBIAS = \frac{\sum_{i=1}^n (O_i - M_i)}{\sum_{i=1}^n (O_i)} \times 100 \quad (3)$$

where, O_i and M_i are the i th reference and modeled climate data values while \bar{O} and \bar{M} are the mean of reference and modeled climate data values, respectively and n refers to the total number of data points (i.e., MSs).

In addition to the assessment of model performance skills based on the individual performance indicators, an aggregated performance index (API) is generated and used to rank the models. To calculate the API, models are ranked three times for each indicator separately (i.e., ranking of all models from best to worst) and three ranks are averaged to find the API of each model. The model with the lowest API is considered to achieve the best performance in the reproduction of spatial variation in climatology in the study area. The mean value of the API is 7.5.

4. Results

4.1. Analysis of climatology

The climatology maps of the SA are developed by the application of the inverse distance weighted (IDW) interpolation method on climatology data of MSs in the SA. The climatology maps in the study region obtained using RD are given in Fig. 2. Accordingly, the coastal stations have the highest seasonality of precipitation in the region. Coastal MSs receive 50% or higher of the annual precipitation during the winter season (Fig. 3); however, for the summer season (June–July–August) precipitation is significantly low. For these MSs, summer is either completely dry or has a very low precipitation rate (Fig. 2(d)). As can be seen in Fig. 2(a), most of these stations also receive higher mean annual precipitation (>2 mm/day) than the rest of the MSs in the study region. For the SA, winter precipitation climatology ranges between 1 and 8 mm/day, with the highest winter precipitation climatology observed at 12 MSs in the region stretching along the Southern Mediterranean coast, from Western Mediterranean to the East of the Middle Mediterranean basin.

The lowest annual precipitation rate is recorded for MSs in Konya Closed Basin, in the hinterland of the coastal Mediterranean region. For these inland stations, particularly for the stations that are not located in the proximity of any inland water body, annual mean precipitation is around 0.8–0.9 mm/day. At this basin, winter (December–January–February) and spring (March–April–May) are rainy seasons, during which around 60% of the annual precipitation is received. Inland MSs in Akarçay and Sakarya basins in western central Anatolia experience the lowest seasonality. These stations receive 30% or less of the annual precipitation during the winter season (Fig. 3). The main wet season for these MSs is spring (Fig. 2(c)). Nevertheless, summer is still the driest season of the year for these MSs (Fig. 2(d)). Summer precipitation forms 15–18% of the annual precipitation. A comparison of the spatial distribution of annual precipitation in different basins shows that Middle Mediterranean Basin receives more annual precipitation compared to neighboring watersheds. However, as can be seen from Fig. 2(a), this basin also has the highest spatial variability regarding precipitation climatology compared to the surrounding watersheds. The reason for its spatial variability is considered to be created by the topography and inland water bodies as well as the shape of the basin stretching out from the Mediterranean coast to farther inland in Anatolia. After the Middle Mediterranean Basin, Eastern Mediterranean Basin is the region with the second-highest spatial variability of precipitation climatology.

4.2. Analysis of the spatial representation skills of climate models

The annual precipitation climatology reproduced with the historical outputs of each climate model is compared with the benchmark RD from 59 MSs to identify the performance skill of the models concerning the distribution of precipitation in the study region. In order to assess the model skills for the reproduction of spatial variability of precipitation in the SA the observed annual precipitation means for all MSs in the SA are compared with the simulated annual means of the closest modeling grid. The data series of the benchmark MSs and the relevant modeling grids are used to determine *Corr*, *RMSE* and *PBIAS* for each climate model.

The best performance indicator values obtained from 14 climate models are indicated in bold in Table 2. Accordingly, NHRCM (M2) is among the top three models that provide the best representation of the spatial change in precipitation climatology with respect to *Corr*, *RMSE* and *PBIAS*.

With respect to the correlation of spatial variation of precipitation climatology, the other two models with the highest skill are EC-EARTH_HIRHAM5 (M7) and HadGEM2-ES_RACMO22E (M13). These three models can represent spatial variation with a correlation coefficient of 0.78. On the other hand, respecting the model bias value EC-EARTH_CCLM4-8-17 (M6) is seen to perform best among all 14

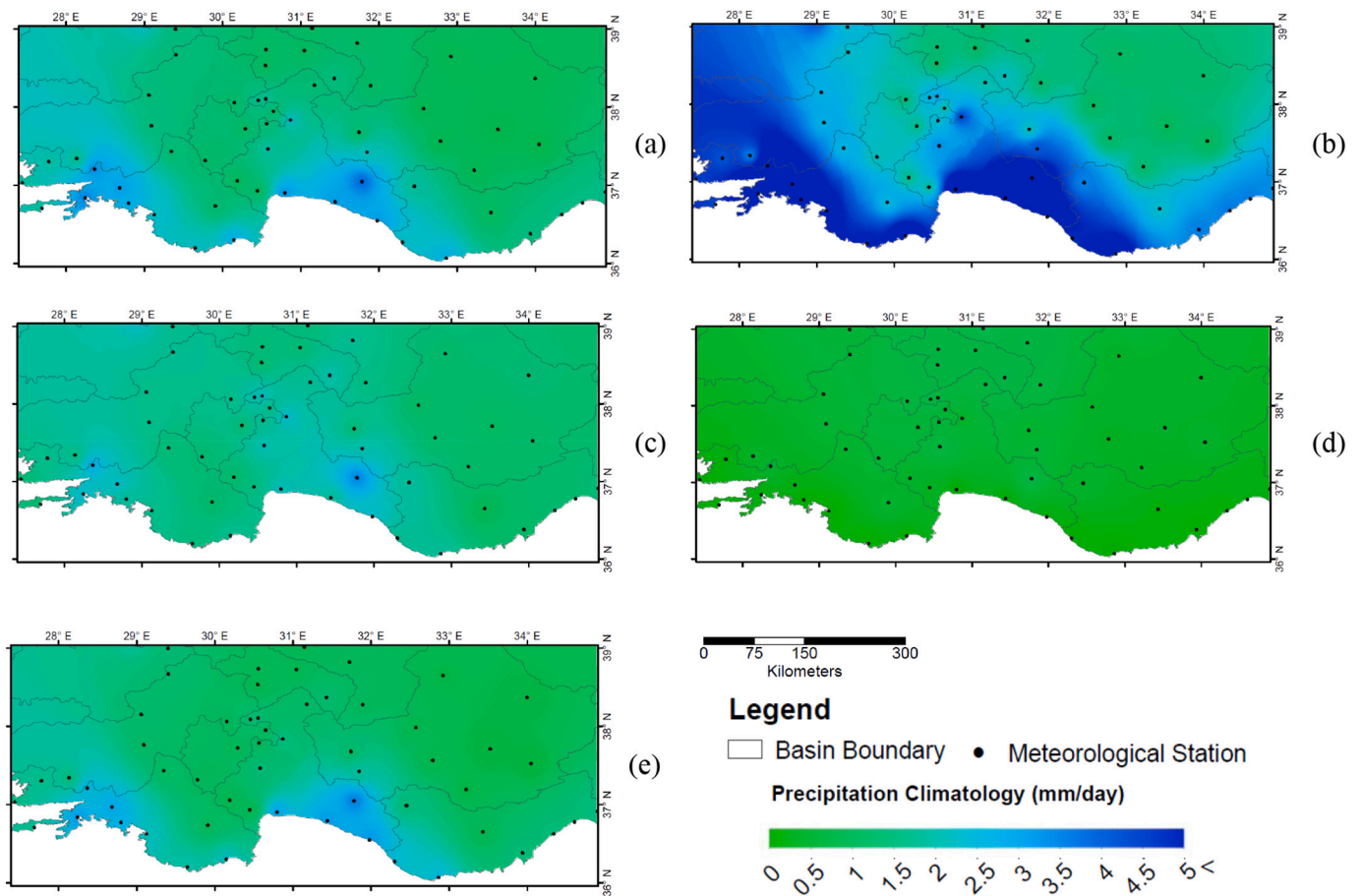


Fig. 2. Baseline precipitation climatology maps of the study area, (a): annual climatology, (b): winter climatology, (c): spring climatology, (d): summer climatology, (e): fall climatology.

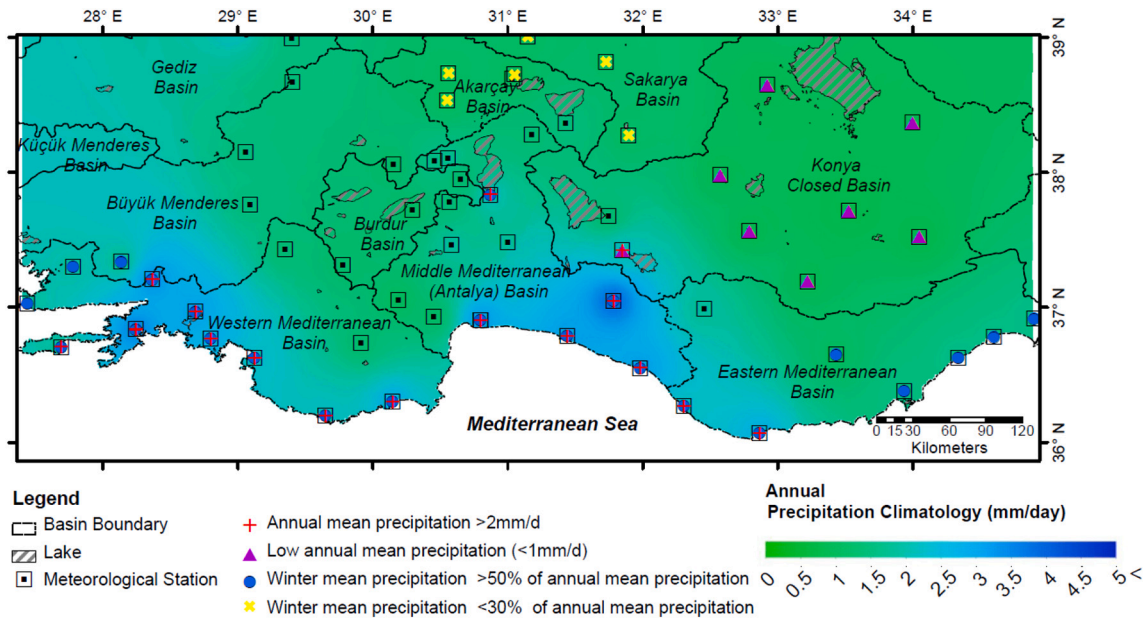


Fig. 3. Analysis of precipitation climatology properties at MSs in the study region.

climate models with 0.51 mm *RMSE* and significantly low (0.52%) *PBIAS*. In the 14-member ensemble of climate models, MRI's NHRCM based on the MRI-AGCM boundary conditions (M2) shows good skill with relatively low bias generating the second-best *RMSE* and *PBIAS*

values after EC-EARTH_CCLM4-8-17. The API calculated for the climate models verifies the best skill of NHRCM (M2) for the replication of the spatial distribution of precipitation in the study region. Other climate models with relatively better performance indexes are M6, M7, M8, and

Table 2
Performance indicator values for climate models.

ID	Model name	Corr	RMSE (mm)	PBIAS (%)	API
M1	MRI-AGCM	0.73	0.76	-20.35	8.00
M2	NHRCM	0.78^a	0.55	2.91	1.67
M3	CNRM-CM5_ALADIN53	0.32	0.92	-17.09	11.67
M4	CNRM-CM5_CCLM4-8-17	0.66	0.90	-35.93	12.67
M5	CNRM-CM5_RCA4	0.67	0.75	-3.25	7.00
M6	EC-EARTH_CCLM4-8-17	0.73	0.51	0.52	3.00
M7	EC-EARTH_HIRHAM5	0.78	0.70	3.80	4.00
M8	EC-EARTH_RACMO22E	0.75	0.59	8.04	5.00
M9	EC-EARTH_RCA4	0.70	0.66	6.26	6.67
M10	CM5A-MR_RCA4	0.68	0.75	28.99	10.00
M11	CM5A-MR_WRF331F	0.61	1.08	-30.05	13.33
M12	HadGEM2-ES_CCLM4-8-17	0.72	0.89	-27.58	10.00
M13	HadGEM2-ES_RACMO22E	0.78	0.87	-25.93	7.67
M14	HadGEM2-ES_RCA4	0.76	0.65	-4.55	4.33

^a The best values are indicated in bold.

M14. Comparison of NHRCM with MRI-AGCM results shows that the downscaled projections obtained by NHRCM have lower bias and better correlation with the RD.

The poorest API values are calculated for M3 (CNRM-CM5_ALADIN53), M4 (CNRM-CM5_CCLM4-8-17), and M11 (CM5A-MR_WRF331F). WRF331F is known to demonstrate poor replication skills for the annual precipitation trend over Greece for historical and RCP8.5 simulations (EURO-CORDEX, 2021). The testing of WRF331F for the SA verifies poor projection skill for precipitation in Turkey. Among the climate models, ALADIN53 has the lowest correlation with the spatial variability of precipitation in the SA. In fact, the poor performance of ALADIN53 is considered to be related to the problematic SST mapping from driving GCM that is expected to cause biased projections of surface temperature, particularly for coastal areas, as reported by EURO-CORDEX (2021). Biased surface temperature projections for coastal stations are likely to create further bias in precipitation projections. Furthermore, among the CORDEX RCMs tested in the study EURO-CORDEX (2021) reported potential weakness of RCA4 in precipitation projections implied by the patchy pattern in the summer/winter rainfall index generated by RCM. However, testing of model performance for the SA has verified that RCA4 shows no particularly significant weakness relative to other climate models. According to the API values, the skill of RCA4 is variable depending on the driving GCM. RCA4 nested in HadGEM2-ES has the highest skill relative to different boundary conditions from EC-EARTH, CNRM-CM5, and CM5A-MR.

The skills in precipitation dynamically downscaled with RCMs depends on lateral boundary conditions derived from GCMs. The performance indicator values, therefore, depends on both RCM and GCMs. As mentioned in 3.1 Data, MRI-AGCM has no biases in SST because of prescribed observed SSTs. However, CMIP5 models tend to contain biases in climatological SST because of SST simulated with ocean models. Indeed, MRI-AGCM generally has good skill in precipitation climatology, but does not always have best skills for some specific regions (Ito et al., 2020). Ito et al. (2020) compared Taylor's skill scores among the CMIP5 models and MRI-AGCM. The scores in the Mediterranean region are distributed in range of 0.72 to 0.96 with the median of 0.90 for the entire CMIP5 models. The subset with high Taylor's skill scores for the regional precipitation has the score range of 0.92 to 0.96 with the median of 0.93. In fact, MRI-AGCM has the lowest score of 0.90 among the 5 CMIP5 models listed in Table 1. Therefore, highest API of NHRCM is not due to a GCM providing the lateral boundary conditions but the dynamical downscaling with NHRCM enhances API.

Examination of the rankings of the climate models regarding API shows that the driving GCMs for the best-performing five models are EC-EARTH and HadGEM2-ES, and the driving GCMs for the worst-performing five models are CM5A-MR, HadGEM2-ES, and CNRM-CM5. Hence, that is to say, EC-EARTH performed well in projection

with all four RCMs (CCLM4-8-17, HIRHAM5, RCA4, and RACMO22E), whereas the projection performance of the climate models with the driving model HadGEM2-ES depends on the regional climate model nested in it. Moreover, CNRM-CM5 and CM5A-MR as the driving models for different RCMs perform relatively poorly for the study area. In that respect, the weak performance of CNRM-CM5 as the driving model of different RCMs might be attributed to the problem with the boundary forcing conditions in CNRM-CM5 for historical runs as reported by EURO-CORDEX (2021). Although it is reported that the influence of the technical error related to the inconsistent boundary forcing use in CNRM-CM5 is expected to be weak on climate scale, the relevant problem might be a factor for relatively low performance of this GCM in historical simulations for the SA.

Regarding climate model performances in the Mediterranean and Aegean Region of Turkey between 1971 and 2005, Aziz and Yucel (2021) reported two RCMs, RACMO22E (M13 of the current study) (from hereafter, the model ID used in the current study is given in parenthesis) and CCLM4-8-17 (M12) (driving GCM: HadGEM2-ES) in the 12-member CORDEX ensemble, to have the best correlation and RMSE values for the replication of the mean daily precipitation climatology and the change in monthly mean precipitation in time. EC-EARTH_RACMO22E (M8), EC-EARTH_RCA4 (M9), and CM5A-MR_RCA4 (M10) are also among the models reported with a relatively better performance ranking. Furthermore, the models CNRM-CM5_ALADIN53 (M3), CNRM-CM5_CCLM4-8-17 (M4), and CM5A-MR_WRF331F (M11) reported by Aziz and Yucel (2021) to be weak in reproduction of the temporal change in precipitation in most of the regions of Turkey are identified to be weak in the representation of spatial variability of precipitation in the SA producing relatively poor API values in our evaluation as well. Hence, the performance indicators including API calculated in our study for the representation of the spatial variability of the precipitation climatology are similar to the findings from that recently published previous study focusing on performance regarding the replication of temporal change of precipitation, although differences exist depending on the differences in criteria and metrics used in this study.

Taylor diagram to compare the model performances is given in Fig. 4. According to Fig. 4, for the study region, four RCMs (M2, M6, M8, and M10) are notable in their better performance skills over the rest of the climate models. According to the overall evaluation based on API and Taylor diagram, three climate models identified with the best performance skill in the spatial representation of climatology at the SA are M2: NHRCM with MRI-AGCM boundary conditions, M6: EC-EARTH - CCLM4-8-17, and M8: EC-EARTH - RACMO22E.

4.3. Future projections on precipitation

For the analysis of future projections, the division of time-series of RCM outputs are done to generate information that might be useful for decision-makers for short-, medium-, and long-term planning against potential water scarcity at different parts of Turkey. Hence, the analysis is focused on the immediate future (2020–2030), medium-term future (2031–2050) that will be the second stage for mitigation planning and the long-term future for mitigation planning in the long horizon. In that scope, the projections of 12 CORDEX RCMs are assessed for short-term (2020–2030), medium-term (2031–2050), and long-term (2051–2100) through a comparison with the annual precipitation climatology of the reference period.

RCP8.5 scenario projections for the 2080–2100 timeframe from two high-resolution MRI climate models are also added to the analysis for the assessment of the potential changes in long-term future precipitation.

The percent change in precipitation for the projection period is calculated as follows:

$$\text{Percent change in precipitation} = \frac{\Delta P}{P_{Ref}} \times 100 \quad (4)$$

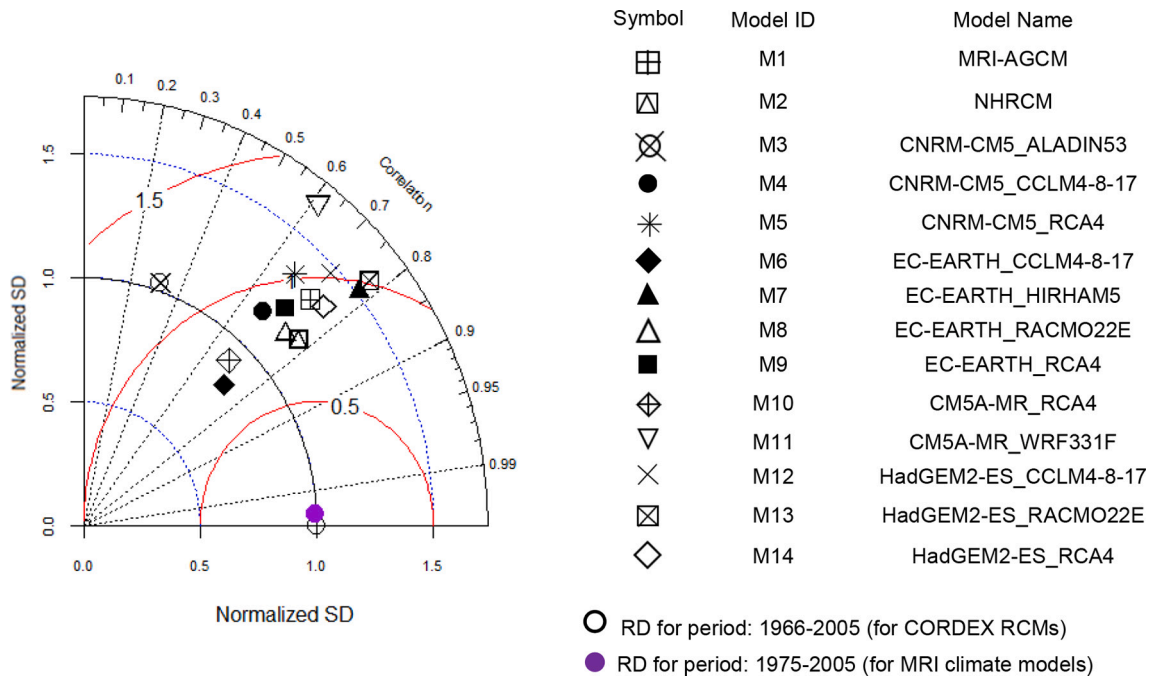


Fig. 4. Taylor diagram of climate models.

where, ΔP is the difference in the precipitation climatology between the projection period (e.g., 2020–2030 for short-term) and reference period, and P_{Ref} is the climatology of the reference period. The data on percent change in precipitation at modeling grids in the SA are processed to obtain spatial variability of the change within the area. For that purpose, point data of grids are converted to surface data using the IDW interpolation method of the Spatial Analyst tool of ArcGIS 10.0. Maps in Fig. 5 to Fig. 11 show the projections on percent change in annual precipitation climatology for 59 MSs in the SA based on 14 climate model outputs. The comparison of results indicates that projections of 14 models for the region include significant variability not only for the quantity but also for the direction of the change in precipitation climatology. To overcome the inter-model variability due to uncertainties, various multi-model ensemble (MME) methodologies can be followed. The selected MME approach might range from simple methods such as multi-model simple averaging, or multi-model weighted averaging based on some model performance metrics (Tebaldi and Knutti, 2007; Christensen et al., 2010), to more complex methodologies such as synthesis of the models using multiple regression (i.e., Superensemble method) (Stefanova and Krishnamurti, 2002; Krishnamurti et al., 2016; Mesta and Kentel, 2021), Artificial Neural Networks (Boulanger et al., 2006, 2007; Cakir et al., 2013), Bayesian hierarchical modeling or Bayesian model averaging (BMA) (Wang et al., 2014, 2016) to achieve probabilistic projections through ensembling. Respecting the main objective of this study, a relatively simple approach, based on weighted averaging constructed according to the simulation skills of the models, is used. Hence, the MME method used in this study is limited to a linear deterministic approach that is referred to as Performance-based Weighted Average (PBWA) and calculated as detailed below. The objective of the use of PBWA is to obtain a general understanding of the range of impact on precipitation that is projected by the individual climate models that are defined to have the highest simulation skills.

The projection maps between Figs. 5 and 10 also provide maps based on PBWA of CORDEX models for the relevant projection periods. The PBWA of projections on percent change in precipitation climatology is calculated as follows:

$$PBWA = \frac{\sum_{i=1}^n \left[\frac{1}{API_i} \times (\text{Percent change in precipitation})_i \right]}{\sum_{i=1}^n \frac{1}{API_i}} \quad (5)$$

where, i is the index for the models used in PBWA of projections on percent change. Here, the best performing five CORDEX models (i.e., $n = 5$) identified according to the API (i.e., M6, M7, M8, M9, M14; see Table 2) are used to generate PBWA. Only for long-term future for the RCP8.5 scenario (Fig. 10), two PBWA of projections are generated, the first (i.e., PBWA-1) using five best performing CORDEX models (i.e., M6, M7, M8, M9, M14) and the second (i.e., PBWA-2) using NHRCM plus four best performing CORDEX models (M6, M7, M8, M14). In Figs. 5 to 10, the map of the PBWA of percent change in precipitation climatology of 59 MSs in the SA is shown in the last row. Additionally, the projection map of the best performing CORDEX model (i.e., M6; see Table 2 and Fig. 4) is written in bold.

The significance of the change in precipitation is tested by the use of Welch’s two-sample t -test (or unequal variances t -test). t -test was applied to annual precipitation time series from the climate model projections for the reference versus future short-, medium- and long-term periods. The results of the test indicating statistically non-significant change according to the 95% confidence level are shown as hatched on the percent precipitation change maps for each climate model. The surface data on the significance of the results are produced by using the IDW method. However, it should be noted that, t -test is not applicable to the PBWA results that are calculated directly from percent change projections and hence is not shown on the relevant maps.

In addition to the analysis of potential changes concerning long-term means of annual total precipitation for short-, medium-, and long-term future, the interannual fluctuations in total precipitation are also assessed to detect any potentially significant change within these periods, particularly for the 50-year long long-term future. For that purpose, smoothing by non-parametric regression is applied to total annual precipitation time-series from RCMs. The LOESS (Locally Estimated Scatterplot Smoothing) is used to filter the annual time series to remove local fluctuations for the assessment of long-term precipitation patterns under the climate change conditions. LOESS is based on iteratively

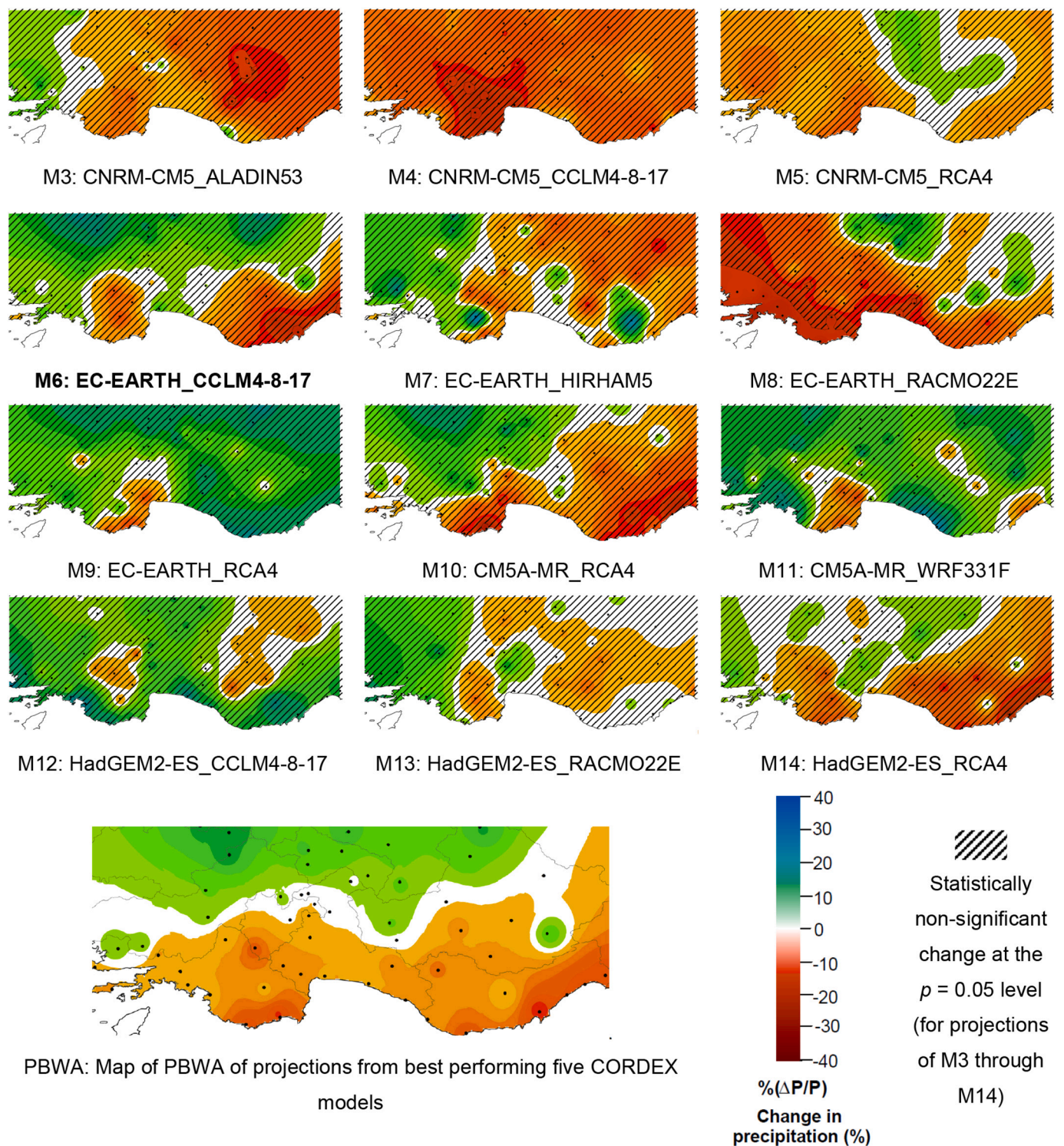


Fig. 5. Climate model projections for percent change in precipitation in short-term future for the RCP4.5 scenario.

applied weighted least squares regression, computed locally to obtain smooth curves from large size data sets (Cleveland, 1979; Cleveland and Devlin, 1988). LOESS is frequently used for the smoothing of climate data sets, and data sets in various fields of study to produce an empirically fitted curve calculated through LOESS regression (Jacoby, 2000; Della-Marta and Wanner, 2006; Toreti et al., 2010; Steinacker, 2021).

For the short-term future under the RCP4.5 scenario, the maximum range for 12-member CORDEX model ensemble shows an increase in precipitation up to 24% and a decrease up to 22% at different locations

in SA (Fig. 5) indicating an intra-regional variability in the size and type of impact on precipitation. As can be seen in the PBWA map of Fig. 5, when the best performing five CORDEX models' predictions are combined, a more uniform map showing mostly a decrease in precipitation at the coastal zones at the south and a gradual increase towards inland is obtained.

As it is seen in Fig. 5, the precipitation climatology for annual mean calculated from the projections of seven of the 12 CORDEX models (M3, M4, M5, M7, M8, M10, M14) indicate a decrease in precipitation in the

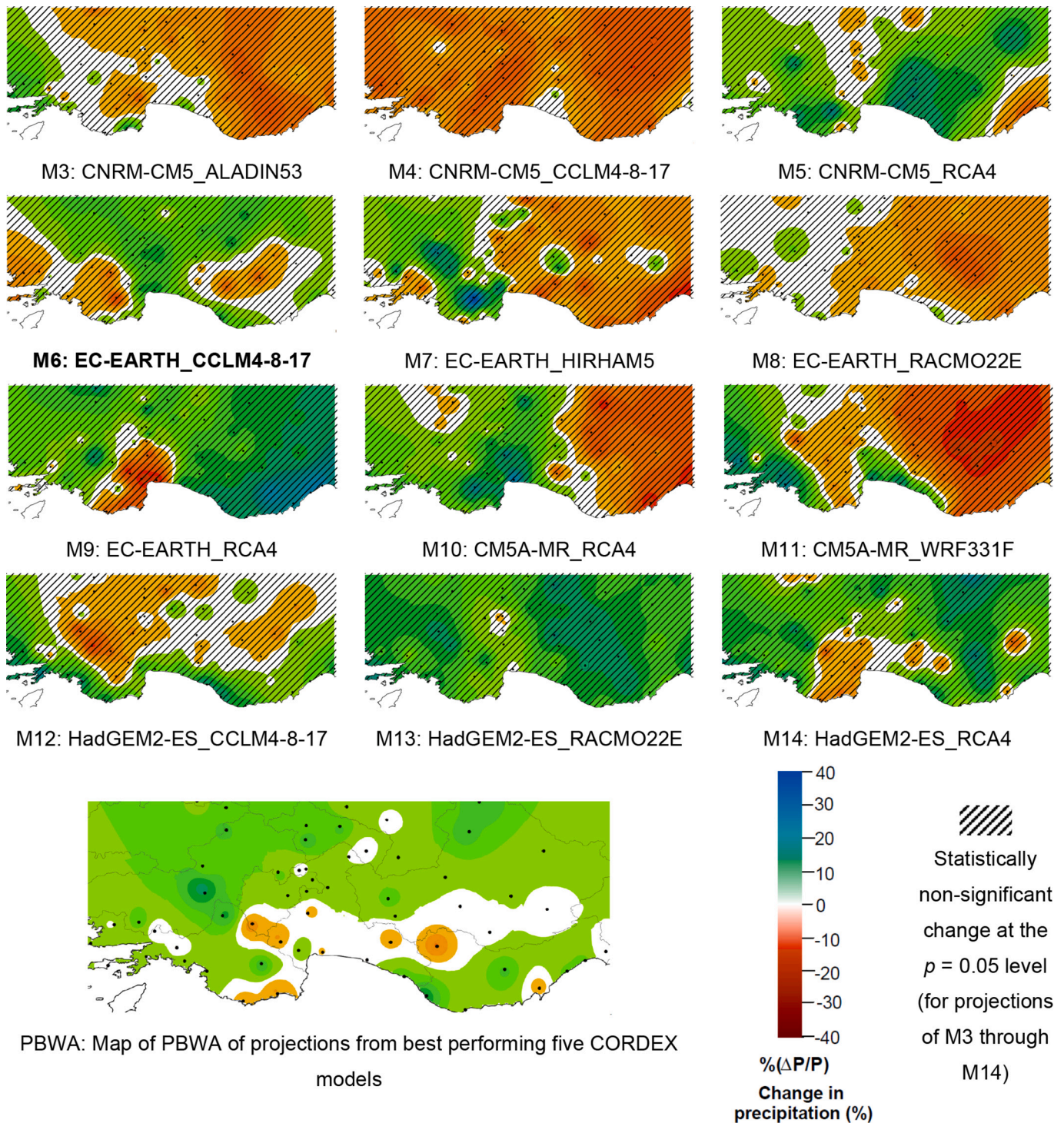


Fig. 6. Climate model projections for percent change in precipitation in short-term future for the RCP8.5 scenario.

short-term future under the RCP4.5 scenario for at least half of the stations in the region. Furthermore, for the SA, the areal average values (mean of 59 stations) calculated for these seven models indicate a decrease in the precipitation. On the other hand, except for M8, CORDEX RCMs project statistically significant change for less than 10% of the stations in SA. M8 projects significant change in precipitation for the coastal stations at the west of SA. M6 (EC-EARTH_CCLM4-8-17) that is defined to have relative best skill in replication of spatial variability of climatology in SA for present conditions, projects a mean increase of 0.7% in precipitation for the short-term under RCP4.5 scenario. The

annual mean precipitation climatology projected by M6 is either at the same level or slightly higher (up to 17%) than the climatology of the reference period for around 60% of the MSs across the SA under the RCP4.5 scenario. The increase in precipitation climatology is calculated mostly for the northern parts of the study region. According to the M6 results, the remaining 40% of MSs with a negative anomaly of precipitation climatology are mostly located at the southern coast of the Mediterranean. However, *t*-test, on M6's projections, indicates statistically significant change ($p < 0.05$) only for two coastal stations in Eastern Mediterranean Basin.

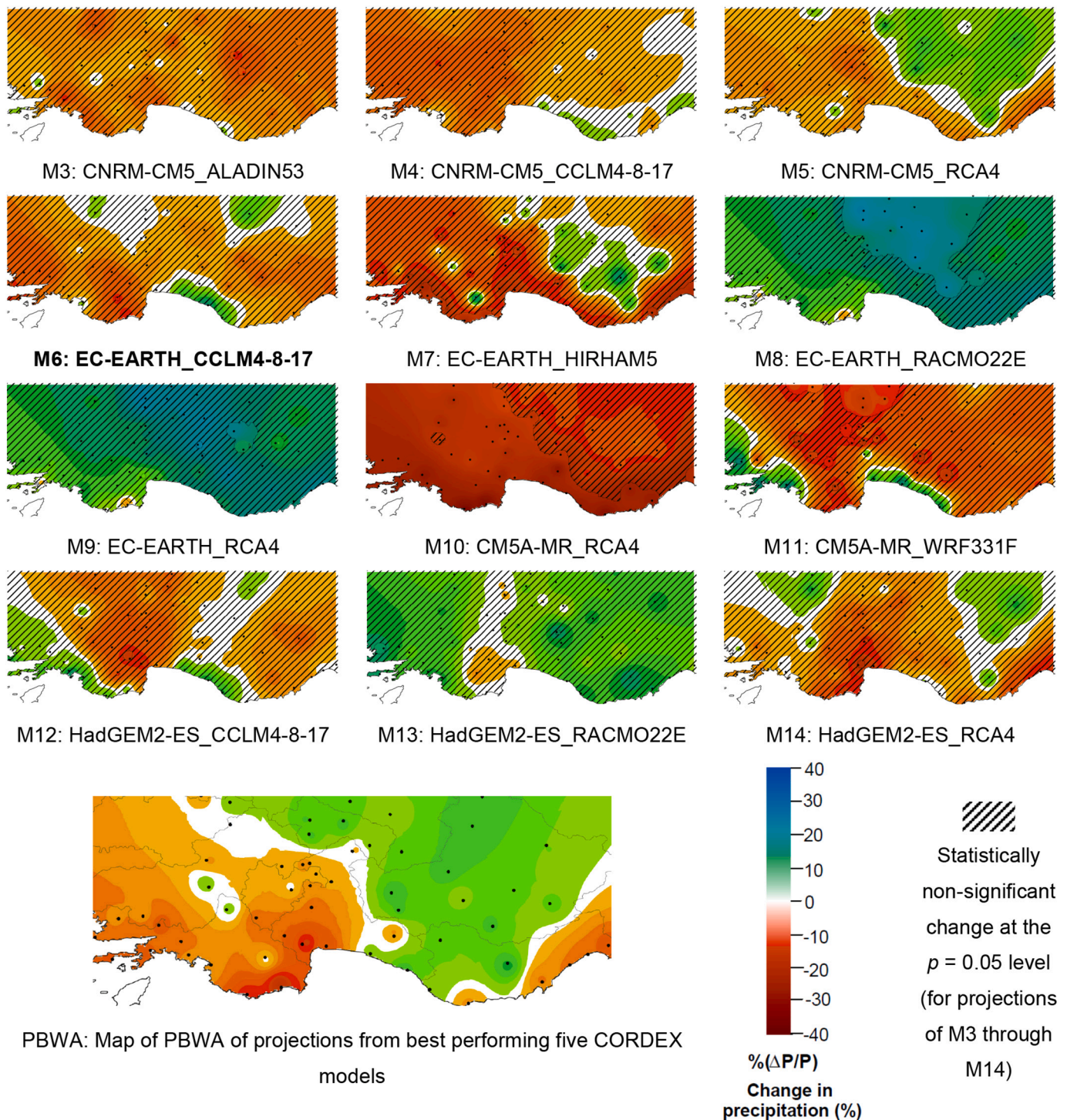


Fig. 7. Climate model projections for percent change in precipitation in medium-term future for the RCP4.5 scenario.

In the short-term future for the RCP8.5 scenario, the maximum range of the ensemble including the entire range of projections all 59 MSs is between -16% and 37% (Fig. 6). Additionally, the means of 12 models at each MS in the SA for the change in precipitation are within the range of -9% to 4.5% for the RCP4.5 and -2% to 6% for RCP8.5 again showing the intra-regional variability. For RCP8.5 scenario, similar to RCP4.5, changes in precipitation is smoother in the PBWA map of Fig. 6, however for this scenario, increase in precipitation is predicted even at some coastal areas. Observing the individual model projections, it is seen that the precipitation climatology calculated for five of the models (M8, M3, M4, M7, M11) show negative anomaly for the majority of the

stations, while M6 projects a decrease in the precipitation mostly for the MSs at the southern coast of the Mediterranean. However, according to M6 the potential decrease in annual precipitation is projected to be less than or equal to 10% (Fig. 6). Furthermore, projections of all CORDEX models including M6 agree on the change in precipitation classified as statistically insignificant in general of the SA.

Figs. 7 and 8 show the medium-term future projections on change in annual precipitation by 12 CORDEX models for RCP4.5 and RCP8.5, respectively. Accordingly, under RCP4.5 most of the models and under RCP8.5 all models except for one (M5) project a decrease in annual precipitation climatology at the majority of MSs. The PBWA map for

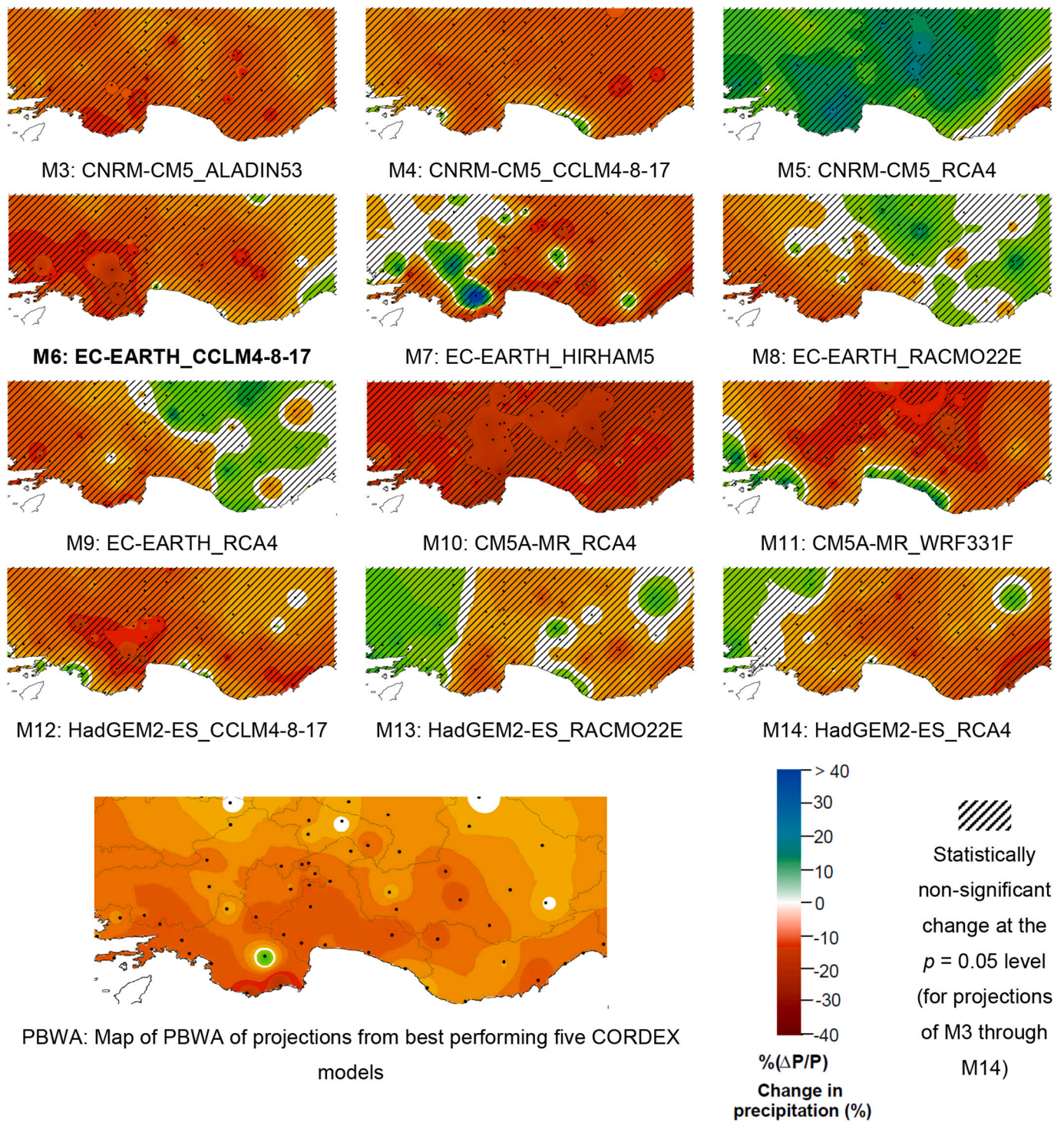


Fig. 8. Climate model projections for percent change in precipitation in medium-term future for the RCP8.5 scenario.

RCP4.5 scenario shows a decrease in the western part of the SA and in a relatively regional section in southeastern coast around Mersin station, while the eastern part, especially the inland will receive more precipitation compared to the reference period.

As it is seen in Fig. 8, M6 projects a decrease in precipitation at most of the MSs. M6 projects a maximum decrease in future precipitation of up to 20% at different MSs across the SA. M6 projects statistically significant change in precipitation for 16 of the MSs. On the other hand, the PBWA map for RCP8.5 scenario shows a decrease in precipitation throughout the whole SA.

Long-term future projections on the percent change in annual precipitation climatology at SA by 12 models are given in Figs. 9 and 10 for RCP4.5 and RCP8.5, respectively. As it is seen in Fig. 9, the analysis of long-term projections for the RCP4.5 scenario indicates a decrease in annual precipitation climatology at the majority of the MSs for most of the models. Additionally, 12-model means indicate a reduction in annual precipitation at all MSs in the SA. For the RCP4.5 scenario, M6 along with the other eight CORDEX RCMs (M5, M8, M9, M10, M11, M12, M13, M14) project further elevation in dryness in the region for the long-term compared to the medium-term future. Although the RCMs

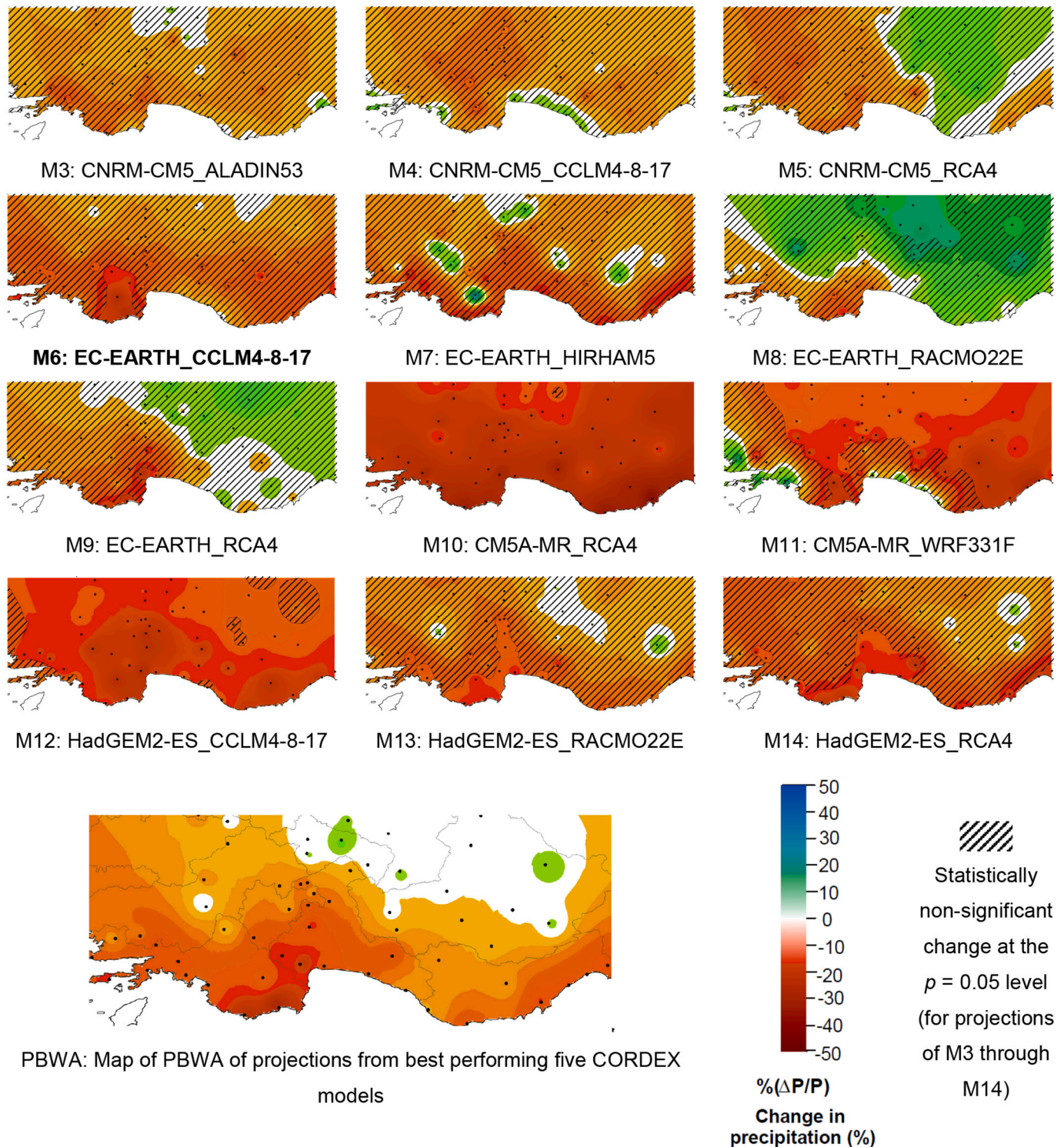


Fig. 9. Climate model projections for percent change in precipitation in long-term future for the RCP4.5 scenario.

using CNRM as the driving GCM (i.e., M3, M4, and M5) project statistically significant change in precipitation for only 10% or less of the MSs, projections by the climate models using other GCMs as the driving model show a statistically significant change for at least one-third of the MSs in SA, in general. Similar to the short-term for RCP4.5 scenario, the PBWA map of Fig. 9 projects a gradual decrease in the change of precipitation from inland towards the coast, reaching 26% decrease around Finike.

The projections for RCP8.5 by all 12 CORDEX RCMs agree on the

projection of a decrease in the precipitation climatology for 27% of the MSs in the region. Though the amount of the likely decrease in climatology at these 16 stations varies in the range of 0.4% to 50% depending on location and projection model. Furthermore, except for M3, all the CORDEX models project an increase in dryness in the long-term future in either entire or most of the SA compared to the medium-term future under the RCP8.5 conditions (Fig. 10). According to the projections by the majority of the models, the change in precipitation is statistically significant for more than 60% of the MSs in SA.

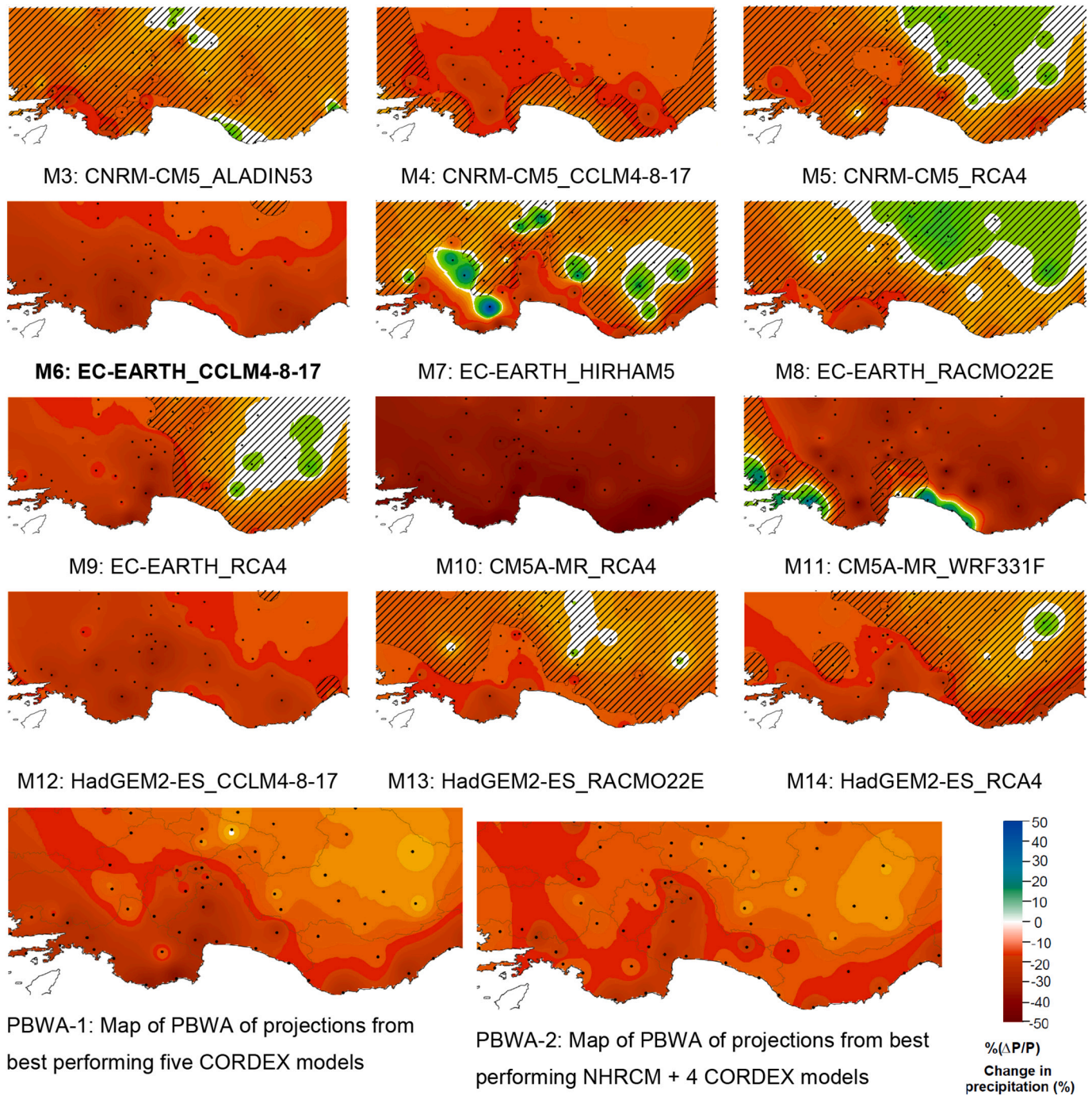


Fig. 10. Climate model projections for percent change in precipitation in long-term future for the RCP8.5 scenario.

Related to the climate change signal indicated by ensemble members it should be noted that for two CORDEX RCMs in the analysis, WRF331F, and HIRHAM5, the assumption on the GHG forcing differs from others. Such difference in the model setup is verified by Jerez et al. (2018) to create a difference from other RCMs in generated climate signal. For WRF331F and HIRHAM5 analyzed in the study the change in GHG concentrations is not included as an additional climate forcing in RCM setup but rather the impact of change in GHG concentrations is inherited from the driving GCM. Analyzing the potential change in precipitation projected by two RCMs against others in the ensemble indicates no

distinct difference from other RCMs for WRF331F projections regarding the change in impact between medium- to long-term future for RCP 4.5 and RCP8.5. On the other hand, for HIRHAM5, the difference in impact size between RCP4.5 and RCP8.5 scenarios for the medium-term future differs from other ensemble members. The distinction might be attributed to the difference in the model setup regarding GHG evolution.

The projection by M6 for the long-term future under the RCP8.5 scenario indicates a decrease in the annual precipitation climatology for all MSs ranging between 8 and 34%. The projection by M6 for precipitation decrease is statistically significant for almost all MSs. The areal

average for SA regarding the decrease in annual precipitation climatology is 19.5% according to M6. Similarly, PBWA-1 (obtained from M6, M7, M8, M9, M14) and PBWA-2 (obtained from NHRCM, M6, M7, M8, M14) generated for RCP8.5 scenario for long-term future agree in a decrease in precipitation for all MSs across SA (Fig. 10). On the other hand, combination of best performing five CORDEX models project higher decrease in precipitation in the long-term compared to the PWBA generated including NHRCM projections. But both PWBA maps show 20–35% or larger decrease in precipitation in the middle section of the SA, for example around Finike. For the coastal regions in SA, PBWA-1 projects a larger decrease relative to the PBWA-2. On the other hand, for the inland stations PBWA-2 projects a larger decrease relative to the PBWA-1.

As it is seen in Fig. 11, MRI-AGCM projects an increase in precipitation climatology at the majority of coastal MSs and a decrease of up to 70% for inland MSs giving an areal average of around 6% increase in the annual precipitation climatology for the SA in the long-term future. The MRI-AGCM projects statistically significant change in precipitation for the majority of the MSs in SA. Except for two stations in southwestern Turkey (Bodrum MS 17290 and Dalaman MS 17294), MRI's NHRCM projects a decrease of up to 32% in annual precipitation climatology at all MSs for the long-term future under the RCP8.5 scenario (Fig. 11). The potential increase in two stations (Bodrum and Dalaman) is projected less than or equal to 5%. Similar to the areal average of the CORDEX mean, the areal average for NHRCM estimates a 14% decrease in the annual precipitation climatology at the SA. According to NHRCM projection statistically significant change in precipitation is likely for over 40% of the MSs in SA.

The range of change in precipitation projected by 12 CORDEX models for RCP4.5 and RCP8.5 scenarios in short-, medium- and long-term future and by MRI models for the RCP8.5 scenario in long-term future at the SA are depicted in the box plots in Fig. 12. The calculated value of the projected percent change in precipitation by each climate model in the ensemble are referred to the Supplementary Material (Appendix C). Box plots show inter-model variability in the projected percent change in annual climatology within the SA.

Regarding the short-term impact on precipitation for the entire SA, the areal average for the CORDEX mean shows a -0.5% (SA median: 0.2%) change in precipitation for the RCP4.5 and a 1.3% (SA median: 0.9%) change for the RCP8.5 scenario (Fig. 12(a)). As it is seen in Fig. 12 (b) for the medium-term future, the mean change in annual precipitation projected by CORDEX RCMs for 59 individual MSs in the SA ranges between -10% and 3.5% in the SA (from hereafter will be referred to as MeanMR meaning the mean model range of 12 models for the potential change in precipitation) for RCP4.5. Considering RCP4.5 the maximum range of ensemble including the entire range of projections for all MSs (from hereafter will be referred to as MaxMR) is between -34% and 23% for RCP4.5. Under RCP8.5, 12-model ensemble indicates MeanMR

between 0.6 and -9.5% and MaxMR from -25% to 55% . Furthermore, the areal average calculated for the SA verify the projection of a decline in annual precipitation of 2.7% and 4.6% (SA median: -3% and -4.6% , See Fig. 12(b)) for RCP4.5 and RCP8.5 scenarios, respectively.

MeanMR of long-term projections is between -17% and -1.5% , while MaxMR is between -38.5% and 21.5% under the RCP4.5 scenario (Fig. 12(c)). For the RCP8.5 scenario, MeanMR and MaxMR are calculated as between -6 and -26% , and between -51.5% and 47% , respectively. The areal averages demonstrate a reduction in precipitation for both scenarios. The decline in annual precipitation is projected as 7% for RCP4.5 and 14% for RCP8.5 at the SA regarding the mean value of 59 stations which is very close to the median value (See Fig. 12 (c)).

Hence, a comparison of projections for RCP4.5 and RCP8.5 regarding the MeanMR and PBWA of climate model projections for short-, medium, and long-term shows that potential decrease in precipitation in the near term under the RCP8.5 scenario is not projected as prominent as it is projected for the RCP4.5 scenario. For the RCP 8.5 scenario, the onset of the decrease in precipitation is projected to be more likely and extensive in the medium- to long-term future. Although not at the statistically significant level most of the climate models project a relatively higher decrease in precipitation under the RCP 4.5 scenario in the short-term compared to RCP8.5. Therefore, the negative impact on the water cycle is expected to be much more prominent in the high emissions scenario with cumulated GHG concentrations by 2100.

The long-term future projections under the RCP8.5 scenario agree on an amplified water scarcity for many mid-latitude regions (IPCC, 2014). However, as highlighted in the Climate Change 2013 report of IPCC (IPCC, 2013), the radiative forcing impacts in the short-term future between different RCP scenarios are expected to be relatively small, but an increasing impact is expected by the end of the 21st century. The local elements such as aerosol emissions are estimated to be still the major control on the climate change impacts in the short-term. Moreover, the impact on the precipitation intensity is likely to be significantly affected by the atmospheric water vapor content (IPCC, 2013). The variability in the short-term projections on the impact on precipitation verified with the findings of this study is interpreted to be related to those above-mentioned factors.

Fig. 13 depicts the comparison of the projections on the percent change in the climatological mean of annual precipitation from all 14 climate models considering the areal averages for each basin located in the study area. As it is seen in Fig. 13 regarding the short-term impacts, the variability in the projections on the change in precipitation among different basins is particularly prominent not just for the quantity but also for the likely type of change (i.e., positive or negative). However, for medium- and long-term future projections areal averages indicate a potential decrease at all basins in the study area. Moreover, in the long-term future, except for MRI-AGCM, the models in the ensemble, in

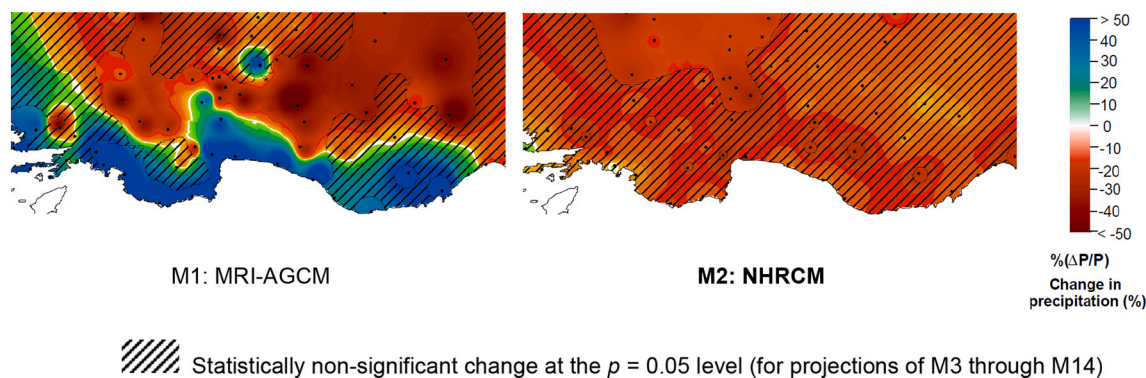


Fig. 11. Climate model projections for percent change in precipitation in long-term future for the RCP8.5 scenario for MRI climate models (the projection map of the best performing climate model M2: MRI-AGCM_NHRCM is written in bold).

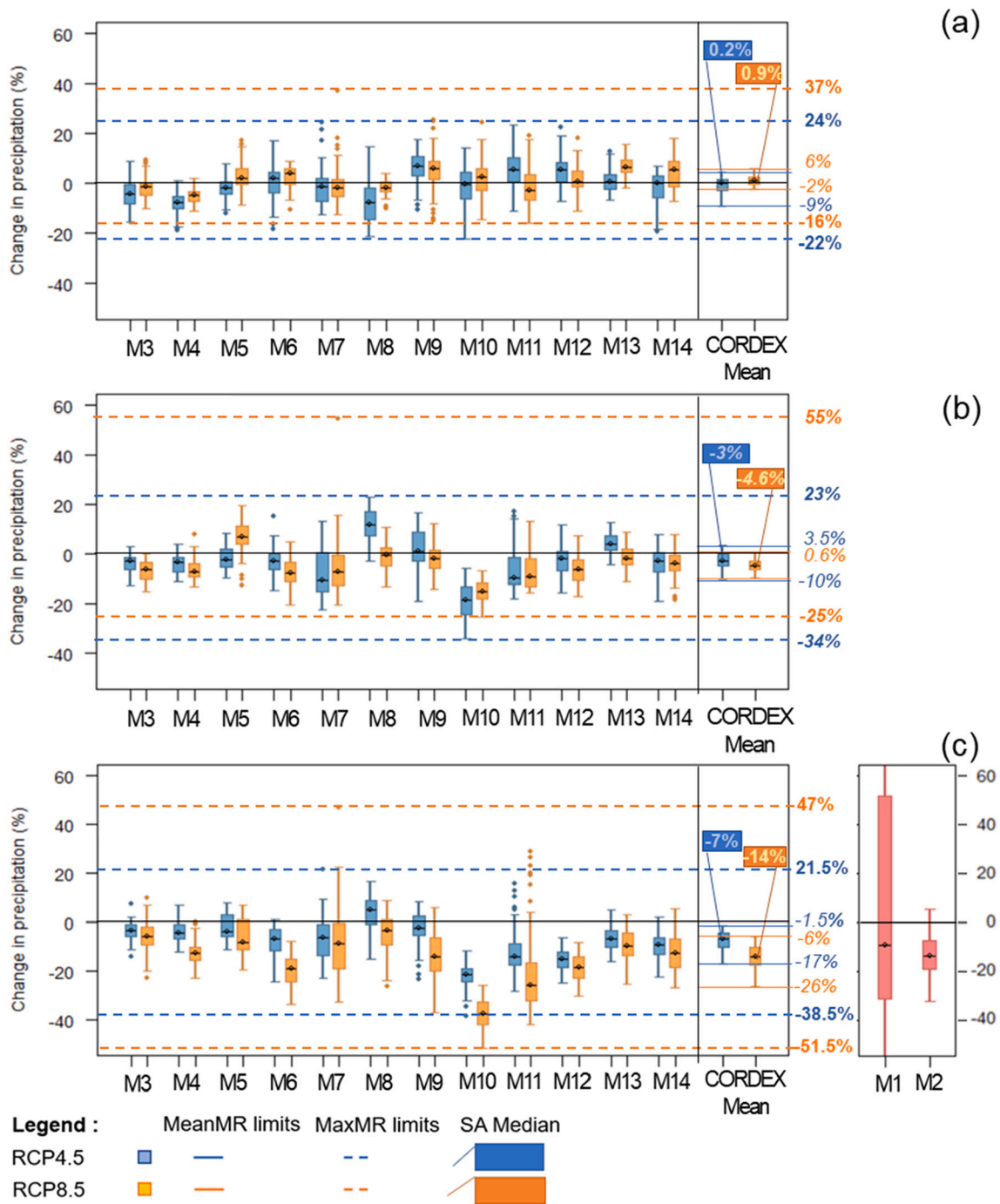


Fig. 12. Boxplot showing percent change in annual precipitation climatology projected by climate models for (a) short-, (b) medium-, (c) long-term future (Upper and lower whisker boundaries of the boxplot are the largest data within 1.5 IQR (interquartile range) above the third quartile and smallest data within 1.5 IQR below the first quartile of the data set, respectively).The box plots of MRI’s AGCM and NHRCM shown in (c) are only for the RCP8.5 scenario outputs. In (c) MRI’s AGCM and NHRCM are shown separately from the CORDEX RCMs because of the difference in the timeframe of projections, max model range for MRI extends beyond the limit of y axis in the plot, it ranges between -69% to 120%).

general, agree on a mean decrease in precipitation at all basins. On the other hand, MRI-AGCM projects an increase in annual mean precipitation for the basins along the Mediterranean coast.

LOESS curves of projections by 12 CORDEX RCMs for RCP4.5 and 8.5 scenarios are provided in Supplementary Material (Appendix B). The LOESS curves of the total annual precipitation time series for basins in the SA are generated by the use of R-Code (Wickham, 2016). The LOESS regression in R-code is applied using the smoothing parameter (α) value of 0.3 and the degree of the local fitted polynomial of 2. The examination

of the interannual changes in precipitation projected for the future between the period 2020–2100 after smoothing with LOESS curve verifies the projected precipitation changes and relevant spatial distribution of potential impact illustrated in Figs. 5 through 10. Under the RCP4.5 scenario, the projections by 12 CORDEX RCMs demonstrating a statistically insignificant change in precipitation for short- and medium-term future at all basins in the SA are generally supported by the smooth LOESS curves obtained by local regression (Relevant figures are presented in Supplementary Material -Appendix B). In the long-term,

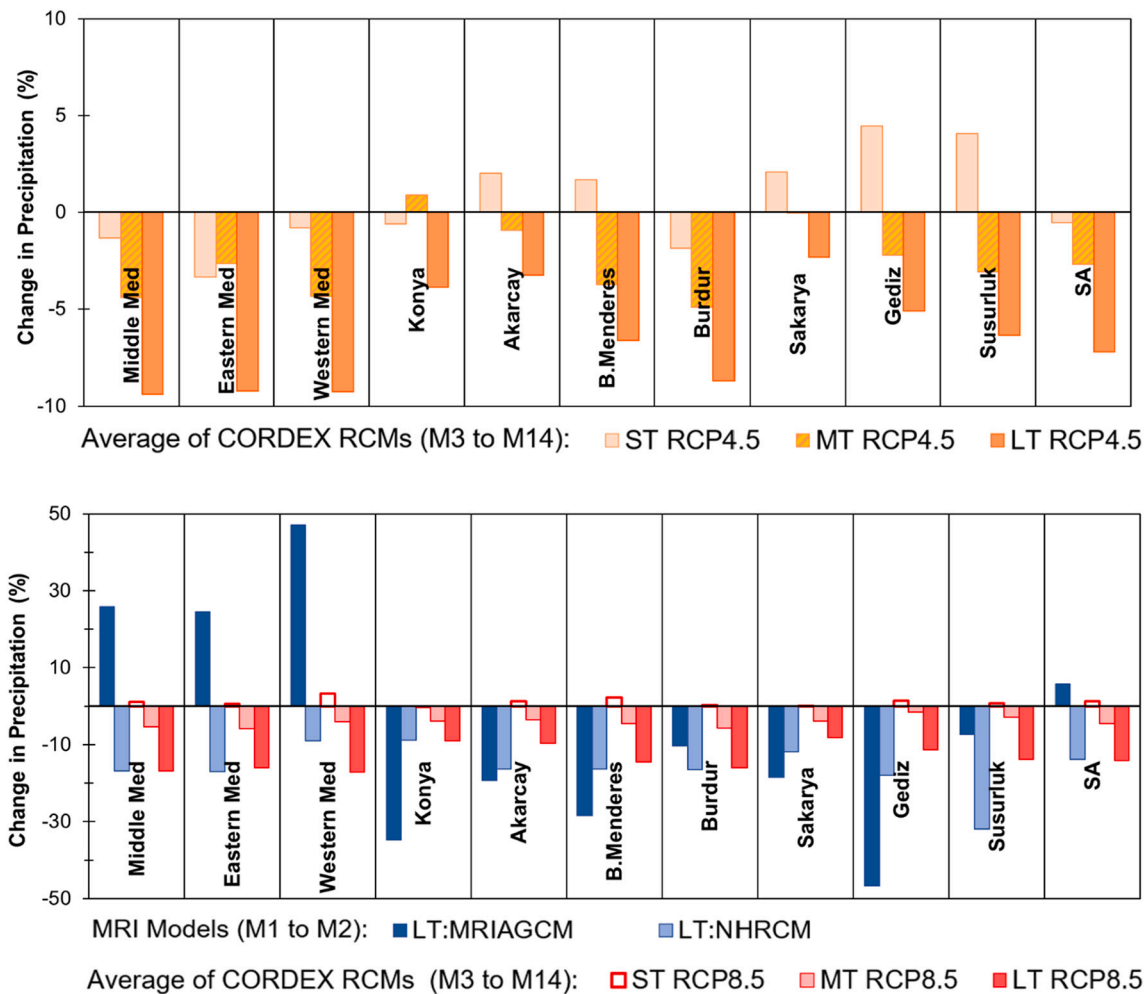


Fig. 13. Comparison of the areal means of short-, medium- and long-term projections on change in precipitation at basins in the SA for RCP4.5 (top graph) and RCP8.5 (bottom graph).

however, the decrease in precipitation and a distinct downward trend creating a gradual decrease in precipitation by the end of the 21st century is seen particularly for projections of RCMs nested in CM5A-MR and HadGEM2-ES. On the other hand, regarding the projections by RCMs nested in EC-EARTH and CNRM-CM5, despite the decadal/bi-decadal variability in precipitation, the general trend is projected to remain relatively stationary.

Furthermore, RCP8.5 scenario projections of RCMs nested in CM5A-MR, and HadGEM2-ES show an evident downward trend in total annual precipitation starting from the first half of the 21st century. Except for M3 (CNRM-CM5_ALADIN53), most of the RCMs agree on a distinct decrease in precipitation, despite the decadal/bi-decadal fluctuations, particularly for Middle and Western Mediterranean basins.

5. Conclusion

The objective of this study is to assess potential future changes in the precipitation climatology in the study area that covers most of the west and southwestern Turkey, partially or fully including 10 of the major watersheds in Turkey. The area is in the eastern part of the greater Mediterranean Basin and is designated among the hotspots concerning climate change impacts. Moreover, location, complex morphology, and interconnecting factors that affect the local climate processes at the study area create challenges in climate projections for the region. At the first stage of the assessment, a 14-member set of high-resolution climate models, that constitutes 12 CORDEX RCMs and two high-resolution

climate models of the Japanese MRI, is analyzed to evaluate their skills to represent the spatial variability of precipitation at the study area with respect to ground-based meteorological stations. The analysis indicated relatively weak performance skills of GCM-RCM combinations of CNRM-CM5/ALADIN53 (M3), CNRM-CM5/CCLM4-8-17 (M4), and CM5A-MR/WRF331F (M11) for the study area regarding the spatial variability of precipitation climatology. On the other hand, MRI's NHRCM with MRI-AGCM boundary conditions (M2), and two CORDEX models, EC-EARTH/CCLM4-8-17 (M6), and EC-EARTH/RACMO22E (M8) are identified as having the best performance skills in the spatial representation of climatology at the region. The ranking based on the API values also indicates that all RCMs (CCLM4-8-17, HIRHAM5, RCA4, and RACMO22E) nested in the EC-EARTH GCM have relatively higher projection skills. However, RCMs nested in CNRM-CM5, and CM5A-MR perform relatively poorly for the study area. Furthermore, the performance of the climate models using HadGEM2-ES as the driving GCM depends on the regional climate model nested on it. The subsequent analysis of the potential changes in precipitation under climate change impacts concerning short-term (2020–2030), medium-term (2031–2050), and long-term (2051–2100) future verified significant inter-model and intra-regional variability not only for the quantity but also for the direction of the change in precipitation climatology.

Under the RCP4.5 scenario, the areal average of potential change in annual precipitation calculated for the mean of 12 CORDEX RCMs indicates a gradual decrease by the end of the century. The projected change in the mean precipitation is -0.5% for short, -2.7% for medium,

and – 7% for the long-term future. For the RCP8.5 scenario, the areal mean demonstrates a slight increase in the near term followed by a decrease by the end of the century. Under RCP8.5 conditions the projection for change in annual precipitation is 1.3%, –4.6%, and –14% for short-, medium-, and long-term future, respectively. According to these findings, 12-member ensemble projects a relatively reprieved decrease in the annual precipitation under the RCP8.5 scenario until the mid-century. Nevertheless, for the second half of the century, a larger reduction is projected for the RCP8.5 than the RCP 4.5 scenario to the extend at which is projected to ultimately create a larger decrease in mean precipitation by the end of the century compared to the RCP4.5 scenario.

Analysis of the projections by high-resolution climate model of MRI, NHRCM for RCP8.5 scenario, shows intra-regional variability in change in precipitation within the range of –32% to 5%. However, the majority of MSS in the SA are projected to experience a decline in mean precipitation in the long-term. Similar to the CORDEX ensemble mean, based on the spatial mean, the potential change in precipitation in SA is projected as –14% by NHRCM.

Consequently;

- The analysis indicates variability in the simulation skills of 14 climate models for the study area regarding the spatial variability of precipitation climatology.
- Projections indicate intra-regional variability in the climate change impacts on precipitation climatology.
- The multi-model ensemble analysis of the projections on precipitation for the long-term future under both RCP4.5 and RCP8.5 scenarios indicates a general decrease in the precipitation at all basins in the study area.
- The short-term impacts are projected to be relatively small and not as significant as the impacts that are potentially expected in longer terms. Nevertheless, medium-, and long-term impacts of climate change are expected to be more prominent and create a relatively larger reduction in mean precipitation.
- Hence, future adaptation strategies are necessary to be designed in a tiered structure so as to minimize the risks not only for the near-term impacts but also for likely risks that may arise in the long-term future.

Declaration of Competing Interest

The authors declare that they have no known competing financial interests or personal relationships that could have appeared to influence the work reported in this paper.

Acknowledgements

The authors thank the Scientific and Technological Research Council of Turkey, TÜBİTAK, and Japan Society for the Promotion of Science, JSPS [Grant Number JPJSBP12019940], for supporting this bilateral research collaborations. The work for the generation of NHRCM simulations was supported by the Integrated Research Program for Advancing Climate Models (TOUGOU) [Grant Number JPMXD0717935561] from the Ministry of Education, Culture, Sports, Science, and Technology (MEXT) of Japan. The research leading to these results is funded by the Scientific and Technological Research Council of Turkey (TÜBİTAK) the project “Assessment of Climate Change Impacts on Streamflow and Hydropower in Antalya, Turkey” [Grant Number 118Y365].

Appendix A. Supplementary data

Supplementary data to this article can be found online at <https://doi.org/10.1016/j.atmosres.2022.106140>.

References

- Aziz, R., Yucel, I., 2021. Assessing nonstationarity impacts for historical and projected extreme precipitation in Turkey. *Theor. Appl. Climatol.* 143, 1213–1226. <https://doi.org/10.1007/s00704-020-03503-x>.
- Boulanger, J.P., Martinez, F., Segura, E.C., 2006. Projection of future climate change conditions using IPCC simulations, neural networks and Bayesian statistics. Part 1: temperature mean state and seasonal cycle in South America. *Clim. Dyn.* 27 (2–3), 233–259.
- Boulanger, J.P., Martinez, F., Segura, E.C., 2007. Projection of future climate change conditions using IPCC simulations, neural networks and Bayesian statistics. Part 2: precipitation mean state and seasonal cycle in South America. *Clim. Dyn.* 28 (2–3), 255–271.
- Bucak, T., Trolle, D., Tavşanoğlu, Ü.N., Çakıroğlu, A.İ., Özen, A., Jeppesen, E., Beklioglu, M., 2018. Modeling the effects of climatic and land use changes on phytoplankton and water quality of the largest Turkish freshwater lake: Lake Beyşehir. *Sci. Total Environ.* 621, 802–816. <https://doi.org/10.1016/j.scitotenv.2017.11.258>.
- Cakir, S., Kadioglu, M., Cubukcu, N., 2013. Multischeme ensemble forecasting of surface temperature using neural network over Turkey. *Theor. Appl. Climatol.* 111 (3–4), 703–711.
- Christensen, J.H., Kjellström, E., Giorgi, F., Lenderink, G., Rummukainen, M., 2010. Weight assignment in regional climate models. *Clim. Res.* 44 (2–3), 179–194.
- Cleveland, W.S., 1979. Robust locally weighted regression and smoothing scatterplots. *J. Am. Stat. Assoc.* 74 (368), 829–836.
- Cleveland, W.S., Devlin, S.J., 1988. Locally weighted regression: an approach to regression analysis by local fitting. *J. Am. Stat. Assoc.* 83 (403), 596–610.
- Cowling, R.M., Rundel, P.W., Lamont, B.B., Arroyo, M.K., Arianoutsou, M., 1996. Plant diversity in mediterranean-climate regions. *Trends Ecol. Evol.* 11 (9), 362–366. [https://doi.org/10.1016/0169-5347\(96\)10044-6](https://doi.org/10.1016/0169-5347(96)10044-6).
- Deidda, R., Marrocu, M., Caroletti, G., Pusceddu, G., Langousis, G., Langousis, A., Lucarini, V., Puliga, M., Speranza, A., 2013. Regional climate models' performance in representing precipitation and temperature over selected Mediterranean areas. *Hydrol. Earth Syst. Sci.* 17, 5041–5059. <https://doi.org/10.5194/hess-17-5041-2013>.
- Della-Marta, P.M., Wanner, H., 2006. A method of homogenizing the extremes and mean of daily temperature measurements. *J. Clim.* 19 (17), 4179–4197.
- Demircan, M., Gürkan, H., Eskioglu, O., Arabaci, H., Coşkun, M., 2017. Climate change projections for Turkey: three models and two scenarios. *Turkish J. Water Sci. Manag.* 1 (1), 22–43.
- Dino, I.G., Akgül, C.M., 2019. Impact of climate change on the existing residential building stock in Turkey: an analysis on energy use, greenhouse gas emissions and occupant comfort. *Renew. Energy* 141, 828–846. <https://doi.org/10.1016/j.renene.2019.03.150>.
- EURO-CORDEX, 2021. EURO-CORDEX Errata Page, Errata Table. <https://www.euro-cordex.net/078730/index.php.en> (accessed 21 December 2021).
- Evans, J.P., 2009. 21st century climate change in the Middle East. *Clim. Chang.* 92 (3–4), 417–432.
- Fujihara, Y., Tanaka, K., Watanabe, T., Nagano, T., Kojiri, T., 2008. Assessing the impacts of climate change on the water resources of the Seyhan River Basin in Turkey: use of dynamically downscaled data for hydrologic simulations. *J. Hydrol.* 353, 33–48.
- Giorgi, F., 2006. Climate change hot-spots. *Geophys. Res. Lett.* 33, 1–4. <https://doi.org/10.1029/2006GL025734>.
- Giorgi, F., Lionello, P., 2008. Climate change projections for the Mediterranean region. *Glob. Planet. Chang.* 63, 90–104. <https://doi.org/10.1016/j.gloplacha.2007.09.005>.
- Gorguner, M., Kavvas, M.L., Ishida, K., 2019. Assessing the impacts of future climate change on the hydroclimatology of the Gediz Basin in Turkey by using dynamically downscaled CMIP5 projections. *Sci. Total Environ.* 648, 481–499. <https://doi.org/10.1016/j.scitotenv.2018.08.167>.
- Guo, J., Huang, G., Wang, X., Li, Y., Yang, L., 2018. Future changes in precipitation extremes over China projected by a regional climate model ensemble. *Atmos. Environ.* 188, 142–156.
- Haarsma, R.J., Roberts, M.J., Vidale, P.L., Senior, C.A., Bellucci, A., Bao, Q., Chang, P., Corti, S., Fućkar, N.S., Guemas, V., von Hardenberg, J., Hazeleger, W., Kodama, C., Koenig, T., Leung, L.R., Lu, J., Luo, J.-J., Mao, J., Mizielinski, M.S., Mizuta, R., Nobre, P., Satoh, M., Scoccimarro, E., Semmler, T., Small, J., von Storch, J.-S., 2016. High resolution model intercomparison project (HighResMIP v1.0) for CMIP6. *Geosci. Model Dev.* 9, 4185–4208. <https://doi.org/10.5194/gmd-9-4185-2016>.
- IPCC, 2013. In: Stocker, T.F., Qin, D., Plattner, G.-K., Tignor, M., Allen, S.K., Boschung, J., Nauels, A., Xia, Y., Bex, V., Midgley, P.M. (Eds.), *Climate Change 2013: The Physical Science Basis. Contribution of Working Group I to the Fifth Assessment Report of the Intergovernmental Panel on Climate Change*. Cambridge University Press, Cambridge, United Kingdom and New York, NY, USA (1535 pp.).
- IPCC, 2014. In: The Core Writing Team, Pachauri, R.K., Meyer, L. (Eds.), *Climate Change 2014 Synthesis Report*. IPCC, Geneva, Switzerland.
- IPCC, 2018. In: Masson-Delmotte, V., Zhai, P., Pörtner, H.-O., Roberts, D., Skea, J., Shukla, P.R., Waterfield, T. (Eds.), *An IPCC Special Report on the Impacts of Global Warming of 1.5°C Above Pre-industrial Levels and Related Global Greenhouse Gas Emission Pathways, in the Context of Strengthening the Global Response to the Threat of Climate Change, Sustainable Development, and Efforts to Eradicate Poverty*.
- Ito, R., Shioyama, H., Nakaegawa, T., Takayabu, I., 2020. Uncertainties in climate change projections covered by the ISIMIP and CORDEX model subsets from CMIP5. *Geosci. Model Dev.* 13 (3), 859–872.
- Jacoby, W.G., 2000. Loess: a nonparametric, graphical tool for depicting relationships between variables. *Elect. Stud.* 19 (4), 577–613.

- Jerez, S., López-Romero, J.M., Turco, M., Jiménez-Guerrero, P., Vautard, R., Montávez, J.P., 2018. Impact of evolving greenhouse gas forcing on the warming signal in regional climate model experiments. *Nat. Commun.* 9 (1), 1–7.
- Kentel, E., Akgun, O.B., Mesta, B., 2019. User-friendly R-code for Data Extraction from CMIP6 outputs. In: *AGU Fall Meeting Abstracts*, 2019 pp. PA33C-1098.
- Kitoh, A., Ose, T., Kurihara, K., Kusunoki, S., Sugi, M., KAKUSHIN Team-3 Modeling Group, 2009. Projection of changes in future weather extremes using super-high-resolution global and regional atmospheric models in the KAKUSHIN Program: results of preliminary experiments. *Hydrol. Res. Lett.* 3, 49–53. <https://doi.org/10.3178/HRL.3.49>.
- Kitoh, A., Ose, T., Takayabu, I., 2016. Dynamical downscaling for climate projection with high-resolution MRI AGCM - RCM. *J. Meteorol. Soc. Jpn.* 94A, 1–16. <https://doi.org/10.2151/jmsj.2015-022>.
- Krichak, S.O., Kishcha, P., Alpert, P., 2002. Decadal trends of main Eurasian oscillations and the Eastern Mediterranean precipitation. *Theor. Appl. Climatol.* 72 (3), 209–220.
- Krishnamurti, T.N., Kumar, V., Simon, A., Bhardwaj, A., Ghosh, T., Ross, R., 2016. A review of multimodel superensemble forecasting for weather, seasonal climate, and hurricanes. *Rev. Geophys.* 54 (2), 336–377.
- Kusunoki, S., 2018. Is the global atmospheric model MRI-AGCM3.2 better than the CMIP5 atmospheric models in simulating precipitation over East Asia? *Clim. Dyn.* 51, 4489–4510. <https://doi.org/10.1007/s00382-016-3335-9>.
- Kusunoki, S., Nakaegawa, T., Pinzón, R., Sanchez-Galan, J.E., Fábrega, J.R., 2019. Future precipitation changes over Panama projected with the atmospheric global model MRI-AGCM3. 2. *Clim. Dyn.* 53 (7), 5019–5034.
- Lionello, P., Malanotte-Rizzoli, P., Boscolo, R., Alpert, P., Artale, V., Li, L., Luterbacher, J., May, W., Trigo, R., Tsimplis, M., Ulbrich, U., Xoplaki, E., 2006. In: Lionello, P., Malanotte-Rizzoli, P., Boscolo, R. (Eds.), *The Mediterranean Climate: An Overview of the Main Characteristics and Issues*, 4. Mediterranean Climate Variability, p. 438.
- McSweeney, C.F., Jones, R.G., Lee, R.W., Rowell, D.P., 2015. Selecting CMIP5 GCMs for downscaling over multiple regions. *Clim. Dyn.* 44 (11), 3237–3260.
- Mehr, A.D., Kahya, E., 2017. Climate change impacts on catchment-scale extreme rainfall variability: case study of Rize Province, Turkey. *J. Hydrol. Eng.* 22 (3), 1–11. [https://doi.org/10.1061/\(ASCE\)HE.1943-5584.0001477](https://doi.org/10.1061/(ASCE)HE.1943-5584.0001477).
- Mesta, B., Kentel, E., 2021. Superensembles of raw and bias-adjusted regional climate models for Mediterranean region, Turkey. *Int. J. Climatol.* 1–20. <https://doi.org/10.1002/joc.7381>. In press.
- Mizuta, R., Oouchi, K., Yoshimura, H., Noda, A., Katayama, K., Yukimoto, S., Hosaka, M., Kusunoki, S., Kawai, H., Nakagawa, M., 2006. 20-km-mesh global climate simulations using JMA-GSM model - mean climate states. *J. Meteorol. Soc. Jpn.* 84 (1), 165–185.
- Mizuta, R., Adachi, Y., Yukimoto, S., Kusunoki, S., 2008. Estimation of future distribution of sea surface temperature and sea ice using CMIP3 multi-model ensemble mean. *Tech. Rep. Meteor. Res. Inst.* 56 (28 pp.).
- Mizuta, R., Arakawa, O., Ose, T., Kusunoki, S., Endo, H., Kitoh, A., 2014. Classification of CMIP5 future climate responses by the tropical sea surface temperature changes. *SOLA* 10, 167–171. <https://doi.org/10.2151/sola.2014-035>.
- Nakaegawa, T., Kitoh, A., Kusunoki, S., Murakami, H., Arakawa, O., 2014. Hydroclimate change over Central America and the Caribbean in a global warming climate projected with 20-km and 60-km mesh MRI atmospheric general circulation models. *Pap. Meteorol. Geophys.* 65, 15.
- Nakaegawa, T., Hibino, K., Takayabu, I., 2017. Identifying climate analogues for cities in Australia by a non-parametric approach using multi-ensemble, high-horizonal-resolution future climate projections by an atmospheric general circulation model, MRI-AGCM3. 2H. *Hydrol. Res. Lett.* 11 (1), 72–78.
- Özdoğan, M., 2011. Modeling the impacts of climate change on wheat yields in Northwestern Turkey. *Agric. Ecosyst. Environ.* 141, 1–12. <https://doi.org/10.1016/j.agee.2011.02.001>.
- Öztürk, T., Ceber, Z.P., Türkeş, M., Kurnaz, M.L., 2015. Projections of climate change in the Mediterranean Basin by using downscaled global climate model outputs. *Int. J. Climatol.* 35, 4276–4292. <https://doi.org/10.1002/joc.4285>.
- Pinzón, R.E., Hibino, K., Takayabu, I., Nakaegawa, T., 2017. Virtually experiencing future climate changes in Central America with MRI-AGCM: climate analogues study. *Hydrol. Res. Lett.* 11 (2), 106–113. <https://doi.org/10.3178/hrl.11.106>.
- Saito, K., Fujita, T., Yamada, Y., Ishida, J.-I., Kumagai, Y., Aranami, K., Shiro, O., Nagasawa, R., Kumagai, S., Muroi, C., Kato, T., Eito, H., Yamazaki, Y., 2006. The operational JMA nonhydrostatic mesoscale model. *Mon. Weather Rev.* 134, 1266–1298.
- Sasaki, H., Kurihara, K., 2008. Relationship between precipitation and elevation in the present climate reproduced by the non-hydrostatic regional climate model. *SOLA* 4, 109–112.
- Sasaki, H., Kurihara, K., Takayabu, I., Uchiyama, T., 2008. Preliminary experiments of reproducing the present climate using the non-hydrostatic regional climate model. *SOLA* 4, 025–028. <https://doi.org/10.2151/sola.2008-007>.
- Sasaki, H., Murata, A., Hanafusa, M., Oh'izumi, M., Kurihara, K., 2011. Reproducibility of present climate in a non-hydrostatic regional climate model nested within an atmosphere general circulation model. *SOLA* 7, 173–176.
- Sasaki, H., Murata, A., Hanafusa, M., Oh'izumi, M., Kurihara, K., 2012. Projection of future climate change in a non-hydrostatic regional climate model nested within an atmospheric general circulation model. *SOLA* 8, 53–56.
- Sasaki, H., Kurihara, K., Murata, A., Hanafusa, M., Oh'izumi, M., 2013. Future changes of snow depth in a non-hydrostatic regional climate model with bias correction. *SOLA* 9, 5–8.
- Sen, B., Topcu, S., Türkeş, M., Sen, B., Warner, J.F., 2012. Projecting climate change, drought conditions and crop productivity in Turkey. *Clim. Res.* 52, 175–191. <https://doi.org/10.3354/cr01074>.
- Spinoni, J., Barbosa, P., Buchignani, E., Cassano, J., Cavazos, T., Christensen, J.H., Christensen, O.B., Coppola, E., Evans, J., Geyer, B., Giorgi, F., Hadjinicolaou, P., Jacob, D., Katzfey, J., Koenigk, T., Laprise, R., Lennard, C.J., Kurnaz, M.L., Li, D., Llopart, M., McCormick, N., Naumann, G., Nikulin, G., Ozturk, T., Panitz, H.J., Porfiro da Rocha, R., Rockel, B., Solman, S.A., Syktus, J., Tangang, F., Teichmann, C., Vautard, R., Vogt, J., Winger, K., Zittis, G., Dosio, A., 2020. Future global meteorological drought hot spots: a study based on CORDEX data. *J. Clim.* 33, 3635–3661. <https://doi.org/10.1175/JCLI-D-19-0084.1>.
- Stefanova, L., Krishnamurti, T.N., 2002. Interpretation of seasonal climate forecast using Brier skill score, the Florida State University superensemble, and the AMIP-I dataset. *J. Clim.* 15 (5), 537–544.
- Steinacker, R., 2021. How to correctly apply Gaussian statistics in a non-stationary climate? *Theor. Appl. Climatol.* 144 (3), 1363–1374.
- Sunyer Pinya, M.A., Hundecha, Y., Lawrence, D., Madsen, H., Willems, P., Martinkova, M., Vormoor, K., Bürger, G., Hanel, M., Kriaciuniene, J., Loukas, A., Osuch, M., Yücel, I., 2015. Inter-comparison of statistical downscaling methods for projection of extreme precipitation in Europe. *Hydrol. Earth Syst. Sci.* 19 (4), 1827–1847. <https://doi.org/10.5194/hess-19-1827-2015>.
- Tebaldi, C., Knutti, R., 2007. The use of the multi-model ensemble in probabilistic climate projections. *Philos. Trans. R. Soc. A Math. Phys. Eng. Sci.* 365 (1857), 2053–2075.
- Toreti, A., Kuglitsch, F.G., Xoplaki, E., Luterbacher, J., Wanner, H., 2010. A novel method for the homogenization of daily temperature series and its relevance for climate change analysis. *J. Clim.* 23 (19), 5325–5331.
- Varghese, S.J., Surendran, S., Rajendran, K., Kitoh, A., 2020. Future projections of Indian Summer Monsoon under multiple RCPs using a high resolution global climate model multiforcing ensemble simulations. *Clim. Dyn.* 54, 1315–1328. <https://doi.org/10.1007/s00382-019-05059-7>.
- Wang, X., Huang, G., Lin, Q., Liu, J., 2014. High-resolution probabilistic projections of temperature changes over Ontario, Canada. *J. Clim.* 27 (14), 5259–5284.
- Wang, X., Huang, G., Baetz, B.W., 2016. Dynamically-downscaled probabilistic projections of precipitation changes: a Canadian case study. *Environ. Res.* 148, 86–101.
- Wickham, H., 2016. *ggplot2: Elegant Graphics for Data Analysis*. Springer-Verlag, New York (ISBN 978-3-319-24277-4, <https://ggplot2.tidyverse.org>).
- Yilmaz, A.G., 2015. The effects of climate change on historical and future extreme rainfall in Antalya, Turkey. *Hydrol. Sci. J.* 60 (12), 2148–2162. <https://doi.org/10.1080/02626667.2014.945455>.
- Yukimoto, S., Adachi, Y., Hosaka, M., Sakami, T., Yoshimura, H., Hirabara, M., Kitoh, A., 2012. A new global climate model of the Meteorological Research Institute: MRI-CGCM3—model description and basic performance. *J. Meteorol. Soc. Jpn. Ser. II* 90, 23–64.

C. PAPER 3: EFFECT OF CLIMATE CHANGE ON SURFACE AIR TEMPERATURE AT EASTERN MEDITERRANEAN, TURKEY

Buket Mesta ^a, Hidetaka Sasaki ^b, Tosiuyuki Nakaegawa ^b, Elçin Kentel ^{c,*}

^a *Department of Earth System Science, Middle East Technical University, Ankara, Turkey*

^b *Department of Applied Meteorology Research, Meteorological Research Institute, Tsukuba, Japan*

^c *Department of Civil Engineering, Middle East Technical University, Ankara, Turkey*

* *Corresponding author. E-mail address: ekentel@metu.edu.tr (E. Kentel). Postal address: Department of Civil Engineering, Water Resources Laboratory, Middle East Technical University, Üniversiteler Mahallesi Dumlupınar Bulvarı No:1 06800, Ankara, Turkey*

Abstract

Critical impacts are expected for the Mediterranean basin due to global climate change. Various interconnected climate drivers on a global to local scale influence the regional climate. Different local climate influences of inland water bodies, complex topography, and surrounding seas cause temperate, arid, and continental climate properties to prevail with local variations in different parts of Turkey, which is located between Europe and the Middle East. Hence, the climatology shows intraregional variability that creates uncertainties and challenges in climate modeling. This study includes an assessment of the climate change impacts on the surface air temperature in western and southwestern Turkey through an ensemble analysis of high-resolution models. For the analysis, surface air temperature projections for the study area by twelve GCM/RCM combinations from the EURO-CORDEX Database and two high-resolution climate models developed by the Japan Meteorological Research Institute (MRI) are used. In the analysis, firstly, climate model outputs are validated through a benchmark of the historical simulation results with the observed data. The daily surface air temperature data from 59 stations are used to determine the skills of models to reproduce the local climatology. Further,

changes in surface air temperature climatology in the short- (2020-2030), medium- (2031-2050), and long-term (2051-2100) future are assessed. The findings verify that among 14 climate models, two models of MRI (MRI-AGCM, NHRCM) and two CORDEX RCMs nested in HadGEM2-ES (RCA4 and CCLM4-8-17) perform best to replicate the spatial variability of surface air temperature in the study area. Additionally, the multi-model ensemble analysis shows a statistically significant, gradual increase in the mean surface air temperature for the entire region under both RCP4.5 and RCP8.5 scenarios by the end of the 21st century. A comparative analysis of the projections by the models in the ensemble regarding surface air temperature and precipitation changes demonstrates that the projections mostly agree on an inverse linear relationship between the two parameters at the entire study area.

Keywords: EURO-CORDEX, NHRCM, MRI-AGCM, surface air temperature, surface air temperature-precipitation relationship, Mediterranean

1. Introduction

The Mediterranean basin that is located on three different continents has its particular features bringing different types of topographic, biogeographic, and societal elements and forms a transition zone between the arid climate of North Africa and the surface air temperature (from here after will be referred to as temperature) and rainy climate of Central Europe. The Mediterranean climate, which is characterized by hot dry summers and humid, cool winters, is expected to be adversely impacted by global climate change (IPCC, 2021). The region is potentially vulnerable to the climatic changes induced by anthropogenic activities causing increasing concentrations of greenhouse gases (Giorgi and Lionello, 2008). The increase in temperatures is expected to exacerbate the existing anthropogenic-induced pressures on the environment and distinct biodiversity of the region. The findings from Giorgi's study (2006) support this argument defining the region as one of the most prominent 'Hot-spots' in terms of the response to global change that will experience a significant decrease in mean precipitation and intensified variability in precipitation, particularly for the dry (warm) season. Furthermore, a larger increase is expected in the regional temperature than that is expected for the global scale, particularly for the dry season. Several studies verified that 1.06°C increase in global mean temperature observed throughout 1850 to 2019, as highlighted in IPCC's 6th Assessment Report (IPCC, 2021), created a rise in maximum and minimum temperatures in the Mediterranean basin (Kostopoulou and Jones, 2005; Kuglitsch et al., 2010; Efthymiadis et al., 2011; Bartolini et al., 2012; Tanarhte et al., 2015). Kuglitsch et al. (2010) identified the eastern parts of the Turkish Black Sea coastline, western, southwestern, and central Turkey, and western Balkans as the "Hot spots" of heatwave changes. Bartolini et al. (2012) studied annual and seasonal long-term trends for temperature in the central Mediterranean and showed an increase of 0.9°C per 50 years in central Italy.

Studies focused on the historical temperature records from meteorological stations across Turkey analyzed the trends in temperature changes, heatwaves, and extreme temperature events (Tayanç et al. 2009; Cagatan and Unal, 2010; Toros, 2012; Unal

et al., 2013; Acar Deniz and Gönençgil, 2015; Gönençgil and Acar Deniz, 2016; Altın and Barak, 2017; Erlat et al., 2021) and verified an increasing trend in temperature in Turkey particularly after the 1990s. Tayanç et al. (2009) demonstrated that the climate signal of temperature showed a continuous warming period for Turkey after 1993 with significant warming for the south and southeastern Turkey featuring increases in maximum and mean temperature series. Furthermore, an increasing trend in heatwaves in western Turkey is identified to be more evident in inland stations (Cagatan and Unal, 2010; Unal et al., 2013). Similarly, Altın and Barak (2017) showed a statistically significant positive anomaly for the number of summer days and tropical days above the long-term average for the duration between 1993 – 2014 in the Adana Sub-region of the Eastern Mediterranean coast of Turkey.

Several studies used projections from the climate models to assess the likely future trends in the temperature in the Mediterranean (Lelieveld et al., 2012; Kostopoulou et al., 2014; Öztürk et al., 2015; Zittis et al., 2016). Lelieveld et al. (2012) studied the projections after dynamical downscaling of 2 different GCMs for the eastern Mediterranean and the Middle East under the SRES A1B (intermediate) scenario. They found gradual and relatively strong warming of about 3.5–7°C by the end of the 21st century. Using the projections on the optimistic (B2), intermediate (A1B), and pessimistic (A2) SRES scenarios from the same climate models, Zittis et al. (2016) revealed that the frequency of heatwaves is likely to increase in the Mediterranean. Öztürk et al. (2015) studied projections of 16 CMIP3 GCMs for the Mediterranean region under SRES A2, A1B, and B1 scenarios after statistical downscaling and found an increase in annual temperature (Öztürk et al., 2015).

Analyses of the potential future trends in temperature for different regions of Turkey support the likelihood of positive anomaly in all parts of the country (Önol and Unal, 2014; Bağçacı et al., 2021). Önol and Unal (2014) studied the climate change impact for seven different geographical regions of Turkey by the use of projections from the RegCM3 regional climate model driven by the NASA Finite Volume GCM (fvGCM) under the SRES A2 scenario. They reported an increase in temperature in the range of 2–5°C by the end of the 21st century. Bağçacı et al. (2021) used the mean

average ensemble of the best-performing four models from CMIP5 and CMIP6 GCMs identified for Turkey and analyzed potential changes in the temperature and precipitation. The analysis revealed a statistically significant positive anomaly for the near-surface temperature projections for RCP4.5 and 8.5 scenarios. For the long-term future (2070-2100), the study revealed an increase in the mean temperature values for all seasons. Aziz et al. (2020) analyzed the climate non-stationarity based on the outputs of 12 CORDEX RCMs under the RCP8.5 scenario in Turkey. The analysis showed inter-regional variability in temperature change across Turkey (Aziz et al., 2020) for the projection period between 2051 and 2100.

Various studies focused on the assessment of potential future climate change impacts at different regions of Turkey. Several studies analyzed the future climate projections to examine potential impacts considering forestry, ecosystem dynamics, crop yield, energy, and tourism activities (Fujihara et al., 2008; Özdoğan, 2011; Sen et al., 2012; Deidda et al., 2013; Öztürk et al., 2015; Sunyer Pinya et al., 2015; Yilmaz, 2015; Demircan et al., 2017; Mehr and Kahya, 2017; Bucak et al., 2018; Dino and Akgül, 2019).

The MRI-AGCM is an atmospheric general circulation model (AGCM) that was developed to improve the regional-scale representation of the climate integrated with the global-scale and long-term mean climate state. The horizontal grid resolution of this model is about 20 km (Mizuta et al., 2006), which corresponds to high-resolution GCM data. MRI-AGCM was used for future climate change studies in various parts of the world, including Central America (Kusunoki et al., 2019; Nakaegawa et al., 2014) and Australia (Nakaegawa et al., 2017). NHRCM is a regional climate model which was developed by enhancing an operational non-hydrostatic model (NHM) of MRI and the Numerical Prediction Division of the Japan Meteorological Agency (NPD/JMA) (Sasaki et al., 2008, 2011). The performance of NHRCM for climate simulations was thoroughly tested by several studies in Japan. Sasaki et al. (2008) demonstrated strong simulation performance of NHRCM to reproduce the precipitation and temperature as well as the inter-annual variation of temperature. Sasaki et al. (2011) demonstrated that NHRCM provides improved skills for local

temperature and precipitation projections compared to AGCM. Additionally, it was tested for its performance for other parameters such as extreme storm events, snow depth, and storm tracks and also for the performance to represent the effect of topography on precipitation (Sasaki and Kurihara, 2008; Sasaki et al., 2011, 2012, 2013).

Furthermore, several studies evaluated model performances of MRI-AGCM and NHRCM for various regions of the world by comparing them to other global and regional models regarding the present and future climate simulations (Saito et al., 2006; Kitoh et al., 2009, 2016; Pinzón et al., 2017; Varghese et al., 2020). Even though Turkey was included in some of these studies, this is the first study that covers a detailed comparison of these two models with CORDEX RCMs for the Mediterranean region. In this study, NHRCM grid data are generated for the domain limited to the study area by nesting within MRI-AGCM with 20-km grid spacing. The horizontal resolution of NHRCM is 5 km in this study. NHRCM integration with MRI-AGCM boundary conditions was conducted for 20-year timeframes to simulate present (1980-2001) and future (2080-2100) climate conditions.

Identification of the climate change impacts for the Mediterranean region of Turkey that has a complex topography and climate features is a challenging task and previous studies verified that the projections by CORDEX RCMs demonstrate inter-regional and inter-model variability (Aziz et al., 2020). Furthermore, to the best of our knowledge, the number of studies that include a comparison of various CORDEX RCMs for the projection skills for Turkey is still limited.

In this study, the climate projections for temperature are analyzed for a study region covering more than 200,000 km² area in the western and southwestern Turkey including the Mediterranean region (from hereafter will be referred to as the study area or SA) using high-resolution climate model projections. Simulations for the EUR-11 domain from 12 CORDEX RCMs, simulations from the super-high-resolution atmospheric climate model (MRI-AGCM) generated by the Japan Meteorological Agency (JMA) Meteorological Research Institute (MRI), and the projections from Non-Hydrostatic Regional Climate Model (NHRCM) of JMA-MRI

with boundary forcing of MRI-AGCM are used in this study . NHRCM is nested in the boundary conditions of the MRI-AGCM. Within that scope, initially, 12 CORDEX RCMs and two MRI climate models are evaluated for their skill of simulation performance regarding the replication of the spatial variability of annual temperature mean at the SA. After that, potential change in temperature under the RCP4.5 and RCP8.5 scenarios in the short-term (2020-2030), medium-term (2031-2050), and long-term (2051-2100) future are assessed through the comparison of the climatology with reference period. Finally, a per basin analysis of the potential temperature change and its relation to the likely change in precipitation is provided. The short-, medium-, and long-term future periods analyzed in this study are selected with the purpose of delineation of likely size of the impact on mean temperature that may be addressed by planning with a tiered approach for future adaptation strategies.

2. Study area

The region of interest in this study covers a considerable portion of Turkey, where the temperate climate conditions, so-called Mediterranean climate features are dominantly observed. The study area (SA) includes partially or wholly, 10 of the major watersheds in Turkey (Fig. 1) and extends through three (Aegean, Mediterranean, and Central Anatolian regions) of seven separate geographical regions of Turkey (Fig. 2). Different climatic conditions prevail in each geographical region due to the diverse topography and effect of the surrounding seas (Sensoy et al., 2008; Sensoy and Demircan, 2016). The complex morphological structure of the region strongly affects the atmospheric circulation in the region (Lionello et al., 2006).

The Mediterranean region covering most of the western, middle, and eastern Mediterranean basins in Turkey is separated from the Central Anatolia region by the Taurus mountains stretching parallel to the southern coastline. The Taurus mountains not only form the water divide for the basins at the south but also create a barrier between the regions making the diversified climatic conditions (Fig. 2). As it is seen in the Köppen Geiger classification of the SA in Fig. 2, the southern and western coastal areas have temperate climate properties typical of the Mediterranean climate with dry and hot summers and mild winters. Higher latitude lands of the mountain ranges have cold climate features with dry summers. Behind the barrier of the mountains, continental features dominate in the arid steppe climate of the Central Anatolia and inland Aegean regions.

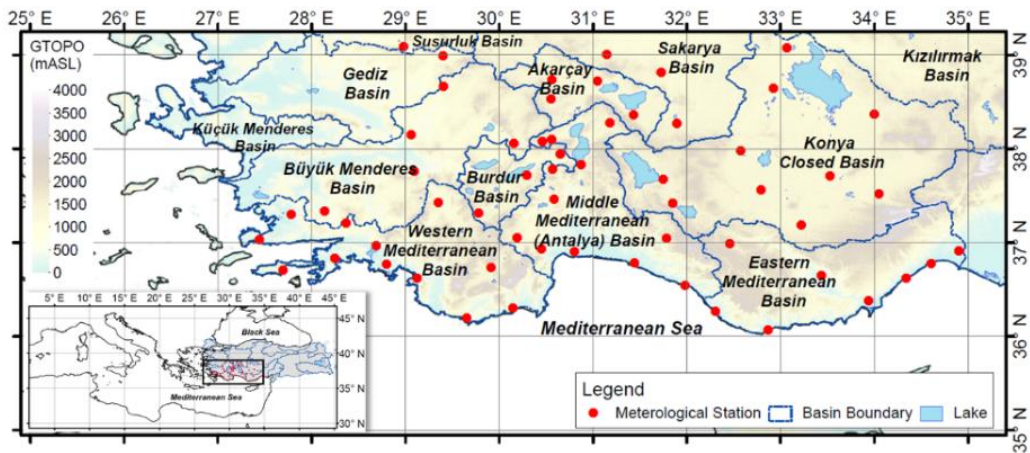


Fig.1. Topographical map of the study area (SA) showing the locations of the meteorological stations used in this study.

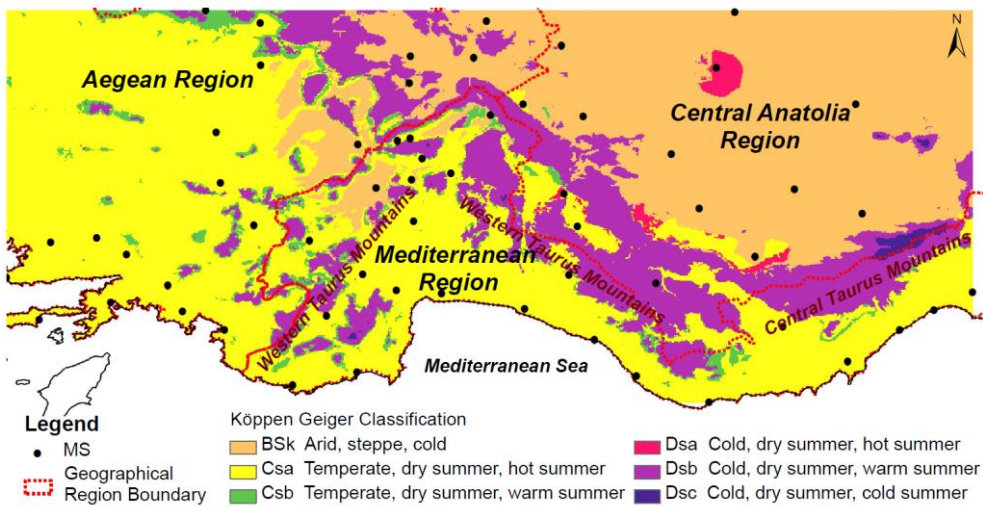


Fig. 2. Map of Köppen Geiger climate zones indicating geographical regions in the SA (adapted from Beck et al., 2018).

3. Data and methods

3.1. Data

The reference data (RD) used for the validation of the historical projection outputs is obtained from the historical daily mean temperature recordings from the meteorological stations (MSs) located across the study area (Fig. 1). The MSs used for the study are ground-based stations operated by the Turkish State Meteorological Service. In total, 59 MSs providing a minimum of 30-year long time series between 1966-2005 are selected for the study. The list of the MSs in the SA is given in Supplementary Material in Appendix A. For the assessment of the baseline climatology at the SA, annual and seasonal climatological temperature means for each station are calculated from the daily mean temperature data. RD for temperature is also used for the comparison with modeled data for the testing of the simulation performance of climate models.

The assessment of the potential change in temperature due to climate change in the SA covers a multi-model analysis of 14 high-resolution climate models (i.e., 12 CORDEX RCMs and two high-resolution climate models developed by MRI). A list of the climate models is given in Table 1. Twelve model outputs of CORDEX RCMs are composed of the combination of five different RCMs (i.e., ALADIN53 of Centre National de Recherches Météorologiques (CNRM), CCLM4-8-17 of Climate Limited-area Modelling Community (CLM-Community), RCA4 of Swedish Meteorological and Hydrological Institute (SMHI), HIRHAM5 of Danish Meteorological Institute (DMI), and RACMO22E of Royal Netherlands Meteorological Institute (KNMI), and WRF331F of Institut Pierre-Simon Laplace (IPSL-INNERIS)) with four different GCMs from CMIP5 as the driving model. The selection of the GCM/RCM combinations producing twelve high-resolution projections is done to enable the assessment of the performance of at least two different RCMs taking the same GCM as the boundary conditions. The outputs of CORDEX models belonging to the EUR-11 Domain (0.11-degree resolution) are obtained from the CORDEX database. The other two model outputs are from super

high-resolution (0.1875-degree) AGCM generated by Japanese MRI, and the MRI's NHRCM (5-km resolution) using the MRI-AGCM as the boundary conditions.

Table 19 List of the climate models used in the study.

Climate Model (RCM/GCM)			Output Period		Resolution	Source	Model Number
Driving Model/ GCM (Institution)	Name	Institution	Historic	Future (Scenarios)			
MRI-AGCM (MRI)		MRI	1979-2003	2075-2100 (RCP8.5)	0.1875*	MRI	M1
MRI-AGCM (MRI)	NHRCM	MRI	1980-2001	2080-2100 (RCP8.5)	5 km	MRI	M2
CNRM-CM5 (CNRM-CERFACS)	ALADIN53	CNRM	1951-2005	2006-2100 (RCP4.5, RCP8.5)	0.11*	CORDEX Db ^a	M3
CNRM-CM5 (CNRM-CERFACS)	CCLM4-8-17	CLM-Community	1950-2005	2006-2100 (RCP4.5, RCP8.5)	0.11*	CORDEX Db ^a	M4
CNRM-CM5 (CNRM-CERFACS)	RCA4	SMHI	1970-2005	2006-2100 (RCP4.5, RCP8.5)	0.11*	CORDEX Db ^a	M5
EC-EARTH (ICHEC)	CCLM4-8-17	CLM-Community	1949-2005	2006-2100 (RCP4.5, RCP8.5)	0.11*	CORDEX Db ^a	M6
EC-EARTH (ICHEC)	HIRHAM5	DMI	1951-2005	2006-2100 (RCP4.5, RCP8.5)	0.11*	CORDEX Db ^a	M7
EC-EARTH (ICHEC)	RACMO22E	KNMI	1950-2005	2006-2100 (RCP4.5, RCP8.5)	0.11*	CORDEX Db ^a	M8
EC-EARTH (ICHEC)	RCA4	SMHI	1970-2005	2006-2100 (RCP4.5, RCP8.5)	0.11*	CORDEX Db ^a	M9
CM5A-MR (IPSL)	RCA4	SMHI	1970-2005	2006-2100 (RCP4.5, RCP8.5)	0.11*	CORDEX Db ^a	M10
CM5A-MR (IPSL)	WRF331F	IPSL-INNERIS	1951-2005	2006-2100 (RCP4.5, RCP8.5)	0.11*	CORDEX Db ^a	M11
HadGEM2-ES (MOHC)	CCLM4-8-17	CLM-Community	1949-2005	2006-2100 (RCP4.5, RCP8.5)	0.11*	CORDEX Db ^a	M12
HadGEM2-ES (MOHC)	RACMO22E	KNMI	1950-2005	2006-2100 (RCP4.5, RCP8.5)	0.11*	CORDEX Db ^a	M13
HadGEM2-ES (MOHC)	RCA4	SMHI	1970-2005	2006-2100 (RCP4.5, RCP8.5)	0.11*	CORDEX Db ^a	M14

^a CORDEX Database: ESGF, Earth System Grid Federation website, <https://esgf-node.llnl.gov/search/esgf-llnl/>, (CoG version v4.0.0b2, ESGF P2P Version v4.0.4)

3.2. Evaluation of performance skills of climate models

The climate models are tested for their skills in the reproduction of the baseline climatological conditions and the spatial variability of the temperature climatology in the study area. For the analysis, the annual climatological means of temperature at 59 stations (i.e., the closest modeling grids) calculated from the historical simulations are compared with the observed values. The performance skill is evaluated by using three statistical performance indicators; Pearson's Correlation Coefficient (*Corr*), Root Mean Square Error (*RMSE*), and Bias (*Bias*). The performance indicators are calculated using the annual mean temperature data series in °C.

In addition to the evaluation of the individual performance indicators, an aggregated performance index (API) is also generated for each model to determine the best climate models for the SA in terms of the efficiency in the simulation of mean

temperature. For the calculation of API, models are ranked three times for each indicator separately (i.e., ranking of all models from best to worst) and three ranks of each model are averaged. The model with the lowest API is considered to achieve the best modeling performance for the SA.

4. Results

4.1. Analysis of climatology

RD from 59 MSs is used to assess the annual and seasonal climatological temperature means at the SA. The annual climatological temperature mean, \overline{AT} is the long-term mean of the annual means of daily average temperatures for each MS. Similarly, the seasonal climatological mean is the long-term mean value of the seasonal temperature means. In order to obtain the climatology maps for the SA, the inverse distance weighted (IDW) interpolation method is applied to the climatology data for the MSs. Fig. 3 displays the relevant climatology maps. The \overline{AT} values range between 10°C and 20°C (Fig. 3(a)) in the SA. In fact, for coastal MSs, \overline{AT} values are greater than or equal to 18°C, whereas, for the remaining two-thirds of the MSs, located inland, it is between 10°C and 17°C (Fig. 4). The highest and lowest \overline{AT} values are observed at coastal Kas MS (MS:17380) in the Middle Mediterranean Basin and at inland Hadim MS (MS: 17928) in the Eastern Mediterranean Basin, respectively (Fig. 4). The coastal stations also have the highest climatological temperature means for all seasons in the region.

The winter temperature means, \overline{WT} at coastal stations ranges between 10°C and 13°C with the highest mean temperature recorded in the Middle Mediterranean Basin (Kas MS, 17380), whereas for the remaining MSs it ranges between -1°C and 7°C (Fig. 3(b)). The areal average of temperature means (the average of climatological temperature means for 59 MSs) for the winter season in the SA is 5°C. The \overline{WT} drops slightly below 0°C for two stations in the SA. These are Hadim MS (MS: 17928) at 1500mASL in the Eastern Mediterranean Basin and Kulu MS (MS: 17754) at

1000mASL in the Central Anatolia region. These two stations also have the lowest spring, summer, and fall season climatological means (Fig. 4). The climatological summer temperature means, \overline{ST} at the MSs in the SA ranges between 19°C (at Hadim MS: 17928) and 28°C (at Mut MS:17956) (Fig. 3(d)). Both stations are located in the eastern Mediterranean Basin (Fig. 4).

To analyze the seasonal fluctuation, the seasonal climatological mean values of the MSs are compared with the annual climatology of each station. Accordingly, in the SA the seasonal climatological temperature means for 59 stations are 7°C to 11°C lower, and 0°C to 2°C lower than \overline{AT} values for winter and spring, respectively. Fall and summer climatological temperature means, \overline{FT} and \overline{ST} , are respectively 0.5°C to 2°C, and 7°C to 10°C higher compared \overline{AT} values for MSs in the SA. Hence, the difference between \overline{WT} and \overline{ST} values range from 14°C to 21°C in the SA.

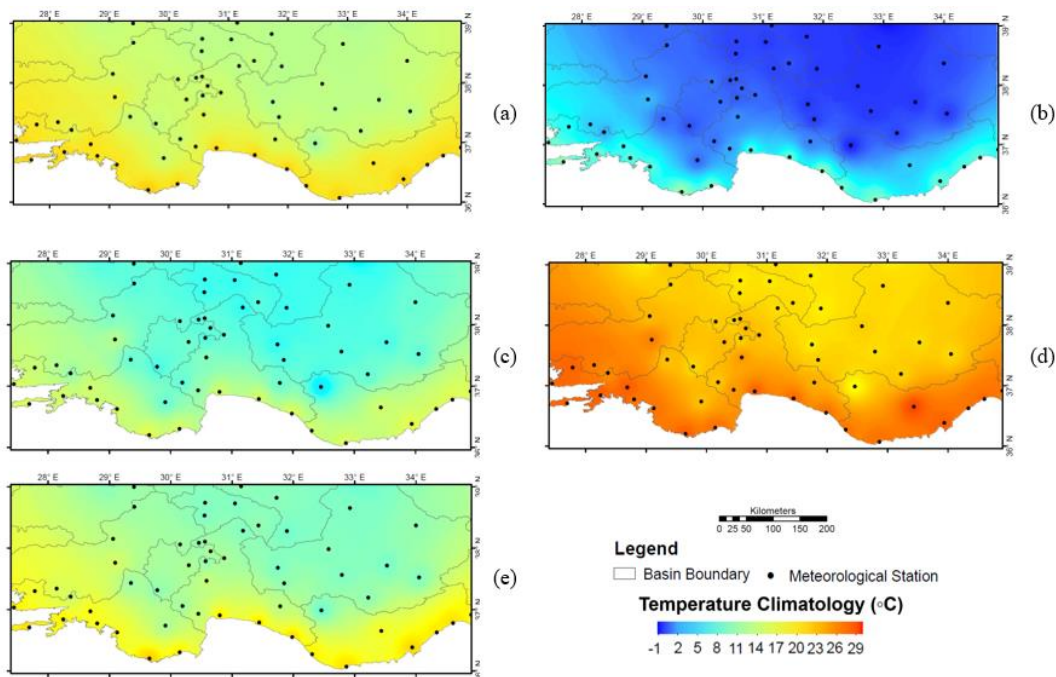


Fig. 3. Baseline temperature climatology maps of the SA for (a) annual climatology, (b) winter climatology, (c) spring climatology, (d) summer climatology, (e) fall climatology.

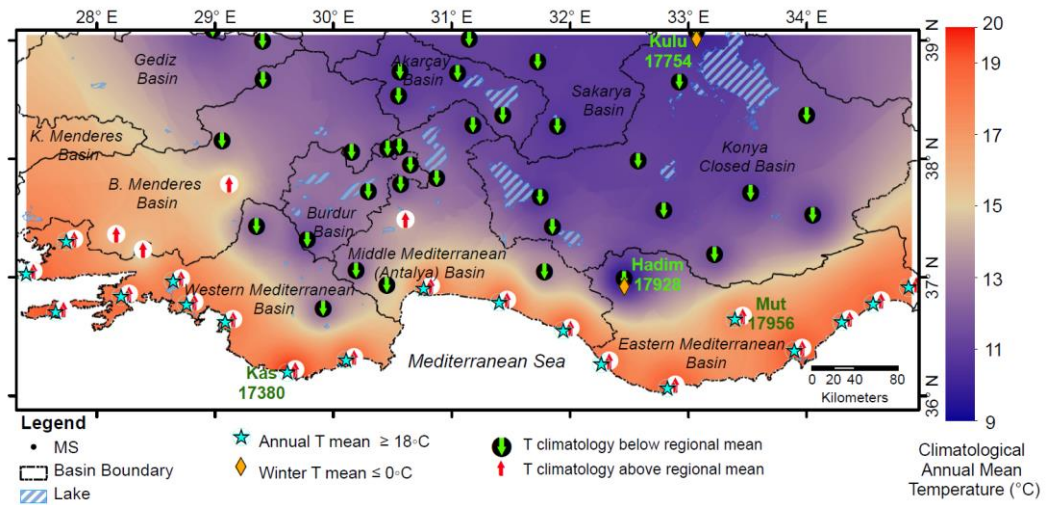


Fig. 4. Analysis of climatological temperature properties at MSs in the SA.

4.2. Analysis of the modeling performance

The simulation skills of climate models are tested through a benchmark with RD from 59 MSs across the study area. Individual performance indicators (*Corr*, *RMSE*, and *Bias*), and APIs calculated for each model regarding the skills in representing spatial variability of temperature in the SA, are given in Table 2. The best performance indicator values are highlighted in bold in the table. Accordingly, all models in the ensemble attain high *Corr* values ranging between 0.86-0.94 to replicate the spatial variability of temperature climatology. *RMSE* values for 14 models range between 1.6 and 4.7°C. The highest variability among the models is seen for *Bias* value. *Bias* varies in the range of 0.05 to 4.2°C for the models.

Taylor diagram in Fig. 5, comparing model simulations of spatial variability in temperature climatology against observed, indicates a relatively similar simulation efficiency for 14 models, in general, except for M3 that is verified to perform weaker than other models.

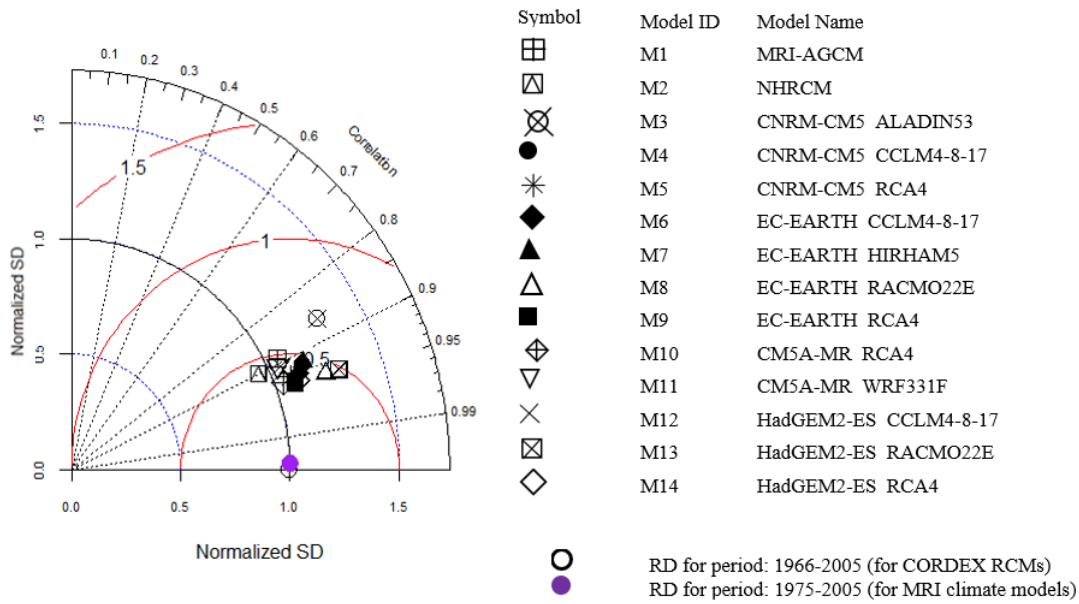


Fig. 5. Taylor diagram of climate models.

Table 2 Performance indicator values for climate models.

ID	Model Name	<i>Corr</i>	<i>RMSE</i> (°C)	<i>Bias</i> ^b (°C)	API
M1	MRI-AGCM	0.89	1.58	0.05	5.00
M2	NHRCM	0.90	1.61	0.73	5.33
M3	CNRM-CM5_ALADIN53	0.86	4.69	4.15	14.00
M4	CNRM-CM5_CCLM4-8-17	0.92	2.83	2.39	8.67
M5	CNRM-CM5_RCA4	0.93	2.90	2.59	9.00
M6	EC-EARTH_CCLM4-8-17	0.93	2.68	2.30	7.67
M7	EC-EARTH_HIRHAM5	0.92	2.00	1.29	5.67
M8	EC-EARTH_RACMO22E	0.94 ^a	4.08	3.80	9.33
M9	EC-EARTH_RCA4	0.94	3.45	3.23	9.00
M10	CM5A-MR_RCA4	0.93	2.59	2.28	6.00
M11	CM5A-MR_WRF331F	0.90	2.62	2.16	8.00
M12	HadGEM2-ES_CCLM4-8-17	0.91	1.82	1.06	5.33
M13	HadGEM2-ES_RACMO22E	0.94	3.04	2.58	7.33
M14	HadGEM2-ES_RCA4	0.94	2.20	1.79	4.67

^aThe best values are indicated in bold

^b absolute value of mean difference between observed and simulated

Taking the API values into consideration five climate models are evaluated to have the best skills in modeling temperature climatology. These are two MRI models M1 and M2, two CORDEX RCMs, M14 (RCA4), M12 (CCLM4-8-17) using HadGEM2-ES as the driving GCM, and M7 (HIRHAM5) using EC-EARTH as the driving GCM. On the other hand, M3 (ALADIN53 using CNRM-CM5 as the driving GCM) has the weakest performance value among 14 climate models. In fact, the poor performance of ALADIN53 is considered to be related to the problematic Sea Surface Temperature (SST) mapping from driving GCMs that is likely to cause biased projections of surface temperature particularly for coastal areas as indicated in the EURO-CORDEX's technical errata webpage (EURO-CORDEX, 2021). Furthermore, although HIRHAM5 (EC-EARTH as driving GCM) is observed to perform relatively well for historical simulations it should still be taken into consideration that among the CORDEX-RCMs certain runs of HIRHAM and WRF use a different assumption on the GHG forcing which potentially has an influence on the surface temperature projections from these RCMs (Jerez et al., 2018). The same issue was also proclaimed by the EURO-CORDEX errata webpage highlighting likely significant impacts of the use of different approaches by these RCMs. The ensemble members M7 and M11 are the RCM simulations with no GHG evolution assumption and involve the GHG change impact projection from driving GCM only.

Among the best-performing five models, in addition to the MRI models, the driving GCMs for the CORDEX RCMs are HadGEM2-ES and EC-EARTH. On the other hand, the driving GCMs for the worst-performing five models are EC-EARTH and CNRM-CM5. Hence, it can be said that as the driving GCM HadGEM2-ES performs relatively well for temperature projections, whereas CNRM-CM5 performs relatively poorly in projections for the study area in combinations with different RCMs. However, the projection skill of EC-EARTH for temperature varies depending on the RCM. In that respect, the weak performance of RCMs using CNRM-CM5 might be attributed to the problem with the boundary forcing conditions in CNRM-CM5 for historical runs as reported by EURO-CORDEX (2021). Although it is reported that the influence on climate scale is expected to be

weak, the relevant problem might be a factor in the relatively lower performance of this GCM in historical simulations of the SA. An additional divergence of CNRM-CM5 from the other three CMIP5 GCMs that may affect the simulation skill is that the forcing agent of land-use change is not included in the model setup (Collins et al. 2013; Boé et al., 2020). Consequently, among four driving GCMs CNRM-CM5 is seen to be relatively poor for temperature climatology as shown above and also regarding the skill for the reproduction of precipitation climatology for SA, as verified by the study of Mesta et al. (2022).

Comparing the simulation performances of 14 climate models for the representation of temperature climatology with the findings from the earlier study by Mesta et al. (2022), it is seen that NHRCM with MRI-AGCM boundary conditions has demonstrated similarly high skill regarding the reproduction of spatial variation of precipitation climatology at the SA. Regarding the simulation performances of different GCMs as driving models of CORDEX RCMs for precipitation the following inferences can be made using Mesta et al. (2022) study outputs: Unlike temperature simulations, the simulation skill for the precipitation climatology is found to depend on the RCMs using HadGEM2-ES as the driving model. On the other hand, RCMs nested in the EC-EARTH model are seen to perform well for precipitation for different RCM (CCLM4-8-17, HIRHAM5, RACMO22E, RCA4) combinations.

4.3. Future projections on temperature

The short-term (2020-2030), medium-term (2031-2050), and long-term (2051-2100) projections of 12 CORDEX RCMs are assessed through a comparison with the annual temperature climatology of the reference period. RCP8.5 scenario projections for the 2080-2100 timeframe from two high-resolution MRI climate models are also added to the analysis for the assessment of the potential changes in long-term future temperature. The change in temperature for the projection period is calculated as follows:

$$\text{Change in temperature } (\Delta T) = T - \overline{AT} \quad (1)$$

where, ΔT is the difference in the temperature climatology between the projection period, T (e.g., 2020-2030 for short-term) and the reference period, \overline{AT} . Maps in Figs. 6 to 12 show the projections of change in annual temperature climatology for 59 MSs in the SA based on 14 climate model outputs. The projection maps between Figs. 6 and 10 also provide maps based on a performance-based weighted average (PBWA) of CORDEX models for the relevant projection periods. The PBWA of projections on percent change in temperature climatology is calculated based on the API values regarding performance skill on spatial variability according to Equation (2).

$$PBWA = \frac{\sum_{i=1}^n \left[\frac{1}{API_i} \times (\Delta T)_i \right]}{\sum_{i=1}^n \frac{1}{API_i}} \quad (2)$$

where, i is the index for the models used in PBWA of projections on temperature change. Here, the best-performing five CORDEX models (i.e., $n = 5$), identified according to the API (i.e., M7, M10, M12, M13, M14; see Table 2) for the reproduction of spatial variability, are used to generate the PBWA. Additionally, for the long-term future under the RCP8.5 scenario (Fig. 11), two PBWA of projections are generated, the first (i.e., PBWA-1) using five best performing CORDEX models (i.e., M7, M10, M12, M13, M14) and the second (i.e., PBWA-2) using two MRI models (M1, and M2) that show best projection skill for temperature in the SA plus three best performing CORDEX models (M7, M12, M14). In Figs. 5 to 10, the map of the PBWA of change in temperature climatology of 59 MSs in the SA is shown in the last row. Additionally, the name of the model for the projection map of the best performing CORDEX model (i.e., M14; see Table 2) is written in bold. The IDW interpolation method is used to convert the potential temperature change and

statistical significance data on modeling grids into surface data illustrated in the maps.

Welch's two-sample T-test (or unequal variances t-test) is applied to the annual temperature time series from the climate model projections to test the significance of the change in temperature at 95% confidence level. The significance of the change in the short-, medium- and long-term future is tested against the reference period. The T-test is used for the projections of individual models, and not for the PBWA results that are calculated from percent change projections.

For the short-term future, the potential change in \overline{AT} under RCP4.5 and RCP8.5 scenarios based on the projections of 12 CORDEX RCMs are shown in Figs. 5 and 6, respectively. Under the RCP4.5 scenario, all models agree on an increase in the \overline{AT} in the entire SA (Fig. 6). Furthermore, with a 95% confidence level, all models agree on a significant change in the temperature at all MSs. The maximum range for the change in temperature at 59 stations projected by 12 models (from hereafter will be referred to as MaxMR) for the RCP4.5 scenario is from 0.6°C to 2.6°C. The mean model range indicated by the 12-member ensemble as for the potential change in temperature at 59 stations across the SA (from hereafter will be referred to as MeanMR) is between 0.9°C and 1.4°C. The 12-member ensemble's projection for the areal average of temperature change in the SA is 1.2°C. Among 12 models, M14 identified to have better simulation skill, projects 1.6°C increase in the areal average of temperature mean. It projects a relatively higher temperature increase for inland areas than coastal, which is also similar to the projection obtained by the weighted average of the five best-performing models in Fig. 6. PBWA map indicates a more uniform impact regarding the temperature increase throughout the SA compared to most of the individual model projections. Nevertheless, an approximately 0.4-0.5°C higher temperature increase is still projected for the inland stations. Higher increase in temperature in inland areas is considered to be originated from the reduction of evaporative cooling due to the depletion of soil moisture in those areas. The amplified increase in temperatures in dryer climate in inland parts of the SA is interpreted to be connected with several physical mechanisms including the increase

in dryness and added positive feedbacks of subsequent decrease in cloud formation that exacerbate the solar radiation effect (Zampieri et al., 2009; Seneviratne et al., 2010, 2013; Selten et al., 2020). The potential evaporative cooling impact at the coastal stations in line with the topographical features is seen to be represented particularly in the projections by M8 through M14. The effect of the Mediterranean Sea is seen to be prevalent in the area along the southern shoreline that is bordered by the impediment of the Taurus Mountains. On the other hand, at the western coast of the Aegean region, effect of sea is seen to reach farther inland due to the stretch of mountains perpendicular to the shoreline which maintains a farther outreach for westerly flow (Önol and Unal, 2014), which is in general more evident in the projections by RC4 (M9, M10, M14).

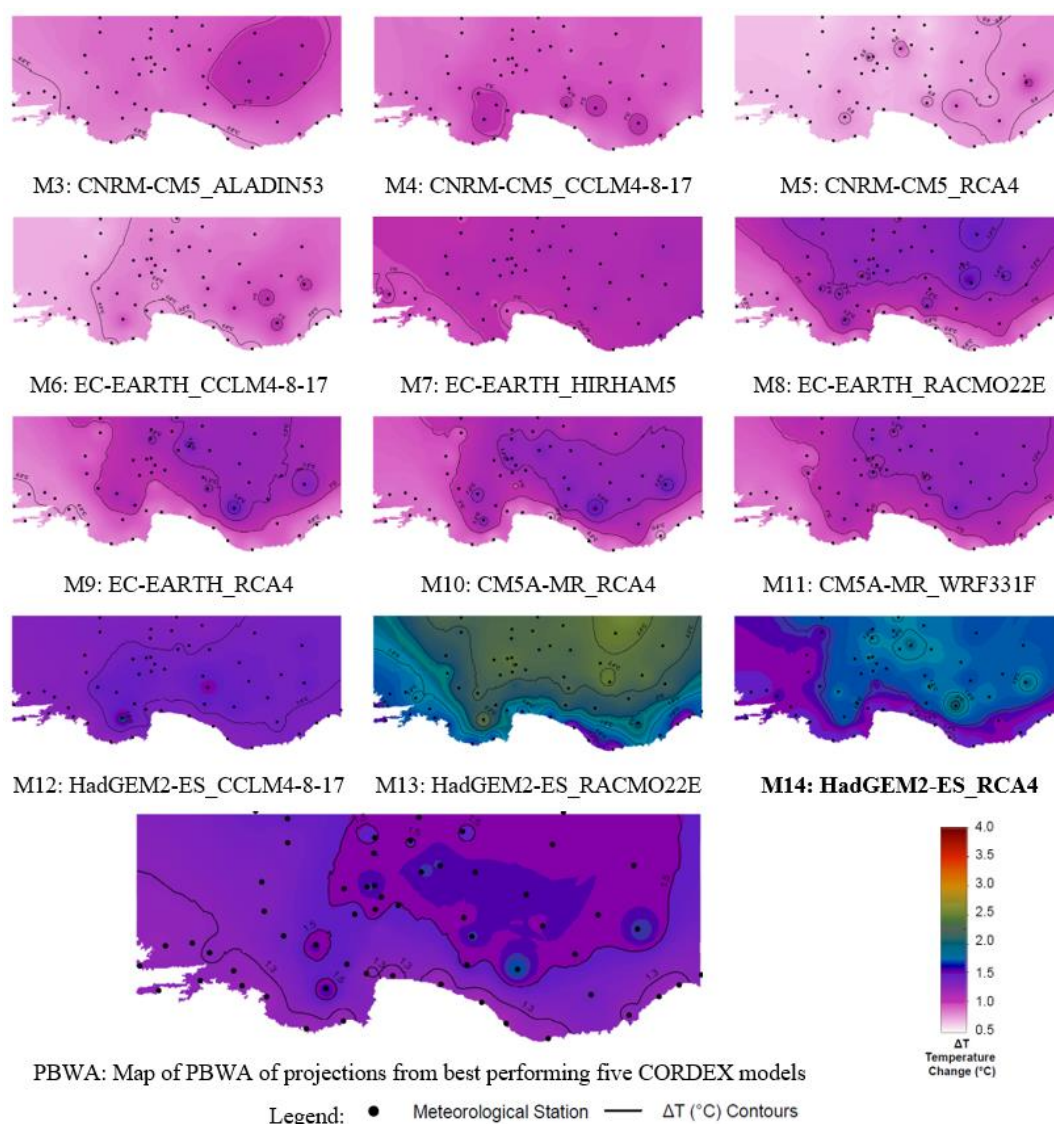


Fig. 6. Projections for temperature change, ΔT ($^{\circ}\text{C}$) in short-term future for RCP4.5 scenario (for models M3 through M14 all changes are statistically significant at the 95% confidence level).

Under the RCP8.5 scenario, analysis of 12-member ensemble indicates MaxMR between 0.9°C and 2.7°C , and MeanMR between 1.2°C and 1.6°C . According to the 12-member ensemble mean, the areal average of the SA is projected as 1.4°C change in temperature. Based on the 95% confidence level, statistically significant temperature change is likely for all MSs in the SA under the RCP8.5 scenario. The

projection by PBWA shows smoother variation in temperature change across the SA with an areal average of 1.6°C (Fig. 7).

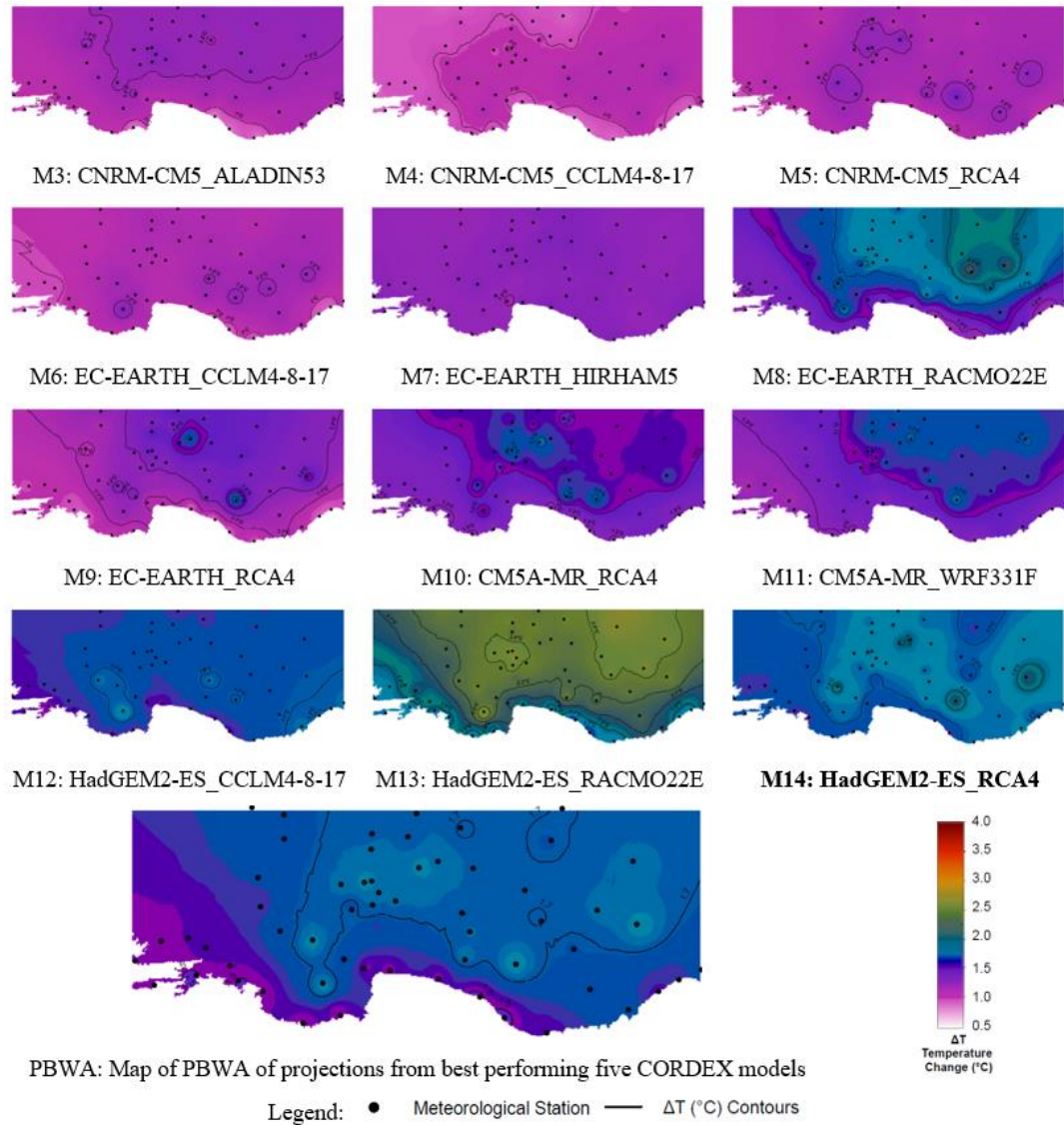


Fig. 7. Projections for temperature change, ΔT (°C) in short-term future for RCP8.5 scenario (for models M3 through M14 all changes are statistically significant at the 95% confidence level).

According to Fig. 8, all members of the ensemble show an increase in temperature for all MSs in the SA under the RCP4.5 scenario. The MaxMR of the ensemble is

between 0.9°C and 3.3°C, and MeanMR is between 1.4°C and 1.8°C. Multi-model ensemble projects a higher temperature increase for inland MSs. The areal average temperature change calculated from the 12-member ensemble mean is 1.6°C, lower than the areal average projected by M14 (2.3°C). PBWA projects a 1.9°C increase in temperature for coastal areas and a 2.1°C increase for inland sections in the SA.

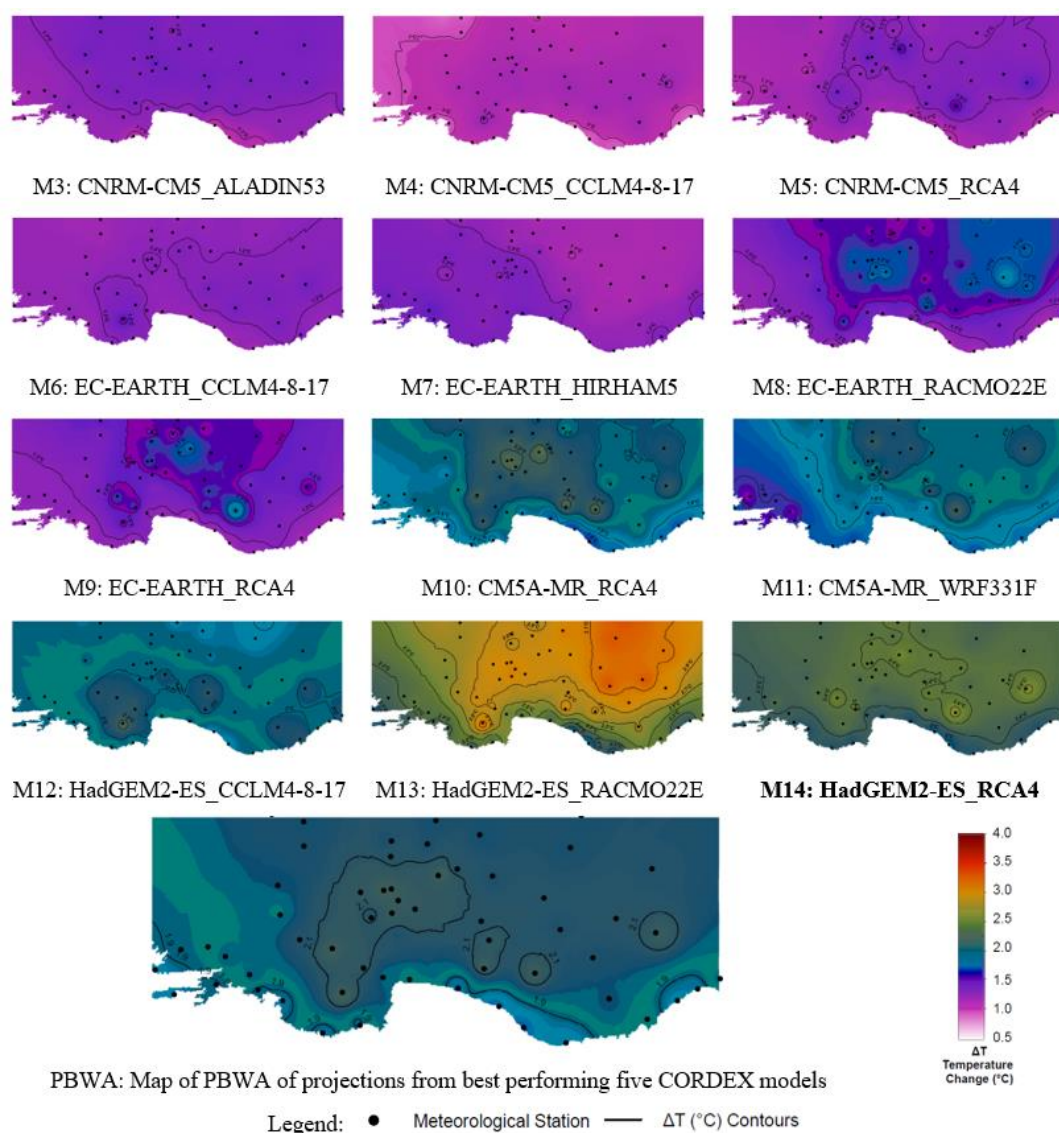


Fig. 8. Projections for temperature change, ΔT (°C) in medium-term future for RCP4.5 scenario (for models M3 through M14 all changes are statistically significant at the 95% confidence level).

Under the RCP8.5 scenario (Fig. 9), 12-member ensemble gives MaxMR between 1.2°C and 4°C, and MeanMR between 1.8°C and 2.3°C. The 12-model mean projects temperature increase at 2.1°C in the average of the SA. The projection obtained from PBWA shows around 2.3-2.4°C increase for coastal and 2.6°C increase for inland areas. All models in the ensemble agree on a statistically significant change in temperature in the medium-term future both under RCP4.5 and 8.5 scenarios in the entire SA.

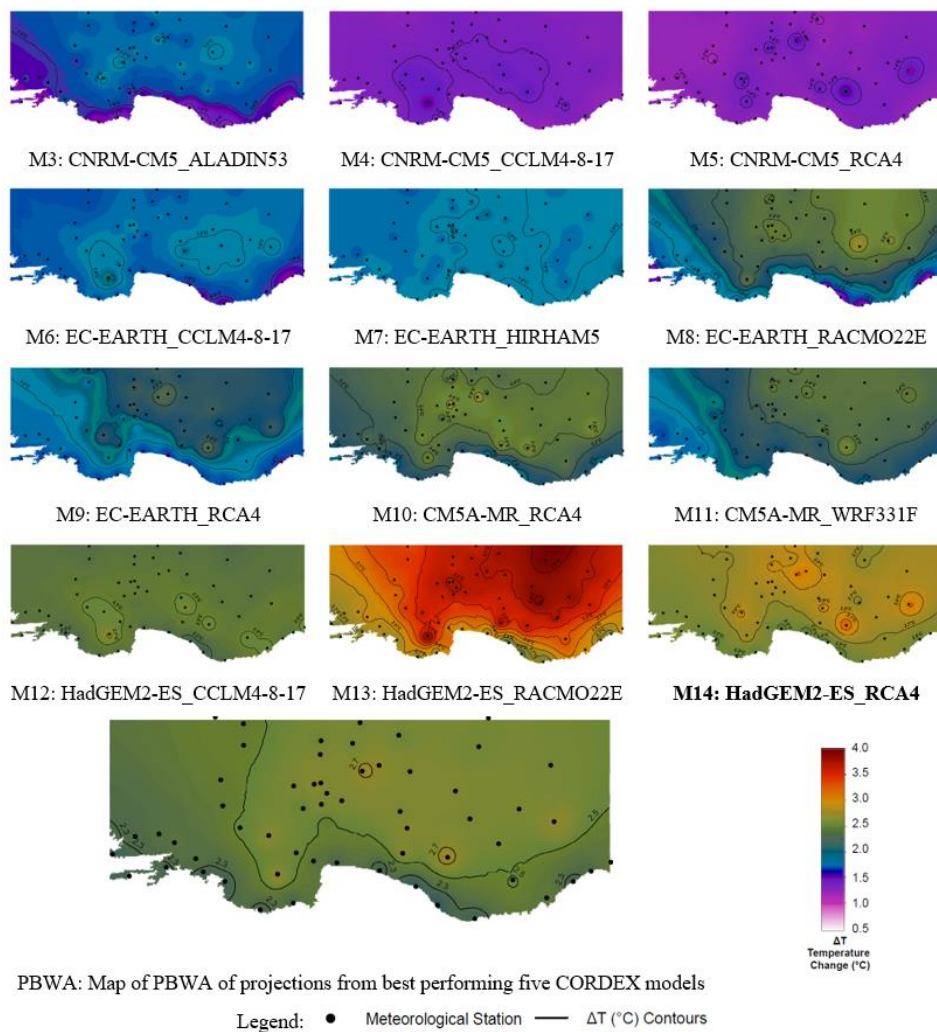


Fig. 9. Projections for temperature change, ΔT (°C) in medium-term future for RCP8.5 scenario (for models M3 through M14 all changes are statistically significant at the 95% confidence level).

The RCP4.5 projections of 12 CORDEX RCMs for the temperature change in the SA are shown in Fig. 10. 12-member ensemble shows a MaxMR between 1.7°C and 4.5°C, and a MeanMR between 2.1°C and 2.8°C and generate an areal average of 2.5°C in long term. Similar to medium-term simulations the projection by M14 (3.2°C) remains slightly over the ensemble mean for the projected temperature change. Unlike the long-term projections of precipitation reported by Mesta et al. (2022) to be statistically significant for approximately 30% or less of the MSs, temperature change is projected at a statistically significant level for the entire SA under the RCP 4.5 scenario by all CORDEX RCMs.

The RCP8.5 projections of 12 CORDEX RCMs on the temperature change in the SA in the long-term future are shown in Fig. 11. As it is seen in Figs. 10 and 11, the impact of temperature increase in the study area for the second half of the 21st century under RCP8.5 conditions becomes much more prominent in comparison to the RCP4.5 scenario, as the result of the higher GHG accumulation creating higher radiative forcing. The MaxMR and MeanMR of the ensemble is 2.8°C to 6.6°C, and 3.5°C to 4.6°C, respectively. The areal average of the ensemble means projects a 4.1°C increase by the end of 2100. The individual model projection by M14 for temperature increase by the end of the century is 4.8°C. For the long-term future, the temperature change is likely to be statistically significant under the RCP8.5 scenario according to all models in the ensemble. Similarly, the previous study on the climate change effect on precipitation verified statistically significant precipitation change for more than 60% of the MSs in the SA for the majority of RCMs (Mesta et al., 2022).

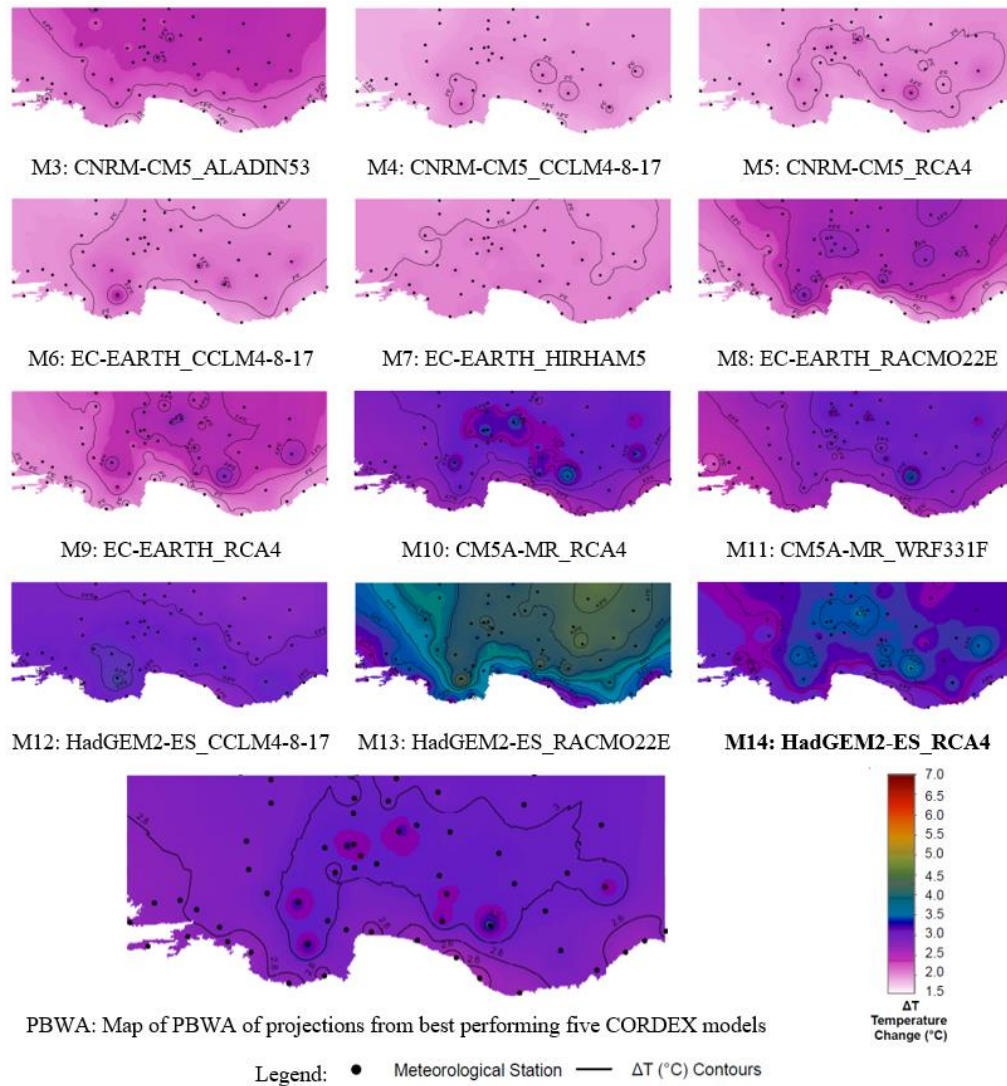


Fig. 10. Projections for temperature change, ΔT (°C) in long-term future for RCP4.5 scenario (for models M3 through M14 all changes are statistically significant at the 95% confidence level).

Regarding the future projections depicted above (Figs. 5 through 10), CM5A-MR and HADGEM2-ES as the driving GCMs of RCMs in the ensemble are seen to project a larger size of the climate change impact (i.e., temperature increase) compared to CNRM-CM5 and EC-EARTH for both RCP4.5 and RCP8.5 scenarios. Furthermore, as regards the long-term temperature increase under RCP4.5 and RCP8.5 scenarios, the difference between the two scenarios concerning the impact

size is projected to be even more pronounced by RCMs nested in CM5A-MR compared to other ensemble members with the same RCMs (i.e., Fig. 10 vs. 11). In comparison to other ensemble members, the projections of models using CNRM-CM5 as the driving model on relatively lower severity of the temperature increase might be attributed to the model setup not including the forcing of land-use change.

The long-term projections on temperature change by two MRI models are shown in Fig. 12. Accordingly, M1 projects a slightly higher temperature increase for the majority of MSs than M2. Although, both models project a similar range for the increase in the temperature mean in the SA. The model ranges of M1 and M2 for change in temperature across the SA are 4°C to 5.2°C and 4°C to 5.4°C, respectively. Moreover, the areal average of temperature increase is projected as 4.9°C by M1 and 4.7°C by M2. Hence, MRI models project a slightly higher SA average for temperature increase than the mean of 12 CORDEX models. Like the CORDEX RCMs, both MRI models project statistically significant changes in temperature in the entire SA. The analysis of MRI's NHRCM projection on change in precipitation climatology indicates a statistically significant change for over 40% of the MSs in the SA (Mesta et al., 2022).

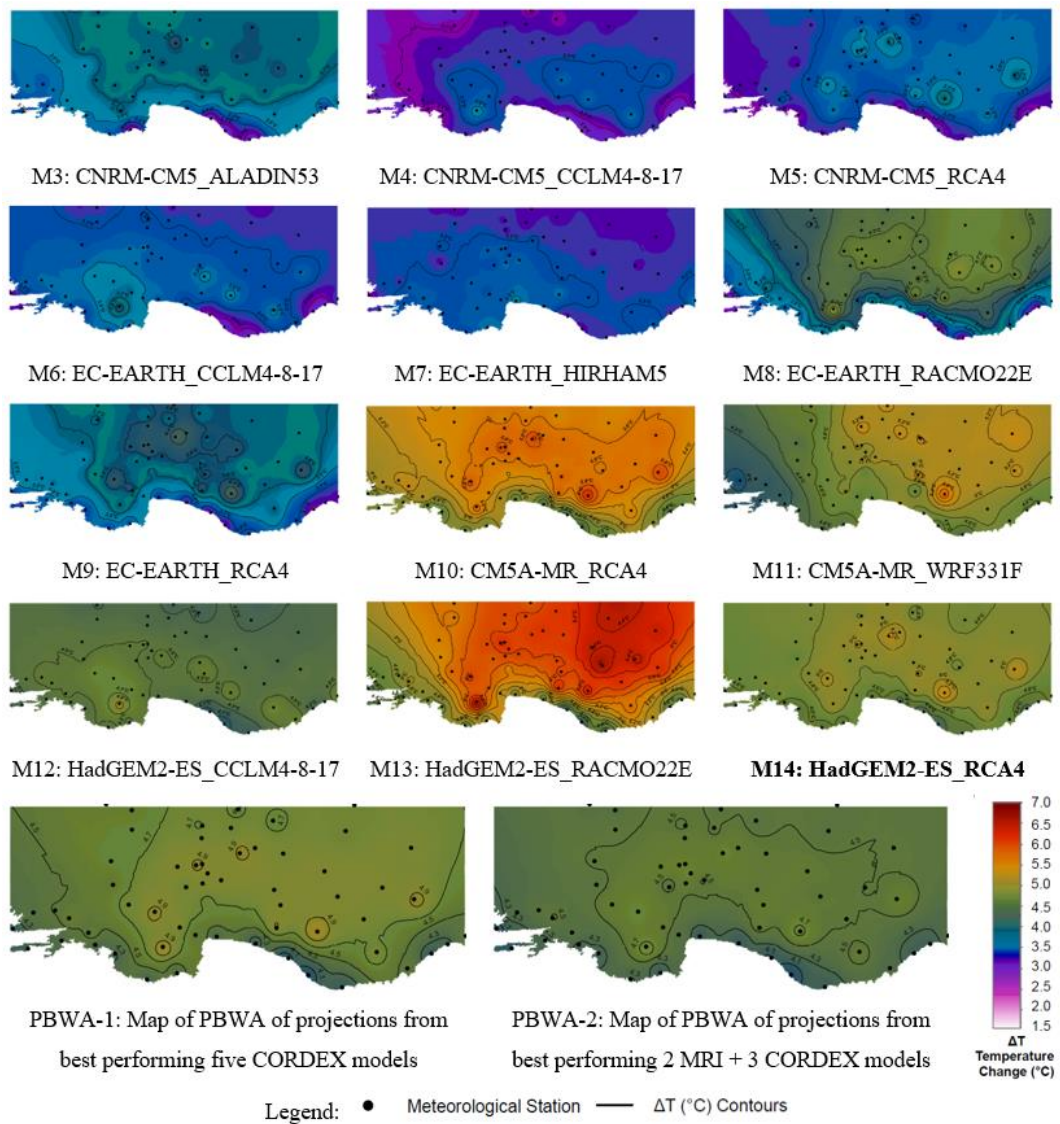


Fig. 11. Projections for temperature change, ΔT ($^{\circ}\text{C}$) in long-term future for RCP8.5 scenario (for models M3 through M14 all changes are statistically significant at the 95% confidence level).

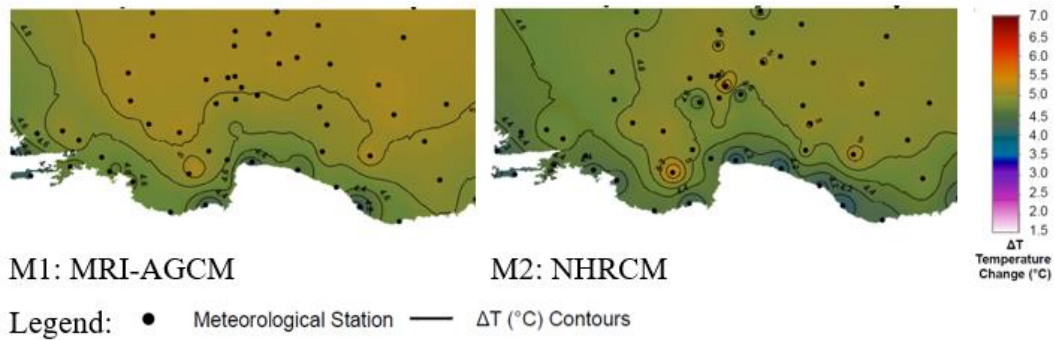


Fig. 12. Projections for temperature change, ΔT ($^{\circ}\text{C}$) in long-term future for RCP8.5 scenario for MRI climate models (for M1 and M2 all changes are statistically significant at the 95% confidence level).

Observation of the inter-model variability in projections shows that relative to other RCMs, among the ensemble members RACMO22E (with EC-EARTH and HadGEM2-ES boundary forcing) displays the highest spatial variability (as can be seen in Fig. 13) in the SA regarding the impact on temperature for all future periods under both scenarios. Additionally, RACMO22E projects the highest level of impact on temperature (Figs. 6 through 11) relative to other RCMs. Hence, it also projects for the most prominent difference in the temperature increase between inland and coastal areas (e.g., Fig. 11, M8, and M13 in comparison to other RCMs nested in the same GCM). On the other hand, HIRHAM5 and CCLM-4-8-17 project relatively lower spatial variability in the SA under both RCP4.5 and RCP8.5 (particularly evident in long-term projections in Figs. 9 and 10). Additionally, RACMO22E nested in EC-EARTH and HadGEM2-ES (M8 and M13) projects a higher difference between the impacts projected under RCP4.5 and RCP8.5 scenarios relative to other RCMs with the same driving GCMs (i.e., difference between Fig. 10 – 11 for long-term, and Fig. 8- 9 for medium-term displayed by M8 and M13 in comparison to other RCMs with same boundary forcing).

A gradual increase in temperature is expected by 2100 under both RCP4.5 and RCP8.5 scenarios across the entire SA. Although, under the RCP4.5 scenario, most of the models agree on a decline in the rate of increase in temperature (increase per

decade) for the second half of the century (i.e., long-term future period). Exceptions are CCLM4-8-17 (nested in CNRM-CM5) that projects a higher rate of increase for the long-term future compared to the medium-term future period for the entire SA, and HIRHAM5 (nested in EC-EARTH) projecting a slightly higher rate of increase for most of the MSs in the SA. For the remaining models, the rate of increase is expected to decline either for the majority or for the entire SA in the long term.

Under the RCP8.5 scenario, all models except for RCMs using HadGEM2-ES as driving GCM project a relatively higher rate of increase for the long-term period compared to the medium-term period for the entire SA. Among the RCMs nested in HadGEM2-ES, RACMO22E and RCA4 (M13 and M14) project a slightly weakened rate of increase for the long term. For CCLM4-8-17 (M12), the rate of increase is projected to be only slightly higher in the long-term period relative to the medium-term for the majority of the MSs. The rest of the models project a higher per decade rate of increase in temperature for more than half of or the entire SA.

The range of projections calculated for the member models in the ensemble for both RCP4.5 and RCP8.5 scenario for short-, medium- and long-term future are demonstrated by box plots provided in Fig. 13.

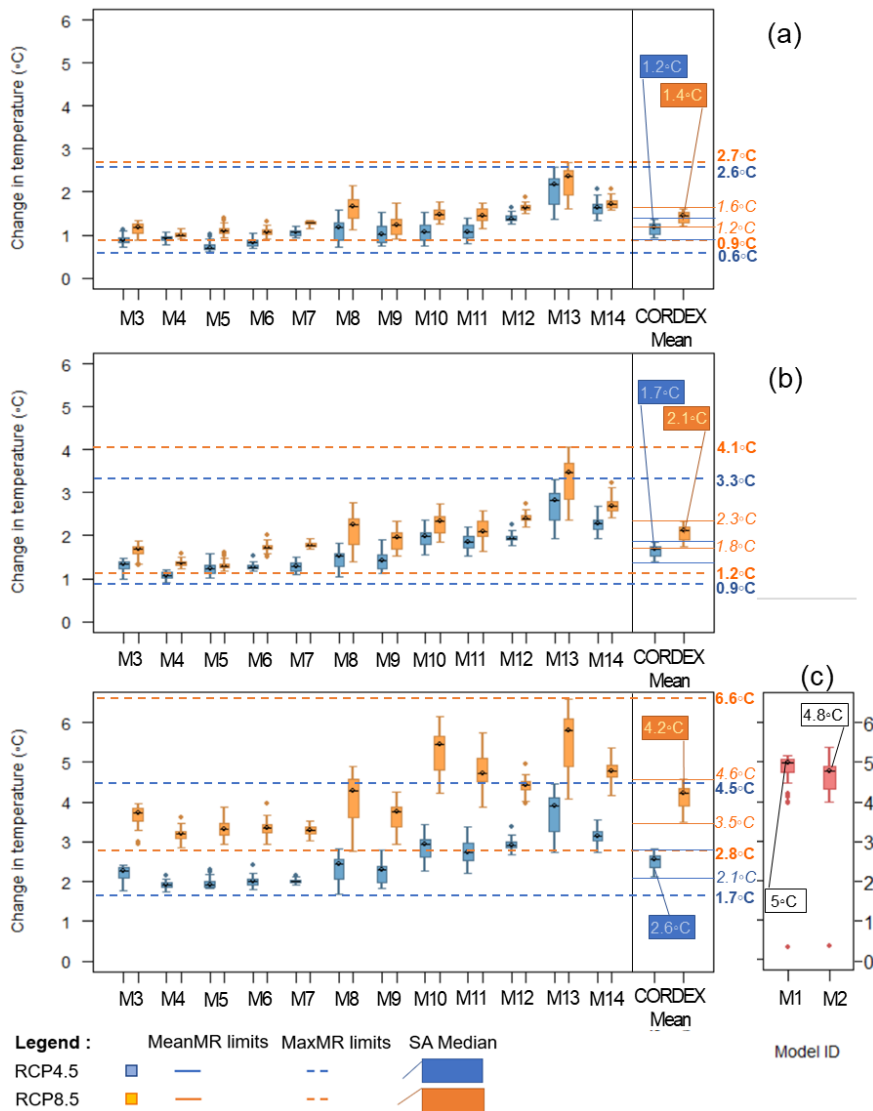


Fig. 13. Boxplot showing projected change in temperature climatology for (a) short-, (b) medium-, (c) long-term future under RCP4.5 and RCP8.5 scenarios (the box plots of MRI’s AGCM and NHRCM shown in (c) are only for the RCP8.5 scenario outputs. In (c) MRI’s AGCM and NHRCM are shown separately from the CORDEX RCMs because of the difference in the timeframe of projections. Upper and lower whisker boundaries of the boxplot are the largest data within 1.5 IQR (interquartile range) above the third quartile and smallest data within 1.5 IQR below the first quartile of the data set, respectively).

Regarding the inter-model variability, a significant divergence in the model setups of RCMs in the ensemble is due to different approaches to the forcing connected with changes in GHGs and aerosols in time. Except for RACMO22E and ALADIN53, CORDEX-RCMs do not include changing aerosol concentrations in the simulations. Therefore, simulations are based on constant aerosol forcings which may have an influence on the temperature projections (Sørland et al., 2020) due to the effect on the simulated solar radiation (Gutiérrez et al., 2020). Furthermore, HIRHAM5 and WRF331F do not include evolution in GHG forcing in time which is verified to have a statistically significant effect on the temperature projections (Jerez, 2018). The analysis of projections on temperature change from each ensemble member for both RCP4.5 and RCP8.5 scenarios (using data series of mean temperature at all MSs) indicates, except for RACMO22E, none of the ensemble members generates outliers (outside ensemble range of $\mu \pm 2\sigma$, where μ : ensemble mean value and σ : ensemble standard deviation). On the other hand, RACMO22E (nested in HadGEM2-ES) has the highest projections for temperature increase in the SA that form outlier values for the majority of the MSs for both scenarios in the short- and medium-term future and for the RCP4.5 scenario in the long-term future. The analysis of the future time-series of annual mean temperature for outliers with respect to the ensemble is provided in Supplementary Material (Appendix B).

Fig. 14 shows the average temperature change with respect to the historic period at each basin and at the entire study area projected by the mean of 12 CORDEX RCMs and two MRI models for short-, medium- and long-term future. Accordingly, a gradual increase in temperature is projected for both RCP4.5 and RCP8.5 scenarios by the end of the century. Four of the inland basins (Konya, Akarcay, Burdur, and Sakarya basins) located behind the topographical boundary formed by the Taurus Mountains are projected to have a slightly higher temperature increase than the general average of the study area for both scenarios and throughout the entire century from short- to long-term. Nevertheless, as it is seen in Fig. 14 similar rate of increase is expected for the \overline{AT} at all basins in the SA particularly for the RCP4.5 scenario. The increase in the \overline{AT} at the SA and at the basins located in it is seen to be

approximately 1°C above the global mean temperature increase demonstrated by AR6 of IPCC for the long-term (2081-2100) compared to the 1850-1900 period under the RCP4.5 scenario (IPCC, 2021). Projections on increase in temperature mean under the RCP8.5 scenario in the SA by the end of the century are similar to the global mean temperature increase defined in AR6 of IPCC for the long-term (2081-2100) compared to the 1850-1900 period (IPCC, 2021).

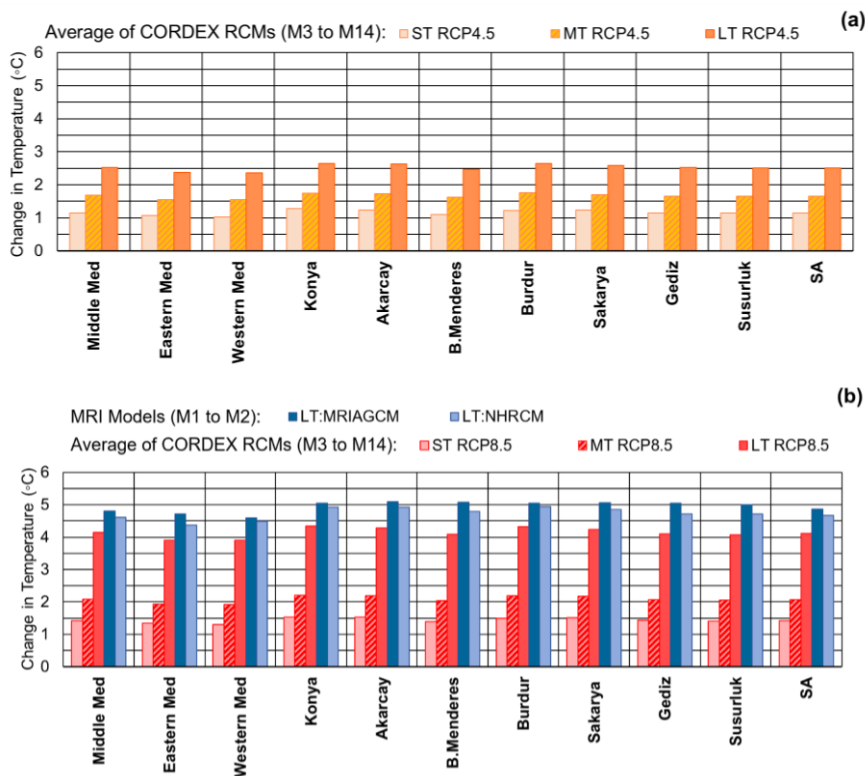


Fig. 14. Comparison of the areal average of short-, medium- and long-term projections on change in temperature with respect to the historic period at basins in the SA (a) for RCP4.5, (b) for RCP8.5.

The amplified temperature increase in inland regions with continental climate characteristics is expected to be the result of the intensification of drought conditions in the area. The soil moisture acts as a control in the sensible to latent heat flux ratio particularly for dry climates and transitional climates between dry and wet (Seneviratne et al., 2010). Increased dryness decreases the latent heat flux and the

cooling effect of evaporation but increases the sensible heat flux that in turn escalates the surface temperature. Haarsma et al. (2009) in their study verified elevated surface air temperature in the Mediterranean region causes decline in latent heat flux although the surface solar radiation in the region remains relatively stable. The increase is related to low soil moisture in semi-arid conditions of the Mediterranean region (Haarsma et al., 2009). The control of soil moisture and climate change-induced dryness is verified to have a strong effect on mean temperature and even on mean precipitation; however, the findings for precipitation are with higher uncertainty (Seneviratne et al., 2013). For areas such as Central Anatolia with semi-arid steppe climate, evapotranspiration is very limited but also closely correlated with the soil moisture. Decrease in soil moisture due to increasing temperature forms positive feedback for the elevated temperatures (Haarsma et al., 2009; Seneviratne et al., 2010, 2013; Byrne and O’Gorman, 2018; Selten et al., 2020). Due to limited evapotranspiration, offset of the drop in soil moisture by enhanced precipitation is not possible. Furthermore, for transitional soil moisture regime or climate (between dry and wet) conditions, soil moisture plays an even more critical role in increasing climate variability (Seneviratne et al., 2013). Hence, projections for aggravated temperature increase in inland areas and the pattern of the intra-regional variability of impact on surface air temperature in the study area, that is particularly displayed by RACMO22E, RCA4, WRF331F, ALADIN53, MRI-AGCM, and NHRCM follow the influence of major local climate drivers.

4.3. Comparison of changes in temperature and precipitation climatologies

The potential short-, medium- and long-term changes in precipitation in the SA have been previously studied in Mesta et al. (2022). The correlation between potential change in temperature and percent change in precipitation according to the average of 12 CORDEX RCMs, and NHRCM as the areal average of each basin under RCP 4.5 and 8.5 scenarios are examined through the graph in Fig. 15. The relation between change in precipitation and temperature in the long term according to the projection of MRI-AGCM is given in Fig. 16.

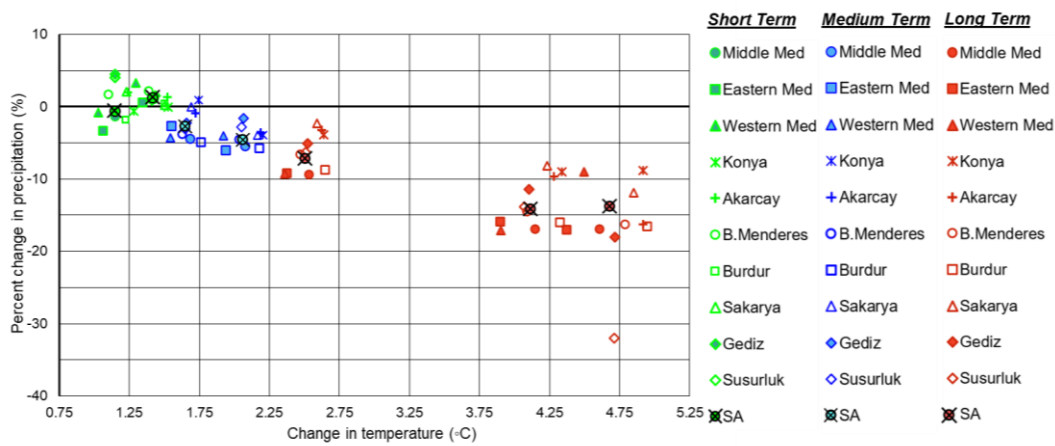


Fig. 15. Areal average changes at basins in the SA projected for short-, medium, and long-term future according to the average projection of 12 CORDEX models, and individual projection of NHRCM (Both RCP4.5 and RCP8.5 projections for the same basin are shown with the same symbol and color).

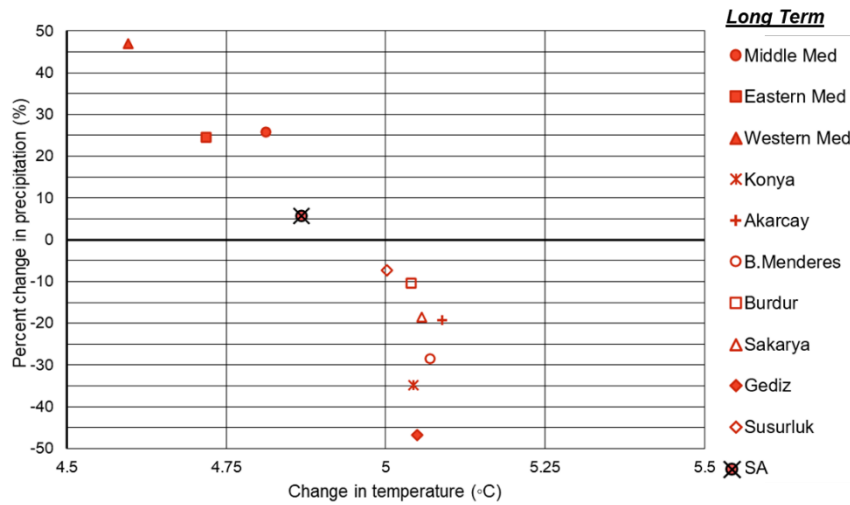


Fig. 16. Areal average changes at basins in the SA long-term future under RCP8.5 scenario according to the MRI-AGCM.

As it is seen in Fig. 15, all RCMs project an inverse linear relationship between temperature and precipitation change at basins and on average of the entire SA. In the long-term future, precipitation is projected to decrease while temperature is projected to increase at all the sub-basins. These two simultaneous changes in climate may cause amplified stress on the water resources of the SA. The results of short-, medium- and long-term projections in precipitation and temperature demonstrates the need of tiered adaptation measures to climate change.

The projections of MRI-AGCM indicate an increase both for precipitation and temperature in long-term for the Mediterranean region of Turkey including West, Middle, and East Mediterranean basins, stretching along the Mediterranean coastline (see Fig. 16). On the other hand, for inland basins around 5°C temperature increase concurrent to various levels of decrease in precipitation in the range of 5 to 50% is projected. The projections by MRI-AGCM are explained by a potential increase in precipitation due to elevated evapotranspiration for the coastal areas where the relative moisture is generally higher. However, the precipitation in areas where semi-

arid continental climate features prevail is expected to drop even more due to the depletion of soil moisture.

5. Conclusions

The analysis of a 14-member ensemble for the simulation skills verified better performance to replicate the spatial variability of annual temperature climatology in the SA for two RCMs (RCA4 and CCLM4-8-17) nested in HadGEM2-ES. This complies with the findings by Aziz et al. (2020) that showed the better skill of two models in the replication of mean daily temperature climatology regarding the regional averages for the Mediterranean, Aegean, and Central Anatolia regions of Turkey. In our study two high-resolution MRI climate models, NHRCM nested on MRI-AGCM and MRI-AGCM without downscaling also show high simulation skills. Although it should be noted that among the driving GCMs used in this study MRI-AGCM uses prescribed observation-based SST that eliminates potential biases in SST, unlike other CMIP5 GCMs.

The RCMs using EC-EARTH as the driving model show varying performance skills for temperature, while CNRM-CM5 as the driving model produced a relatively poor performance for the SA. For RCMs with CM5A-MR forcing, simulation performances are found not to be either significantly strong or weak relative to other models, although according to the analysis by McSweeney et al. (2015) CM5A-MR was shown to have weak performance particularly for the replication of the annual temperature and precipitation cycles in the Mediterranean. Regarding other driving GCMs in our study, McSweeney et al. (2015) also found that CNRM-CM5, EC-EARTH, HadGEM2-ES are satisfactory for the simulation in the EURO domain regarding the replication of the annual cycles of temperature and precipitation, circulation patterns, and storm tracks. Nevertheless, the poor performance of CNRM-CM5 as driving GCM for simulation of our SA temperature is interpreted to be connected to the technical problem in the model related to the boundary forcing conditions (EURO-CORDEX, 2021). Furthermore, unlike other driving GCMs in

this study, CNRM-CM5 do not include forcing for land-use change (Collins et al. 2013; Boé et al., 2020) which may be another factor for its relatively weak performance particularly considering that none of the CORDEX RCMs in this study includes forcing of land cover changes (Boé et al., 2020).

The analysis of potential change in annual mean temperature for short-, medium-, and long- term future demonstrated a statistically significant temperature increase by the end of the 21st century for the entire SA and for all three future periods under both moderate (RCP4.5) and high (RCP8.5) CO₂ emission scenarios. For both scenario conditions and in all three future periods RACMO22E, RCA4, WRF331F, ALADIN53, MRI-AGCM, and NHRCM are seen to project a more pronounced increase in annual temperature for inland parts of the SA compared to the coastal parts. This is considered to be connected with the influence of the Mediterranean (and Aegean) Sea and the dry climate in inland regions which is most pronounced in the Central Anatolia region with very low annual mean precipitation (<1mm/d) (Mesta et al., 2022).

All models in the 14 member ensemble agree on a gradual and statistically significant increase in temperature under both RCP4.5 and RCP8.5 scenarios across the entire SA. Under the RCP4.5 scenario, most of the models indicate a decline in the rate of increase in temperature (increase per decade) for the long term in the second half of the century, whereas under the RCP8.5 scenario, models mostly show a relatively higher rate of increase for the long-term period compared to the medium-term period.

Based on the average of 12 CORDEX RCMs, under the RCP4.5 scenario, a likely increase in the areal average of temperature means (\overline{AT}) of is projected for the in the entire SA as 1.2°C, 1.6°C, and 2.5°C for short-, medium-, and long-term future, respectively. The likely temperature increase under the RCP8.5 scenario is 1.4°C, 2.1°C, and 4.1°C for the short-, medium-, and long-term future, respectively. Additionally, MRI's MRI-AGCM and NHRCM project 4.9°C, and 4.7°C increase in the areal average of \overline{AT} in the study area for 20 years period at the end of 21st century.

Combined analysis of the projections on the increase in temperature and decrease in percent precipitation on basins in the SA supports an inverse linear relationship. Hence, climate change is expected to amplify drought particularly in inland basins with increased temperature due to the prevailing dry climate.

Based on the findings from the study;

- The analysis indicates variability in the simulation skills of 14 climate models for the study area regarding the spatial variability of temperature climatology.
- The multi-model ensemble analysis verifies a gradual increase in the temperature by 2100 under both RCP4.5 and RCP8.5 scenarios at the entire study area.
- Under the RCP4.5 scenario, most models in the ensemble agree that the warming will continue, although the rate of increase is expected to diminish. On the other hand, for the RCP8.5 scenario, the projections mostly agree on an increase with an even more elevated rate at the second half of the 21st century.
- The temperature increase at the inland basins is likely to be more pronounced than the coastal areas, which is interpreted to be connected to the drying effect of climate change.
- The simultaneous decrease in precipitation with the increase in temperature at all basins in the SA is expected to aggravate the impacts on water resources in the SA which necessitate tiered adaptation measures to be put into use.

CRedit authorship contribution statement

Buket Mesta: Conceptualization, methodology, data curation, formal analysis, validation, writing - original draft, funding acquisition

Hidetaka Sasaki: Methodology, writing – review & editing, project administration, funding acquisition

Tosiyuki Nakaegawa: Methodology, writing – review & editing, project administration, funding acquisition

Elçin Kentel: Conceptualization, methodology, writing – review & editing, supervision, project administration, funding acquisition

Declaration of Competing Interest

The authors declare that they have no known competing financial interests or personal relationships that could have appeared to influence the work reported in this paper.

Acknowledgements

The authors thank the Scientific and Technological Research Council of Turkey, TUBITAK, and Japan Society for the Promotion of Science, JSPS [Grant Number JPJSBP12019940], for supporting this bilateral research collaborations. The work for the generation of NHRCM simulations was supported by the Integrated Research Program for Advancing Climate Models (TOUGOU) [Grant Number JPMXD0717935561] from the Ministry of Education, Culture, Sports, Science, and Technology (MEXT) of Japan. The research leading to these results is funded by the Scientific and Technological Research Council of Turkey (TÜBİTAK) the project “Assessment of Climate Change Impacts on Streamflow and Hydropower in Antalya, Turkey” [Grant Number 118Y365].

Appendix A. Supplementary data

Supplementary data to this article can be found in the attached file (Appendices_SupplementaryData.docx)

References

- Acar Deniz, Z.A., Gönençgil, B., 2015. Trends of summer daily maximum temperature extremes in Turkey. *Physical Geography*. 36(4), 268-281. <https://doi.org/10.1080/02723646.2015.1045285>.
- Altın, T. B., Barak, B., 2017. Trends and changes in tropical and summer days at the Adana Sub-Region of the Mediterranean Region, Southern Turkey. *Atmospheric Research*. 196, 182-199.
- Aziz, R., Yucel, I., Yozgatligil, C., 2020. Nonstationarity impacts on frequency analysis of yearly and seasonal extreme temperature in Turkey. *Atmospheric Research*. 238, 104875.
- Bağçacı, S. Ç., Yucel, I., Duzenli, E., Yilmaz, M. T., 2021. Intercomparison of the expected change in the temperature and the precipitation retrieved from CMIP6 and CMIP5 climate projections: A Mediterranean hot spot case, Turkey. *Atmospheric Research*. 256, 105576.
- Bartolini, G., Di Stefano, V., Maracchi, G., Orlandini, S., 2012. Mediterranean warming is especially due to summer season. *Theoretical and Applied Climatology*. 107(1), 279-295.
- Beck, H.E., Zimmermann, N.E., McVicar, T.R., Vergopolan, N., Berg, A., Wood, E.F., 2018. Present and future Köppen-Geiger climate classification maps at 1-km resolution. *Sci. Data*. 5:180214. <https://doi:10.1038/sdata.2018.214>.
- Boé, J., Somot, S., Corre, L., Nabat, P., 2020. Large discrepancies in summer climate change over Europe as projected by global and regional climate models: causes and consequences. *Climate Dynamics*. 54(5), 2981-3002.

- Bucak, T., Trolle, D., Tavşanoğlu, Ü. N., Çakıroğlu, A. İ., Özen, A., Jeppesen, E., Beklioğlu, M., 2018. Modeling the effects of climatic and land use changes on phytoplankton and water quality of the largest Turkish freshwater lake: Lake Beyşehir. *Sci. Total Environ.* 621, 802–816. doi:10.1016/j.scitotenv.2017.11.258.
- Byrne, M. P., & O’Gorman, P. A., 2018. Trends in continental temperature and humidity directly linked to ocean warming. *Proceedings of the National Academy of Sciences.* 115(19), 4863-4868.
- Cagatan, K., Unal, Y., 2010, May. Heat Wave Tendency in the Western Part of Turkey and Its Relation to Circulation Patterns. In EGU General Assembly Conference Abstracts (p. 8507).
- Collins, M., Knutti, R., Arblaster, J., Dufresne, J.-L., Fichet, T., Friedlingstein, P., Gao, X., Gutowski, W.J., Johns, T., Krinner, G., Shongwe, M., Tebaldi, C., Weaver, A.J., and Wehner, M., 2013. Long-term climate change: Projections, commitments and irreversibility, in: *Climate Change 2013: The Physical Science Basis. Contribution of Working Group I to the Fifth Assessment Report of the Intergovernmental Panel on Climate Change.* T.F. Stocker, D. Qin, G.-K. Plattner, M. Tignor, S.K. Allen, J. Doschung, A. Nauels, Y. Xia, V. Bex, and P.M. Midgley, Eds. Cambridge University Press, pp. 1029-1136, doi:10.1017/CBO9781107415324.024.
- Deidda, R., Marrocu, M., Caroletti, G., Pusceddu, G., Langousis, G., Langousis, A., Lucarini, V., Puliga, M., Speranza, A., 2013. Regional climate models’ performance in representing precipitation and temperature over selected Mediterranean areas. *Hydrol. Earth Syst. Sci.* 17, 5041–5059. <https://doi.org/10.5194/hess-17-5041-2013>.
- Demircan, M., Gürkan, H., Eskioğlu, O., Arabacı, H., Coşkun, M., 2017. Climate Change Projections for Turkey: Three Models and Two Scenarios. *Turkish Journal of Water Science & Management.* 1(1), 22-43.

- Dino, I.G., Akgül, C.M., 2019. Impact of climate change on the existing residential building stock in Turkey: an analysis on energy use, greenhouse gas emissions and occupant comfort. *Renew. Energy*. 141, 828–846. <https://doi.org/10.1016/j.renene.2019.03.150>.
- Efthymiadis, D., Goodess, C. M., Jones, P. D., 2011. Trends in Mediterranean gridded temperature extremes and large-scale circulation influences. *Natural Hazards and Earth System Sciences*. 11(8), 2199-2214.
- Erlat, E., Türkeş, M., Aydın-Kandemir, F., 2021. Observed changes and trends in heatwave characteristics in Turkey since 1950. *Theoretical and Applied Climatology*. 145(1), 137-157.
- EURO-CORDEX, 2021. EURO-CORDEX Errata Page, Errata Table. <https://www.euro-cordex.net/078730/index.php.en> (accessed 21 December 2021).
- Fujihara, Y., Tanaka, K., Watanabe, T., Nagano, T., Kojiri, T., 2008. Assessing the impacts of climate change on the water resources of the Seyhan River Basin in Turkey: use of dynamically downscaled data for hydrologic simulations. *J. Hydrol.* 353, 33–48.
- Giorgi, F., 2006. Climate change hot-spots. *Geophys. Res. Lett.* 33, 1–4. <https://doi.org/10.1029/2006GL025734>.
- Giorgi, F., Lionello, P., 2008. Climate change projections for the Mediterranean region. *Glob. Planet. Chang.* 63, 90–104. <https://doi.org/10.1016/j.gloplacha.2007.09.005>.
- Gönençgil, B., Acar Deniz, Z. A., 2016. Extreme maximum and minimum air temperature in Mediterranean coasts in Turkey. *Geography, Environment, Sustainability*. 9(1), 59-70. https://doi.org/10.15356/2071-9388_01v09_2016_05.
- Gutiérrez, C., Somot, S., Nabat, P., Mallet, M., Corre, L., van Meijgaard, E., ... & Gaertner, M. Á., 2020. Future evolution of surface solar radiation and

photovoltaic potential in Europe: investigating the role of aerosols. *Environmental Research Letters*. 15(3), 034035.

Haarsma, R. J., Selten, F., Hurk, B. V., Hazeleger, W., Wang, X., 2009. Drier Mediterranean soils due to greenhouse warming bring easterly winds over summertime central Europe. *Geophysical research letters*. 36(4).

IPCC, 2021. *Climate Change 2021: The Physical Science Basis. Contribution of Working Group I to the Sixth Assessment Report of the Intergovernmental Panel on Climate Change*, in: Masson-Delmotte, V., P. Zhai, A. Pirani, S.L. Connors, C. Péan, S. Berger, N. Caud, Y. Chen, L. Goldfarb, M.I. Gomis, M. Huang, K. Leitzell, E. Lonnoy, J.B.R. Matthews, T.K. Maycock, T. Waterfield, O. Yelekçi, R. Yu, and B. Zhou (eds.). Cambridge University Press. In Press.

Jerez, S., L'opez-Romero, J.M., Turco, M., Jim'enez-Guerrero, P., Vautard, R., Mont'avez, J.P., 2018. Impact of evolving greenhouse gas forcing on the warming signal in regional climate model experiments. *Nat. Commun.* 9 (1), 1–7.

Kitoh, A., Ose, T., Kurihara, K., Kusunoki, S., Sugi, M., KAKUSHIN Team-3 Modeling Group, 2009. Projection of changes in future weather extremes using super-highresolution global and regional atmospheric models in the KAKUSHIN Program: results of preliminary experiments. *Hydrol. Res. Lett.* 3, 49–53. <https://doi.org/10.3178/HRL.3.49>.

Kitoh, A., Ose, T., Takayabu, I., 2016. Dynamical downscaling for climate projection with high-resolution MRI AGCM - RCM. *J. Meteorol. Soc. Jpn.* 94A, 1–16. <https://doi.org/10.2151/jmsj.2015-022>.

Kostopoulou, E., Jones, P. D., 2005. Assessment of climate extremes in the Eastern Mediterranean. *Meteorology and Atmospheric Physics*. 89(1), 69-85.

Kostopoulou, E., Giannakopoulos, C., Hatzaki, M., Karali, A., Hadjinicolaou, P., Lelieveld, J., Lange, M. A., 2014. Spatio-temporal patterns of recent and

- future climate extremes in the eastern Mediterranean and Middle East region. *Natural Hazards and Earth System Sciences*. 14(6), 1565-1577.
- Kuglitsch, F. G., Toreti, A., Xoplaki, E., Della-Marta, P. M., Zerefos, C. S., Türkeş, M., Luterbacher, J., 2010. Heat wave changes in the eastern Mediterranean since 1960. *Geophysical Research Letters*. 37(4).
- Kusunoki, S., Nakaegawa, T., Pinzón, R., Sanchez-Galan, J.E., F'abrega, J.R., 2019. Future precipitation changes over Panama projected with the atmospheric global model MRI-AGCM3. 2. *Clim. Dyn.* 53 (7), 5019–5034.
- Lelieveld, J., Hadjinicolaou, P., Kostopoulou, E., Chenoweth, J., El Maayar, M., Giannakopoulos, C., Hannides, C., Lange, M. A., Tanarhte, M., Tyrllis, E., Xoplaki, E., 2012. Climate change and impacts in the Eastern Mediterranean and the Middle East. *Climatic change*. 114(3), 667-687.
- Lionello, P., Malanotte-Rizzoli, P., Boscolo, R., Alpert, P., Artale, V., Li, L., Luterbacher, J., May, W., Trigo, R., Tsimplis, M., Ulbrich, U., Xoplaki, E., 2006. In: Lionello, P., Malanotte-Rizzoli, P., Boscolo, R. (Eds.), *The Mediterranean Climate: An Overview of the Main Characteristics and Issues*, 4. *Mediterranean Climate Variability*. p. 438.
- McSweeney, C.F., Jones, R.G., Lee, R.W., Rowell, D.P., 2015. Selecting CMIP5 GCMs for downscaling over multiple regions. *Clim. Dyn.* 44 (11), 3237–3260.
- Mehr, A.D., Kahya, E., 2017. Climate change impacts on catchment-scale extreme rainfall variability: case study of Rize Province, Turkey. *J. Hydrol. Eng.* 22 (3), 1–11. [https://doi.org/10.1061/\(ASCE\)HE.1943-5584.0001477](https://doi.org/10.1061/(ASCE)HE.1943-5584.0001477).
- Mesta, B., Sasaki, H., Nakaegawa, T., Kentel, E., 2022. Changes in precipitation climatology for the Eastern Mediterranean using CORDEX RCMs, NHRCM and MRI-AGCM. *Atmospheric Research*. 106140.
- Mizuta, R., Oouchi, K., Yoshimura, H., Noda, A., Katayama, K., Yukimoto, S., Hosaka, M., Kusunoki, S., Kawai, H., Nakagawa, M., 2006. 20-km-mesh

- global climate simulations using JMA-GSM model - mean climate states. *J. Meteorol. Soc. Jpn.* 84 (1), 165–185.
- Nakaegawa, T., Kitoh, A., Kusunoki, S., Murakami, H., Arakawa, O., 2014. Hydroclimate change over Central America and the Caribbean in a global warming climate projected with 20-km and 60-km mesh MRI atmospheric general circulation models. *Pap. Meteorol. Geophys.* 65, 15.
- Nakaegawa, T., Hibino, K., Takayabu, I., 2017. Identifying climate analogues for cities in Australia by a non-parametric approach using multi-ensemble, high-horizontal resolution future climate projections by an atmospheric general circulation model, MRI-AGCM3. 2H. *Hydrol. Res. Lett.* 11 (1), 72–78.
- Önol, B., Unal, Y. S., 2014. Assessment of climate change simulations over climate zones of Turkey. *Regional Environmental Change.* 14(5), 1921-1935.
- Özdoğan, M., 2011. Modeling the impacts of climate change on wheat yields in Northwestern Turkey. *Agriculture, Ecosystems and Environment.* 141, 1-12. doi:10.1016/j.agee.2011.02.001
- Öztürk, T., Ceber, Z.P., Türkes, M., Kurnaz, M.L., 2015. Projections of climate change in the Mediterranean Basin by using downscaled global climate model outputs. *Int. J. Climatol.* 35, 4276–4292. <https://doi.org/10.1002/joc.4285>.
- Pinzón, R.E., Hibino, K., Takayabu, I., Nakaegawa, T., 2017. Virtually experiencing future climate changes in Central America with MRI-AGCM: climate analogues study. *Hydrol. Res. Lett.* 11 (2), 106–113. <https://doi.org/10.3178/hrl.11.106>.
- Saito, K., Fujita, T., Yamada, Y., Ishida, J.-I., Kumagai, Y., Aranami, K., Ohmori, S., Nagasawa, R., Kumagai, S., Muroi, C., Kato, T., Eito, H., Yamazaki, Y., 2006. The Operational JMA Nonhydrostatic Mesoscale Model. *Monthly Weather Review.* 134, 1266-1298.

- Sasaki, H., Kurihara, K., 2008. Relationship between precipitation and elevation in the present climate reproduced by the non-hydrostatic regional climate model. SOLA. 4, 109–112.
- Sasaki, H., Kurihara, K., Takayabu, I., Uchiyama, T., 2008. Preliminary experiments of reproducing the present climate using the non-hydrostatic regional climate model. SOLA. 4, 025–028. <https://doi.org/10.2151/sola.2008-007>.
- Sasaki, H., Murata, A., Hanafusa, M., Oh'izumi, M., Kurihara, K., 2011. Reproducibility of present climate in a non-hydrostatic regional climate model nested within an atmosphere general circulation model. SOLA. 7, 173–176.
- Sasaki, H., Murata, A., Hanafusa, M., Oh'izumi, M., Kurihara, K., 2012. Projection of future climate change in a non-hydrostatic regional climate model nested within an atmospheric general circulation model. SOLA. 8, 53–56.
- Sasaki, H., Kurihara, K., Murata, A., Hanafusa, M., Oh'izumi, M., 2013. Future changes of snow depth in a non-hydrostatic regional climate model with bias correction. SOLA. 9, 5–8.
- Selten, F. M., Bintanja, R., Vautard, R., & van den Hurk, B. J. J. M., 2020. Future continental summer warming constrained by the present-day seasonal cycle of surface hydrology. *Scientific reports*. 10(1), 1-7.
- Sen, B., Topcu, S., Türkeş, M., Sen, B., Warner, J.F., 2012. Projecting climate change, drought conditions and crop productivity in Turkey. *Clim. Res.* 52, 175–191. <https://doi.org/10.3354/cr01074>.
- Seneviratne, S. I., Corti, T., Davin, E. L., Hirschi, M., Jaeger, E. B., Lehner, I., Orlowsky, B., Teuling, A. J., 2010. Investigating soil moisture–climate interactions in a changing climate: A review. *Earth Sci. Rev.*, 99(3-4), 125–161. <https://doi.org/10.1016/j.earscirev.2010.02.004>.
- Seneviratne, S. I., Wilhelm, M., Stanelle, T., van den Hurk, B., Hagemann, S., Berg, A., Cheruy, F., Matthew, E., Higgins, M.E., Meier, A., Brovkin, V.,

- Claussen, M., Ducharne, A., Dufresne, J.L., Findell, K.L., Ghattas, J., Lawrence, D.M., Malyshev, S., Rummukainen, M., Smith, <https://agupubs.onlinelibrary.wiley.com/doi/full/10.1002/grl.50956>
B., 2013. Impact of soil moisture-climate feedbacks on CMIP5 projections: First results from the GLACE-CMIP5 experiment. *Geophysical Research Letters*. 40(19), 5212–5217. <https://doi.org/10.1002/grl.50956>
- Sensoy, S., Demircan, M., Ulupinar, Y., Balta, I., 2008. Climate of Turkey. Turkish State Meteorological Service, 401. http://212.174.109.9/FILES/genel/makale/31_climateofturkey.pdf.
- Sensoy, S., Demircan, M., 2016. Climate of Turkey. Turkish State Meteorological Service, Ankara, Turkey. https://www.researchgate.net/publication/296597022_Climate_of_Turkey.
- Sørland, S. L., Fischer, A. M., Kotlarski, S., Künsch, H. R., Liniger, M. A., Rajczak, J., ... & Knutti, R., 2020. CH2018–National climate scenarios for Switzerland: How to construct consistent multi-model projections from ensembles of opportunity. *Climate Services*. 20, 100196.
- Sunyer Pinya, M.A., Hundecha, Y., Lawrence, D., Madsen, H., Willems, P., Martinkova, M., Vormoor, K., Bürger, G., Hanel, M., Kriaučiuniene, J., Loukas, A., Osuch, M., Yücel, I., 2015. Inter-comparison of statistical downscaling methods for projection of extreme precipitation in Europe. *Hydrol. Earth Syst. Sci.* 19 (4), 1827–1847. <https://doi.org/10.5194/hess-19-1827-2015>.
- Tanarhte, M., Hadjinicolaou, P., Lelieveld, J., 2015. Heat wave characteristics in the eastern Mediterranean and Middle East using extreme value theory. *Climate Research*. 63(2), 99-113.
- Tayanç, M., İm, U., Doğruel, M., Karaca, M., 2009. Climate change in Turkey for the last half century. *Climatic Change*. 94(3), 483-502.

- Toros, H., 2012. Spatio-temporal variation of daily extreme temperatures over Turkey. *International Journal of Climatology*. 32(7), 1047-1055.
- Unal, Y. S., Tan, E., Montes, S.S., 2013. Summer heat waves over western Turkey between 1965 and 2006. *Theoretical and Applied Climatology*. 112(1), 339-350.
- Varghese, S.J., Surendran, S., Rajendran, K., Kitoh, A., 2020. Future projections of Indian Summer Monsoon under multiple RCPs using a high resolution global climate model multiforcing ensemble simulations. *Clim. Dyn.* 54, 1315–1328. <https://doi.org/10.1007/s00382-019-05059-7>.
- Yilmaz, A.G., 2015. The effects of climate change on historical and future extreme rainfall in Antalya, Turkey. *Hydrol. Sci. J.* 60 (12), 2148–2162. <https://doi.org/10.1080/02626667.2014.945455>.
- Zampieri, M., D'andrea, F., Vautard, R., Ciais, P., de Noblet-Ducoudré, N., Yiou, P., 2009. Hot European summers and the role of soil moisture in the propagation of Mediterranean drought. *Journal of Climate*. 22(18), 4747-4758.
- Zittis, G., Hadjinicolaou, P., Fnais, M., Lelieveld, J., 2016. Projected changes in heat wave characteristics in the eastern Mediterranean and the Middle East. *Regional environmental change*. 16(7), 1863-1876.

**D. PAPER 4: IMPROVING PRECIPITATION ESTIMATES FOR TURKEY
WITH MULTIMODEL ENSEMBLE: A COMPARISON OF
NONLINEAR ARTIFICIAL NEURAL NETWORK METHOD WITH
LINEAR METHODS**

Buket Mesta¹, O. Burak Akgun², Elcin Kentel^{2*}

¹Middle East Technical University, Department of Earth System Science, Ankara, Turkey

²Middle East Technical University, Department of Civil Engineering, Ankara, Turkey

*Corresponding Author: Middle East Technical University, Department of Civil Engineering, Water Resources Laboratory, K4 Bldg., 06800 Ankara, Turkey

Tel.: +90 312 210 5412

E-mail address: ekentel@metu.edu.tr

Abstract

Ensemble analysis is proven to provide advantages in climate change impact assessment based on outputs from climate models. Ensembled series are shown to outperform single model assessments through increased consistency and stability. This study aims to test the improvement of precipitation estimates through the use of ensemble analysis for south and southwestern Turkey that is known to have complex

climatic features due to varying topography and interacting climate forcings. The analysis covers an evaluation of the performance of eight regional climate models (RCMs) from EUR11 Domain available from the CORDEX database. The historical outputs are evaluated for their representativeness of the current climate of the Mediterranean region and its surroundings in Turkey through a comparison with long term monthly precipitation time series obtained from ground-based precipitation observations by the use of statistical performance indicators and Taylor Diagrams. This is followed by a comparative evaluation of three ensemble methodologies, Simple Average of the Models, Multiple Linear Regression for Superensemble, and Artificial Neural Networks (ANN). The analysis results show that the overall performance of ensembled time series is better compared to individual RCMs. ANN generally provided the best performance when all RCMs are used as inputs instead of selected three best performing RCMs. However, extreme events are poorly represented in the ensembled time series, and this may result in inefficient design of various water structures such as spillways and storm water drainage systems that are based on high return period events.

Key words: Precipitation, RCM, Artificial Neural Network, Multiple Linear Regression

1. Introduction

The Mediterranean region is expected to be affected most by climate change impacts (Gao and Giorgi, 2008). The Mediterranean basin including southern Europe, Anatolia, and the Middle East has a very complex topography resulting in a milder climate in coastal areas while inland Anatolia experiences extreme weather conditions (Sensoy, 2004). Moreover, the climate processes in that region are affected by teleconnections and regional processes, the interactions of which are not well understood (Hemming et al., 2010; Palatella et al., 2010). The local processes and the teleconnections (e.g., North Atlantic Oscillation, North Sea-Caspian) interacting those, the effects of the varying topography and the Mediterranean Sea itself create large inter-annual and intra-annual variability in the region which also shows significant spatial variability depending on local properties (Black, 2010; Hemming et al., 2010; Palatella et al., 2010; Bozkurt and Sen, 2011; Onol and Unal, 2014; Mascaro et al., 2018).

For the assessment of climate change impacts including impacts on hydrology, regional climate models (RCMs) with high resolution are used for local-scale assessments (Maharana et al., 2021) and for parameters such as precipitation that are mainly controlled by local processes, particularly for regions with a complex orography (Sunyer Pinya et al., 2015; Lun et al., 2021; Park et al., 2021). However, RCM outputs may contain systematic errors or biases (Stocker et al., 2015; Gutiérrez et al., 2019) due to the boundary conditions or imperfect conceptualization, discretization, and spatial averaging within grid cells (Fujihara et al., 2008; López - Moreno et al., 2008; Teutschbein and Seibert, 2012; Kara and Yucel, 2015). Furthermore, studies indicate uncertainties and significant inter-model variability for RCM outputs (López - Moreno et al., 2008; Sunyer Pinya et al., 2015) which are even more pronounced for regions with complex terrain features (Evans, 2009). Various factors such as the multiplicity of model designs or assumptions amplify the

variability and divergence in outputs, particularly for evaluations based on single models. Hence, the uncertainties and significant divergence in precipitation outputs by various climate models create challenges in impact assessment and planning for adaptation.

To overcome the limitations of the single model assessment in dealing with uncertainties multimodel ensemble (MME) assessment is preferred over single model assessments. MME approach has been used in various fields such as finance (Zhang and Berardi, 2001), ecology (Araújo and New, 2007), atmospheric air quality (Galmarini et al., 2004), streamflow forecasting (Ajami et al., 2006), weather prediction (Krishnamurti et al., 2000; Roebber et al., 2007), and for climate simulations (Kotlarski et al., 2014). Studies have shown that ensemble analysis helps to improve the statistical indicators relative to single model analysis, provides more consistency and reliability in simulations, and can enable a better understanding of uncertainties (Hagedorn et al., 2005; Tebaldi and Knutti, 2007; Sunyer Pinya et al., 2015; Vautard et al., 2021). The MME approach is based on the use of a set of models (Tebaldi and Knutti, 2007; Knutti et al., 2010) and it overcomes the disadvantages of single-model-based assessments by using different models with different mechanisms that eliminate or reduce poorly represented processes through better-represented processes from other models in the ensemble group.

The most common approach of MME is ensemble averaging. In this approach, weights are assigned to each member of the ensemble either equally to obtain a multimodel simple average (will be referred to as the simple average of the models, SAM) or according to some predefined criteria (e.g., weights for relative model performances or weights defined by certain statistical techniques) to obtain a multimodel weighted average (Giorgi and Mearns, 2002, 2003; Tebaldi and Knutti, 2007; Christensen et al., 2010).

A linear statistical MME approach, Superensemble (SE) method uses Multiple Linear Regression (MLR) to assign a suitable weight for each model to build an ensemble model with a minimized deviation from observations (Krishnamurti et al.,

1999; 2000; 2016; Stefanova and Krishnamurti, 2002). Studies verify that SE provides a better simulation efficiency than single models and SAM (Krishnamurti et al., 1999, 2000, 2016; Yun et al., 2005; Cane and Milelli, 2010) by providing a bias correction in ensembling. Comparison of SE with “individual bias removed ensemble mean” is reported to verify the better performance of SE providing a collective bias removal by assigning different weights on member models depending on the degree of convergence to observations (Krishnamurti et al., 1999, 2000; Yun et al., 2005). Sirdas et al. (2007) tested the efficiency of SE, for the Euro-Mediterranean region, by the use of monthly and seasonal forecasts of precipitation, sea surface temperature (SST), and surface air temperature (SAT) from 13 Global Climate Models (GCMs). The outputs obtained with the synthetic SE method for winter SST and SAT provided satisfactory results concerning the root mean square error (RMSE) and anomaly correlation (AC) coefficient values.

Another methodology for MME is the Artificial Neural Network (ANN) approach (Boulanger et al., 2006; 2007; Krasnopolsky and Lin, 2012; Fan et al., 2021) which is also frequently used for statistical downscaling of climate models (Mendes and Marengo, 2010; Kang et al., 2015; Okkan, 2015; Okkan and Inan, 2015; Campozano et al., 2016; Okkan and Kirdemir, 2016; Vu et al., 2016). For example, Campozano et al. (2016) compared the performances of two artificial intelligence methods, namely ANN and least squares support vector machines in downscaling of monthly precipitation, and the authors concluded that they performed equally well. Regarding the use of neural networks in MME, Boulanger et al. (2006, 2007) worked on the ensembling of seven Atmospheric-Ocean Global Circulation Models (AOGCMs). They used ANN and Bayesian statistics to attain MME with higher efficiency than single models for the simulations on temperature and precipitation in South America. Krasnopolsky and Lin (2012) developed an ANN model for MME of 24-hour precipitation forecasts and demonstrated improvements in the forecasts over Continental US. Furthermore, their findings verified superior results of the nonlinear ANN approach compared to the linear approaches (including MLR) in MME for forecasting. In a more recent study, Fan et al. (2021) used ANN to improve the

Climate Forecast System (CFS) of the US National Oceanic and Atmospheric Administration (NOAA) for week 3-4 precipitation and 2-meter air temperature forecasts. The study developed an ANN model for MME by the use of a set of predictors and the predictand. The study results revealed that MLR and ANN provided superior results over bias-adjusted CFS, and MME through ANN improved forecasts better than MLR in many aspects. However, despite improvements in forecasting skills through MME with ANN, some weaknesses regarding RMSE and AC skills are still notified (Fan et al., 2021).

Studies on local impacts of climate change regarding hydrology, crop yields, and reservoir inflows for various basins in Turkey use the benefit of the ensemble approach by including the SAM in the analysis (Kitoh, 2007; Ozdogan, 2011; Okkan and Inan, 2015). In their study, on climate change in Gediz Basin in western Turkey, Okkan and Kirdemir (2016) used a multi-GCM ensemble based on Bayesian Model Averaging (BMA) for 12 GCMs from Coupled Model Inter-comparison Project Phase 5 (CMIP5) after statistical downscaling with ANN and least squares support vector machine methods. In another study, Cakir et al. (2013) used historical records from 50 meteorological stations across Turkey to test the ANN ensemble approach for temperature. Their study verified that the ANN ensemble generates more accurate results compared to the simple bias-corrected ensemble mean. On the other hand, the study does not provide any evaluation for a comparison of the nonlinear ANN approach with the linear MLR approach and concludes the necessity of comparison for future studies.

To the best of our knowledge, the use of ANN for MME for the Mediterranean region is very limited and only a few studies are published on the use of ANN for ensemble analysis for Turkey. Moreover, for Turkey, there are still not many studies using multiple high-resolution CORDEX RCMs to evaluate relative model performances in comparison to MME. Therefore, the objective of our study is to evaluate the efficiency of ensemble analysis with the nonlinear ANN approach and to compare it with conventional linear MME methodologies, namely SAM and SE. The study uses CORDEX data of RCM outputs. The evaluation is done through comparison with

reference data from local stations in the south and southwestern Turkey that provide long-term daily precipitation time series. The comparison of the efficiencies of ANN, SAM, and SE showed that for most stations, correlation and normalized root-mean-square difference (RMSD) values improved by MME compared to the best performing individual RCM and the ANN approach showed relatively best skills, in general. However, certain weaknesses to represent the variability of precipitation due to the reduction of the extreme or low-frequency events are also detected for ANN, SAM, and SE through the analysis.

2. Case Study

2.1. Study Area

In this study, the historical simulation results of eight RCMs are used for the multimodel ensemble analysis. This paper makes a comparison of the efficiency of the linear and nonlinear ANN ensembling methodologies relative to the individual raw RCM outputs regarding the replication of the historical precipitation. For the analysis, the observed and simulated daily total precipitation for 14 meteorological stations (MSs) throughout south and southwestern Turkey including the Mediterranean coast and its hinterland are used (Figure 1). The meteorological stations are selected from different climatologic regions (i.e., coastal and inland Mediterranean, inland Aegean and Central Anatolian regions) and major basins of Turkey to assess the potential effect of spatial differences. The characteristics of these MSs are given in Table 1.

[Figure 1. The Study Region and the locations of Meteorological Stations]

[Table 1. The characteristics of Meteorological Stations (MSs) used in this study]

2.2. Data

For the ensemble analysis, the daily precipitation data for the closest grid to the MSs (See Table 1, the last column gives the distance between MS and center of the nearest model grid) are extracted from the historic simulation results of eight RCMs for the EUR-11 Domain (with the horizontal grid spacing of 0.11°) available from the CORDEX database (ESGF, 2020). RCMs used in this study together with their driving GCMs are given in Table 2. All of the eight RCMs have daily historical simulation outputs for the period between 1951 and 2005. The historical daily total precipitation time series from 1951 to 2005 are extracted for the relevant modeling grids by the use of the R code developed by Kentel et al. (2019). The daily time series are converted to monthly mean precipitation time series to be used in ensembling. These will be referred to as RCM Time Series (RCMTS) from hereafter.

[Table 2. Overview of RCMs used in the study]

The observed daily total precipitation data for the same historical period (1951 to 2005) from 14 meteorological stations operated by the Turkish State Meteorological Service are used as reference data in the study. The observed precipitation is used for the training of SE and ANN models and for the testing of the simulation efficiency of the ensembled time series. For this purpose, the observation data is initially screened through a Quality Check (QC) process (Figure 2). In the QC, the observation data are initially screened for continuous data gaps. The months, that are identified to have more than ten days of missing records are removed from the dataset. The observed monthly mean precipitation time series is formed by the use of the remaining months. As a second stage of the QC, the data for the months with

less than 0.1 mm precipitation record outside the dry season raised an error flag and are excluded from the data series as well.

In the study region, July, August, and September are the main dry months during which monthly mean precipitation is likely to drop to distinctly low levels or even to zero. Hence, annual precipitation is mostly received during the remaining months. Therefore, monthly mean precipitation records of zero for the months outside of the dry season raised an error flag. After the removal of the months with long data gaps and monthly means with an error flag, the final Quality Checked Dataset (QCD) of the observed precipitation is obtained. Time series of observed precipitation generated using QCD will be referred to as the Observed Time Series (OTS) from hereafter. The OTS is used for the application and testing of ensemble methodologies.

3. Methodology

3.1. Formation of Training and Validation Data Sets

The analysis includes a comparison of the efficiencies of linear methodologies with the nonlinear ANN approach for ensembling of the climate simulation outputs to replicate the observed precipitation. The use of linear and nonlinear methodologies for ensembling of eight RCMTS is based on a benchmark with the aforementioned OTS. Training and validation data sets that are used in SE and ANN methodologies are formed from the randomly selected data points of eight RCMTS and OTS. The relevant data sets include the same data points (from the same grid point and same point in time) of all time series. To test the robustness of the linear and nonlinear approaches, 5-fold cross-validation (80% for training and 20% for validation) is used. Training and subsequent validation for the ensemble time series are done for each fold separately. Log transformation and normalization are applied to data sets before ensembling to improve efficiency.

Ensembling is carried out for two different sets of inputs. The first set is composed of all eight RCMTS (referred to as AllMs in Figure 2). The second set is composed of three best-performing RCMTS selected among available eight RCMTS (referred to as SMs in Figure 2). However, as mentioned above, due to the multidimensional variability of climate outputs, the selection of the best or most representative model is a challenging task. Although there is an ample number of metrics that provide an evaluation from different aspects of climate features (Knutti et al., 2010), no standard set of performance metrics is defined for specific assessment purposes (Baker and Taylor, 2016). Taylor diagram (Taylor, 2001) is among the most common means of depicting the relative performance skill of models. Thus, in this study, Taylor Diagrams are used to select three best-performing RCMTS (see Figure 2) for each MS.

As an example, Figure 3 provides the Taylor Diagram for Usak MS (17188) comparing the OTS with eight RCMTS for the entire period between 1951 to 2005. Each RCMTS is represented by a symbol on the Taylor Diagram. The correlation coefficient, which is represented by the azimuthal angle, the centered RMSD which is represented by the distance from the OTS (i.e., the point marked with a plus in a circle on the x-axis) to the symbol of the RCMTS and the standard deviation (SD) which is represented by the radial distance from the origin are plotted on the Taylor Diagram. The position of each symbol indicates how similar that RCMTS and OTS are. Euclidian distance from the OTS to the symbol of the RCMTS is calculated and three best performing RCMs are identified as the models having three shortest Euclidian distances. For Usak MS, the best-performing three RCMs are M4, M7, and M3. Table 3 gives three best-performing RCMs for each MS in the descending order of simulation skills based on the corresponding Taylor Diagrams. In this study, two types of MMEs (i.e., MME of all RCMs, and MME of best-performing three RCMs) are generated by using ANN, SE, and SAM methods as shown in Figure 2.

[Figure 2. Flowchart of the methodology]

[Figure 3. Taylor Diagram of Usak MS (17188)]

[Table 3. Selected Models (SMs) for Meteorological Stations (MSs)]

3.2. Artificial Neural Networks for Ensembling

The ensembling process used to simulate monthly mean precipitation values at a selected grid i using RCMTS at the same grid using all models (AllMs) or only the selected three models (SMs) can be mathematically represented as follows:

$$ANN_{i,t}^{AllM} = f(RCM_{i,t}^1, RCM_{i,t}^2, \dots, RCM_{i,t}^8), \forall i, \forall t \quad (1)$$

$$ANN_{i,t}^{SM} = f(RCM_{i,t}^1, RCM_{i,t}^2, RCM_{i,t}^3), \forall i, \forall t \quad (2)$$

where $ANN_{i,t}^{AllM}$ is the ANN ensemble generated using all RCMs at grid i for month t , $RCM_{i,t}^j$ is the j^{th} RCMs at grid i for month t . When all models are used in generating the ensemble, $j = 1, 2, \dots, 8$. $ANN_{i,t}^{SM}$ is the ANN ensemble generated using three selected RCMs based on Taylor Diagrams at grid i for month t . For each MS, selected three RCMs are given in Table 3. In this study, 14 MSs are used; thus, $i = 1, 2, \dots, 14$. The simulation period is from 1951 to 2005, but the months that could not pass the quality check are eliminated, thus ensembles are calculated for $t = 1, 2, \dots, T$ where T is at most 660.

As can be seen in Figure 2, two ANN models – one using eight RCMs (i.e., 8 input nodes) and the other using outputs of three selected RCMs (i.e., 3 input nodes) as

inputs – are built for each MS. One hidden layer with six and two hidden nodes for AllMs and SMs, respectively are used in all ANN models in this study. The number of hidden nodes is selected after multiple trials to avoid overfitting. The architecture for the ANN model built for Anamur MS (17320) which uses all RCMs as inputs is shown in Figure 4. In this study, the Sigmoid activation function is used in all ANN models and all data is scaled to 0.1-0.9 range. The momentum, the learning rate and maximum iterations are identified through trial and error. Various combinations of momentum and learning rate from the ranges of 0.001 to 0.9 and 0.001 to 0.5, respectively are tested. Finally, the momentum and learning rates are selected as 0.5 and 0.05, respectively. The maximum number of iterations is set to 2000 for all ANN models. Larger number of iterations have been tested however no significant improvement is achieved when all cross-validation runs are considered.

[Figure 4. ANN model architecture for Anamur MS (17320)]

3.3. Simple Average of the Models for Ensembling

SAM of all models (Equation 3) and best-performing three models (Equation 4) are calculated based on the arithmetic average of the anomalies simulated by the RCMs by the use of the following equations (Cane and Milelli, 2010):

$$SAM_{i,t}^{AllM} = \bar{O}_i + \frac{1}{8} \sum_{j=1}^8 (RCM_{i,t}^j - \overline{RCM_t^j}) , \forall i, \forall t \quad (3)$$

$$SAM_{i,t}^{SM} = \bar{O}_i + \frac{1}{3} \sum_{j=1}^3 (RCM_{i,t}^j - \overline{RCM_t^j}) , \forall i, \forall t \quad (4)$$

where $SAM_{i,t}^{AllM}$ is the SAM ensemble generated using all RCMs at grid i for month t , $SAM_{i,t}^{SM}$ is the SAM ensemble generated using three best-performing RCM outputs at grid i for month t , \overline{RCM}_i^j is the climatology determined by RCM j , and \overline{O}_i is the mean observation or observed climatology value at grid i .

$$\overline{RCM}_i^j = \frac{1}{T} \sum_{t=1}^T RCM_{i,t}^j, \forall i, \forall j$$

$$\overline{O}_i = \frac{1}{T} \sum_{t=1}^T O_{i,t}, \forall i$$

where $O_{i,t}$ is the observed precipitation at grid i at month t .

3.4. Multiple Linear Regression for Ensembling

The use of MLR for ensembling is done based on the Superensemble method suggested by Krishnamurti et al. (1999, 2000):

$$SE_{i,t}^{AllM} = \overline{O}_i + \sum_{j=1}^8 a_j (RCM_{i,t}^j - \overline{RCM}_i^j), \forall i, \forall t \quad (5)$$

$$SE_{i,t}^{SM} = \overline{O}_i + \sum_{j=1}^3 a_j (RCM_{i,t}^j - \overline{RCM}_i^j), \forall i, \forall t \quad (6)$$

where $SE_{i,t}^{AllM}$ is the SE generated using all RCMs at grid i for month t , $SE_{i,t}^{SM}$ is the SE generated using three selected RCMs at grid i for month t , a_j is the weight of RCM j optimized for the training period to minimize the difference between observed and modeled precipitation at grid i based on the conventional MLR. In

order to enable benchmarking between three methods, the same training and validation datasets are used for all three ensemble approaches for each fold.

4. Results and Discussion

In the tables and figures given in this section, MSs are sorted based on their proximity to the sea, in order to observe the potential spatial effect. 5-fold validation is used to test the performance of each approach (i.e., each data point is used in one of the validation data sets). The comparison of the performance ranges of ensembles with the performance range of individual RCMs regarding five validation data sets are given in Figures 5 and 6 for SMs and AllMs, respectively. The performance ranges in Figures 5 and 6 represent the range of correlation (Pearson correlation coefficient) values of each ensemble method (ANN, SE, SAM) with the observed for *SMs* and *AllMs*, respectively.

[Figure 5. Comparison of correlation performances when selected models (SMs) are used as inputs]

[Figure 6. Comparison of correlation performances when all models (AllMs) are used as inputs]

As can be seen from Figures 5 and 6, ensembling with ANN, SE, or SAM improves the correlations for most of the validation data sets. Moreover, more consistent estimates are obtained from ensembling compared to the single RCMs in terms of correlations. Better improvement is achieved when all the models are used in the ensemble. Although the model performances generally are better for MSs closer to the sea, variation of the correlation of the models varies regardless to spatial characteristics of the MSs.

In the rest of this study, the Ensembled Time Series (ETS) is used to evaluate the ensemble performance of each approach (i.e., ANN, SE, and SAM). The ETS is generated by combining together the validation data sets of five folds. The Correlation, RMSD and Percent Bias (PBIAS) values of the best and the worst performing RCMs, the ETS obtained from ANN, SE, and SAM approaches with selected and all models are given in Tables 4, 5 and 6, respectively. Stations are listed according to their approximate distances from the sea (see Table 3) and the best performing model for each station is given in bold.

[Table 4. Correlation values of the best and the worst RCMTS and the ETS obtained from ANN, SE, SAM approaches]

As can be seen in Table 4, the ETS obtained from ANN_AllMs generally resulted in the best correlations, except for two stations (i.e., 17238 and 17240) for which ANN_SMs, and for two other stations (i.e., 17340 and 17330) for which SAM_AllMs provided the best correlations. The performances of both ANN models (selected and all) are very similar to each other. For all stations, other than 17238, 17239 and 17240, when all models are used, correlations improved but less than 5%. On the other hand, for SE, correlation values improved more than 5% for eight of the stations when all models are used instead of three best-performing RCMs as inputs. The improvement is more pronounced for SAM. When all models are used instead of three selected models, correlations of 11 stations improved more than 5%. In fact, for 17340 and 17239, the improvement was more than 20%. Thus, it can be concluded that generally, performance in terms of correlations is better when all models instead of the selected three best-performing models are used as inputs and SAM benefits the most from ensembling all available RCMs.

For correlation, the ETS, generated using all models or selected three models, perform better than the best RCMTS for all stations. As can be seen in the third and

fifth columns of Table 4, RCMTS has a large range of correlation performances. The difference in model performance according to the atmospheric instability in local scale is also reported in the study conducted by Baghanam et al. (2020). Thus, utilization of a single RCM for future precipitation projections is prone to high uncertainty. Moreover, stations closer to the sea generally perform better compared to the inland ones (i.e., correlations have a decreasing trend from the top to the bottom in Table 4). Milder climatologic conditions experienced in Mediterranean coasts compared to the inland Anatolia might be the reason of it. As seen in Figure 6, the performance of the ETS is influenced by the performance of the RCMTS in the ensemble set. Hence, using better performing RCMs as inputs results in the ETS to have better performance in terms of correlations. Percent improvements in correlation when the ETS is evaluated with respect to the best RCMTS are given in columns 2, 3 and 4 of Table 7 for ANN, SE and SAM, respectively. Up to 38% improvement is achieved due to ensembling.

[Table 5. RMSD values of the best and the worst RCMTS and the ETS obtained from the ANN, SE, SAM approaches.]

Similar to correlations, the ETS obtained from ANN_AllMs generally resulted in the best RMSD values (see Table 5). For 17340, 17240, 17239, and 17190 either SE or SAM with all models resulted in better RMSD values, while for 17238, SE_SMs provided the minimum RMSD. The performances of both ANN models are very similar to each other. Improvements in RMSD when all models are used instead of selected three are less than 3% for all stations, other than 17290, 17292 and 17300. Similarly, for SE, improvements are less than 3% for all the stations and in fact for 17320, 17238 and 17188 SE_SMs performed better than SE_AllMs. On the contrary, improvement in RMSD is more than 5% for 12 stations when SAM is used for ensembling. Thus, it can be concluded that generally, all methods perform better in

terms of RMSD when all models instead of the selected three models are used as inputs, but SAM benefits the most from ensembling larger number of inputs.

For RMSD, the ETS, generated using all models or selected three models, perform better than the best RCMTS for all stations. Percent improvements in RMSD (i.e., decrease in RMSD) when the ensembled VTS is evaluated with respect to the best RCM are given in columns 5, 6 and 7 of Table 7 for ANN, SE and SAM, respectively. The improvements in RMSD range between 9% to 28% when the ETS are used instead of the best RCMTS.

[Table 6. PBIAS values of the best and the worst RCMTS and the ETS obtained from the ANN, SE, SAM approaches.]

As can be seen from Table 6, bias correction performance of ensembling is not as good as those of Correlation and RMSD. All ensemble results are in the range of Best and Worst RCMTS performances for all stations. Thus, the ETS perform better than some of RCMTS but generally not as good as the Best RCMTS. PBIAS values of the best RCMTS is better than all the ETS for all the stations other than 17238, 17240, 17244, 17188 and 17190. For ANN, utilization of all models compared to selected models improves PBIAS values for all the stations other than 17239 and 17188, but not to the level of the best RCMTS. For SE, PBIAS values improve when all models are used for half of the stations. In contrast, PBIAS values are better when selected models are used for all stations other than 17296 and 17300 for SAM. So, it can be concluded that PBIAS values of the best RCMTS cannot be achieved with either of the three ensembling methods with all or selected models. Thus, when the goal is to obtain precipitation time series with minimum bias, the best performing RCMTS should be preferred over the ETS.

Percent deterioration in PBIAS when the ETS obtained by using the better of the selected or all models are evaluated with respect to the best RCMTS and are given

in the last three columns of Table 7. For most of the stations, higher PBIAS values are obtained for the ETS compared to those obtained for the best RCMTS. This outcome does not support the literature where multi model ensemble is reported to reduce model biases (Krishnamurti et al., 1999, 2016; Tebaldi and Knutti, 2007). In this study, we believe that poor performance of ensembling for PBIAS is partially due to utilization of log-transformed inputs. In order to test this hypothesis, the ETS are generated for MS 17320 which has the worst PBIAS performance (see Table 7) using only normalized RCMTS as inputs (i.e., log-transformation is not applied to input data). AllMs are used to generate the ETS and the results are given in Table 8. Log-transformation does not significantly affect correlation and RMSD performances of ensembling. However, PBIAS values decrease significantly, almost to the level of the best performing RCMTS, when log-transformation is not used. Thus, when the goal is to reduce biases, it is beneficial to use RCMTS directly, without log-transformation.

The superior results for simulation skills regarding correlation and RMSD indicate the advantage of the use of MME over single model analysis for long-term climate assessments. Furthermore, the MME obtained by the use of the nonlinear ANN method has a relatively better performance compared to the linear ensembling methods regarding both MLR and simple ensemble averaging. Hence, the improved representation skills by nonlinear ANN over linear methods obtained as a result are in agreement with the findings from a study by Krasnopolsky and Lin (2012) for the continental US. Krasnopolsky and Lin (2012) denote that, nonlinear approaches provide better representation for long term simulations, and for precipitation fields with high gradients and sharp, localized features for which the linearity assumption is not applicable, and therefore ANN generates better skills compared to the conventional linear methods.

[Table 7. Percent changes in Correlation, RMSD and PBIAS values of the ETS relative to the best RCMTS]

[Table 8. Effect of log-transformation on ensemble performance for Anamur MS (17320)]

To provide a visual comparison of RCMTS and ETS Taylor Diagrams for all MSs are given in Figure 7. The legend is given at the bottom right corner of the figure. The outputs that are close to the reference/observed are the better performing ones. As can be seen from Figure 7, RCMTS (marked with grey circles) always have lower correlation and higher RMSD values compared to those of the ensembled outputs as demonstrated in Tables 4 and 5. However, improvement in correlation and RMSD is maintained with ensembling at the cost of losing variance (see Normalized Standard Deviation performances in Figure 7).

To represent the performance of ensembling in terms of reproducing the mean and variation of the OTS, the relative mean (i.e., the mean of RCMTS or ETS divided by the mean of the OTS) versus the relative standard deviation (i.e., the standard deviation of RCMTS or ETS divided by the standard deviation of the OTS) plots are given in Figure 8. The relative mean values of the ETS are bounded between 0.75-1.00, while relative standard deviations are around 0.5 for all MSs. On the other hand, the relative standard deviations of RCMTS are between 0.5-1.5, while the relative means of RCMTS are highly scattered (especially for MS 17240 and 17190). One noteworthy drawback of ensembling is that it causes time series to accumulate around mean as can be seen in Figure 8. Moreover, the standard deviation values of the ETS are significantly lower than those of the RCMTS in comparison with the OTS (see Figure 7 and 8). Thus, it can be concluded that through ensembling, higher variations in RCMTS are mapped into ETS with lower variations.

The ETS obtained by ANN_AllIMs for 17290 which has a very good performance (i.e., correlation=0.67, RMSD=1.85 mm, PBIAS=14.2) is given in Figure 9. Eight RCMTS used in ensembling and the OTS are marked with grey and dashed black,

respectively. As can be seen in Figure 9, despite following the general trend, the ETS obtained by ANN_AllMs do not show the variation that exists in the OTS. For MS 17290, the relative standard deviations for four RCMTS (M1, M2, M3, M7) have similar values to those of the ETS, but three RCMTS (M4, M5, M8) have the normalized standard deviations very close to the OTS (see Figure 8). Although, their correlation and RMSD values are lower than those of the ETS, these three RCMTS which have higher normalized standard deviations represent the variability in observed precipitation better. Hence, a set of individual climate models with different mechanisms provides a better representation of the potential variability in observations. The cumulative distribution functions of the ETS obtained from ANN_AllMs, observations, and RCMTS demonstrate this behavior (Figure 10). As shown in Figure 10, the cumulative distribution functions of three RCMTS (M4, M5 and M8) are more similar to that of the OTS compared to the ANN_AllMs for MS 17290. However, as reported in Mascaro et al. (2018) the performance skills of RCMs in capturing the variation of climatological precipitation patterns at small temporal scales are limited. Hence, the use of a single model for the assessment may cause higher biases in evaluations due to unconsidered uncertainties, especially for regions having complex spatial characteristics like the Mediterranean region. Given that, ensembled data series can be considered to be particularly useful in assessment when evaluated in integration with the likely ranges including relatively low frequency and/or extreme events identified through a large ensemble set of individual models with diverse approaches or assumptions.

Providing more consistent estimates, ensembling is advisable for station simulation (Xu et al., 2020). Ensembling, on the other hand, improves correlation and RMSD performances at the cost of reducing the variability in the precipitation. Thus, it can be concluded that in the estimation of the total depth/volume of precipitation over a long period of time, utilization of ensembled results will be beneficial. However, when the goal is to select extreme precipitations to be used in design discharge calculations of water structures, peak values of individual RCMs will be more conservative; thus, may be better preferred.

[Figure 7. Taylor Diagram of RCMTS and the ETS obtained from ANN, SE, SAM for all MSs (legend and explanation of axis are provided on the bottom right diagram)]

[Figure 8. The relative mean versus relative standard deviation of RCMTS and the ETS obtained from ANN_AllMs, SE_AllMs, SAM_AllMs for all MSs]

[Figure 9. ETS obtained from ANN_AllMs, observations, and eight input RCMs for Bodrum MS (17290)]

[Figure 10. Cumulative distribution functions for the ETS obtained from ANN_AllMs, observations, and eight input RCMs for Bodrum MS (17290)]

5. Conclusions

The objective of this study is to examine the effect of the multimodel ensembling on the precipitation simulations for a study region in the south and southwestern Turkey with complex climatic features. In the analysis, three ensembling approaches, namely SAM, SE and ANN, are applied by the use of the historical outputs of eight RCMs from the CORDEX database. Long term monthly precipitation time series obtained from ground-based precipitation observations from fourteen meteorological stations is used as the benchmark. This study provides a comparison of the improvement in replication skills of historical precipitation simulations from individual RCMs by the use of linear and nonlinear MME methods. Main findings of the study are as follows:

- The analysis results show that the overall performance of the ensemble time series is better compared to individual RCMs. Generally, stations in the coastal strip have better performing RCMs, thus ensemble works better for these stations compared to the inland ones.
- ANN generally provided the best performance among the three ensemble methodologies, particularly regarding the correlation and RMSD values calculated for the test data series. Additionally, it is seen to perform better when all RCMTS are used as inputs instead of selected three best performing RCMTS as inputs.
- Analysis of the individual RCMTS in a multimodel analysis generates a wide range of correlations and RMSD, hence, high uncertainty, however, the use of multimodel ensemble reduces the model uncertainty. On the other hand, PBIAS values for MME are seen to be higher than the value for the best individual model. It is observed that bias reduction, almost to the level of the best RCMTS performance, is achieved when input time series are directly used (i.e., without log-transformation) in ensemble.
- Despite the advantages in reducing uncertainty and improvement in correlation and RMSD values, ensemble is verified to increase the simulation performance at the cost of reducing the variability in the precipitation. It should be realized that extreme events are poorly represented in the ensemble time series, and this may result in inefficient design of various water structures such as spillways and storm water drainage systems that are based on high return period events. Thus, it can be concluded that ensemble is more useful in estimation of the total depth/volume of precipitation over long time periods, rather than for the simulation of extreme precipitations.

CRedit

Buket Mesta: Conceptualization, methodology, formal analysis, validation, writing - original draft, funding acquisition

O. Burak Akgun: Conceptualization, methodology, data curation, formal analysis, visualization, writing - original draft

Elcin Kentel: Conceptualization, methodology, formal analysis, validation, writing - original draft, supervision, project administration, funding acquisition

Acknowledgement

The research leading to these results is funded by the Scientific and Technological Research Council of Turkey (TÜBİTAK) and an on-going project “Assessment of Climate Change Impacts on Streamflow and Hydropower in Antalya, Turkey” (Project ID: 118Y365).

References

- Ajami, N. K., Duan, Q., Gao, X., & Sorooshian, S. (2006). Multimodel combination techniques for analysis of hydrological simulations: Application to distributed model intercomparison project results. *Journal of Hydrometeorology*, 7(4), 755-768.
- Araújo, M. B., & New, M. (2007). Ensemble forecasting of species distributions. *Trends in Ecology & Evolution*, 22(1), 42–47.
- Baghanam, A. H., Eslahi, M., Sheikhabaei, A., & Seifi, A. J. (2020). Assessing the impact of climate change over the northwest of Iran: an overview of statistical downscaling methods. *Theoretical and Applied Climatology*, 141(3), 1135-1150.
- Baker, N. C., & Taylor, P. C. (2016). A framework for evaluating climate model performance metrics. *Journal of Climate*, 29(5), 1773-1782.
- Black, E., Brayshaw, D. J., & Rambeau, C. M. (2010). Past, present and future precipitation in the Middle East: insights from models and observations. *Philosophical Transactions of the Royal Society A: Mathematical, Physical and Engineering Sciences*, 368(1931), 5173-5184.
- Boulangier, J. P., Martinez, F., & Segura, E. C. (2006). Projection of future climate change conditions using IPCC simulations, neural networks and Bayesian statistics. Part 1: Temperature mean state and seasonal cycle in South America. *Climate Dynamics*, 27(2-3), 233-259.
- Boulangier, J. P., Martinez, F., & Segura, E. C. (2007). Projection of future climate change conditions using IPCC simulations, neural networks and Bayesian statistics. Part 2: precipitation mean state and seasonal cycle in South America. *Climate Dynamics*, 28(2-3), 255-271.

- Bozkurt, D., & Sen, O. L. (2011). Precipitation in the Anatolian Peninsula: sensitivity to increased SSTs in the surrounding seas. *Climate dynamics*, 36(3-4), 711-726.
- Cakir, S., Kadioglu, M., & Cubukcu, N. (2013). Multischeme ensemble forecasting of surface temperature using neural network over Turkey. *Theoretical and applied climatology*, 111(3-4), 703-711.
- Campozano, L., Tenelanda, D., Sanchez, E., Samaniego, E., & Feyen, J. (2016). Comparison of statistical downscaling methods for monthly total precipitation: case study for the paute river basin in Southern Ecuador. *Advances in Meteorology*, 2016.
- Cane, D., & Milelli, M. (2010). Multimodel SuperEnsemble technique for quantitative precipitation forecasts in Piemonte region. *Natural Hazards & Earth System Sciences*, 10(2).
- Christensen, J. H., Kjellström, E., Giorgi, F., Lenderink, G., & Rummukainen, M. (2010). Weight assignment in regional climate models. *Climate Research*, 44(2-3), 179-194.
- Evans, J. P. (2009). 21st century climate change in the Middle East. *Climatic Change*, 92(3-4), 417-432.
- Fan, Y., Krasnopolsky, V. M., van den Dool, H., W, Ch-Y., and Gottschalck, J. (2021) Using Artificial Neural Networks to Improve CFS Week 3-4 Precipitation and 2-Meter Air Temperature Forecasts. *Weather and Forecasting*, <https://doi.org/10.1175/WAF-D-20-0014.1>.
- Fujihara, Y., Tanaka, K., Watanabe, T., Nagano, T., & Kojiri, T. (2008). Assessing the impacts of climate change on the water resources of the Seyhan River Basin in Turkey: Use of dynamically downscaled data for hydrologic simulations. *Journal of Hydrology*, 353(1-2), 33-48.

- Galmarini, S., Bianconi, R., Klug, W., Mikkelsen, T., Addis, R., Andronopoulos, S., ... & Bellasio, R. (2004). Ensemble dispersion forecasting—Part I: concept, approach and indicators. *Atmospheric Environment*, 38(28), 4607-4617.
- Gao, X., & Giorgi, F. (2008). Increased aridity in the Mediterranean region under greenhouse gas forcing estimated from high resolution simulations with a regional climate model. *Global and Planetary Change*, 62(3-4), 195-209.
- Giorgi, F., & Mearns, L. O. (2002). Calculation of average, uncertainty range, and reliability of regional climate changes from AOGCM simulations via the Reliability Ensemble Averaging (REA) method. *Journal of Climate*, 15(10), 1141-1158.
- Giorgi, F., & Mearns, L. O. (2003). Probability of regional climate change based on the Reliability Ensemble Averaging (REA) method. *Geophysical research letters*, 30(12).
- Gutiérrez, J. M., Maraun, D., Widmann, M., Huth, R., Hertig, E., Benestad, R., ... & San Martin, D. (2019). An intercomparison of a large ensemble of statistical downscaling methods over Europe: Results from the VALUE perfect predictor cross - validation experiment. *International journal of climatology*, 39(9), 3750-3785.
- Hagedorn, R., Doblas-Reyes, F. J., & Palmer, T. N. (2005). The rationale behind the success of multi-model ensembles in seasonal forecasting—I. Basic concept. *Tellus A: Dynamic Meteorology and Oceanography*, 57(3), 219-233.
- Hemming, D., Buontempo, C., Burke, E., Collins, M., & Kaye, N. (2010). How uncertain are climate model projections of water availability indicators across the Middle East? *Philosophical Transactions of the Royal Society A: Mathematical, Physical and Engineering Sciences*, 368(1931), 5117-5135.
- Kang, B., Do Kim, Y., Lee, J. M., & Kim, S. J. (2015). Hydro-environmental runoff projection under GCM scenario downscaled by Artificial Neural Network in

the Namgang Dam watershed, Korea. *KSCE Journal of Civil Engineering*, 19(2), 434-445.

Kara, F., & Yucel, I. (2015). Climate change effects on extreme flows of water supply area in Istanbul: utility of regional climate models and downscaling method. *Environmental monitoring and assessment*, 187(9), 580.

Kentel, E., Akgun, O. B., & Mesta, B. (2019, December). User-Friendly R-Code for Data Extraction from CMIP6 outputs. In *AGU Fall Meeting Abstracts (Vol. 2019, pp. PA33C-1098)*.

Krasnopolsky, V. M., & Lin, Y. (2012). A Neural Network Nonlinear Multimodel Ensemble to Improve Precipitation Forecasts over Continental US. *Advances in Meteorology*, Volume 2012, Article ID 649450.

Kitoh, A. (2007). Future climate projections around Turkey by global climate models. Final report of ICCAP.

Knutti, R., Furrer, R., Tebaldi, C., Cermak, J., & Meehl, G. A. (2010). Challenges in combining projections from multiple climate models. *Journal of Climate*, 23(10), 2739-2758.

Kotlarski, S., Keuler, K., Christensen, O. B., Colette, A., Déqué, M., Gobiet, A., ... & Nikulin, G. (2014). Regional climate modeling on European scales: a joint standard evaluation of the EURO-CORDEX RCM ensemble. *Geoscientific Model Development*, 7, 1297-1333.

Krishnamurti, T. N., Kishtawal, C. M., LaRow, T. E., Bachiochi, D. R., Zhang, Z., Williford, C. E., ... & Surendran, S. (1999). Improved weather and seasonal climate forecasts from multimodel superensemble. *Science*, 285(5433), 1548-1550.

Krishnamurti, T. N., Kishtawal, C. M., Zhang, Z., LaRow, T., Bachiochi, D., Williford, E., ... & Surendran, S. (2000). Multimodel ensemble forecasts for weather and seasonal climate. *Journal of Climate*, 13(23), 4196-4216.

- Krishnamurti, T. N., Kumar, V., Simon, A., Bhardwaj, A., Ghosh, T., & Ross, R. (2016). A review of multimodel superensemble forecasting for weather, seasonal climate, and hurricanes. *Reviews of Geophysics*, 54(2), 336-377.
- López - Moreno, J. I., Goyette, S., & Beniston, M. (2008). Climate change prediction over complex areas: spatial variability of uncertainties and predictions over the Pyrenees from a set of regional climate models. *International Journal of Climatology: A Journal of the Royal Meteorological Society*, 28(11), 1535-1550.
- Lun, Y., Liu, L., Cheng, L., Li, X., Li, H., & Xu, Z. (2021). Assessment of GCMs simulation performance for precipitation and temperature from CMIP5 to CMIP6 over the Tibetan Plateau. *International Journal of Climatology*
- Maharana, P., Kumar, D., Das, S., & Tiwari, P. R. (2021). Present and future changes in precipitation characteristics during Indian summer monsoon in CORDEX - CORE simulations. *International Journal of Climatology*, 41(3), 2137-2153.
- Mascaro, G., Viola, F., & Deidda, R. (2018). Evaluation of Precipitation From EURO - CORDEX Regional Climate Simulations in a Small - Scale Mediterranean Site. *Journal of Geophysical Research: Atmospheres*, 123(3), 1604-1625.
- Mendes, D., & Marengo, J. A. (2010). Temporal downscaling: a comparison between artificial neural network and autocorrelation techniques over the Amazon Basin in present and future climate change scenarios. *Theoretical and Applied Climatology*, 100(3), 413-421.
- Okkan, U. (2015). Assessing the effects of climate change on monthly precipitation: proposing of a downscaling strategy through a case study in Turkey. *KSCE Journal of Civil Engineering*, 19(4), 1150-1156.

- Okkan, U., & Inan, G. (2015). Statistical downscaling of monthly reservoir inflows for Kemer watershed in Turkey: use of machine learning methods, multiple GCMs and emission scenarios. *International Journal of Climatology*, 35(11), 3274-3295.
- Okkan, U., & Kirdemir, U. (2016). Downscaling of monthly precipitation using CMIP5 climate models operated under RCPs. *Meteorological Applications*, 23(3), 514-528.
- Onol, B., & Unal, Y. S. (2014). Assessment of climate change simulations over climate zones of Turkey. *Regional Environmental Change*, 14(5), 1921-1935.
- Ozdogan, M. (2011). Modeling the impacts of climate change on wheat yields in Northwestern Turkey. *Agriculture, ecosystems & environment*, 141(1-2), 1-12.
- Palatella, L., Miglietta, M. M., Paradisi, P., & Lionello, P. (2010). Climate change assessment for Mediterranean agricultural areas by statistical downscaling. *Natural Hazards and Earth System Sciences*, 10(7), 1647.
- Park, C., Lee, G., Kim, G., & Cha, D. H. (2021). Future changes in precipitation for identified sub - regions in East Asia using bias - corrected multi - RCMs. *International Journal of Climatology*, 41(3), 1889-1904.
- Roebber, P. J., Butt, M. R., Reinke, S. J., & Grafenauer, T. J. (2007). Real-time forecasting of snowfall using a neural network. *Weather and Forecasting*, 22(3), 676–684.
- Sensoy, S. (2004). The mountains influence on Turkey climate. In Balwois Conference on Water Observation and Information System for Decision Support.
- Sirdas, S., Ross, R. S., Krishnamurti, T. N., & Chakraborty, A. (2007). Evaluation of the FSU synthetic superensemble performance for seasonal forecasts over

- the Euro-Mediterranean region. *Tellus A: Dynamic Meteorology and Oceanography*, 59(1), 50-70.
- Stefanova, L., & Krishnamurti, T. N. (2002). Interpretation of seasonal climate forecast using Brier skill score, the Florida State University superensemble, and the AMIP-I dataset. *Journal of Climate*, 15(5), 537-544.
- Stocker, T. F., Dahe, Q., Plattner, G. K., & Tignor, M. (2015, September). IPCC Workshop on Regional Climate Projections and their Use in Impacts and Risk Analysis Studies. In *Workshop Report (Vol. 15, p. 18)*.
- Sunyer Pinya, M. A., Hundedcha, Y., Lawrence, D., Madsen, H., Willems, P., Martinkova, M., Vormoor, K., Bürger, G., Hanel, M., Kriaučiuniene, J., Loukas, A., Osuch, M., & Yücel, I. (2015). Inter-comparison of statistical downscaling methods for projection of extreme precipitation in Europe. *Hydrology and Earth System Sciences*, 19(4), 1827-1847. <https://doi.org/10.5194/hess-19-1827-2015>
- Taylor, K. E. (2001). Summarizing multiple aspects of model performance in a single diagram. *Journal of Geophysical Research: Atmospheres*, 106(D7), 7183-7192.
- Tebaldi, C., & Knutti, R. (2007). The use of the multi-model ensemble in probabilistic climate projections. *Philosophical transactions of the royal society A: mathematical, physical and engineering sciences*, 365(1857), 2053-2075.
- Teutschbein, C., & Seibert, J. (2012). Bias correction of regional climate model simulations for hydrological climate-change impact studies: Review and evaluation of different methods. *Journal of hydrology*, 456, 12-29.
- Vautard, R., Kadyrov, N., Iles, C., Boberg, F., Buonomo, E., Bülow, K., ... & Wulfmeyer, V. (2021). Evaluation of the large EURO - CORDEX regional

- climate model ensemble. *Journal of Geophysical Research: Atmospheres*, 126(17), e2019JD032344.
- Vu, M. T., Aribarg, T., Supratid, S., Raghavan, S. V., & Liang, S. Y. (2016). Statistical downscaling rainfall using artificial neural network: significantly wetter Bangkok? *Theoretical and applied climatology*, 126(3-4), 453-467.
- Xu, R., Chen, N., Chen, Y., & Chen, Z. (2020). Downscaling and projection of multi-CMIP5 Precipitation using machine learning methods in the upper Han River Basin. *Advances in Meteorology*, 2020.
- Yun, W. T., Stefanova, L., Mitra, A. K., Vijaya Kumar, T. S. V., Dewar, W., & Krishnamurti, T. N. (2005). A multi-model superensemble algorithm for seasonal climate prediction using DEMETER forecasts. *Tellus A: Dynamic Meteorology and Oceanography*, 57(3), 280-289.
- Zhang, G. P., & Berardi, V. L. (2001). Time series forecasting with neural network ensembles: an application for exchange rate prediction. *Journal of the Operational Research Society*, 52(6), 652-664, DOI: 10.1057/palgrave.jors.2601133.
- ESGF, Earth System Grid Federation website. (CoG version v4.0.0b2, ESGF P2P Version v4.0.4). <https://esgf-node.llnl.gov/search/esgf-llnl/> Latest Access: 5th June 2020]

TABLES IN MANUSCRIPT

Table 1. The characteristics of Meteorological Stations (MSs) used in this study

MS ID*	MS Name	Elevation (m ASL)	Latitude (DD)	Longitude (DD)	Distance to the sea (km)	Distance to the center of the nearest RCM grid (km)
17290	BODRUM	26	37.03	27.44	0	4.4
17296	FETHIYE	3	36.63	29.12	0	5.3
17320	ANAMUR	2	36.07	32.86	0	3.8
17340	MERSIN	7	36.78	34.6	0	4.8
17300	ANTALYA	64	36.91	30.8	6	2.4
17330	SILIFKE	10	36.38	33.94	7	3.7
17292	MUGLA	646	37.21	28.37	17	3.3
17238	BURDUR	957	37.72	30.29	100	5.6
17240	ISPARTA	997	37.78	30.57	100	5.6
17246	KARAMAN	1018	37.19	33.22	115	4.2
17244	KONYA	1031	37.98	32.57	165	2.2
17239	AKSEHIR	1002	38.37	31.43	170	4.3
17188	USAK	919	38.67	29.4	195	3.9
17190	AFYON	1034	38.74	30.56	205	5.6

*MS ID: Meteorological Station ID used by the Turkish State Meteorological Service

Table 2. Overview of RCMs used in the study

Driving GCM	RCM		Model ID*
	Name	Institution	
CNRM-CM5 (CNRM-CERFACS)	CCLM4-8-17	Climate Limited-area Modelling Community (CLM-Community)	M1
CNRM-CM5 (CNRM-CERFACS)	ALADIN53	Centre National de Recherches Météorologiques (CNRM)	M2
EC-EARTH (ICHEC)	CCLM4-8-17	Climate Limited-area Modelling Community (CLM-Community)	M3
EC-EARTH (ICHEC)	RACMO22E	Royal Netherlands Meteorological Institute (KNMI)	M4
EC-EARTH (ICHEC)	HIRHAM5	Danish Meteorological Institute (DMI)	M5
CM5A-MR (IPSL)	WRF331F	Institut Pierre-Simon Laplace (IPSL-INERIS)	M6
HadGEM2-ES (MOHC)	CCLM4-8-17	Climate Limited-area Modelling Community (CLM-Community)	M7
HadGEM2-ES (MOHC)	RACMO22E	Royal Netherlands Meteorological Institute (KNMI)	M8

*Climate model ID used in this study.

Table 3. Selected Models (SMs) for Meteorological Stations (MSs)

MS ID	MS Name	SMs		
17290	BODRUM	M7	M3	M4
17296	FETHIYE	M5	M4	M2
17320	ANAMUR	M5	M4	M8
17340	MERSIN	M4	M6	M5
17300	ANTALYA AIRPORT	M2	M4	M6
17330	SILIFKE	M5	M4	M6
17292	MUGLA	M7	M3	M4
17238	BURDUR	M5	M4	M8
17240	ISPARTA	M4	M3	M7
17246	KARAMAN	M5	M4	M8
17244	KONYA AIRPORT	M5	M4	M8
17239	AKSEHIR	M4	M3	M8
17188	USAK	M4	M7	M3

Table 4. Correlation values of the best and the worst RCMTS and the ETS obtained from ANN, SE, SAM approaches

Correlation										
MS ID*	RCMTS				ETS					
	Best RCM		Worst RCM		ANN		SE		SAM	
	Model	Value	Model	Value	SMs	AllMs	SMs	AllMs	SMs	AllMs
17290	M4	0.57	M1	0.25	0.64	0.67**	0.62	0.66	0.61	0.66
17296	M5	0.52	M2	0.16	0.60	0.62	0.57	0.61	0.54	0.61
17320	M5	0.53	M2	0.26	0.66	0.66	0.61	0.62	0.60	0.62
17340	M7	0.46	M2	-0.02	0.51	0.52	0.47	0.51	0.45	0.54
17300	M4	0.43	M6	0.19	0.54	0.56	0.51	0.55	0.48	0.55
17330	M8	0.45	M2	0.17	0.56	0.57	0.54	0.56	0.51	0.58
17292	M8	0.57	M2	0.30	0.61	0.66	0.61	0.64	0.59	0.65
17238	M8	0.37	M6	0.11	0.47	0.45	0.45	0.43	0.42	0.45
17240	M4	0.40	M2	0.15	0.47	0.46	0.43	0.47	0.46	0.45
17246	M7	0.42	M2	0.14	0.54	0.55	0.48	0.50	0.47	0.51
17244	M7	0.35	M2	0.07	0.46	0.48	0.44	0.47	0.44	0.46
17239	M7	0.35	M2	0.04	0.41	0.44	0.39	0.44	0.37	0.45
17188	M8	0.42	M2	-0.14	0.51	0.53	0.51	0.49	0.48	0.53
17190	M3	0.29	M2	0.12	0.39	0.40	0.36	0.40	0.37	0.40

*MSs are given in the order of proximity to the sea, **The best performing model for each station is given in bold.

Table 5. RMSD values of the best and the worst RCMTS and the ETS obtained from the ANN, SE, SAM approaches

RMSD (mm)										
MS ID*	RCMTS				ETS					
	Best RCM		Worst RCM		ANN		SE		SAM	
	Model	Value	Model	Value	SMs	AllMs	SMs	AllMs	SMs	AllMs
17290	M4	2.26	M6	2.94	2.00	1.85**	1.97	1.94	1.99	1.89
17296	M5	2.76	M7	4.10	2.49	2.43	2.56	2.51	2.62	2.45
17320	M8	3.12	M7	3.86	2.68	2.66	2.79	2.81	2.81	2.75
17340	M4	2.25	M1	3.06	1.96	1.93	2.01	1.96	2.05	1.91
17300	M4	4.16	M7	6.71	3.79	3.67	3.84	3.79	3.91	3.70
17330	M5	2.15	M8	2.81	1.83	1.81	1.89	1.87	1.95	1.82
17292	M7	3.59	M6	6.53	3.13	2.93	3.09	3.05	3.13	2.96
17238	M4	1.11	M1	1.61	0.96	0.96	0.93	0.95	1.00	0.93
17240	M4	1.72	M2	3.12	1.32	1.32	1.34	1.31	1.41	1.31
17246	M8	0.86	M1	1.19	0.70	0.69	0.72	0.71	0.74	0.71
17244	M5	0.83	M2	1.27	0.67	0.66	0.69	0.67	0.72	0.68
17239	M4	1.44	M2	2.18	1.25	1.23	1.27	1.24	1.37	1.22
17188	M4	1.49	M2	2.31	1.09	1.07	1.09	1.11	1.20	1.07
17190	M4	0.96	M2	2.21	0.79	0.79	0.80	0.80	0.85	0.78

*MSs are given in the order of proximity to the sea, **The best performing model for each station is given in bold.

Table 6. PBIAS values of the best and the worst RCMTS and the ETS obtained from the ANN, SE, SAM approaches

PBIAS										
MS ID	RCMTS				ETS					
	Best RCM		Worst RCM		ANN		SE		SAM	
	Model	Value	Model	Value	SMs	AllMs	SMs	AllMs	SMs	AllMs
17290	M5	4.07**	M6	-48.64	25.12	14.20	17.91	21.11	13.33	15.40
17296	M6	-3.13	M7	-47.57	18.30	15.11	19.71	22.84	21.57	18.56
17320	M1	-0.06	M4	47.21	21.10	19.15	17.47	23.91	15.74	16.88
17340	M3	6.61	M6	45.79	20.77	19.85	21.27	20.72	15.27	19.47
17300	M3	-3.81	M7	-66.78	26.61	23.10	25.59	29.06	26.54	22.71
17330	M4	-0.37	M8	-52.73	9.11	6.94	19.18	20.69	13.91	17.90
17292	M2	-2.14	M6	-100.89	23.48	17.03	21.14	22.10	13.48	18.63
17238	M2	-7.05	M1	-52.07	23.01	22.47	12.31	9.33	5.33	11.97
17240	M3	-16.99	M6	-121.52	20.37	17.64	12.05	9.11	1.39	12.54
17246	M6	0.40	M5	57.04	18.06	15.51	10.43	10.42	6.65	11.44
17244	M8	-3.55	M5	24.21	-1.93	1.97	10.85	9.06	4.82	10.33
17239	M8	1.58	M2	-34.38	13.28	13.48	14.21	10.03	4.83	13.03
17188	M4	-6.73	M6	-79.15	9.33	9.80	12.68	10.72	2.56	12.09
17190	M8	-2.88	M2	-116.00	12.56	11.72	9.87	7.16	4.80	10.34

*MSs are given in the order of proximity to the sea, **The best performing model for each station is given in bold.

Table 7. Percent changes in Correlation, RMSD and PBIAS values of the ETS relative to the best RCMTS

MS ID*	Correlation			RMSD			PBIAS		
	ANN	SE	SAM	ANN	SE	SAM	ANN	SE	SAM
17290	17.5**	15.8	15.8	-18.1	-14.2	-16.4	248.9	418.7	278.4
17296	19.2	17.3	17.3	-12.0	-9.1	-11.2	382.7	629.7	493.0
17320	24.5	17.0	17.0	-14.7	-9.9	-11.9	31816.7	39750.0	28033.3
17340	13.0	10.9	17.4	-14.2	-12.9	-15.1	200.3	213.5	194.6
17300	30.2	27.9	27.9	-11.8	-8.9	-11.1	506.3	662.7	496.1
17330	26.7	24.4	28.9	-15.8	-13.0	-15.3	1775.7	5491.9	4737.8
17292	15.8	12.3	14.0	-18.4	-15.0	-17.5	695.8	932.7	770.6
17238	21.6	16.2	21.6	-13.5	-14.4	-16.2	218.7	32.3	69.8
17240	15.0	17.5	12.5	-23.3	-23.8	-23.8	3.8	-46.4	-26.2
17246	31.0	19.0	21.4	-19.8	-17.4	-17.4	3777.5	2505.0	2760.0
17244	37.1	34.3	31.4	-20.5	-19.3	-18.1	-44.5	155.2	191.0
17239	25.7	25.7	28.6	-14.6	-13.9	-15.3	753.2	534.8	724.7
17188	26.2	16.7	26.2	-28.2	-25.5	-28.2	45.6	59.3	79.6
17190	37.9	37.9	37.9	-17.7	-16.7	-18.8	306.9	148.6	259.0

*MSs are given in the order of proximity to the sea, **Improved values are given in bold

Table 8. Effect of log-transformation on ensemble performance for Anamur MS (17320)

	Best RCM	Worst RCM	Log-transformed			Without Log-transformation		
			ANN	SE	SAM	ANN	SE	SAM
Corr	0.53	0.26	0.66	0.62	0.62	0.64	0.62	0.61
RMSD	3.12	3.86	2.66	2.81	2.75	2.65	2.70	2.72
PBIAS	-0.06	47.21	19.15	23.91	16.88	-0.33	-0.56	-0.29

FIGURES IN MANUSCRIPT

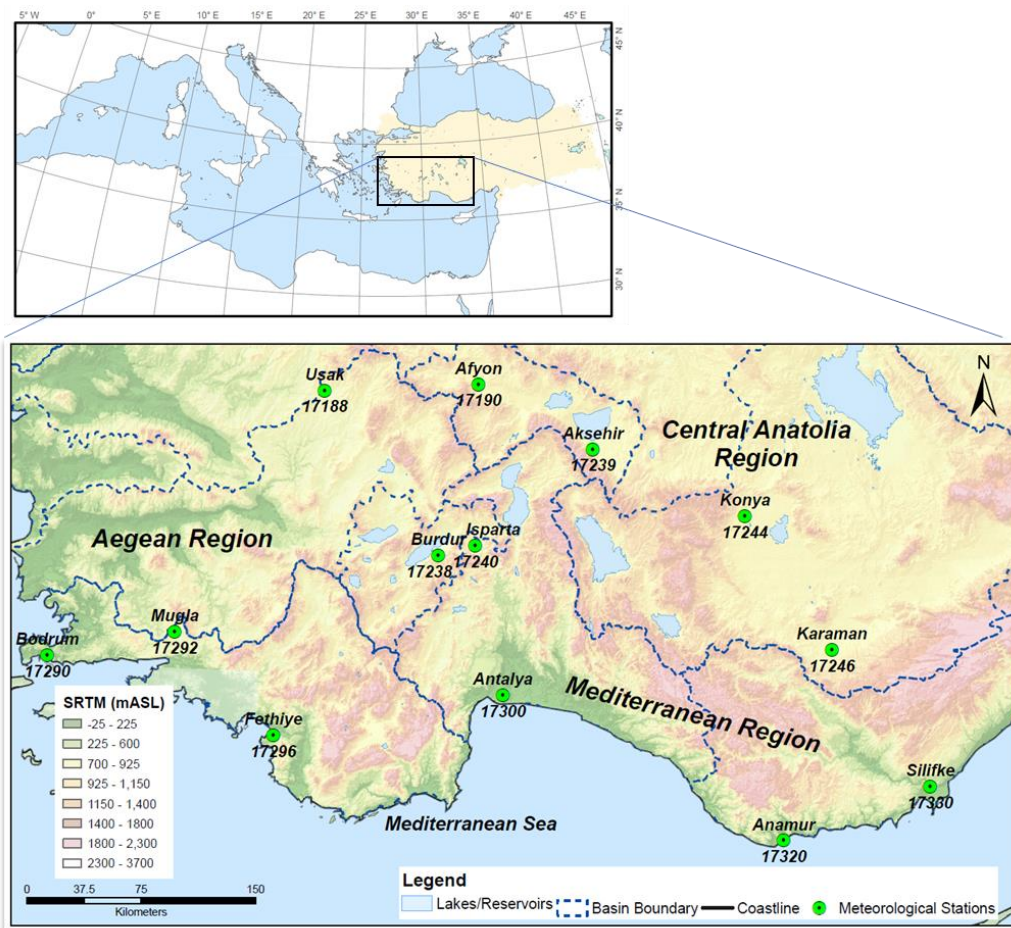


Figure 1. The Study Region and the locations of Meteorological Stations

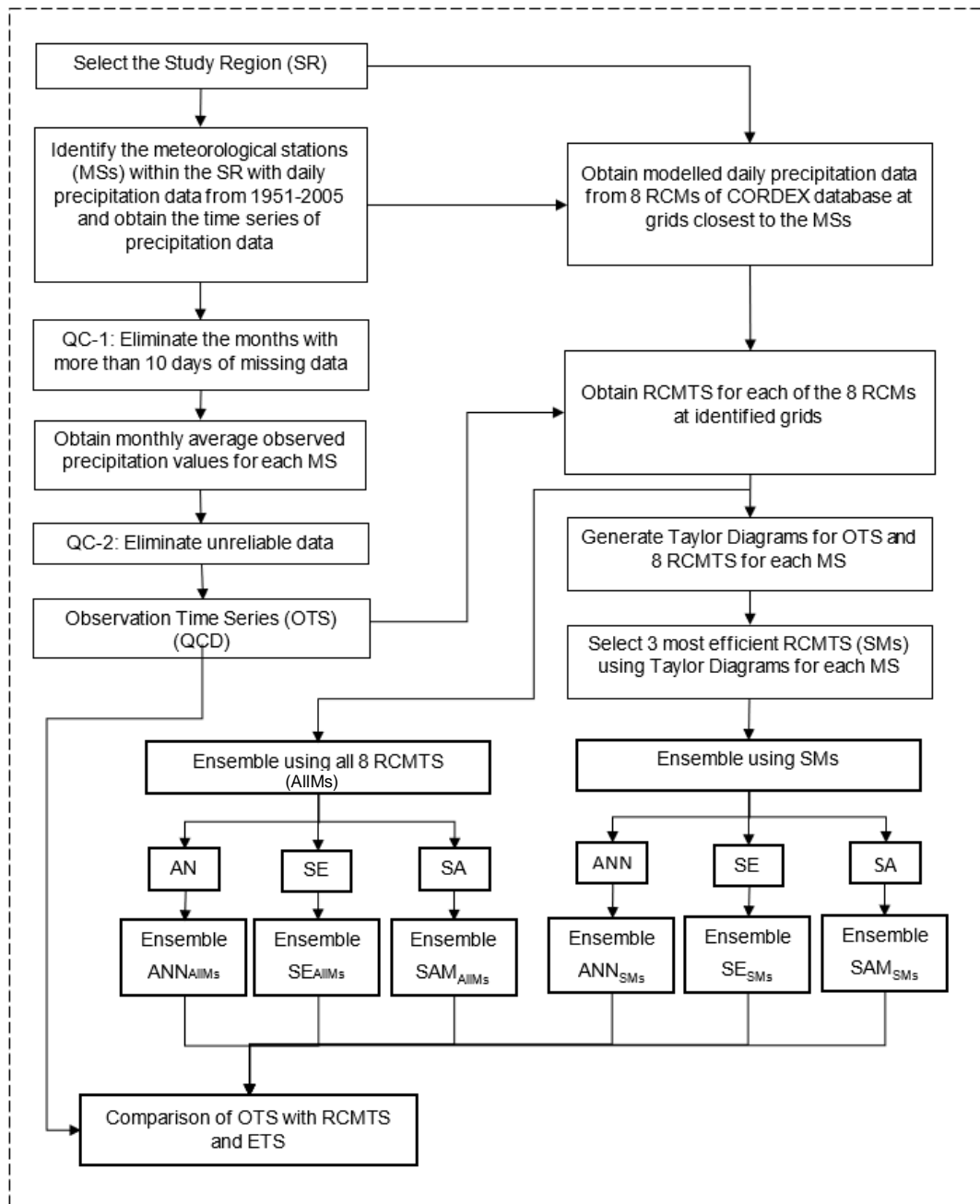


Figure 2. Flowchart of the methodology

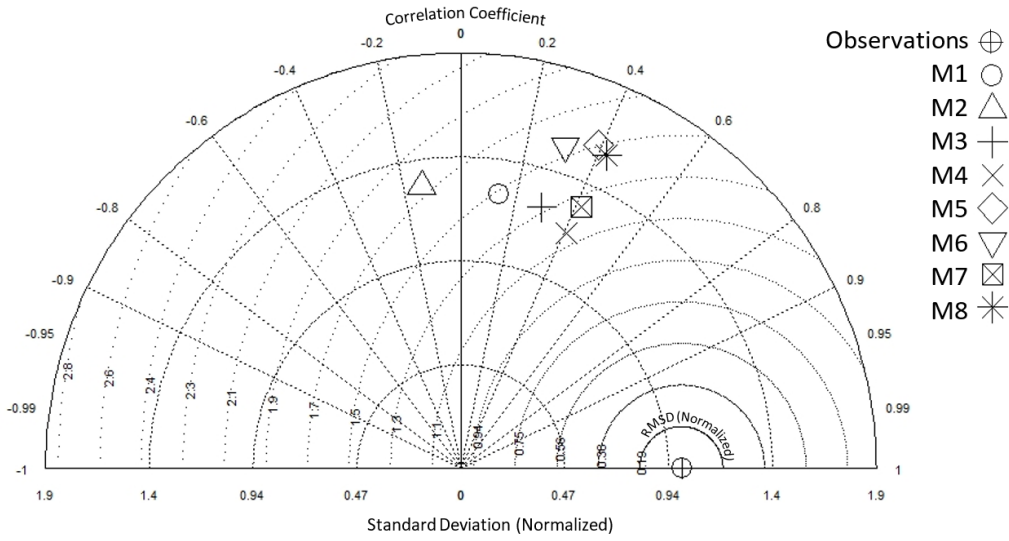


Figure 3. Taylor Diagram of Usak MS (17188)

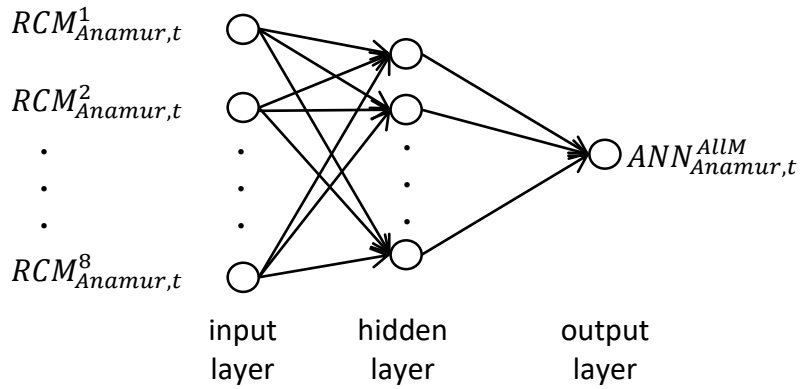


Figure 4. ANN model architecture for Anamur MS (17320)

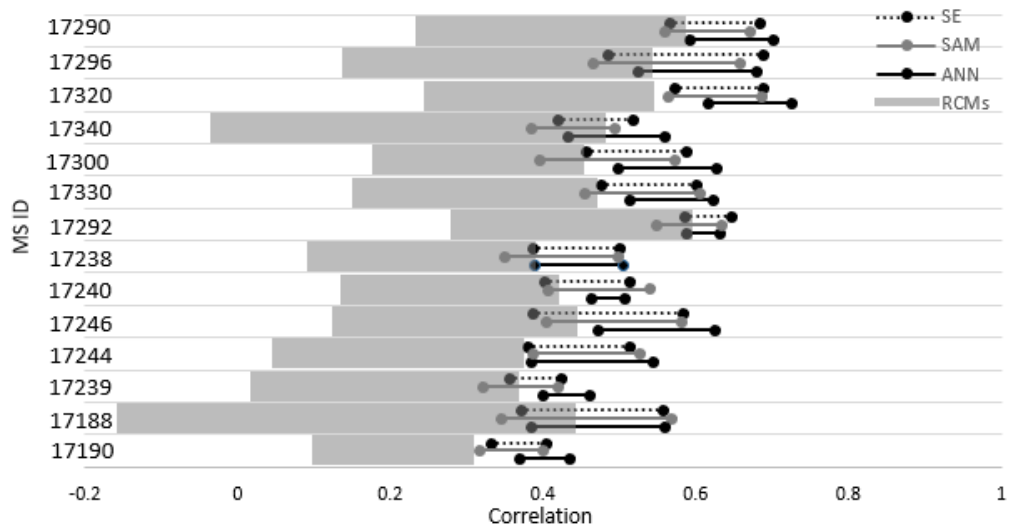


Figure 5. Comparison of correlation performances when selected models (SMs) are used as inputs

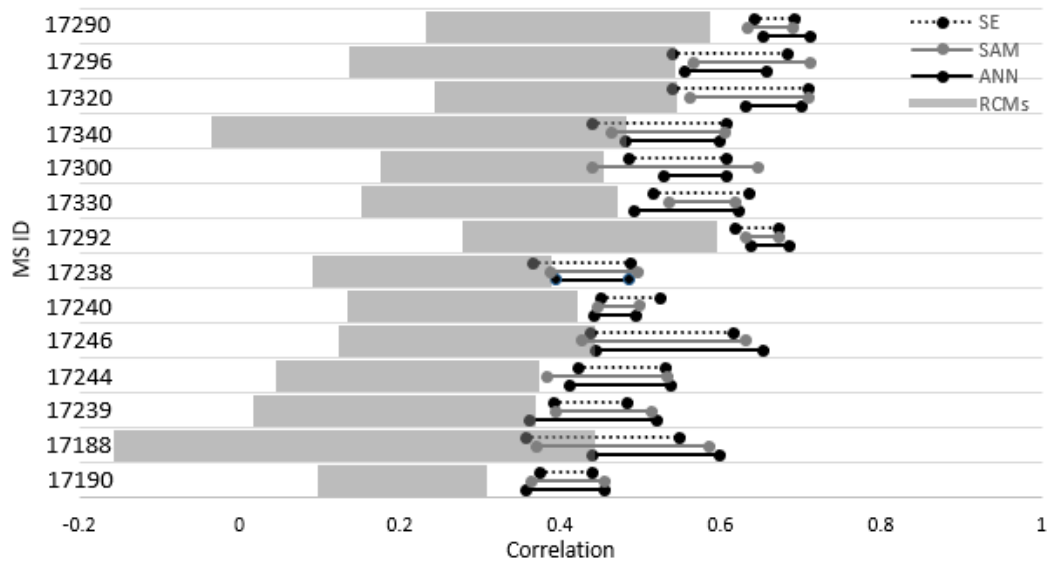


Figure 6. Comparison of correlation performances when all models (AllMs) are used as inputs

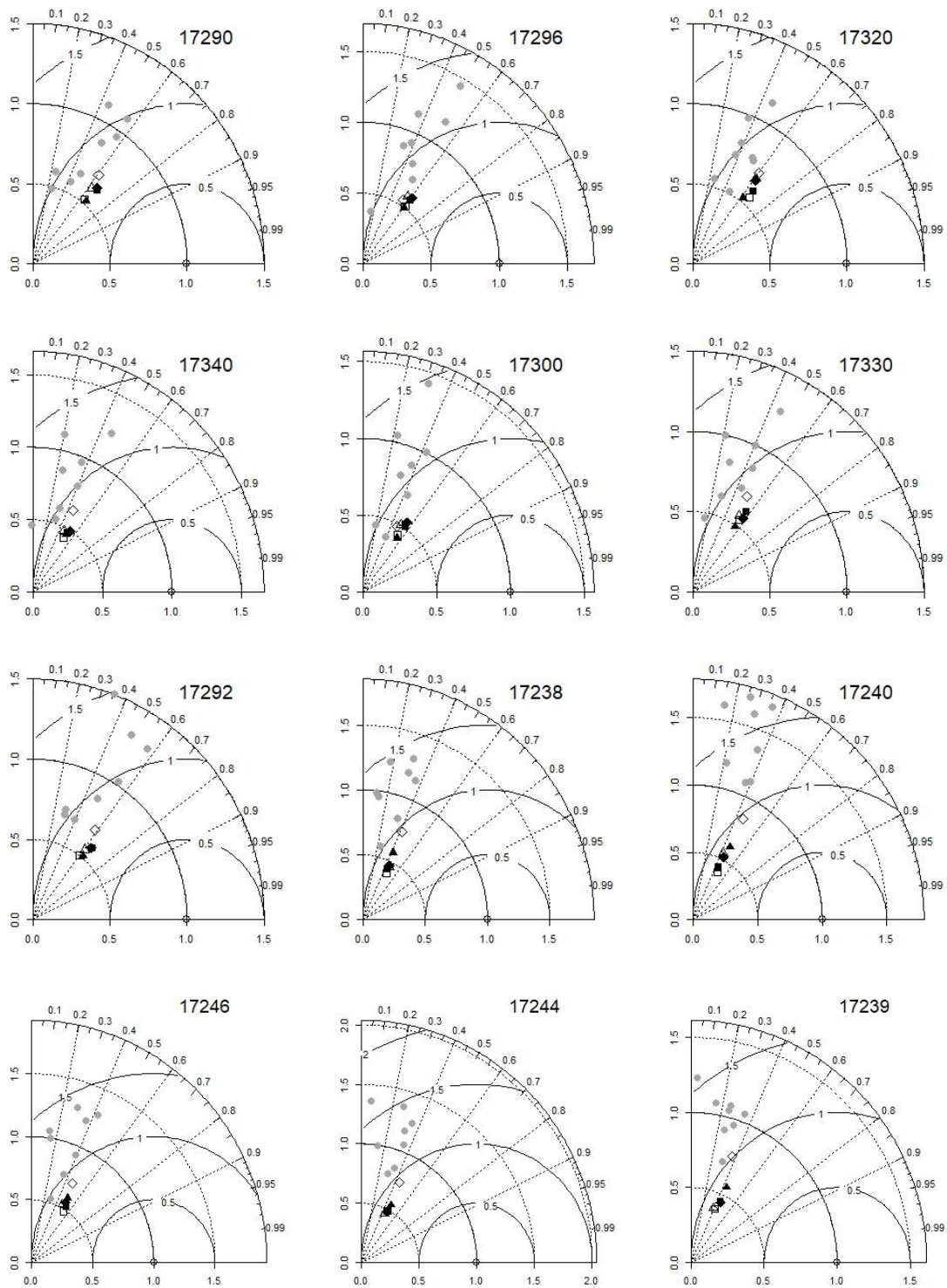


Figure 7. Taylor Diagram of RCMTS and the ETS obtained from ANN, SE, SAM for all MSs (legend and explanation of axis are provided on the bottom right diagram)

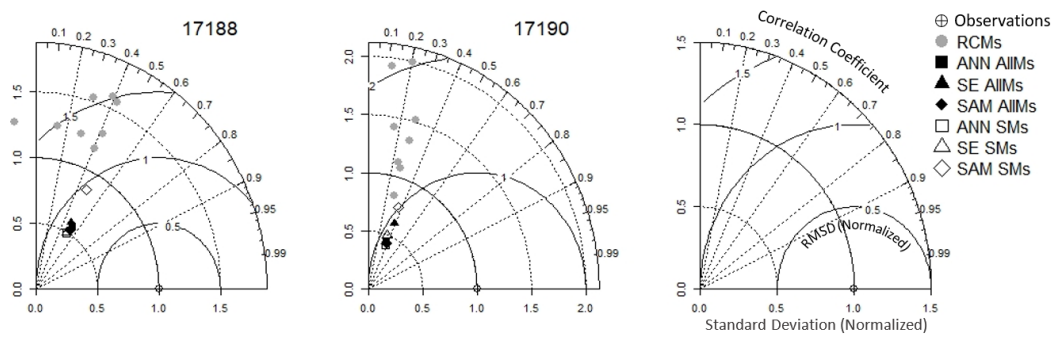


Figure 7. (continued)

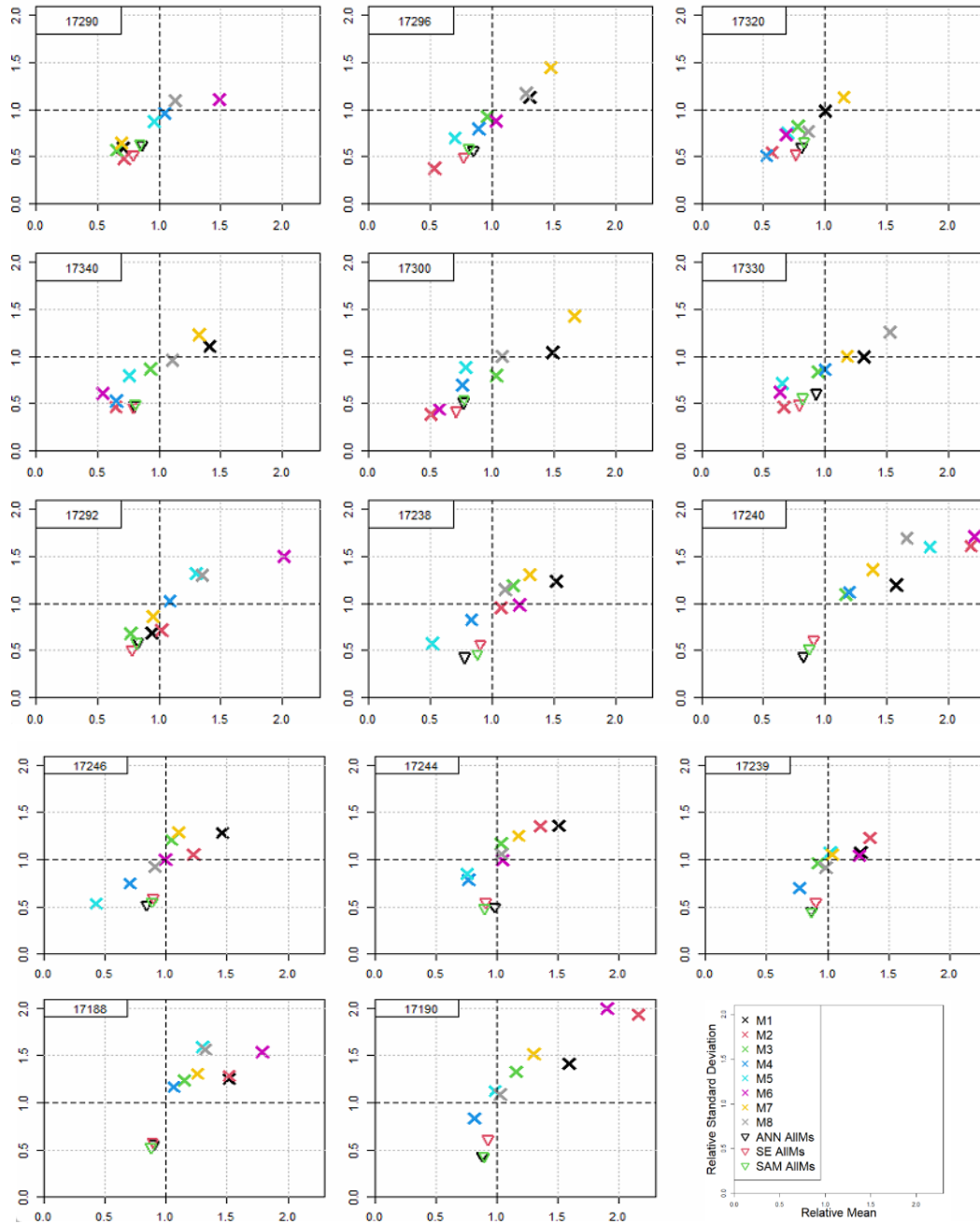


Figure 8. The relative mean versus relative standard deviation of RCMTS and the ETS obtained from ANN_AllMs, SE_AllMs, SAM_AllMs for all MSs (legend and explanation of axis are provided on the bottom right diagram)

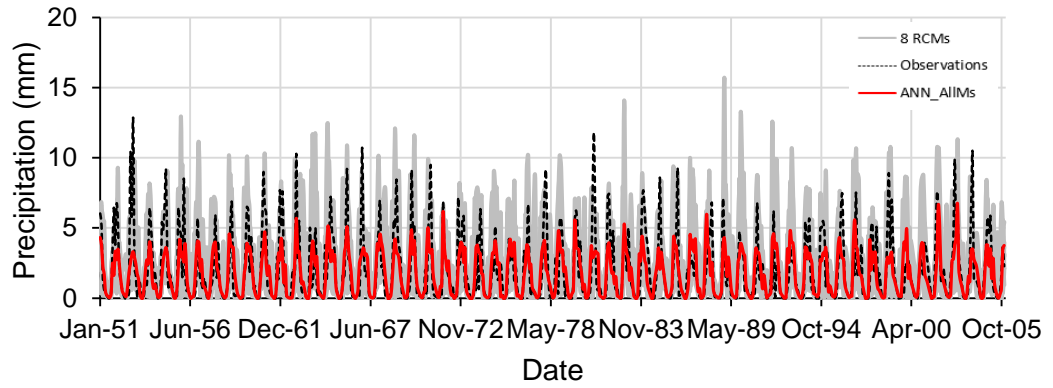


Figure 9. ETS obtained from ANN_AII Ms, observations, and eight input RCMs for Bodrum MS (17290)

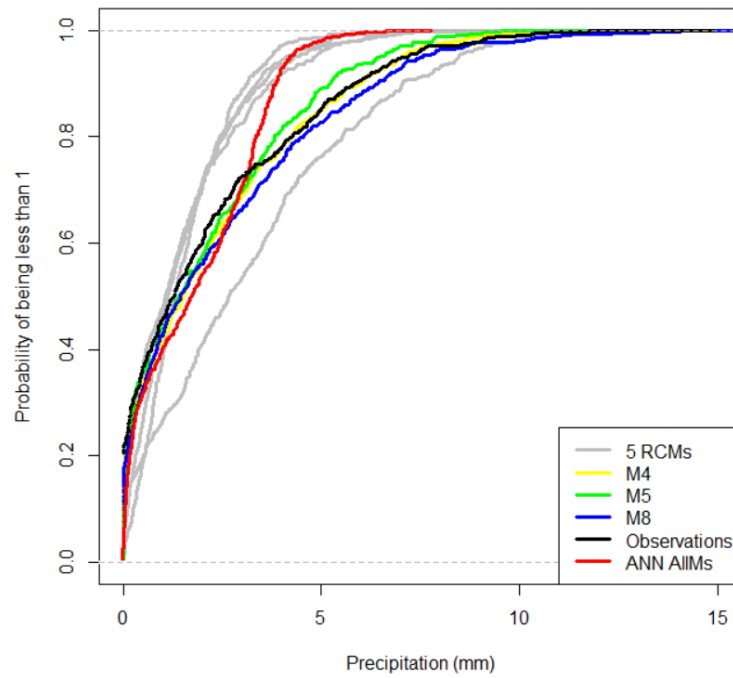


Figure 10. Cumulative distribution functions for the ETS obtained from ANN_AII Ms, observations, and eight input RCMs for Bodrum MS (17290)

**E. DAILY HYDROGRAPHS FROM HISTORICAL (1971-2005)
STREAMFLOW SIMULATIONS (Q1 TO Q12)**

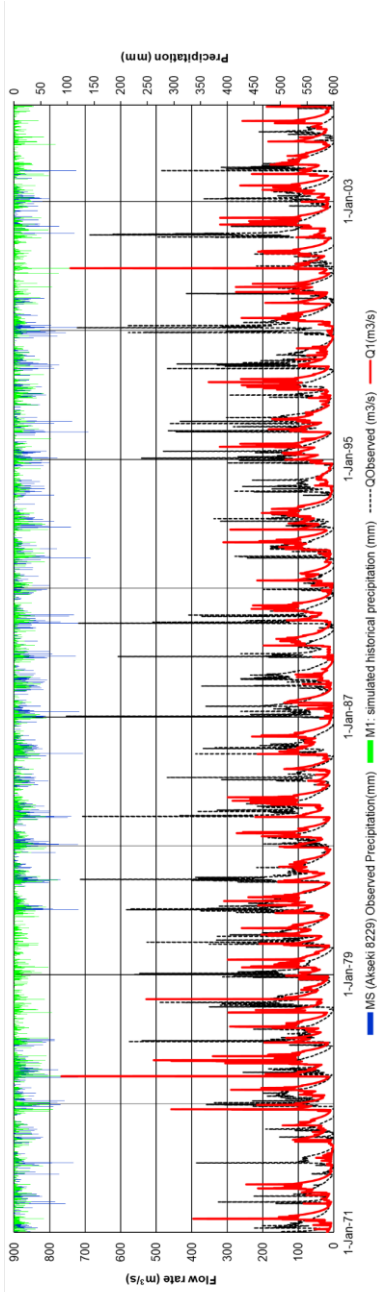


Figure E.1. Comparison of daily observed and simulated (i.e., Q1 based on CNRM-CM5_ALADIN53) hydrographs

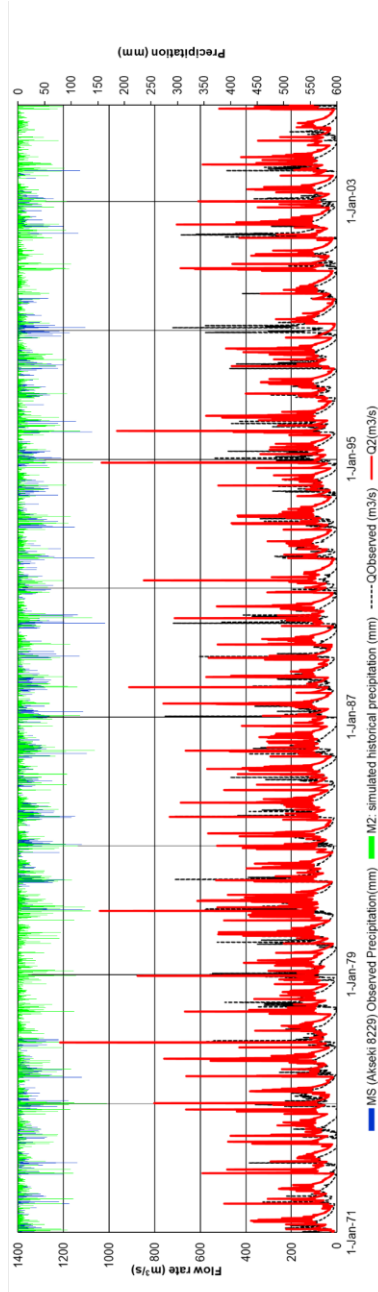


Figure E.2. Comparison of daily observed and simulated (i.e., Q2 based on CNRM-CM5_CCLM4-8-17) hydrographs

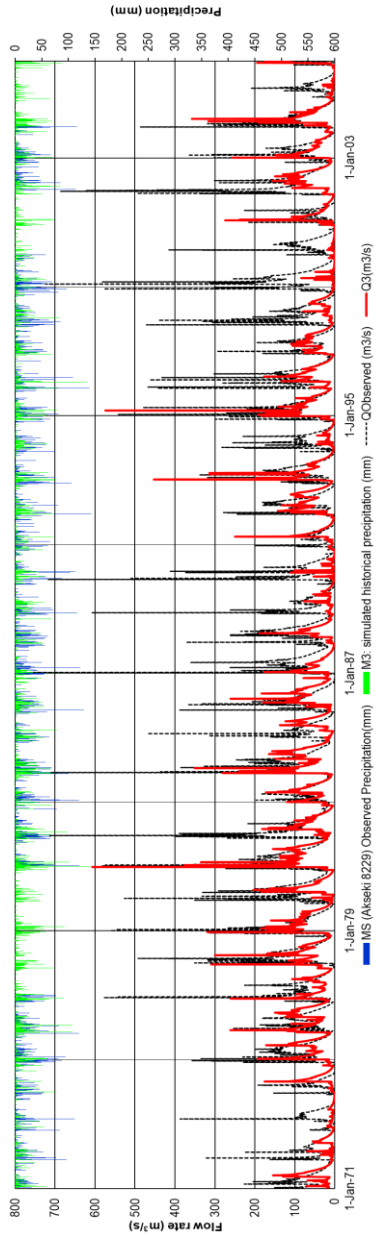


Figure E.3. Comparison of daily observed and simulated (i.e., Q3 based on CNRM-CM5_RCA4) hydrographs

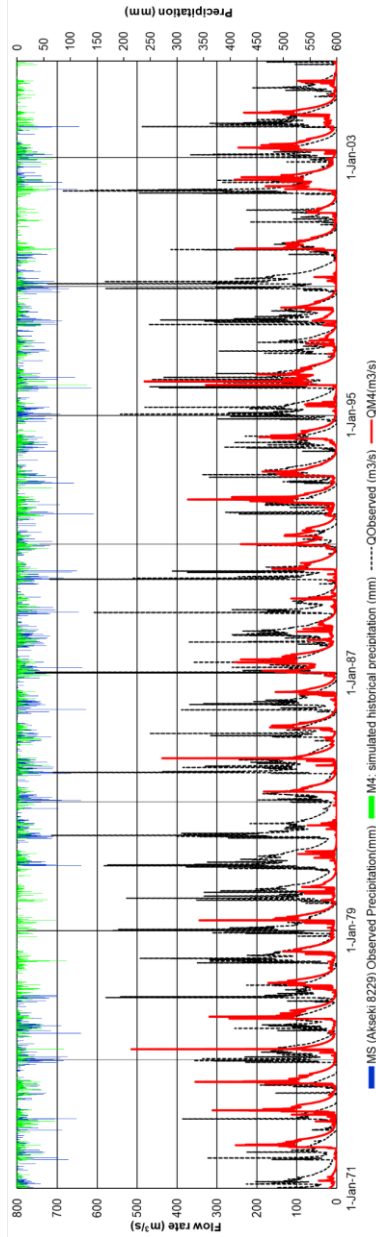


Figure E.4. Comparison of daily observed and simulated (i.e., Q4 based on EC-EARTH_CCLM4-8-17) hydrographs

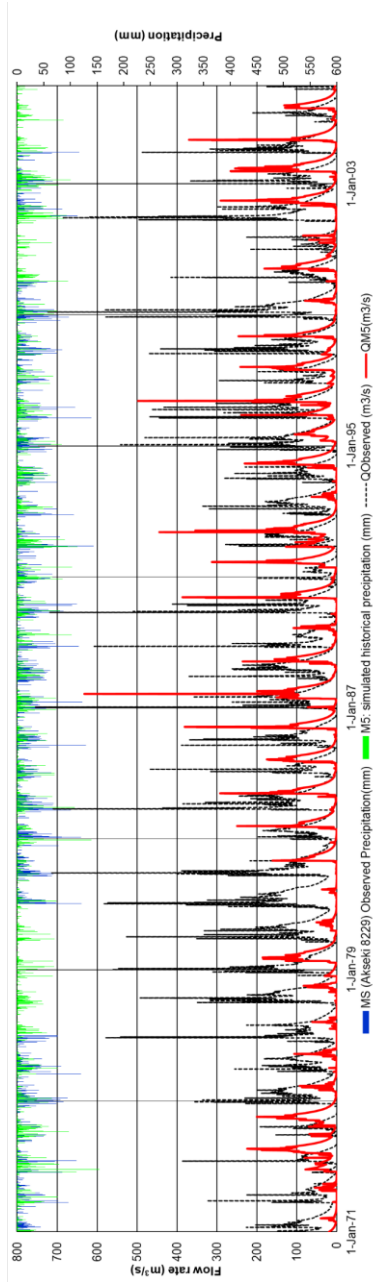


Figure E.5. Comparison of daily observed and simulated (i.e., Q5 based on EC-EARTH_HIRHAM5) hydrographs

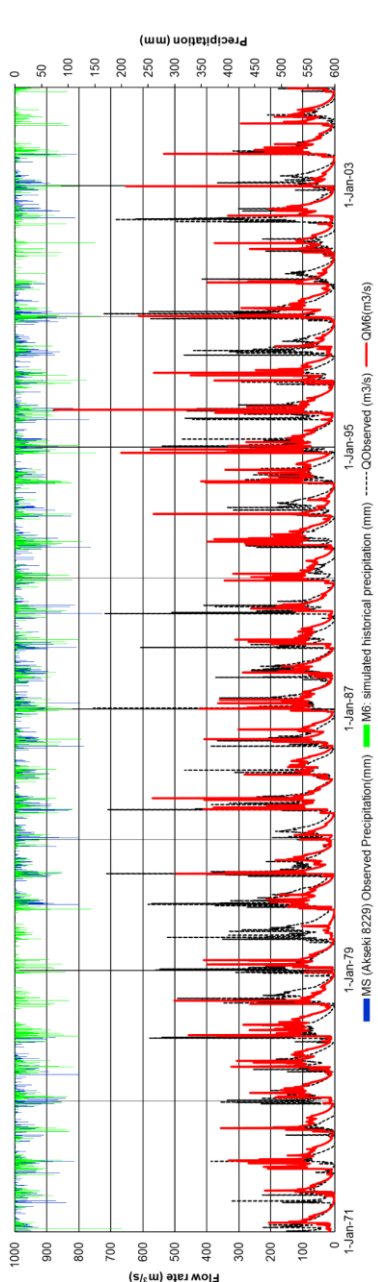


Figure E.6. Comparison of daily observed and simulated (i.e., Q6 based on EC-EARTH_RACMO22E) hydrographs

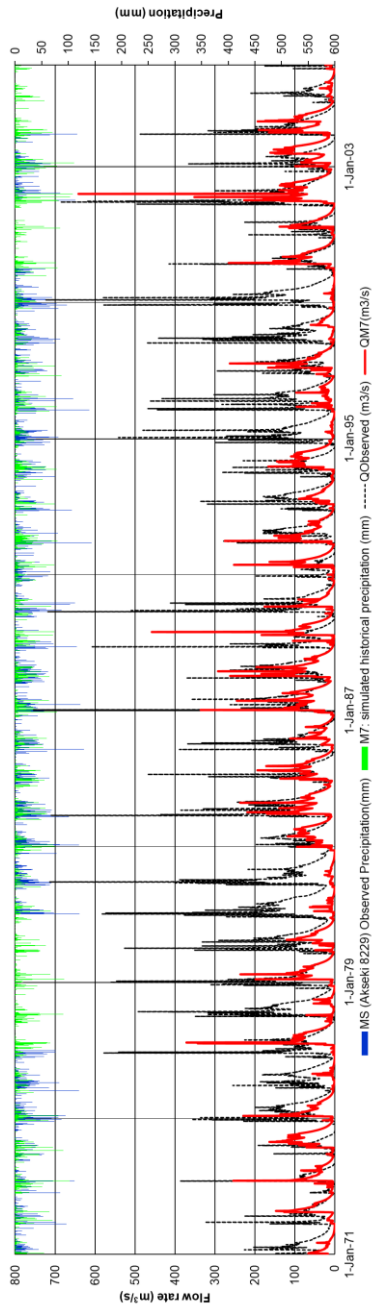


Figure E.7. Comparison of daily observed and simulated (i.e., Q7 based on EC-EARTH_RCA4) hydrographs

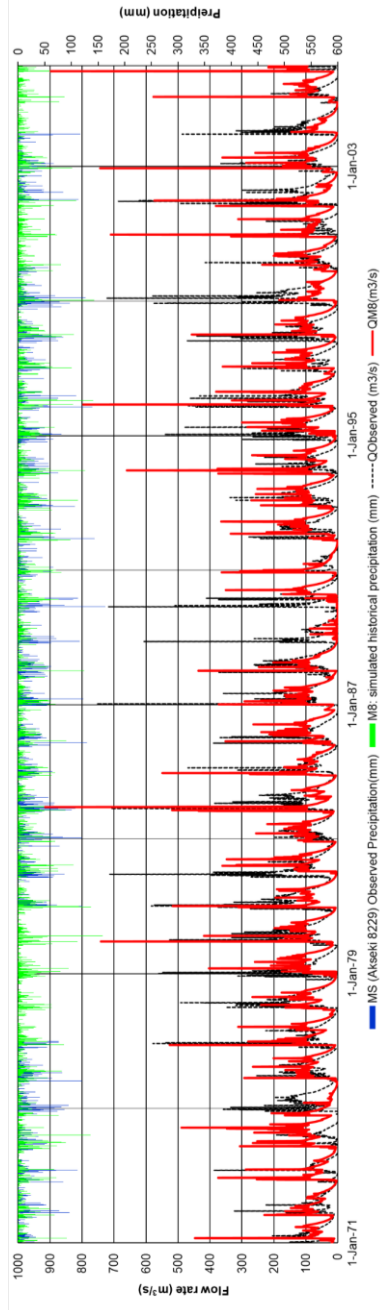


Figure E.8. Comparison of daily observed and simulated (i.e., Q8 based on CM5A-MR_RCA4) hydrographs

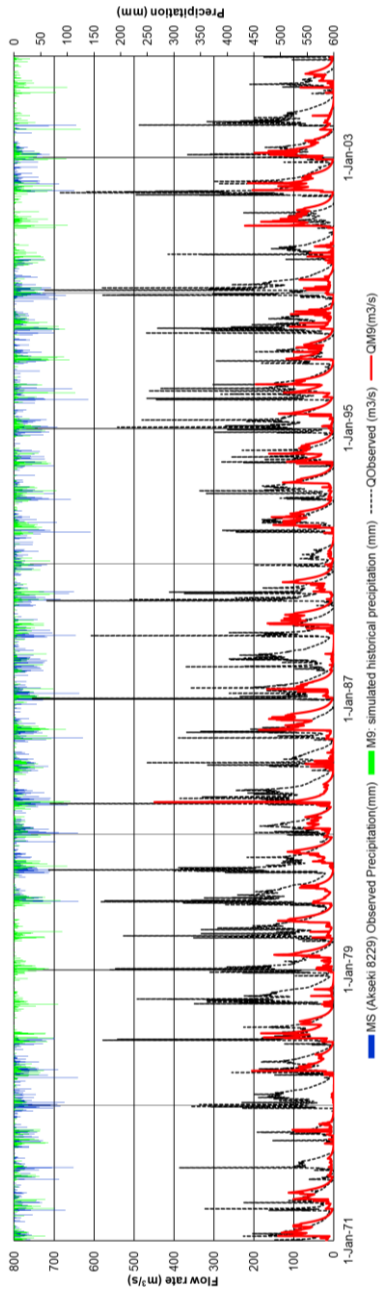


Figure E.9. Comparison of daily observed and simulated (i.e., Q9 based on CM5A-MR_WRF331F) hydrographs

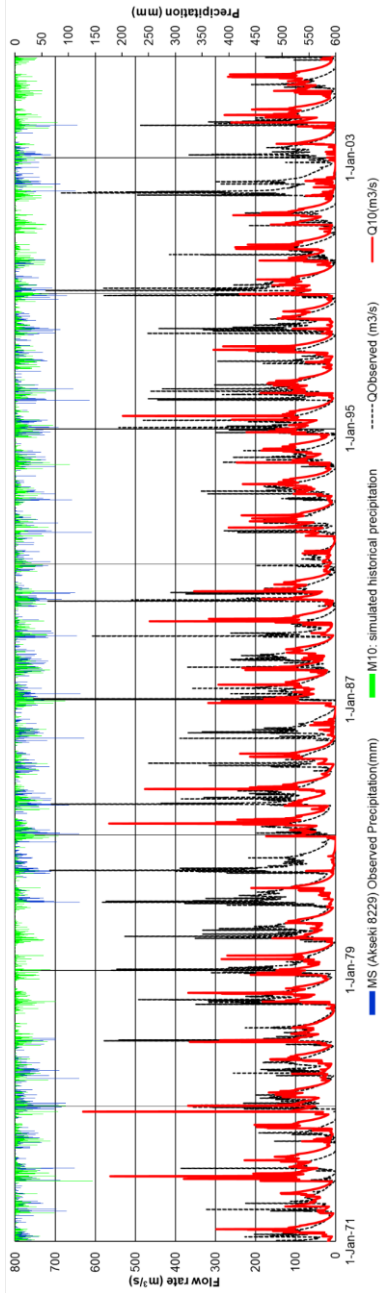


Figure E.10. Comparison of daily observed and simulated (i.e., Q10 based on HadGEM2-ES_CCLM4-8-17) hydrographs

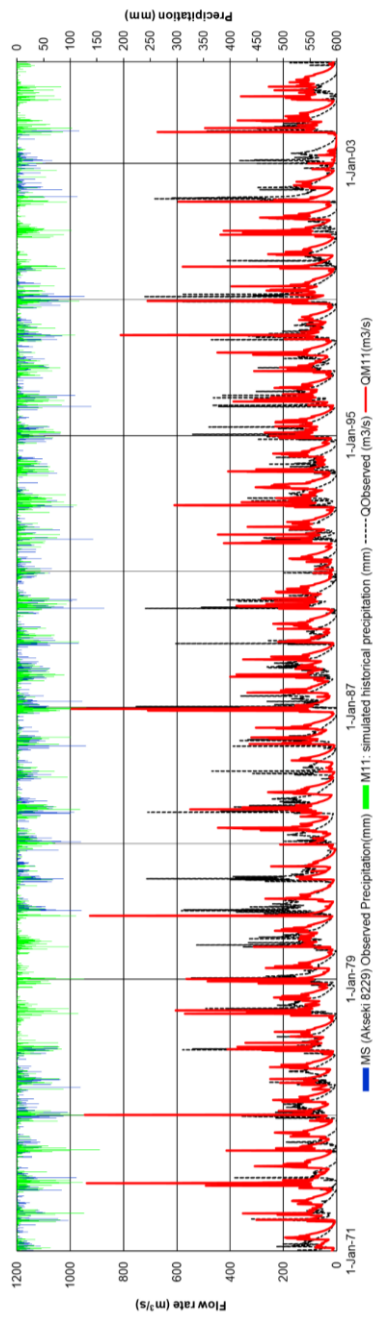


Figure E.11. Comparison of daily observed and simulated (i.e., Q11 based on HadGEM2-ES_RACMO22E) hydrographs

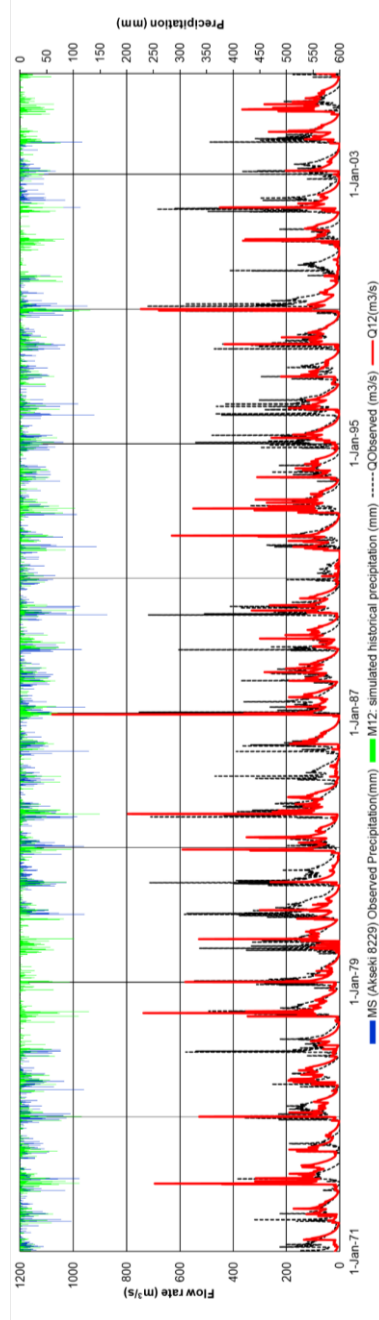


Figure E.12. Comparison of daily observed and simulated (i.e., Q12 based on HadGEM2-ES_RCA4) hydrographs

**F. DAILY HYDROGRAPHS FROM HISTORICAL (1971-2005)
 STREAMFLOW SIMULATIONS USING ENSEMBLED
 TEMPERATURE AND PRECIPITATION (Q13 AND Q14)**

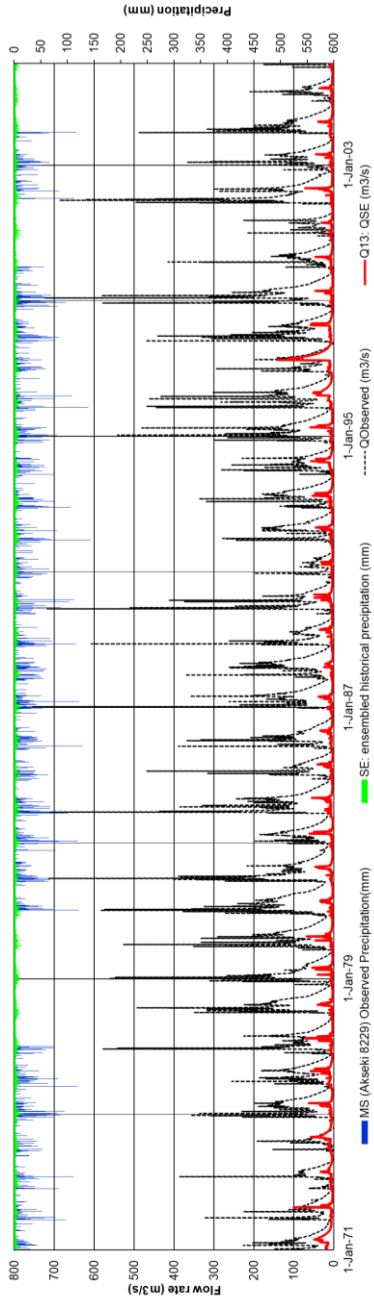


Figure F.1. Comparison of daily observed and simulated (i.e., Q13 based on ensemble temperature and precipitation with SE method) hydrographs

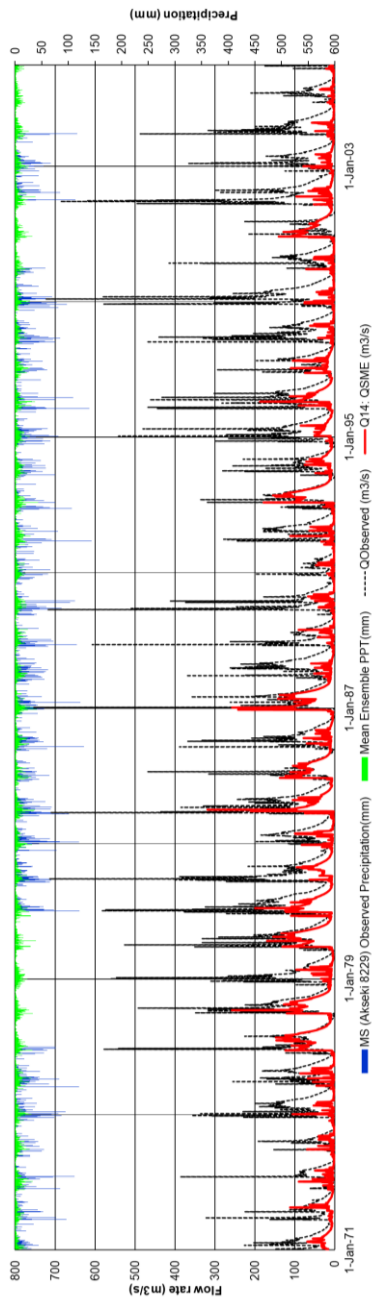


Figure F.2. Comparison of daily observed and simulated (i.e., Q14 based on ensemble temperature and precipitation with SME method) hydrographs

CURRICULUM VITAE

Surname, Name: Mesta Yoleri, Buket

EDUCATION

Degree	Institution	Year of Graduation
MS	University of Newcastle upon Tyne, Newcastle upon Tyne, UK Environmental Engineering	2002
BS	METU Environmental Engineering, Ankara	2000
Minor BS	METU Business Administration, Ankara	2000
High School	Ankara Anadolu High School, Ankara	1995

FOREIGN LANGUAGES

Fluent English

WORK EXPERIENCE

Job Title	Employer	Years
Environmental Consultant (Independent)	Freelance	2015-
Senior Environmental Engineer (Geoenvironment)	SRK Turkey, Ankara	2008- 2015

Project Technical Coordinator	ENCON Environmental Consultancy, Ankara	2007-2008
Environmental Specialist	İstanbul Governorate, İstanbul Project Coordination Unit (IPCU), İstanbul	2006-2007
Project Technical Coordinator	Encon Environmental Consultancy, Ankara	2002-2006

PUBLICATIONS

1. Mesta, B., Sasaki, H., Nakaegawa, T., & Kentel, E. (2022). Changes in precipitation climatology for the Eastern Mediterranean using CORDEX RCMs, NHRCM and MRI-AGCM. *Atmospheric Research*, 106140.
2. Mesta, B., & Kentel, E. (2021). Superensembles of raw and bias-adjusted regional climate models for Mediterranean region, Turkey. *International Journal of Climatology*.
3. Mesta, B., Akgun, O. B., & Kentel, E. (2021). Alternative solutions for long missing streamflow data for sustainable water resources management. *International Journal of Water Resources Development*, 37(5), 882-905.
4. Mesta, B., Kargi, P. G., Tezyapar, İ., Ayvaz, M. T., Göktaş, R. K., Kentel, E., & Tezel, U. (2019). Determination of Rainfall–Runoff Relationship in Yenicegoruce Basin with HEC-HMS Hydrologic Model. *Pamukkale Üniversitesi Mühendislik Bilimleri Dergisi*, 25(8), 949-955.

CONFERENCE PAPERS AND PRESENTATIONS

1. Kentel, E., Mesta, B., & Akgun, O. B. (2019, December). Multi-model analysis of bias corrected and non-bias corrected RCM simulations for the assessment of uncertainties and representation of orographic impacts in Mediterranean Region. In *AGU Fall Meeting Abstracts (Vol. 2019, pp. A51Q-2824)*.

2. Kentel, E., Akgun, O. B., & Mesta, B. (2019, December). User-Friendly R-Code for Data Extraction from CMIP6 outputs. In AGU Fall Meeting Abstracts (Vol. 2019, pp. PA33C-1098).
3. Kaya Göktaş, R., Ayvaz, T., Gökçe Kargı, P., Kentel, E., Mesta, B., Tezyapar, İ., & Tezel, U. (2018, April). Effect of land surface elevation data availability on river hydraulic model output. In EGU General Assembly Conference Abstracts (p. 14885).
4. Mesta, B., & Kentel, E. (2018, April). Inflow Analysis of a Hydropower Plant Reservoir. In EGU General Assembly Conference Abstracts (p. 18299).
5. Mesta Yoleri B., Kentel Erdogan E., Durgut P. G., Ayvaz M. T., Tezyapar İ., & Göktaş R. K. (2018, October). Yenigörüş Havzasındaki Yağış-Akış İlişkisinin HEC-HMS Hidrolojik Modeli ile Belirlenmesi, Poster Presentation, Uluslararası Kentsel Su ve Atıksu Yönetimi Sempozyumu (UKSAY)-2018, 25 October 2018, 27 October 2018, 1061 - 1068.
6. Goktas, R. K., Tezel, U., Kargı, P. G., Ayvaz, T., Tezyapar, I., Mesta, B., & Kentel, E. (2017, December). Effect of Using Extreme Years in Hydrologic Model Calibration Performance. In AGU Fall Meeting Abstracts (Vol. 2017, pp. H43B-1620).

RESEARCH PROJECTS

- PhD. Student Scholarship for TÜBİTAK Project No: 118Y365, Project Title: “Assessment of Climate Change Impacts on Streamflow and Hydropower in Antalya, Turkey (Antalya Havzasında İklim Değişikliğinin Debi ve HES Enerji Üretimine Etkilerinin İncelenmesi)”.

Project Type and Category: 2544 Project, International Project with Bilateral Collaboration with Japan Society for the Promotion of Science (JSPS)

Project Partners: METU, Japan Meteorological Research Institution, Hirosaki University

Project Start and End dates: 01.08.2019 - 01.08.2021.

- MSc. Student Scholarship for TÜBİTAK Project No: 115Y064, Project Title: “Development of a geographical information systems based decision-making tool for water quality management of Ergene watershed using pollutant fingerprints (Ergene Havzası Su Kalitesi Yönetimi İçin Kirletici Parmak İzine Bağlı Coğrafi Bilgi Sistemi Bazlı Karar Destek Sistemleri Geliştirilmesi)”

Project Type and Category: 1003 Project

Project Start and End dates: 01.03.2016 - 01.03.2019.